Rutherford
Appleton
Laboratory

RAL-85-110
Volume I

Proceedings of the Eighth Meeting of the International Collaboration
on Advanced Neutron Sources 8 — 12 July 1985

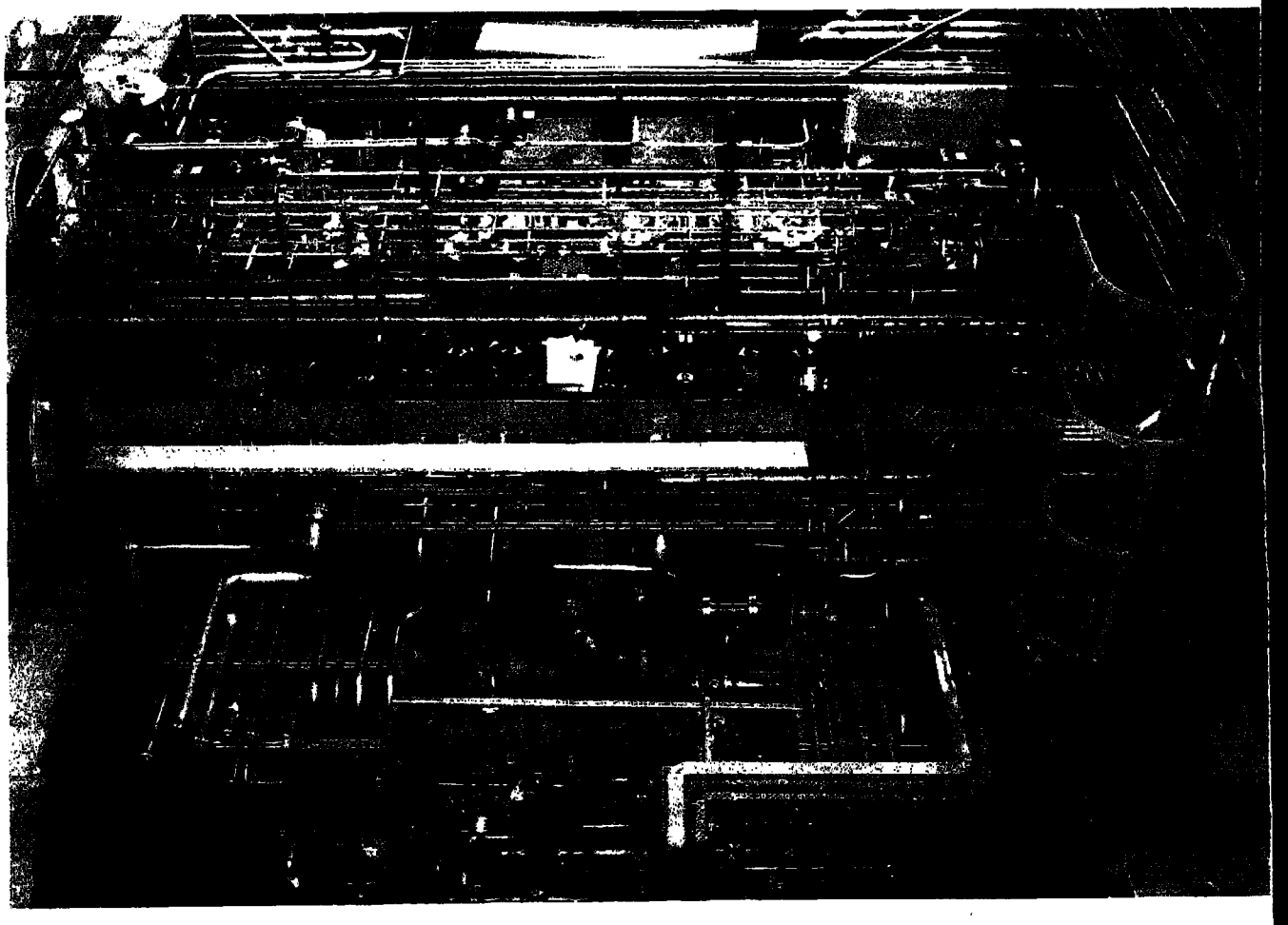

ICANS - VIII

Volume I
Status reports
Target systems
Moderators

RAL-85-110

ICANS-VIII

Proceedings of the Eighth Meeting of the International Collaboration on Advanced Neutron Sources

8-12 July 1985

VOLUME I

Status reports
Target systems
Moderators

Rutherford Appleton Laboratory
Chilton
DIDCOT
Oxfordshire

November 1985

Cover: The H_2O/D_2O cooling plant for the SNS target moderator system (see p 264)

PREFACE

The eighth meeting of the International Collaboration on Advanced Neutron Sources was hosted by the Rutherford Appleton Laboratory and held at Keble College Oxford, from the 8th to 12th July 1985. The timing, and venue in the UK, were particularly appropriate in view of the contemporaneous start-up of RAL's spallation neutron source.

Following the traditional cycle of programming, ICANS-VIII concentrated on target and moderator systems for accelerator-based sources, and on neutron-scattering instrumentation. Continuing the trend of recent meetings, there was an increasing emphasis on data and results from operating facilities, but amidst the success stories came the announcement of the demise of the SNQ project. The achievements of the Jülich team have been quite remarkable, and other ICANS laboratories will continue to benefit from their work for many years to come.

The meeting also noted with regret the recent passing of Rex Fluharty, formerly of Los Alamos. Rex had been involved with ICANS since its inception, and with his breadth of experience had been a stalwart of the Collaboration, and a valued colleague at numerous international meetings and workshops.

These ICANS-VIII proceedings follow a familiar format, opening with status reports from the participating laboratories. The presentation of subsequent papers adheres more or less to the organisation of the meeting; there has been minimal editing of individual papers in order to facilitate reproduction procedures. Two *ad hoc* workshop sessions held during the meeting, on "Boosters and Delayed Neutrons" and "The Second User Revolution" led by John Carpenter and Peter Egelstaff respectively, have not been recorded here. These sessions highlighted two important issues facing the neutron-scattering community at this time. With many of the new generation sources now becoming operational alongside the more conventional reactor sources, it is timely to ask how we proceed towards the next generation of advanced facilities, while at the same time reappraising the optimal means of exploiting their potential. It was appropriate that the present meeting chose to address these problems, which are certain to feature even more prominantly in future ICANS programmes.

GEORGE C STIRLING
Rutherford Appleton Laboratory
November 1985

Eighth Meeting of the International Collaboration on Advanced Neutron Sources (ICANS-VIII), Oxford, 8-12 July 1985

REGISTERED PARTICIPANTS

B Alefeld	Jülich	M Kohgi	Tohoku
C Andreani	Rome	J Laakmann	Jülich
T W Armstrong	La Jolla	A J Leadbetter	RAL
F Atchison	SIN	G Manning	RAL
J R J Bennett	RAL	F A Morse	LANL
S Biggin	Bristol	R O Nelson	LANL
D E Bohringer	ANL	K Neumann	IKE Stuttgart
T A Broome	RAL	R J Newport	RAL
F Brumwell	ANL	T G Perring	Cambridge
C J Carlile	RAL	G E Ostrowski	ANL
J M Carpenter	ANL	M Paoli	Oxford
B G Chidley	CRNL	J Penfold	RAL
F Cilloco	Frascati	C Petrillo	Perugia
P Cloth	Jülich	D J Picton	Birmingham
H Conrad	Jülich	B H Poulten	RAL
R Cywinski	RAL	V T Pugh	RAL
W I F David	RAL	A V Rauchas	ANL
M Davidovic	Vinca	R A Robinson	LANL
V Drüke	Jülich	H Robinson	LANL
P A Egelstaff	Guelph	G J Russell	LANL
D Filges	Jülich	F Sacchetti	Perugia
W E Fischer	SIN	A W Schulke Jr	ANL
J B Forsyth	RAL	P A Seeger	LANL
R Geick	Würzburg	R N Silver	LANL
P S Goyal	BARC Bombay	H Stechemesser	Jülich
D A Gray	RAL	H Stiller	Jülich
R K Heenan	RAL	G C Stirling	RAL
A W Hewat	ILL	Y Takeda	SIN
W S Howells	RAL	A D Taylor	RAL
Y Ishikawa	Tohoku	I M Thorson	TRIUMF
M W Johnson	RAL	Ch Tschalär	SIN
T J L Jones	RAL	H Tietze	Würzburg
M Kimura	Sendai	R C Ward	RAL
W Kley	JRC Ispra	W G Williams	RAL
K J Knowles	RAL	C G Windsor	AERE
A Kollmar	Jülich	H Wroe	RAL

TABLE OF CONTENTS

VOLUME 1

STATUS REPORTS, NEW CONCEPTS

TARGET SYSTEMS

VOLUME III

SHIELDING, BEAM DEFINITION

CHOPPER SYSTEMS

DETECTORS

DATA ACQUISITION

ANCILLARY DEVICES AND EQUIPMENT

Proceedings of the Eighth Meeting of the International Collaboration on Advanced Neutron Sources (ICANS-VIII)
8-12 July 1985, Rutherford Appleton Laboratory Report RAL-85-110

Status of the Intense Pulsed Neutron Source*

John M. Carpenter, Bruce S. Brown,
Robert L. Kustom, Gerard H. Lander,
Charles W. Potts, August W. Schulke
Argonne National Laboratory
Argonne, Illinois 60439 USA

and

Gödehard Wüstefeld
Argonne National Laboratory and KFA Jülich

Introduction

Fortunately in spite of some premature reports of its impending demise, IPNS has passed the fourth anniversary of the first delivery of protons to the targets (May 5, 1981) and is approaching the fourth anniversary of its operation as a scattering facility (August 4, 1981). On June 10, 1984, the RCS delivered its one billionth pulse to the IPNS target--the total number of protons delivered to the targets amounted then to 75 stp cm^3 of H_2 gas! Since startup IPNS has improved steadily in terms of the performance of the Rapid Cycling Synchrotron, the source and its moderators and the scattering instruments, and a substantial and productive user program has evolved.

This report summarizes the current status of the Intense Pulsed Neutron Source at Argonne National Laboratory. We include reference to recent accelerator operating experience, neutron facility operating experience, improvements to these systems, design work on the ASPUN high-current facility, booster target design, the new solid methane moderator, characterization of the room temperature moderators, and provide some examples of recent results from several of the spectrometers.

Status of the Rapid Cycling Synchrotron

Recently RCS has run with high reliability and delivered time-average currents of 12 μA (see Figures 1 and 2). Our standard operating mode is to accelerate to 450 MeV, since the increased reliability at that energy compensates for the higher neutron yield at the design energy of 500 MeV. In the October 1984 running period RCS suffered a leak in the cooling line of the extraction septum magnet, which cost several months of availability which have been made up in the succeeding months. Recent developments have improved the performance of the accelerator, namely the installation of a new clock which enables the accelerator to run almost synchronously with the power line while still allowing the choppers to operate with high reliability, and the use of carbon stripping foils which require less conditioning than the polymer foils used until now, and seem to live longer. These improvements have led to average currents near 13 μA. At the time of shutdown for the summer on 3 July, 1985, the current was 14 μA! Other contributions [1,2] in this Meeting describe these developments in greater detail.

* Work Supported by U. S. Department of Energy

Status of the ASPUN-FFAG

Argonne is developing the design for an advanced super pulsed-spallation neutron source called ASPUN that uses a fixed-field alternating-gradient accelerator as the proton source. Work on this design has gone on at a somewhat reduced pace in the past months, due to the work on other accelerator projects of importance to the Laboratory.

The design goal for ASPUN is to deliver a peak flux greater than 1×10^{17} thermal neutrons/cm^{2}sec at the beam target with a repetition rate of somewhere between 10 Hz and 100 Hz. If a direct scaling from the IPNS target, which is currently in operation at Argonne, is reasonable, an average beam current of 1380 μA at 1500 MeV would be sufficient to achieve this neutron flux. In order to provide a sizeable safety margin in startup, the design goal for ASPUN is 3800 μA. Table 1 shows a summary of the main-ring parameters.

Table 1

ASPUN Main Ring Parameters

Injection Frequency	240 Hz
Extraction frequency	40 Hz
Injection energy (H^-)	200 MeV
Extraction energy	1500 MeV
Injection radius	25.888 m
Extraction radius	28.139 m
Number of sector magnets	20
Magnetic field (injection/extraction)	0.413 T/1.327 T
Field index k = (R/B) (dB/dR)	14
Spiral angle	61°
Horizontal acceptance	650 π mm-mrad
Vertical acceptance	500 π mm-mrad
Betatron tunes ν_x/ν_z	4.25/3.3
RF frequencies (2nd harmonic)	2.08/3.09 MHz
(1st harmonic)	1.54/1.57 MHz
Peak RF voltage per turn	400 kV
Protons per pulse (design goal) (injection/extraction)	$1 \times 10^{14}/6 \times 10^{14}$

The plans are to accelerate on the second harmonic two bunches from the injection energy to 1250 MeV. At this energy a stack of altogether 12 bunches is built up and finally accelerated as a single bunch to 1500 MeV. Extraction is accomplished in one turn with a fast kicker magnet. The pulse length of the single extracted bunch which is transported to the target is about 325 ns.

There are two possible approaches for the FFAG to get the transverse focusing (see Figures 3 and 4). Up to now, mainly the spiral focusing with normal conducting magnets was studied[3]. Recently, an investigation of radial focusing with reversed field magnets[4] showed several important advantages compared to the earlier studies. By using superconducting coils with a peak field of about 4 T, the radial FFAG can be built with the same radius as the spiral machine but with much longer effective straight sections between the magnets. Therefore, the rf cavity gap can be placed perpendicular to the beam orbit. Additionally, the stability region in the phase space will be larger and therefore the machine will be less sensitive to field and alignment errors. Nearly all the machine parameters from Table I will be unchanged. The magnetic field distribution along the azimuthal direction is given in Figure 5. The maximum positive field on the extraction orbit will be 4 T and the minimum negative field along the same orbit will be -1.3 T. The spiral angle will be zero.

Further topics which are under study and basically identical for both types of machines are beam loading and collective phenomena. First calculations show that beam loading can be controlled by a cathode follower; alternatively a feedback amplifier operating on the second harmonic could correct the waveform distortion. The transverse coherent instability is a critical issue and needs to be studied in much more detail. The outcome of this study might indicate an increase in the injection energy.

Target Station Developments

It is a pleasure to report that the target and its cooling, monitoring and other associated systems have continued to operate with no significant problems. Two of the most significant accomplishments of the past year which relate to the neutron source itself, are the installation of a new solid methane moderator, and the characterization of the pulse shapes of the room temperature polyethylene moderators.

Continuing what is now a long sequence of moderator developments at IPNS, we have installed a grooved, solid methane moderator which operatoes at a physical temperature of 12 K, and produces a spectrum with a temperature of 20 K. The system has operated quite well since its installation in January, 1985, and the increased intensity of long wavelength neutrons has brought our cold neutron instruments up to a high level of performance. Figure 6 shows the spectrum of neutrons from the new moderator. Another paper provides more details on the new system[5].

With Susumu Ikeda, who visited us from KEK, we have performed careful measurements of the pulse shapes as a function of energy for the two ambient-temperature polyethylene moderators. The result is a new set of functions which fit the pulse shapes in a simple and intuitively-appealing way. Ikeda's pulse shape function is of the form

$$i(v,t) = \alpha/2 \{ (1-R)(\alpha t)^2 \exp(-\alpha t) + 2\alpha^2\beta R/(\alpha-\beta)^3 [\exp(-\beta t)-\exp(-\alpha t)(1+(\alpha-\beta)t+1/2(\alpha-\beta)^2 t^2)]\} \; ; \; t>0 \qquad (1)$$

where $\int_0^\infty i(v,t)dt = 1$, $\alpha = v\Sigma$ in the slowing down time distribution, β is the decay constant of the fundamental eigenfunction (Maxwellian), and R is the ratio of the area of the second term (the "storage term") to the total area. The constants have simple wavelength dependence,

$$\Sigma = (S_1^2 + S_2^2\lambda^2)^{1/2}, \qquad (2)$$

S_1, S_2, and β are constants, and the ratio R can be represented

$$R = \exp(-E/E_o). \qquad (3)$$

For one 10x10x5 cm^3, heavily-irradiated, ambient temperature (~50 C), polyethylene moderator poisoned at 2.5 cm depth with 0.5 mm Cd, we found S_1 = 0.98 cm^{-1}, S_2 = 0.27 cm^{-1}, $1/\beta$ = 24.1 μsec and E_o = 190. meV. In Equation 1 the first term represents the escape of neutrons from the moderator while they are slowing down; the second term represents the escape of thermalized neutrons, whose exponentially-decaying population is fed by the slowing-down time distribution. The mean emission time derived from the distribution (1) is

$$\bar{t} = 3/2\alpha + R/\beta. \qquad (4)$$

Figure 7 shows the time dependence of the neutron pulse as a function of energy, resulting from a least-squares fit of Equation 1 to data between .00253 eV and 0.648 eV. A complete description of the work[6] will soon appear. These results already provide the basis for complete understanding of the chopper spectrometer resolution functions and energy transfer scales. We hope that they may also provide better profile functions and time scale calibrations for time-of-flight diffractometers.

Booster Target Development

In order to supply greater neutron beam intensities, we have launhced a program to produce an enriched uranium booster target for IPNS. The principles guiding the development have been to provide a modest gain while imposing no requirements for major changes in the target station, and producing no significant increase in the width of the primary source neutron pulse. This led to the choice of a nominal gain factor of 5, (k_{eff} = 0.80) in a fast, subcritical arrangement. The total power , about 90 kW compared to the present 10 kW, can be handled by the present cooling systems, and no major shielding changes will be needed. The neutron beam intensity gain due to the booster will be a factor of about 3, mostly because the spallation source does not couple perfectly to the most nearly critical mode of the booster. The delayed neutron background will increase from the present roughly 0.5% to about 3.0%, which we believe will require only modest measures to overcome. Figure 8 shows a cross sectional view of the booster target.

The booster design program has been in progress for about one year and we expect to install the new system to operate in Fall, 1986. Another paper[7] describes the booster project in greater detail.

Scattering Instruments and Experimental Facilities

We have made a number of improvements, modifications and additions to the scattering instruments and the facilities available to the users. Table 2 summarizes the most significant ones.

Table 2.

Summary of Improvements and Modifications of

IPNS Scattering Instruments and Experimental Facilities

Large-angle ($90^\circ < \phi < 140^\circ$) flight path installed in HRMECS

Dead time in the Anger camera of SCD improved from 15 μs to 3μs, and dead time measuring system improved

Remote-window sample chamber installed on SCD--sliding seals permit full rotation of the sample

Misplaced shielding wedge relocated in SEPD--produced ×2 intensity increase

Multiple Converging Aperture collimation installed in SAD, and sample-to detector distance shortened from 3 m to 1.5 m

Additional sample environment equipment provided

New VAX 11/750 computer installed

Figure 9 shows the new large-angle flight path of the High Resolution Medium Energy Chopper Spectrometer.

Figure 10 shows the collimating system of the Small Angle Diffractometer. The converging apertures are formed by a pair of converging Soller collimators, one vertical, the other horizontal, with approximately 1.- mm exit slits, tapered to converge at the location of the detector. CIDIC of UK produced these to our specifications, using slats of ^{11}B-painted aluminium. These work quite well in spite of a small halo (actually appears like a four-petaled flower) outside the penumbra due to internal reflections. This effect seems to be controllable by additional roughening of the surfaces, which we are investigating.

We pursue a continuing effort to provide a greater range of sample environments for research at IPNS. Table 3 summarizes the present complement of pressure cells, cryostats and ovens available at IPNS. Another paper [8] deals more completely with the peripheral equipment.

Table 3.

Equipment for Special Sample Environments at IPNS

Low Temperatures
(Adaptable to most instruments)

Displex Refrigerators	$T \geq 10$ K
^{4}He Cryostat	$1.5 \leq T \leq 200$ K

High Temperatures

Diffractometer and Chopper Spectrometer Furnaces	$T \leq 1400$ C
Small-Angle Diffractometer Furnace	$T \leq 1000$ C

High Pressures
(Special Environment Powder Diffractometer, $2\theta = 90°$)

	Pressure	Volume	Temperature
Piston-Cylinder	35 Kbar	0.25 cm^3	300 K
Gas-Pressurized Cells	6 Kbar	2.0 cm^3	10 K
Clamped Piston-Cylinder	25 Kbar	1.5 cm^3	10 K

Examples of Some Recent Scientific Results

To illustrate the performance of some of the IPNS scattering instruments, we provide some examples of recent experimental results. Figure 11 shows the scattering from superfluid Helium, measured at the Low Resolution Medium Energy Chopper Spectrometer, with incident energy E_o = 160 meV and a the scattering angle ϕ = 116 . The measurements were performed by P. Sokol, R. Simmons, D. Price and R. Hilleke. Plotted is the difference between data taken in the superfluid phase at 1.0 K, and in the normal phase at the same atom density, $1/\rho$ = 27. cm^3/mole. (We have found that the mean kinetic energy in the normal substance depends almost exclusively on the density.) The wave vector change at the peak of the scattering is about 13. $Å^{-1}$. The positive component is the resolution-broadened scattering from the zero-momentum Bose condensate. The fitted function is the difference of two gaussians; the result of the fit is that the integrated difference is zero, indicating that the area lost from the broad, normal component appears in the condensate peak. Figure 12 shows the condensate fraction n_o measured in this way.

Figure 13 shows a plot of the diffracted intensity distribution in the (4.93,k.1) plane of $(BEDT\text{-}TTF)_2I_3$, [bis(ethylenedithio)tetrathiafulvalene triiodide] at 20 K, measured at the Single Crystal Diffractometer; by Emge, et al.[8]. The sample mass was 2 mg, and the counting time for these data was 24 hours. Superlattice peaks with indices (hkl) $\pm$ q, where q = (0.08, 0.27,0.205) appear below 200 K.

Figure 14 illustrates the result of the measurement **in situ** of the scattering from CoO(1-x)O, slightly non-stoichiometric Cobalt Oxide, at 1100 C under a small partial pressure of CO. The data are those of John Faber and his colleagues. The main figure shows the data from scattering angle $2\Theta = 90°$, the Rietveld refinement, the location of the Bragg peaks and the residual of the fit. The inset shows the variation of the lattic parameter with defect concentration x (note the very small values of x). The high resolution of the instrument allowed determination of the changes in lattice parameter on the order of one part in 10^4. The inset also shows the variation of the isotropic thermal parameters of the Co and O atoms as a function of x, made possible by the measurements a small d spacings.

Figures 15a and 15b show the diffraction pattern of the collagen of kangaroo tail tendon reconstituted in D_2O, compiled from the 14. Å wavelength bin (15a) and from the 7. Å wavelength bin (15b) The long-wavelength data illustrate the low-Q range accessible ($Q_{min} = 0.0036$ Å^{-1}) and the resolution of the instrument. The shorter-wavelength data show the first six orders of reflection from the structure (the second order structure factor is zero). The instrument is now very effective, with good Q_{min} and good resolution, and the wide Q range which is characteristic of TOF Small Angle Scattering instruments; these result from the installation of the new converging aperture collimation and the new solid methane moderator.

User Program

The use of IPNS continues to increase, as do the number of users and total amount of instrument time requested. Figure 16 shows the total number of requested instrument days, those requested by non-Argonne scientists as principal investigator and the (smaller) number of instrument days available for each six month proposal period. Table 4 shows the distribution of requests for instrument time for the January 1984 proposal period. We are oversubscribed by a factor of 2.5 on average, and a factor of more than 3. on the chopper spectrometers.

Table 4.

	Requested				
	Non-ANL	ANL Instrument Scientist	ANL Other	Total	
Powder diffractometers (SEPD & GPPD)	179	11	38	227	86
Single crystal diffractometer	105	0	1	106	43
Small-angle diffractometer	36	41	16	93	43
Chopper spectrometers (HRMECS & LRMECS)	240	7	26	273	86
Crystal analyzer spectrometer	59	0	0	59	43
	619	59	80	758	301

Table 5.

	FY 1983	FY 1984
Weeks of operation	26	29
Number of experiments performed	110	210
Visitors to IPNS for at least one experiment:		
DOE labs - ANL	41	49
DOE labs - other	7	7
Other government labs	2	1
Universities	33	45
Industry	5	9
Foreign	18	39
	106	150

The users come from many institutions; Table 5 shows the distribution according to types of institution for the years 1983 and 1984. The table entries do not include multiple visits by one person in one year.

Conclusions

IPNS continues to improve and to serve a useful role in the community of facilities for condensed matter science.

References

1. A. Rauchas, F. Brumwell, C. Potts, V. Stipp and G. Volk, "Status of the Intense Pulsed Neutron Source Accelerator System", these proceedings.

2. G. E. Ostrowski, L. I. Donley, A. V. Rauchas, G. J. Volk, E. A. Jung, J. R. Haumann and C. A. Pelizzari, "The IPNS Chopper Control and Accelerator Interface Systems", these proceedings.

3. R. L. Kustom, T. K. Khoe and E. A. Crosbie, "A 1500 MeV Fixed-Field Alternating Gradient Synchrotron for a Pulsed Spallation Neutron Source", to be published in the proceedings of the Particle Accelerator Conference, Vancouver, Canada, 13 - 16 May, 1985.

4. P. F. Meads and G. Wüstefeld, "An FFAG Compressor and Accelerator Ring Studied for the German Spallation Neutron Source", to be published in the proceedings of the Particle Accelerator Conference, Vancouver, Canada, 13 - 16 May, 1985.

5. John M. Carpenter, August W. Schulke, Terry L. Scott, Denis G. Wozniak, Burton O. Benson and Bryan D. Leyda, "The IPNS Grooved, Solid Methane Moderator", these proceedings.

6. Susumu Ikeda and John M. Carpenter, "Wide-Energy-Range, High-Resolution Measurements of Neutron Pulse Shapes of Polyethylene Moderators", to be published in Nuclear Instruments and Methods in Physics Research (1985).

7. A. W. Schulke, Jr. for the IPNS Enriched Uranium Booster Target Design Team, "IPNS Enriched Uranium Booster Target", these proceedings.

8. D. E. Bohringer and R. K. Crawford, "Sample-related Peripheral Equipment at IPNS", these proceedings.

9. T. Emge, P. Leung, M. Beno, A. Schultz, L. Sowa and J. M. Williams, Phys Rev B 30, 6780 (1984).

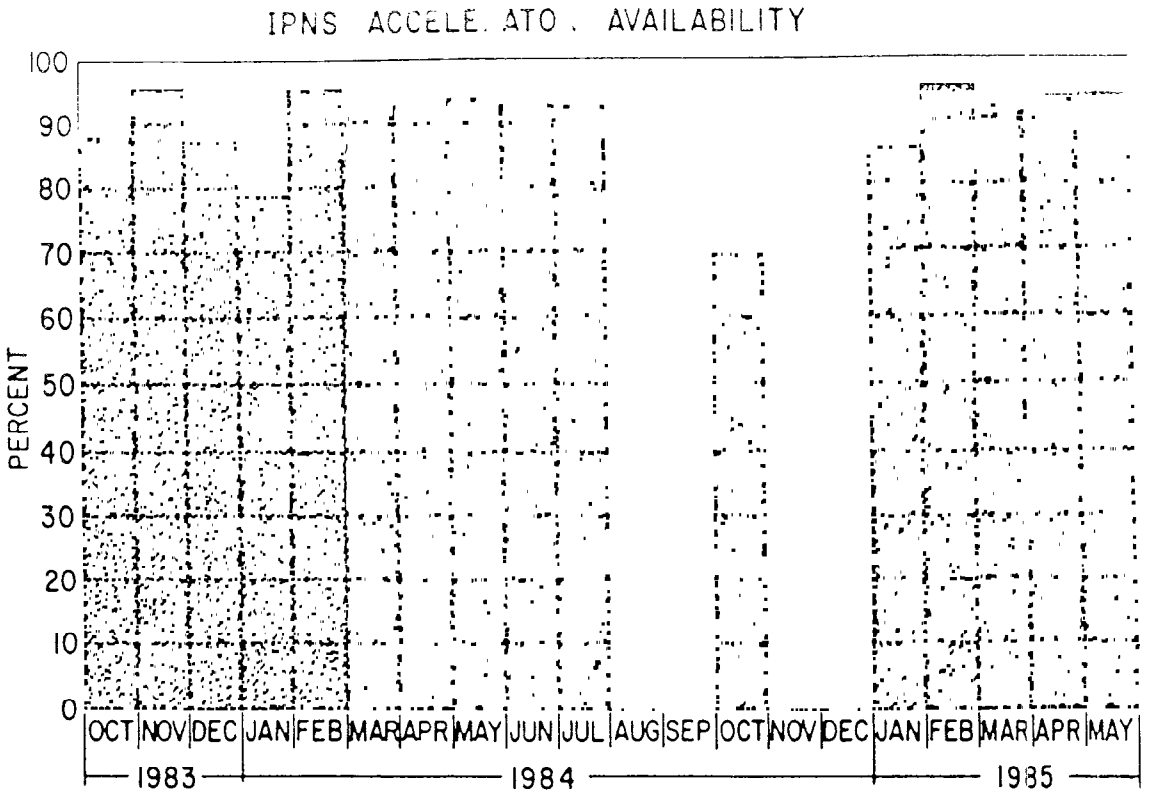

1. Availability of the Rapid Cycling Synchrotron.

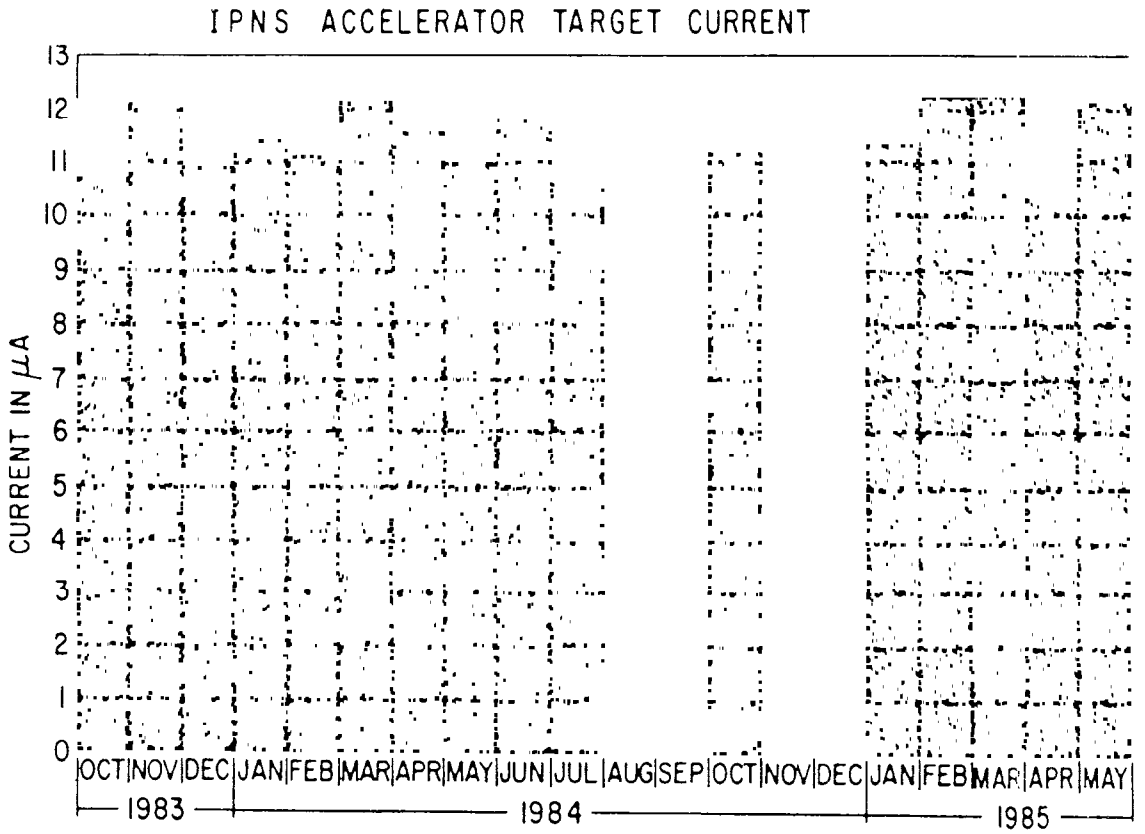

2. Average current delivered by RCS to the IPNS target (30 Hz).

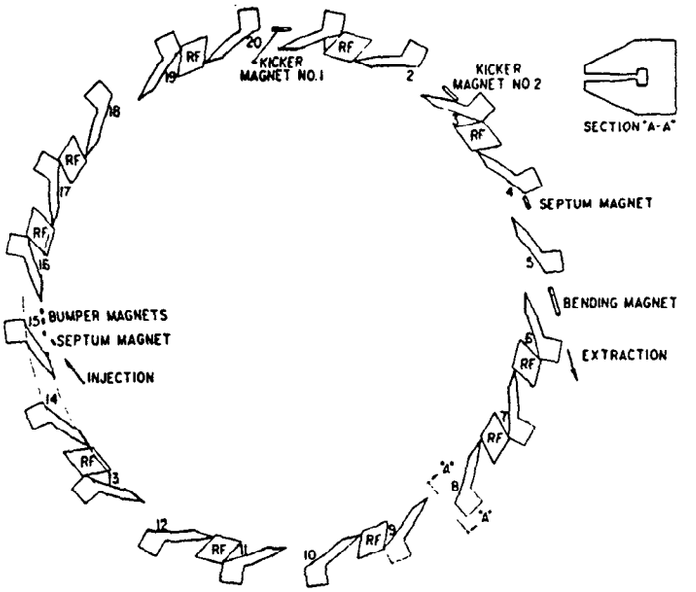

3. Schematic view of the 1500 MeV FFAG, spiral type.

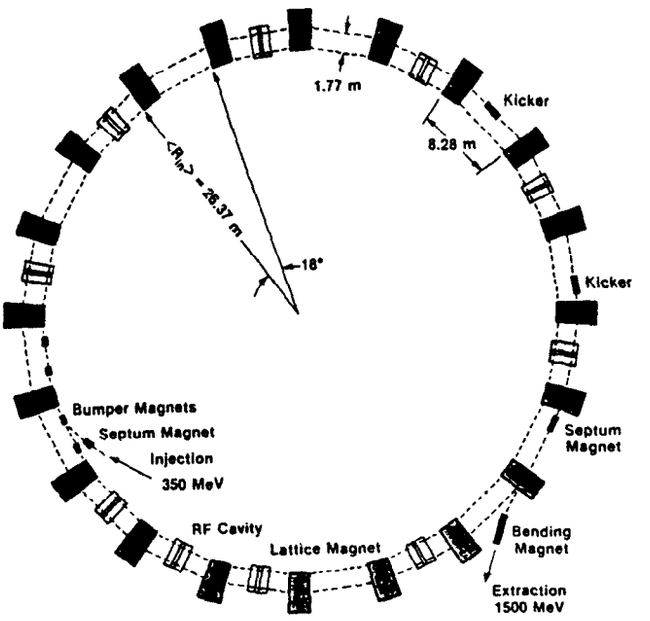

4. Schematic view of the 1500 MeV FFAG, radial type.

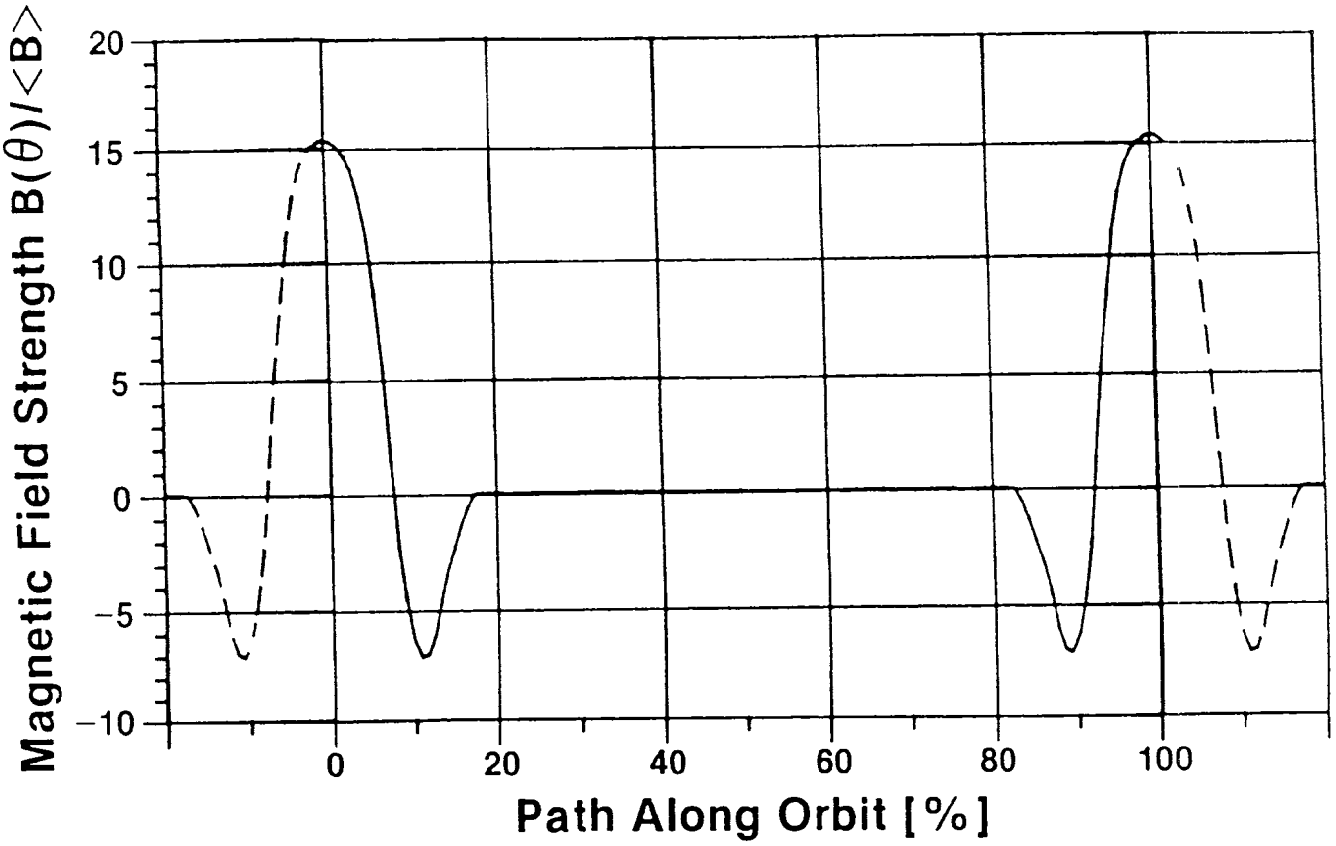

5. The azimuthal profile of the magnetic field along one lattice cell.

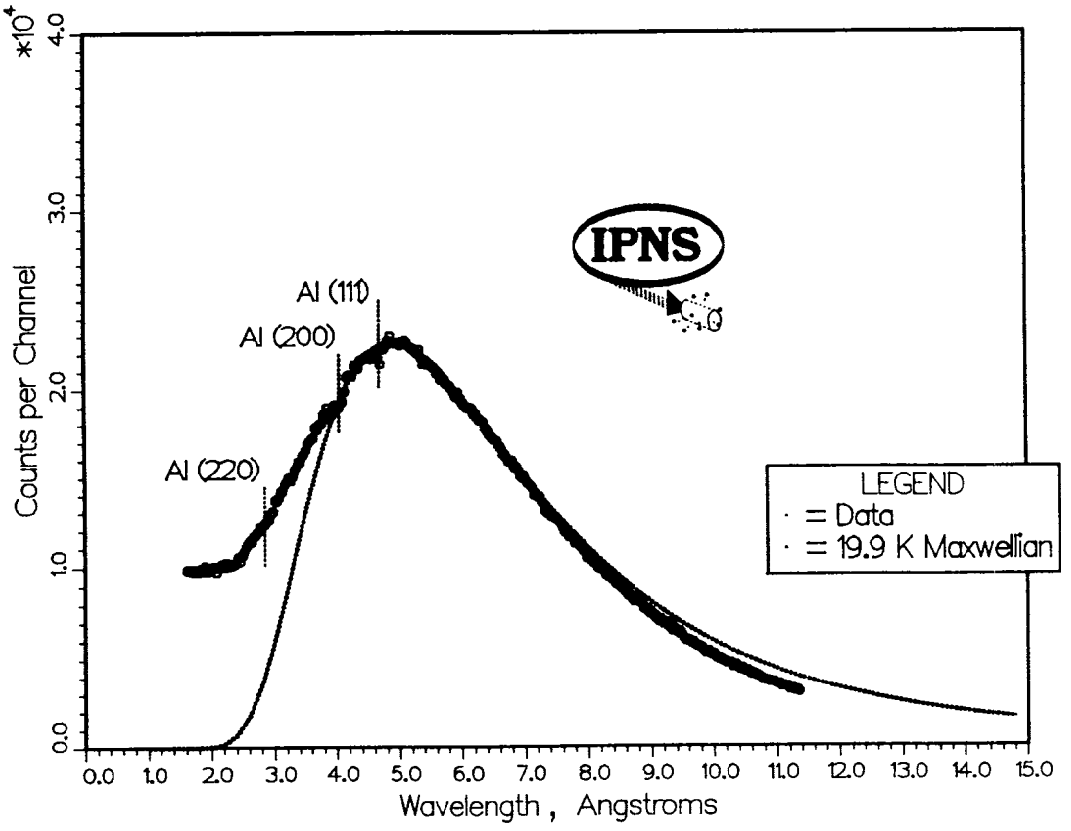

6. The counting rate distribution in a "1/v" detector from the 12 K solid methane moderator.

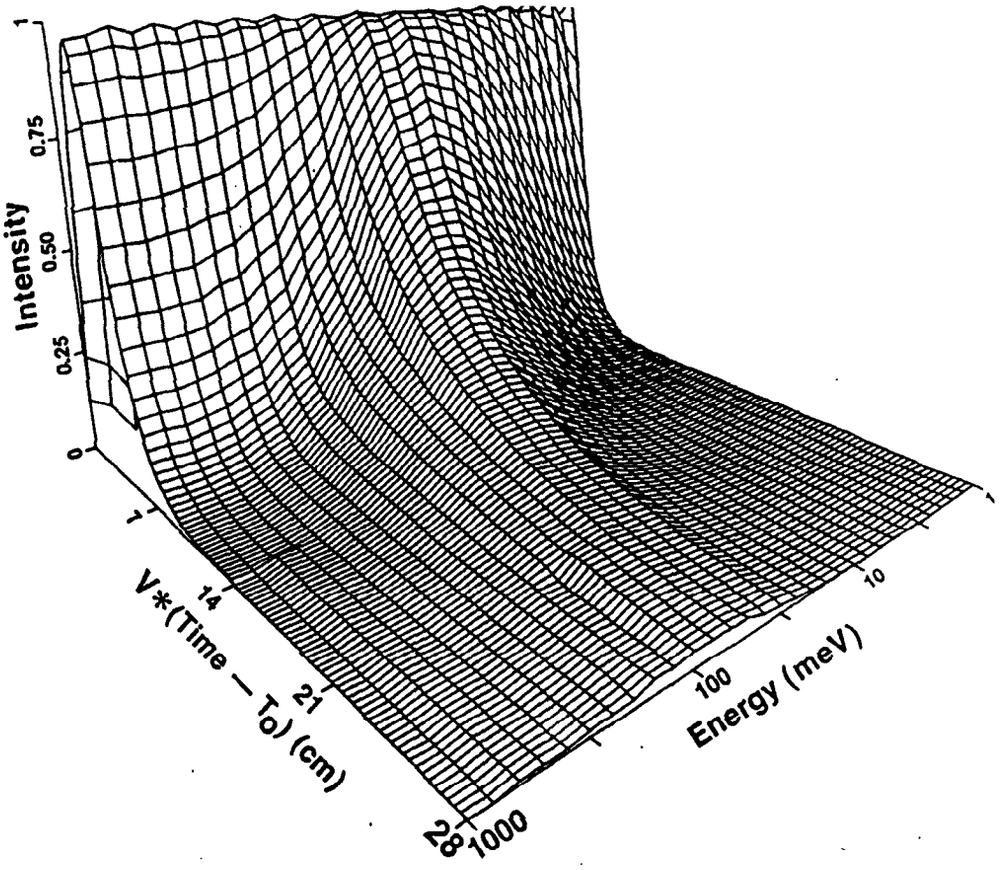

7. The pulse shape of the IPNS "H" moderator as a function of energy. Time is represented in length units $v*(t - t_o)$.

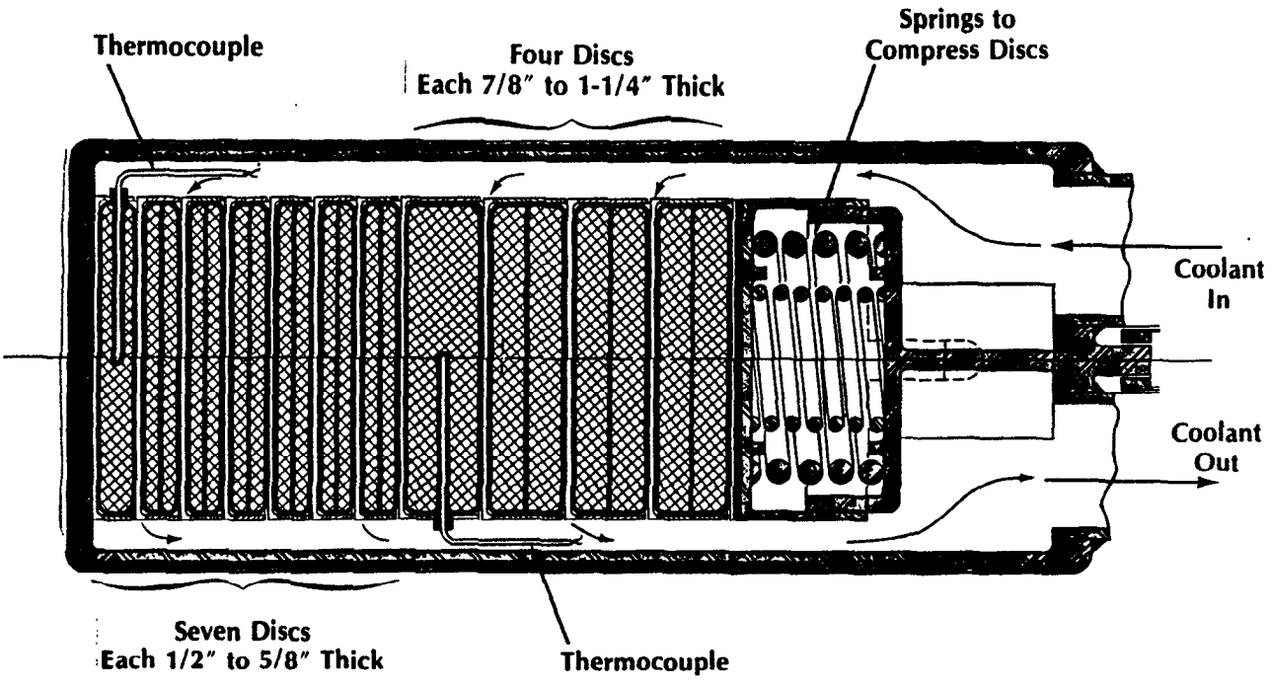

8. Cross sectional view of the Enriched Uranium Booster Target.

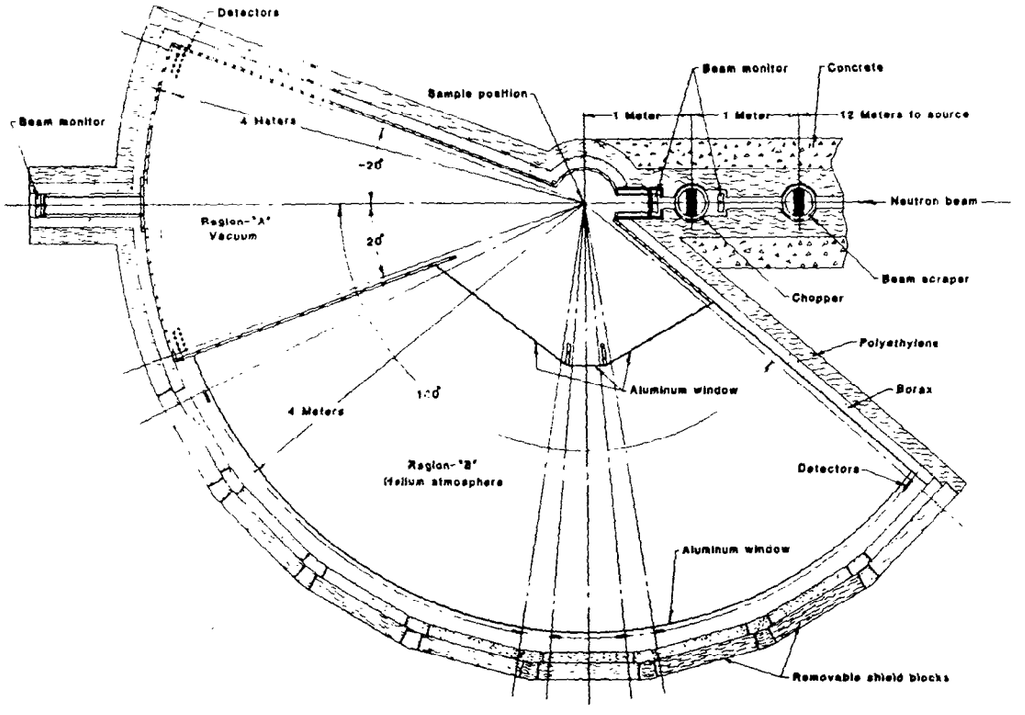

9. The High Resolution Medium Energy Chopper Spectrometer. The new flight path provides scattering angles between 90° and 140°.

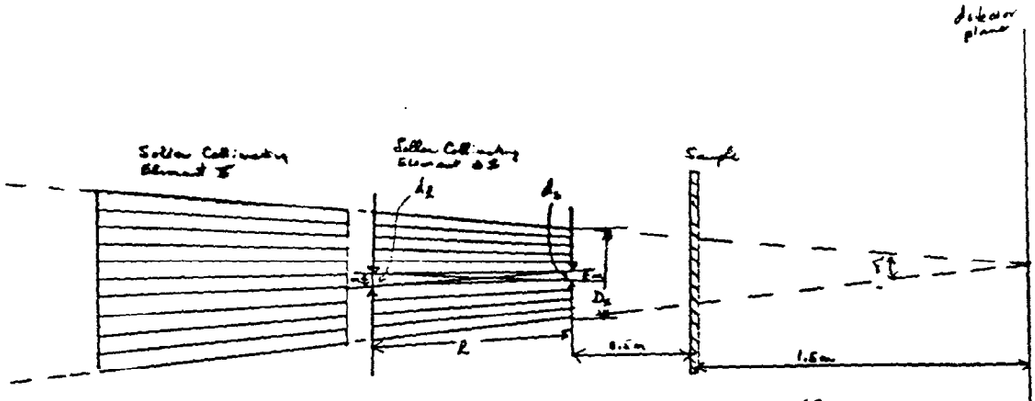

Focusing Soller Collimators, Aluminum coated with $^{10}_{5}B$

	d_s(mm)	d_ℓ(mm)	ℓ(cm)	D_s(cm)	δ(deg)	α(deg)
I).	0.750	0.844	25.0	1.63	0.4663	0.3653
II).	0.851	0.974	32.8	1.85	0.4663	0.3187

10. The multiple converging aperture collimator of the Small Angle Diffractometer.

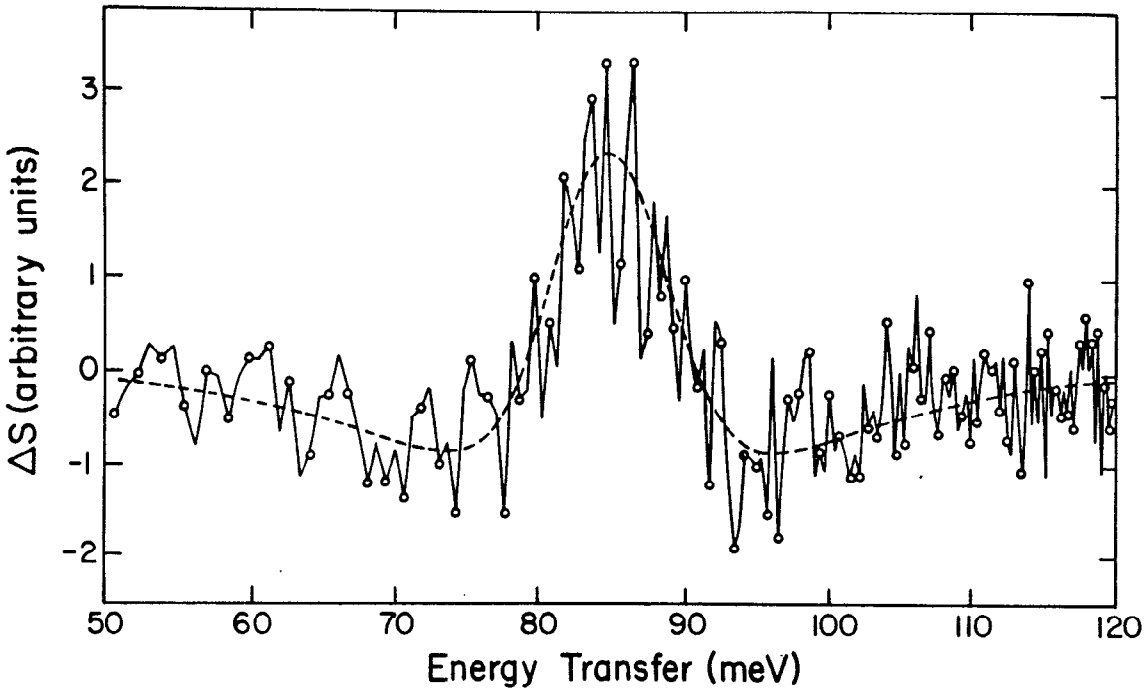

11. Difference between the inelastic scattering functions $S(Q,\varepsilon)$ of superfluid and normal liquid Helium, measured at the Low Resolution Medium Energy Chopper Spectrometer. The sharp peak is due to the Bose condensate.

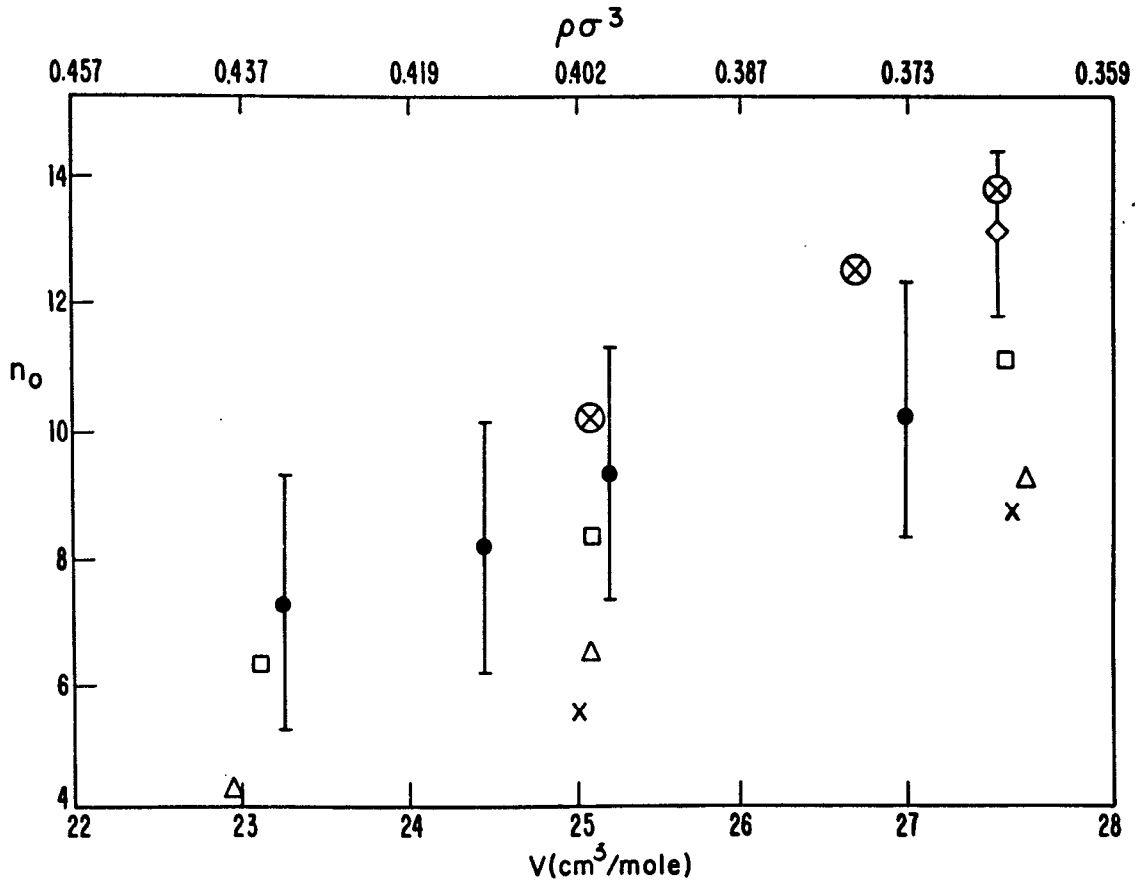

12. The Bose condensate fraction n_o of superfluid helium vs specific volume. Solid points with error bars are from LRMECS.

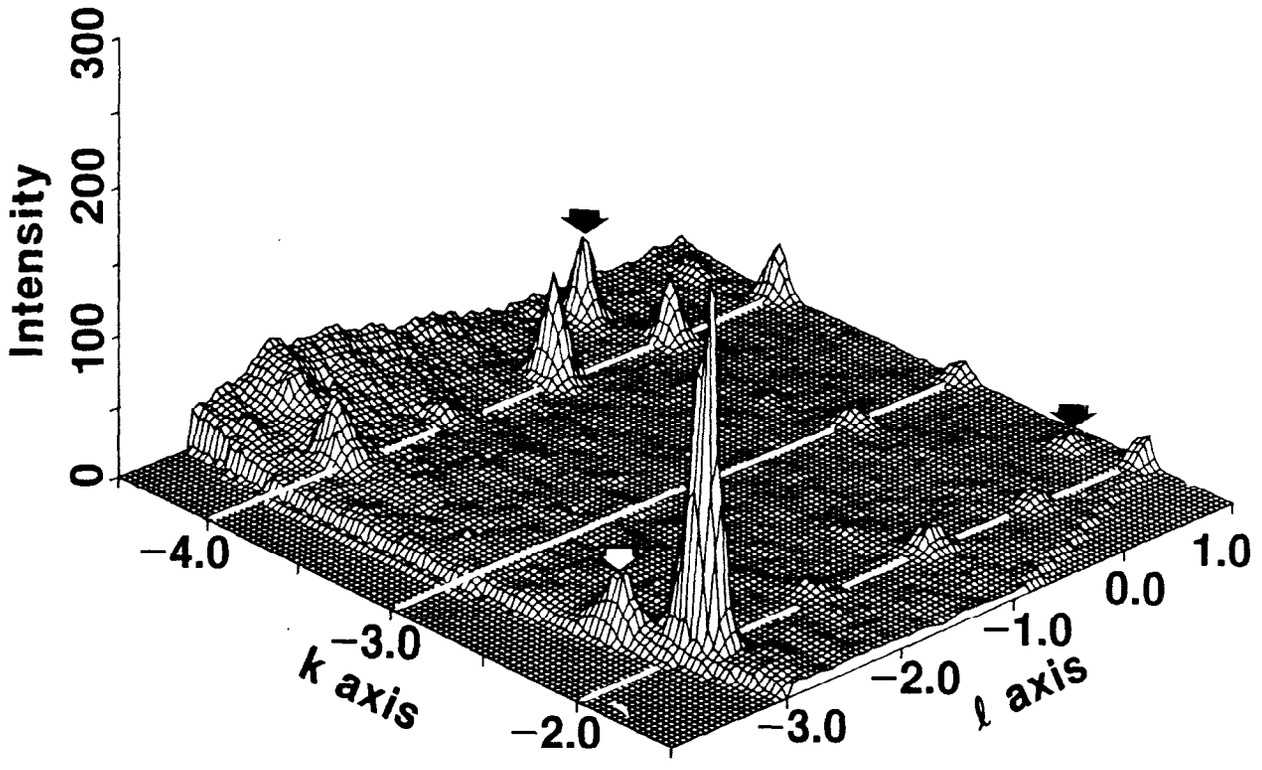

13. The diffracted intensity of $(BEDT\text{-}TTF)_2I_3$ at 20 K, in the (4.93,k,l) plane, measured on the Single Crystal Diffractometer. Arrows indicate superlattice peaks.

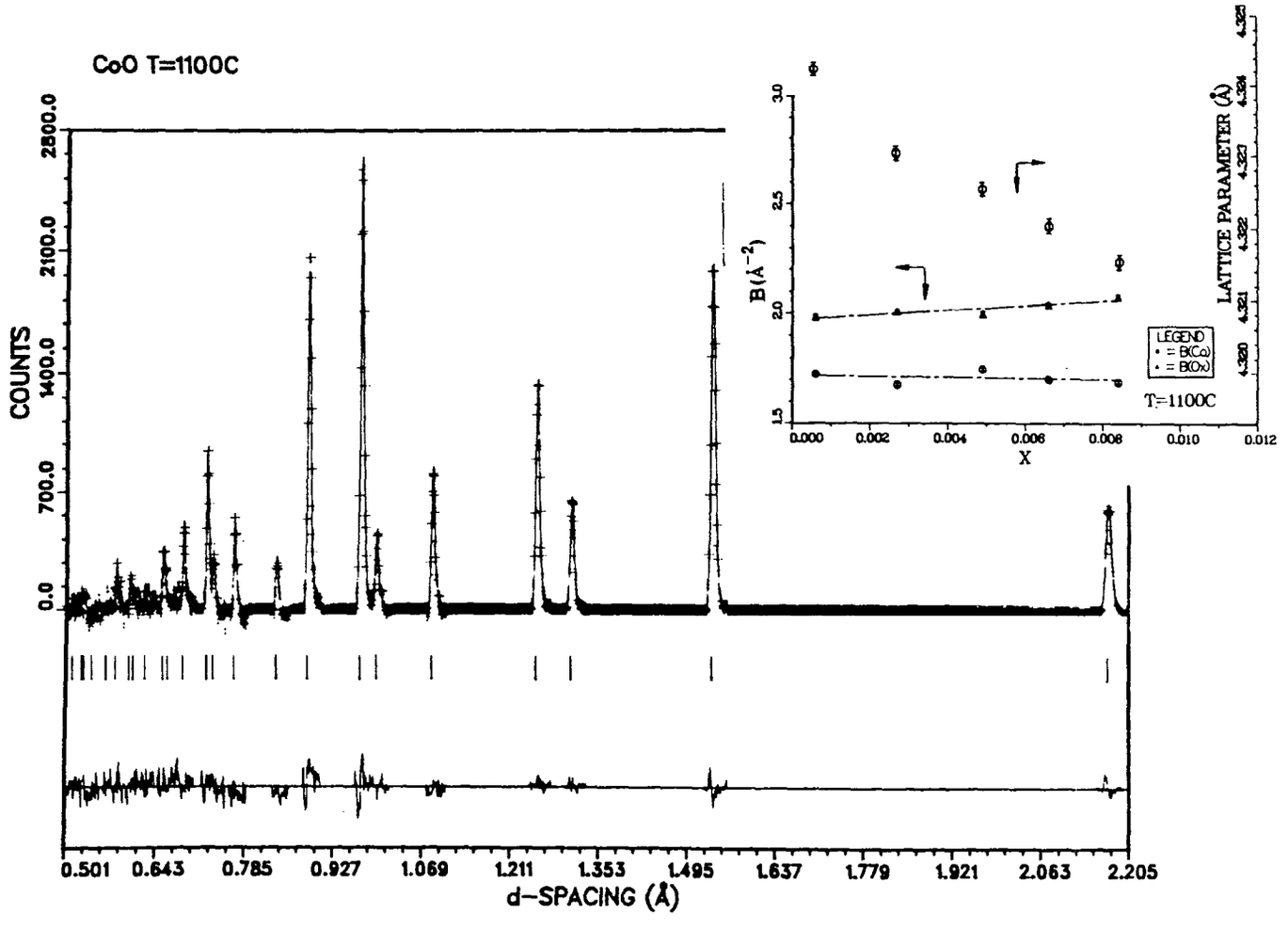

14. Powder diffraction pattern measured at $2\Theta = 90°$ on CoO(1-x)O at 1100 C in the General Purpose Powder Diffractometer. The inset shows the variation of lattice parameter and of the isotropic thermal parameters of Co and O.

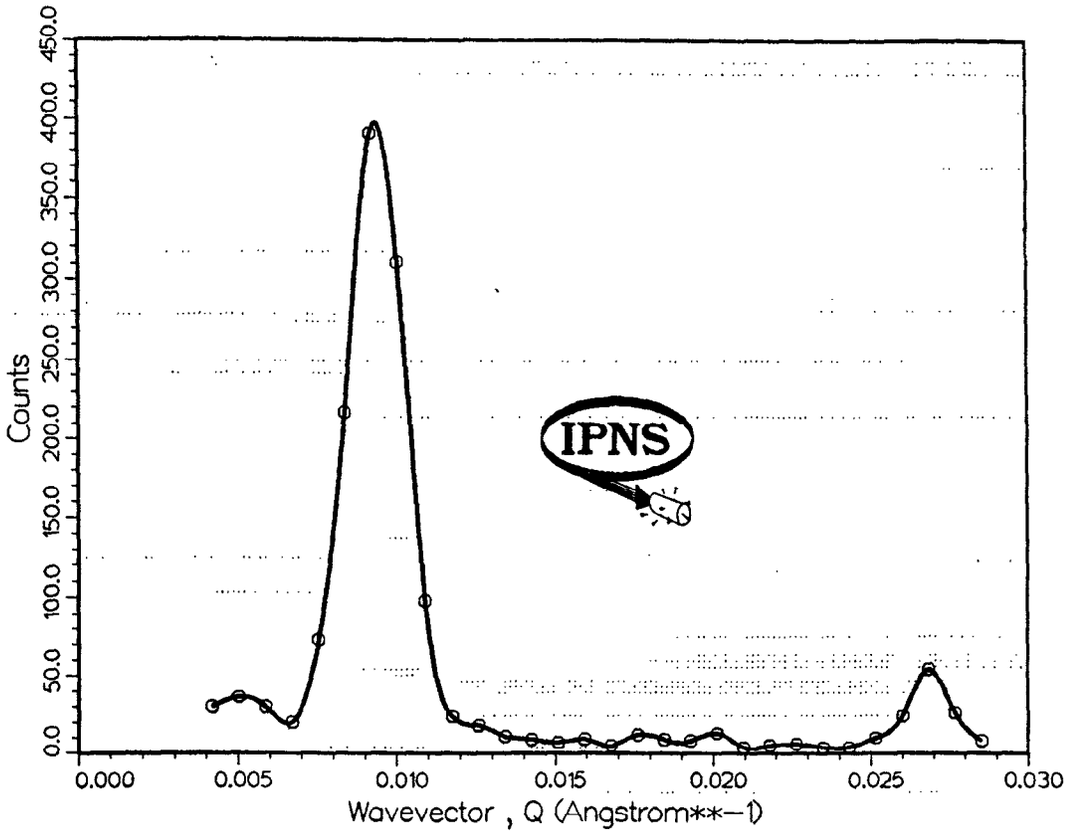

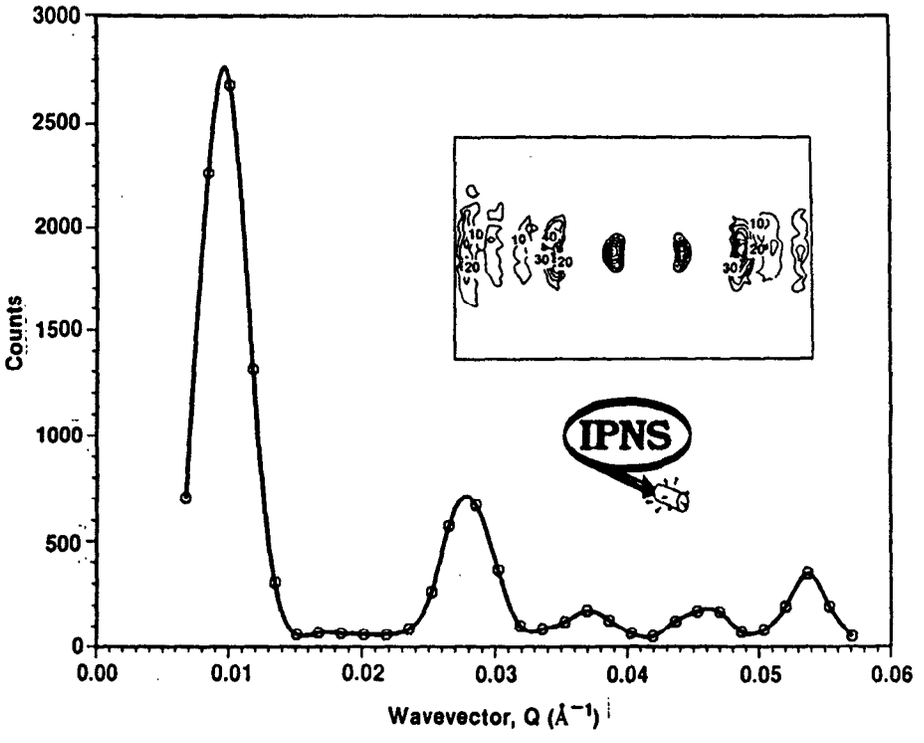

15. The Diffracted intensity from collagen of kangaroo tail tendon reconstituted in D_2O, measured on the Small Angle Diffractometer. a. From the 14. Å wavelength bin. b. From the 7. Å wavelength bin. The inset shows the intensity contours on the detector.

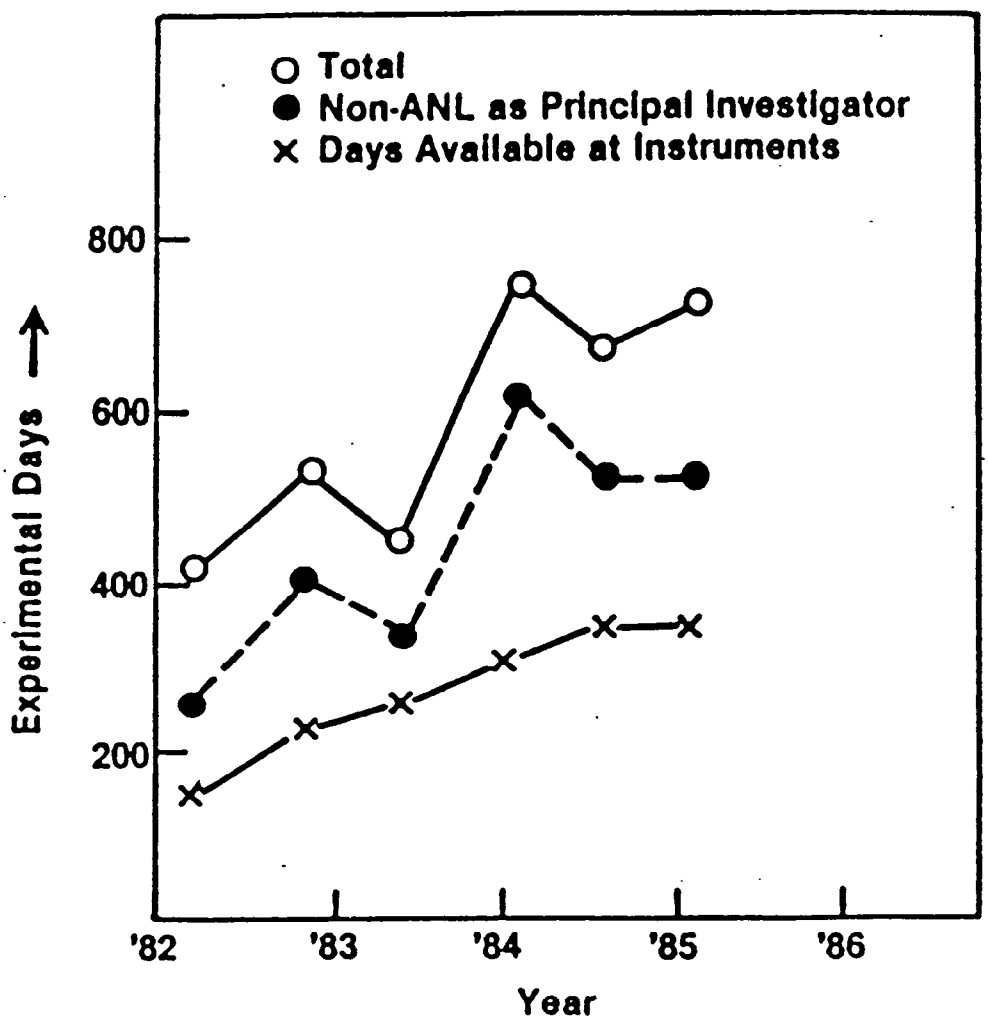

16. The number of experiment days requested and available for each six-month proposal period of IPNS.

Proceedings of the Eighth Meeting of the International Collaboration on Advanced Neutron Sources (ICANS-VIII)
8-12 July 1985, Rutherford Appleton Laboratory Report RAL-85-110

PRESENT STATUS AND FUTURE PROJECT OF KENS FACILITY

Y. Ishikawa and the KENS group
Physics Department, Tohoku University 980 Japan
National Laboratory for High Energy Physics

1. Introduction

The KENS facility restarted the operation on 17 June 1985 after a long shut down of more than one year. Although no neutron scattering researches were carried out in our facility during the last fiscal year, many efforts have been paid for realization of the KENS-I', the second phase of KENS, in this period. A number of new spectrometers has also been installed and there is now no vacant beam hole left unused in our facility. Fig. 1 is the latest version of the layout of the KENS facility. The machine groups worked to improve the spectrometers, particularly their data acquisition systems, while the users were busy for analyzing the data they accumulated before the shut-down. Therefore many papers on the scientific yields from KENS-I have been or are going to be published. A publication list will be distributed in the ICANS meeting. This report summarizes the present status of the KENS-I' as well as the point of improvement of each spectrometer.

The future project of the Booster Synchrotron Utilization Facility, GEMINI, has started to be discussed formally as one of the important candidate of the next projects of our laboratory, KEK, which is discussed in the last section.

2. KENS-I' Facility

The KENS-I' is a project which aims to increase the neutron beam intensity by one order of magnitude by upgrading the present

accelerator and converting the tungsten target to a depleted uranium target for neutron production. The project is now underway as described below.

2.1 Increase of 500 MeV proton beam intensity

The increase of the proton beam intensity was planned to be achieved (i) by converting the 20 MeV injection system from the original multi-turn injection to the H^- charge-exchange injection system [1),2)] and (ii) by increasing the injection energy from 20 MeV to 40 MeV[3)]. The final beam current we can expect by this modification is about four times of the original intensity in an ideal situation.

H^- charge-exchange injection

The first trial on the H^- charge-exchange injection at the Booster Synchrotron had been carried out during three weeks from the end of September 1983 preceding the long shut-down of the 12 GeV Proton Synchrotron through 1984. More than 20 mA H^- ion beam was extracted from a newly developed multi-cusp ion source, and 18 mA was injected into the 20 MeV linac. At the end of the test period, the H^- ion beam delivered from the linac reached 8 mA. The maximum stacked beam intensity of 2.1×10^{12} protons just after completion of the injection process has been attained by the new injection method with a 8 mA, 100 μs wide H^- ion beam and a 120 $\mu g/cm^2$ thick carbon stripper while the stacked beam by the original multi-turn injection method with proton beam was at around 1.4×10^{12} protons in the typical operation. The maximum output intensity of 7.1×10^{11} protons per pulse was recorded, which was a new record in the booster. The test experiment proved that in spite of such low injection energy as 20 MeV this injection method appeared to be quite promising for increasing the beam intensity of the Booster Synchrotron.

Operation of the 12 GeV Proton Synchrotron has reopened in the early of this June with commissioning of the new H^- charge-exchange injection system in place of the original system for the proton multi-turn injection. The intensity record of the Booster Synchrotron has been rewritten and reached more than 9×10^{11} proton per pulse at

the end of the last June, which is up about 50 % from the original case of the proton beam injection.

Upgrading of the injector linac

Extension of the present injector linac from 20 MeV to 40 MeV was undertaken. Construction of an additional Alvarez linac is under way. By this upgrading, the space-charge limit of the Booster Synchrotron is raised by a factor of two. Furthermore, it is beneficial to the H^- charge-exchange injection scheme applied to the booster. Energy loss and multiple scattering caused by passing through a charge stripping foil are considerably reduced. Especially the multiple scattering will be reduced to about a half when the proton energy increases from 20 MeV to 40 MeV. Thus, combining the charge-exchange injection with the linac upgrading, higher beam intensity of the booster can be attained with lower beam loss at injection.

Parameters of the new Alvarez linac are listed in Table 1.

The new linac will be installed by the end of this October, and come into operation in November.

2.2 Conversion to U target

The uranium target we finally got for KENS-I' consists of four blocks of Zircaloy-2 cladded depleted uranium metal which were fabricated at Argonne National Laboratory. Figure 2 shows a photography of the target blocks with an illustration of the designed target assembly. The traditional rectangular shape of KENS-I target is inherited to keep the better target-moderator coupling. A new target cooling system has been manufactured, a photograph of which is shown in Fig. 3. A mock-up experiment of the new target system proved that the flow rate of cooling water 60 ℓ/min can keep the maximum temperature at the center of uranium block at about 230°C for heat generation of 7.5 kW (500 MeV, 10 μA). The target-moderator-reflector assembly will be modified slightly in order to install the new target, but the overall configuration will be maintained. A lead cask to handle the irradiated uranium target, which is located in

front of the target shielding will be renewed. The air filled target environment as well as the last two meters section of the proton beam line will be replaced by helium atmosphere in order to protect the uranium target from serious erosion caused by NO_x produced by the proton beam, on which we have a bitter experience. The new uranium target system is now under severe examination and the installation of the system will be completed at the end of this October.

2.3 Target Shielding

Shielding power of the existing bulk shield for the target station is very close to the upper limit of the dose rate regulation for accepting the upgraded proten beam of 10 μA, but still within allowable level. Preshielding around the exits of the neutron beam holes is, however, not sufficient and a substantial improvement of the preshielding is indispensable. In addition to it, most of spectrometers have hitherto been operated without overhead shields for convenience sakes, which should be inhibited in KENS-I'. Neutrons scattered upward from the spectrometers will not only give serious radiation level inside the experimental hall, particularly at the position of the second floor of 2 m high, newly installed for easy access to the spectrometers, but also contribute significantly to the neutron skyshine at the nearest site boundary. It has been proved that the overhead shield reduces the radiation level within an allowable level. The experimental hall was surrounded by 1 meter thick concrete wall up to 4 m height. For the wall which borders the Particle Radiation Medical Science Center (PRMSC), the height was extended to 5 m to reduce the radiation level at the control room of PRMSC.

Quite recently with the new start of our facility, we encountered a serious problem of the unexpected increase of radiation level around the bulk shield. The increase of the proton beam was about by 1.5 times, but the radiation level at the top of the overhead shield of the entrance to the target station attained already to 26 mrem/hr. We expect it due to the unexpected proton beam loss around the entrance the target shielding (about 1.6 m up-stream of the target).

It is not clear whether it is due to the increase of proton beam size or other reasons and a careful survey of the origins is now under way. This is the first difficulty we have had since the construction of KENS-I, but should be overcome in order to accomplish the KENS-I'.

2.4 Cold Moderator of KENS-I'

Since the intensity of neutron will increase about by a factor 8 in KENS-I', the new cold moderator should have a cooling power to remove the heat deposit of the order of 15 W (flat moderator) to 50 W (grooved moderator). (We should note here that our previous report[4] on the heat deposit in the KENS-I cold moderator may not be accurate enough because we have now an indication that the tail of proton beams hits the cold moderator at the end of the KENS-I operation , which was clearly not the case at the beginning). Therefore mock-up experiments were carried out for the KENS-I' cold moderator and the details are discussed in a separate paper presented in this ICANS meeting . Here we briefly summarizes the results obtained.

The mock-up experiments were practiced with a flat moderator (12 x 5 x 15 cm^3) of solid methane using the cooling system of the KENS-I. Heat generation by neutrons was simulated by a heater of resistive wire embedded inside solid methane so that the same temperature distribution as the neutron heating could be attained. The results of the experiments are shown in Figs 4(a) and (b). It is clear from these figures that the increase of heat deposit to 15 W in the present cold moderator results in increasing the maximum temperature to 60 K, but the temperature increase can be reduced by introducing 1 mmϕ Aℓ wire lattice (1 x 1 cm^2) inside solid methane as shown in Fig. 4(b). We also found a significant temperature difference between the cooling head and the wall of the moderator case for the 15 W heating. A simple three dimensional calculation based on the differential equation of heat transportation was found to give a good agreement with the observation. After making a series of simulation calculation as displayed in Fig. 5 and also by taking into account curious phenomena ("Burp") Argonne cold moderator exhibits, we attained to the following conclusions.

1) The best way to cool the moderator is to insert Aℓ plates (0.5 mm thin at the distance of 10 mm). Aℓ sponge would not be recommended because it has a possibility to promote the H_2 decomposition.

2) The moderator case should be cooled directly by coolant of refrigerator, instead of adopting the indirect method we used for KENS-I, but the present refrigerator (PGH 105, 40 W cooling power at 20 K) can be employed even for KENS-I'.

3) We need to give up the grooved moderator mainly because of lack of cooling power with the present refrigerator as well as for the difficulty of cooling effectively solid methane. In addition to it, it was found that the grooved moderator does not give benefits to the high resolution powder spectroscopy. The decrease of the intensity by adopting the flat moderator can be partly compensated by improving the reflector system.

Finally we should note that in KENS-I' both thermal and cold neutron intensities on the sample position will be significantly larger than the equivalent neutron sources because of its tight configuration.

3. Installation and Improvement of Spectrometers

The total number of spectrometers installed at KENS reaches to fifteen as is shown in Fig. 1. Two new spectrometers, WIT and INC which were approved to be installed after the last ICANS meeting is still under construction. All other spectrometers are under operation for the users. We have now six elastic scattering machines (FOX, WIT, HIT, MRP, HRP), seven inelastic scattering spectrometers (MAX, LAM-80, LAM-40, LAM-D, CAT, RAT, INC) and two spectrometers for polarized neutron scattering (PEN, TOP). The characteristics or recent progress of these spectrometers will be discussed briefly below.

3.1 Four Circle Single Crystal Diffractometer FOX

A new one dimensional ^{6}Li loaded glass scintillation position sensitive detector using encode method was developed for the FOX, was attached to the diffractometer. A preliminary measurement detected Bragg reflections with a good S/N ratio, but still high back ground level.

3.2 Thermal Neutron Small Angle Scattering Instrument WIT

The WIT is a new type small angle scattering instrument installed at the thermal neutron beam hole in order to increase the total machine time of neutron small angle scattering. The instrument is equipped with a two dimensional converging grid collimator and 14 ring ^{6}Li loaded glass scintillation detectors. The spectrometer is particularly suitable for the simultaneous measurement of the wide range of momentum transfers Q between 0.01 A^{-1} and 25 A^{-1} from isotropic scattering media. A recent preliminary measurement indicates that the converging grid collimator works satisfactorily. We are particularly interested in the back ground level of our glass scintillators.

3.3 Liquid and Amorphous Diffractometer HIT

It is well known that the HIT has made a significant contribution to the structural determination of a number of liquid and amorphous materials. The recent interest is focussed on glass transition[5].

As the second stage, two improvements are now in progress, one is a development of the electrical hardware focussing and another is a scintillation detector system introduced as lower angle counters. In the first stage, we adopted a traditional geometrical focussing for high angle counters and off-line focussing was performed on analysis for lower angle counters. This was because the instantaneous counting rate exceeded the processing time of the computer for the programmed forcusing. Recently, however, we have developed a new CAMAC module which enables us to accumulate the high counting rate of neutron signals, 170 ns in separation with the time focussing. Block diagram of the module is shown in Fig. 6.

For the measurements of S(Q) from liquids and amorphous solids containing light atoms such as water (D_2O) solution, lower angle counters, say $2\Theta < 30°$, becomes indispensable to avoid enormous Placzek corrections, Sometimes S(Q) up to 70 A^{-1} is required with $2\Theta \simeq 30°$. This means that epithermal neutrons up to 37 eV must be detected with a reasonable efficiency. A scintillation detector system using ^6Li loaded glass, 5 to 10 mm thick is now under development for this purpose. In addition to these counters, three scintillation rings are going to be installed at $2\Theta = 2.6° \sim 4°$ in order to extend the momentum transfers range down to $Q = 0.05\ A^{-1}$.

3.4 Powder Diffractometers HRP/MRP

Two powder diffractometers have been in operation since 1983. The HRP is a high resolution diffractometer realized by utilizing narrow thermal neutron pulses from the solid methane moderator, having a 20 meters long flight path and backward counters. Resolution $\Delta d/d$ achieved by HRP is almost the same as that of GPPD at IPNS ($\Delta d/d \sim 0.3$ %). Fig. 7 shows a typical example of the result obtained for Bi_2O_3 at room temperature with the Rietveld profile[6]. Counting time was one day which is adequate for Rietveld refinement. A problem we need to resolve now is how to describe the burst shape of neutrons from the grooved solid methane moderator by a simple set of parameters, covering an entire range of neutron wavelength from cold Maxwellian to epithermal region, which is now under consideration.

3.5 Small Angle Cold Neutron Scattering Instrument SAN

The SAN is a cold neutron small angle scattering machine, having made an important contribution to various problems as phase separation[7], spin glass, polymer science and structural studies of biological substances because of its unique characteristics of wide dynamical range of Q measurements and of employing neutrons with a band of wavelength. The characteristics of the spectrometer as well as the design principle are discussed in detail in a separate paper presented in this meeting[8]. A very recent progress we made is that the minimum Q range which was designed to be $3 \times 10^{-3}\ A^{-1}$ by employing the wave lengths between 3 to 11 A is now extended to $2 \times 10^{-3}\ A^{-1}$ by

shifting the employing wavelength region from 3 to 9 A to 9 to 15 A as shown in Fig. 7. Another important result we got is that the magnon scattering can now be separated from small angle scattering of static origin without making energy analysis. The technique is found to be quite promissing for studying the ferromagnetic system.

3.6 Coherent Inelastic Scattering Spectrometer MAX

The MAX was most successfully used to study the low energy spin dynamics in a quasi-2D antiferromagnet, $MnTiO_3$[9] and has proved that the anisotropic magnon dispersions can be measured with almost the same efficiency and resolution as our triple axis spectrometer TUNS at JRR-2 (10 MW Reactor). However for the high energy excitation studies the resolution problem is much more severe in the MAX than the three axis spectrometer in the reactor and we need further technical development for it. One of the important progresses we made was the development of Si wafer monochromators[10]. By employing commercially available Si wafers, we fabricated bent packet Si wafer monochromators having the reflectivity more than 70 % of PG (200). Since the monochromator does not suffer from higher order contamination and a good number of large monochromators can be obtained with a reasonable price, the Si wafer monochromator would give a promissing aspect for the MAX type spectrometer.

3.7 Incoherent Inelastic Scattering Spectrometers LAM-80, LAM-40, LAM-D

Three LAM-Type spectrometers with different dynamical range of measurements have finally been installed at KENS which were found quite useful for studying the molecular dynamics in various chemical compounds by covering a wide range of energy transfers between 100 meV and 1 μeV. If combined further with CAT, the dynamical range of measurements for the incoherent inelastic scattering can be extended up to 1 eV. The LAM type spectrometer is characterized by (i) its simple structure, (ii) easy to modify the energy resolution, (iii) a good scattering intensity profile for the quasi-elastic scattering which makes easy the profile analysis and particularly (iv) the wide dynamical range of measurement for the inelastic scattering. The

detailed discussions of the characteristics are found in a separate paper[11]. We can conclude that the LAM is quite suitable for the pulsed neutron source. Fig. 9 displays an example of the energy spectra measured with LAM-40 and LAM-80.

3.8 eV Spectrometer RAT

Resonance Detector Spectrometer RAT attracted a world wide attention because of its clear detection of Bose condensation state in superfluid helium[12]. The measurements of momentum distribution from solids and liquids including superfluid ^{4}He will be continued for coming months with an improvement for increasing statistics, but a developing study for low Q and high energy transfer measurements with RAT will soon be started, for which the development of the sum coincidence method is indispensable, which is now in progress.

3.9 Epithermal Neutron Polarizer PEN

The PEN, the spectrometer to polarize epithermal neutrons by means of polarized proton filter is a unique machine which continued the operation even in the shut-down period. The most significant progress we made during this period is the success of cooling the polarized proton filter by liquid ^{4}He which were cooled by pumped liquid ^{3}He down to 0.4 K (^{3}He/^{4}He Heat Exchange Method)[13]. This success overcame a difficulty of presence of ^{3}He in the neutron path and enabled us to enlarge the filter area. The maximum proton polarization of the filter of 30 x 40 x 15 mm^3 attained by means of dynamical polarization was 50 %, which can polarize the neutrons of 1 eV to 75 %. A higher proton polarization would be obtained if the cooling power is improved, which is now under examination. In Fig. 10 is plotted the quality factor η of the polarized proton filter defined as $\eta = P^2 TA$ (P=neutron polarization, T=neutron transmission, A=neutron beam area) determined experimentally for different filters against the year of measurement, indicating a continuous improvement of the factor. A more detailed description will be given in a separate paper presented in this meeting.

3.10 Cold Polarized Neutron Spectrometer TOP

The TOP is the cold neutron scattering spectrometer with polarization analyzer employing polarized neutrons with λ ranging from 3 to 9 A. Recent interests have been focussed on the transmission measurements where the wavelength dependence of the depolarization was found to give new information on domain sizes in the ferromagnetic materials[14]. A peculiar phenomenon of damped oscillation type depolarization was observed in the re-entrant spin glass system as $Fe_{0.7}Al_{0.3}$ or $Fe_{0.22}Cr_{0.78}$. In order to pursue further these phenomena, a three dimensional polarization analyzer is installed to the spectrometer. Fig. 11 displays a preliminary result we got with this analyzer. A frame shape sample of $Fe_{0.7}Al_{0.3}$ was used for the measurement. No oscillatory depolarization was found for the Z-Z polarization in a magnetic field of 100 Oe.

4. Future Project - KENS-II

The GEMINI project consisting of the projects of intense neutron scattering facility, KENS-II and intense pulsed meson facility Super BOOM was officially proposed to KEK in 1984 as the next project of the Booster Synchrotron Utilization Facility.

The GEMINI (Generator of Meson Intense and Neutron Intense Beam) is an 800 MeV rapid-cycling proton synchrotron with two bunched beams, each of which is planed to be delivered to each facility. The total time averaged current is aimed to be 500 μA and the KENS-II will get the proton beams of 250 μA in time average continuously. Layout of the GEMINI project is displayed in Fig. 12.

The project has been discussed in various places including among the neutron scattering community or nuclear physicist group. On the other hand, the KEK started the discussions on the post TRISTAN project and the GEMINI is considered as a good candidate for it. The neutron scattering committee agrees that the pulsed spallation neutron source would be the next national project of neutron source in Japan and the GEMINI-KENS-II project satisfies their requirements. However the nuclear and high energy physics groups consider that the GEMINI should have a potential to link to a higher energy accelerator so as

to promote the hadron project as a Kaon factory. In this connection, a project to increase a current intensity of the existing 12 GeV Proton Synchrotron (PS) has also been discussed in KEK and the combination of the GEMINI with the future project of the 12 GeV proton accelerator is one possibility to realize the GEMINI in KEK. These projects are going to be discussed in some authorized committees from more general stand point of view.

Under these circumstances the GEMINI project is planed to be modified to satisfy the severe requirements imposed by muon group coupled with the nuclear and high energy physics groups; the increase of the beam energy to higher than 1 GeV, the decrease of the beam emittance in addition to the sharp bunched beam. Since it is difficult to compromise these requirements with those of neutron group by upgrading the original GEMINI accelerator itself, accelerator group made an interesting proposal to add a 1.5 GeV FFAG synchrotron to the GEMINI project, whose average radius at injection is just a half of the original synchrotron's. One of the bunches accelerated by the 800 MeV synchrotron is injected into the FFAG synchrotron, and is accelerated up to 1.5 GeV. The preliminary design parameters are listed in Table 2. The circumference of the extraction orbit is larger than that of the injection only by 5 %. The extracted beam can be injected into the present 12 GeV PS at KEK, which makes possible to increase the beam intensity of the PS by fifteen times of the present intensity. Moreover, the beam from the FFAG synchrotron may also be a source of kaon and anti-proton factory, which might be built in future. Additional cost of the GEMINI project due to the construction of the FFAG synchrotron is estimated to be 25 to 30 % up of the construction money of the 800 MeV rapid-cycling synchrotron.

One of the recent topics in the GEMINI design study is the development of a world highest field permanent quadrupole magnet, and the development of a stranded cable for the exciting coil of the rapid-cycling GEMINI magnet. The segmented ring-shaped quadrupole magnet, whose bore radius is 6 mm, will be set in the drift tube of a 400 MHz, 100 MeV Alvarez injector linac. It has been realized that the maximum field gradient and pole-tip field are 160T/m and 1.2T with core material of SmCo, and 260T/m and 1.6T with Nd-Fe-B, respectively. The transverse acceptance of the linac will be considerably increased by using those permanent magnets. A proto-type bending magnet for the

GEMINI synchrotron has been completed. In place of conventional hollow conductor, a stranded cable with a water-cooling pipe is used as an exciting coil. The cross section of the cable is 30 mm x 30 mm. The cable consists of 84 Al-wires of 3 mm in diameter and a 14 mm dia. and 1.5 mm thick copper pipe, carrying 1,650 A DC current and 880 A peak AC current (50 Hz). By applying such a stranded cable, the rapid-cycling magnet is completely free from the power dissipation due to the induced eddy current in coil conductor. Fig. 18 and 19 show the ring-shaped quadrupole magnet made of Nd-Fe-B and the cross sectional view of the stranded cable for exciting GEMINI synchrotron magnet respectively.

We would express our sincere thanks to Prof. T. Nishikawa, Director General of National Laboratory for High Energy Physics for his continuous interests and encouragement.

References

1) H. Sasaki, Proc. ICANS-VII (Chalk River) 1983. Report ADCL-8488 P. 14
2) T. Kawakubo, I. Sakai, M. Suetake and H. Sasaki, KEK Report 84-6 (1984) A
3) S. Fukumoto et al., KEK Preprint 85-9 (1985)
4) Y. Ishikawa, et al., Proc. ICANS-VII (Chalk River). 1983 Report AECL-8488 P.
5) M. Misawa and N. Watanabe KENS Report-IV (1983) 18
6) F. Izumi et al., to be published, (preminary, KENS Report-V (1984) 105)
7) M. Furusaka, Y. Ishikawa and M. Mera, Phys. Rev. Lett. 17 (1985) 2611
8) Y. Ishikawa et al., J. Appl. Cryst (1985) to be published
9) Y. Todate, Y. Ishikawa, S. Tomiyoshi and K. Tajima, J. Phys. Soc. Jpn (1985) to be published
10) S. Tomiyoshi, Y. Ishikawa and K. Tajima, KENS Report-IV 154
11) K. Inoue et al., Nucl. Inst. Methods (1985) in press
12) N. Watanabe, Neutron Scattering in the 'Ninties, IAEA Vienna (1985) 279
13) M. Kohgi et al., a paper presented in ICANS-III meeting
14) S. Mitsuda and Y. Endoh, J. Phys. Soc. Jpn. 54 (1985) 1570

Table 1. Parameters of new linac

Kinetic Energy	20.60 - 40.46 MeV
Frequency	201.070 MHz
Tank	Copper-plated steel
Length	12.84 m
Inside diameter	0.90 m
Number of cells	35
Drift tube	Copper-plated stainless steel
Length	23.32 - 28.79 cm
Outer diameter	16 cm
Bore diameter	3 cm
Stem diameter	3.6 cm
Quadrupole magnet	Permanent (ALNICO-9)
Aperture	3.4 cm
Length	16 cm
Outer diameter	13.5 cm
Field gradient	2.0 - 2.05 kG/cm
Synchronous phase	-30°
Average axial field	2.1 MV/m
Shunt impedance	70.33 - 68.71 MΩ/m
Transit time factor	0.8699 - 0.8143
Effective shunt impedance	53.22 - 45.56 MΩ/m
RF System	
Excitation power	1.078 MW
Coupling	Loop, two feeds
Stabilizer	Post couplers
Post diameter	3.0 cm
Vacuum system	
Main pump	Ion pump (1.000 l/s x 7)
Roughing pump	Turbomolecular pump (500 l/s x 1)

Table 2. A 1.5 GeV FFAG Synchrotron

Max. kinetic energy	1.5 GeV
Max. intensity	3×10^{13} p/p
Max. repetition rate	50 Hz
Average beam current	250 μA
Injection energy	800 MeV
Number of sectors	16
Circumference factor	2.5
Pole radius	
at injection	13.49 m
at max. energy	14.15 m
Injection field	0.904 T
Max. field	1.324 T
Spiral angle	64.6°
Field index	8.0
Radial betatron oscillation frequency	
horizontal	3.24
vertical	3.25
Max. beta-function over radius of curvature	
holizontal	1.4
vertical	1.6
Momentum compaction factor	0.111
Max. momentum dispersion over radius of curvature	0.34
Beam emittance	
at 800 MeV	290 x 160 $(mm \cdot mrad)^2$
at 1.5 GeV	190 x 100 $(mm \cdot mrad)^2$
Frequency range of RF acceleration	2.98-3.11 MHZ
Harmonic number	1
RF bucket area at injection	4.1 ev•sec
Peak RF voltage	40 kV
RF voltage at injection	21 kV
Number of cavities	2
Transition energy over rest mass energy	3.0
Weight of sector magnets	
iron	590 tons
copper	24 tons

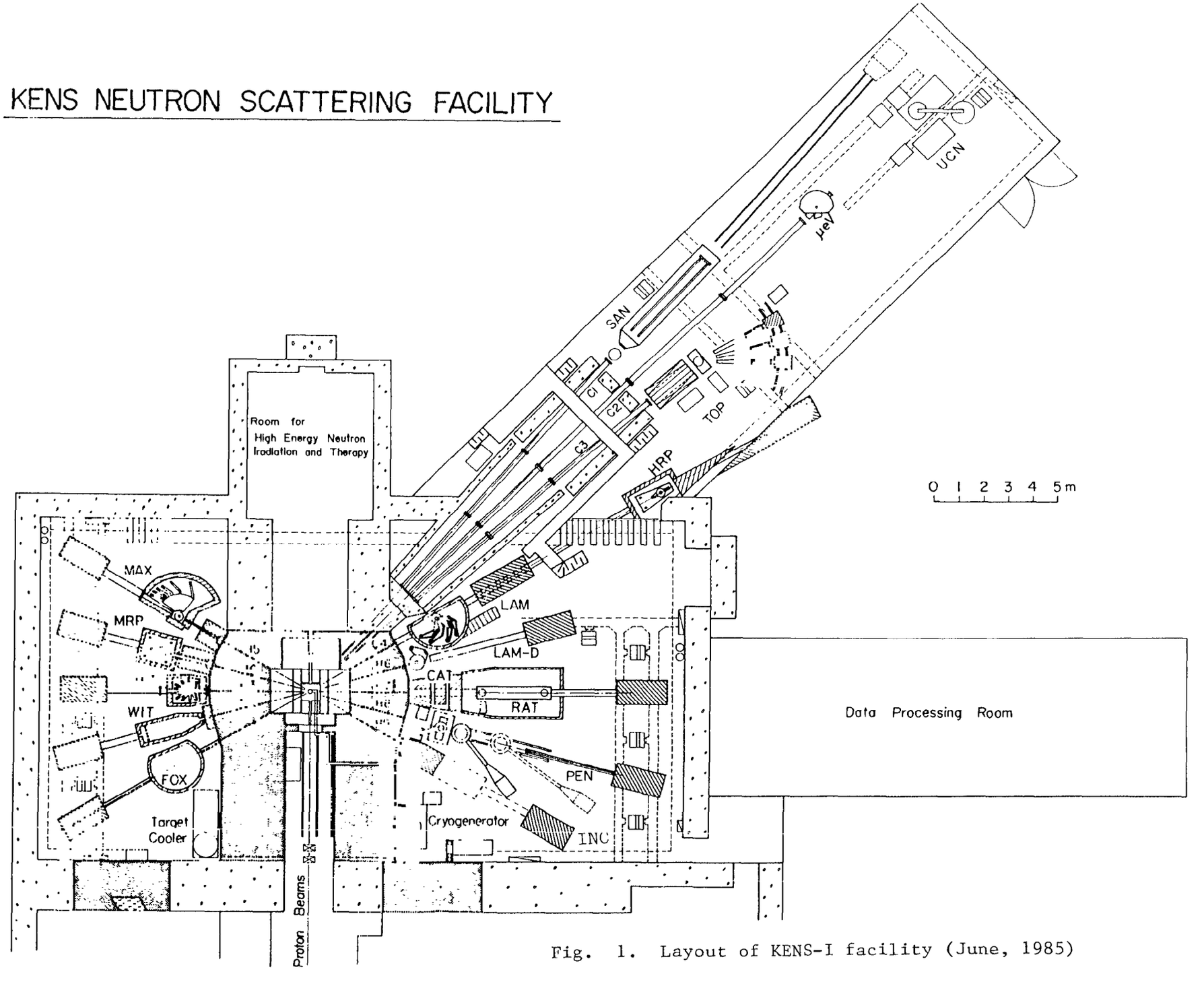

Fig. 1. Layout of KENS-I facility (June, 1985)

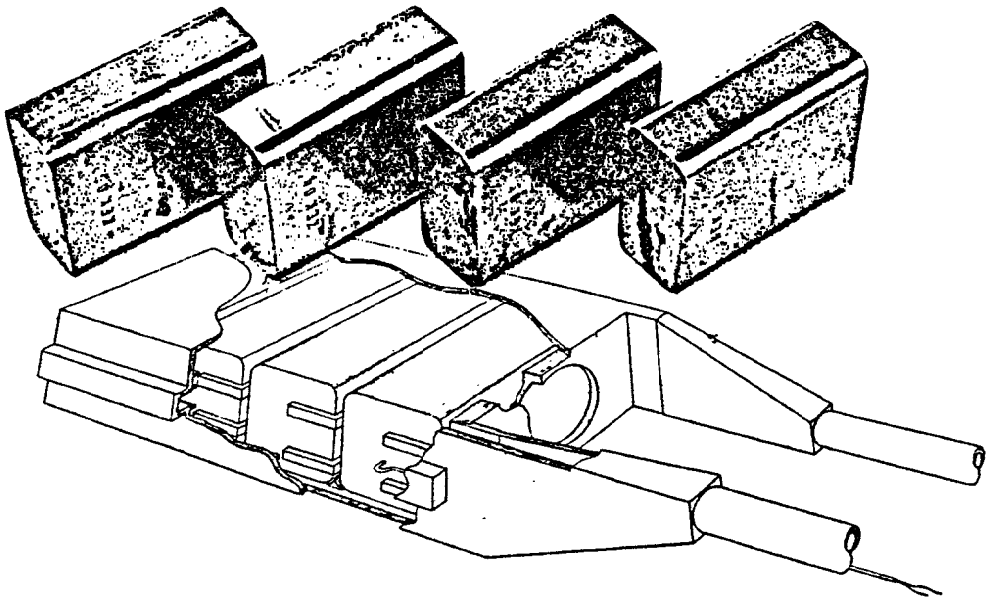

Fig. 2. Uranium target blocks for KENS-I' with an illustration of target assembly

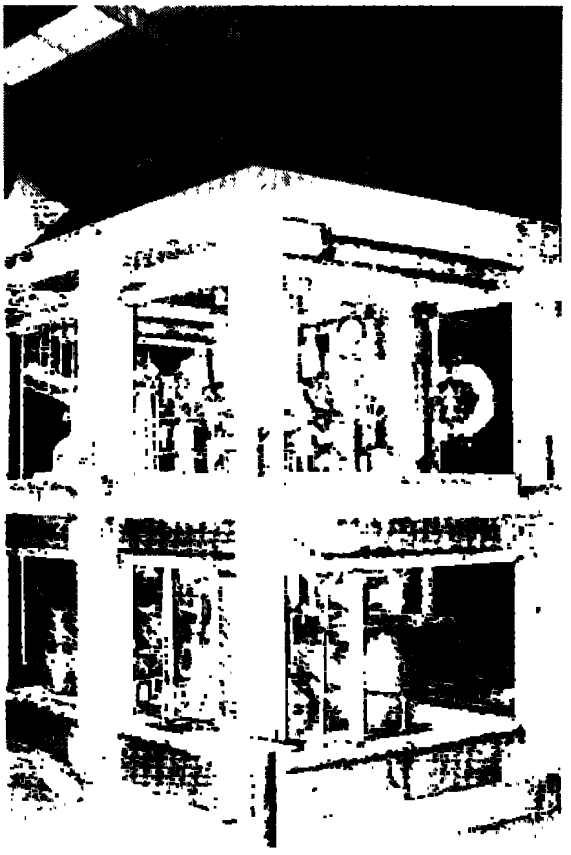

Fig. 3. Photograph of target cooling system

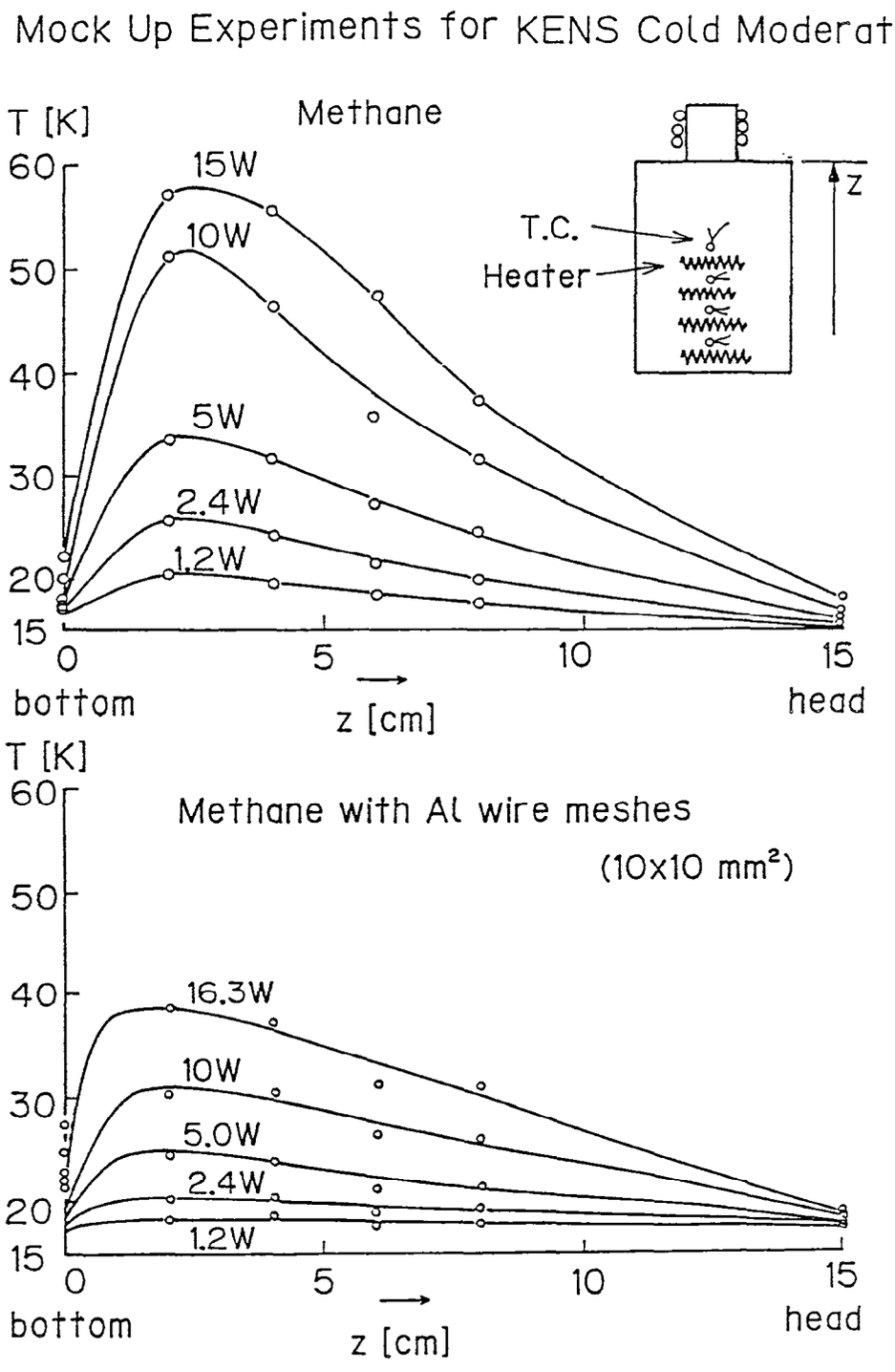

Fig. 4. Temperature distribution inside KENS-I methane cold moderator in case of higher heat deposit (a) without Aℓ wires. (b) with 1 mm ϕ Aℓ wire lattice (10 x 10 mm^2)

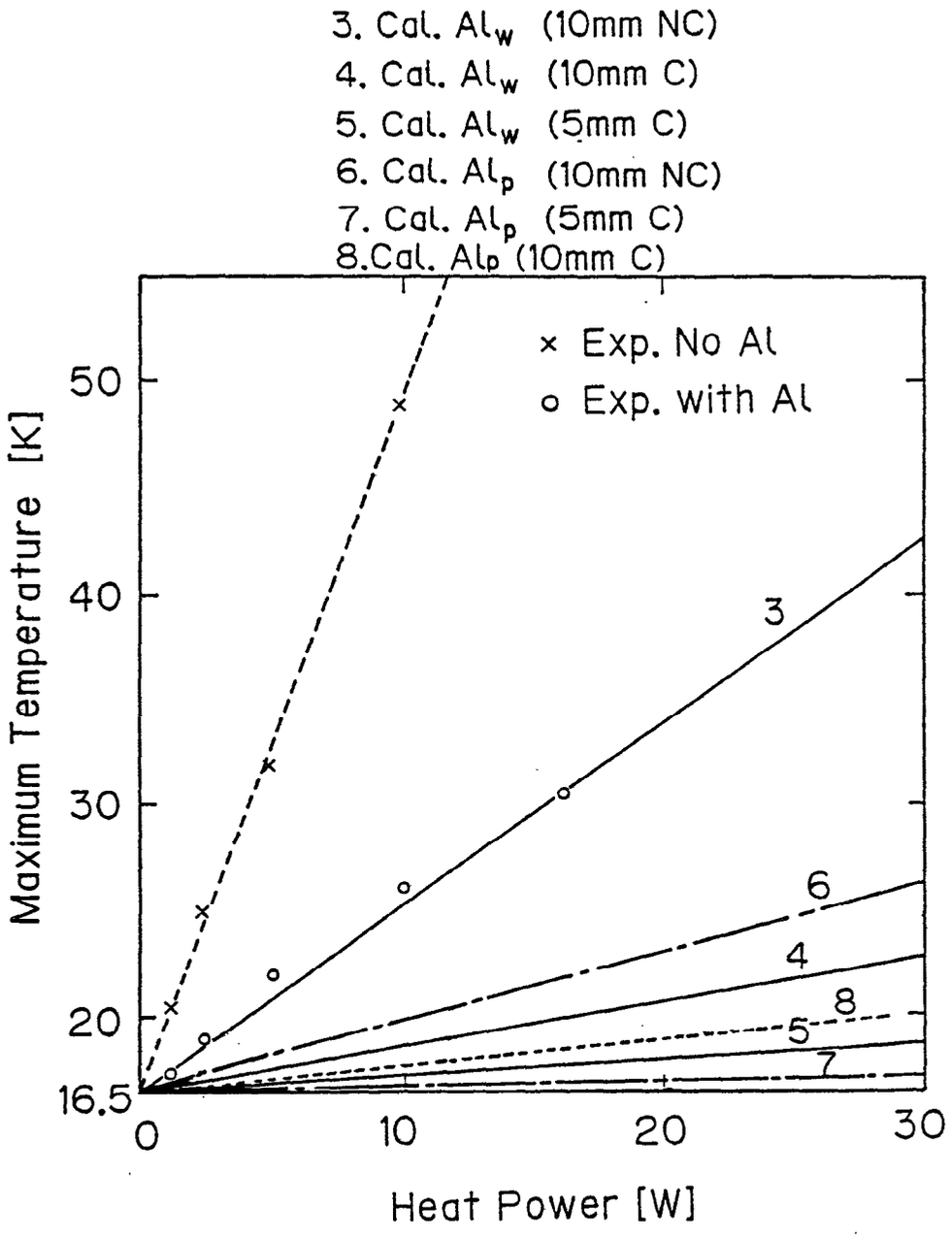

Fig. 5. Simulation calculation of maximum temperature inside solid methane for several different cases and comparison with the experimental results
Alw (10 mm NC): 1 mm ϕ Al wires lattice 10 x 10 mm^2 with poor thermal contact with the refrigerator
Al P (5 mm C) 0.5 mm thick Al plate lattice 5 mm apart with good contact with the refrigerator

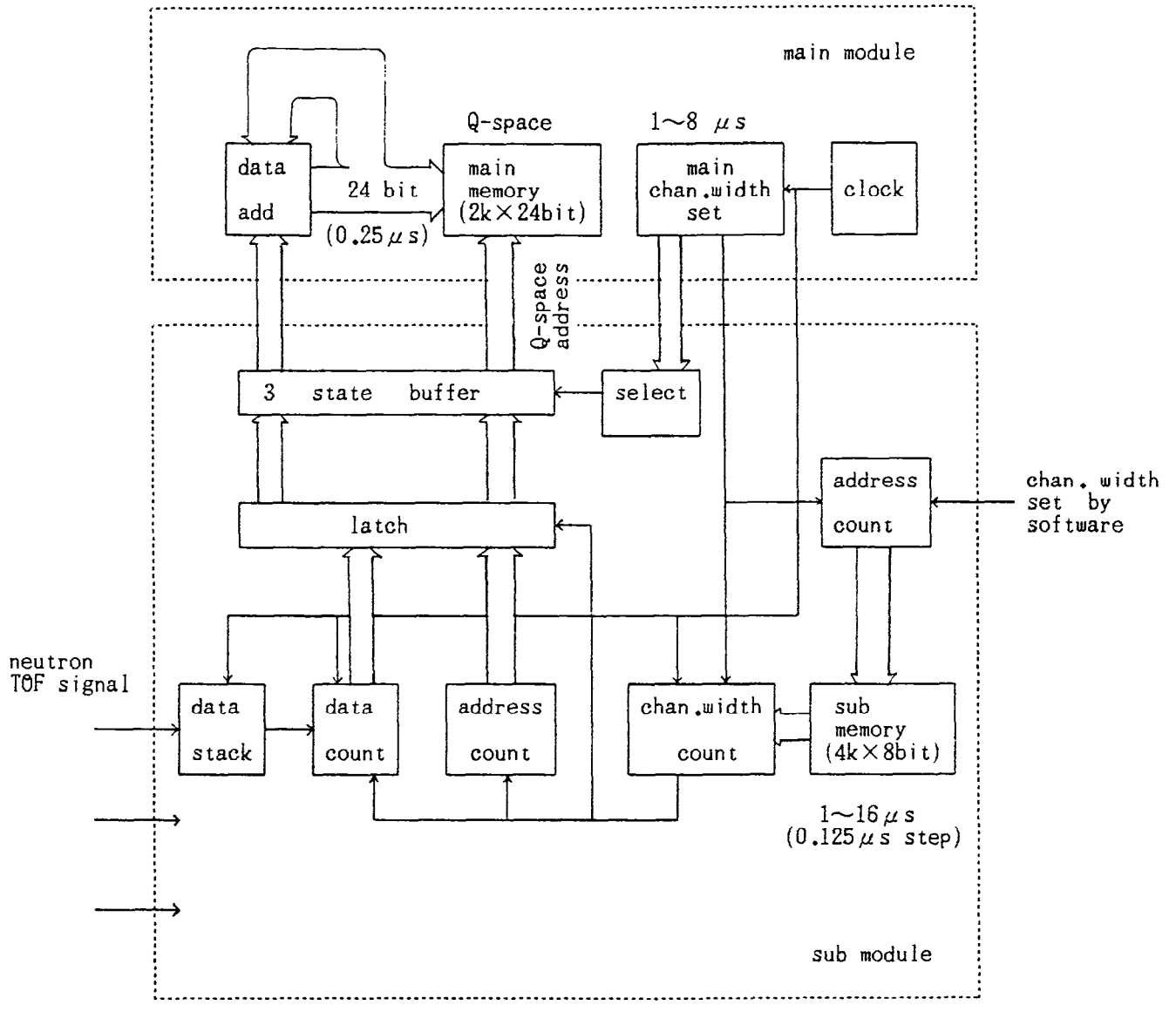

Fig. 6. Block diagram of CAMAC module for hardware time-focussing

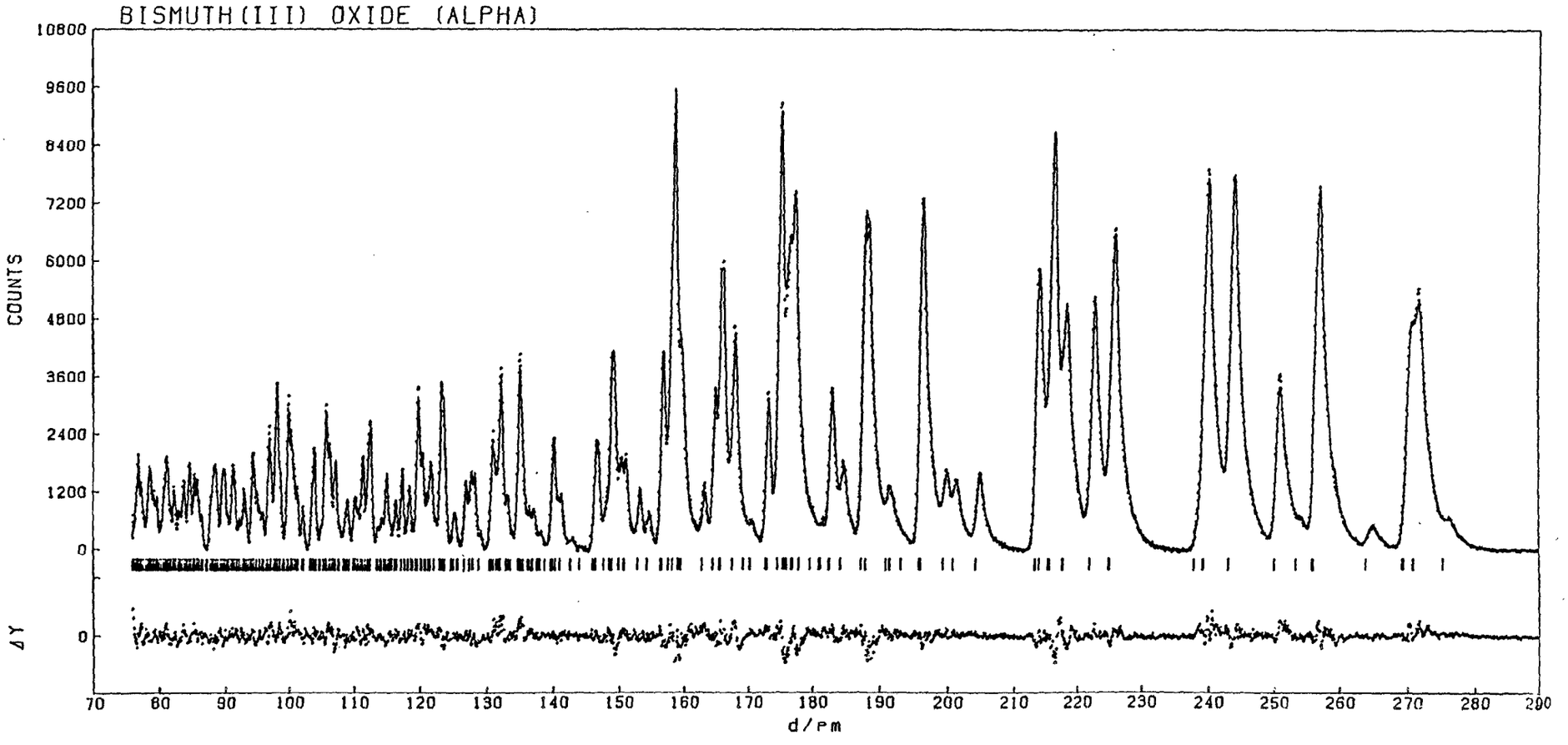

Fig. 7. Powder diffraction patterns taken by HRP with Riesvelt profile

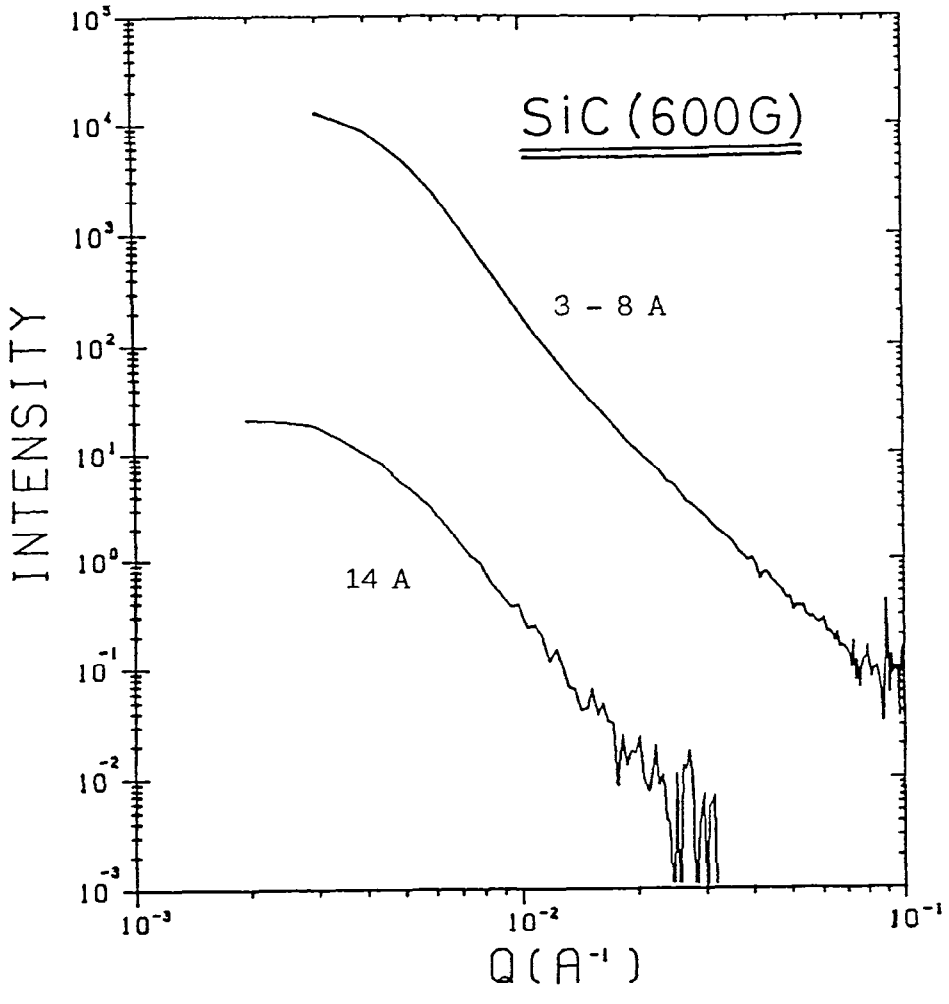

Fig. 8. A preliminary result of small angle scattering from SiC (600 G) measured by employing a band of wavelength between 9 and 15 A can comparison with a previous measurement

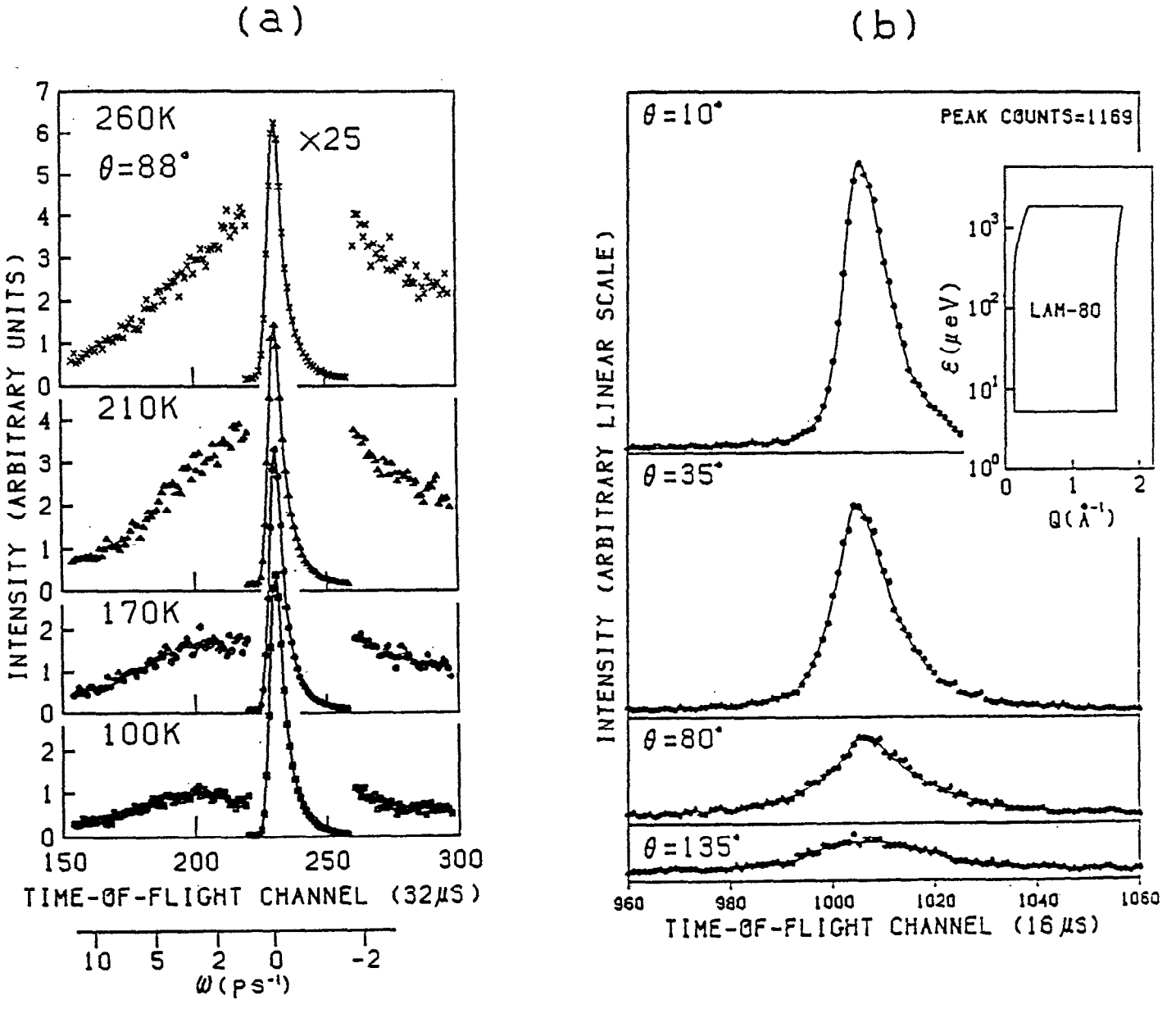

Fig. 9. Time of flight spectra from poly (butadience), measured (a) with LAM-40 at various temperatures, and (b) with LAM-80 at a temperature below meeting point

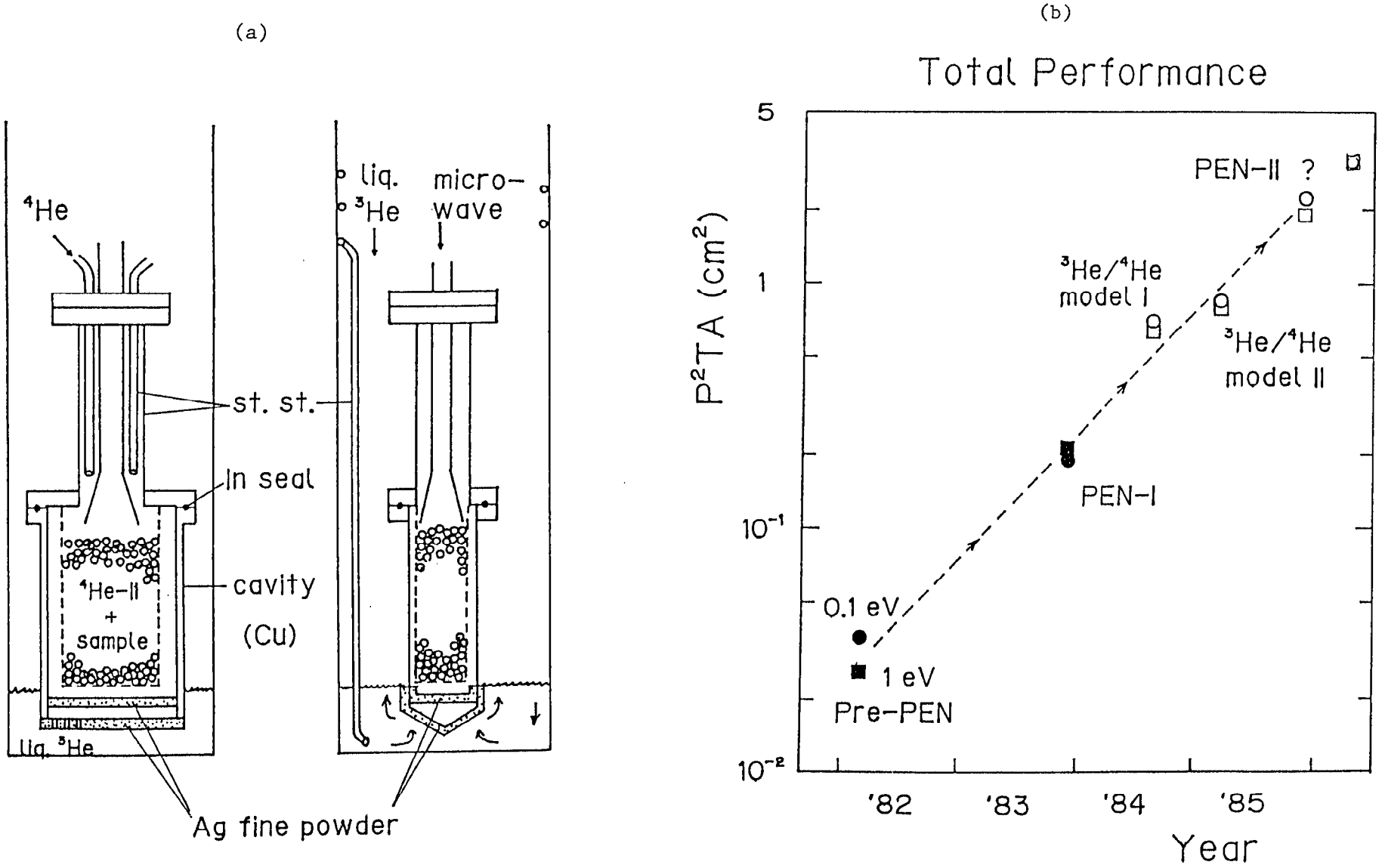

Fig. 10. ^{3}He/^{4}He heat exchange cooling system newly adopted for polarizing proton filter of PEN (a) and improvement of quality factor $\eta = P^2TA$ of polarizing proton filter plotted against the year of measurement (b)

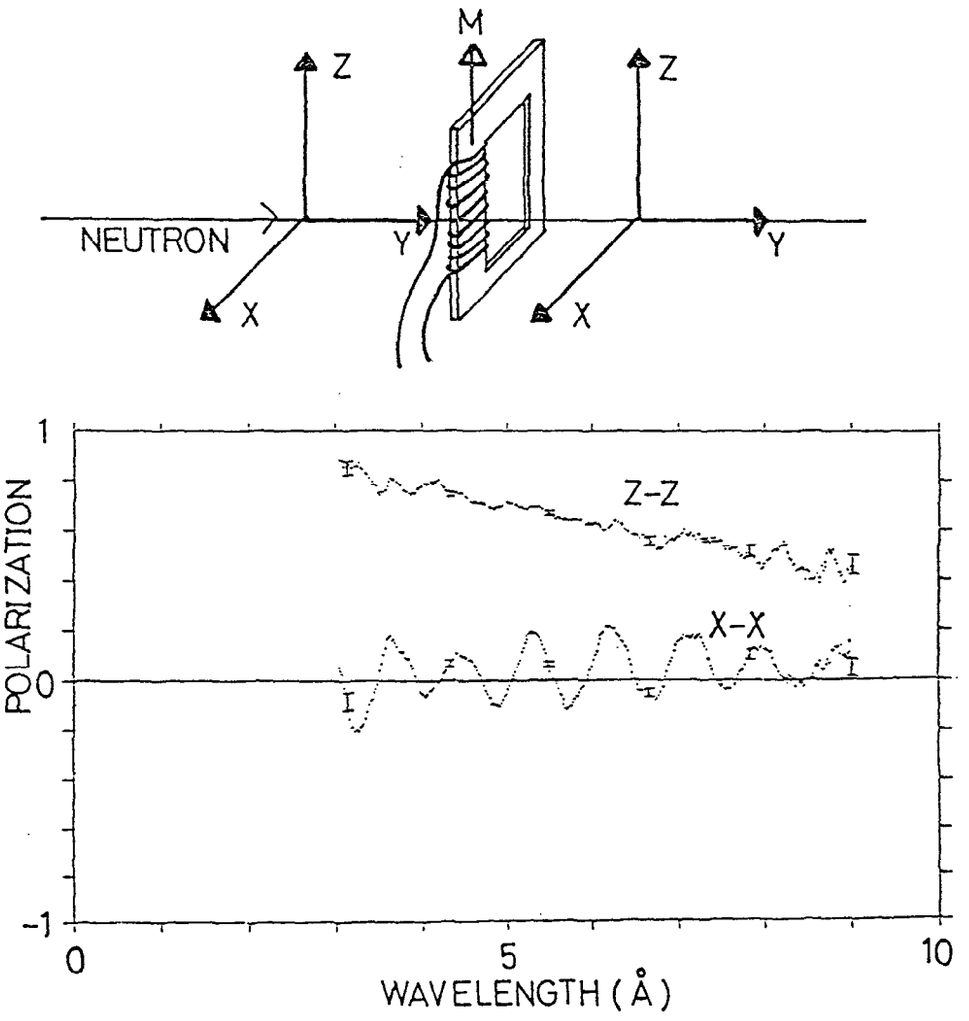

Fig. 11. A preliminary result of three dimensional polarization analyses of polarized neutrons transmitted through the frame shape re-entrant spin glass $Fe_{0.7}Al_{0.3}$

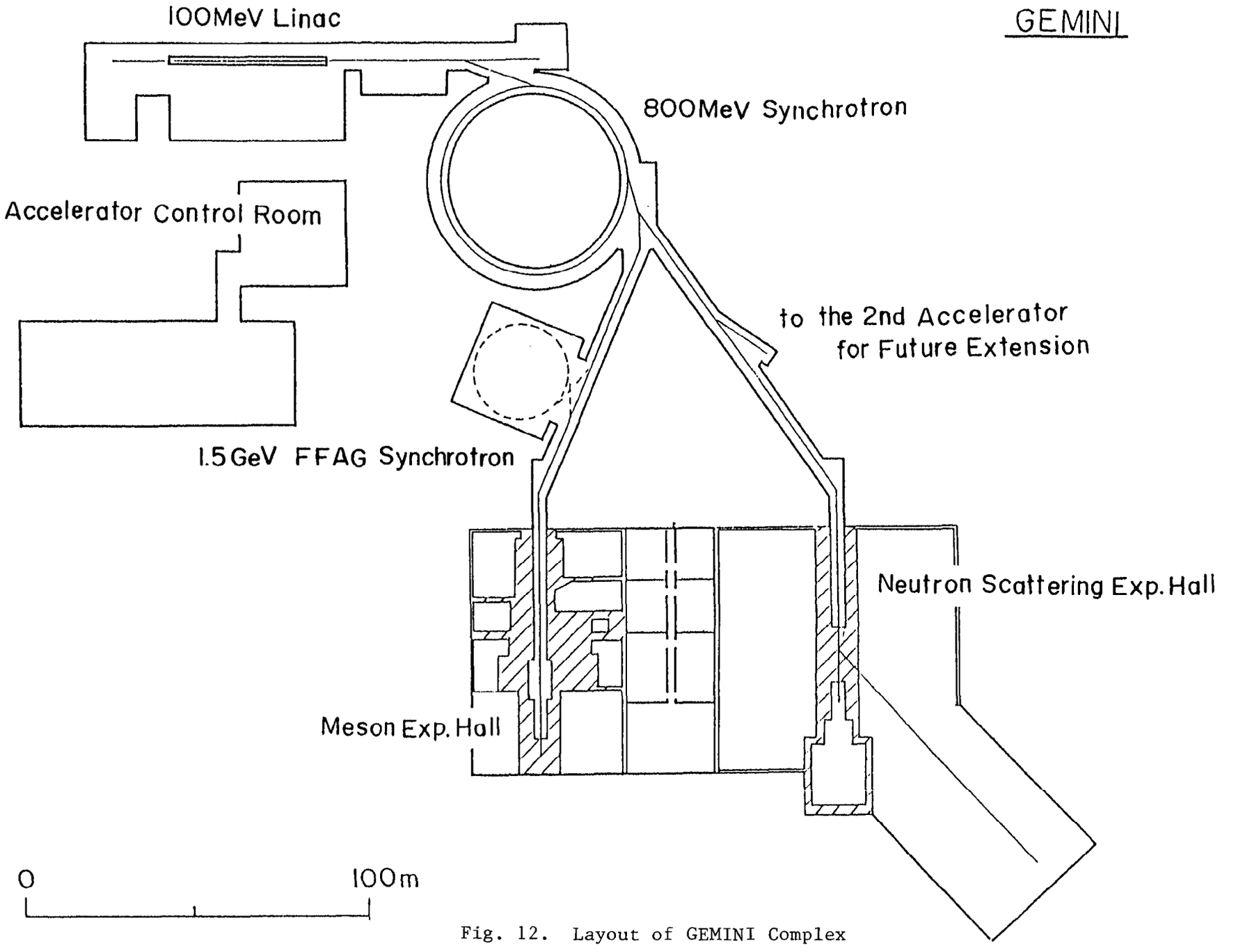

Fig. 12. Layout of GEMINI Complex

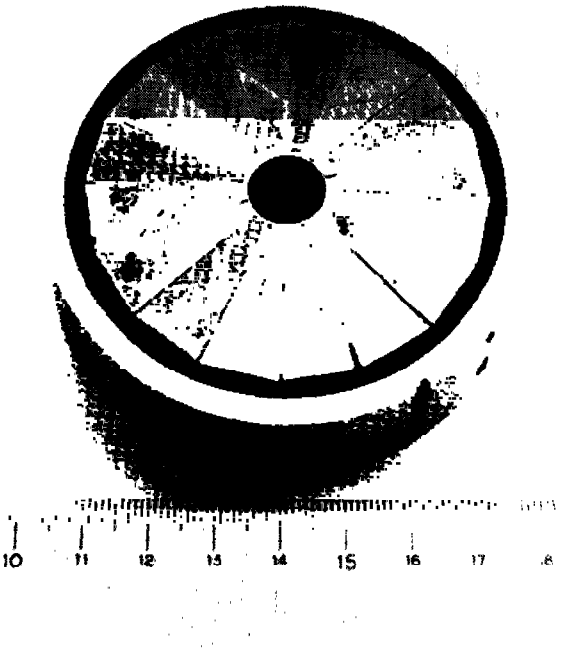

Fig. 13. A segmented ring-shaped permanent quadrupole magnet built in the drift tube of the 400 MHz 100 MeV injector linac

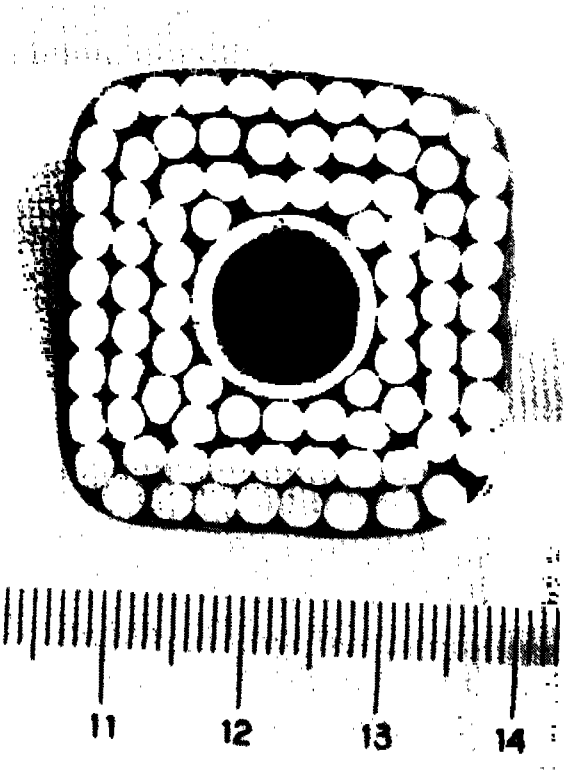

Fig. 14. Cross sectional view of the stranded cable for exciting GEMINI synchrotron magnet

Proceedings of the Eighth Meeting of the International Collaboration on Advanced Neutron Sources (ICANS-VIII)
8-12 July 1985, Rutherford Appleton Laboratory Report RAL-85-110

State of the SNQ Project

Hans Stiller
Kernforschungsanlage Jülilch

The state of the SNQ project can be stated in 6 words: the SNQ will not be built.

This decision was taken only two weeks ago by the Supervisory Board of our laboratory, based on a recommendation by a commission of the federal German parliament, the commission for research and technology. The decisive paragraph of the decision reads:

> "The Supervisory Board has noted that the KFA associates do not see any possibility of realizing the project under the present circumstances in view of the high amount of funds required for the construction of the SNQ spallation neutron source. It, therefore, decides that the project be terminated by December 31, 1985 in accordance with Art. 7, para. 2a of the partnership agreement. The Supervisory Board requests the Board of Directors to complete any work still under way for the SNQ project during this period and to document the results also with a view to a potential revival of such a project at a later date. The Supervisory Board notes that the Federal Minister for Research and Technology intends to set up an advisory committee in order to clarify the question of future research opportunities for German scientists working with neutrons. The KFA is requested to support the activities of this committee by making available its expertise and the experience gained in handling the SNQ project."

The associates mentioned here are the German federal goverment which provides 90% of the laboratory budget and the government of the land Northrhine-Westfalia which contributes 10% of the budget. The decision was taken in spite of the unanimous positive votes by two scientific bodies, the SNQ Scientific Council and the German Advisory Board on Basic Research in Natural Sciences.

Now, though the SNQ is dead we decided to come to this meeting and to present our contributions, because we think that at least some of them may be of interest to the design of other spallation sources or for the utilization of spallation sources.

Thus, first I will describe briefly once more the basic concept of SNQ. Then, in the workshops, we will present some special aspects; 8 contributions related to the target, with its special features resulting from the high power density we had planned, and 2 on ideas and development work for neutron scattering instrumentation. A rather large amount of work done about instrumentation for pulsed sources has been published as a report entitled "Proceedings of the Workshop on Neutron Scattering Instrumentation for SNQ" /1/.

The Basic SNQ Concept

The primary goal of our project has been: to create a facility for neutron scattering which goes beyond a high flux reactor. I still am convinced

- in the first place, that - at least virtually - neutron scattering is the very best tool for condensed matter research, where by condensed matter I mean not only solids and liquids but also and in particular biological matter,
- secondly, that in order to apply this tool to more and more complex and interesting systems and more complex and more interesting phenomena more beam intensity is required than presently available even with high flux reactors, and
- in the third place, that the only way to make substantial progress in this direction is the development of sources based on spallation.

The advantage of spallation lies not only in the possibility it provides for an optimal time structure of the neutron beams but also in the fact that the heat produced per released neutron is considerably smaller than with fission and can be removed more easily. Yet, also for spallation sources, the final limit for attainable flux strengthes will be given not by the achievable proton beam power but again by heat, by the heat production in the target. If one considers a hybrid target, a booster, combining spallation and fission, obviously the more fission one allows for the sooner one will reach the final limit. A booster may be a sensible option for a given accelerator; the optimal solution will be a pure spallation source.

By "beyond a high flux reactor" I mean here: not only for hot and epithermal but also for thermal and subthermal neutrons and not only for time-of-flight measurements but for as many types of measurements as possible.

We had many and long discussions on what types of measurements should be performable with a spallation source. We finally agreed to distinguish 3 classes:

1. Steady state measurements (dc-measurements like with a triple axis spectrometer). For such measurements, going beyond a high flux reactor for thermal neutron beams must mean, of course:

$$\Phi_{th} > \Phi_{th}^{HFR} \qquad (1)$$

where Φ_{th} is the thermal neutron flux from the spallation source in time average.

2. Time-of-flight measurements, mostly of the type you would or could do at a reactor too. Here, going beyond a reactor must mean:

$$\nu_s \cdot \hat{\Phi}_{th} > \nu_{tof} \cdot \Phi_{th}^{HFR} \qquad (2)$$

where $\hat{\Phi}_{th}$ is the peak thermal flux, ν_s the source repetition rate and ν_{tof} the time-of-flight pulse frequency you would use for the same measurement at a reactor.

3. Multiplexing measurements.

By "multiplexing" we mean measurements for which the time structure of the source does not determine the resolution. The time structure is used only to carry out a number of scans simultaneously. - This is illustrated in fig. 1, the well-known time-distance diagram for neutron flight. The different slopes of the obligue lines correspond to different neutron velocities or neutron wavelengthes. In time intervals T, the source provides pulses of duration τ. For a multiplexing measurement, you accept in a time fraction Δt a wavelength band which is as broad as possible (the shaded area in fig. 1), much broader than the resolution you need, and you then later, in front of the sample or behind it, subdivide this band into sections corresponding to your resolution requirements so that you perform n measurements in the interval between two pulses. You can do this by time-of-flight but also by other means, by crystals for instance.

I consider the exploitation of this possibility most important for steps beyond high flux reactors. Fig. 2 illustrates the principle with the simplest example: a measurement on diffuse elastic scattering. By elastic I mean, without energy analysis; the scattering is known to be elastic. If the incident beam is open for a time interval Δt, then we have in a distance l after a time A_M a wavelength band

$$\Delta\lambda = \lambda_1 - \lambda_2 = \Delta t \cdot \frac{\lambda_M}{A_M}$$

centered around λ_M, if $A_M = l/v_M$. If a scattering number resolution δQ is required, we need a wavelength resolution

$$\frac{\delta\lambda}{\lambda} = \frac{\delta Q}{Q} - \frac{1}{2}\cot\frac{\vartheta}{2} \cdot \delta\vartheta$$

if ϑ is the scattering angle. To achieve this resolution, for instance by time-of-flight, we require

$$\frac{\delta t}{T_M} = \frac{\delta\lambda}{\lambda_M}$$

with $T_M = L/v_M$, L being the flight path. We then get an intensity

$$I_{pulsed} = \hat{\Phi}_{th} \cdot \frac{\tau}{T} \cdot P_c \cdot \delta\Omega \cdot \frac{\Delta\lambda}{\lambda} \frac{\delta t}{\Delta t}$$

where P_c is the transmission of the chopper placed at distance l and open at time A_M for an interval δt and $\delta\Omega$ is the solid angle element for the scattered beam. For comparison, with a similar experiment at a high flux reactor, we would obtain

$$I_{HFR} = \Phi_{th}^{HFR} \cdot P_x \cdot \delta\Omega \cdot \frac{\delta\lambda}{\lambda}$$

P_x being the reflectivity of a monochromizing crystal. Assuming $\Phi_{th}^{HFR} = \hat{\Phi}_{th} \cdot \frac{\tau}{T}$ and $P_c \simeq P_x$, we get

$$\frac{I_{pulsed}}{I_{HFR}} = \frac{\Delta\lambda}{\delta\lambda} \cdot \frac{\delta t}{\Delta t} = \frac{L}{T}$$

which may be 10 or 20, depending on overlap conditions. We performed 10 to 20 measurements at the same time. There are many other examples for

multiplexing: a multi-crystal back scattering spectrometer, time-of-flight small angle scattering, a time-of-flight spin echo instrument, etc.

For the multiplexing type of measurements, going beyond a HFR means:

$$\Delta t \cdot \Phi_{th} > \delta t \cdot \Phi_{th}^{HFR} \tag{3}$$

where the fullfillment of this requirement will be constrained by considerations on the avoidance of overlap of beams from different pulses, just as the fullfillment of requirement (2) must be limited by such considerations which are specific to each measurement, of course.

The requirement (1) was specified for SNQ to be:

$$\Phi_{th} = 1.2\ \Phi_{th}^{HFR} = 1.2 \times 10^{15}\ cm^{-2}s^{-1} \tag{1a}$$

With protons as primary particles and U^{238} as spallation material this means a beam power of 5.5 MW. The energy was chosen to be 1.1 GeV, because at this energy the heat produced per released neutron has a minimum. Then a time-average current

$$\bar{I}_p = 5\ mA \tag{1b}$$

is required. For the repetition rate, ν_s, we got requests between 25 and 400 Hz from different users,

$$\nu_s = 100\ s^{-1} \tag{2a}$$

appeared as a reasonable compromise. The requirements (1b) and (2a) can be fullfilled with a linear accelerator or, possibly, with a FFAG synchrotron only.

With a linear accelerator of the high frequency type

$$\hat{I}_p = 200\ mA \tag{2b}$$

is feasible with present-day technology without too large beam losses. This yields

$$\hat{\Phi}_{th} = 4.5 \times 10^{16}\ cm^{-2}\ s^{-1} \qquad (2c)$$

$$\nu_s \cdot \hat{\Phi}_{th} = 4.5 \times 10^{18}\ cm^{-2}\ s^{-2}$$

From (1a), (2a) and (2b) it then follows that the pulse width must be $\tau_p = 250\ \mu s$.

The values for $\bar{\Phi}_{th}$, equ. (1a), and for $\hat{\Phi}_{th}$, equ. (2c), refer to a H_2O moderator without poison and fully coupled to the target. With τ_p = 250 μs the neutron pulse width is

$$\tau_{th} = 280\ \mu s. \qquad (3a)$$

To make the pulses shorter would require not only shorter proton pulses but also poisoning and decoupling of the moderators which in turn would reduce $\bar{\Phi}_{th}$ by more than an order of magnitude and $\hat{\Phi}_{th}$ by about factor 2. And, moreover, a Δt_{th} of 280 μs is a good value for many kinds of multiplexing instruments. Other instruments, of course, need shorter pulses. They then must use individual pulse shapers, to be placed in the beam ports as close as possible to the moderators, balancing for each individual measurement resolution against intensity. Considerable effort has been spent to develop such choppers. We are confident that this can be accomplished with the help of magnetic bearings.

Many studies, in some cases very elaborate ones, have been carried out last year to optimize existing instruments and to conceive and develop entirely novel ones with regard to a pulsed source of the SNQ type. For 15 kinds of measurements the gain to be expected with such instruments in comparison to similar measurements at the ILL has been calculated on the basis of the source specifications (1a), (2a), (2c) and (3a). The results are summarized in table 1. The numbers for the gain actually ought to be multiplied by 1.2 as all calculations were done with $\bar{\Phi}_{th} = \Phi_{th}^{HFR}$ rather than with (1a).

As an option for shorter pulses - of about 200 ns duration - a compressor ring has been conceived as has been done with LAMPF. It has been proposed as an

option only because:

i) for funding reasons, we wished to build the facility in two steps;

ii) we wished to await the development of demand for very short pulses as it may arise from operation of the SNS,

iii) we did not have the time or the manpower to design the ring in sufficient detail and to develop a solution to the problems arising from the short-pulsed heat generation in the target.

Reference:

(1) Proceedings of the Workshop on Neutron Scattering Instrumentation for SNQ, Jül-1954, Oct. 1984

Type of Measurement	Gain with SNQ	Reference
Time-of-Flight Powder Diffractometer with 2×10^{-4} resolution	35	(1)
Time-of-Flight Single Crystal Diffractometer a) small unit cell ($LiSO_4 \cdot H_2O$) b) large unit cell c) magnetic structures	6 9-35 10	(10) (2) (10)
Small Angle Diffraction	4-6	(3)
Small Angle Scattering a) with 10 mm beam diameter, 10 % resolution b) with 10 mm beam diameter, 1 % resolution c) with 1 mm beam diameter, 10 % resolution	1-2 20 14	(4) (4) (5)
Triple Axis Spectrometer	1	
Time-of-Flight a) at thermal moderator with ν = 250 Hz b) at cold moderator with ν = 100 Hz	14 17	
Inverted Time-of-Flight with Multi-Arm-Crystal Analyser (MAX)	10	(6)
Inverted Time-of-Flight Back Scattering (IRIS) for 10-50μeV res.	12 - 15	(7)
Multi-Crystal Backscattering for 0.1 to 1 μeV resolution Spin Echo for 20 neV resolution	12 3-6	(7), (8) (9)

Table 1: Intensity gain for various types of measurement at the SNQ in comparison to the ILL high flux reactor. The references for the detailed calculations are to be found in /1/.

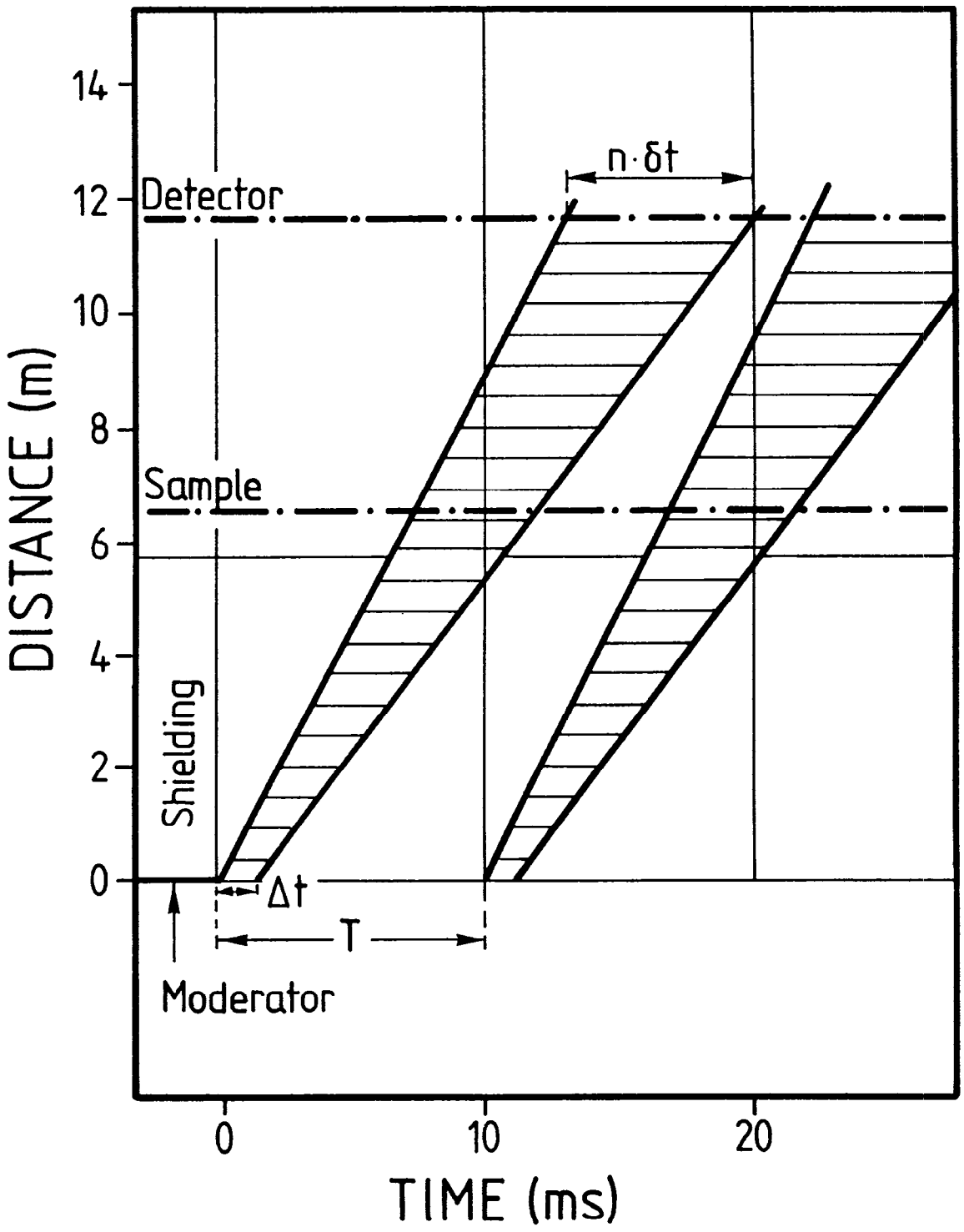

Fig. 1: The source provides pulses of duration τ in intervals T. A fraction Δt of τ is accepted to the measurement. Δt contains a neutron velocity band $\Delta v = v_1 - v_2$ which subsequently is subdivided into n elements δt, each containing a velocity band δv as required for resolution.

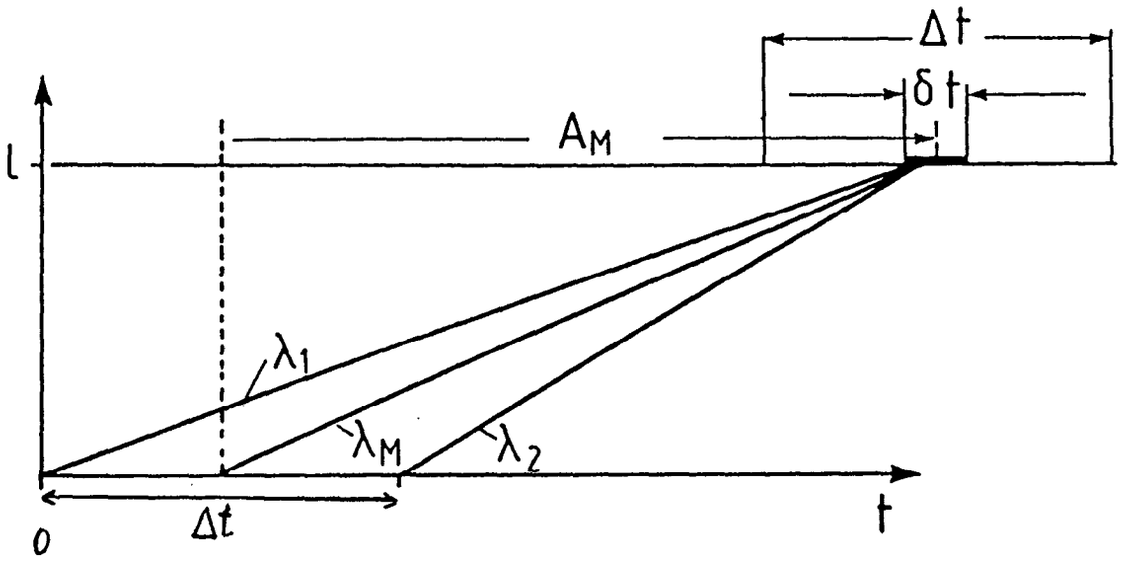

Fig. 2: Distance l between the moderator and a chopper to be open at time A_M for an interval δt in a measurement of elastic diffuse scattering (see text).

Proceedings of the Eighth Meeting of the International Collaboration on Advanced Neutron Sources (ICANS-VIII)
8-12 July 1985, Rutherford Appleton Laboratory Report RAL-85-110

STATUS OF THE COMMISSIONING OF THE LOS ALAMOS NEUTRON SCATTERING CENTER, LANSCE

by
Fred A. Morse
Los Alamos National Laboratory

INTRODUCTION

The Los Alamos spallation neutron source, formerly referred to as the Weapons Neutron Research facility has been upgraded through the use of a proton storage ring. The new capability has been referred to as the WNR/PSR facility which is at least difficult to pronounce and at worst somewhat misleading since we have several target areas associated with the entire facility. Consequently, we have chosen to give the name in the title, LANSCE, to the target area and experimental hall devoted primarily to materials. The other areas in the larger complex are principally used for nuclear and particle physics research. These areas will retain the designation WNR. The LANSCE has been in effect, separated from the WNR functionally, organizationally, and in name.

The first vugraph shows the relation of LANSCE to the Los Alamos Meson Physics Facility (LAMPF), and to the WNR complex.

UPGRADE

The LANSCE has been undergoing an upgrade from the capability we had when LAMPF beam was simply delivered to the spallation source. The addition of the proton storage ring (PSR, it really is an accumulator), permits us to increase the neutron flux delivered to an instrument as shown in Figure 2. The Table also shows projected capability as compared to the capability of SNS as reported by A.J. Leadbetter et al. It can be seen that the two facilities will be offering very similar neutron fluxes.

The improvement at Los Alamos is obtained by a substantial change to the LAMPF injector as well as by the addition of the PSR. The LAMPF injector has been modified to increase the H^- current from 100μa to 1ma. The LAMPF pulses are schematically shown in Figure 3. Each of the 750μs long macro pulses tailored for injection into the PSR consists of 2000 ea. 0.270 μs long packets of micropulses. These packets are injected into the storage ring, one after another. The timing is such that each packet is inserted on top of the pulse preceding it until the current density within the storage ring reaches 45A, at which time it is expelled from the ring and directed to the spallation target. At this point, the proton current is 100 μamps, has a pulse width of 0.27μs and a repetition rate of 12 Hz.

In order to insert the H^- beam into the ring, it is necessary to strip the H^- to H^o, then to ionize the H^o to produce protons. These operations take place as shown in Figure 4. The H^- beam is stripped by the use of an intense magnetic field, the neutral beam is then reionized with a carbon stripper foil. The H^- to H^o conversion is measured to be 100%, the H^o to H^+ is measured to be 98% efficient.

COMMISSIONING

Figure 5 is a picture of the storage ring under vacuum before first beam. The status of our work in shown in Figure 6. We are on schedule. Beam current we have extracted so far from the storage ring is 0.5 Amp.

We are projecting 20/μA for use this year and full current by the fall of 1986 and operational use of full current by October 1986.

EXPERIMENTAL FACILITIES

Figure 7 shows the existing layout of the experimental area with a list of operational instruments. Figures 8 shows the proposed expansion of the experimental hall and office space. The request is still under review in Washington D.C.

The moderators we've used in the past, expect to use this year, and those we expect to have operational by 1986 are given in Figure 9.

FUTURE

Future upgrades include, of course, the new hall. We are studying the appropriateness and design of a booster target and the utility of increasing the pulse frequency by a factor of two. The existing instrumentation will easily permit these changes. The new instruments on the drawing boards are given in Figure 10.

I show in figure 11, those people most responsible for these exciting new capabilities.

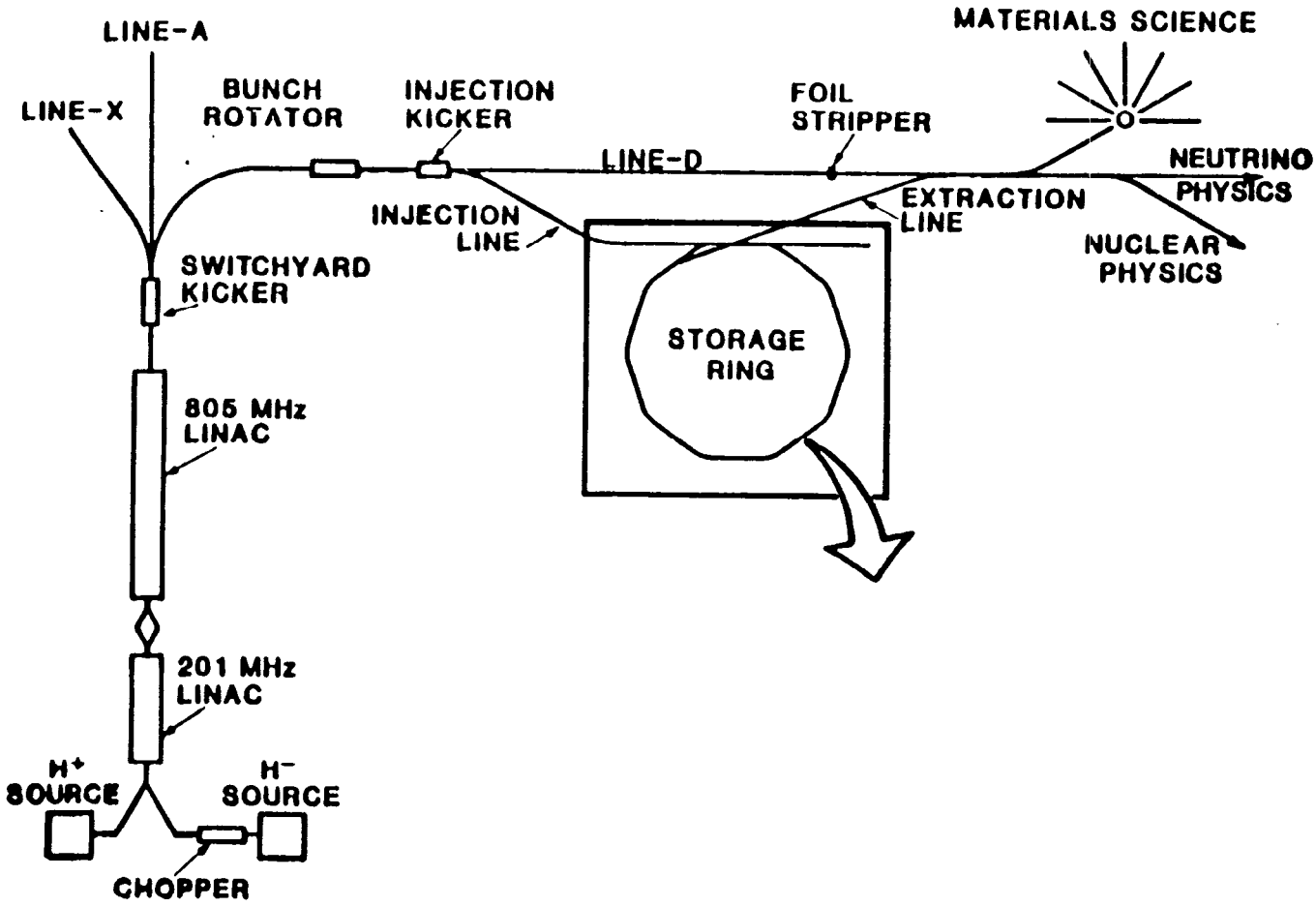
LINE-A
LINE-X
BUNCH ROTATOR
INJECTION KICKER
FOIL STRIPPER
MATERIALS SCIENCE
LINE-D
NEUTRINO PHYSICS
INJECTION LINE
EXTRACTION LINE
NUCLEAR PHYSICS
SWITCHYARD KICKER
STORAGE RING
805 MHz LINAC
201 MHz LINAC
H+ SOURCE
H- SOURCE
CHOPPER

Figure 1

BASIC CHARACTERISTICS OF LANSCE BEAM COMPARED TO THE SNS

	LANSCE				SNS
	1984	MAY 1985	SEP 85	PROJECTED SEP 86	PROJECTED AT COMPLETION
Beam Energy	800 MeV	800 MeV	800 MeV	800 MeV	800 MeV
Protons/Pulse	2.8×10^{11}	2.6×10^{11}	1×10^{13}	5×10^{13}	2.5×10^{13}
Pulse Width	5 μs	.2 μs	.27 μs	.27 μs	.4 μs
Repetition Rate	120 Hz	12 Hz	12 Hz	12 Hz	50 Hz
Average Proton/Sec	3.4×10^{13}	3×10^{12}	1.2×10^{14}	6×10^{14}	1.2×10^{15}
Peak Current	10 mA	.2 A	6 A	30 A	10 A
Average Current	5.4 μA	.5 μA	20 μA	100 μA	200 μA
Moderators					
Ambient Poisoned Mod					✓
Liq H_2, Moderator				25°	25°
H_2O Ambient Temp				✓	✓
Liquid Methane				•	100°

• SEE FIGURE 9

(FIGURE 2)

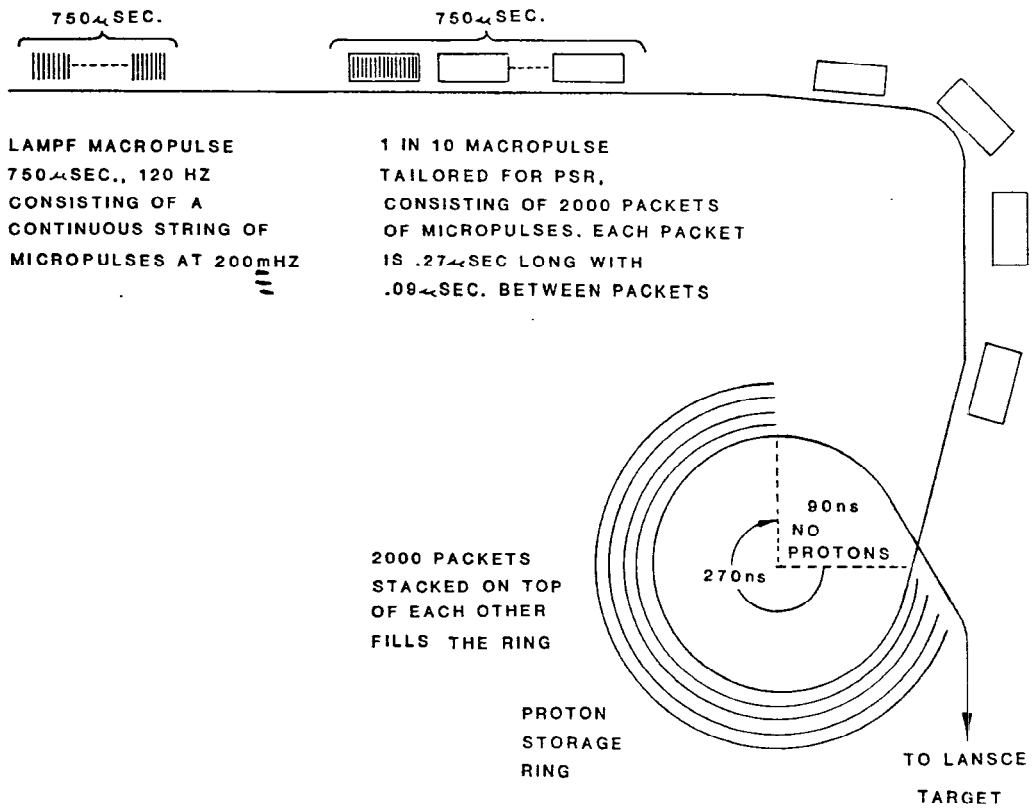

PROTON STORAGE RING PULSE CONFIGURATION

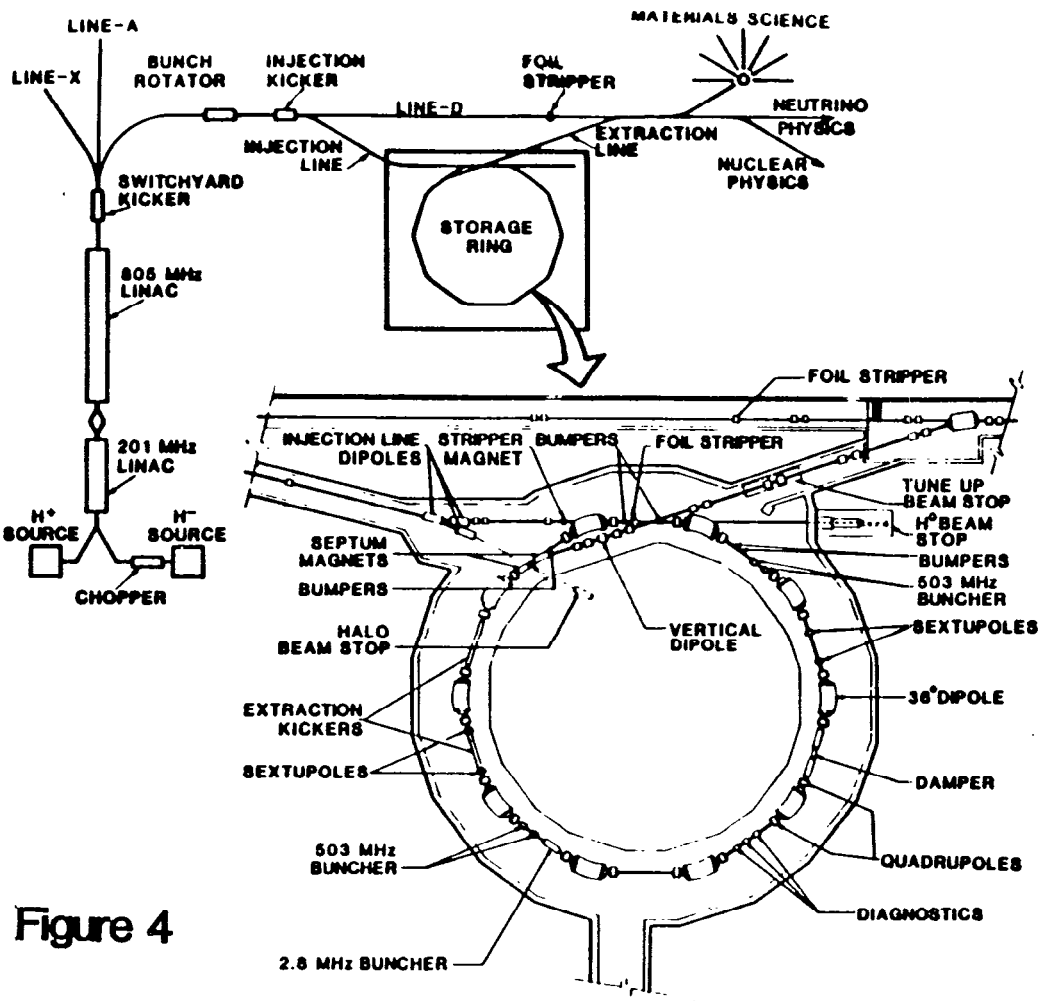

Figure 4

PSR MILESTONES

September 1979	Project authorized by Congress.
October 1980	Project reestimated and scheduled.
January 1981	$5M construction funds released. Start construction of staging building. Increased R and D activity.
July 1981	Occupy staging building.
September 1981	Major dipole magnet order placed.
May 1982	Start construction of ring and equipment building.
August 1982	Beneficial occupancy of ring tunnel. Start equipment installation.
February 1984	Beneficial occupancy of equipment building. Start equipment installation.
October 1984	LAMPF shutdown. Start final switchyard and Line-D installation.
March 1985	Ready for first beam into ring.
March 1986	Initial shakedown complete.

FIGURE 6A

PSR/WNR SCHEDULE

1985	
3/31	LAMPF and PSR ready for beam.
4/22	LAMPF starts production.
4/25	First beam in PSR.
4/25-6/3	Low current tuning < 100 nA avg.
6/3-7/22	Tuning at up to 1 x e13 ppp.
7/1	WNR high-current target ready.
7/15	Beam-on-target demo at 20 μA.
7/25-8/30	PSR tuning at up to 20 μA avg. Some beam for friendly users.
9/1-12/15	Production at 20 μA (70% time). PSR tuning at > 1 x E13 ppp (30%)
1986	
5/86-9/86	PSR tuning to 100 μA avg. Production at increasing flux.
9/86	100 μA production at 12 Hz
9/87	Upgrade to 200 μA at 24 Hz
9/88	Upgrade to 400 μA at 48 Hz

FIGURE 6B

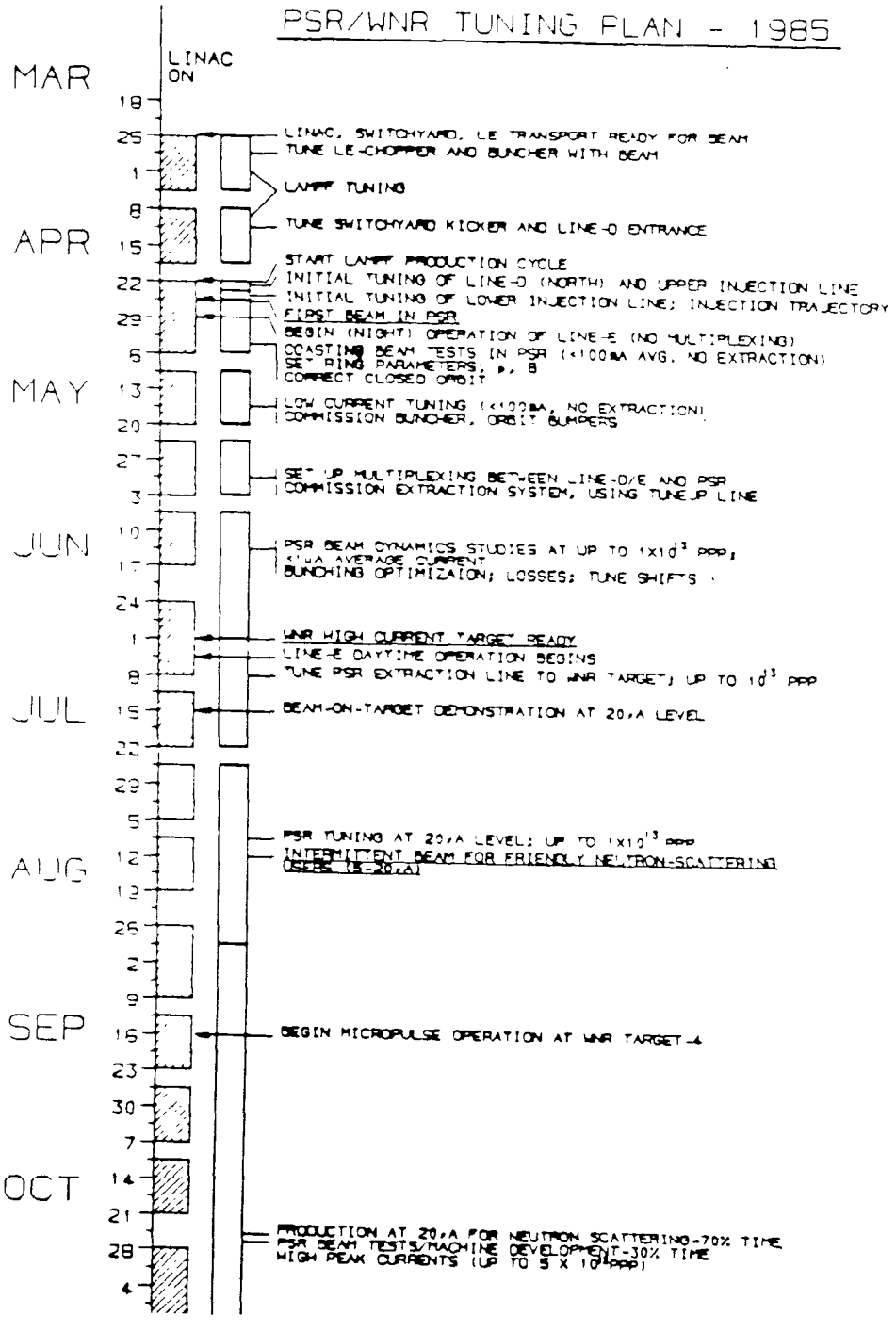
PSR/WNR TUNING PLAN - 1985
MAR
APR
MAY
JUN
JUL
AUG
SEP
OCT
LINAC ON
18
25
1
8
15
22
29
6
13
20
27
3
10
17
24
1
8
15
22
29
5
12
19
26
2
9
16
23
30
7
14
21
28
4
LINAC, SWITCHYARD, LE TRANSPORT READY FOR BEAM
TUNE LE-CHOPPER AND BUNCHER WITH BEAM
LAMPF TUNING
TUNE SWITCHYARD KICKER AND LINE-D ENTRANCE
START LAMPF PRODUCTION CYCLE
INITIAL TUNING OF LINE-D (NORTH) AND UPPER INJECTION LINE
INITIAL TUNING OF LOWER INJECTION LINE; INJECTION TRAJECTORY
FIRST BEAM IN PSR
BEGIN (NIGHT) OPERATION OF LINE-E (NO MULTIPLEXING)
COASTING BEAM TESTS IN PSR (<100nA AVG. NO EXTRACTION)
SET RING PARAMETERS; ν, β
CORRECT CLOSED ORBIT
LOW CURRENT TUNING (<100nA, NO EXTRACTION)
COMMISSION BUNCHER, ORBIT BUMPERS
SET UP MULTIPLEXING BETWEEN LINE-D/E AND PSR
COMMISSION EXTRACTION SYSTEM, USING TUNE-UP LINE
PSR BEAM DYNAMICS STUDIES AT UP TO 1x10^13 PPP;
<1μA AVERAGE CURRENT
BUNCHING OPTIMIZATION; LOSSES; TUNE SHIFTS
WNR HIGH CURRENT TARGET READY
LINE-E DAYTIME OPERATION BEGINS
TUNE PSR EXTRACTION LINE TO WNR TARGET; UP TO 10^13 PPP
BEAM-ON-TARGET DEMONSTRATION AT 20μA LEVEL
PSR TUNING AT 20μA LEVEL; UP TO 1x10^13 PPP
INTERMITTENT BEAM FOR FRIENDLY NEUTRON-SCATTERING USERS (5-20μA)
BEGIN MICROPULSE OPERATION AT WNR TARGET-4
PRODUCTION AT 20μA FOR NEUTRON SCATTERING-70% TIME
PSR BEAM TESTS/MACHINE DEVELOPMENT-30% TIME
HIGH PEAK CURRENTS (UP TO 5 x 10^13 PPP)

Figure 6C

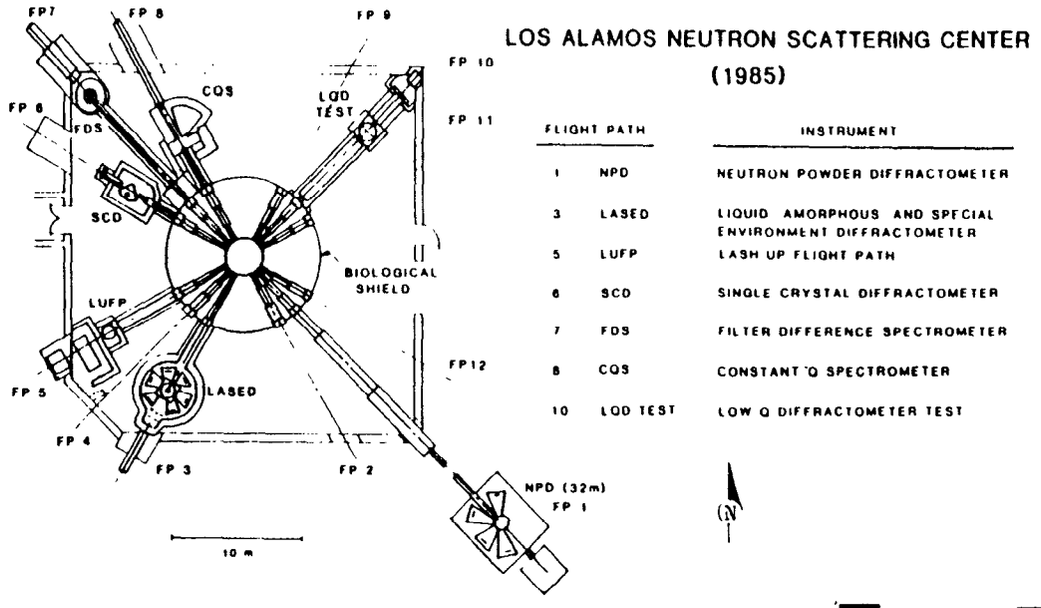

LOS ALAMOS NEUTRON SCATTERING CENTER (1985)

FLIGHT PATH		INSTRUMENT
1	NPD	NEUTRON POWDER DIFFRACTOMETER
3	LASED	LIQUID AMORPHOUS AND SPECIAL ENVIRONMENT DIFFRACTOMETER
5	LUFP	LASH UP FLIGHT PATH
6	SCD	SINGLE CRYSTAL DIFFRACTOMETER
7	FDS	FILTER DIFFERENCE SPECTROMETER
8	CQS	CONSTANT Q SPECTROMETER
10	LOD TEST	LOW Q DIFFRACTOMETER TEST

Figure 7

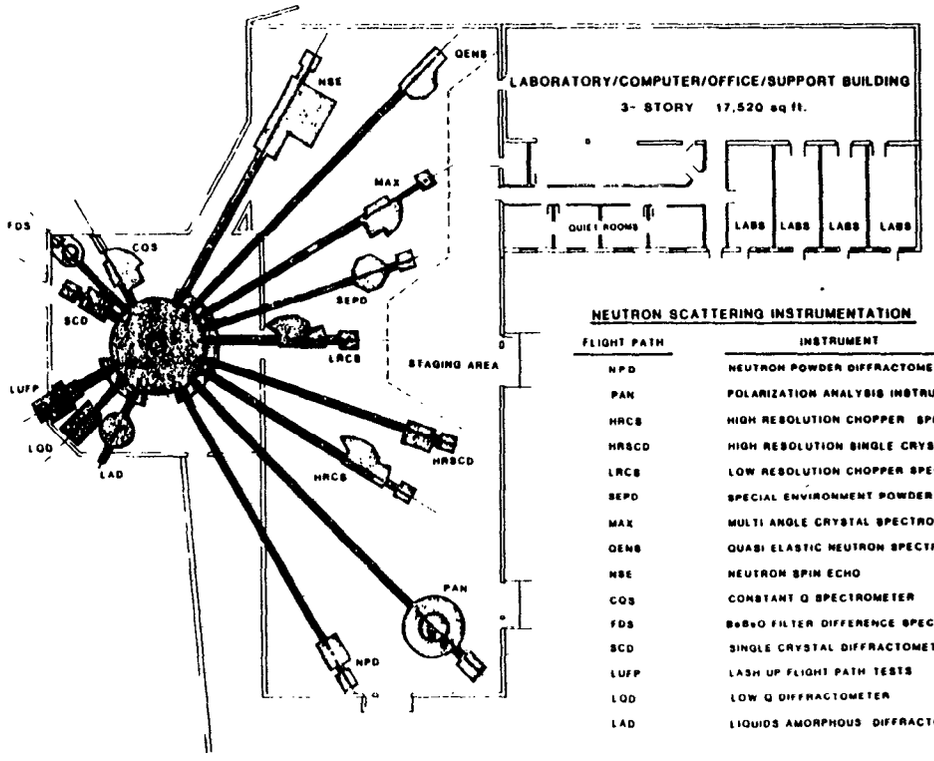

NEUTRON SCATTERING INSTRUMENTATION

FLIGHT PATH	INSTRUMENT
NPD	NEUTRON POWDER DIFFRACTOMETER
PAN	POLARIZATION ANALYSIS INSTRUMENT
HRCS	HIGH RESOLUTION CHOPPER SPECTROMETER
HRSCD	HIGH RESOLUTION SINGLE CRYSTAL DIFFRACTOMETER
LRCS	LOW RESOLUTION CHOPPER SPECTROMETER
SEPD	SPECIAL ENVIRONMENT POWDER DIFFRACTOMETER
MAX	MULTI ANGLE CRYSTAL SPECTROMETER
QENS	QUASI ELASTIC NEUTRON SPECTROMETER
NSE	NEUTRON SPIN ECHO
CQS	CONSTANT Q SPECTROMETER
FDS	BeSeO FILTER DIFFERENCE SPECTROMETER
SCD	SINGLE CRYSTAL DIFFRACTOMETER
LUFP	LASH UP FLIGHT PATH TESTS
LOD	LOW Q DIFFRACTOMETER
LAD	LIQUIDS AMORPHOUS DIFFRACTOMETER

Figure 8

LANSCE MODERATOR CAPABILITY

	#	TYPE	TEMP	BEAM LINES SERVED
WNR 1984	3	H_2O	AMBIENT	8
LANCE 1985–86	3	H_2O	316 ± .5K	9
	1	H_2	25 ± 1K	3
WITH NEW	4	H_2O	316 ± .5K	12
EXPERIMENTAL	1	H_2O	25 ± 1K	3
HALL	1	CH_4	96 ± 1K	3

FIGURE 9

INSTRUMENT STATUS

NAME	STATUS	INST. RESPONSIBLE
● Be–BeO Filter Difference Spectrometer	Operational	J. Eckert
● Single Crystal Diffractometer	Operational	P. Vergamini/ G. Christoph
● Liquids, Amorphous; Special Environment Diffractometer (9m)	Operational	A. Williams
● Neutron Powder Diffractometer	Operational, Reconfigure to 32 m	J. Goldstone
● Constant Q Spectrometer	Development	R. Robinson
● Low Q Diffractometer (1986)	Design, Anger Camera Development	P. Seeger
● Chopper Spectrometer (1986–87)	Design, Magnetic Bearing Operational	R. Silver/ R. Heffner
● High Resolution Powder Diffractometer (1988)	Workshop Planned	----
● Quasielastic Neutron Spectrometer (10 μeV) (1988)	Nat'l Lab–Industry Collaboration Begun	----
● Polarization Analysis Instrument (1988)	F. Mezei Conceptual Design	----
● Lash Up Flight Path (Tests)	To Be Operational (1985)	M. Nutter

FIGURE 10

J. Browne – Associate Director for Experimental Physics
G. Sawyer – Construction Project Manager

Accelerator Technology Division

G. Lawrence
R. Hardekopf
P. Clout
A. Jason

Physics Division

C. Bowman
R. Woods
R. Ryder
G. Russell
D. Clark
H. Robinson

LAMPF

D. Hagerman
O. Van Dyck
D. Fitzgerald
R. Macek
H. Butler
R. Stevens

FIGURE 11

Proceedings of the Eighth Meeting of the International Collaboration on Advanced Neutron Sources (ICANS-VIII)
8-12 July 1985, Rutherford Appleton Laboratory Report RAL-85-110

STATUS OF THE SNS

D A Gray

Rutherford Appleton Laboratory, Chilton, Didcot, Oxfordshire, England

1. INTRODUCTION

Reports at past ICANS meetings have been on the state of construction of the SNS. It is a pleasure to report at this meeting preliminary experiences in producing neutrons. During June 1985 the SNS started on a routine schedule of operating 2 weeks for neutrons and 1 week for machine and target station development and maintenance. A description of commissioning highlights is given together with the general status of the neutron scattering instruments. Details of the state of machine and target station equipment as at May 1985 are given in ref (1).

2. COMMISSIONING

Highlights of commissioning are as follows:

Jan 84 - 1 μs long 70 MeV beam pulses injected into the main ring (with dc excitation of the magnets) and several hundred turns circulated at the first attempt.

Mar 84 - 0.8 μs, 70 MeV beam pulses successfully circulated with ac + dc excitation of the main ring magnets.

Apr 84 - 10 μs beam pulses successfully accelerated at the first attempt to 140 MeV using 2 rf cavities. With longer injected beam pulses the maximum accelerated beam intensity was 2.8×10^{12} protons per pulse (ppp) or about 10% of full intensity per pulse.

Jun 84 - 1.2×10^{12} ppp accelerated, at the first attempt using 4 rf cavities, to an energy of 550 MeV.

Sep 84 - 1.5×10^{12} ppp successfully extracted into a graphite beam dump, again at the first attempt.

Dec 84 First neutrons.

For all commissioning work repetition rates of about 1 per second have been used to minimise induced activity of components. The physics processes are independent of repetition rate.

3. THE DECEMBER 84 RUN

For the December run the following equipment was available for the first time:

- Extracted proton beam line, 150 m in length with 65 magnets
- Uranium target cooled by static D_2O
- The 2 ambient temperature moderators
- The 100K liquid methane moderator
- The 25K liquid hydrogen moderator
- Beryllium reflectors cooled by static D_2O
- Six neutron shutters open
- Six instrumental measuring stations
- 95 m neutron guide to High Resolution Powder Diffractometer
- 35 m neutron guide to Indian instrument, High Resolution Inelastic Spectrometer
- Data collection electronics and computer systems.

Neutrons were first produced at 19.16 hrs on Sunday 16 December 1984 (see Figures 1 - 4). Following this 2 to 5 x 10^{11} protons per pulse at 1 Hz were run into the target for a period of about 3 hours. The neutronic properties of the final target/moderator/reflector system were measured. These are reported fully in RAL Report RAL-85-030 (2) and together with reports on instruments are the subject of a number of papers at this meeting.

The basic design and performance of the system was as predicted.

4. PROGRESS DURING 1985

4.1 Installation and commissioning

The period until June was spent on the following installation and development work:

Target Station

- Completion of shielding
- Improvement to controls of cryogenic moderator systems
- Commissioning of cooling system for target and moderator
- Repair of small leak between circuits on the target module
- Commissioning of the Remote Handling Cell.

Machine

- Increasing repetition rate on injector
- Increasing repetition rate on injection kicker magnets
- Increasing repetition rate on extraction kickers
- Improvement on controls

Instruments

- Completion of installation to first stage for the 5 initial engineered instruments
- Preparation for installation of the 3 development instruments

The performance reached on various parts of the machine is as follows:

	Design			Performance		
	Energy	Rep rate Hz	Intensity per pulse	Energy	Rep rate Hz	Intensity per pulse
Ion source	18 keV	50	10^{14}	18 keV	50	2.5×10^{13}
Pre-injector	665 keV	50	10^{14}	665 keV	50/4	5×10^{12}
Linac RF system		50			50/4	
Injection kickers		50			50/2	
Synchrotron and magnet RF	800 MeV level	50		550 MeV level	50	
Synchrotron	800 MeV	50	2.5×10^{13}	550 Mev	50/16	2.5×10^{12}
Extraction kickers	800 MeV level	50		550 level	50	

The target/moderator/reflector system will take the full power. The policy on shielding is to make measurements as intensity is raised and to increase shielding to match personnel protection and backgrounds as required. Initial experience shows the shielding to perform as expected.

4.2 Scheduled running

Scheduled running started on 26 June 1985. Various items in the target station were brought on as follows:

June 26 Target and reflectors cooled with light water.
Two ambient temperature moderators.
550 MeV beam, 50/64 pps and 10^{12} ppp on to target.

June 30 Hydrogen moderator at 21K.

July 3 Methane moderator at 100K.
Target system was therefore all working.

July 5 550 MeV beam, 50/16 and 1.8×10^{12} ppp on to target.

At this stage typical intensities were:

Injection line	2.4×10^{12} ppp
Accelerated to 550 MeV	1.8×10^{12}
On target	1.8×10^{12}

The losses are consistent with what is expected and are such that the repetition rates can be increased without undue induced activity on accelerator components.

Target cooling will be changed to D_2O after a period of running with light water.

Commissioning of the installed spectrometers is under way, as is being reported at this meeting. The instruments are:

- High energy transfer spectrometer (HET) 0.1 - 1 eV
- High resolution powder diffractometer (HRPD) $\Delta d/d \sim 4 \times 10^{-4}$
- High resolution inelastic spectrometer (IRIS) 50 μeV resolution
- Liquids and amorphous diffractometer (LAD)
- Time focussed crystal analyser (TFXA) $\sim$ 1 eV

The small angle scattering instrument LOWQ is being installed as are the 3 development instruments:

- Polarised beams (POLARIS)
- Electron-volt spectrometer (eVS)
- Single crystal diffractometer (SXD)

5. OTHER USES OF THE SNS

KfK, Karlsruhe, are providing the main part of the funds for the neutrino physics facility, KARMEN, at SNS (3). The foundation for the 2.2 m thick, 5500 tonne, steel blockhouse and its walls and first part of the roof and its moveable shielding door have been installed.

The European Community, France and West Germany have provided funds for the installation of an intermediate target in the extracted proton beam some 20 m before the neutron target and a muon beam for tests on the technique of using pulsed muons for condensed matter research (4).

A test beam is being installed which will use a needle target which intercepts the edges of the beam in the synchrotron from which protons would normally be lost. The secondary particles will be used by particle physicists to test equipment destined to be used at other accelerator installations.

There has been some use of 70 MeV protons from the injector for irradiation of electronic components.

A pipe has been installed in the target station which allows irradiation of samples close to the neutron production target where the proportion of high energy neutrons is high.

6. INTERNATIONAL INVOLVEMENT IN THE SNS

The Bhahba Atomic Research Centre, India, has provided the IRIS instrument. The provision of the neutrino physics facility and the muon beam have already been mentioned. Italy has begun construction of the instrument PRISMA for studying single crystal excitations and it is planned to instal this in 1986. Sweden has provided funds for Swedish scientists to use the SNS.

Discussions are being held with France, Italy, West Germany, and others about a wider involvement of the European neutron scattering community in the SNS.

7. DEVELOPMENT OF THE SNS

We are clearly at the stage where our main priority is to get the SNS up to full performance and to equip it with a suitable range and number of spectrometers with appropriate support to provide efficient utilisation. Some thought has been given to uprating the present target by the use of enriched material in the target. Also it is feasible to multiplex the extracted proton beam to a second target station in a separate hall. These studies have been carried out in conjunction with KfA, Julich, and Birmingham University and are being reported at this meeting.

ACKNOWLEDGEMENT

The achievement of first neutrons and the start of scheduled operation on the SNS has been made possible by the enormous efforts of a large number of people at RAL. This is a further opportunity to record my appreciation of those efforts.

REFERENCES

(1) Initial operation of the SNS. D A Gray. 1985 Particle Accelerator Conference, Vancouver, May 1985.

(2) First neutron results from SNS. A J Leadbetter et al. RAL Report RAL-85-030, May 1985.

(3) Low energy neutrino physics at high intensity pulsed proton accelerators. B Zeitnitz, KfK, Germany. Progress in Particle and Nuclear Physics, Vol 13. Proc Intern School of Nuclear Physics, 445-78, 1985.

(4) A pulsed surface muon beam/pion beam for the RAL Spallation Neutron Source. G H Eaton et al. Nuclear Instr & Methods, 214(1983) 151-167.

FIG 1

Before 19.16 hrs
on 16.12.84

FIG 2

After 19.16 hrs
on 16.12.84

SNS Control Centre

FIG 3

FIG 4

SNS Target Station Control Room

Proceedings of the Eighth Meeting of the International Collaboration on Advanced Neutron Sources (ICANS-VIII)
8-12 July 1985, Rutherford Appleton Laboratory Report RAL-85-110

STATUS REPORT ON THE SIN-NEUTRON SOURCE (July 1985)

F. Atchison, W.E. Fischer, M. Pepin, D. Renker,
Y. Takeda, Ch. Tschalaer
SIN, Swiss Institute for Nuclear Research,
CH-5234 Villigen, Switzerland

ABSTRACT

SINQ is a continuous spallation neutron source which is planned to be attached to the existing accelerator at SIN after its upgrading to higher currents. The overall project aims to provide the Swiss neutron user community with the facilities necessary to carry out scattering experiments in the wavelength range 1 to 10 Å; that is, the neutron source itself, experimental areas, sample conditioning apparatus, sample preparation areas and scattering instruments. Construction is planned to start in 1987, with the first neutron expected in early 1990. Total costs (excluding spectrometers) are estimated to be 27 Mio. SFr.

1. INTRODUCTION

The Swiss Institute for Nuclear Research (SIN) operates a cyclotron system that produces a high-intensity proton beam of 592 MeV. The beam intensity available at present is about 150 μA, and mainly used for meson production at two special target stations. The secondary meson beams are used for nuclear and particle physics. This research forms the main activity for SIN, although some condensed matter physics is done at a muon beam.

After having passed through the meson target, about 70 % of the power of the original primary proton beam is still left. This beam is at present stopped in a beam dump.

A new injector system is now being commissioned to allow routine operation of the SIN experimental programme with a proton current in excess of 1 mA. With such beam current, the construction of a spallation neutron source with a performance comparable to that of a medium-flux reactor becomes feasible. Owing to the absence of any macro-pulse structure in the extracted proton beam this neutron source will be of the continuous type.

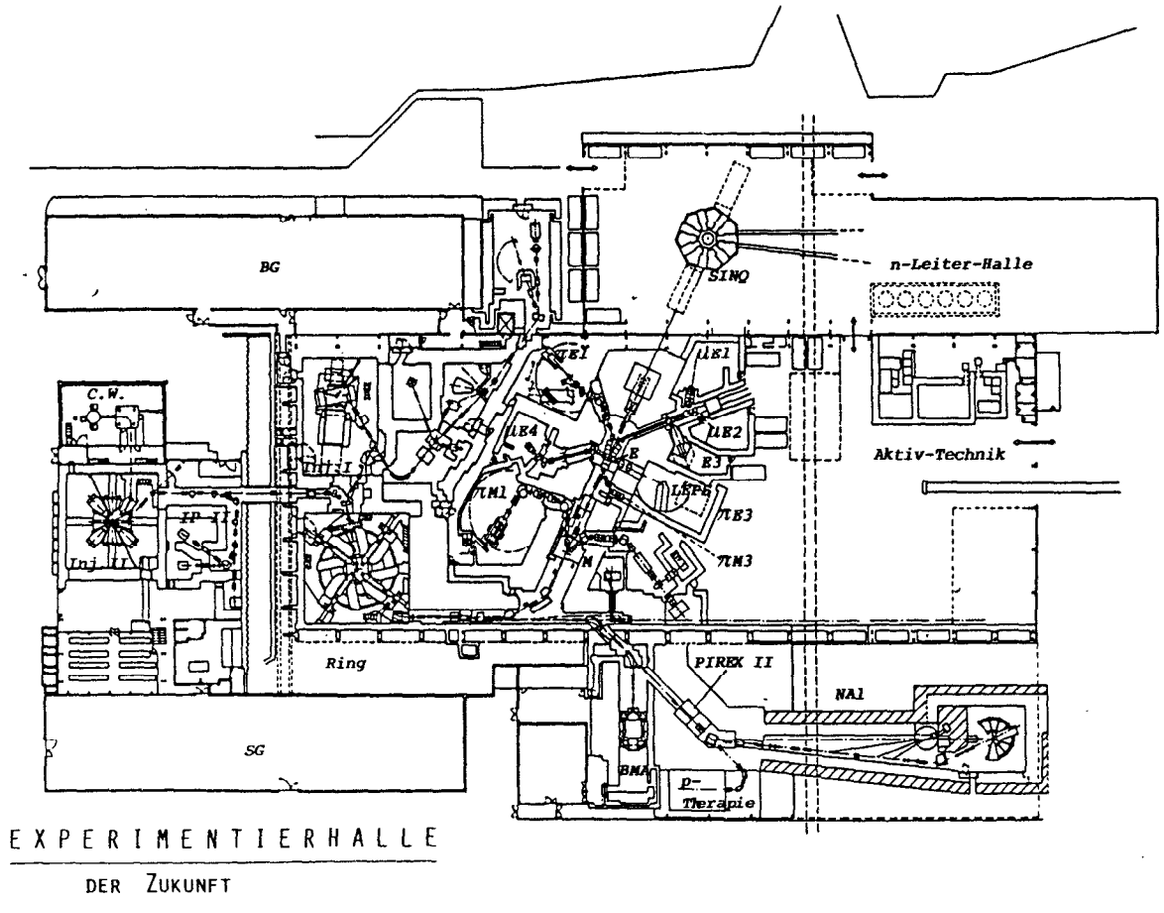

Fig. 1 Layout of the SIN-accelerator system and the experimental facilities. The location of the neutron hall, containing SINQ, and the guide hall is at the upper right of the picture.

The layout of the accelerator system and experimental facilities, following completion of the upgrade programme and including SINQ, is shown in Fig. 1. The major components of SINQ are (I) an extension of the present proton channel, (II) the neutron source itself, (III) the building for the source and neutron beam-tube experimental area, (IV) the neutron guide hall, and (V) the scattering instruments.

2. STATUS OF INJECTOR II

The pre-accelerator (Cockcroft-Walton) of Injector II contains a multi-cusp ion source with an extraction voltage of 60 keV. A short beam line, where the H^+ beam is cleared of other hydrogen ions, is followed by an acceleration tube of 800 keV. The 860 keV beam is then axially injected into the injector cyclotron, which is - like the main ring accelerator - of the isochronous type. Approximately 10 % of the injected DC-beam is accepted by the RF-system of the cyclotron for further acceleration up to 72 MeV. A view of Injector II with the 860 keV beam line, axial injection and the extraction for the 72 MeV beam is presented in Fig. 2.

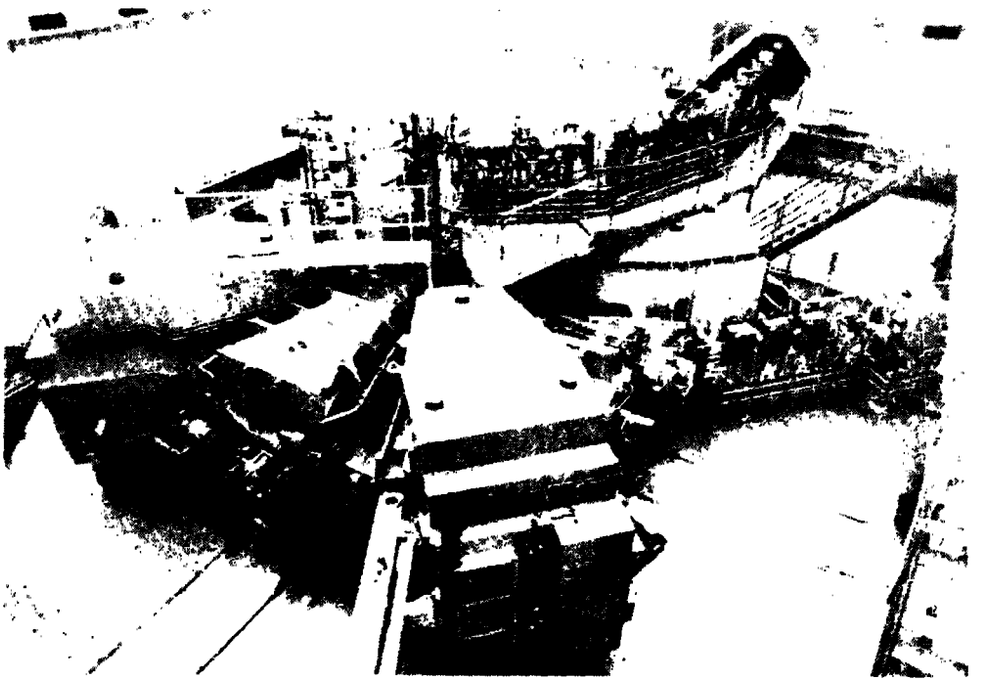

Fig. 2 A view of Injector II with the 860 keV beam line, axial injection and the extraction region for the 72 MeV beam line.

The status of this accelerator is as follows:

I) A maximum current of Ø.55 mA has been extracted. Beam losses were smaller than Ø.1 %. For a high extraction efficiency, a good separation of the final turns is essential. Fig. 3 shows the pattern of the last turns before extraction.

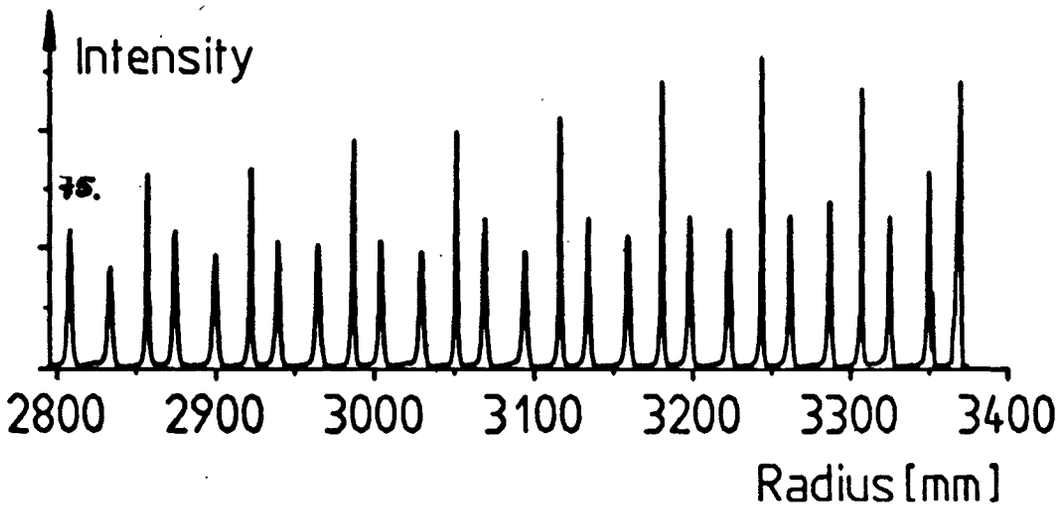

Fig. 3 Pattern of the last turns in Injector II before extraction. A superperiod of three turns (due to a small phase space mismatch) and the horizontal focusing frequency close to Q=4/3 is clearly visible.

II) In order to investigate space charge effects, a 1 : 6 pulse suppression system has been installed. By suppression of 5 out of 6 micropulses, the space charge effects of high currents can be produced at only 1/6-th of the corresponding beam power. In this mode, a current which corresponds to 72Ø μA has been extracted.

III) During 1985, Injector II will be used for routine operation at currents of circa 2ØØ μA. This limitation is given by the second meson target station which has not yet been upgraded for higher currents.

The ultimate intensity limit will probably be determined by longitudinal space charge effects at the low energy orbits (7 MeV) just after injection into this machine /1/. It is of vital interest to show soon the feasibility of currents of the order of 1.5 mA, since both the spallation neutron source project as well as the possible extension of the SIN facilities towards higher energies /2/ rely on this beam current.

3. THE SPALLATION SOURCE - SINQ

a) Principle

The source is to be mounted on an extension of the present proton channel beyond target 'E' in a new building on the east side of the experimental hall. This building is to contain the source itself and the experimental area for instruments requiring beam tubes. The non-interacting part of the proton beam will be collected beyond target 'E', deflected downwards to pass under the beam-tube area, hence to the centre of the source and finally pitched vertically upwards to the spallation target.

The proton energy at the spallation target will range from 560 to 590 MeV (depending on the thickness of target 'E') with an initial intensity of 1 mA.

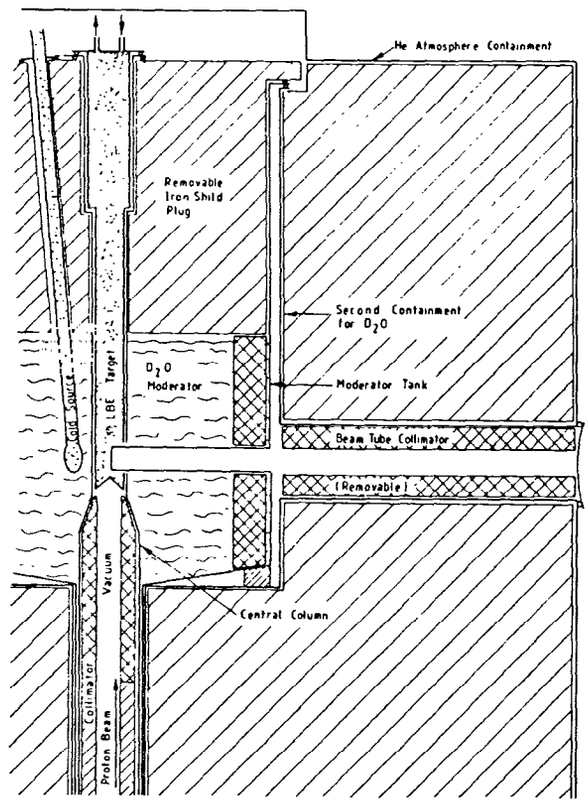

Fig. 4 Schematic view of the vertical section through the central region of the source.

A vertical section through the central region of the source is shown in Fig. 4. The target consists of a 'pot' of Pb/Bi eutectic

mixture (molten) of inner diameter about 15 cm and 2 to 4 m high. Most of the beam power is deposited in the bottom 30 cm of the target. Natural convection is to be used to transport this heat to an exchanger mounted at the top of the target and hence away from the source /3/. The 'active' region of the target (the bottom 30 cm) is located at the centre of a tank of D_2O with a diameter and height of about 2 m. The D_2O thermalizes the fast neutrons resulting from high-energy proton interactions with the Pb/Bi in the target.

Design work is presently particularly active for

I) The target plug including the heat exchanger and the cold traps for volatile spallation products /4/. This whole system is being designed as an entity and to have a lifetime of more than one operational year.

II) The beam entrance collimator system in front of the spallation target.

III) Flasks for the exchange and disposal of the target plug and the collimator system

IV) The D_2O-system.

V) The proton beam extension to the spallation target.

Since in many projects for spallation neutron sources the primary proton beam is also to be exploited for other purposes, e.g. μSR, it might be of general interest to describe our beam transport line after the last meson target in more detail.

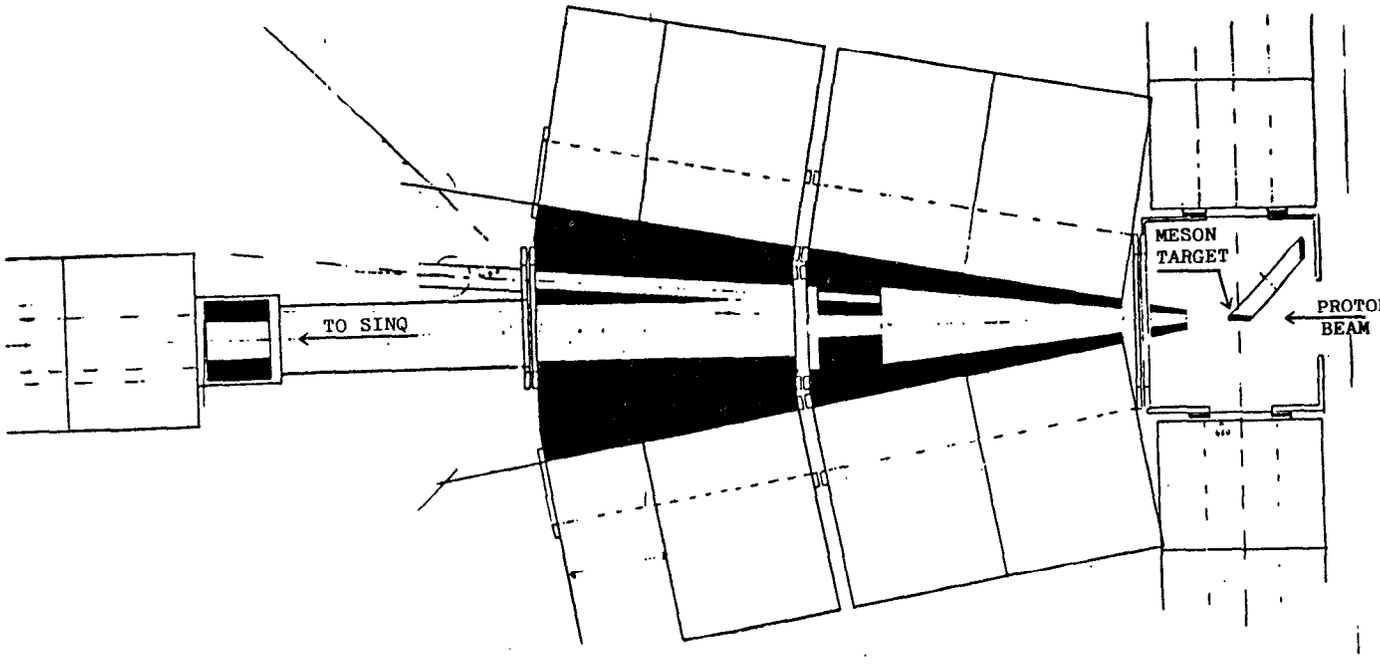

Fig. 5 The collimator system for cleaning up the transmitted proton beam at the last meson-target station.

b) Proton Beam Injection

Fig. 5 shows the collimator system which has to remove the halo of the proton beam, produced by scattering in the meson target. The transport of the proton beam through the target and the collimator system leads to the beam losses listed in Table I. The thickness of the target used for this estimate corresponds to 12 g Carbon, which is certainly an upper limit for a meson target bombarded by a proton beam with a power larger then 1 Mw:. The feasibility of a recovery of the proton beam under these extreme conditions gives us confidence in the chosen concept.

Table I

	loss (% of primary beam intensity)
Meson Target	11
Collimator I	6
II	14
III	1
Total	32

After passing through the meson target, the beam has a somewhat peculiar energy structure: Those parts which have missed the target, passing on its left or right side, have the original energy of 590 MeV, but the main part has been degraded by the target material to the range 570 -540 MeV.

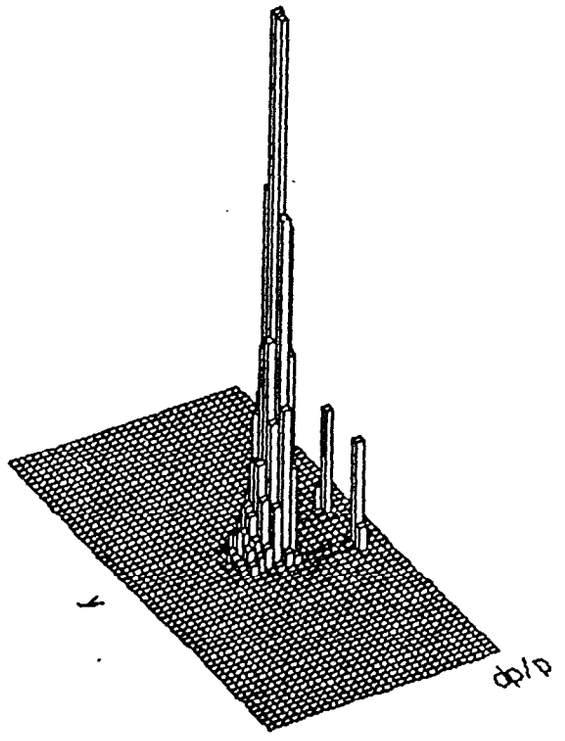

Fig. 6 Energy distribution of the proton beam after the meson target. A small part of the beam is passing to the left and right side of the target without interaction.

This distribution is shown in Fig. 6. Due to the relatively large energy spread, the beam line to the spallation target has to be of the achromatic type.

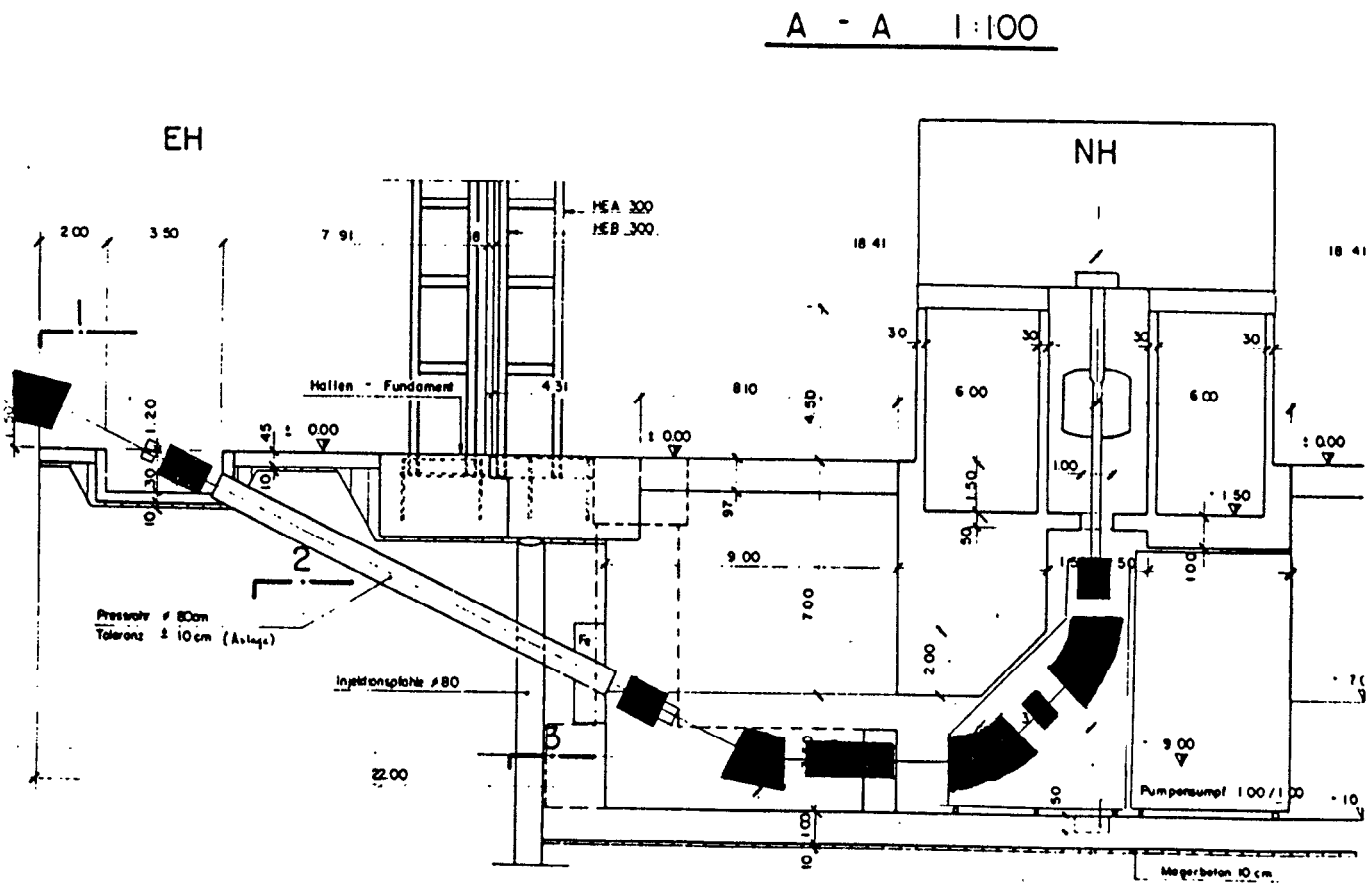

Fig. 7 Beam transport line between the meson target and the spallation source target. The sloping drift section passes the beam under the foundations of the present experimental hall. This concept also avoids excavating in the position where the present beam dump is located.

The present layout for the beam line is shown in Fig. 7. The proton beam will be refocused by a pair of quadrupoles placed after the collimator region, deflected downwards to pass under the neutron hall and hence into the cave below the centre of the source and finally pitched vertically upwards to the spallation target.

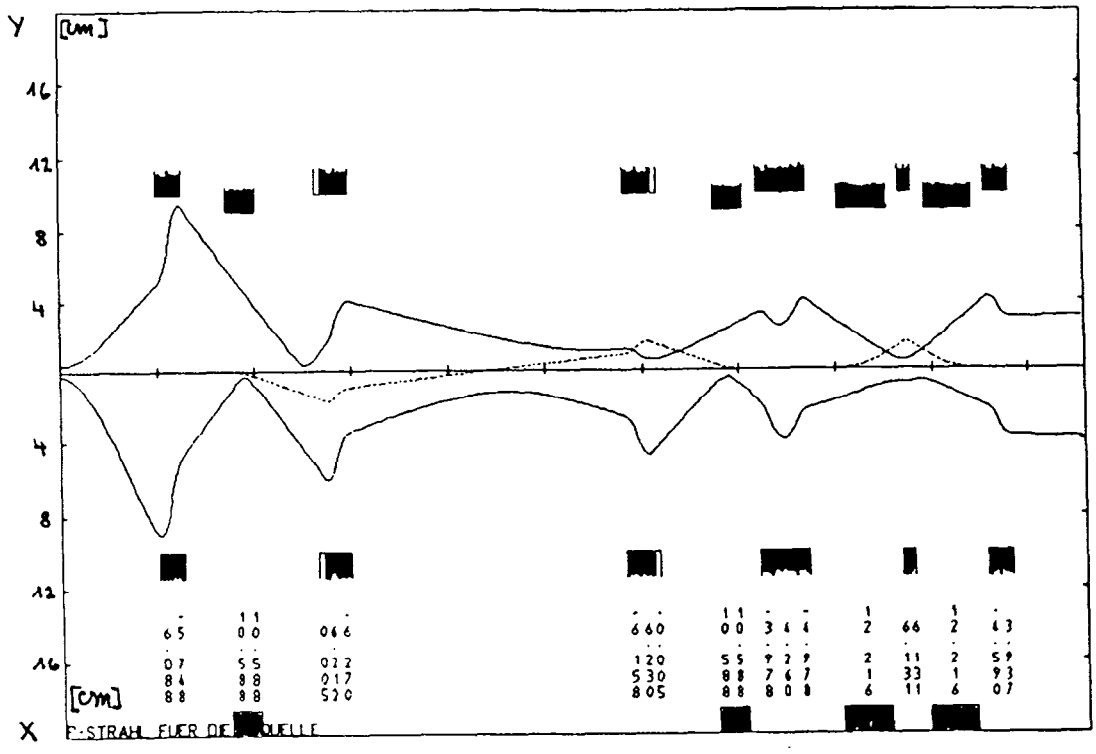

Fig. 8 Proton beam envelope and dispersion path for the injection line. This envelope contains the whole energy width of the beam indicated in Fig. 6.

The horizontal and vertical beam envelope as well as the dispersion path through the transport system are shown in Fig. 8. Beam losses are predicted to be less than 10^{-4} and located mainly in the region of the quadrupole doublet after the long drift tube, where the beam dispersion is rather high. This low beam loss gives us the possibility to design the undersource cave as a region with limited access and avoid an expensive remote handling system.

The beam spot on the target is relatively large, with a diameter of 6-8 cm. This size is a compromise between the following demands:

I) Optimal neutron production in the target

II) Efficient driving of the natural convection of the liquid metal in the target

III) Limitation of the power density in the material of the target window.

A collimator system in the vertical part of the beam line will protect equipment in this region (vacuum system, magnets etc.) against beam mis-steering. Special precautions will have to be taken to prevent incorrect focusing onto the beam window.

c) Neutron Flux and Source Performance

The design and performance of SINQ are based on results from an experimental programme for the investigation of the neutronics. This programme has been realized by a Julich-SIN collaboration on a secondary proton beam at SIN with a one-to-one mock-up model of the source /5/.

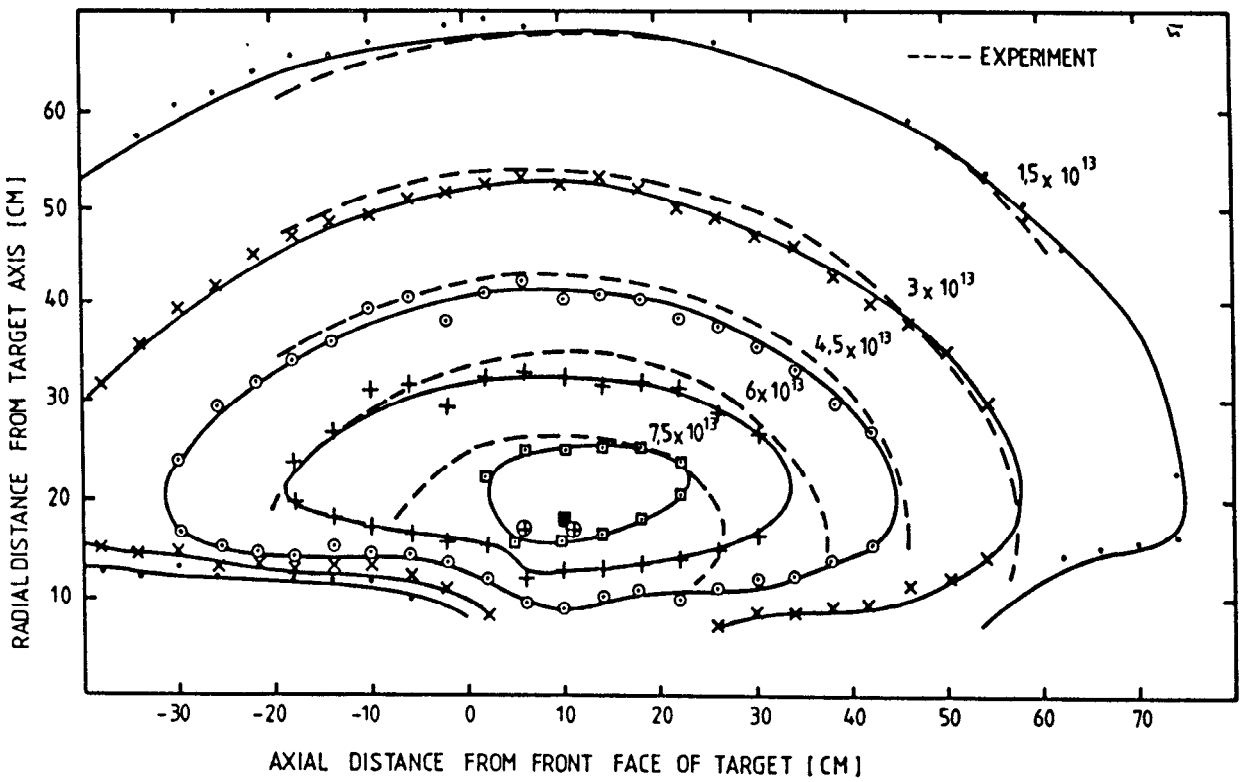

Fig. 9 Flux map for thermal neutrons in the D2O-moderator for 1 mA proton beam current.

Dashed lines: Mock up experiment

Solid lines: Monte Carlo simulation.

One of the flux maps, relevant to the planned SIN source, is shown together with its comparison with a Monte-Carlo simulation in Fig. 9. By means of flux distributions such as these, the optimal position of the cold source as well as the position and size of the beam tubes, may be determined. The last experiments at the mock-up model examined several configurations of cold hydrogen sources and their spectra /6/.

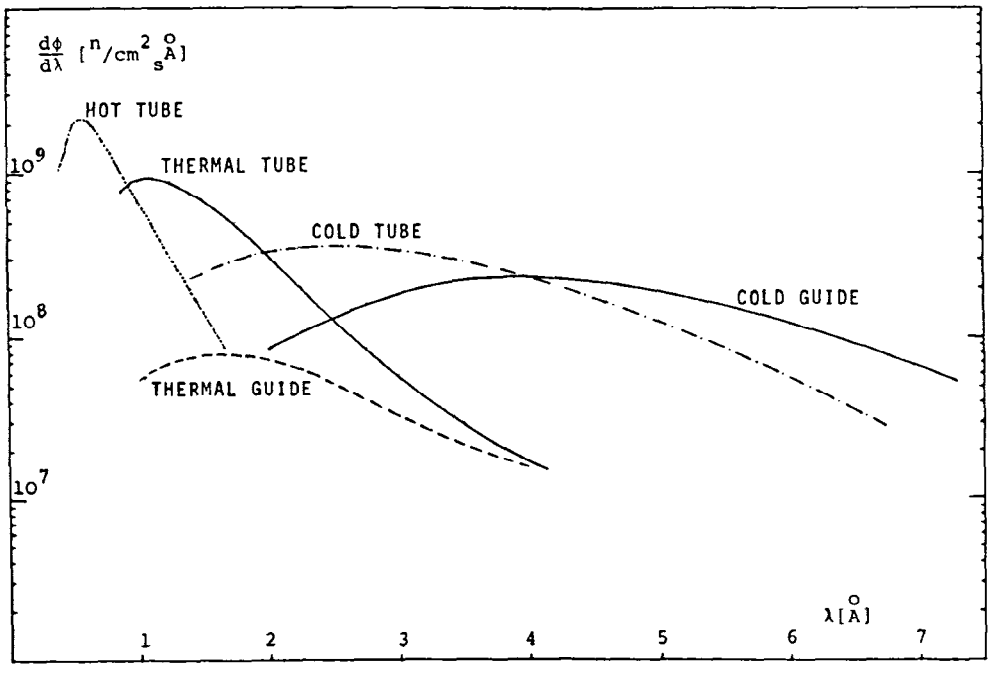

Fig. 10 Spectral fluxes at monochromator positions of SINQ for tubes and guides. The primary proton beam current is 1.5 mA.

From these data we can estimate the spectral fluxes at monochromator (or velocity selector) positions of beam tubes and neutron guides. The spectral fluxes shown in Fig. 10 are based on the following tube and guide cross sections and a primary beam current of 1.5 mA (1 Mw beam power):

height h = 10 cm width d = 5 cm

Furthermore the guides are assumed to be straight and plated with ^{58}Ni. For background /7/ suppression, we will need to install benders into the guides; as a result, the flux at the guides of the actual source will be somewhat lower and the spectrum will cut off at short wavelength. It is evident from Fig. 10 that experiments using a wavelength region of 2Å – 4Å should be installed at beam tubes viewing one of the cold sources: For wavelength above 4Å, the guides give a higher flux.

The flux at a thermal guide is given for reference only; it is not planned to install these at SINQ.

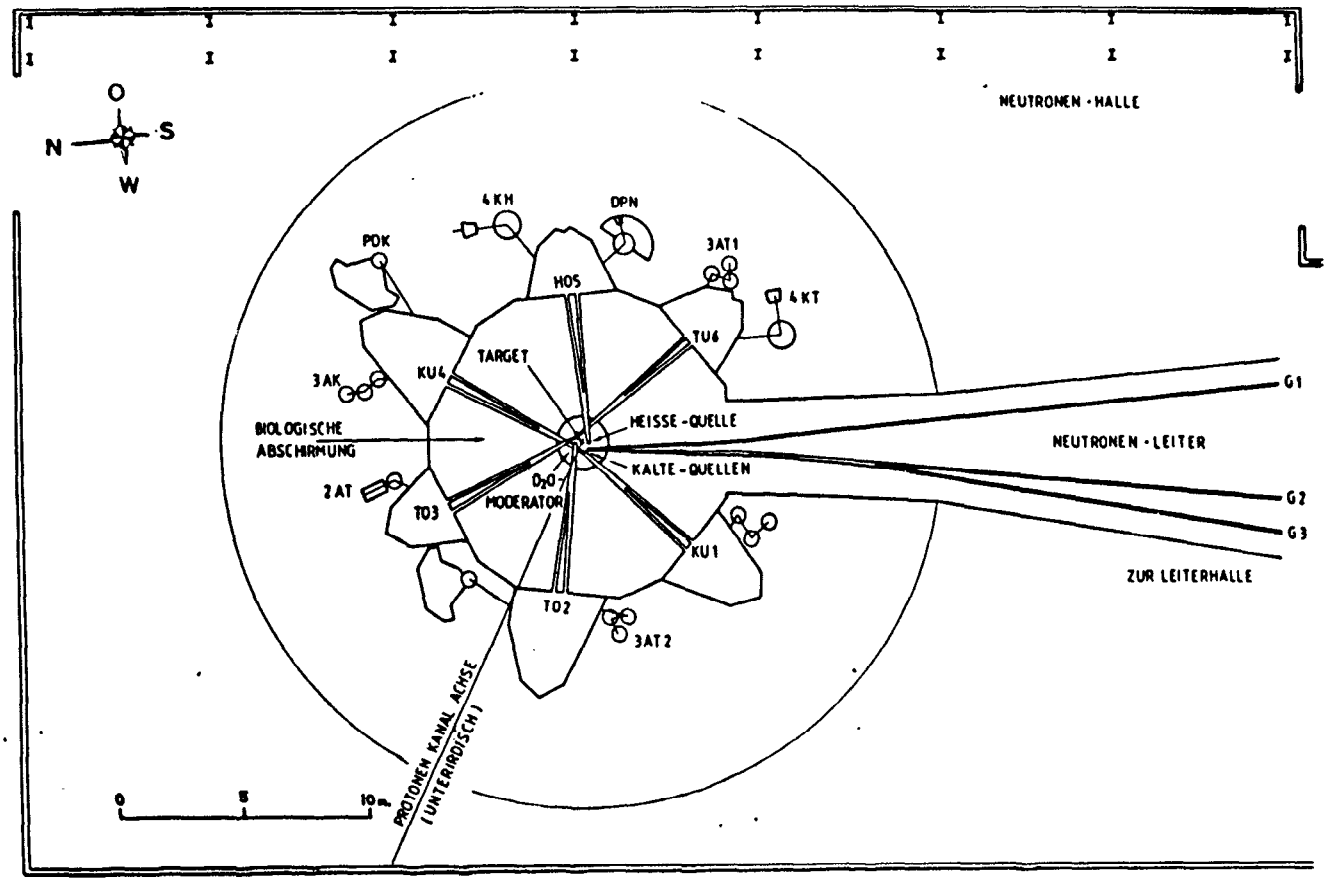

Fig. 11 Horizontal cut through the source, showing the layout for beam tubes and instruments.

d) Beam Tube Lay-out and Instrumentation

A horizontal cut through the source, showing the layout for the beam-tubes is shown in Fig. 11. The truncated heptagon is the fixed part of the source but with the shielding around the beam tubes mounted in boxes to allow this to be rearranged as the source develops during operation. External to the source will be mounted monochromators; these will require shielding which is more easily constructed onto flat faces (hence the heptagon).

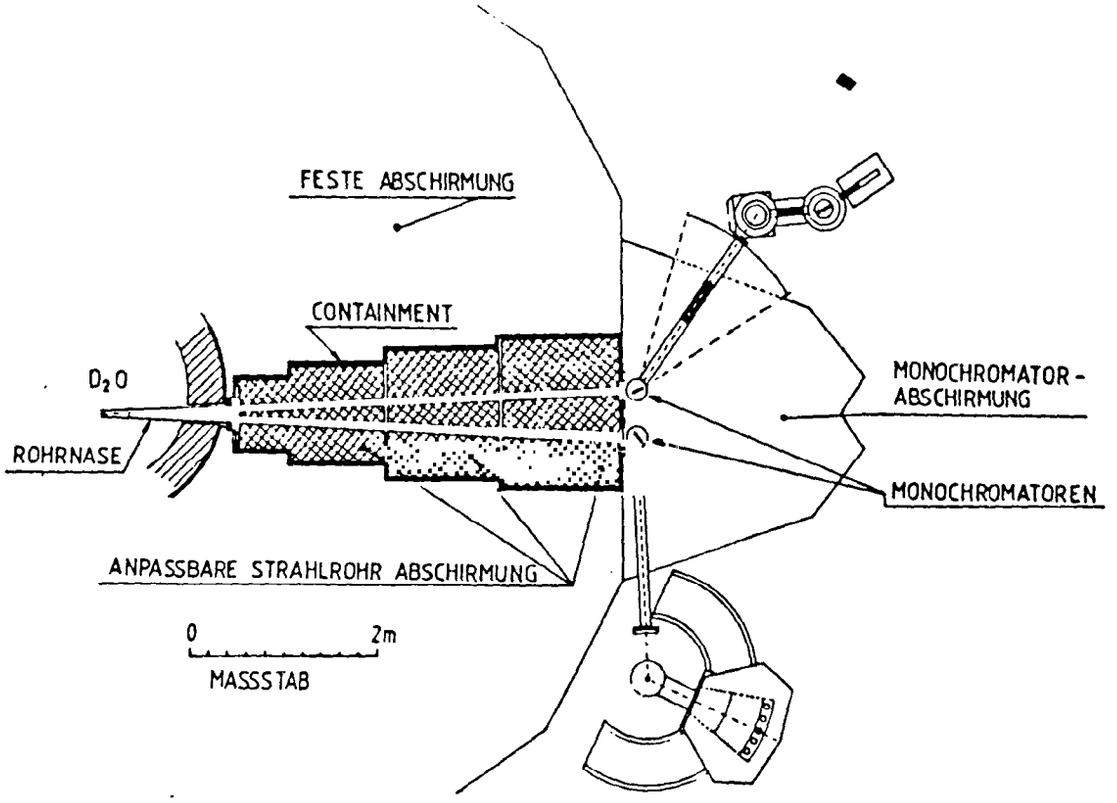

Fig. 12 Beam tube pair with monochromator shield and instruments.

A schematic picture of a beam-tube pair with their monochromators, external shielding and instruments is shown in Fig. 12.

A list of instruments, divided between thermal, hot and cold tubes and cold guides, is given in Table II.

Table II Neutron Scattering Instruments for SINQ

1. Thermal-neutron beam tube
   - Two-axis spectrometer with adjustable detector
   - Multidetector powder diffractometer
   - Two-off three-axis spectrometers
   - Four-circle goniometer

2. Hot-neutron beam tubes
   - Polarized-neutron spectrometer
   - Three-axis spectrometer for high energy-transfer

3. Cold-neutron beam tubes
   - Three-axis spectrometer
   - High energy-resolution three-axis spectrometer (with neutron turbine)

4. Cold-neutron guides
   - High resolution powder-spectrometer
   - Small angle scattering spectrometer for biological applications
   - Small angle scattering spectrometer for materials and polymer science
   - High resolution three-axis spectrometer
   - Spin-echo spectrometer

References

1) S. Adam

"Calculation of space charge effects in isochronous cyclotrons", Proc. Part. Accel. Conf. May 1985, Vancouver

2) W. Joho

Proc. 10th Int. Conf. on Cyclotrons and their Applications,

East Lansing Michigan USA, 1984, p. 195

3) Y. Takeda, Ch. Gerber

"The development work on the liquid lead-bismuth target for SINQ", these proceedings (1985)

4) F. Atchison, W.E. Fischer

Status report, ICANS-VII, September 1983 Chalk-River Rep. AECL-8488

5) G.S. Bauer, W.E. Fischer, F. Gompf, M. Kuchle, W. Reichardt, W. Spitzer

Proc. ICANS-V 1981 Julich

6) G.S. Bauer, H. Conrad, W.E. Fischer, K. Grunhagen, H. Spitzer

"Leakage Flux, Life-Time and Spectra of Cold Neutrons from H2-Moderators with various Reflectors", these proceedings (1985)

7) F. Atchison

"Considerations on Backgrounds at SINQ", these proceedings (1985)

Proceedings of the Eighth Meeting of the International Collaboration on Advanced Neutron Sources (ICANS-VIII)
8-12 July 1985, Rutherford Appleton Laboratory Report RAL-85-110

Neutron Facility Possibilities with the TRIUMF Kaon Factory

I.M. Thorson

TRIUMF
4004 Wesbrook Mall, Vancouver, B.C., Canada V6T 2A3

I. INTRODUCTION

The accelerator options for a TRIUMF Kaon Factory reported at the ICANS VII meeting[1] have now been resolved in favour of a two stage rapid cycling synchrotron system to be fed by the existing 500 MeV H^- cyclotron facility. The formal proposal[2] for the facility to support a request to the Canadian Government for funding is essentially complete and will be available shortly; it deals exclusively with the accelerator and experimental nuclear, meson and particle physics facilities. The possibilities for a pulsed neutron facility that could be associated with this complex have not been examined in detail although some of the established accelerator characteristics are similar to those of an optimum facility like the SNS.[2] This report will outline the facility that is being proposed and sketch the incremental requirements for a useful pulsed neutron source.

II. PROPOSED ACCELERATORS

The proposed facility for the TRIUMF Kaon Factory is shown in Fig. 1. It consists of five accelerator/storage rings in addition to the present TRIUMF 500 MeV H^- isochronous cyclotron. The H^- ions will be extracted directly without changing their charge state at 440 MeV by a series of orbit perturbing elements and septa and transported (gently) to

the beam accumulator (A) ring; the full ($\gtrsim$100 μA) beam current from the cyclotron will be collected for 20 ms periods and injected into the accumulator ring by stripping the H^- ions to protons. At the end of the accumulation cycle the beam is transferred in one turn to the adjacent booster (B) ring shown in Fig. 2 and accelerated to 3 GeV proton energy. At the end of the booster acceleration cycle the protons are transferred, again in one cycle of the accelerating ring, into 1/5 of the circumference in the collector (C) ring in the main accelerator tunnel. Five such cycles are collected in the five circumferential positions in the C-ring; they are then transferred, again in one cycle of the C-ring, to the driver (D) ring that accelerates the protons to 30 GeV. At the end of the acceleration stage the protons can be extracted (again in one turn) either into the fast extraction line for experiments requiring a low duty factor or transferred to the extender (E) ring for slow — essentially continuous — ejection into experimental facilities requiring large duty factors. The proposed initial configuration for the pion, kaon, neutrino, etc. experimental facilities is shown in Fig. 3. Because the various rings all operate simultaneously, with only brief interruptions for the transfer of protons between rings the full 100 μA cyclotron output can be accelerated to 30 GeV.

For a neutron facility the interest is centered on the 3 GeV stage. The output from the booster acceleration stage (B-ring) could be channeled directly to a pulsed neutron facility. As a dedicated facility the pulse repetition rate (50 Hz) and pulse length (0.74 μs) are close to optimum for thermal and near epithermal neutrons. For higher neutron energies the pulse length could be shortened, at the price of correspondingly lower intensity, by chopping the cyclotron output at extraction or the cyclotron input at the ion source-injection system. The limiting case for this technique is the use of only 1 of the 45 phase slots in the accumulator (A-ring) and the booster (B-ring). At the full nominal design intensity this would produce a time averaged beam current

of 100/45 = 2.2 μA in ~8 ns wide pulses at 50 Hz repetition rate; this is approximately a factor 6 lower intensity than the Los Alamos PSR,[4] reflecting mostly the lower repetition rate. Correspondingly higher intensities can be obtained by filling more of the 22 ns phase slots in the accumulator ring from the cyclotron; the macro-pulse width is now, however, a multiple of the micro-pulse period rather than the micro-pulse width.

III. ADDITIONAL REQUIREMENTS FOR A NEUTRON FACILITY

The additional hardware required to feed a neutron facility from the booster ring in a dedicated alternate mode will be almost trivial; to provide simultaneous feeds to both a neutron facility and the C-ring of the Kaon facility will not likely present any serious difficulties. The beam line to the center of a 50 m diameter experimental hall and vertical injection into a target assembly could provide horizontal neutron beams over most of the 360° azimuth at, or near, ground level. It would be imprudent however not to leave space between the booster extractor and the neutron facility for a pulsed muon facility and a consolidater (C') storage ring that could multiply the available intensity in either the single or multiple micro-pulse/macro-pulse modes.

No study has been carried out on the design of neutron production targets that would be required for the relatively high proton energy (3 GeV) available from the booster. Although this energy is probably higher than optimum it will not likely present any difficulties significant enough to indicate reduction, although this might be possible at the cost of a more expensive circuit for tailoring the power wave form to the booster accelerator ring.

IV. CONCLUSIONS

The accelerator complex being proposed for the TRIUMF Kaon Factory has intensity, pulse width and repetition rates from the 3 GeV booster stage that make it very interesting as a source of protons for a pulsed spallation neutron facility. A conceptual design with enough detail to make reliable cost estimates is required for the additional components

needed for such a facility. Because of the obvious competition for the available intensity that this addition would produce with the primary Kaon facility all design parameters affecting intensity in the present proposal should be examined closely, e.g., booster synchrotron cycling frequency. One obvious advantage of this additional component would be the earlier potential research yield from the construction of the lower energy stage.

V. ACKNOWLEDGEMENTS

I would like to thank M.K. Craddock, chairman of Kaon Factory design study group, E.W. Blackmore, J.R. Richardson, W.K. Dawson and D.A. Garner for helpful discussions during the preparation of this report.

REFERENCES

[1]E.W. Blackmore, TRIUMF Kaon Factory as a Potential Neutron Source, p.55, AECL-8488, Proceedings of the Seventh Meeting of the International Collaboration on Advanced Neutron Sources, Chalk River Nuclear Laboratory, Sept. 13-16, 1983. Edited by S.O. Schriber.

[2]TRIUMF Proposal for a KAON Factory, June, 1985, M.K. Craddock, Editor.

[3]G. Manning, Progress on Construction and Commissioning of the Spallation Neutron Source at the Rutherford Appleton Laboratory, p.34, AECL-8488, 1983.

[4]C. Bowman, Status Report on the WNR/PSR Pulsed Spallation Neutron Source at the Los Alamos National Laboratory, p.9, AECL-8488, 1983.

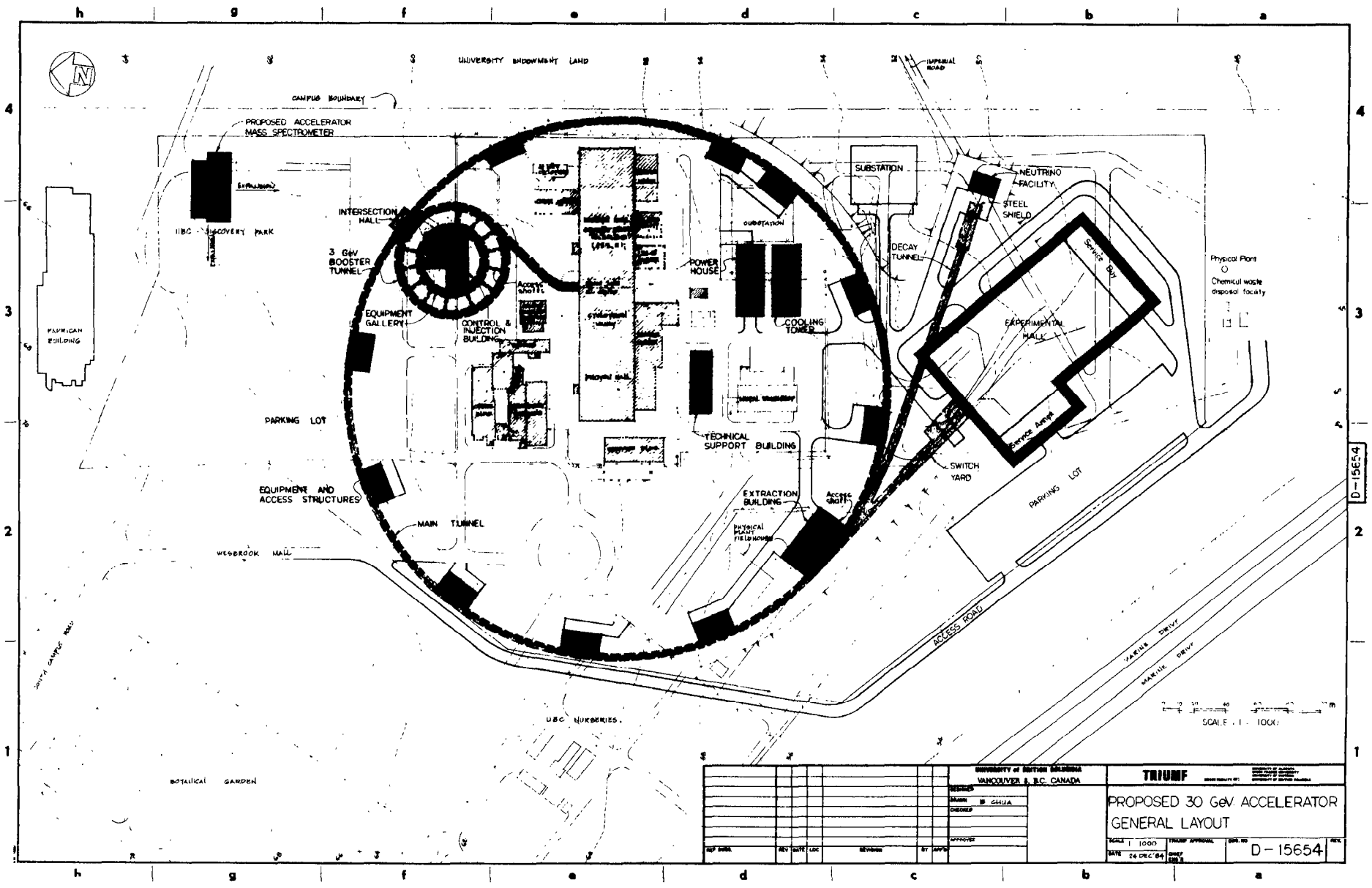

Fig. 1. The layout of the proposed TRIUMF KAON factory accelerators and experimental facilities

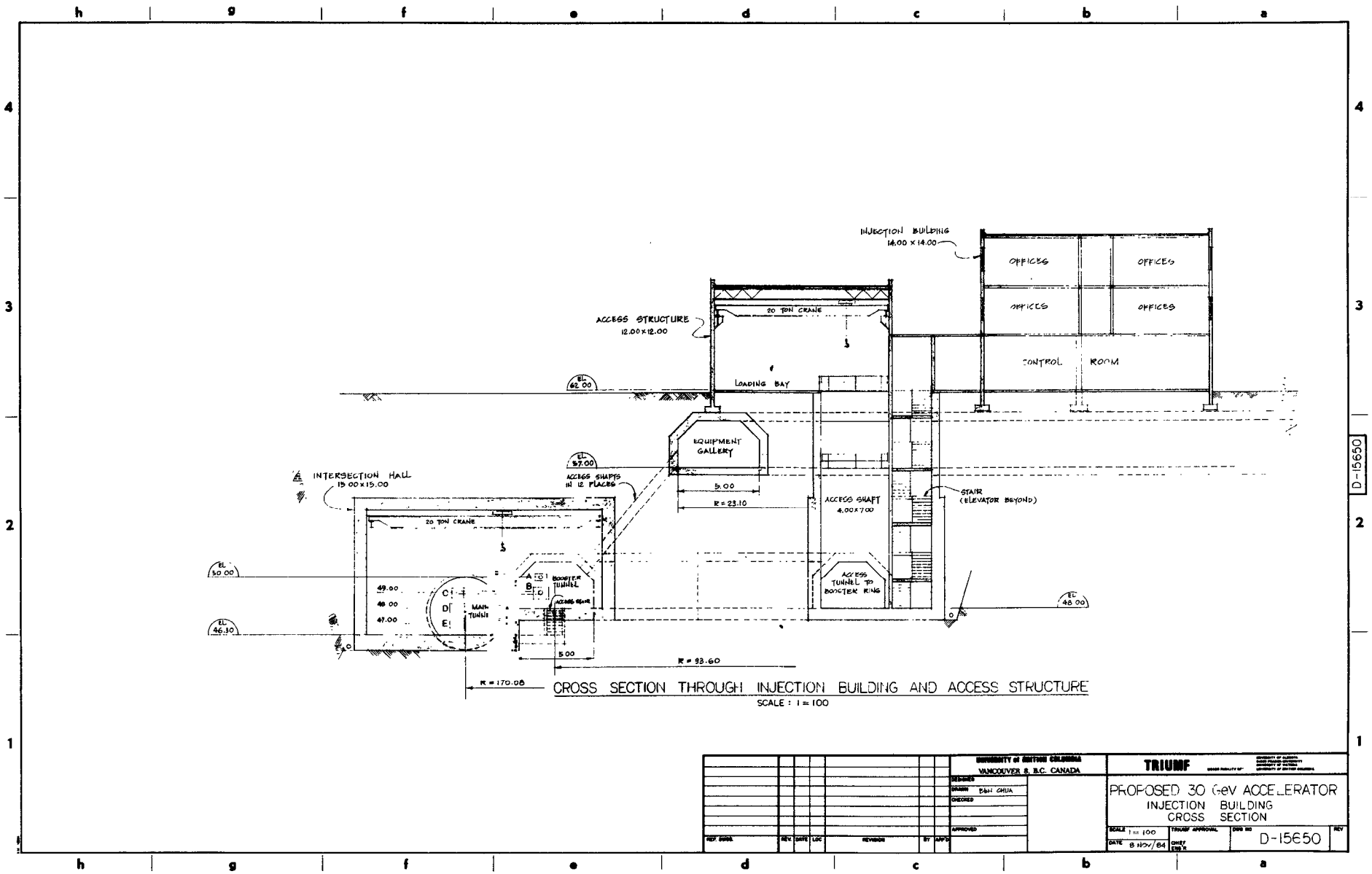

Fig. 2. Section through injector and booster/main ring intersection structure of TRIUMF KAON Factory

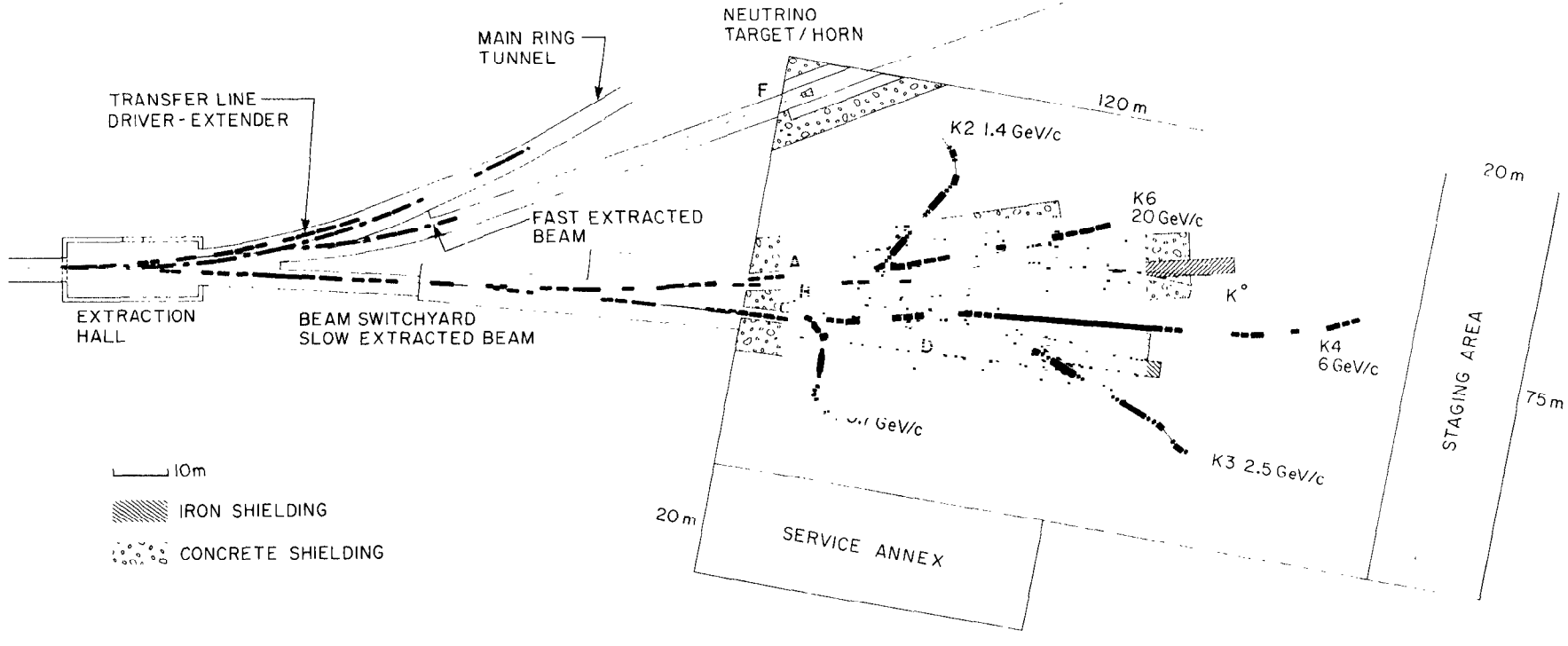

Fig. 3. TRIUMF KAON Factory extraction hall and experimental facilities

Proceedings of the Eighth Meeting of the International Collaboration on Advanced Neutron Sources (ICANS-VIII)
8-12 July 1985, Rutherford Appleton Laboratory Report RAL-85-110

Status of the Intense Pulsed Neutron Source Accelerator System*

A. Rauchas, F. Brumwell, C. Potts, V. Stipp and G. Volk
Argonne National Laboratory
Argonne, Illinois 60439 USA

Introduction

The Intense Pulsed Neutron Source (IPNS) Accelerator System has been operating since 1977. The first two years were as part of the innovative ZING-P′ program. Since that time the performance of the accelerator system has constantly improved and present currents exceed those of ZING-P′ days by 250%. The accelerator availability, long the pride of the accelerator operations group, has remained excellent, averaging over 90%. Problems with equipment and beam handling have been encountered and have been surmounted. The remainder of the text covers the high points as well as the low of the last two years of the IPNS Accelerator System operation.

Operating Summary

The performance of the IPNS Accelerator System continues to set milestones for proton synchrotrons. At 8:24 a.m. on Sunday, June 10, 1984, the accelerator delivered the billionth pulse of protons to the neutron generating target. At the present time, over 1.3 billion pulses have been delivered. A new record monthly average of 12.5 μA time averaged beam current on target was achieved during February of 1985. That same month, peak currents of 15.6 μA were reached. The following month, March, 1985, accelerator availability hit a peak of 97.3%. During the week of June 20-26, 1985, a new high weekly average of 13.6 μA was achieved. These are not isolated records! Since the last status report at the International Cooperation on Advanced Neutron Sources (ICANS-VII) at Chalk River[1] held in September of 1983, the time averaged beam current on target has increased by almost 40%. Figure 1 shows a more detailed record of target current for that period of time. Figure 2 shows accelerator availability during the same period. An operating summary from the start of IPNS operation in November 1981, until the time of writing is shown in Table I.

With the higher intensity operation, even more emphasis has been placed on keeping the beam losses in the accelerator as low as possible. The reason for this is clearly evident in Fig. 3, which shows that the largest amount of downtime during the past year is due to cooldown - the time required for residual radioactivity to decrease to a low enough level so that a fault in the accelerator tunnel can be repaired. The accelerator current we achieve is limited by the losses we allow. We do not strive for higher currents until the losses are under control. The average beam losses in the accelerator are held

*Work supported by the U.S. Department of Energy.

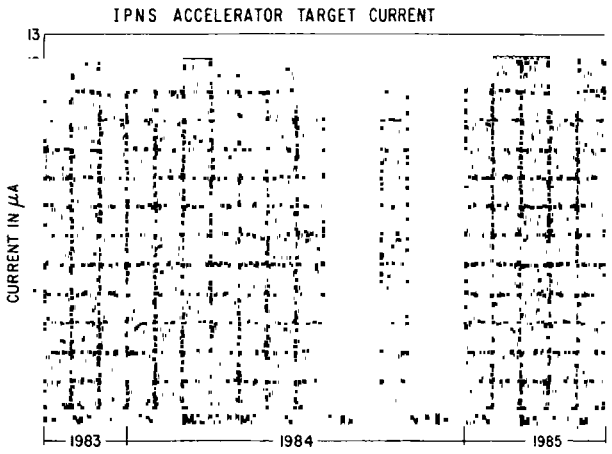

Fig. 1.

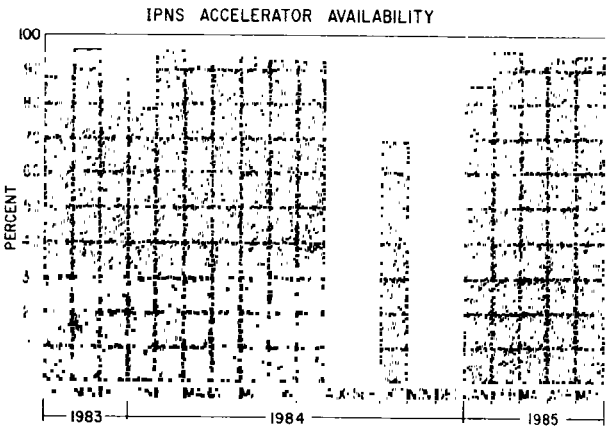

Fig. 2.

below 3.5 x 10^{11} protons per pulse (1.7 μA time averaged current). The majority of the beam losses (approximately 80%) occur below 60 MeV. Automatic protective interlocks will inhibit the beam if 2 x 10^{13} protons are lost in a second. Twenty new scintillation beam loss monitors provide detailed loss information to the operators from various parts of the accelerator. These loss monitors provide much more sensitivity than any of the other diagnostics. Losses of <<1% can be easily observed. The accelerator lattice lacks trim dipole magnets which are required for good loss control. Manipulation of the beam injection quality with 50 MeV transport magnets is a complex and inexact method of loss control, but it is the one we use most.

The quest for both higher intensity as well as high availability is not an easy one and always requires control of the impulse to try for record beams. Maintainability is uppermost on our priority list. In a facility of this type, some experiments last only a few hours and lost experimental time is not easily rescheduled. But even the best laid plans sometimes fail. In November 1984, the pulsed extraction septum magnet failed when a water leak developed in one of the cooling loops. This magnet had pulsed for over 1.5 billion pulses. In fact from a mechanical stress aspect, one can consider 3 billion pulses, since

Table I.

Accelerator Operating Summary

	Nov. 1981-July 1982	Oct. 1982-July 1983	Oct. 1983-July 1984	Oct. 1984-June 1985
Proton beam energy (MeV)	400	450	450-500	450
Average beam current (μA)	8.02	9.21	11.46	11.93
Operating efficiency (%)	88.9	90.2	90.4	91.1
Scheduled operating time (hrs)	3358	3833	4750	2797
Available operating time (hrs)	2985	3458	4294	2547
Total pulses on target	2.94×10^{8}	3.33×10^{8}	4.23×10^{8}	2.66×10^{8}
Total protons on target	4.44×10^{20}	6.39×10^{20}	1.01×10^{21}	6.61×10^{20}

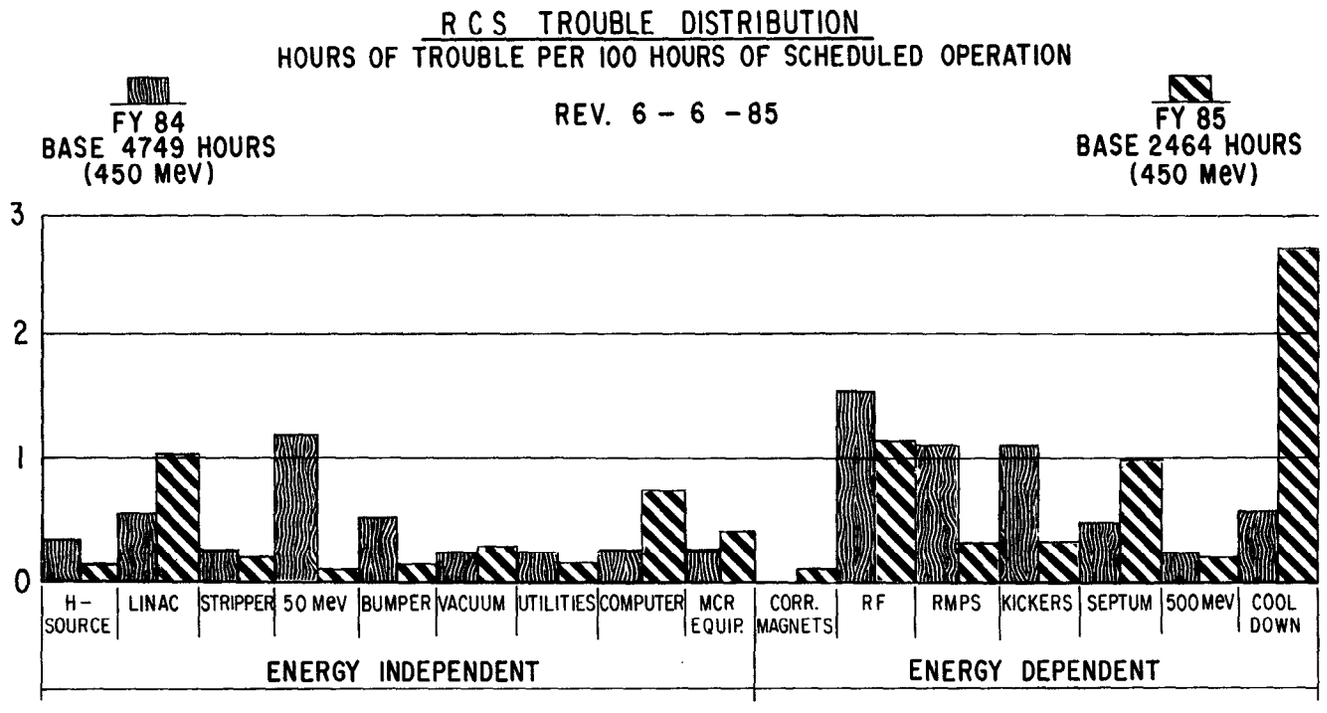

Fig. 3.

after each pulse, the magnet is pulsed with a reverse current pulse at approximately 80% of peak current to reset the core of the transformer type magnet[2]. Although the magnet was designed for relatively easy removal from the vacuum box (fast disconnect power and water feeds), the small size of the synchrotron tunnel did not allow for the installation of the required additional rigging equipment. In addition, the magnet was highly radioactive (20 R/hr after six weeks cooldown) further complicating the repair. A shutdown of ten weeks was required to repair the magnet although the actual repair took less than two weeks. This was the first time since the start of IPNS operation in 1981 that an accelerator problem forced a change in the neutron science operating schedule. No experimental time was lost since the lost time was made up by additional running after the repair.

Another problem occurred on April 7, 1985, when after completing the repair of a minor extraction kicker problem, only 50% of the normal beam could be accelerated. Subsequent observations revealed high losses in the fifth short and long straight sections. Vertical aperture measurements indicated a restriction of approximately 15 mm out of a total half vertical aperture of 26 mm. The problem cleared itself for no apparent reason several times, once for a period of two days, but then returned with no hint of clearing again. Background radiation studies in the accelerator tunnel indicated that the problem was in singlet magnet #5. The problem appeared to be a repeat of the incident of May 1983, when several "hoops" of the rf liner in singlet magnet #5 and triplet magnet #6 were damaged by the beam and dropped into the aperture[1]. The accelerator continued operation at reduced current until the next scheduled shutdown. By careful tuning, the accelerator operators were able to restore operation to the 8 μA level. During the shutdown, inspection of the magnet revealed that one of the rf hoops was indeed blocking part of the aperture. Because of the short, one week long, scheduled shutdown, only a temporary repair was made by pushing the hoop back up and reforming into place with a remotely operated pneumatic device inserted into the ring magnet. The repair appears to have worked and a more careful inspection and complete repair will be made during the long summer shutdown.

Recent Improvements

The synchrotron exhibited an intensity dependent high energy instability from its earliest days. It was controlled to the 8-9 μA level by careful dynamic chromaticity adjustment. Above 10 μA this was not by itself sufficient. A combination of two simple techniques has raised the instability threshold above 15 μA. These are discussed in detail in Ref. 3 and will only be briefly discussed here. The instability manifests itself as a beam loss of up to 70% during the last two milliseconds of the acceleration cycle. The intensity threshold at which the loss occurred is roughly proportional to the available rf voltage at $\dot{B}$(max). The cause appears to be a resistive wall instability producing vertical dipole oscillations. One of the solutions is to dilute the beam bunch by modulating the net rf voltage amplitude slightly near the second harmonic of the synchrotoron frequency at $\dot{B}$(max). The other solution requires extraction of the beam 2 ms before B(max), at a time when the $\dot{B}$ is not equal to zero. The peak field is raised to ensure that the energy at extraction remains the same. There is little change in beam energy during the last two milliseconds of the sinusoidal acceleration cycle so it is an ideal time for resonance growth. This technique increases the instability threshold by apparently reducing the allowable resonance growth time.

The accelerator was designed to operate phase-locked to the power mains and only minimal filtering was supplied with some of the power supplies. Therefore, any existing ripple had minimal affect on the accelerator performance since its effect was the same each beam pulse. However, neutron choppers had to be synchronized to the accelerator but could not track the variation of the power main, so the accelerator and choppers were each phase locked to the same stable oscillator.[4,5] This caused the accelerator to slip in phase in respect to the power main and now power supply ripple became a factor. Adding additional filtering on the many power supplies was prohibitively expensive but four major problem areas were identified and feedback loops were designed to minimize the effect of the phase shift.[6] The feedback loops were designed to maintain the stability of 1) the linear accelerator tank rf gradient level, 2) the beam intensity injected into the synchrotron, 3) the injected beam position and 4) the injection field of the synchrotron main ring magnets. These feedback loops have improved the accelerator operators' ability to tune the accelerator for minimum beam losses and maximum intensity without continuously correcting the variations of the previously mentioned parameters. Figure 4 is a plot of weekly averages of time averaged current on target per current of beam loss. The weekly averages begin

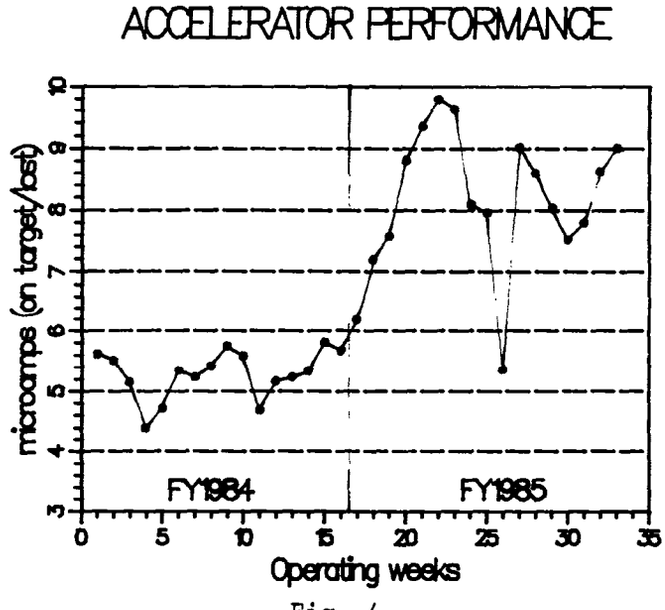

Fig. 4.

in November of 1983, and cover the weeks of neutron chopper synchronized operation through June 1985. It is clearly evident that the accelerator performance improved significantly shortly after the feedback loops were installed at the end fiscal year 1984 (FY1984). The decrease shown for week number 26 was caused by the aperture restriction described earlier. The operators are looking forward to neutron chopper system improvements[7] which will allow the choppers to track the variation of the power main.

Remotely adjustable vertical collimators have been installed in one of the synchrotron straight sections. Their primary objective is to protect the rf liner from further damage after the initial May 1983 failures. Unfortunately, they did not prevent the more recent damage to the liners described in the previous section. They have also been used as diagnostic devices to study the vertical beam size. These studies will be described later.

A recent improvement to the extraction kicker system has not affected the beam intensity, but has improved the system reliability and therefore accelerator availability. One recurring problem with the kicker system had been the interconnecting cables between the magnet coils and the terminating resistive loads. The major source of problem was the termination of the cable itself which was prone to high voltage breakdown failures after about 30 million pulses. The system manager for the kicker system devised a new terminating load, making use of the existing load components, which mounted directly on the magnet coil and eliminated the troublesome cable terminations. This new improvement has significantly reduced kicker system failures as Fig. 3 shows. In addition, several suggestions from the engineers of the thyratron switch manufacturer, English Electric Valve, Ltd., have extended the useful life of the thyratron switches. In fact, one of the four has now operated reliably for over 500 million pulses.

Ongoing Studies

H^- Stripping Foil

The problems with the stripping foils that have been described in the past have not been completely resolved. The standard plastic stripping foils with a thin deposit of aluminum have been used since the start of the accelerator operation. However, the foil lifetimes are not consistent, with some foils lasting tens of millions of pulses and others, only a million or so. Since the normal conditioning of the foils requires operation at reduced intensity for approximately six hours, this reduces the average current. In an attempt to reduce this impact, studies are continuing with other types of stripping foils. Through the cooperation of the SNS staff, several of their aluminum oxide foils had been hand carried to IPNS. Unfortunately, the foils did not fare well during the trans-Atlantic flight and arrived slightly damaged. Enough were salvaged to run some tests and even though the stripping efficiency and scattering effects were good, the oxide foils lasted less than 1 million pulses. Clearly the test was inconclusive due to the less than perfect condition of the foils. Plastic foils with other metal coatings have not improved foil life. A significant step forward has been made with the use of pure carbon foils. These foils have a density of 60 $\mu g/cm^2$ and have been very difficult to mount with one edge of the foil unsupported. A technique has been developed to mount these foils, but with a reduced usable foil aperture. The initial attempts with the carbon foils are very promising with good stripping efficiency, minimal scattering and minimum foil lifetimes of 20 million pulses. The reduced foil aperture did affect accelerator performance somewhat since some of the recirculating beam struck the foil holder. Mounting techniques have since been improved to allow for larger apertures. It is hoped that once the mounting technique has been completely developed, minimum conditioning time will be required with these carbon foils.

Vertical Aperture

Measurements of beam size during capture in the synchrotron using the remotely controlled vertical collimators have shown that at 50 MeV the vertical midplane of the beam is 5 mm above the physical center of the aperture.

Studies conducted with the injection segmented Faraday cups have also shown that the first three injection orbits are also high in those two regions by the same amount. This has raised speculation that if the beam is indeed above the vertical midplane, this could be the cause of the problems with the rf liners. Some additional confirmation of this is a discoloration visible on the liners around the synchrotron above the beam plane, but none visible on the liners below. However, after the rf liner failure in 1983, the upper collimator was positioned within 0.5 mm of the beam to protect the liner. Loss monitor signals indicate that this does protect the liner in triplet magnet #6, but it failed in singlet magnet #5, bringing up the possibility of the existance of vertical orbit warps. Vertical position signals do not show any warps once the beam is bunched, but the possibility of warps during the first 200 turns before the beam is bunched cannot be neglected. The loss monitors, which cannot discriminate between horizontal and vertical losses, do not provide any clues. Studies are planned to investigate this further.

Synchrotron Working Point

During the early days of synchrotron operation, the relatively low intensities did not require working point corrections. Two sets of trim quadrupoles had been provided, but were not used. In an early attempt at eliminating beam instabilities, one of the quadrupole sets was replaced with octupole correction magnets. These magnets were unsuccessful at eliminating the instabilities and are not used. The present higher intensity operation requires the operation of the trim quadrupoles to shift the working point. This correction is provided by the single set of magnets. Computer simulation of the effect on the vertical β function of applying the correction at only one location in the synchrotron lattice indicates the possibility of severe distortions; strangely however, not in the areas where the liner damage has occurred. Nonetheless, the other set of quadrupoles will be installed in place of the octupoles during the summer shutdown. The computer studies indicate that this will reduce the distortion in five out of six locations where the vertical β function reaches a maximum. During the working point studies, another effect became apparent. When the current in the upstream vertical trim quadrupole was reversed to lower the vertical tune, the beam capture efficiency decreased; however, the beam losses during the latter half of the cycle were reduced. Further studies are being conducted, and power supply modifications are underway to dynamically reverse the trim quadrupole currents.

Planned Improvements

Beam Loss Monitoring

The new beam loss monitoring system has become very useful at the present level of operation. However, the day to day variation of these signals is subtle and makes it difficult to determine trends and anticipate potential problems. A new system is being constructed to allow computer sampling of all the loss monitors throughout the acceleration cycle and storing hourly averages of the losses in the control computer memory. The system will allow varied manipulation of the data sets to permit comparisons of the loss patterns on a hourly, daily, weekly and operating cycle basis. In addition, the recording and plotting of vacuum readings by the control computer from 7 locations in the synchrotron and 6 locations in the beam lines has been completed. Since beam losses and vacuum readings are closely linked, the vacuum plots have proved invaluable together with the loss monitor signals for monitoring accelerator performance.

Improved Data Acquisition

A CAMAC based data acquisition system, installed in 1981, is used for monitoring the proton transport system to the target as well as the target parameters. It has operated extremely reliably and provides some very useful additions. One is the ability to notify the accelerator operators of variation in any of the parameters in the data base. The injector and synchrotron data acquisition system does not have this capability, and it is one that is sorely needed. This system is being upgraded to allow this flexibility.

Conclusion

The IPNS Accelerator System has maintained continuous improvement of its operating performance under the difficult conditions of a busy operating schedule and tightly constrained budget. Most of the programmatic resources have gone toward improvement in the scattering instruments and to low temperature moderators. Budgetary limitations have prevented the implementation of most of the long-term improvements mentioned in the ICANS-VII report, most notably, the planned replacement of the ring magnet tuning choke, construction and installation of a third rf accelerating cavity and construction and installation of horizontal and vertical trim dipoles. The Accelerator Operations Group has tried to make improvements in other, less expensive, ways. The records show that it has been successful.

References

[1] C. W. Potts, F. R. Brumwell and V. F. Stipp, "Intense Pulsed Neutron Source Accelerator Status," Proceedings of International Collaboration on Advanced Neutron Sources (ICANS-VII), Atomic Energy of Canada Limited, Report AECL-8488 (Sept. 13-16, 1983) 144.

[2] M. Foss, et al., "A Transformer Septum Magnet," IEEE Transactions on Nuclear Science, Vol. NS-26, No. 3 (June 1979) 4024.

[3] C. Potts, et al., "Beam Intensity Increases at the Intense Pulsed Neutron Source Accelerator," to be published in proceedings of the 1985 Particle Accelerator Conference.

[4] A. Rauchas, et al., "IPNS Accelerator System and Neutron Chopper Synchronization," Proceedings of International Collaboration on Advanced Neutron Sources (ICANS-VII), Atomic Energy of Canada Limited, Report AECL-8488 (Sept. 13-16, 1983) 157.

[5] G. Ostrowski, et al., "The IPNS Chopper Control and Accelerator Interface Systems," proceedings of this conference.

[6] A. Rauchas, et al., "Intensity Stability Improvement for the Intense Pulsed Neutron Source Accelerator System," to be published in proceedings of the 1985 Particle Accelerator Conference.

[7] L. Donley, "Phase Locking the IPNS Neutron Chopper to the 60 Hz Power Line," proceedings of this conference.

Proceedings of the Eighth Meeting of the International Collaboration on Advanced Neutron Sources (ICANS-VIII)
8-12 July 1985, Rutherford Appleton Laboratory Report RAL-85-110

E U R A C

THE JRC PROPOSAL FOR A EUROPEAN FUSION REACTOR MATERIALS TEST AND DEVELOPMENT FACILITY

W. Kley and G.R. Bishop
Commission of the European Communities
Joint Research Centre - Ispra Establishment
21020 Ispra (Va) - Italy

SUMMARY

The United States Department of Energy has spent in the last 10 years more than 100 Mill U.S.$ for the development of intense neutron sources for a fusion reactor material test and development programme based on the D^+-T and D^+-Li stripping reactions. The final design parameters for the large Fusion Materials Irradiator Test (FMIT) facility are:

- Linear Accelerator: . 35 MeV, 100 mA-deuteron-beam on a liquid lithium target
- Irradiation parameters: . 83 dpa/year* in 10 cm^3
  . 11 He appm/dpa*.

*dpa is displacements per atom; appm is atoms parts per million.

**A value of 6.4 is obtained if all neutrons above 30 MeV are collected in the energy group between 29.95 - 30 MeV and their He-production estimated with $\sigma_{n,\alpha}$ (30 MeV). A value of 13 is obtained if the He-production is calculated with estimated $\sigma_{n,\alpha}$-cross sections for neutrons up to 400 MeV and measured neutron spectrum in excellent agreement with Fusion Reactor First Wall conditions.

For the last 6 years we examined the use of a Spallation Neutron Source (SNS) as an alternative European Option to FMIT. For an optimized spallation neutron source design we find now for the same beam power as FMIT the following design parameters:

- Linear Accelerator: . 600 MeV, 6 m-A-proton beam on liquid lead target
- Irradiation parameters: . 320 dpa/year in 20 cm^3 or 274 dpa/year in 31.5 cm^3
  . 6 < He appm/dpa $\leq$ 13**

For a Tokamak Experimental Power Reactor such as INTOR (1.3 MWatt/m^2 wall loading) the design parameters are:

15 dpa/year and 11 He appl/dpa.

If we compare FMIT with an optimized spallation neutron source of equal beam-power or neutron production cost, we arrive at the following Figure of Merit:

$$FM = \frac{(dpa.volume)^{SNS}}{(dpa.volume)^{FMIT}} = \frac{274x31.5}{83x10} \approx 10.4.$$

The present conceptual spallation neutron source target would allow us to use a 1200 MeV, 24 mA-proton beam, if required. The Ispra SNS-Target Station will be designed for these parameters.

For synergetic experiments concerning fatigue and radiation damage the continuous proton beam will be periodically deflected on the target:

$$\Delta t = 9 \text{ sec}, \qquad f = 10^{-1} \text{ sec}^{-1}$$

in order to simulate the Pulsed Mode of Tokamak Power Reactors. The deflected beam can be used for other experiments.

1. INTRODUCTION

The plasma physicists may realize Lawson's break-even condition in their large Tokamak fusion test facilities, such as JET, towards the end of the 1980s. This situation indicates that after 30 years of plasma physics research, the design and construction of future fusion power reactors may be considered now more realistically. However, the technical and economic success of fusion power reactors will depend on the endurance and availability of materials suitable for the radiation environment of a fusion reactor. For the evaluation of the technical and economic feasibility, predictions are needed concerning the evolution of the mechanical properties of materials being exposed to the complex radiation field of a future fusion reactor.

It is now the general understanding of the fusion materials research community that the end-of-life of the first wall or blanket materials is determined by a considerable number of complex and competing phenomena. Due to non-linear effects in the evolution towards end-of-life conditions and due to the absence of a synergetic theory on how damage energy is being stored in a material, one cannot extrapolate from low dose irradiations to end-of-life conditions. Neutron induced radiation damage can be simulated to a certain extent by energetic charged particle beam experiments. However, they have limited reliability if the primary recoil energy spectrum, the production of transmutation products (impurity atoms), dpa-rate effects and typical bulk properties are important parameters in the evolution of the mechanical properties towards end-of-life (e.g. if niobium is exposed to a fluence of 10^{23} n/cm^2, 20 percent (!) of the niobium atoms will be transformed into impurity atoms). Therefore, we need neutron irradiations up to the end-of-life that may occur between 20 and 100 dpa (displacements per atom) or at the respective fluences between 10^{22} to 10^{23} n/cm^2 (fluence = neutron flux · time: $\varphi = \phi \cdot t$ (n/cm^2)). Since one year has about $\pi \cdot 10^7$ sec, we need at least a fast neutron flux of 10^{15} n/cm^2 sec in order to reach in one year irradiation time end-of-life conditions for a typical material.

It can be shown [1-4] that only accelerator based neutron sources can provide the necessary source strength with the required neutron energy distribution. Irradiations in high flux reactors and fast reactors are not valid for fusion reactor conditions with one exception: the nickel based alloys, which are of very limited value and interest for fusion reactors because of the residual radioactivity and Helium production. Therefore, the availability of an accelerator based neutron source is mandatory for a reliable prediction of the technical and economic feasibility of fusion power reactors.

There are essentially only two competing nuclear reactions that might be used for the production of an intense neutron source: they are based either on the D^+-Li stripping, or on the spallation reaction. 35 MeV deuterons, impinging on a lithium target, produce a considerably harder neutron spectrum (average neutron energy: $\bar{E}_n \approx 9$ MeV) than in a first wall fusion reactor ($\bar{E}_n \approx 4$ MeV). On the contrary, spallation neutrons, produced by 600 MeV protons impinging on a lead target, have a somewhat softer spectrum ($\bar{E}_n \approx 6$ MeV) than the D^+-Li neutrons. Therefore, both neutron spectra deviate strongly from the one in the first wall of a fusion reactor. However, for simulating first wall conditions, it is sufficient to show that the ratio of the spectrum averaged properties:

$$\langle\sigma\phi\rangle_{n,p} : \langle\sigma\phi\rangle_{n,d} : \langle\sigma\phi\rangle_{n,t} : \langle\sigma\phi\rangle_{n,\alpha} : \langle\sigma\phi\rangle_{n,2n} : \ldots : \langle\sigma\phi\rangle_{n,\text{rest nuclei}} : P(T)$$

are similar to the one in the fusion reactor. σ stands for $\sigma(E)$, the energy dependent production cross section; $\phi \equiv \phi(E)$, the neutron spectrum; and $P(T)$ stands for the primary recoil energy spectrum; and T for the recoil energy in the laboratory system.

For the evaluation of the spectrum averaged parameters for five neutron sources (fission, 14 MeV, Fusion Reactor First Wall, D^+-Li and spallation neutron source), we need the associated cross sections up to 30 and 40 MeV, often not available for the elements of interest to material scientists. For that reason, cross section calculations have been performed for such a programme up to 30 MeV and are now being extended

up to 40 MeV for ^{52}Cr, ^{56}Fe, ^{55}Mn, ^{58}Ni and ^{60}Ni by the "Institut für Radiumforschung und Kernphysik" of the University of Viennw [5], including the production of transmutation products as well as the Primary Recoil Energy Spectrum P(T) for elastic and inelastic events, and the effects of the transmutation products. A study programme at the Swiss Institute for Nuclear Research (SIN) at Villigen has been completed for various spallation neutron source configurations, for the Fusion First Wall, the 14 MeV, the fission and the D^+-Li neutron spectrum, the spectrum averaged cross sections for chromium, iron, manganese and nickel, the main constituent of 316 stainless steel and the corresponding Primary Recoil Energy spectra. The results from F. Atchison et al. [6] show that the dimensionless ratio

$$\psi_i = \frac{\langle\sigma\phi\rangle^{\text{spallation neutron source}}}{\langle\sigma\phi\rangle^{\text{fusion first wall}}} = 1 \pm 0.3$$

for hydrogen, helium, the transmutation products, the damage energy cross section and dpa; in excellent agreement considering the very different neutron spectra.

Traditionally ψ_i-values have not been used for the intercomparison of different neutron sources but rather the corresponding He to dpa ratio. F. Atchison et al. [6] and V. Herrnberger et al. [7] obtained for stainless steel

$$6 < \frac{\text{He appm}}{\text{dpa}} \leq 13.$$

A value of 6.4 is obtained if all neutrons above 30 MeV are put in the last energy group from 29.75 to 30 MeV and weighted with $\sigma_{n,\alpha}$ (30 MeV). For estimated $\sigma_{n,\alpha}$-cross sections up to 400 MeV and measured spallation neutron spectrum [8] Herrnberger et al. obtained a value of 13. For the INTOR-Tokamak Concept a value of 11 is found for the first wall.

We conclude that spallation neutrons are simulating the Fusion Reactor First Wall conditions as well as the D^+-Li or the 14 MeV neutron sources.

Therefore, we propose the construction of a spallation neutron source based on a 600 MeV, 6 mA linear proton accelerator. If we compare the U.S. Fusion Materials Irradiation Test (FMIT) facility with an optimized spallation neutron source of equal beam power or neutron production cost, we arrive at the following Figure of Merit:

$$FM = \frac{(dpa.volume)^{SNS}}{(dpa.volume)^{FMIT}} = \frac{274 \times 31.5}{83 \times 10} \approx 10.4.$$

The present conceptual spallation neutron source target, described in the following, would allow us to use a beam energy up to 1200 MeV and a beam current up to 24 mA, equivalent to a beam power of 29 MWatt, if required.

2. SPALLATION NEUTRONS - A TOOL TO SIMULATE FIRST WALL CONDITIONS

2.1 The 1978 Hypothesis

The number of neutrons produced per second in a target is a limited criterion for an irradiation test facility. What counts is the highest accessible neutron density or neutron flux and the corresponding energy distributions of these neutrons. In a large water-cooled target such as the beam dump of LAMPF (Los Alamos Meson Physics Factory), the average neutron energy tends to be $\lesssim$ 2 MeV, while in an unperturbed spallation neutron spectrum, at 90° to the impinging proton beam and at the point of the highest neutron density, the mean neutron energy is about 6 - 7 MeV, for 600 MeV protons, well above the mean neutron energy ($\approx$ 4 MeV) of the first wall. Therefore, we have to get as close as possible to an impinging proton beam that has the highest tolerable proton beam density. At this position we have even in a totally reflected system a mean neutron energy of about 4 MeV as in the first wall. In our 1978 hypothesis we assumed that the H, D, T, He^3, He^4, ..., the rest nuclei and the dpa-production is hopefully proportional to the mean neutron energy since the $\sigma_{n,p}(E)$ and $\sigma_{n,\alpha}(E)$ cross sections

have their thresholds around 2 - 4 MeV and their maximum around 13 - 16 MeV, depending on the nuclei considered.

F. Atchison et al. [6] proved that for 20 different neutron spectra with mean neutron energies lying between 1 and 14 MeV, the spectrum averaged He to dpa ratio and the spectrum averaged displacement cross sections are really proportional to the mean neutron energy. Hence, spallation neutrons are a tool to simulate first wall conditions!

2.2 Results of the Theoretical Program and Conclusions

The guiding principle has been outlined above. However, for a well founded decision we needed more precise information on high energy cross sections not available at that time. For that reason we signed a first contract in 1979 with Prof. Dr. H. Vonach, Director of the "Institut für Radiumforschung und Kernphysik" of the University of Vienna. Cross section calculations have been performed by W. Reiter, B. Strohmaier and M. Uhl [5] for such a program between 10 and 30 MeV and are now being extended in a second contract (1984-1985) up to 40 MeV for ^{52}Cr, ^{56}Fe, ^{55}Mn, ^{58}Ni and ^{60}Ni, including the production of transmutation products as well as the Primary Recoil Energy Spectrum P(T) for elastic and inelastic events, and the effects of the transmutation products. In 1982 a contract was signed with the Swiss Institute for Nuclear Research (SIN) at Villigen, in order to obtain, for various spallation neutron source configurations, for the Fusion First Wall, the 14 MeV, the fission and the D^+-Li neutron spectrum, the spectrum averaged production cross sections for chromium, iron, manganese and nickel, the main constituent of 316 stainless steel and the corresponding Primary Recoil Energy Spectra. The geometry and parameters of the theoretical program are given in Fig. 1. The most relevant results of the First and Second Interim and of the Final Report from F. Atchison, W.E. Fischer and M. Pepin [6] are reproduced in Figs. 2 to 9. The results from F. Atchison et al. [6] show that for a spallation neutron source, based on 600 MeV protons, the dimensionless ratio

$$\psi_i = \frac{\langle \sigma_i \phi \rangle^{\text{spallation neutron source}}}{\langle \sigma_i \phi \rangle^{\text{fusion first wall}}} = 1 \pm 0.3$$

for hydrogen, helium, the transmutation products, the damage energy cross section, dpa and the mean neutron energy; in excellent agreement considering the very different neutron spectra.

Traditionally [1-4,7] ψ_i-values have not been used for the intercomparison of different neutron sources but rather the corresponding He to dpa ratio. F. Atchison et al. [6] and V. Herrnberger et al. [7] obtained for stainless steel

$$6 < \frac{\text{He appm}}{\text{dpa}} \leq 13.$$

A value of 6.4 is obtained if all neutrons above 30 MeV are put in the last energy group from 29.75 to 30 MeV and weighted with $\sigma_{n,\alpha}$ (30 MeV). For estimated $\sigma_{n,\alpha}$ cross sections up to 400 MeV and measured spallation neutron spectrum [8] Herrnberger et al. obtained a value of 13.

For the INTOR-Tokamak Concept a value of 11 is found for the first wall. However, we do not believe that the He to dpa ratio is a very sensitive parameter for the intercomparison. A He appm to dpa ratio of 10 means that we have one helium atom for 10^5 vacancies as initial conditions. In addition, "dpa" is used here as a measure for the deposited damage energy that is certainly not only stored in point defects but also in cascades, voids, interstitial and vacancy loops, as well as in precipitates and in the microchemical evolution in general. Any slowing down helium atom is going to be trapped in its own damaged zone that does not necessarily "feel" all the other far away damaged zones which do not contain helium. Therefore, it seems to us that the total helium content or the corresponding ψ_i-value is more important than the actual He to dpa ratio. Since the He-atoms carry a certain fraction of the total damage energy, a certain lower limit of the He to dpa ratio must be respected by the neutron source designer.

We have not yet received any definite answer from material scientists if the mechanical properties of an irradiated material are the same at different dose but the same helium content. There is some speculation that the He:dpa ratio may vary by a factor of 5 without having any considerable influence on the mechanical properties as a function of the total helium content. In other words, the helium content is the more sensitive parameter in respect to DPA. Furthermore, we could not get an answer for the upper limit of the dpa-rate in a neutron source. In our present proposal we are already 20 times higher than in the first wall. What is the lower and upper limit for the He:dpa and dpa-rate, respectively?

Fig. 6 shows that the spectrum averaged <dpa> and <He:dpa> values are really proportional to the mean neutron energy, as assumed in our 1978 hypothesis.
Figs. 7 and 8 display the Primary Recoil Energy Spectra in SS-316 and iron, respectively, for neutron sources based on 600 and 1200 MeV protons, in the Fusion First Wall and FMIT (perturbed). It demonstrates clearly that spallation neutrons are simulating the Fusion First Wall conditions as well as the D^+-Li or the 14 MeV neutron sources.
Fig. 9 shows the neutron spectra for 600 and 1200 MeV protons. Increasing the proton energy does not change the neutron spectrum below 10 MeV, where the evaporation neutrons play a dominant part, while the cascade neutrons are considerably enhanced. Therefore, the spectrum averaged helium production cross sections increases from 9.655 mbarns for 600 MeV protons to 15.061 mbarns for 1200 MeV protons. Most of the damage is produced by the evaporation neutrons while the cascade and knock-on neutrons are predominantly producing helium.

In spite of the close fit of the Primary Recoil Energy Spectrum for 600 and 1200 MeV protons, as shown in Figs. 7 and 8, with the one in the Fusion First Wall, many scientists argue that the very high energy spallation neutrons, even if few in number, will produce very large damage cascades which will give rise to unpredictable problems. To disprove this argument we calculated the Lindhard Efficiency Factor

and the corresponding Damage Energy up to 40 MeV recoil energy which corresponds to an elastic scattering process of a 600 MeV neutron on an iron atom. Fig. 10 shows that the damage energy g(T) of a 100 MeV neutron is only a factor 2 higher than of a 14 MeV neutron; the corresponding recoil energies are 7 and 1 MeV, respectively. Therefore, we have the paradox that the damage energy density, or subcascade density, is smaller for high than for low energy recoils. This is even more true for 600 MeV neutrons since g(T) is saturating; most of the recoil energy is transformed into heat and not into damage. Therefore, we have no problem with high energy neutrons. Mr. W. Matthes from Ispra is working on a detailed analysis of the primary damage energy deposition, to prove quantitatively our qualitative argument.

From the above follows that we can use without any difficulty also 1200 MeV protons. Using 1200 instead of 600 MeV protons the peak neutron flux increases by 37%, the mean neutron energy by 33%, the He production density by a factor 2.13 and the total helium production by a factor 3,5;see Table 1. Therefore, optimum conditions are being achieved at 1200 MeV with an increase in heat deposition density only of 40%, important for the target design.

3. THE CONCEPTUAL DESIGN OF THE SNS FACILITY

3.1 The Target

In Fig. 11 the vertical cross section of a liquid lead target is shown which can tolerate a beam power density of 15 MWatt/cm^2 and more. The fins are guiding the liquid lead in such a way that along the beam axis the centrifugal forces are generating an increasing pressure in the liquid lead suppressing any violent boiling of the lead. But, in contrast to the FMIT target, explosive boiling is not dangerous since the target can be made long enough and consequently the proton beam does not hit a solid wall.

3.2 The Irradiation Test Section

Figs. 12 and 13 show the horizontal and vertical cross section of the irradiation test section. The first three rows of Li or $Li_{17}Pb_{83}$ cooled channels are the fusion reactor materials test zone. In the first row along the beam, 320 dpa per year are generated in a volume of 20 cm^3, allowing 50 percent coolant volume, excluding the structural material of target and test section, which have an even higher dpa-rate. The neutrons leaking from the test zone are driving a subcritical booster ($\lesssim$ 10 MWatt) which provides a thermal neutron flux trap with a liquid hydrogen moderator in the centre. The ZrH_2-thermal neutron moderator will be gas cooled in order to avoid any light or heavy water in the liquid metal cooled target station. Close to the booster target large irradiation test sections (for the development of fast breeder construction materials) and isotope producing rigs can be installed (not shown in Figs. 11 and 12). Thermal and cold neutrons are leaking from the moderator into bent neutron guide tubes, providing intense neutron beams to the neutron scattering spectrometers, used as analytical instruments for the non-destructive testing of highly radioactive samples.

3.3 The Target Station

Fig. 14 shows the lay-out of the Neutron Target Station. The large iron shield will have a diameter $\leq$ 14 metres, depending on the desired maximum beam power in the future. Six thermal and cold neutron beam ports are foreseen for the analytical instruments, designed particularly for highly radioactive samples.

3.4 The Fusion Reactor Materials Test and Development Facility

Fig. 15 shows the lay-out of the facility. H^+- and H^--ion sources are 1200 metres distant from the target station. The 600 MeV proton linear accelerator occupies the first 600 metres. A beam transport system guides the proton beam to the target station. Hence, at a later time, if desired, the proton beam can be brought to an energy of 1200 MeV. For synergetic experiments concerning fatigue and radiation damage the

continuous proton beam will be periodically deflected on the target:

$$\Delta t = 9 \text{ sec}, \qquad f = 10^{-1} \text{ Herz}$$

in order to simulate the Pulsed Mode of Tokamak Power Reactors. The deflected beam will be used for a:

- Nuclear Physics Programme;
- Solid State Physics and a Bio-Medical Research Programme;
- Health Physics Research Programme;
- Special Isotope Production for medical, biological, agricultural and industrial application;
- μ-meson Fusion Programme;
- Breeding or Incineration with neutrons.

3.5 EURAC: The European Accelerator Neutron Source

Drs. R.A. Jameson and S.O. Schriber [10] informed us that for reasons of efficiency and economy, a pulsed proton linear accelerator feeding a pulse stretcher ring must be considered instead of a continuous wave accelerator, at least for the average proton current of 6 to 24 mA, which is our case. An optimalization study will have to be performed to find the crossing point at what beam current the continuous wave accelerator is more economic than the pulsed proton linear accelerator with a pulse stretcher ring. For a number of very important reasons we believe now that we must consider a 12 (24) mA, 1200 MeV pulsed proton linear accelerator, delivering 100 pps of 250 μsec pulse width, as the basis for the future European Neutron Sources. A conceptual scheme of EURAC is given in Fig. 16. EURAC can provide simultaneously a pulsed thermal and cold neutron source, as pioneered by the SNQ-Project Group at Jülich, FRG, and a continuous fast neutron beam for a Fusion Reactor Materials Test and Development programme, as pioneered at the JRC-Ispra, Italy. It can serve many other areas of research from particle physics to medical, biological, agricultural and industrial application, to energy strategies including μ-meson - Fusion, Electrobreeding and Incineration of very long-living radioisotopes.

It may be remarked that muon - Fusion is making remarkable progress [11-15] and it has to be considered seriously as a possible solution to our future energy requirements. To produce one μ-meson an energy of about 5 GeV is necessary, therefore "break even" would be reached at around 300 catalytic D-T muon reactions. Recently at LANL [16], 200 muon catalytic reactions have been measured per μ-meson. This is more than expected from the theoretical sticking factor, describing the probability of attachment of the μ-meson to the α-particle in the D-T muon catalytic fusion process, that predicts about 100 reactions per muon. Two hundred reactions would be sufficient for a Hybrid-Fusion Reactor. However, the problem remains how to collect the muons efficiently from a target and to transfer them to a reaction chamber. It seems a difficult but solveable problem. Therefore, more theoretical and experimental work must be devoted to the collection of μ-mesons.

Fig. 17 shows the artistic view of a Material Science Spectrometer [17] of which a 90 metre long version was designed for the SNS Rutherford Appleton Laboratory, UK, and a 150 metre long version for the SNQ Jülich. The foundations and the beam port insert have been constructed at RAL and a considerable part of the detectors have been purchased. The spectrometer is capable to measure simultaneously Small Angle Scattering (SAS), Elastic Diffuse Scattering (EDS), Quasi Elastic Scattering (QES) and Bragg Scattering (BS). Therefore, the spectrometer is capable to measure simultaneously the density of point defects, the density and size distribution of precipitates, damage cascades and voids, the texture, the stress and strain distributions, the mobility of hydrogen as well as the microchemical evolution of candidate materials irradiated to end-of-life conditions. The high resolution neutron spectrometer will complement the conventional analytical instruments.

Fig. 18 gives an outlook why fusion-fission hybrid power stations might be more economic than pure fusion reactors. The SNS-Ispra is a miniaturized form of a fusion-fission hybrid reactor system. In Table 2 the various neutron source parameters, of interest in our context, are listed.

REFERENCES

1. M.T. Robinson, "The energy dependence of neutron radiation damage in solids", BNES Nuclear Fusion Reactor Conf. at Culham Laboratory, September 1969.

2. Don M. Parkin and Allen N. Goland, "Calculation of radiation effects as a function of incident neutron spectrum", BNL-report, BNL-50434 (1974) and in: Radiation Effects, 1976, Vol. 28, pp. 31-42.

3. P. Grand, K. Batchelor, J.P. Blewett, A. Goland, D. Gurinsky, J. Kukkonen and C.L. Snead, Jr., "An intense Li (d,n) neutron radiation test facility for controlled thermonuclear reactor materials testing", Nuclear Technology, Vol. 29, June 1976, pp.327-336.

4. E.K. Opperman, HEDL-TME81-45 UC-20, January 1982.

5. W. Reiter, B. Strohmair and M. Uhl, "Final report", on work under Euratom contract No.1125-79-97 SISP C.

6. F. Atchison, W.E. Fischer and M. Pepin, "First and second interim reports and final report" on work carried out for contract No. 2007-82-12 ED ISP, CH.

7. V. Herrnberger, P. Stiller and M. Victoria, "Some estimates of the fusion radiation damage simulation by spallation neutrons", Workshop on Evaluation of Simulation Techniques for Radiation Damage in the Bulk of Fusion First Wall Materials, Interlaken, Switzerland, June 27-30, 1983.

8. S. Cierjacks et al., "Messungen der absoluten Ausbeuten ...", 11.04.05 012A KFK-Karlsruhe, February 1980.

9. W. Kley and G.R. Bishop, "The JRC-Ispra fusion reactor materials test and development facility", Nuclear Science and Technology, November 1984, EUR 9753EN.

10. R.A. Jameson and S.O. Schriber, private communication, May 1985.

11. Yu. V. Petrov, Yu. M. Shabel'skii: Sov. J. Nucl. Phys. 30 (1), (1979) 66.

12. L. Bracci, B. Fiorentini, "Mesic molecules and muon catalyzed fusion", Physics Report 86, No.4 (1982).

13. S.E. Jones, A.J. Caffrey, J.B. Walter, A.N. Anderson, J.N. Bradburg, P.A. Gram, M. Leon and M.A. Paciotti, in: Muon - Catalyzed Fusion Workshop, Jackson Hole, WY, June 7-8, 1984, EG&G Idaho Inc.

14. H. Takahashi and A. Moats, Atomkernenergie-Kerntechnik, Vol.43 (1983) No.3, pp.188-190.

15. H. Takahashi, "Reactivation coefficient of muon catalyzed D-T fusion and its enhancement", BNL-report 35543, October 1984.

16. Dr. Louis Rosen, Director of LANL, private communication, May 1985.

17. W. Kley, "Design proposal for a material science spectrometer at the SNQ Jülich, FRG", invited contribution to the SNQ Workshop at Maria Laach, September 3-5, 1984, Jül-1954, ISSN 0366-0885, October 1984, KFA Jülich, F.R.G.

TABLE 1 - Neutron source performance data for 600 and 1200 MeV protons

Proton energy : 600 Mev Sample position: Z = 3.75 cm			Proton energy : 1200 MeV Sample position: Z = 3.75 cm		
Flux/proton (n/cm^2)	$\bar{E}n$ MeV	<He> mbarns	Flux/proton (n/cm^2)	$\bar{E}n$ MeV	<He> mbarns
0.065	4.75	9.655	0.089	6.31	15.061

Conclusion:

Switching from 600 to 1200 MeV protons increases:

1. (dpa.volume) by a factor 2,64
2. Peak neutron flux by 37%
3. Mean neutron energy by 33%
4. He-production density by a factor 2.13
5. Total helium production by a factor 3,5

TABLE 2 - Intercomparison of existing and projected neutron sources

Neutron-Sources	RTNS-II LLL-USA	FMIT HEDL-USA	SNS-RAL Rutherford App. Lab. GB	SNS-LASL WNR USA	LAMPF-Beam-Stop USA	SNS-CH Villigen Switzerland	SNQ-Jülich FRG	SNS-JRC-Ispra	Fusion' 1. Wall "INTOR"
Nuclear Reaction	D^+-T Fusion Reaction	D^+-Li-Stripping-Reaction	800 MeV-Protons; U-238-Target spallation	800 MeV-Protons; U-238 Target spallation	500 - 800 MeV Protons on Cu spallation	590 Mev-Protons on liquid Pb spallation	1100 MeV-Protons on solid W, Pb, U-238 spallation	600 MeV-Protons on liquid Pb spallation	D^+-T^+ Fusion
Beam Energy	400 keV	35 MeV	800 MeV	800 MeV	800 MeV	590 MeV	1100 MeV	600 MeV	
Beam Current	D^+: 150 mA	D^+: 100 mA	$\overline{P^+}$: 0.2 mA	$\overline{P^+}$: 0.1 mA	$\overline{P^+}$: 1 mA	$\overline{P^+}$: 2 mA	$\overline{P^+}$: 5 mA	$\overline{P^+}$: 6 mA	
Beam Power	60 kWatt	3.5 MWatt	160 kWatt	80 kWatt	800 kWatt	1.18 MWatt	5.5 MWatt	3.6 MWatt	1.3 MW/m²
Estimated Beam Power Density	$\frac{60\ kWatt}{cm^2}$	$\frac{1.2\ MWatt}{cm^2}$	$\approx \frac{6.4\ kWatt}{cm^2}$	$\approx \frac{3.2\ kWatt}{cm^2}$	$\approx \frac{8\ kWatt}{cm^2}$	$\lesssim \frac{50\ kWatt}{cm^2}$	$\approx \frac{250\ kWatt}{cm^2}$	$\frac{15\ MWatt}{cm^2}$	$\approx \frac{130\ Watt}{cm^2}$
Mode of Operation	Continuous	Quasi-continuous	Pulsed $\Delta t \approx 0.4\ \mu sec$ $f = 50$ Herz $\Delta t \cdot f = 2 \cdot 10^{-5}$	Pulsed $\Delta t \approx 0.4\ \mu sec$ $f = 12$ Herz $\Delta t \cdot f = 4.8 \cdot 10^{-6}$	Pulsed $\Delta t = 500\ \mu sec$ $f = 120$ Herz $\Delta t \cdot f = 6 \cdot 10^{-2}$	Continuous	Pulsed $\Delta t = 250\ \mu sec$ $f \leqslant 100$ Herz $\Delta t \cdot f = 2.5 \cdot 10^{-2}$	Quasi-continuous; $\Delta t = 9$ sec, $f = 0.1$ Herz $\Delta t \cdot f = 0.9$	Quasi-continuous; $\Delta t \leqslant 3000$ sec, $f \leqslant 10^4$ per year
Number of Neutrons produced per sec in Target	$4 \cdot 10^{13}$ n/sec TiT	10^{16} n/sec Li	$4 \cdot 10^{16}$ n/sec U-238	$2 \cdot 10^{16}$ n/sec U-238	$\lesssim 10^{17}$ n/sec Cu/U-238	$1.2 \cdot 10^{17}$ n/sec Pb	$1.4 \cdot 10^{18}$ n/sec U-238	$9 \cdot 10^{17}$ *n/sec Pb reflected Pb-target	$5.5 \cdot 10^{14}$ n/cm².sec
Estimated accessible average fast neutron-energy	14 MeV $E_n^{max} = 14.1$ MeV	9 MeV $E_n^{max} \lesssim 40$ MeV	$\lesssim 0.5$ MeV $E_n^{max} \lesssim 800$ MeV	$\lesssim 0.5$ MeV $E_n^{max} \lesssim 800$ MeV	$\lesssim 1$ MeV $E_n^{max} \lesssim 800$ MeV	$\lesssim 0.5$ MeV $E_n^{max} \lesssim 590$ MeV	$\lesssim 0.5$ MeV $E_n^{max} \lesssim 1100$ MeV	6 - 7 MeV unrefl. 4 MeV Pb-refl. $E_n^{max} \lesssim 600$ MeV	4 MeV
Accessible Fast Neutron Flux	$1.5 \cdot 10^{13}$ n/cm².sec	$1.4 \cdot 10^{15}$ n/cm².sec			$\lesssim 10^{13}$ n/cm².sec			$\approx 2 \cdot 10^{16}$ n/cm².sec	$5.5 \cdot 10^{14}$ n/cm².sec
dpa/year	0.2	83 (10 cm³)			≈ 0.2			320 (20 cm³)	15
He appm/dpa	15	11			< 1			$6 < \frac{He\ appm}{dpa} \leqslant 13$**	11

* The apparent source strength of the Pb reflected Pb-target. A uranium-238 bare target would deliver $9 \cdot 10^{17}$ n/sec. A 10 MW-Booster target will deliver $1.7 \cdot 10^{18}$ n/sec.

Note: D^+-Li produces: $2{,}85 \cdot 10^{15}$ n/sec.MWatt; P^+-Spallation prod.: $2.5 \cdot 10^{17}$ n/sec.MWatt in U-238.

For an irradiation damage program the beam power density is the decisive parameter that is translated to fast neutron flux and correspondingly to dpa and He appm/dpa, the important parameters.

SNS-LASL, SNS-RAL, SNS-CH and SNQ-Jülich are designed for thermal and cold neutron production. They cannot be compared with SNS-Ispra, designed primarily for radiation damage, including thermal and cold neutron production.

** A value of 6.4 is obtained if all neutrons above 30 MeV are collected in the energy group between 29.75-30 MeV and their He production estimated with $\sigma_{n,\alpha}$ (30 MeV). A value of 13 is obtained if the He-production is calculated with estimated $\sigma_{n,\alpha}$ cross sections for neutrons up to 400 MeV and measured spallation neutron spectrum, in excellent agreement with Fusion Reactor First Wall conditions.

FIGURE CAPTIONS

Fig. 1 Geometry and parameters of the theoretical program.

Fig. 2 ψ_i-values in SS-316 as a function of sample position for an iron shielded neutron source: E_p = 600 MeV.

Fig. 3 ψ_i-values for transmutation products in SS-316 as a function of sample position for an iron shielded neutron. Source: E_p = 600 MeV.

Fig. 4 ψ_i-values in SS-316 as a function of sample position for an iron shielded neutron source: E_p = 1200 MeV.

Fig. 5 ψ_i-values for transmutation products in SS-316 as a function of sample position for an iron shielded neutron source: E_p = 1200 MeV.

Fig. 6 Spectrum averaged <dpa>- and <He:dpa>-values as a function of mean neutron energy.

Fig. 7 Primary recoil energy spectra for SS-316 for neutron sources based on 600 and 1200 MeV protons, fusion first wall and FMIT (perturbed).

Fig. 8 Primary recoil energy spectra for iron for neutron sources based on 600 MeV and 1200 MeV protons, fusion first wall and FMIT (perturbed).

Fig. 9 Neutron spectra at 3.75 cm for iron shielded neutron sources based on 600 and 1200 MeV protons.

Fig. 10 Damage efficiency in iron.

Fig. 11 The conceptional design of the liquid lead target; vertical cross section.

Fig. 12 Conceptional design of target-station; 1/2 horizontal cross section.

Fig. 13 Vertical cross section of conceptual SNS target station.

Fig. 14 Lay-out of the neutron target station.

Fig. 15 Lay-out of the fusion reactor materials test and development facility, based on a continuous wave 600 MeV, 6 mA proton linear accelerator.

Fig. 16 EURAC: a European solution to future needs of neutrons.

Fig. 17 The material science spectrometer.

Fig. 18 Fusion hybrid energy strategy.

Fig. 19 Time schedule for EURAC.

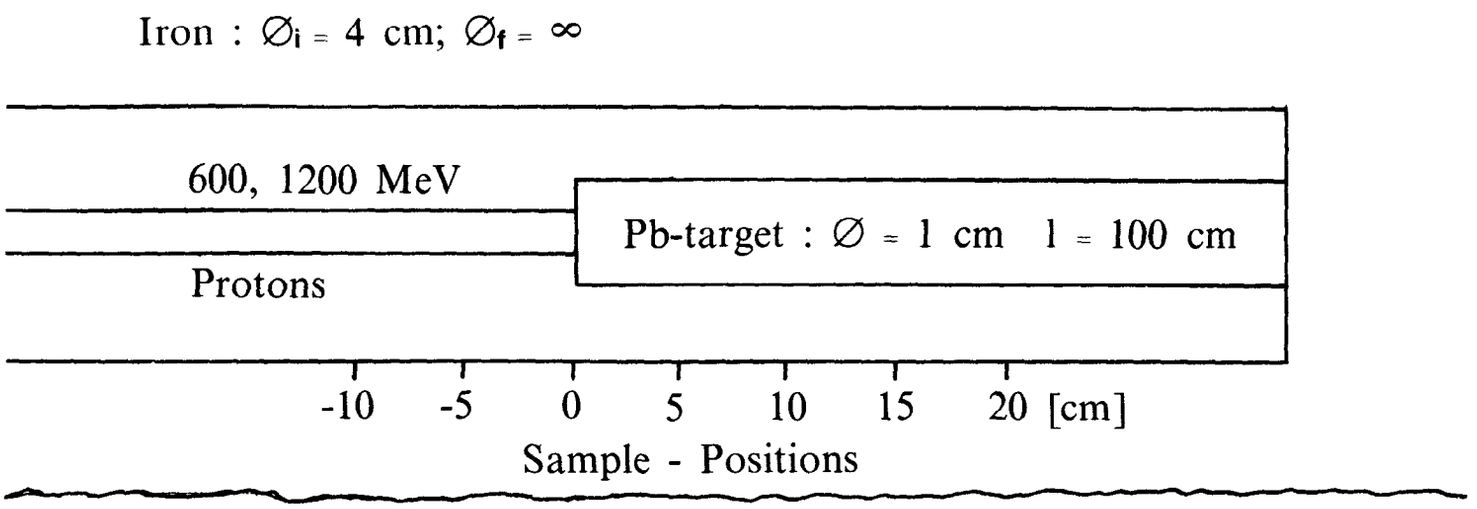

$$\Psi_i = \frac{<\sigma\ (E)\ \varnothing\ (E) > \text{Neutron Source}}{<\sigma\ (E)\ \varnothing\ (E) > \text{Fusion 1. Wall}}$$

P(T) : Primary Recoil Energy Spectrum

Damage Energy : g(T) = T - U = T L(T)

L(T) = Lindhard's Damage Efficiency Factor

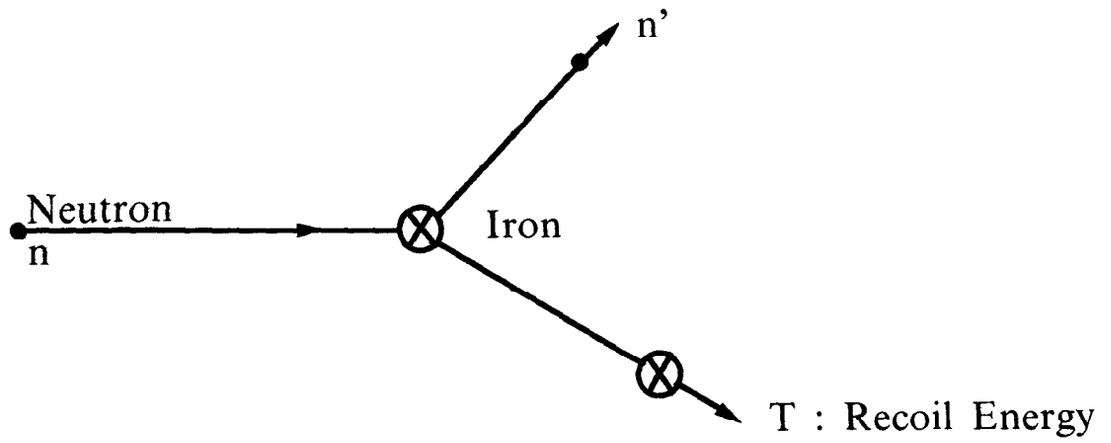

Fig. 1 : Geometry and Parameters of the Theoretical Program.

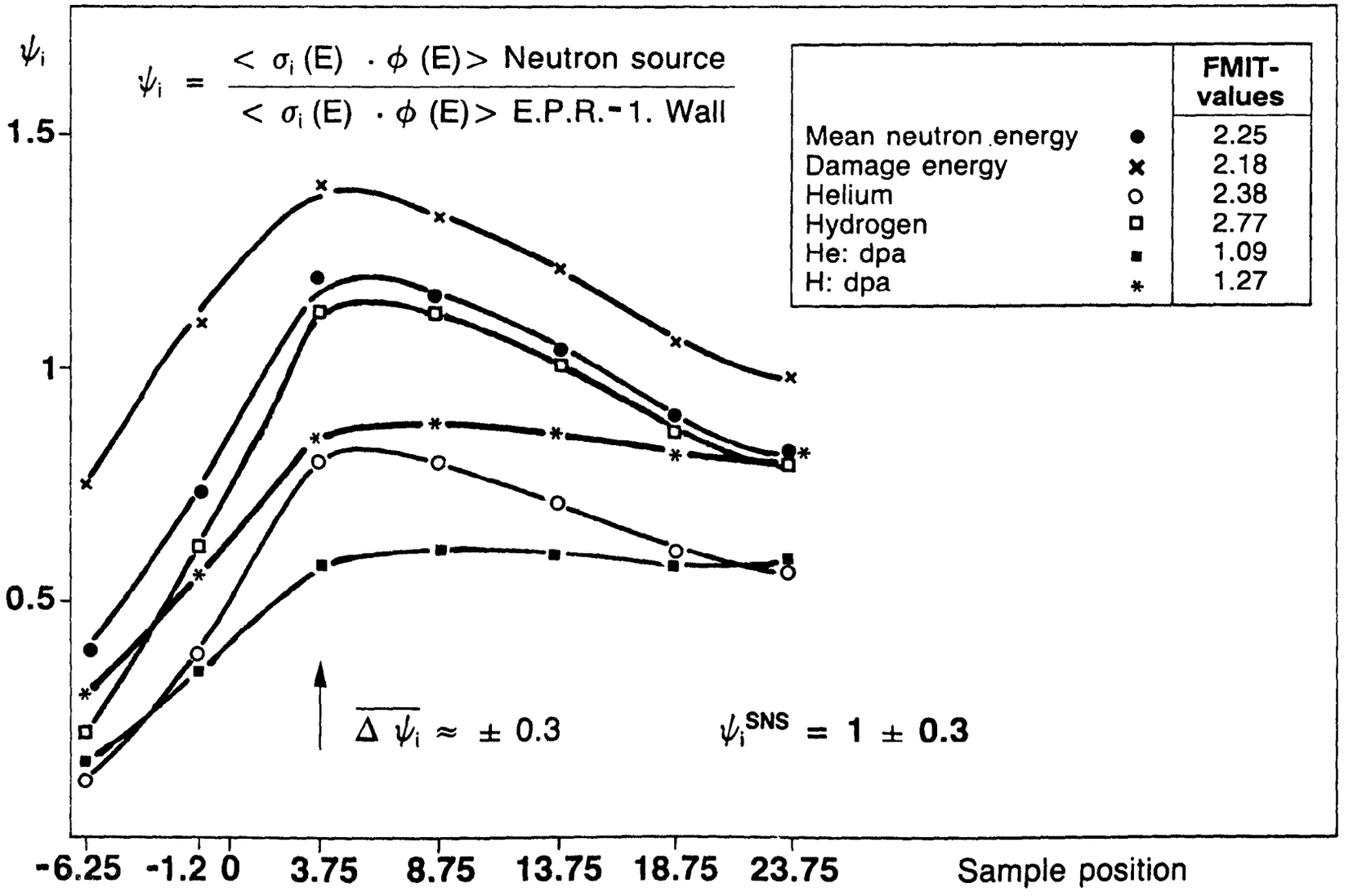

Fig. 2 : Ψ_i -Values in SS-316 as a Function of Sample Position for an Iron Shielded Neutron Source : Ep = 600 MeV.

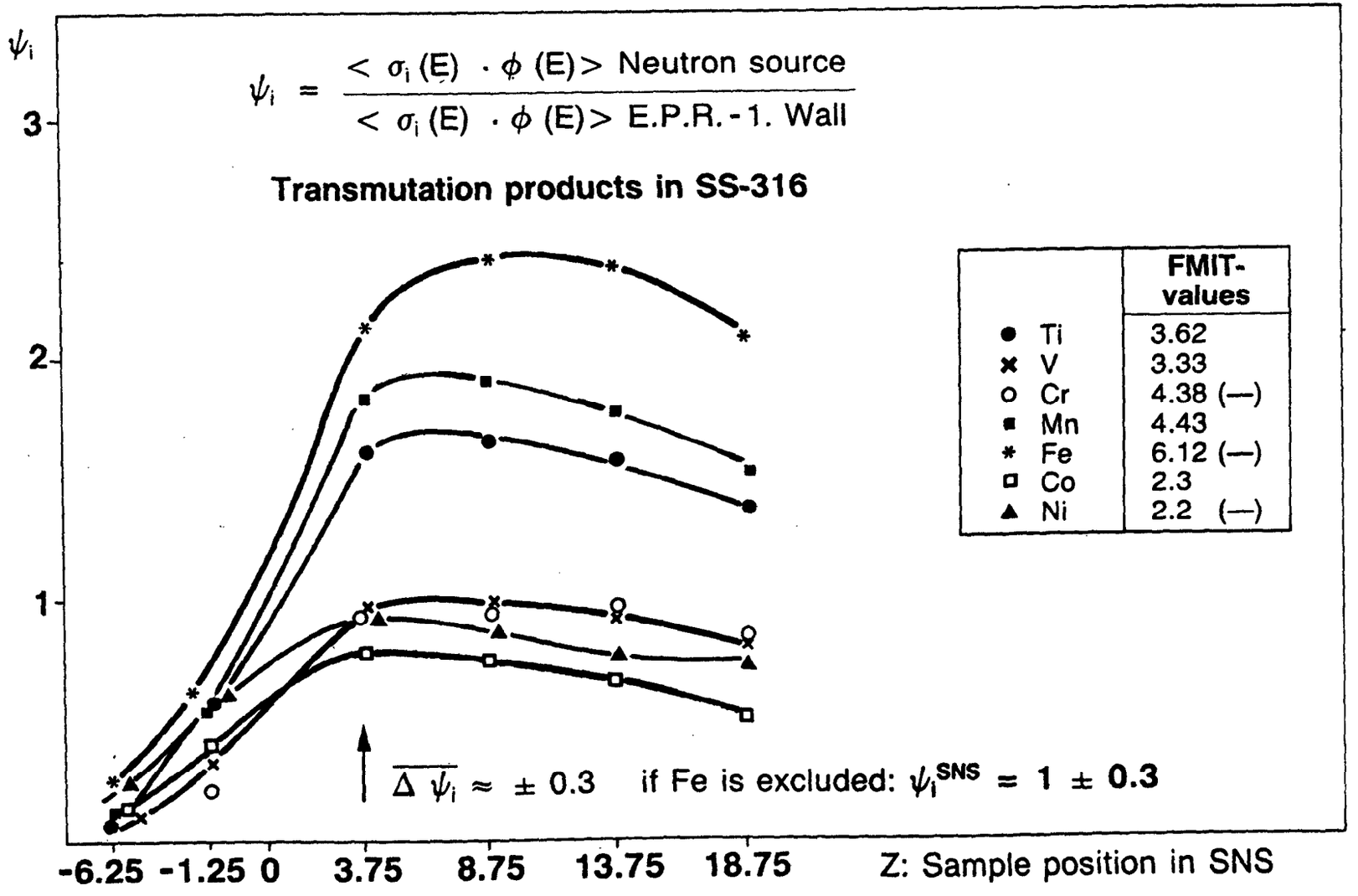

Fig. 3 : Ψ_i -Values for Transmutation Products in SS-316 as a Function of Sample Position for an Iron Shielded Neutron Source : Ep = 600 MeV.

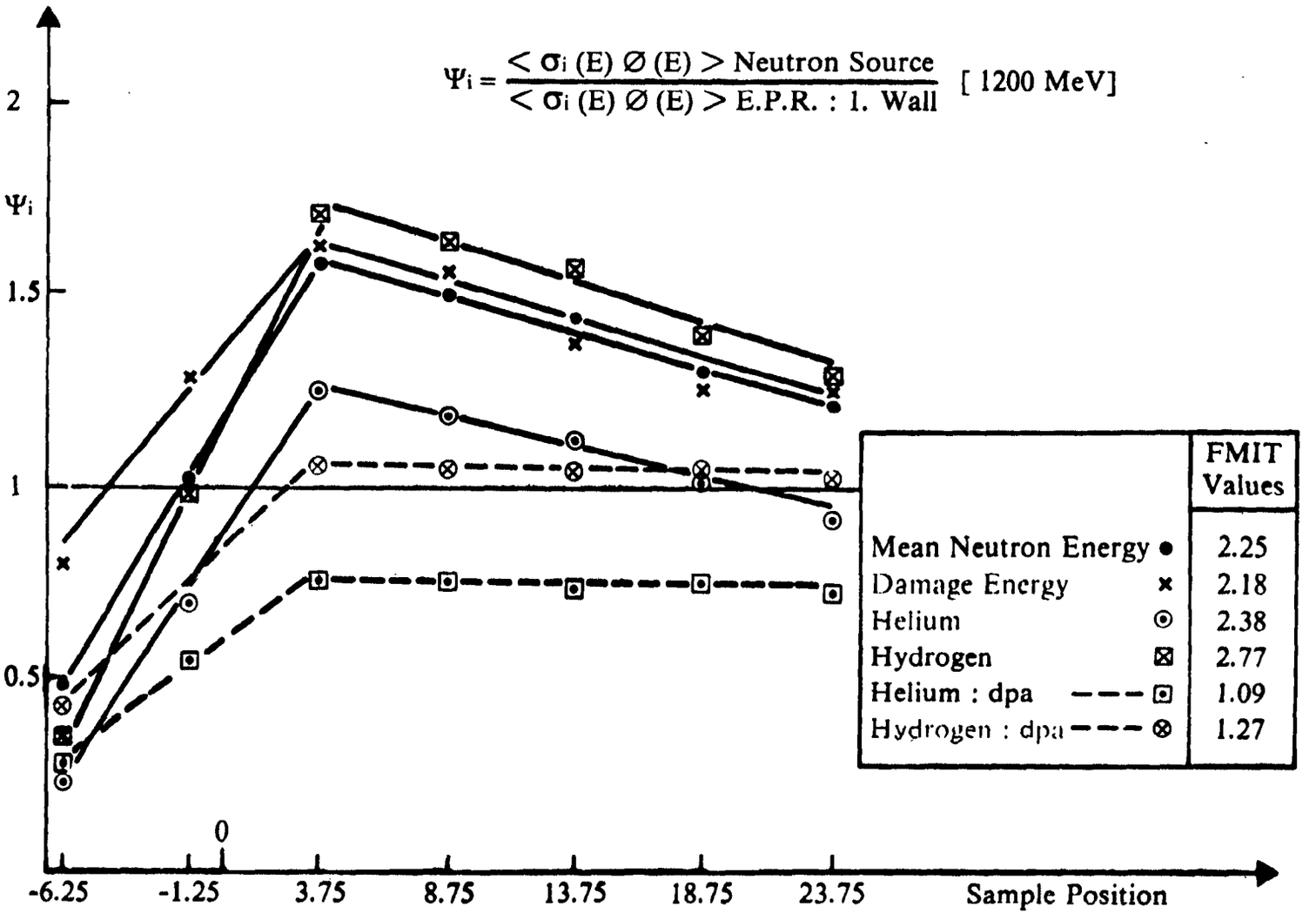

Fig. 4 : Ψ_i -Values in SS-316 as a Function of Sample Position for an Iron Shielded Neutron Source : Ep = 1200 MeV.

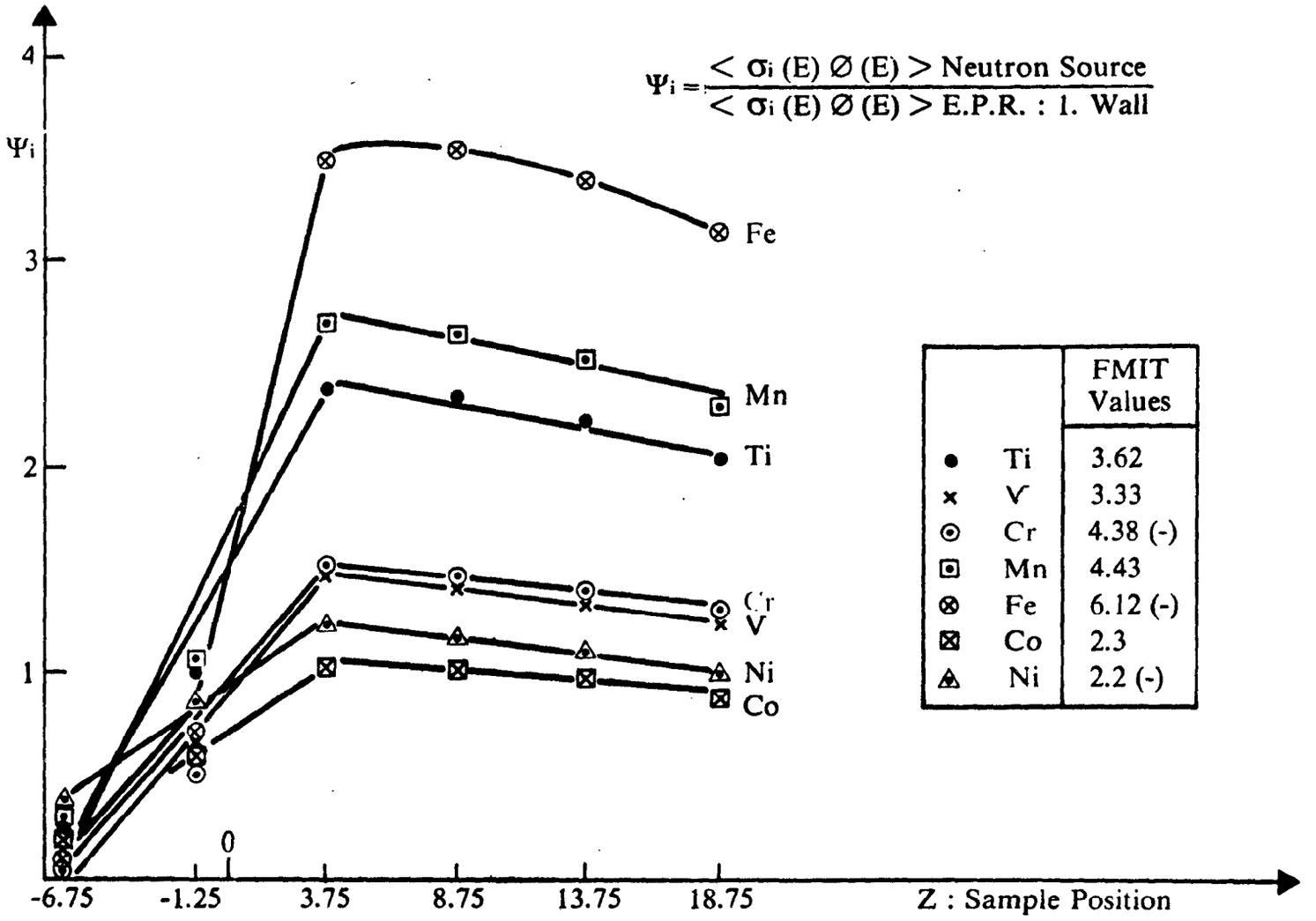

Fig. 5 : Ψ_i -Values for Transmutation Products in SS-316 as a Function of Sample Position for an Iron Shielded Neutron Source : Ep = 1200 MeV.

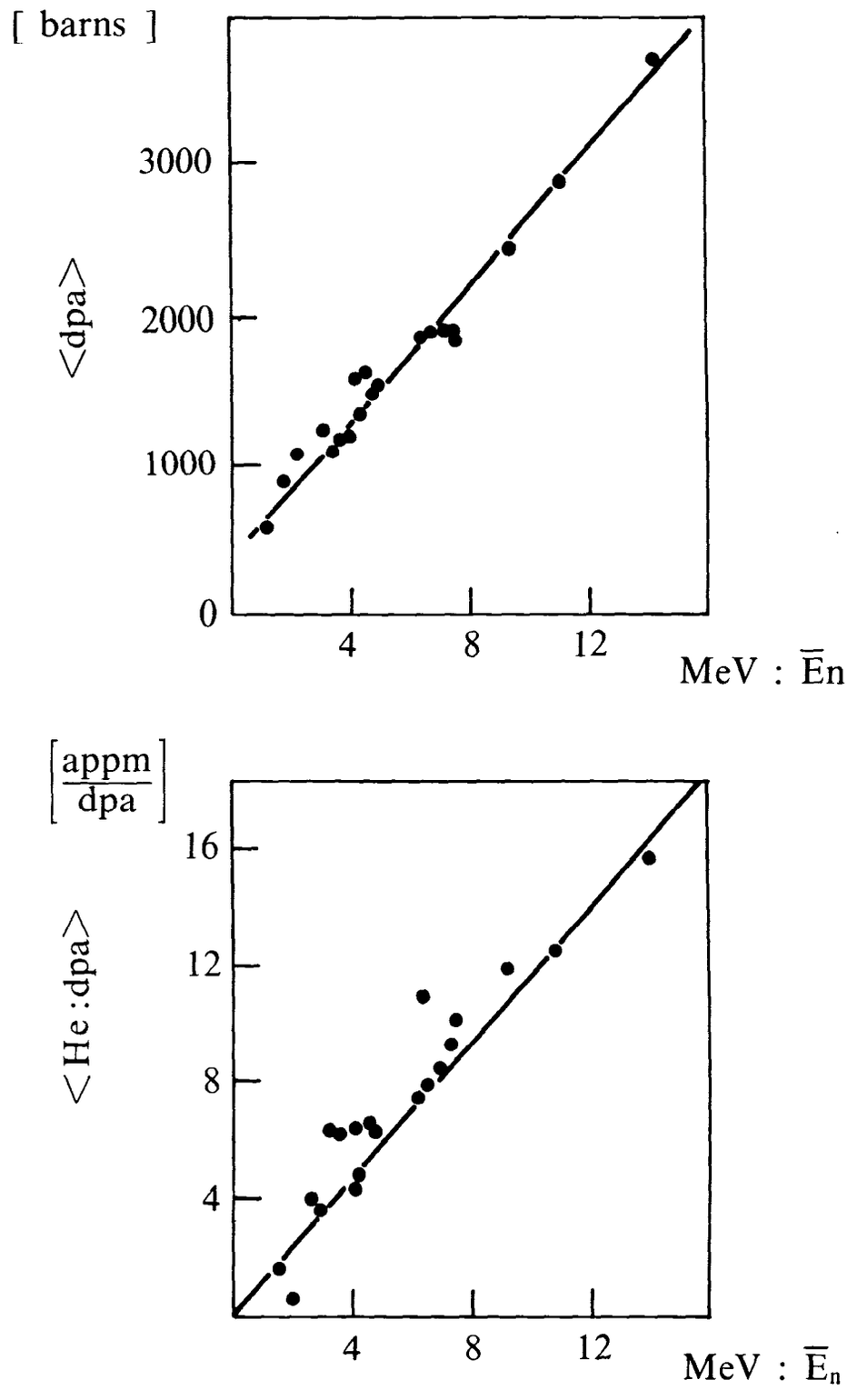

Fig. 6 : Spectrum Averaged <dpa> and <He : dpa> Values as a Function of Mean Neutron Energy.

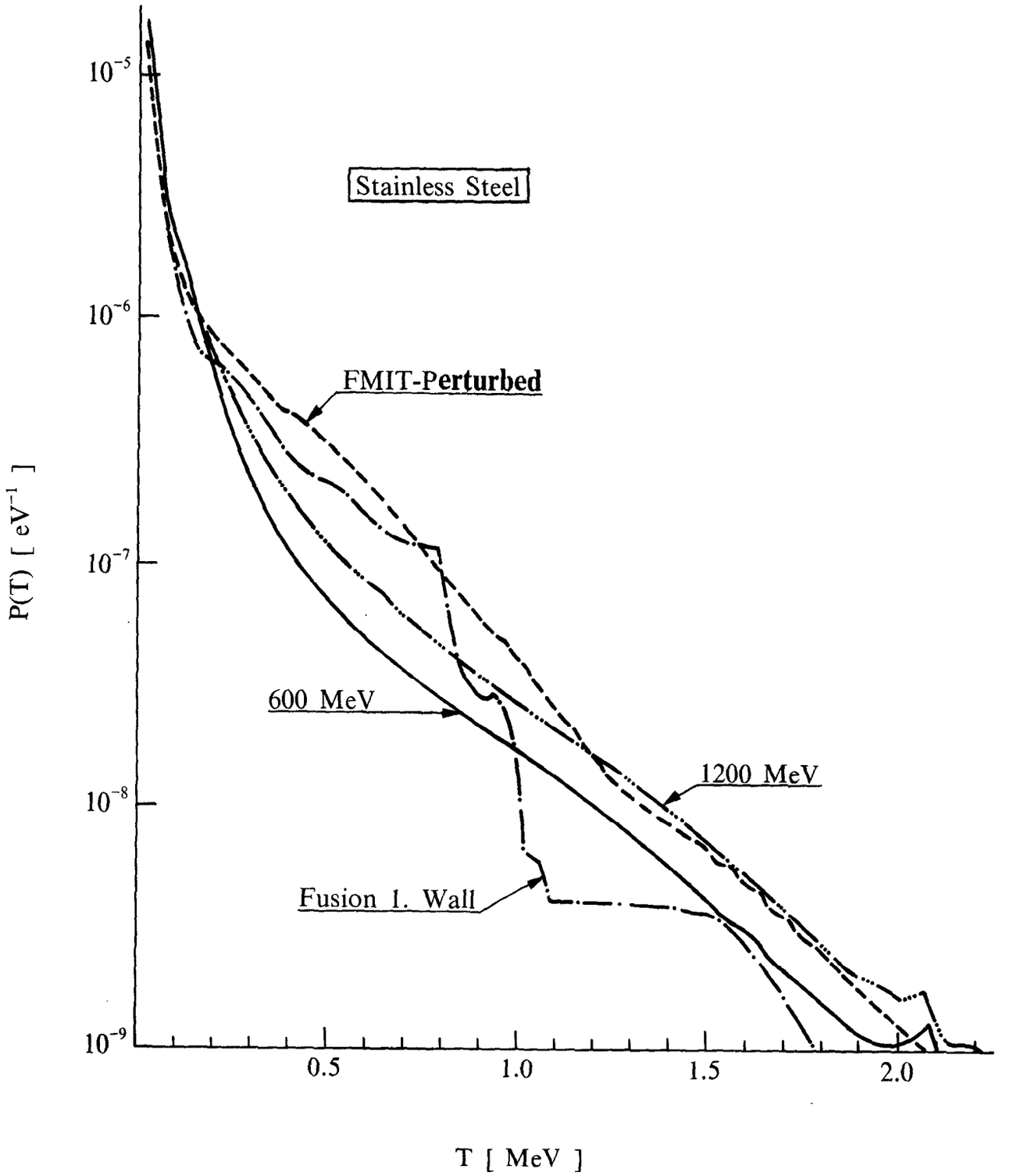

Fig. 7 : Primary Recoil Energy Spectra for SS-316 for Neutron Sources Based on 600 and 1200 MeV Protons, Fusion 1. Wall and FMIT (perturbed).

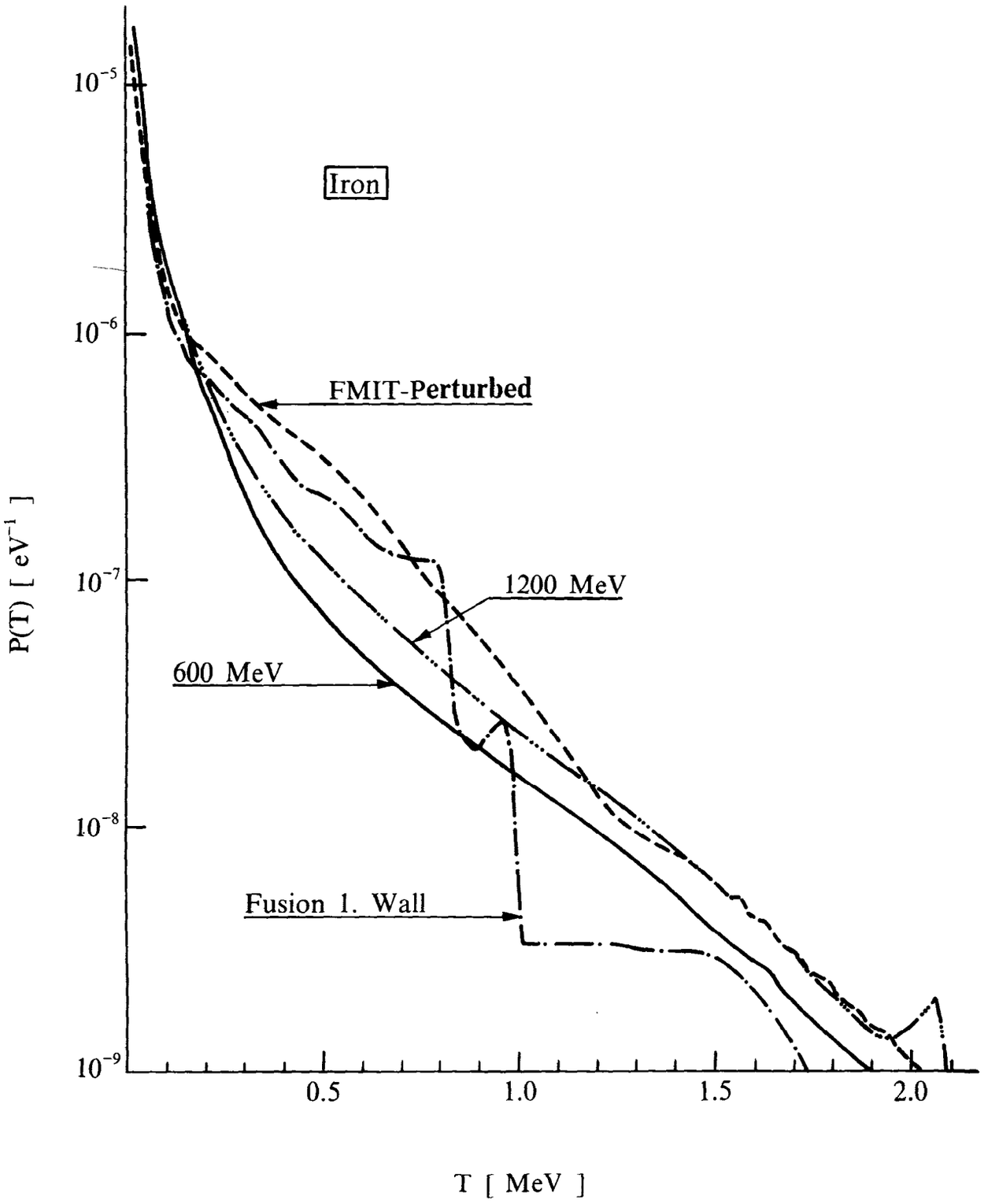

Fig. 8 : Primary Recoil Energy Spectra for Iron for Neutron Sources Based on 600 MeV and 1200 MeV Protons, Fusion 1. Wall and FMIT (perturbed).

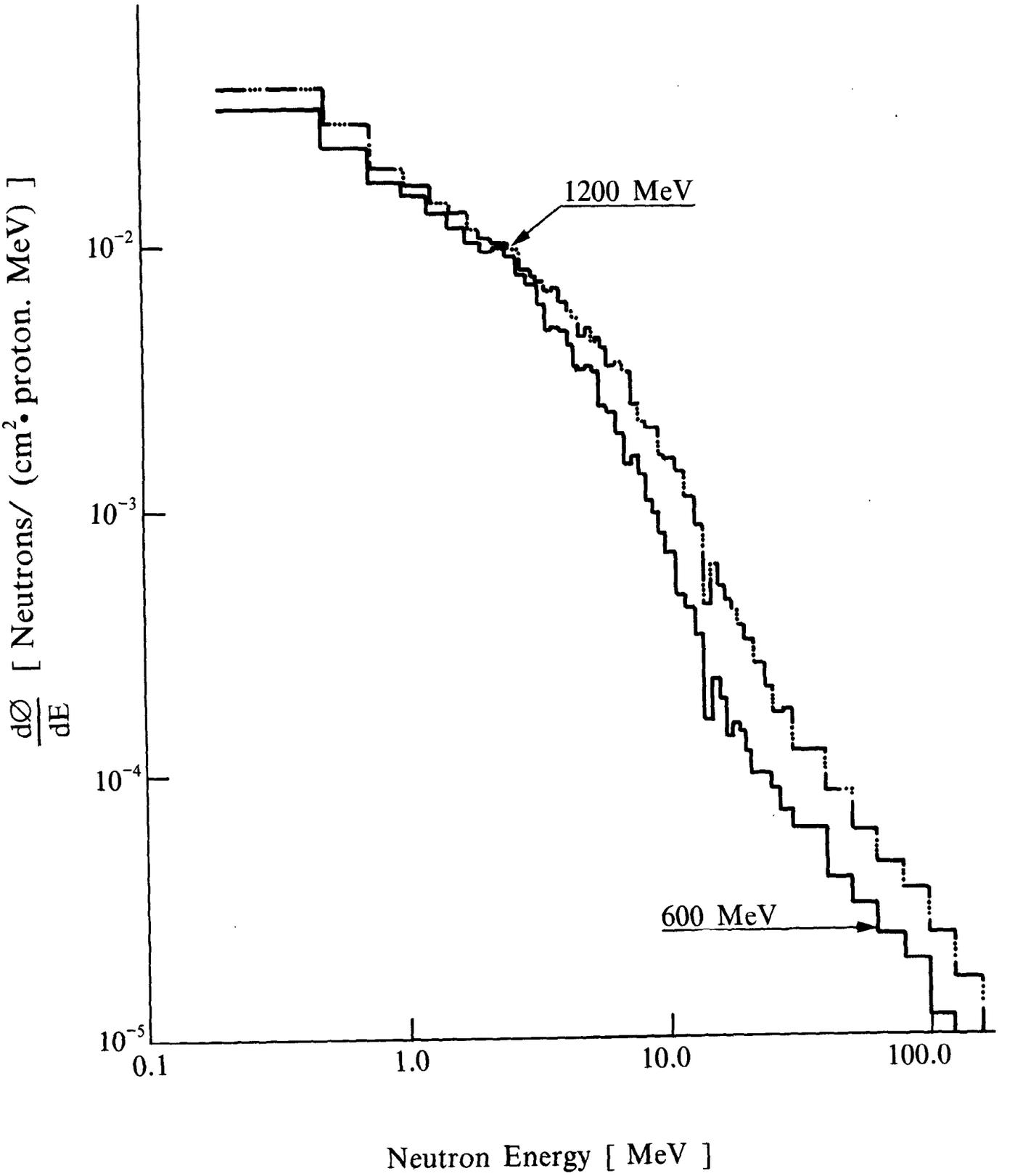

Fig. 9 : Neutron Spectra at 3.75 cm for Iron Shielded Neutron Source Based on 600 and 1200 MeV Protons.

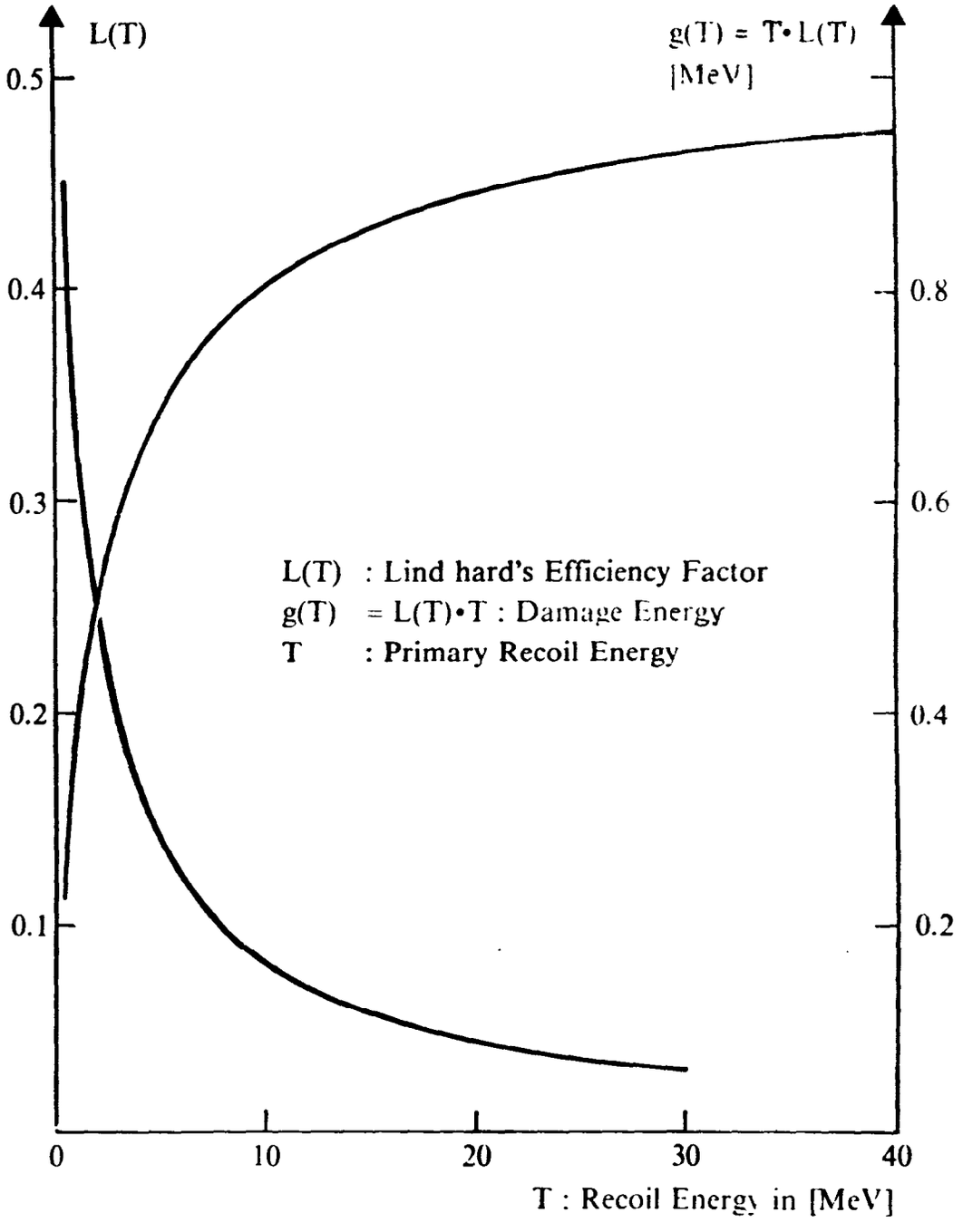

Fig.10 Damage Efficiency in Iron

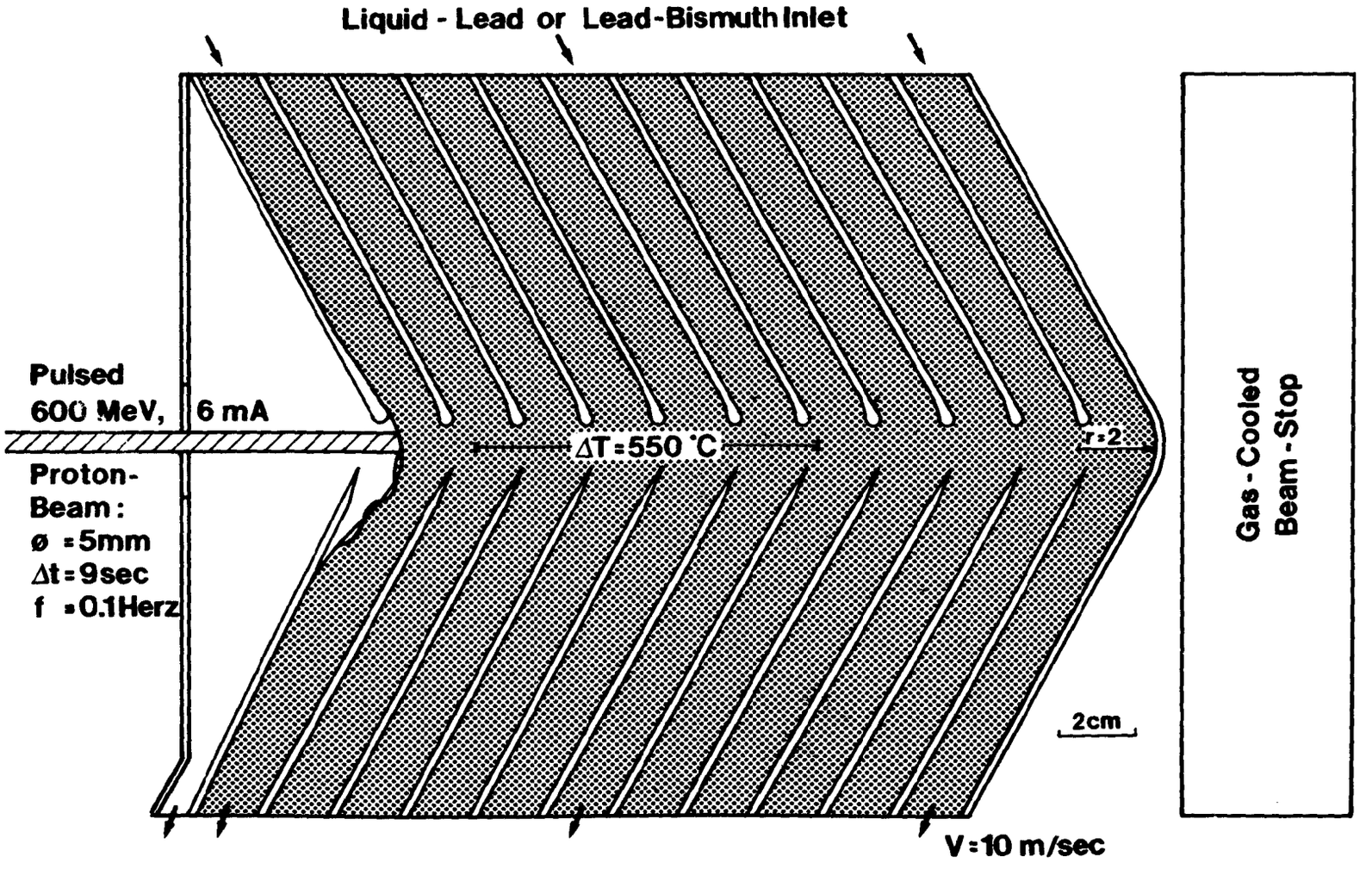

Fig. 11 : The Conceptional Design of the Liquid Lead Target; Vertical Cross Section.

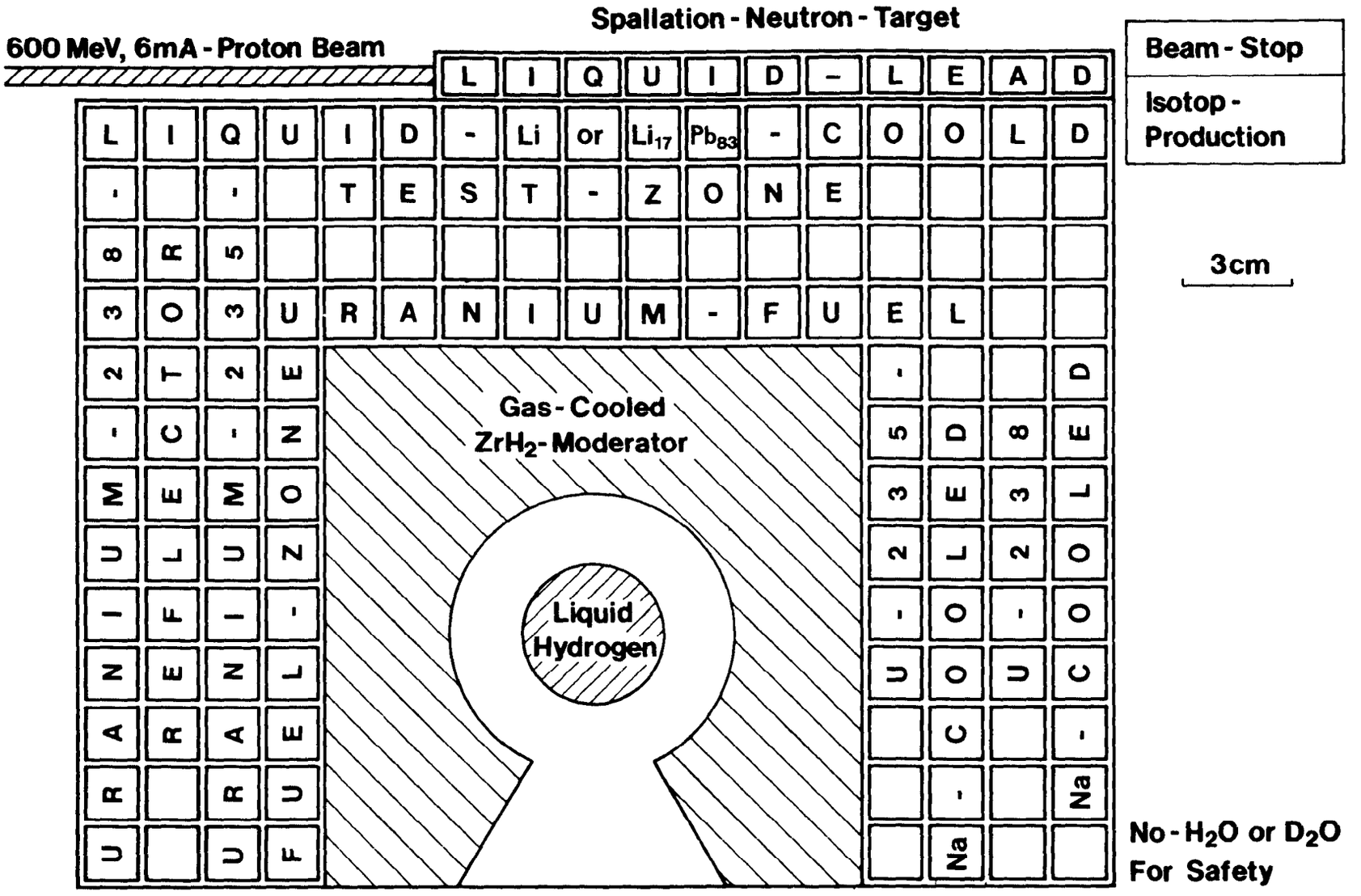

Fig. 12 : Conceptional Design of Target-Station; 1/2-Horizontal Cross Section.

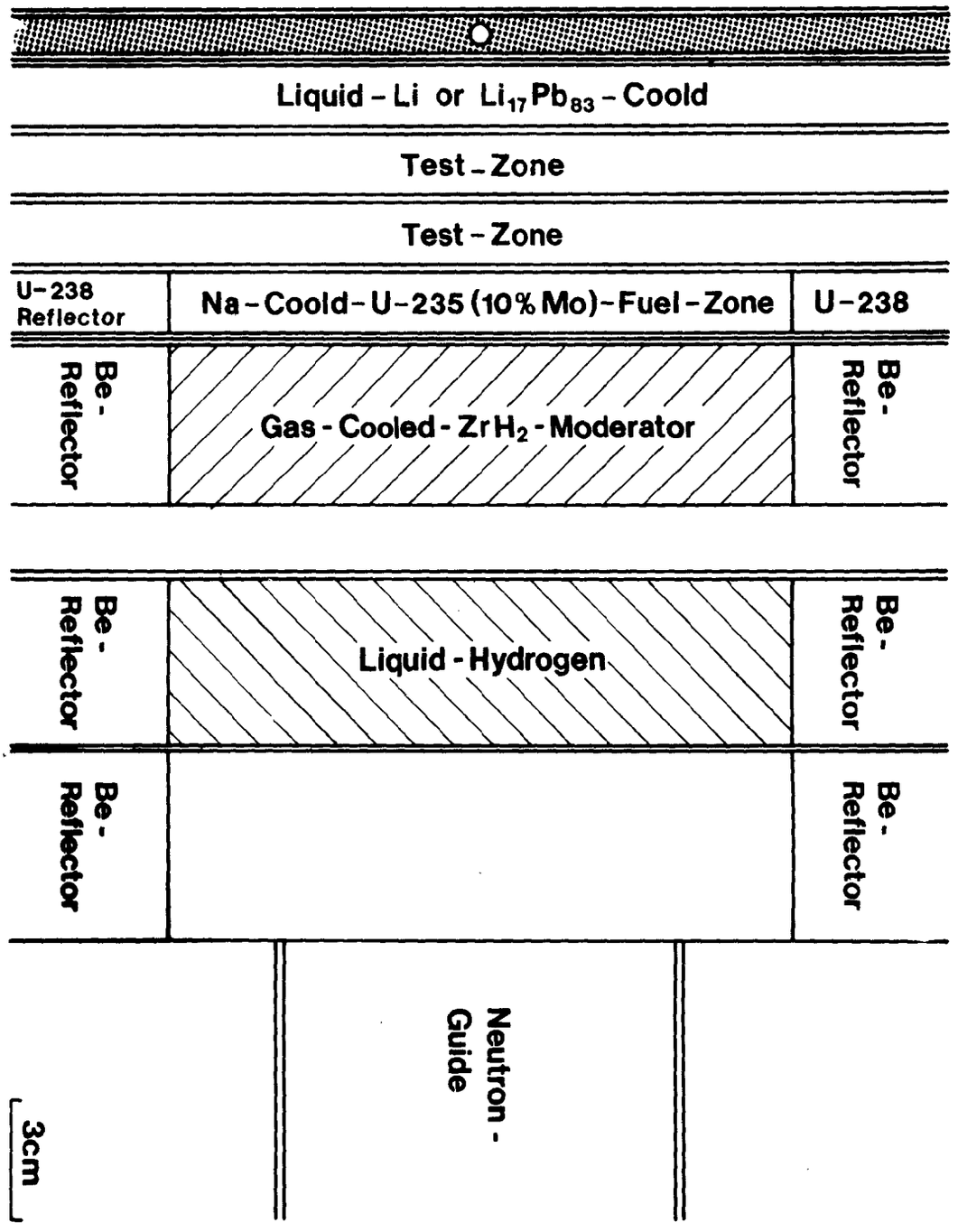

Fig. 13 : Vertical Cross Section of Conceptional SNS Target Station.

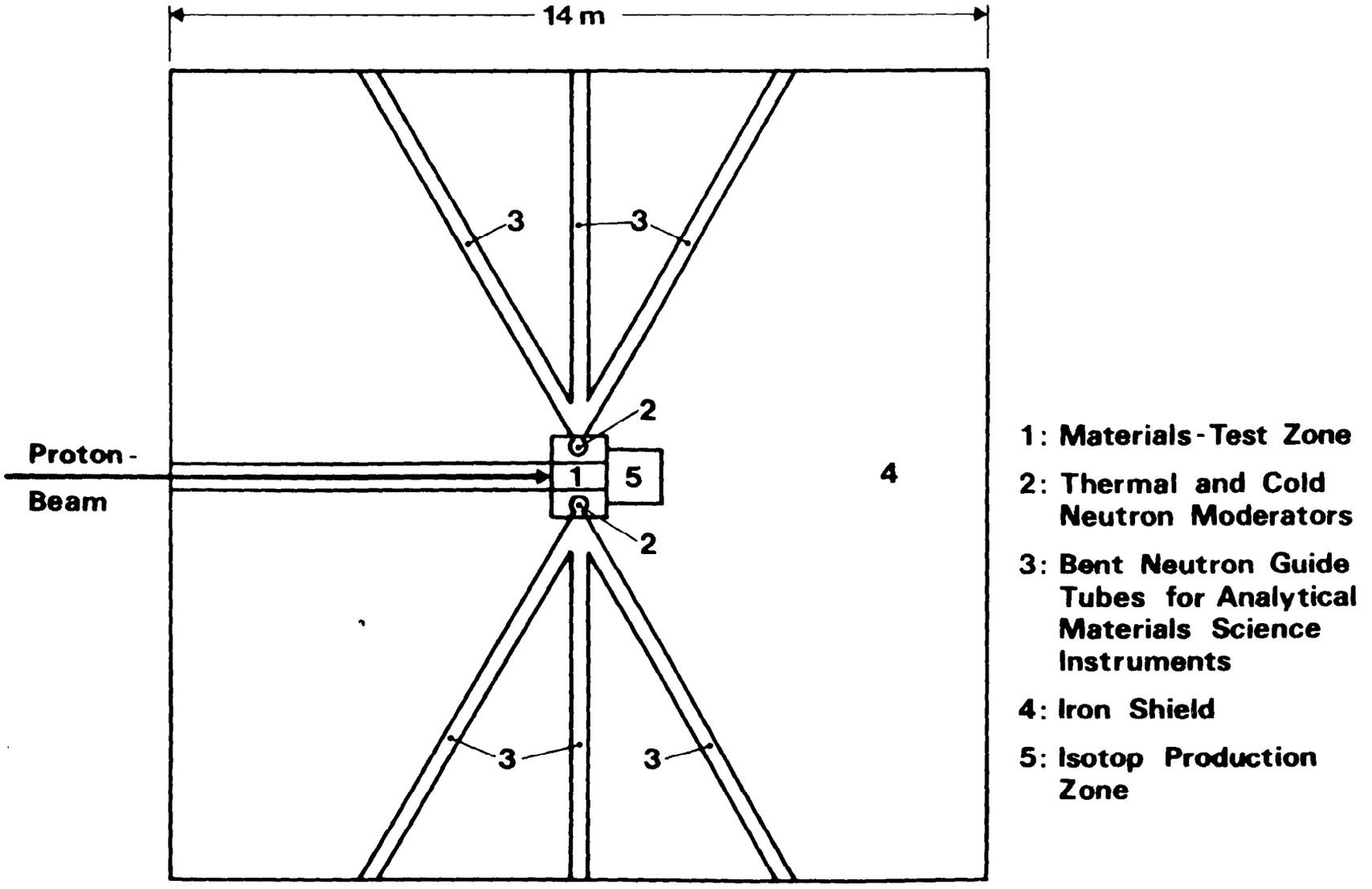

Fig. 14 : Lay-Out of the Neutron Target Station.

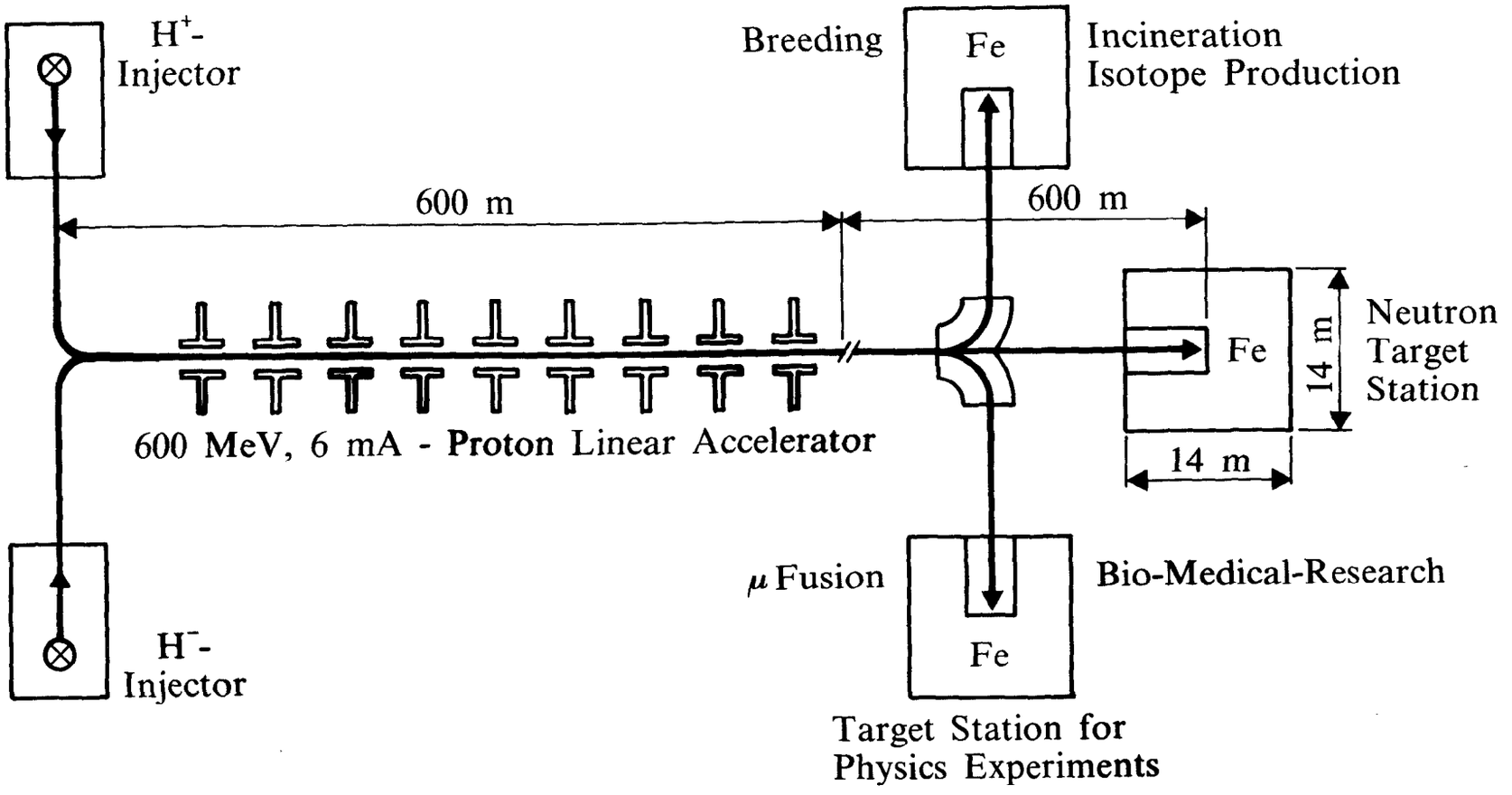

Fig. 15 : Lay-Out of the Fusion Reactor Materials Test and Development Facility, Based on a Continuous Wave 600 MeV, 6 mA Proton Linear Accelerator.

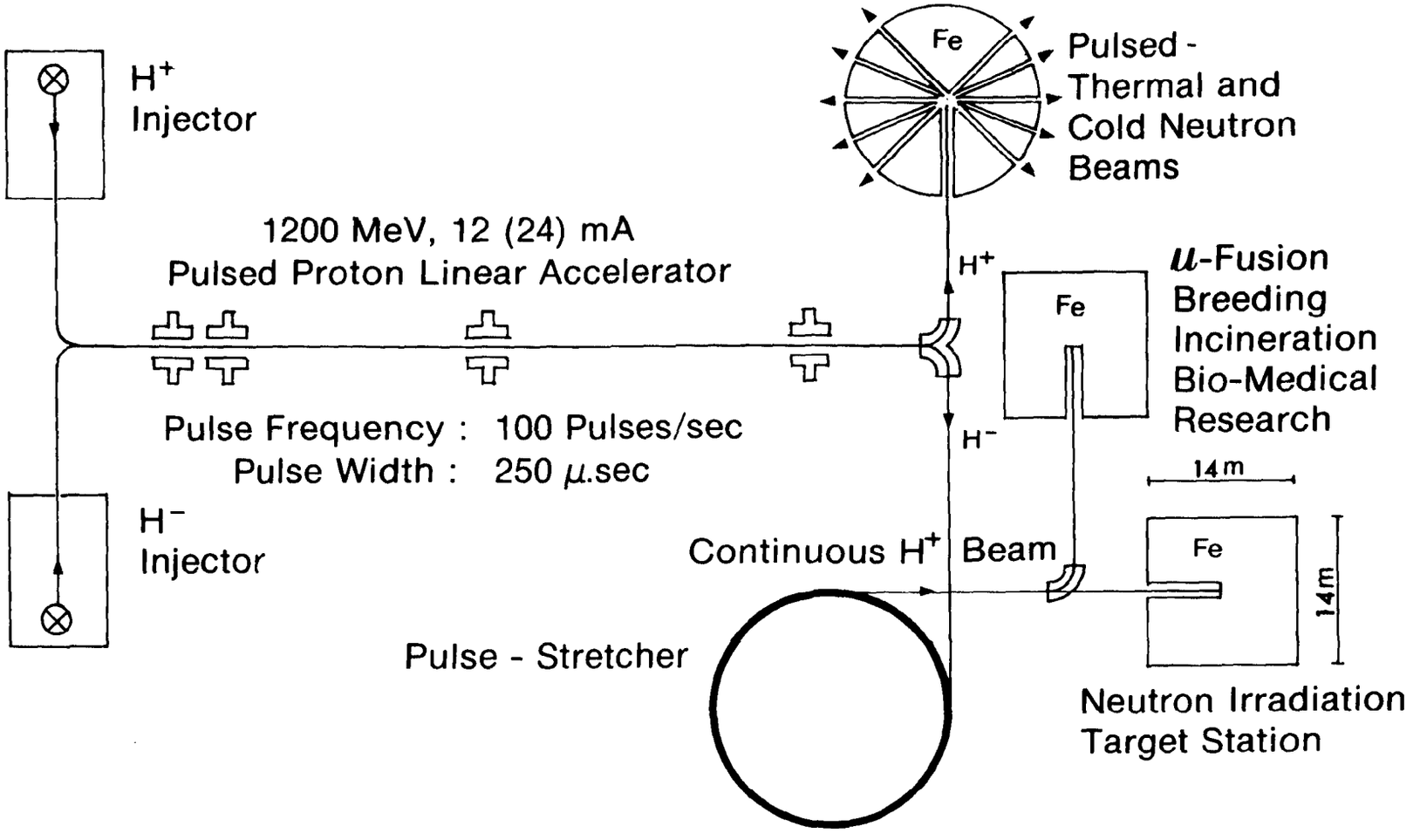

Fig. 16 : EURAC : A European Solution to Future Needs of Neutrons

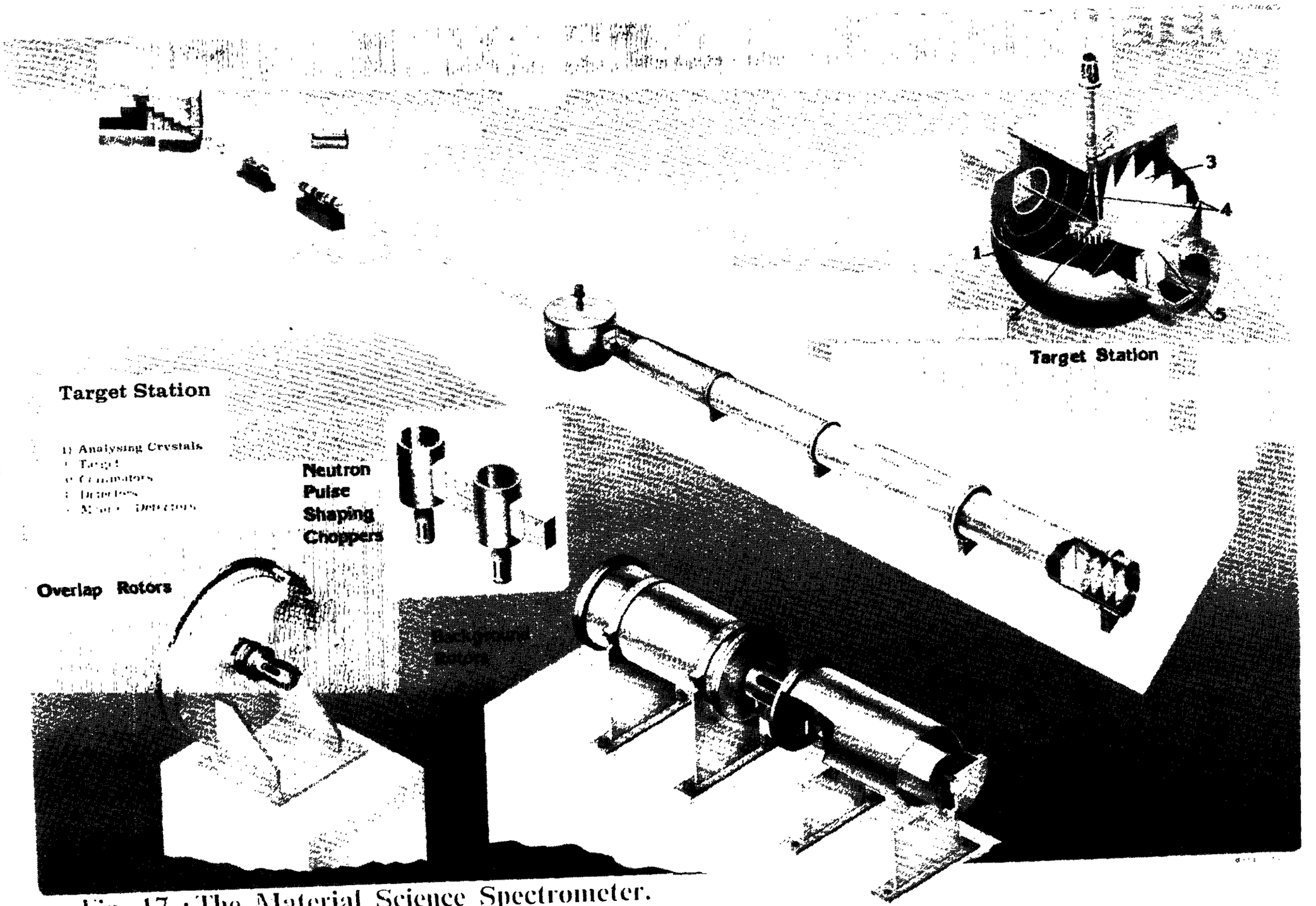

Fig. 17 : The Material Science Spectrometer.

Future Power Stations ?

The physicist's answer :

Subcritical Fast Fission Reactors driven by Fusion Neutrons !

Why ?

$D^+(E \geqslant 10\ KeV) + T^+(E \geqslant 10\ keV) \rightarrow He\ (3.5\ MeV) + n(14.1\ MeV)$

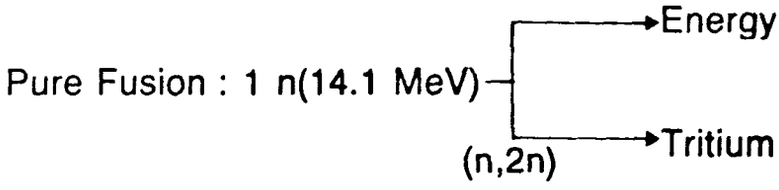

does it breed ?

Hybrid Fusion : 1 n(14.1 MeV) → U^{238} (Th^{232}) + 2.5 n
200 MeV fast fission

energy and neutron multiplier

SNS-Ispra a miniaturized form of the subcritical Fast Fission Power Reactor driven by Fusion-Neutrons

Fig. 18 : Fusion-Hybrid Energy Strategy.

Time Schedule for EURAC*

1986 : Final Layout Design

1987-88 : Industrial Design

1989 : Improve Industrial Design - Decision - Procedure by Council of Ministers

1990-93 : 4 year Construction Period

1994-95 : Start up Period to Full Power

1996 : Start of Routine Operation
[LAMPF has now an availability of 85%]

*European Accelerator Neutron Source : **EURAC**

Fig. 19 : Time Schedule for EURAC

Proceedings of the Eighth Meeting of the International Collaboration on Advanced Neutron Sources (ICANS-VIII)
8-12 July 1985, Rutherford Appleton Laboratory Report RAL-85-110

Remote Temperature Measurement Using Resonant Epithermal Neutrons and the Need for a Compact Pulsed Source

P.H. Fowler
H.H. Wills Physics Laboratory
University of Bristol

My work in this area arose out of a visit I made to Rolls Royce in Spring 1984 to see how the Bristol University Physics Department might play a part in the developments in Rolls Royce. A need for a non-invasive measurement of temperature of critical parts of aero-engines while running was stressed upon me. As a result a test exposure was made in September to epithermal neutrons at Los Alamos by Dr. A.D. Taylor of Rutherford Appleton Laboratory (RAL) and myself using test specimens of Tantalum and a high temperature alloy MARM 002 that contained W, Ta and Hf in suitable proportions. The specimens were held in an evacuated instrumented oven - and held at several temperatures up to 1,000^{o}K.

As an introduction to results we obtained from these test exposures Fig. 1a sketches the main components of the beam line, and Fig. 1b shows a typical time of flight spectrum with a thin tantalum foil in the oven that was in this case at room temperature. The most prominent feature at 1111μsec corresponds to the 4.28eV tantalum resonance, and that at 718μsec to the 10.6eV resonance. Many of the remaining features are due to cadmium in the beam line employed to remove thermal neutrons - the strongest being at 440 sec. Figure 2 shows the effective cross section for the 4.28eV tantalum resonance for five different temperatures spaced by 200^{o}K. The effect of temperature is due to the well known phenomenon of Doppler broadening which is pronounced on the intrinsically narrow resonances of the heavy elements. Also shown is the difference in cross section for a change of 200^{o}K in temperature. The sensitivity to temperature change takes the approximate form of the second derivative of the cross section with energy. Two of the main measurements are displayed in Fig. 3 which shows time of flight spectra at two temperatures using 8mm of MARM 002 as the specimen. Direct comparison with Fig. 1b shows at once the presence of many additional deep resonances due to the hafnium and tungsten, as well as those due to the tantalum in the specimen. However casual inspection of the two spectra

shows little obvious difference with temperature. The differences can however, be vividly revealed by dividing one spectrum by the other bin by bin. Clearly, if nothing had changed, the ratio should be a constant, and unity if the exposures were the same. What is seen is displayed in Fig. 4a. Each well separated resonance is replaced by the form indicated in Fig. 2b, and the effects are quite large - in some bins up to a factor of two either way. Fig. 4b shows an enlarged version of the 1.10 eV Hf^{177} resonance, together with the counting errors in each bin. Our analysis of this resonance yields an estimated accuracy ΔT of $\pm$ 11°K, which is reduced to $\pm$ 5°K when one includes the information contained in the other resonances. The six most informative resonances are tabulated below, two pairs overlap and each yield one estimate.

TABLE

E_o eV	Nuclide	Flight time μ sec	μ_o Attenuation lengths	ΔT °K	
1.10	Hf^{177}	2194	2.4	$\pm$ 11.1	
2.38	Hf^{177}	1489	4.9	$\pm$ 10.4	
4.16	W^{182}	1127	5.6	$\pm$ 8.3	Overlapping
4.28	Ta^{181}	1111	14.6		
7.65	W^{183}	831	2.2	$\pm$ 14.2	Overlapping
7.78	Hf^{178}	824	8.0		

μ_o is the number of attenuation lengths that the specimen presented at the centre of the resonance in the absence of any Doppler broadening.

The temperature measurements described above are in detail the mean temperature of the atoms of the particular nuclide that forms the resonance, the mean being taken over the neutron path. If, say, tantalum is present in a blade - and not in any other material in the beam - the temperature applies to the blade only. If, for a special purpose, one was allowed to coat several particular surfaces one could get several temperature measurements from the same exposure for each pixel. Such a case might occur, for example, for a static blade in an engine where one could use for the front surface Hf, for the inside of the air vents Re, and the rear Pt; with the blade itself containing W and Ta one could form a potentially most informative picture of the temperature distribution.

The detector employed in the measurements was 15 metres away from the oven as shown in Fig. 1, thus the measurements outlined briefly above met the requirement of a "remote and non-invasive temperature measurement", and we viewed the specimen through about 2 cm of stainless steel. The accuracy of temperature assignment demonstrated was $\sim \pm 5^{o}K$ at all temperatures covered $\sim 300^{o}$-$1000^{o}K$.

At Los Alamos each time of flight spectrum took us about 8 hours to accumulate, a feature which must be remedied. A higher neutron flux and an improved detector are clearly called for. During the early commissioning phase the SNS will give us more neutrons than were available at Los Alamos in 1984. (Considerable enhancement has also taken place there in the intervening period), and that will increase by a further factor approaching 10^{2}. The SNS at the Rutherford Appleton Laboratory can provide us not only with adequate neutron fluxes, but also with an ideal environment for the development of the technique so as to prove (or otherwise!) its practicability.

With regards to the detector system - much must be done to improve performance. For a start I am proposing an instrument based on scintillators whose form is as approximated in Figs. 5 and 6. The initial specifications I have in mind are along the following lines:-

a) A high neutron count rate capability - initially at an instantaneous rate $> 10^{5}$/sec in each independent detector element - i.e. $> 10^{2}$ neutrons per pulse per detector. This should be increased to $\sim 10^{6}$/sec for the next phase.

b) A reasonable position sensitivity $\sim \pm$ 1mm FWHM for both Δx and Δy. Δx is given by the partition of light between the pairs of photomultipliers that view each scintillator. Y is determined from the actual detector in which the neutron is in fact captured. With a scintillator thickness of 1 mm the effective value of FWHM for Y is $\sim$ 0.8 mm. The white device will have $\sim$ 2000 such pixels.

c) The expected good time resolution for each neutron giving an energy estimate accurate to one part in 1000.

d) Adequate defences against background γ-rays from the target - delayed by β-decay. To this end Li^{6} is superior to glass scintillators as a neutron has the same pulse height as an electron of $\sim$ 4 MeV. In the glass the neutron appears similar to an electron depositing an energy of $\sim$ 1 MeV only.

This brings me to the second part of this talk. There is an additional constraint that Rolls Royce feels to be essential. If this technique - or any related one - is to be of quite widespread use in Industry - then the neutron source must be where the work is - and not the other way round. This implies

for Rolls Royce that the neutron source be

compact and possibly mobile

cheapish

and be sited at Bristol and/or Derby.

The SNS does not appear to approach this Rolls Royce wish! But is there a possible system when one tailors the accelerator to meet the main requirement. The SNS is designed to produce $\sim 4.10^{16}$ neutrons/sec. I believe that a yield $\sim 10^{14}$/sec of pulsed epithermal neutrons would be of great use. It is however the brightness of the neutron source (n/cm^2.sec.sterad.) that is the most important characteristic - and not the yield.

In Fig. 7 I give a rough sketch of a possible compact system for producing a suitable neutron beam. The following comments apply to the various elements:-

a) In the accelerator area one has the choice of energy, the higher the energy the better the figure for joules/neutron that is to be traded off with the increase of cost and size with energy. Deuterons must also be considered for their higher neutron yields at a given speed and their lower sensitivity to synchrotron stripping of the negative ion.

b) To get the pulsed beam a storage ring may be necessary, separated as suggested in the figure, but also the storage could be made in the outer regions of the accelerator. The maximum storable current increases with increasing energy. The amount of storage required is reduced if one can operate at $\sim$ 1 kHz which is possible if a short flight path D $\sim$ 10 m is satisfactory. As drawn in Fig. 7 a superconducting cyclotron offers the possibility of a compact accelerator.

c) In the target and moderator areas the difference in emphasis occurs because of the need for a bright source. With any energy $\lesssim$ 100 MeV the range of the accelerated beam in the target is small, say $\lesssim$ 1 cm. This enables the moderator to be well coupled to the target. The neutrons are peaked forward at production which helps. So possible target materials are, say, Li or Be for either D or low energy H beams, and perhaps U if a higher energy is chosen - say, $\gtrsim$ 40 MeV.

d) The moderator needs to have as high a figure as possible for the density of H, possible materials that come to mind are VH_2, dense polyethylene or solid unbranched paraffins, or even $N_2H_4.H_2O$. With the much lower energy input heat problems for the moderator should not be a problem so that the overall H density can remain high. The desired energy band for which one is aiming to optimise the brightness is $1 < E < 100$ eV, and not thermal energies, so the amount of moderator necessary is not as large as in the SNS systems.

e) One is also aiming to feed one beam line only so reflectors of say, natural Ni (or even Ni^{58}) all around the moderator will help. The neutrons enter the moderator with E $\sim$ 1 MeV where the cross section is low ($\sigma\sim$ 3 barns), and after a few collisions on H their energy is ideally so reduced that the "reflector" has become efficient - as the cross section of Ni is $\sim$ 17 barns. The reflector may also with advantage incorporate a thin layer of Mn, V and Co to take advantage of their very large resonant scattering cross sections in the range $100 < E < 20000$ eV.

f) Outside the nickel reflector U^{238} could usefully be employed as an additional blanket, especially in the beam direction where most of the high energy neutrons go, to help the neutron economy by fission.

The aim of this neutron system when feeding an appropriate detector is to give an exposure E_x given by

$$E_x \sim 10^7 \frac{dE}{E} \quad \text{detected neutrons/cm}^2,$$

in a "reasonable" time, say, $< 10^3$ sec,

with an angular spread at the detector $\theta_{max} < 10^{-3}$ radians,

and with a flight path D $\sim$ 10 metres.

A yield from the target of N neutrons/sec should produce a moderated spectrum at the exit slit of:

$$dN_E = \frac{N}{18} \cdot \frac{f g}{4\pi^2 a^2} \cdot \frac{dE}{E} \quad \text{neutrons/cm}^2\text{.sec.ster},$$

where $4\pi a^2$ is the surface area of an assumed spherical moderator, with a $\sim$ the RMS migration of a neutron in moderation to $\sim$ 10 eV, the factor 18 normalises the dE/E spectrum from thermal energies to 1 MeV, the extra π is of course the effective number of steradians fed by the output, and the factors f and g are "fudge factors".
The factor f is concerned with the coupling of the target to the moderator and allows both for the forward peaking of the neutrons and for the penetration of a fraction without interaction. The factor g applies to the moderator and its coupling to the exit slit, it represents the enhancement over a spherical moderator due to the Ni reflectors, for losses due to escape and capture, and for an extra contribution to the neutrons from fission in the uranium blanket backing up the nickel. A plausible range for each of the factors f and g seems to be $1 \lesssim f, g \leq 3$.

To meet our requirements at the detector, we must restrict the aperture to $\theta_{max}^2 D^2$ cm^2 if D, the flight path, is measured in centimetres; the value for the solid angle is then fixed at $1/D^2$ per cm^2 of detector. Thus at the detector we can expect to have

$$dN_d = \theta_{max}^2 \frac{N}{18} \frac{f\,g}{4\pi^2 a^2} \frac{dE}{E} \quad \text{neutrons/cm}^2\text{,sec.}$$

Substituting $f = g = 1$, $N = 10^{14}$, $\theta_{max} = 10^{-3}$ and $a = 4$ cm,

we obtain as an approximate estimate for the neutron flux at the detector;

$$dN_d \sim 10^4 \frac{dE}{E} \quad \text{neutrons/cm}^2\text{,sec.}$$

Thus we could hope to meet our target exposure E_x in a time of less than 1000 seconds. Such an exposure would - with a suitable specimen - give temperature estimates accurate to $\pm 5^{\circ}$K for each cm^2. Clearly, there is considerable work to do so as to approach the most suitable system - and realise a practical compact pulsed neutron source. I believe these aims to be within reach, and if so the system could have quite widespread use. I therefore invite your comments.

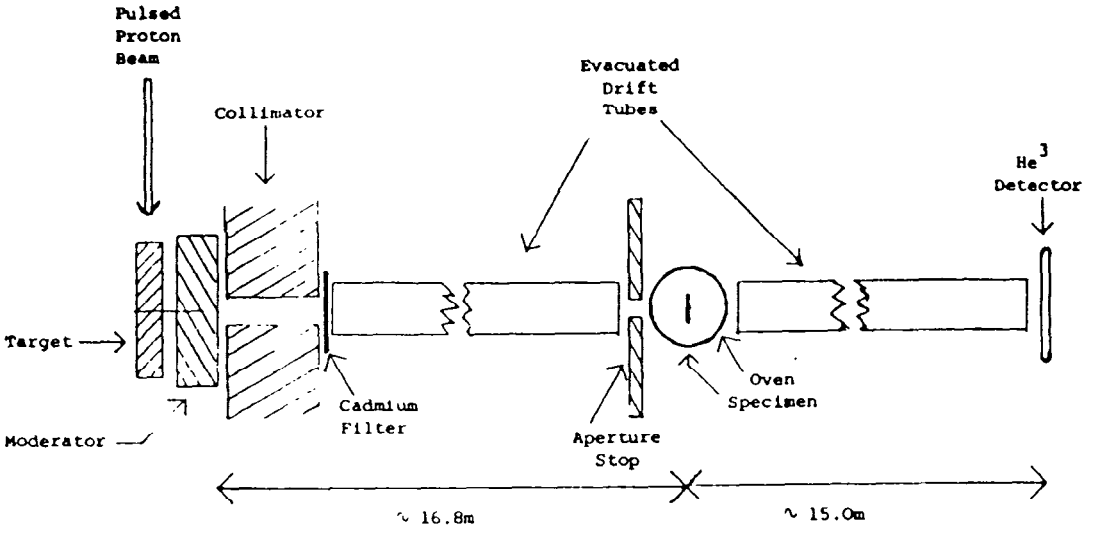

Fig. 1a Sketch of the experimental arrangement used at Los Alamos

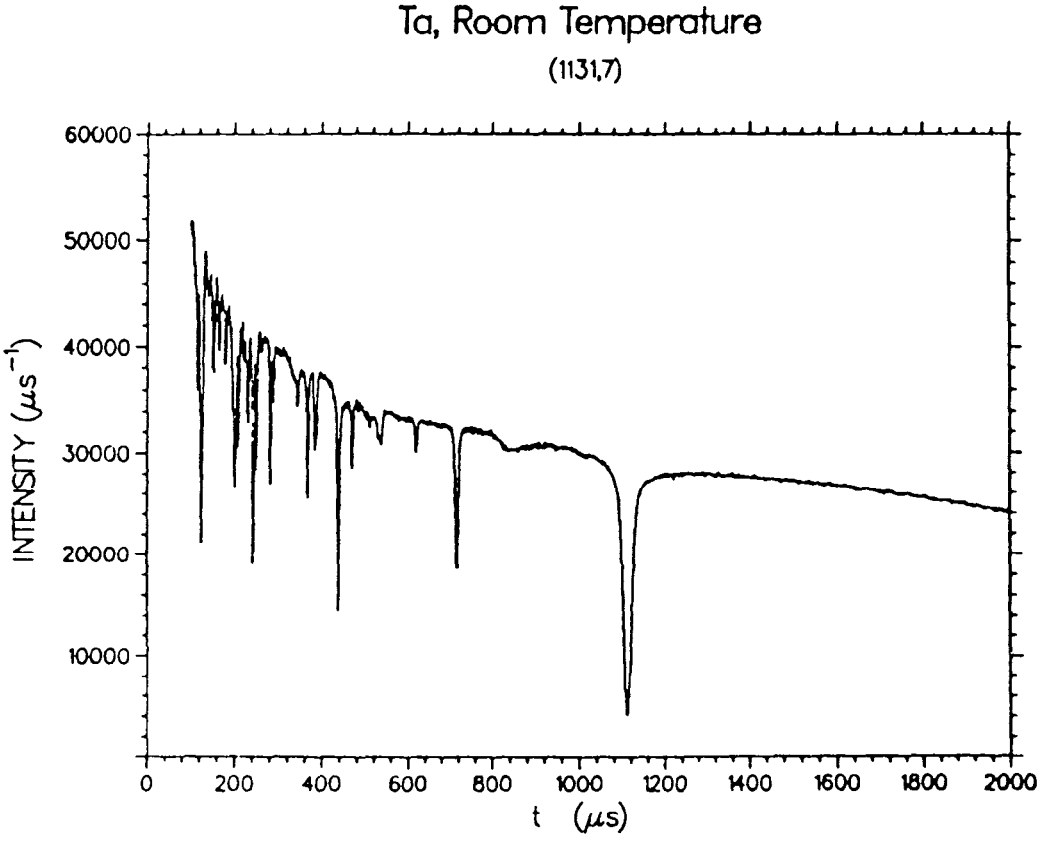

Fig. 1b The time of flight spectrum using a thin (27 μm) Tantalum foil

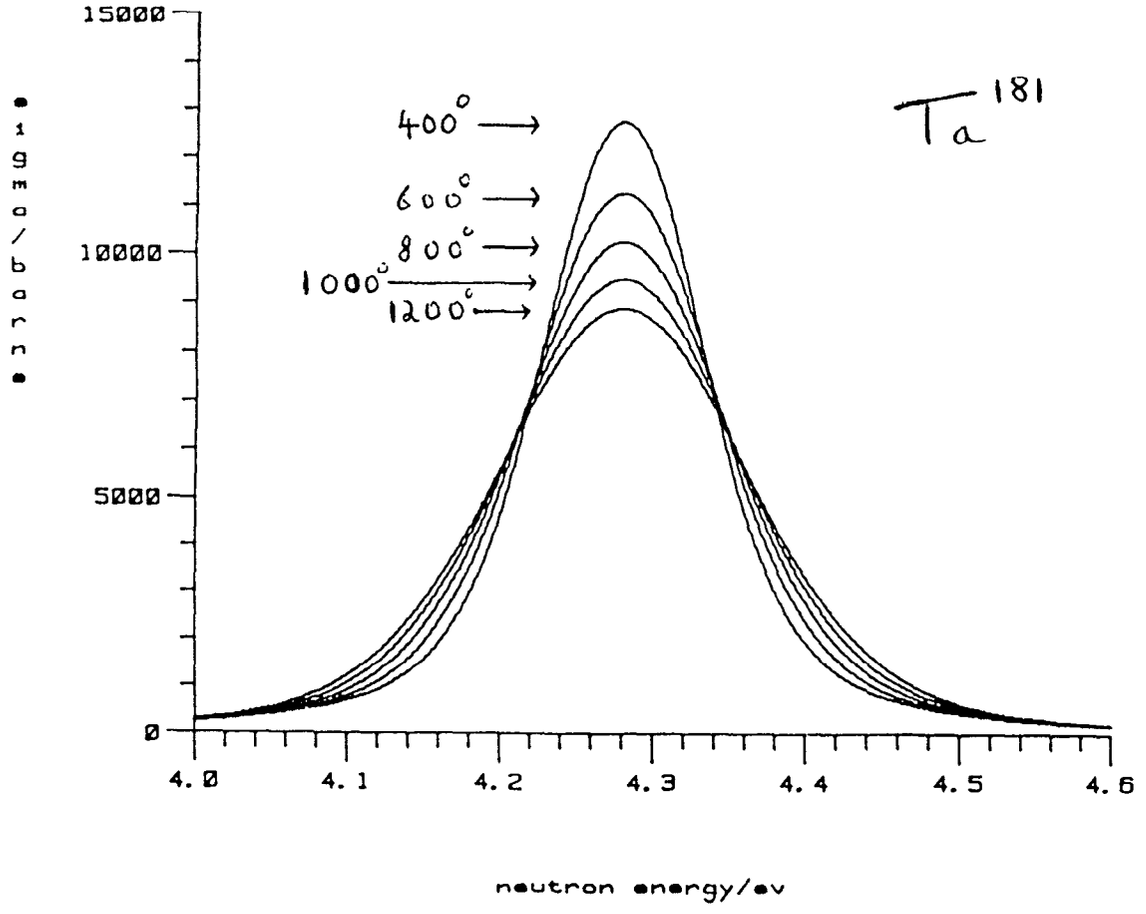

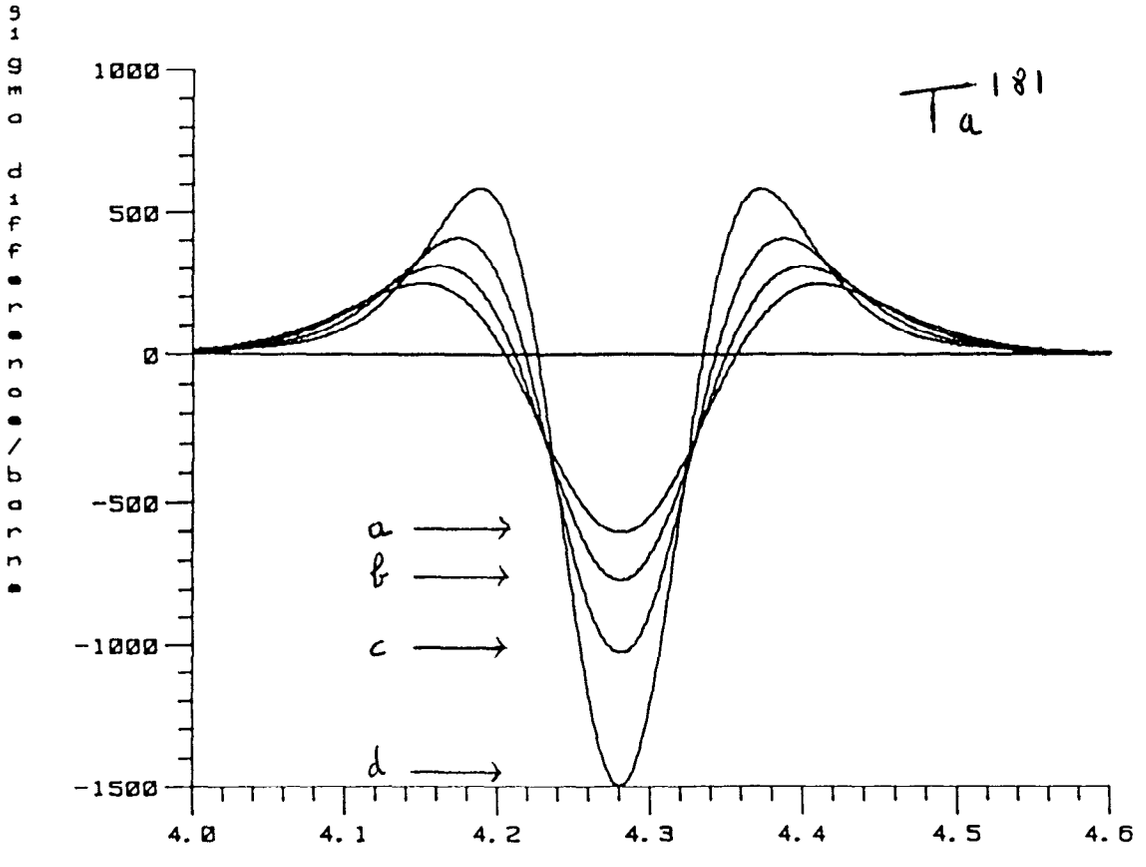

Fig. 2a,b Computed cross sections at 5 temperatures for the 4.28 eV Tantalum resonance, and the change in cross section for successive 200°K temperature increases.

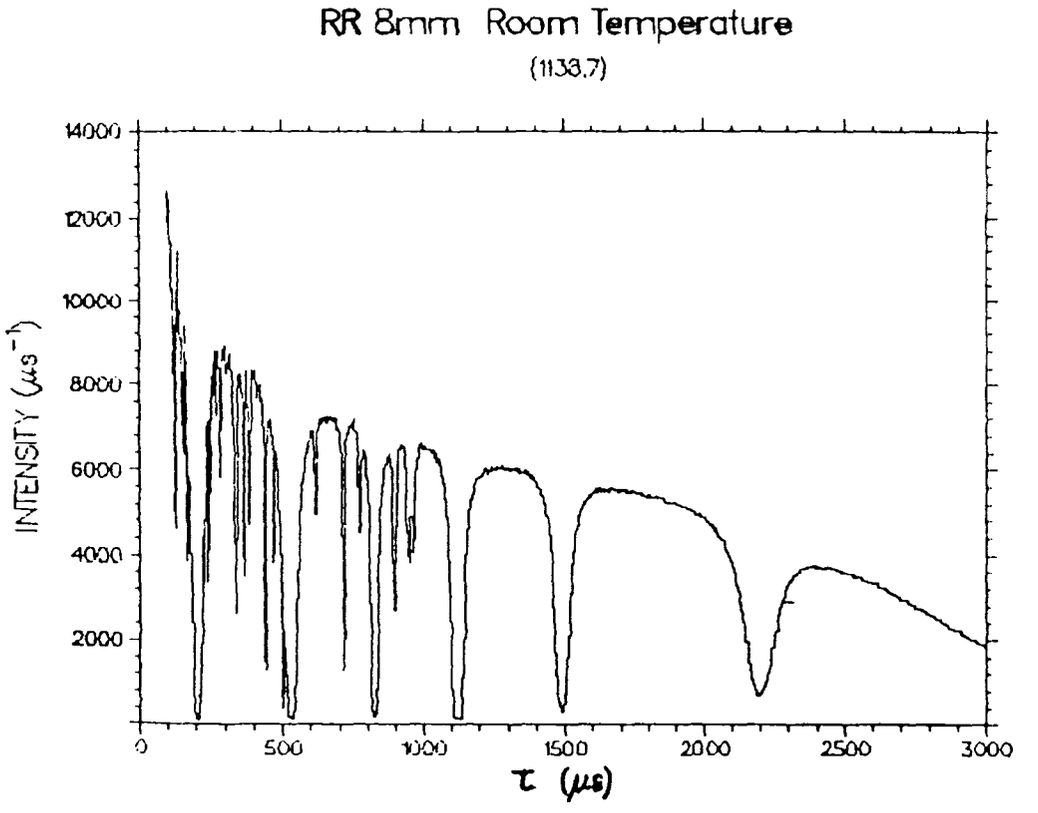

INTENSITY VERSUS DRIFT TIME

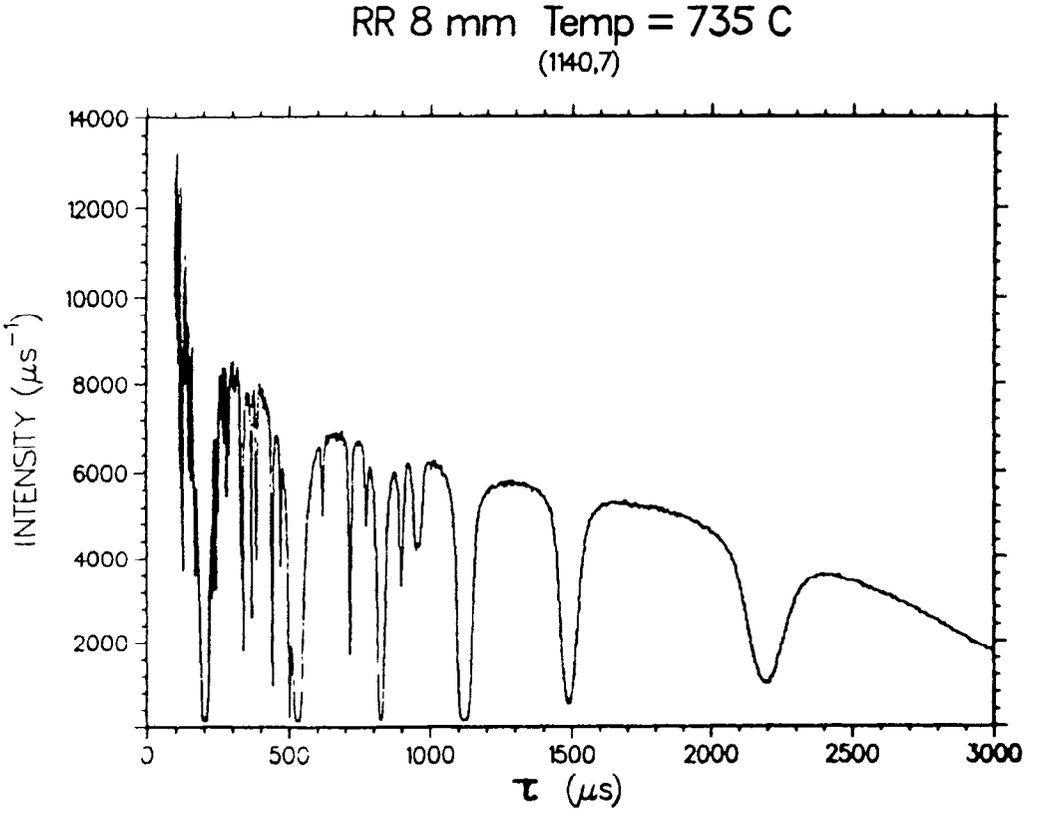

Fig. 3a,b **Time of flight spectra at 20°C and 735°C using 8 mms of MARM 002**

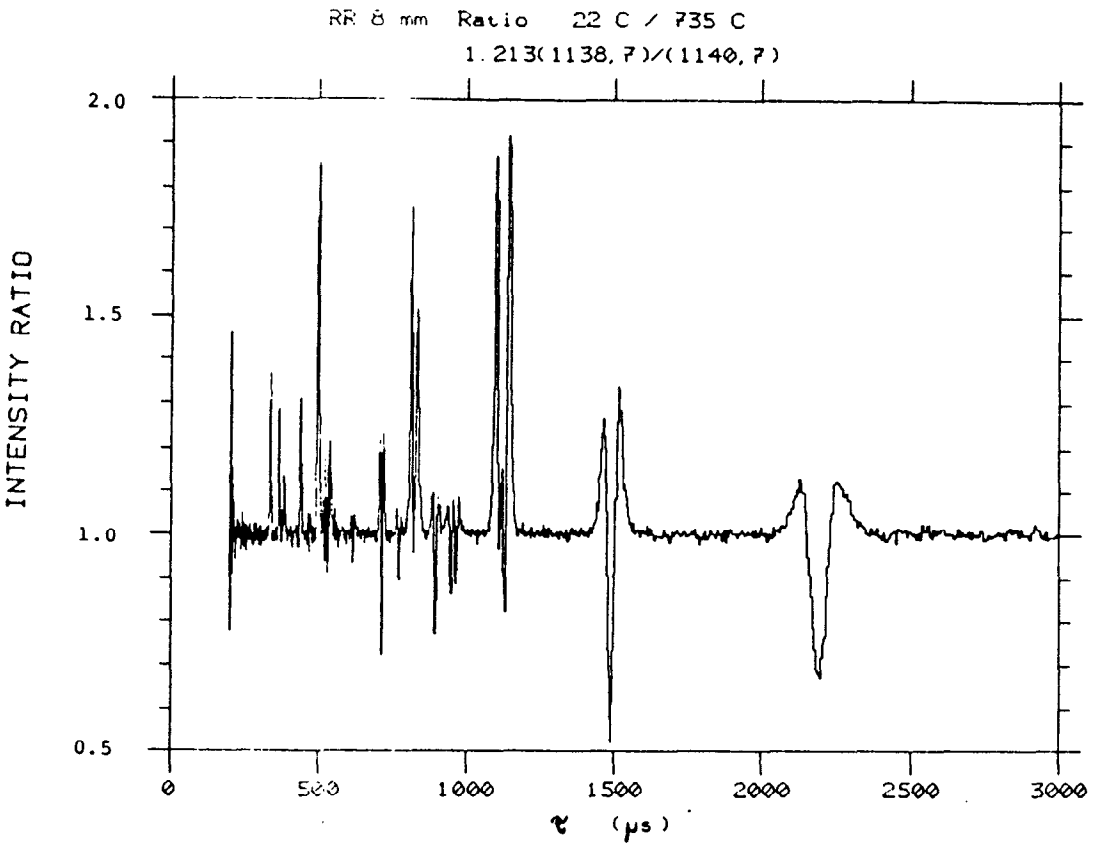

Fig. 4a The intensity ratio versus time of flight from the data given in Figs. 3a and b.

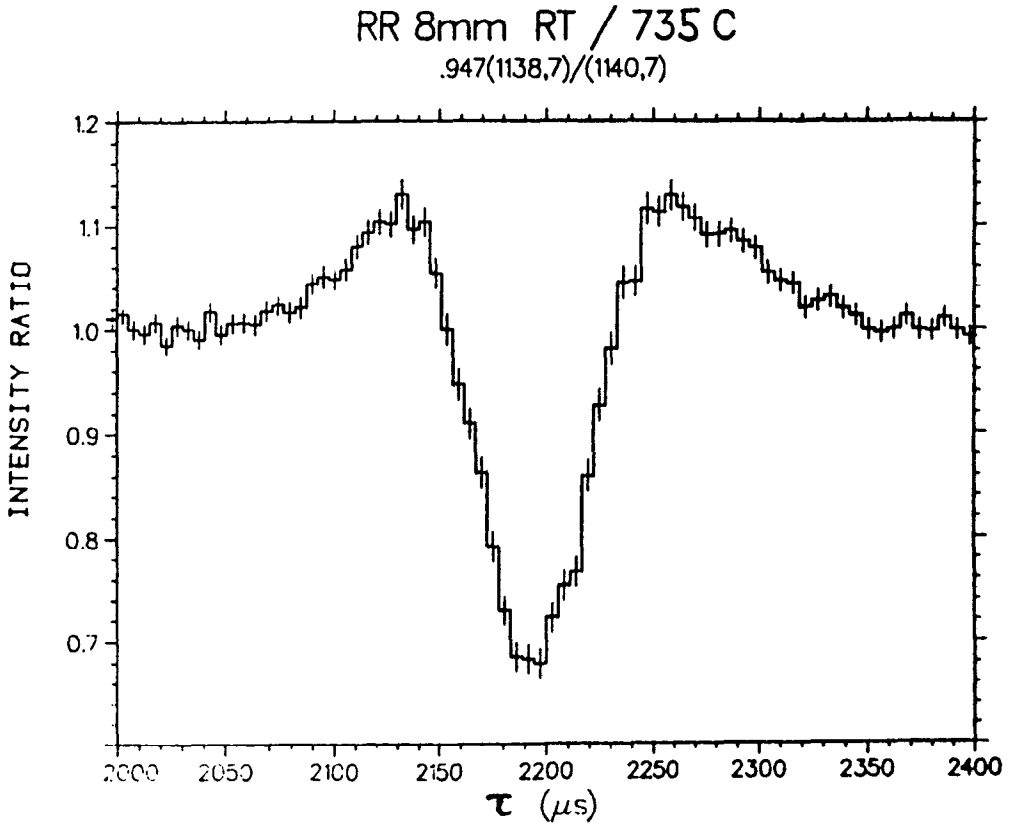

Fig. 4b Details of the intensity ratio from Fig. 4a above for the resonance at ~ 2200 μsec due to Hf^{177}. Statistical errors are given for each bin.

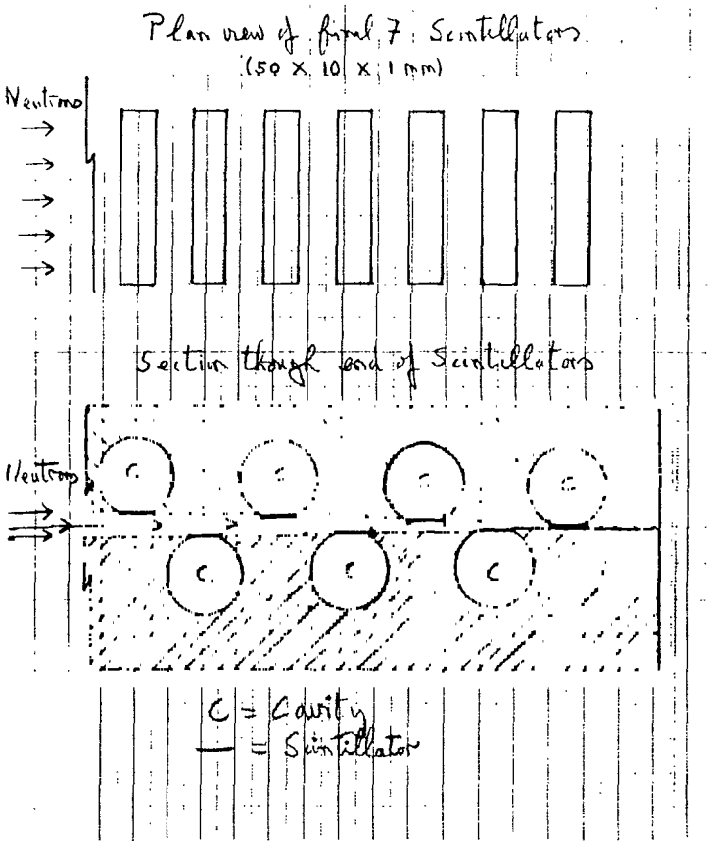

Fig. 5 The plan and side views

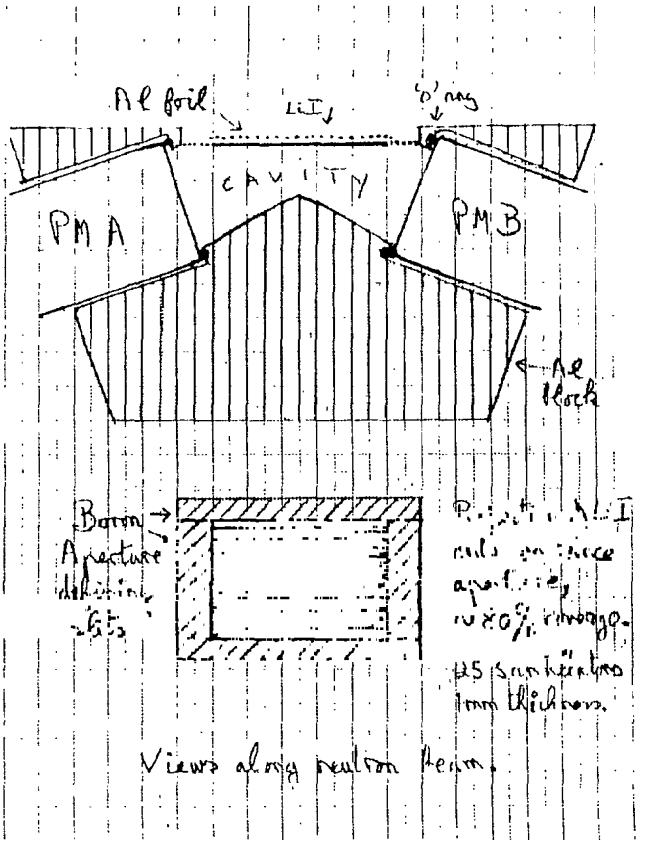

Fig. 6 Two sections as viewed along the neutron beam axis

Figs. 5 and 6. Suggested arrangement for an efficient positional sensitive epithermal neutron detector based on scintillators

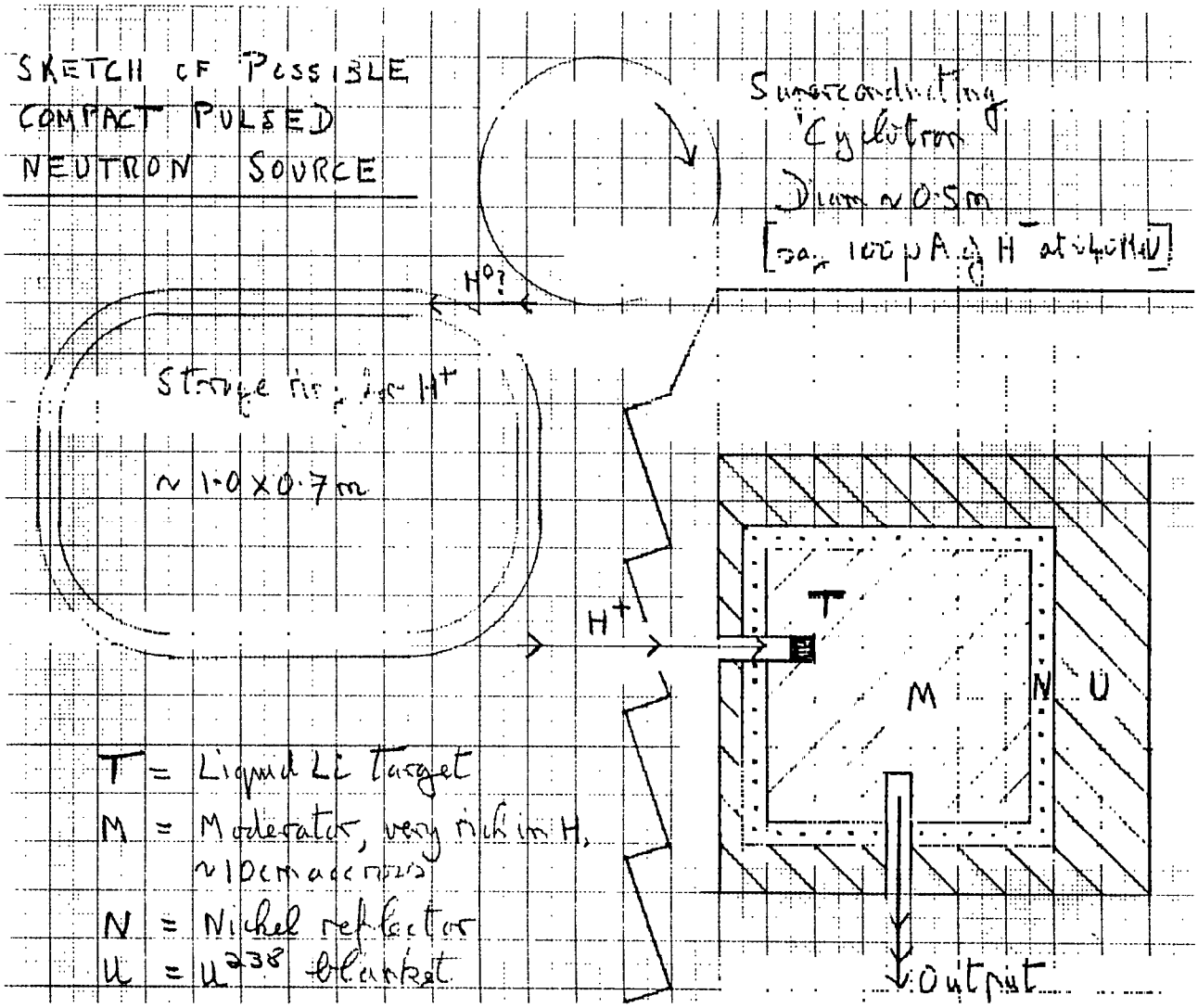
SKETCH OF POSSIBLE
COMPACT PULSED
NEUTRON SOURCE
Superconducting
Cyclotron
Diam ~ 0.5m
[ca. 100 μA of H⁻ at 4 MeV]
H⁰?
Stripper for H⁺
~ 1.0 × 0.7 m
H⁺
T
M
N
U
T = Liquid Li Target
M = Moderator, very rich in H,
~ 1 Dem accuracy
N = Nickel reflector
U = U²³⁸ blanket
Output

FIGURE 7

Proceedings of the Eighth Meeting of the International Collaboration on Advanced Neutron Sources (ICANS-VIII)
8-12 July 1985, Rutherford Appleton Laboratory Report RAL-85-110

NUCLEAR ASPECTS OF THE SNQ TARGET DESIGN

D. Filges, P. Cloth, R.D. Neef, H. Schaal
Institut für Reaktorentwicklung, Kernforschungsanlage Jülich

Very detailed nuclear aspects for the SNQ target-moderator-reflector systems were studied for engineering and safety purposes. In this paper only some important aspects are shown. For further details see Ref. /1/.

Computational Models and Methods

The latest state of the art of radiation transport codes and methods treating the various types of interaction mechanisms were further developed and now in such a state that very sophisticated and detailed nuclear aspects can be considered. The scheme of performance with the capabilities is given in Figure 1. The most advanced Monte Carlo codes like a special version of the high energy transport code HETC-KFA and MORSE are running on KFA's CRAY-XMP. 3-D computer models of the SNQ target-moderator-reflector system for the calculations were used taking into account all necessary material and geometrical conditions /2/. A vertical cut is shown in Figure 2.

Energy Deposition for SNQ Targets

Spatial dependent energy deposition calculations in fine radial and axial mesh intervalls for tungsten and uranium target

systems were performed to assist in designing cooling circuits and thermal cycling calculations. In Figure 3 a horizontal and vertical cut of the mesh grid is given. In Table 1 and 2 the total energy deposition and the peak energy deposition for 1100 MeV proton beam energy for a SNQ tungsten and uranium targets are given. Figure 4 shows the depth dependent energy deposition in the target wheel for two radial intervalls (radius = 0.0 - 1.0 cm and radius = 1.0 - 2.5 cm) about the proton beam axis.

Table 1: Total energy deposition in target for 1100 MeV proton beam energy

	Deposition Power MeV per Proton High Energy $E > 15$ MeV	Low Energy $E \leqq 15$ MeV	Total Power MW per 5 mA
U_{dep}-Target	945	1263	11.4
W-Target	620	65	3.4

Table 2: Peak* energy deposition in target for 1100 MeV proton beam energy

	Deposition Power MeV per Proton		Total Peek Deposition
	High Energy $E > 15$ MeV	Low Energy $E \leqq 15$ MeV	kJ/cm^3 per pulse**
U_{dep}-Target	2.62	0.73	0.168
W-Target	2.04	5.0×10^{-2}	0.105

* for radial intervall about beam axis r = 1.0 cm

** assumed $\hat{I}$ = 200 mA, pulse width 250 µs pulse frequency 100 s^{-1}

Induced Radioactivity and Afterheat Production of Uranium Target Wheel

A detailed procedure to calculate in a spallation facility the time behaviour of radioactivity, thermal power, nuclide numbers etc. caused by a proton beam on a uranium target has been developed /3/.

All calculations were performed for the target area of the SNQ. This means that the target wheel contains depleted uranium, that the proton beam energy is 1100 MeV, and that the beam current is 5 mA. The geometry of the target station - consisting of target wheel, D_2O-tank, neutron beam tubes, moderators etc. - used for the Monte-Carlo-calculations is described above.

For the calculations of the nuclide generation and depletion the codes ORIGEN /4/ and ORIHET /5/ were used. Only the geometry of the wheel is of interest. The model for this target wheel is shown in Fig. 5. It can be seen that the active target zone has a height of 10 cm and a depth of about 40 cm. In Fig. 5 this zone is described by the regions 1 to 4. It should be mentioned that the active target zone consists of uranium pins with aluminum cladding. These pins have got diameters from 1.824 cm up to 2.4 cm. The pins are surrounded by the cooling water. In the calculations the uranium, the aluminum, and the water are described as one homogeneous mixture of the target region /3/.

For the SNQ target wheel an irradiation time of two years is proposed with two operation periods of about 6000 hours. The calculations were performed assuming 12000 hours of operation without any shutdown of the beam. This procedure leads to the highest possible values of radioactivity and of afterheat production. The results are separately given for the products

arising from spallation effects, i.e. calculated by code HETC, and those arising from the neutron flux with neutron energies less than 15 MeV, i.e. calculated by code MORSE.

Integral results after 1200 hours at operation are given in Table 3 and zone dependent results after 1200 hours of operation are given in Table 4. From Table 3 the total amount of radioactivity for t=0 is 45.1 MCi, where 7.5 MCi stem from spallation and 37.6 MCi from neutron flux and here 22.5 MCi from the chain ^{239}U - ^{239}Np - ^{239}Pu. The time behaviour of radioactivity is shown in Fig. 6 for spallation, for neutron flux, and for total. It can be seen that one day after shut down of the beam the sum is decreased to 12.6 MCi.

Table 3: Integral results after 12000 hours of operation

Radioactivity total	: 45.1	MCi
- caused by spallation	: 7.5	MCi
- caused by neutrons $E_n < 15$ MeV	: 37.6	MCi
- maximum per target pin	: 21	kCi
Afterheat total	: 415	kWatts
- caused by spallation	: 120	kWatts
- caused by neutrons	: 295	kWatts
- maximum per target pin	: 0.19	kWatts
Gaseous products		
- total amount	: 3.42	g-atoms
- maximum per target pin	: 1.6×10^{-3}	g-atoms

Maximum thermal power (after heat) is 415 kW, were 120 kW stem from spallation and 295 kW from the neutron flux. The time behaviour of the thermal power for spallation reactions, for the neutron flux reactions, and for the total thermal power is shown in Fig. 7. From this figure it can be seen that the total thermal power after 1 day (10^5 sec) is decreased to 49 kW.

From Table 4 it can be seen that in region 2, i.e. about 8 cm inside the target wheel, we find the maxima of the densities of thermal power, radioactivity, and gas amount. Now we can roughly estimate the maximum amounts per pin.

Table 4: Zone dependent results (zones 1-4) after 12000 hours of operation

	Target region number			
	1	2	3	4
Thermal power (kW)	15.50	133.00	228.00	38.50
Thermal power density (W/cm^3)	1.60	2.10	1.70	0.90
Activity (MCi)	1.68	14.40	24.80	4.20
Activity density (Ci/cm^3)	171.00	229.00	185.00	92.80
Gas amount (g-atoms)	0.13	1.09	1.88	0.32
Gas amount density (10^{-5} g-atoms/cm^3)	1.30	1.73	1.40	0.70

It should be emphasized once more that all results given here do not take into account the influence of cladding material (aluminum) and of the cooling water because of lack of data in the libraries of the code ORIHET.

Calculation of the Time Dependent Dose Rate of the SNQ-Target Cooling Water for Radiolysis Considerations

The irradiation history of the SNQ-target wheel cooling water is due to the motion through the radiation field in azimutal direction by the spinning of the target wheel and radially by the flow of water from the axle to the circumference and back. For the calculational procedure the wheel was azimutally divided into 200 sectors corresponding each to a time interval of 0.01 s or one proton beam pulse.

The flow path can be described by a sequence of meshes. The 200 different partial flows are described simply by rotating the azimutal indices of that mesh sequence. The turn around time of the water flow from entering the wheel into a certain sector and appearing at the outlet within an other sector is 0.56 s or exactly 56 in terms of proton pulses. In Figure 8 the mesh grid and the water flow path through the mesh grid is shown.

The necessary nuclear calculations were performed using the HETC-KFA-1 code and the evaluation code SIMPEL for the radiation energy region above 15 MeV /1/. At low energies (up to 15 MeV) MORSE was run for neutrons and gammas using the 100 neutron and 21 gamma group cross section library EPR /6/. Calculations of stopping powers were performed by the SPAR code /7/. In Table 5 the total deposition powers of different radiation types are given.

Table 5: Total deposition power of different radiation types

type of radiation	total average deposition power	energy range
neutrons	110 kW	0.41 eV - 15 MeV
γ-rays	30 kW	0 - 14 MeV
protons	68 kW	0 - 1100 MeV
pions	2 kW	15 - 400 MeV
heavy ions	3 kW	all energies
all radiation	213 kW	

In Figure 9 the energy deposition power of neutrons are given as an example in the sectors 156-165. This is the situation when the partial flow goes through the primary proton beam near the target circumference. Figure 10 shows the averaged deposition power for neutrons over all sectors. All power deposition curves of all particle types are fed into the

FACSIMILE code in order to obtain time dependent densities of radiolysis products. This has been done by W.G. Burns, Harwell. A report about the details of these calculations will be published /8/. Figure 11 shows as an example the H_2 concentration in Mol per litre.

References

/1/ Physics for Relevant SNQ Target Systems
To be published as Jül-Report

/2/ P. Cloth, D. Filges, R.D. Neef, H. Schaal
Recent Target Design Calculations at KFA
Proceedings ICANS-VII, 1983 Chalk River,
AECL-8488-1984

/3/ H. Schaal, G. Sterzenbach
Internal Report, SNQ 3J./BH 271184, Nov. 1984

/4/ V.J. Bell
ORNL-4628 (1973)

/5/ F. Atchison
Private communication

/6/ EPR data Package, RSIC Data Library Collection
DLC-37

/7/ T.W. Armstrong, K.C. Chandler
ORNL-RSIC-228 (1973)

/8/ W.G. Burns et al.
To be published

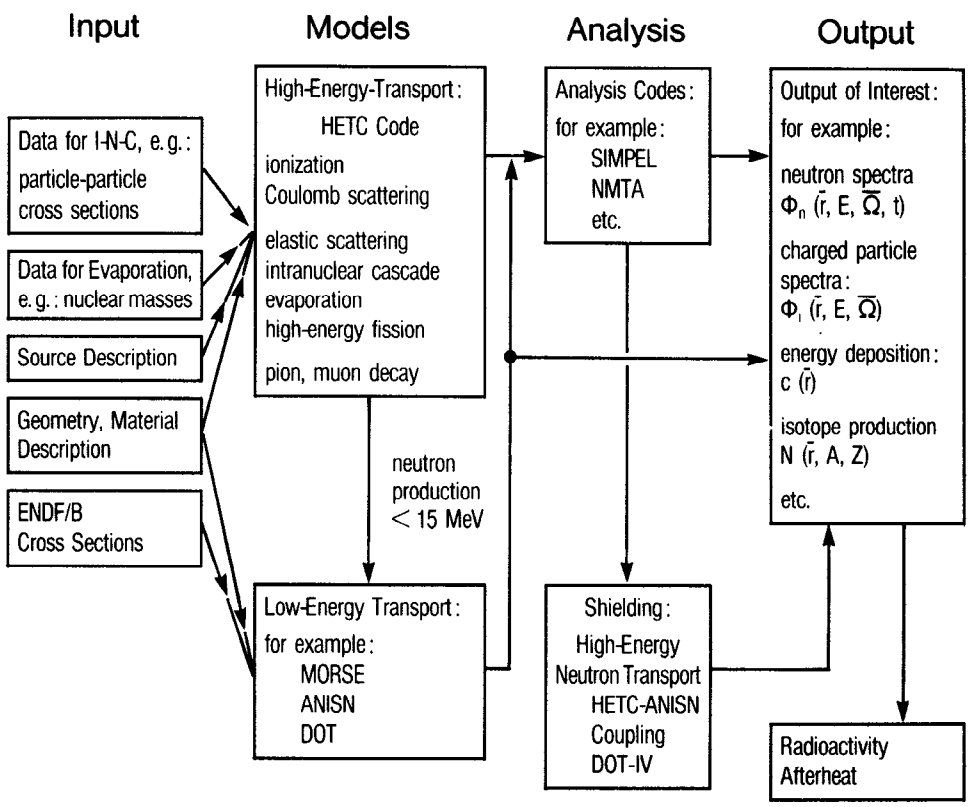

Fig. 1: Scheme of performance of radiation transport codes

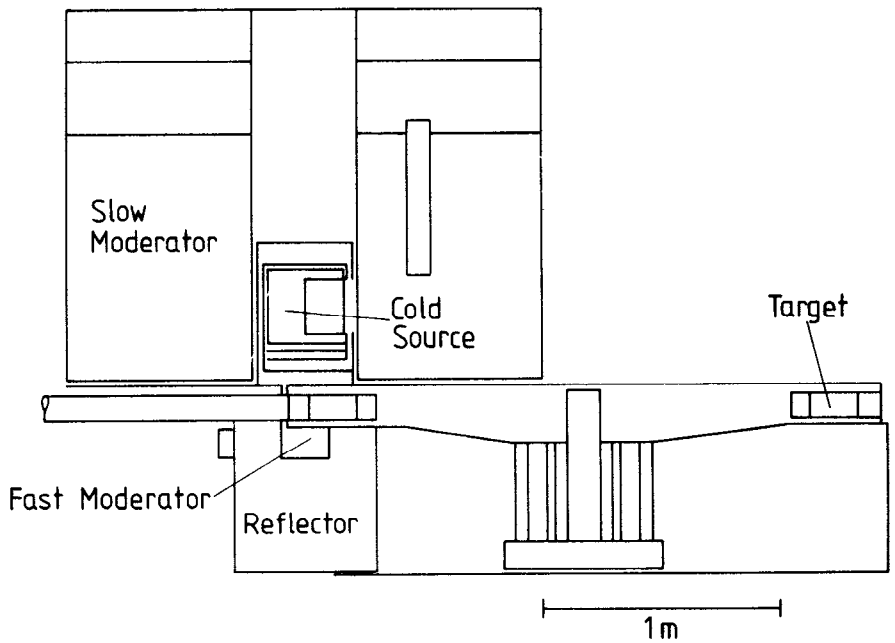

Fig. 2: Vertical cut of target-moderator-reflector-system

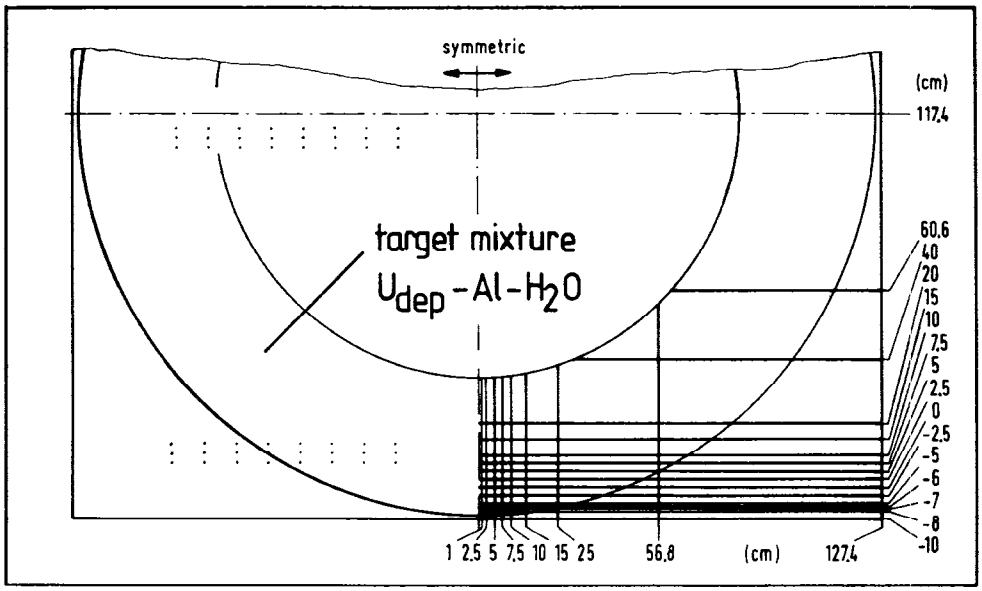

Horizontal cut

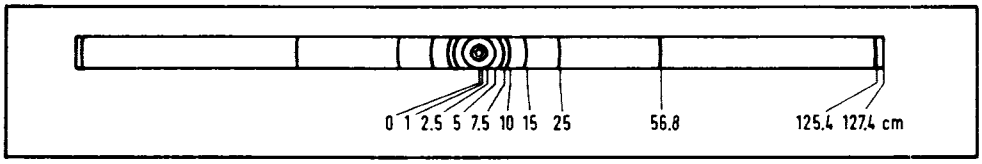

Vertical cut perpendicular to proton beam

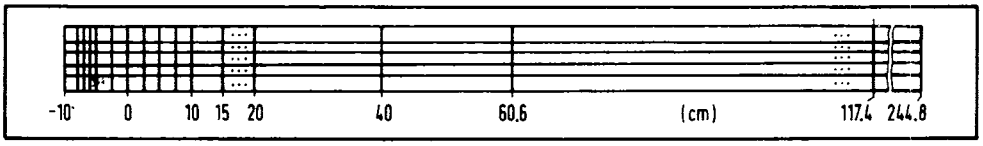

Vertical cut in beam direction

Fig. 3: Mesh grid of the target for spatial energy deposition calculations

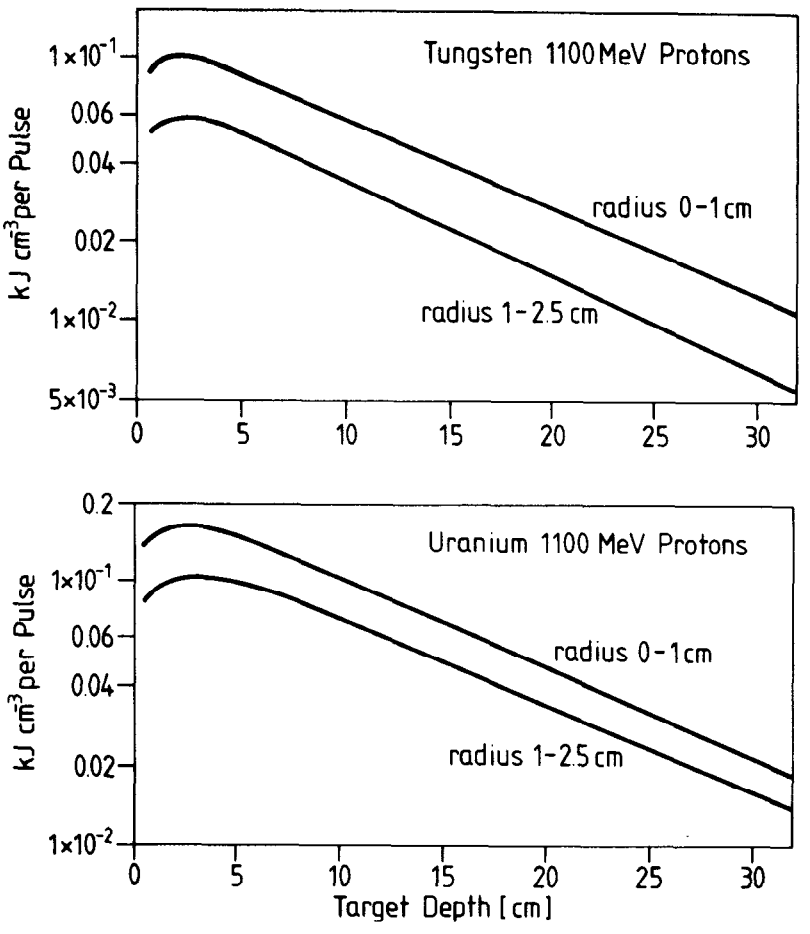

Fig. 4: Depth dependent energy deposition inside target wheel for two radial intervalls about proton beam axis

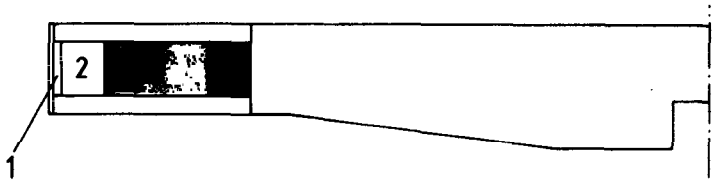

Fig. 5: Three zone model of target wheel with active zone 1-4

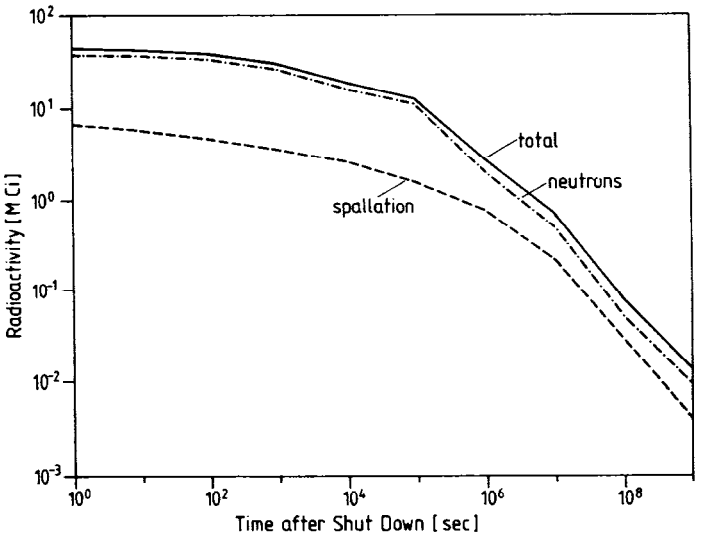

Fig. 6: Time behaviour of activity in uranium after 12000 hours irradiation

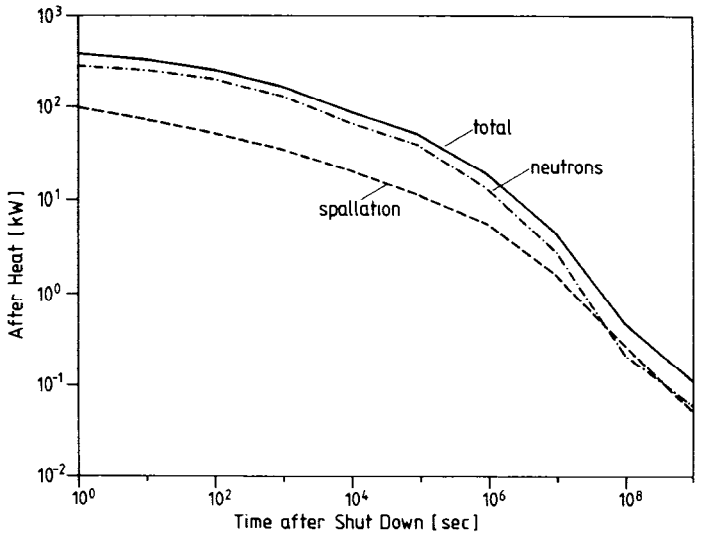

Fig. 7: Time behaviour of thermal power in uranium after 12000 hours irradiation

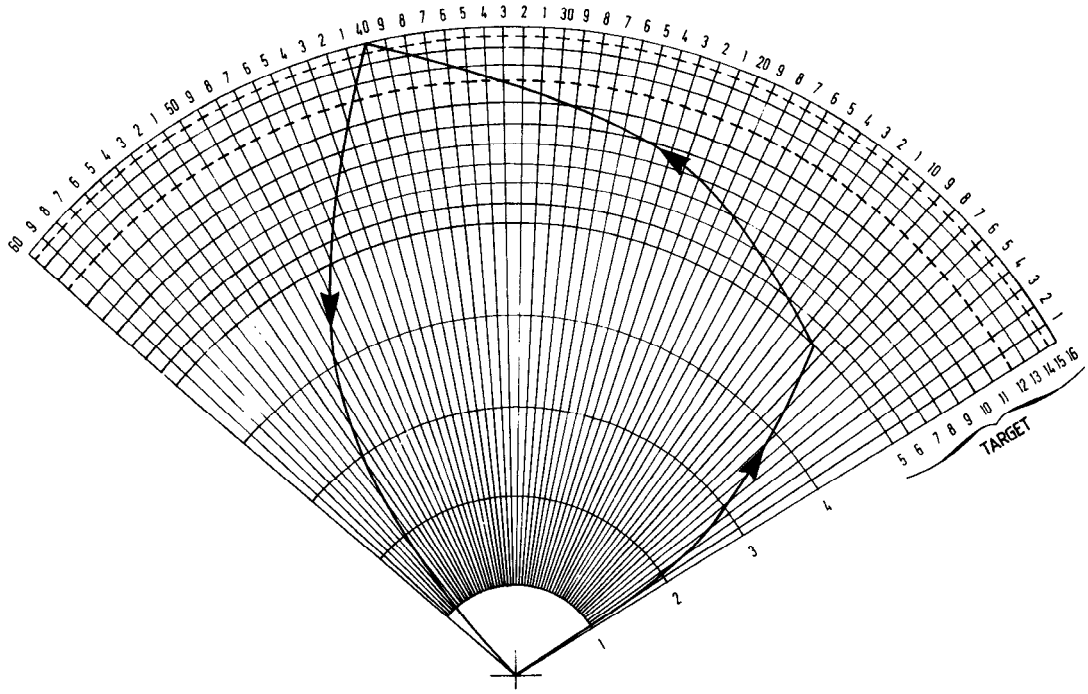

Fig. 8: Water flow path through mesh grid

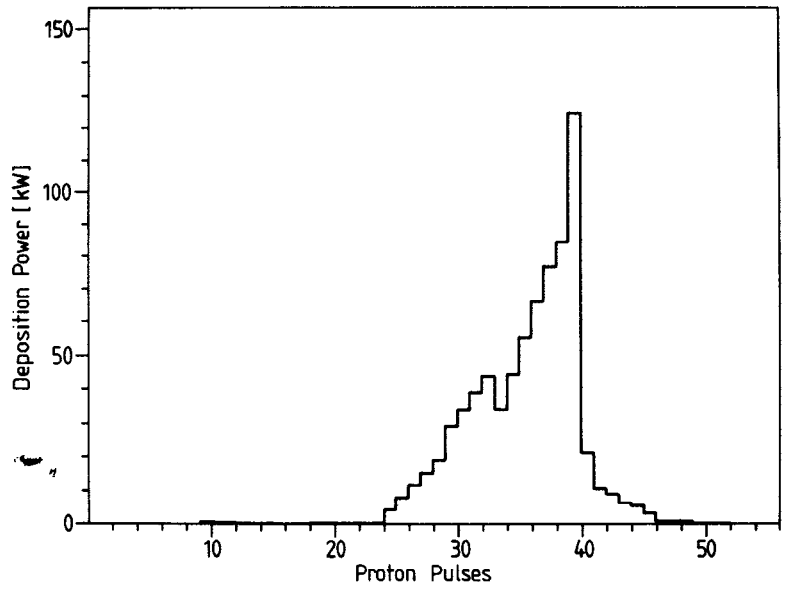

Fig. 9: Energy deposition power of neutrons (energy group 1.35-15.0 MeV) in sectors 156-165

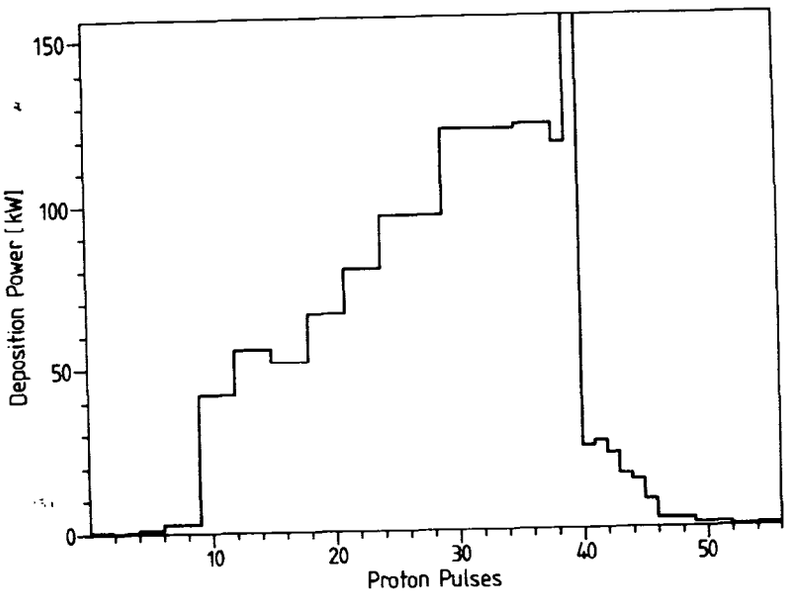

Fig. 10: Averaged deposition power of neutrons (energy group 1.35-15.0 MeV) over all sectors

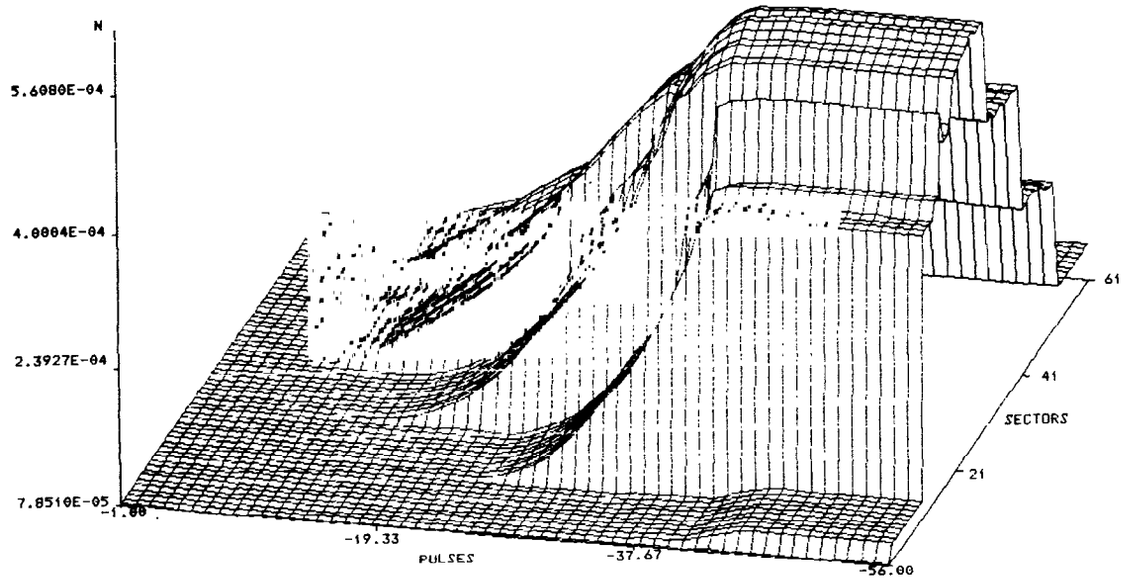

Fig. 11: H_2 concentration in mol per litre/sector/time

Proceedings of the Eighth Meeting of the International Collaboration on Advanced Neutron Sources (ICANS-VIII)
8-12 July 1985, Rutherford Appleton Laboratory Report RAL-85-110

POISONING EFFECTS IN SPALLATION NEUTRON SOURCES.

F. Atchison
Swiss Institute for Nuclear Research
CH-5234 Villigen, Switzerland

1 INTRODUCTION.

The practical design for a continuous spallation neutron source needs to take proper note of neutron economy. The critical region in and around the moderator should avoid the use of materials with a high thermal neutron capture cross-section, as far as this is practicable; for example, the excellent performance of heavy-water as a moderator stems largely from its very low capture cross-section and among many reasons why depleted Uranium is not used in the SINQ design is that the roughly factor-of-two gain of fast-neutron intensity is largely eroded by its high thermal capture probability. The actual choice of material is based on the absorption probability; the mechanical properties (strength of the material and the job it has to do) determine the thickness and it is this times the macroscopic cross-section which needs to be used in any comparison.

During operation, high-energy nucleon induced spallation reactions lead to production of nuclides which have a large thermal capture cross-section. A list of nuclides with σ_{cap} greater than 50b is given in Table I: The high-mass nuclides are spallation products of Lead & Bismuth, also the weak fission in these elements leads to the presence of nuclides in the medium mass range; the lower mass nuclides are possible products from structure materials.

Rather small quantities of material with cross-section in the kilo-barn range will lead to significant increase of absorption. The build-up rates of absorption in some materials considered for use in SINQ have been estimated and will be presented in the next section.

TABLE I

Nuclides with a thermal-neutron capture cross-section of > 50b.

	$t\frac{1}{2}$	σ_c	e		$t\frac{1}{2}$	σ_c	e		$t\frac{1}{2}$	σ_c	e
^{3}He	S	5327	1.8	^{6}Li	S	940	0.4	^{7}Be	53.29d	48000	19
^{10}B	S	3837	0.2	^{22}Na	2.602y	29000	3.4	^{39}Ar	269y	600	50
^{50}V	S	70	47.0	^{58}Co	9.1h	136000	7.3	^{58}Co	71.3d	1880	6.4
^{60}Co	10.48m	58	14	^{59}Ni	75ky	104	3.8	^{66}Cu	5.1m	135	7.4
^{74}Se	S	51.8	2.3	^{76}Se	S	85	8.2	^{83}Kr	S	200	15
^{87}Kr	76.3m	<600		^{103}Rh	S	150	3.3	^{104m}Rh	4.4m	800	13
^{105}Rh	35.5h	16000	9.4	^{109}Ag	S	91	3.3	^{110}Ag	249.9d	82	13
^{109}Cd	435d	650	15	^{113}Cd	S	19910	1.5	^{115}In	S	202	1.0
^{115}Sn	S	50	40	^{123}Te	S	406	7.4	^{125}I	60.14d	894	10
^{126}I	13d	5960		^{124}Xe	S	128		^{125}Xe	16.8h	<5600	
^{131}Xe	S	90	11	^{133}Xe	5.25d	190	47	^{135}Xe	9.1h	2650000	7.5
^{134}Cs	2.06y	140	8.6	^{138}La	S	172		^{143}Pr	13.58d	89	11
^{143}Nd	S	342	2.9	^{146}Pm	5.53y	8400	20	^{147}Pm	2.62y	181	3.9
^{148}Pm	5.37d	2000	50	^{148m}Pm	41.3d	22000	11	^{149}Pm	53.1h	1400	21
^{151}Pm	28h	<700		^{145}Sm	340d	110		^{147}Sm	S	64	7.8
^{149}Sm	S	41000	4.9	^{150}Sm	S	102	4.9	^{151}Sm	93y	15000	12
^{152}Sm	S	206	2.9	^{151}Eu	S	9200	11	^{152}Eu	13.3y	2300	43
^{153}Eu	S	390	7.7	^{154}Eu	8.8y	1500	27	^{155}Eu	4.96y	4040	3.1
^{152}Gd	S	1100	9.1	^{154}Gd	S	85	14	^{155}Gd	S	61000	0.8
^{157}Gd	S	254000	0.8	^{161}Gd	3.6m	31000	39	^{160}Tb	72.1d	525	19
^{160}Dy	S	61	9.8	^{161}Dy	S	585	5.1	^{162}Dy	S	180	11
^{163}Dy	S	130	7.7	^{164}Dy	S	2700	2.8	^{165}Dy	2.35h	3900	7.7
^{165}Ho	S	66.5	5.0	^{167}Er	S	670	4.5	^{171}Er	7.5h	280	11
^{169}Tm	S	103	2.9	^{170}Tm	128.6d	92	4.3	^{168}Yb	S	3470	2.9
^{171}Yb	S	50	8.0	^{174}Yb	S	65	7.7	^{176}Lu	S	2100	2.4
^{174}Hf	S	390	14.0	^{177}Hf	S	365	5.5	^{178}Hf	S	86	8.1
^{180}Ta	S	700	29.0	^{182}Ta	114.4d	8200	7	^{187}W	23.8h	64	16
^{185}Re	S	112	2.7	^{187}Re	S	74	5.4	^{184}Os	S	3000	5.0
^{187}Os	S	336	5.0	^{193}Os	30h	1540		^{191}Ir	S	924	5.7
^{192}Ir	74d	1100	36.0	^{193}Ir	S	112.5	6.7	^{197}Au	S	98.8	0.3
^{198}Au	2.7d	25800	4.7	^{196}Hg	S	3300	6.5	^{199}Hg	S	2000	50
^{200}Hg	S	<60		^{201}Hg	S	<61					

** For the half-life units, m= mins, h= hours, y= years, ky= 1000's of years and S= stable or very long.

e is the percentage error.

2 ESTIMATES FOR THE BUILD-UP OF ABSORPTION CROSS-SECTION.

The effect of thermal-neutron capture in the region of the target on the flux is illustrated in Fig 1: The thermal flux maps for the SINQ moderator with and without a 2cm thick Iron sleeve around the target (σ_{cap} circa 2b), show that in the latter case a flux depression of about 25% results.

The estimates for thermal-capture cross-section build-up are based on calculations using the HETC [1] code and, in the case of the target, with chain-yield analysis using the ORIHET [2] code. The materials have been selected from those which might be used for SINQ in the region of the moderator; the layout of this region of the source is sketched in Fig 2.

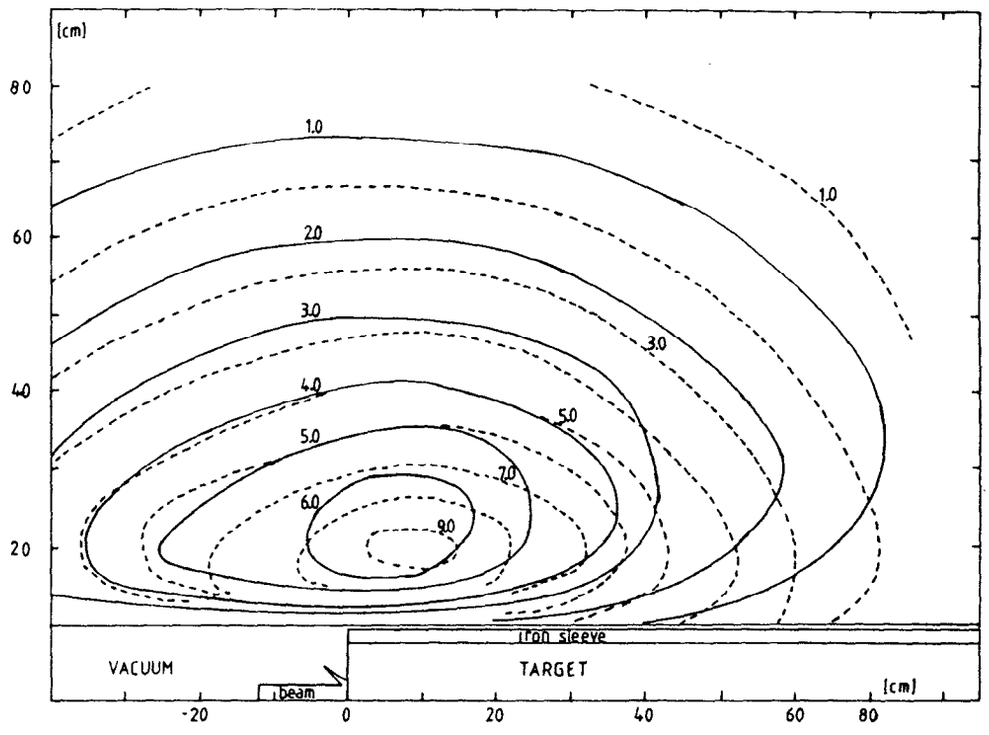

Fig 1: Flux maps for the SINQ moderator with (solid lines) and without (dashed lines) an absorbing Iron sleeve around the target. The diagram is cylindrically symmetric about the axis of the target. The flux intensities are in units of 10^{13} neutrons/(cm^2.sec) and correspond to 1mA at the target.

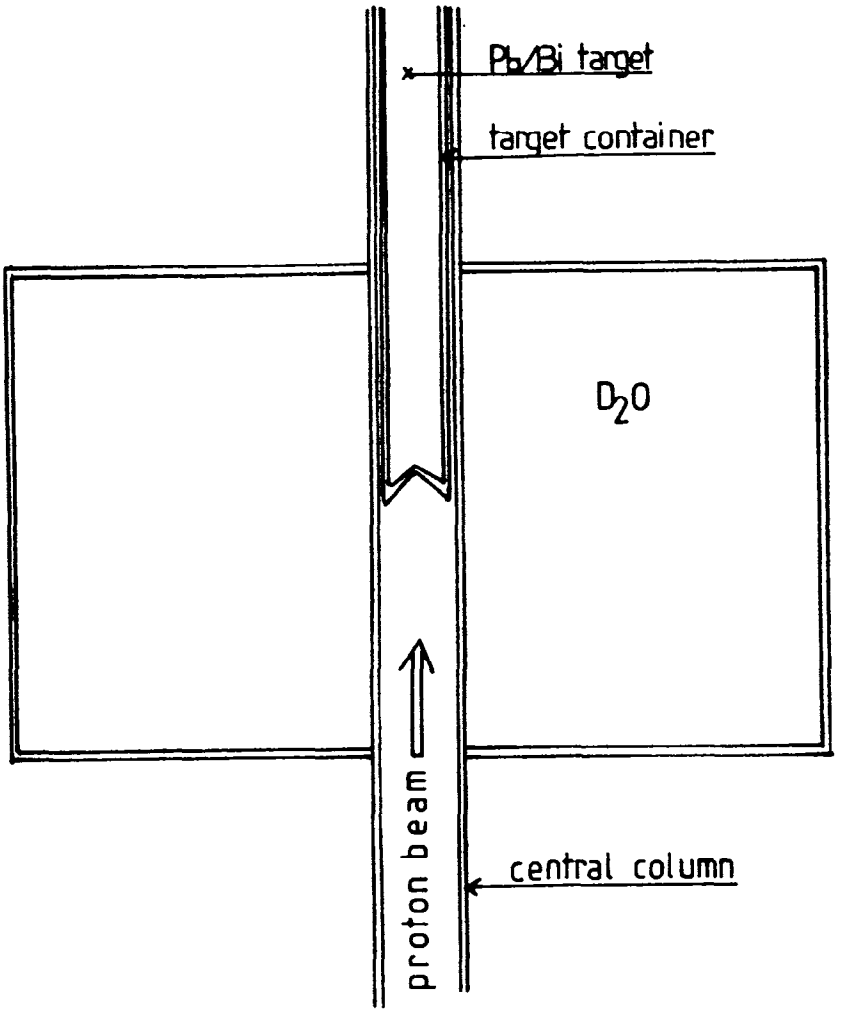

Fig 2: Sketch of the layout for SINQ in the region of the moderator. The principal material choices are for that of the target container and the central column; this latter is the barrier between the heavy-water and the proton channel vacuum.

2.1 Absorption cross-section for Lead-Bismuth under irradiation.

The Lead-Bismuth for the target has an unirradiated capture cross-section of 90mb. The nuclides produced include 57 giving a noticeable contribution to the increase of capture cross-section; the calculation includes fast-fission and chain-yield analysis. About 90% of the overall increase of capture cross-section comes from 9 nuclides and a further 11 contribute another 8%; these nuclides are listed in TABLE-II together with the calculated production rate, g, (grams after 10^7 seconds irradiation by a 1 mA 590 MeV proton beam), the thermal neutron capture cross-section for the product, σc, and the relative contribution to the increase (= g x σ_c/A, A is the mass number).

The increase of capture cross-section is given by:

$$\Delta\sigma_{abs} = \frac{20.8}{V} \sum_{n} \frac{9n \cdot \sigma_c}{An}$$

Where V is the total volume of the target and the sum is over the relative contribution for each of the nuclides produced. The numerical factor 20.8 is A/density for the Lead-Bismuth. The target is in the liquid state with motion from natural convection; it is assumed that the products will be uniformly dispersed throughout the total amount of material (0.25 m^3 in the current design).

TABLE-II

The high capture cross-section products in the SINQ target.

NUCLIDE	THERMAL CAPTURE CX (σ_c barns).	PRODUCTION AT 10^7 sec. and 1 mA (g grams).	$\frac{\sigma_c \, g}{A}$
^{199}Hg	2000	1.0	10.1
^{196}Hg	3080	.65	10.3
^{191}Ir	924	.45	2.2
^{184}Os	3000	.17	2.8
^{168}Yb	3470	.045	0.9
^{157}Gd	254000	.002	3.2
^{155}Gd	61000	.0059	2.3
^{113}Cd	19910	.021	3.7
^{58}Co	136000	.00064	1.5
^{201}Hg	<61	1.29	0.4
^{200}Hg	<60	1.20	0.4
^{197}Au	98.8	.825	0.4
^{187}Os	336	.313	0.6
^{177}Hf	365	.13	0.3
^{174}Hf	390	.085	0.2
^{167}Er	670	.049	0.2
^{149}Sm	41000	.0042	0.3
^{145}Sm	110	.00089	0.3
^{135}Xe	2650000	.0000089	0.2
^{104}Rh	800	.021	0.2

The increase of absorption cross-section after 10^7 seconds irradiation at 1 mA proton current is 3.4 mb and after one year irradiation at 3 mA (the lifetime and maximum current for SINQ targets), 30 mb or one third of the unirradiated cross-section value.

The extra volume of target material (included for technical reasons concerned with the cooling system) dilutes the produced nuclides about 50 times more than if its size were limited to that required by neutron production; were this factor not present, an expected increase of about 1.5 b would result, which in view of the results shown in Fig 1 would lead to a significant degradation of performance during operation.

2.2 Heavy-water moderator and structural materials.

The average high-energy neutron intensity leaving the first 30 cm of the target (the important region from the absorption point of view) is $5.5 \times 10^{-4}/(cm^2.sec.proton)$. The peak flux is about 30% higher. The build-up of absorption cross-section for material irradiated in this region is given by:

$$\frac{d\sigma_{abs}}{dt} = C \times \phi \quad \langle \sigma_p^i(E) \rangle \times \sigma^i_{abs}$$

Where $\langle \sigma_p^i(E) \rangle$ is the production cross-section for nuclide i averaged over the incident neutron spectrum, σ^i_{abs} is the absorption cross-section for product i and ϕ is the neutron flux. The value for $C \times \phi$ is 1.03×10^{-14} /(mb.sec) at 3 mA for the surface of the target. All results to be quoted will be for a proton beam-current of 3 mA at the target. The spectrum averaged production cross-sections have been computed by direct Monte-Carlo using the spectrum shown in Fig 3.

2.2.1 Heavy-water.

The build-up of absorption cross-section comes from the spallation products of oxygen and the results are summarised in Table-III.

TABLE-III

The build-up of absorbing nuclei in heavy-water.

Nuclide	$\langle \sigma_p^i(E) \rangle$ mb	σ_{abs} b	$\langle \sigma_p^i(E) \rangle \times \sigma_{abs}$ mbxb
^3He	0.8	5327	4262
^6Li	4.2	940	3948
^7Be	0.3	48000	14400
^{10}B	0.9	3837	3453

The absorption cross-section initially increases at the rate of 2.7×10^{-7} mb/sec. ^7Be has a half-life of 53.4 days and reaches an equilibrium absorption cross-section of about 1.0 mb and the build-up rate for stable nuclides is 1.2×10^{-7} mb/sec.

This will cause no problem for SINQ because of dilution through mixing into the large volume of heavy-water (about 8 m^3) and removal of some of these nuclides by the processing plant.

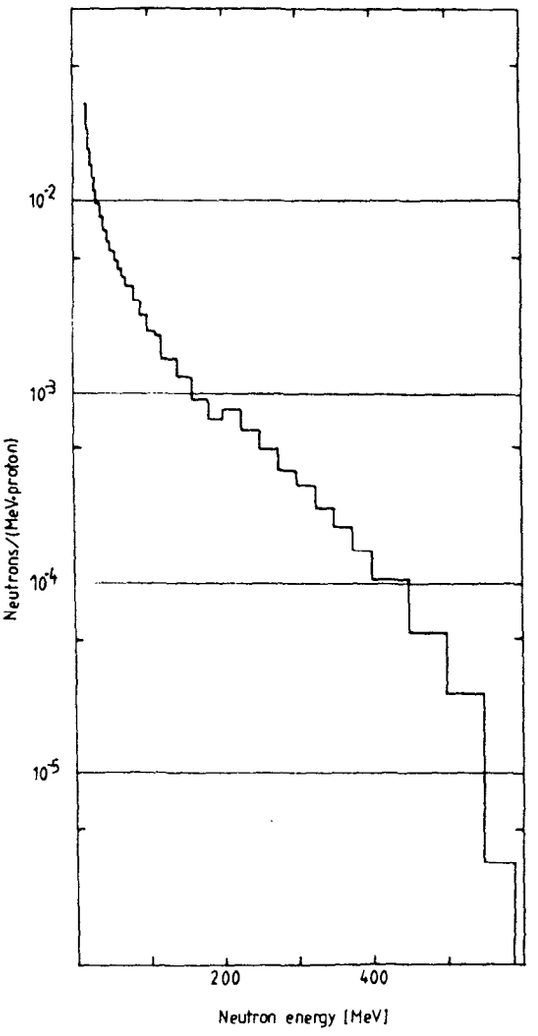

Fig 3: Energy spectrum for HE neutrons from the SINQ Pb/Bi target averaged over the length and all production angles. The spectrum has been calculated using HETC [1].

2.2.2 Structural materials.

The following materials are candidates for either the target container or the central column (see Fig 2).

(a) Carbon.

NUCLIDE	$\langle\sigma_p^i(E)\rangle$ mb	$\langle\sigma_p^i(E)\rangle \times \sigma_{abs}$ mb x b
^3He	1.8	9889
^6Li	20.0	18800
^7Be	3.9	187200
^{10}B	14.0	53718

The predicted initial increase rate of absorption cross-section is 9.2×10^{-7} mb/sec. Again, the ^7Be will come to equilibrium and reaches a value of 13 mb with the stable products giving an increase rate of 8.5×10^{-7} mb/sec. The absorption cross-section for carbon close to the target will rise from an initial 3.4 mb to about 43 mb at 1 year. There might be some slight reduction due to the ^3He diffusing out of the material. The increase of absorption cross-section does not exclude carbon as a target container material.

(b) Iron and Steel.

The production cross-sections of high-absorption cross-section nuclides for the principal constituents of stainless-steel are given in Table-IV.

TABLE IV

Spectrum average production cross-sections (mb) for high absorption cross-section nuclides in constituents of stainless-steel.

PRODUCT / MATERIAL*	^3He	^{50}V	^{36}Ar	^{39}Ar	^{58}Co	^{60}Co	^{59}Ni
Fe	1.3	1.6		0.1			
Ni	1.8	2.9			52.0	4.3	27.0
Cr	1.0	104.0	0.07	0.4			
Mo	0.7		<0.1				
S/S	1.2	28.0		0.12	6.5	0.5	3.4

* The cross-sections are averaged over natural isotopic mixtures and stainless-steel is taken to contain 68.5% Fe, 12.5% Ni, 16.5% Cr and 2.5% Mo.

For pure Iron, the unirradiated absorption cross-section will rise at a rate of 7.3×10^{-8} mb/sec; this has a small effect on the unirradiated absorption cross-section of about 2 b.

In stainless-steel, the ^{58}Co & ^{60}Co both reach equilibrium absorption cross-sections of 0.42 to 1.1 mb and 270pb respectively (^{58}Co has two states, 9.1 hr (0.136 Mb) and 71.3 days (1880 b) half-lives and the two values are for 100% of each state). The increase of absorption cross-section is predicted to be 8.7×10^{-8} mb/sec. At one year an increase of 3.2 mb in the absorption cross-section would result; this is small compared to the unirradiated value of 3.4 b.

(c) Aluminium.

The two high-absorption cross-section nuclides produced are ^{3}He and 2.6 year ^{22}Na. The spectrum averaged production cross-sections are 7 and 14 mb respectively. The ^{22}Na causes an increase of the absorption cross-section of 4.2×10^{-6} mb/sec at 1mA and reaches an equilibrium value of 490 mb. The increase from the ^{3}He is 5.4×10^{-8} mb/sec and gives a contribution at 1 year of about 17 mb. The unirradiated absorption cross-section of 230 mb will increase by a factor of about 3.

3 CONCLUSIONS AND DISCUSSION.

The increase of thermal neutron absorption cross-section, although noticeable, does not seem a major problem for SINQ operation. The use of a large volume liquid-metal target mitigates what could have been a significant degradation of performance as operation proceded. Similarly for the heavy-water, the large volume plus the processing avoids another source of performance reduction.

The carbon results are of more general interest as it is a possible candidate as a material to be used as the moderator. Unirradiated carbon is a good moderating material and has some attractions compared to heavy-water from a safety point of view as it is less easily dispersed. The increase of absorption cross-section causes the moderating ratio (average logarithmic energy loss times scattering cross-section divided by the absorption cross-section) to decrease by a factor of 5 during operation at positions close to the target but (obviously) more slowly at larger distances. This first look at the problem indicates a more careful study of the performance of a carbon moderator would be required before it could be accepted as an alternative to heavy-water.

On a more philosophical note, in 1834, Lenz deduced the law that in electromagnetism an induced current flows in a direction such that it opposes the change that produces it. This is a manifestation of a more general principle, that effects produced tend to oppose that which causes them and finds many examples in Physics and other systems: Seebeck and Peltier effects, the poisoning in reactors etc. We could translate the principle into the vernacular as "This looks wonderful, but what is the catch?".

What about spallation sources? They look wonderful, more proton current more neutron flux! What is the catch? Poisoning?

ACKNOWLEDGEMENT.

This paper is the result of the author annoying his group leader, Walter Fischer, with safety problems concerning the tritiation of the heavy-water moderator. His counter to these quibbles was to suggest the use of a Carbon moderator and was coupled with a request that such a moderator be examined. The author being somewhat reluctant, managed to generate this poisoning argument. WEF then asked "What about the target?" - hence this paper and my grateful thanks.

REFERENCES.

[1] Radiation Shielding Information Centre code package CCC-178, HETC.

[2] ORIHET is a modified version of the ORIGEN code, RSIC code package CCC-217.

M J Bell ORNL-4628 (1973)

Proceedings of the Eighth Meeting of the International Collaboration on Advanced Neutron Sources (ICANS-VIII)
8-12 July 1985, Rutherford Appleton Laboratory Report RAL-85-110

Materials Irradiation Experiments for the SNQ-Target

K.H. Graf[1], J. Laakmann[1], W. Lohmann[1], A. Ribbens[1], W.F. Sommer[2]

[1] Kernforschungsanlage Jülich, D-5170 Jülich, FRG

[2] Los Alamos National Laboratory, Los Alamos, USA

Abstract

Commercial AlMg3 and AlMgSi, both in a high strength and an annealed condition have been irradiated

a) with 760 MeV protons to a fluence of 3.2×10^{20} p/cm^2 yielding a calculated radiation damage of 0.2 dpa (displacement per atom) and 67 appm He.

b) with 28 MeV He^{++}-ions yielding 170 appm helium.

Tensile tests at RT, 100°C after helium implantation and at RT, 100, 200, and 300°C after p-irradiation show

a) no influence of p-irradiation on the 0.2% flow stress and the ultimate tensile strength of the annealed materials.

b) in case of the hardened alloys those values are reduced to those of the annealed alloys

c) no significant influence of helium implantation on tensile data.

1. Introduction

In case of the proposed german spallation neutron source (SNQ) the spallation neutrons will be created by a proton beam characterized by an energy of 1.1 GeV and a time averaged current of 5 mA. Because of the high heat deposition by the beam the target was designed as a rotatable wheel (Fig. 1) carrying a few thousend individually cladded targetelements cooled by water. Those elements will be build of tungsten, uranium or, as a back-up material, lead.

Different Al-alloys as AlMgSi or AlMg3 are favourable to the general structure of the target wheel and to the cladding of these materials. The advantages of these materials are

- high thermal conductivity, i.e. low thermal stresses
- low neutron absorption
- fast decaying neutron induced activity
- low void
- well known technology

The importance of these properties underlined by regarding the conditions for SNQ-operation:

- Creation of radiation damage
- production of large amounts H of helium mainly by (p,)-reactions
- introduction of thermomechanical stresses due to the heat deposition by the p-beam and
- fatigue

A material research program has been established to examine the material behaviour under conditions close to real SNQ operating conditions /1/. This paper reports some results of this program.

2. The influence of helium implantation and proton irradiation on the mechanical properties of two Al-alloys.

We compared, by tensile testing, the 0.2 % flow strength and the ultimate tensile strength of specimens without any pretreatment, after helium implantation and after p-irradiation.

Two different Al-alloys were used: AlMg3 and an AlMgSi-alloy (US Al 6061). Both alloys, delivered as sheets of 0.5 mm thickness, were rolled to foils of 250 µm thickness. In order to establish a hardened (abbreviation h) as well as a soft (abbreviation s) condition of these materials, they were heat treated in the following manner.

AlMgSi (h) - annealed for 15 minutes at 530°C, quenched in water.
- aged for 16 hours at 160°C (precipitation hardening)

AlMgSi (s) - annealed for 3.5 hours at 380°C

AlMg3 (h) - no heat-treatment (cold-worked)

AlMg3 (s) - annealed for 3.5 hours at 350°C

After this treatment specimen of the geometries as shown in Fig. 2 and 3 were punched out of these foils.

2.1 Helium implantation: IBES

A He^{++}-implantation was carried out using the SNQ-irradiation chamber IBES (Ispra Bestrahlungsexperiment SNQ) at the compact cyclotron of CCR Euratom, Ispra (Italia). A schematical sketch is given in Fig. 4.

IBES consists mainly of the following details. A beam window separating the vacuum of the cyclotron from the cooling helium gas in the chamber, a rotatable beam stop also serving as an aperture in the open position, a degrader wheel made of Al-foils of different thickness allowing to implant the specimen homogeneous through their thickness and the sample clamped on a water cooled holder. The Al-alloys were irradiated at 100°C with 28 MeV-He^{++} particles at beam currents of 2.5 µA leading to a nominal helium content of 170 appm after 3 hours. A thermal release measurement yielded 158 ± 13 appm He. The standard deviation of 13 appm has been determined by thermal release of 3 different specimens. These data are in good agreement with the nominal ones.

2.2 The proton irradiation SNQ

The proton irrediations were carried out 1983/84 in Los Alamos at the ISORAD the facility at LAMPF, (Fig.5), which was the only one available at this time.

To transport the specimen to the irradiation position they had to be first transferred from a cask to a cart, then from the cart to stringers. This procedure didn't allow to have a dynamic temperature measurement. To minimize corrosion effects and to assure good heat transfer 7 of the samples were packaged in an Al envelope and sealed (Fig. 6).

16 of these envelopes were then placed in a water cooled specimen holder as shown in Fig. 7.

The irradiation parameters are listed below:

Temperature 40-50—C (calculated; certainly not exceeding 100—C)
Proton energy: 760 MeV
Beam spot: gaussian profile, 2σ ~ 5 cm
Average beam current: 570 µA
Irradiation time: 705 h
Fluence: 3.2×10^{20} p/cm^2
radiation damage: 0.2 dpa (calculated)
He-content: 67 appm (calculated)

2.3 Tensile testing

An Instron Typ 1122 tensile test machine with a temperature cabinet was used to determine the 0.2% flow strengh and the ultimate tensile strength as a function of temperature (23 and 100°C in case of the He^{++}-implanted specimen and 23, 100, 200 and 300°C in case of the p-irradiated materials). All specimen were tensile tested with a strain rate of 2.8×10^{-4} sec^{-1}.

3. Results

Fig. 8-11 show the measured dependence of the 0.2 % flow strength and the ultimate tensile strengh from the testing temperature for Al 6061 and AlMg3, respectively. The soft canditions are denoted with "S", the hardened conditions by "h".

The symbols and their meaning are summarized in Tab. 1.

Taking into account the different geometry of our specimens, we have two references in both conditions and materials - one denoted by "LAMPF" (reference for the p-irradiated samples) and another one denoted by "KFA" (reference for He^{++}-implanted samples)

Table 1:

Symbol	Tensile testing	after
*	"LAMPF"-reference	(h)
H	"KFA"-reference	(h)
+	p-irradiation	(h)
y	He^{++}-implantation	(h)
x	"LAMPF"-reference	(s)
#	"KFA"-reference	(s)
O	p-irradiation	(s)
8	He^{++}-implantation	(s)

One recognizes (by comparison of the symboles # and 8) that helium implantation does not influence the tensile properties in case of the soft alloys. Tensile testing proves that p-irradiation does only slightly affect these properties (x and O). This is true - within the experimental errors being about 10% - for all test-temperatures. In case of the hardened alloys, however, we have a different situation. While helium implantation does not affect the 0.2 % flow strength and the ultimate tensile strenght (H and Y) after p-irradiation a strong reduction of the mechanical properties is observed (* and +). Moreover - by comparison of the symbols + and O one sees, that this reduction leads to the values of the soft alloys.

4. Discussion

The most suprising result is the p-irradiation induced loss of strength in case of the hardened materials. Normally one would expect an irradiation induced hardening as has been published by Farrell and King /2/ in a paper about the tensile properties of neutron irradiated 6061-Al alloy in annealed and precipitation hardened conditions.

The irradiation was performed at $55^{o}C$ to fast ($E > 0.1$ MeV) fluences up to 1.8×10^{27} n/m^2 and thermal ($E < 0.025$ eV fluences) up to 7.0×10^{27} n/m^2 yielding a radiation damage of 260 dpa. The results were that the 0.2 % flow strength and the ultimate tensile strength raised by 45 to 60%. The explanation given by the authors was that this hardening was caused by creation of 7 wt% Si from transmutation reactions.

This result suggests:

a) n-irradiation is not comparable with p-irradiation

b) different microstructural processes become effective under p-irradiation.

References

/1/ W. Lohmann: ICANS VII, Proceedings of the 7th International Collaboration on Advanced Neutron Sources, Chela River Nuclear Laboratories, 1983, Sept. 13-16, Chalk River, Ontario, Canada, p. 274-78. "Irradiation effects in candiate materials for the SNQ"

/2/ K. Ferrell, R.T. King: "Tensile Properties of Neutron Irradiated 6061 Aluminium Alloy in Annealed and Precipitation Hardened Conditions", Effects of Radiation on Structural Materials A51M-51:, 683 61979) 440.

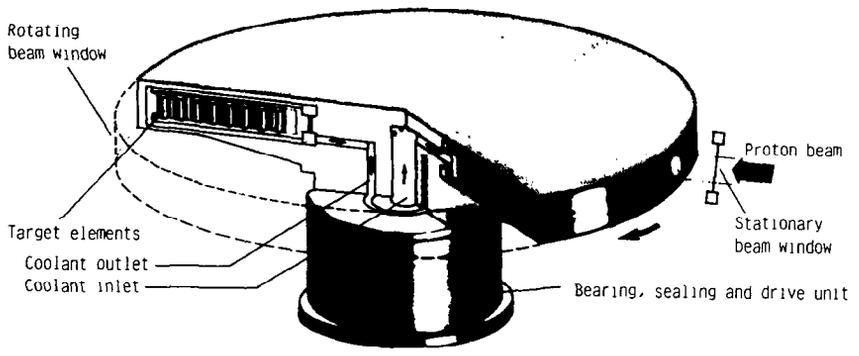

Fig. 1: The SNQ-target wheel

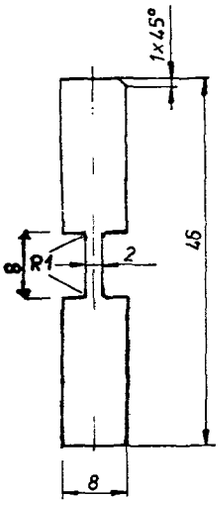

Fig. 2: Geometry of specimens used for helium implantation (all dimensions in mm), thickness = 0.25 mm

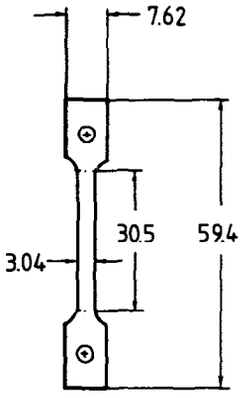

Fig. 3: Geometry of specimens used for p-irradiation (all dimensions in mm, thickness = 0.2 - 0.3 mm)

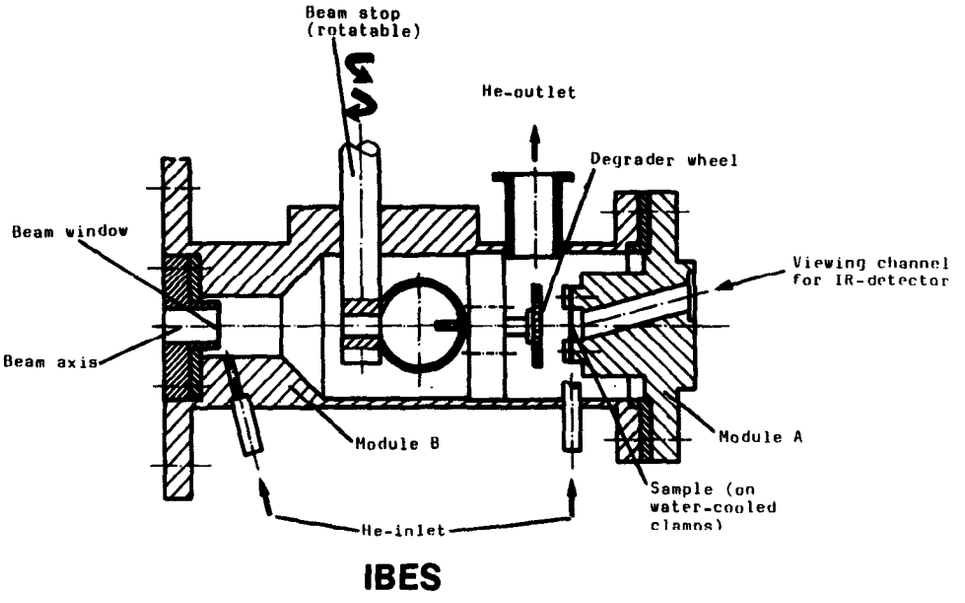

Fig. 4: The irradiation chamber IBES (schematically)

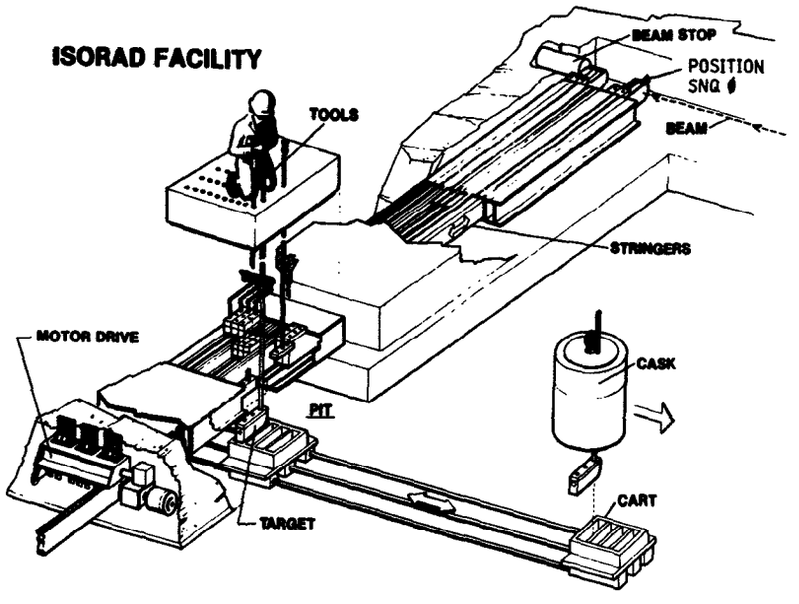

Fig. 5: The LAMPF isotope Production Facility

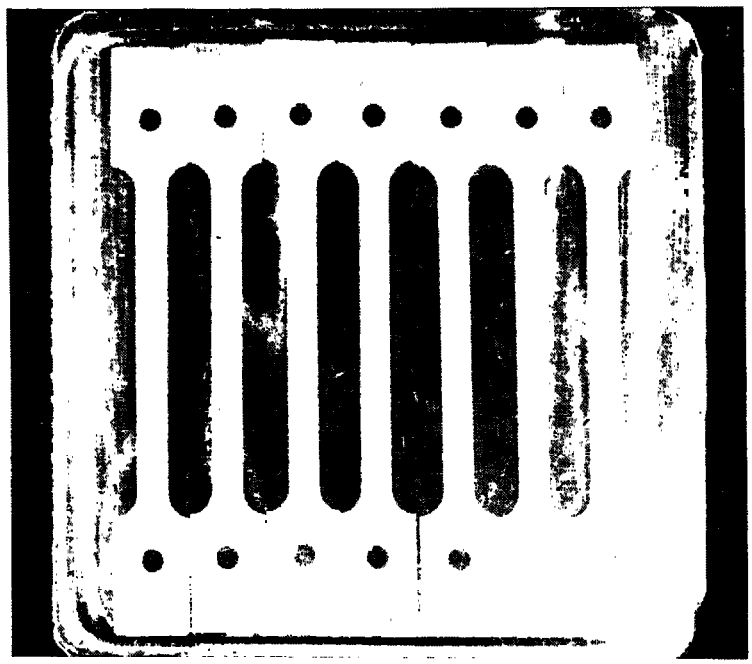

Fig. 6: SNQ O samples in the open envelope

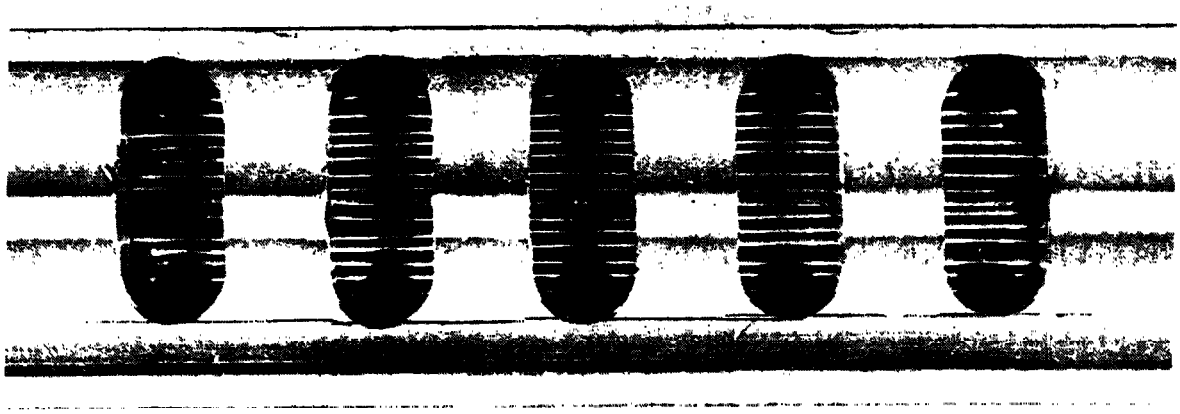

Fig. 7: The SNQ-O specimen holder

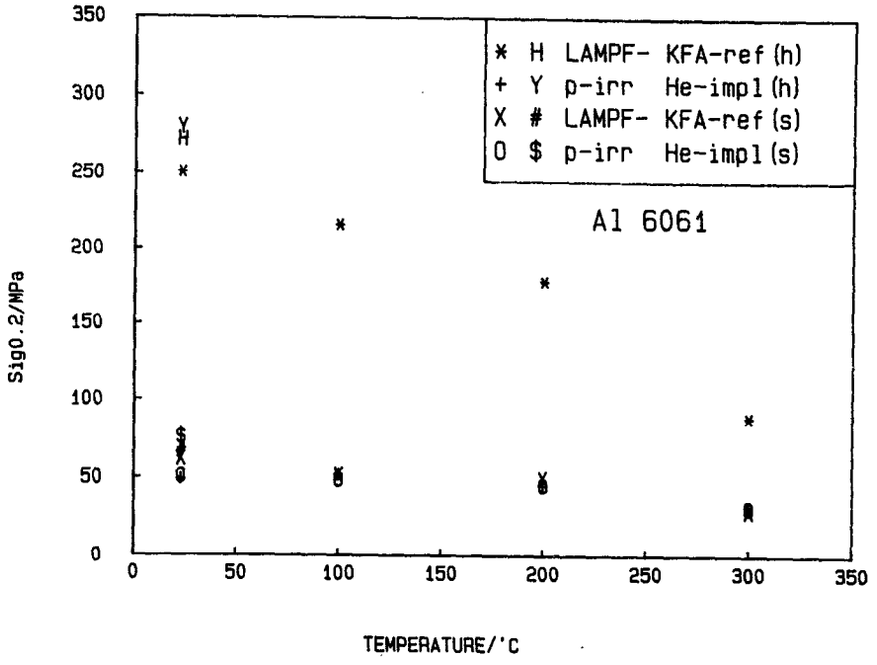

Fig. 8: Temperature-dependent 0.2 % low stress of Al6061 (anneald and percipitation hardened) unirradiated, He^{++}-implanted and 800 MeV-protron irradiated.

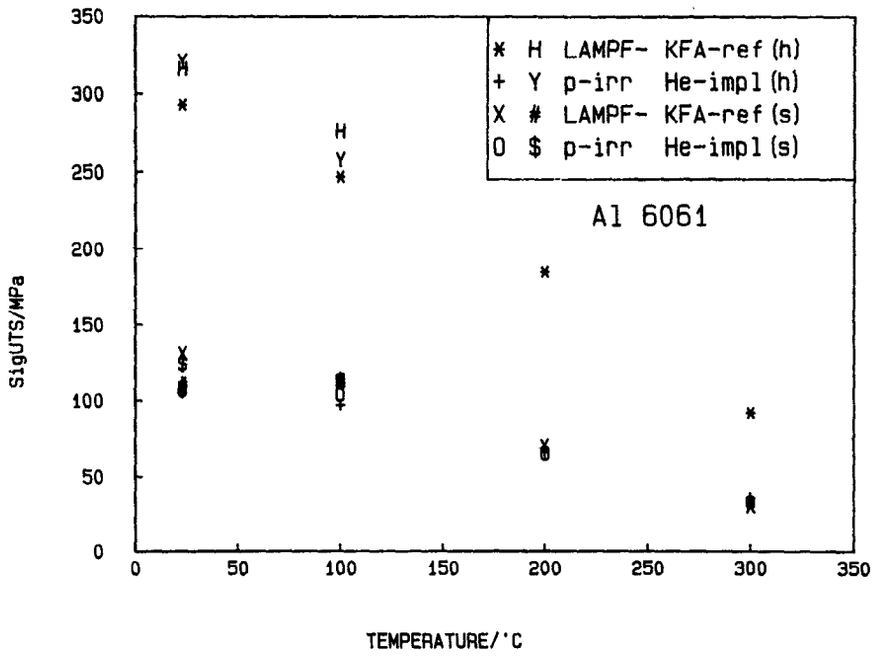

Fig. 9: Temperature-dependent ultimate tensile strength of Al6061 (annealed and percipatation hardened) unirradiated, He^{++}-implanted and 800 MeV-proton irradiated.

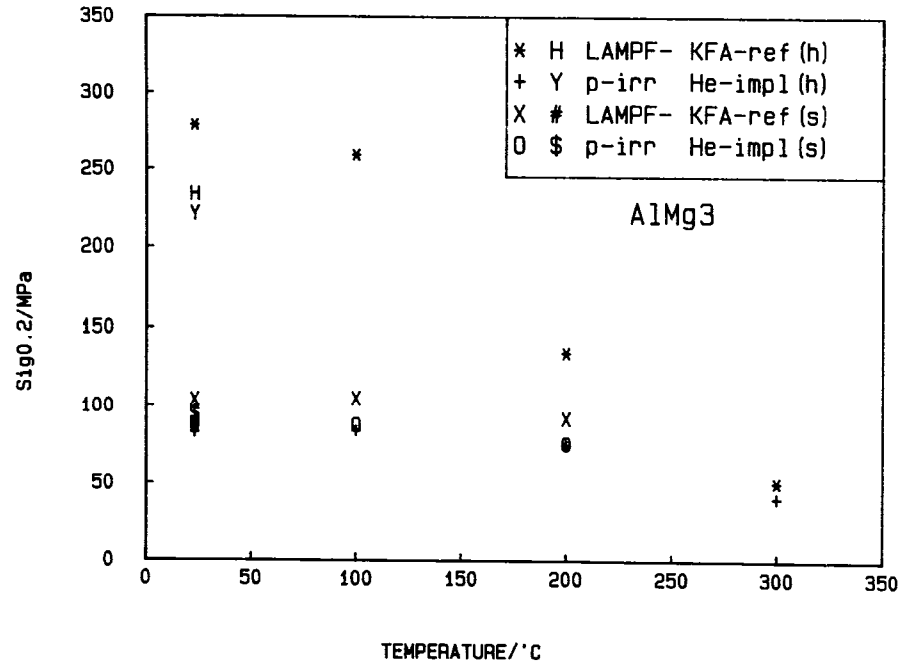

Fig. 10: Temperature dependent 0.2% flow stress of AlMg3 (annealed and cold worked) unirradiated He^{++} implanted and 800 MeV proton irradiated.

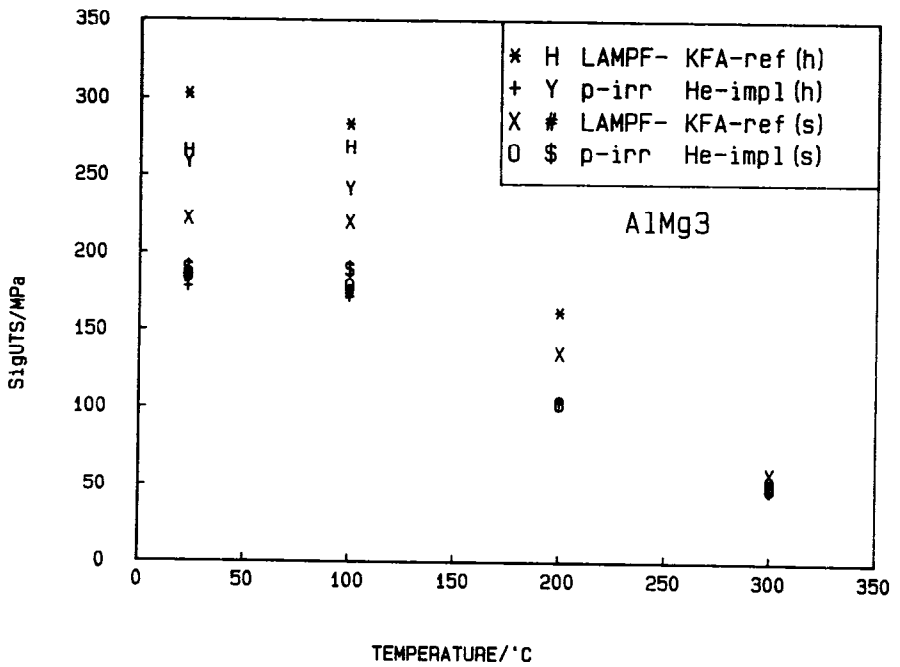

Fig. 11: Temperature dependent ultimate tensile stress of AlMg3 (annealed and cold worked) unirradiated He^{++} implanted and 800 MeV proton irrdiated.

Proceedings of the Eighth Meeting of the International Collaboration on Advanced Neutron Sources (ICANS-VIII)
8-12 July 1985, Rutherford Appleton Laboratory Report RAL-85-110

State of Design of the SNQ-Target

H. Stechemesser 1), G. Thamm 2),

KFA Jülich, D-5170 Jülich,
1) Zentralabteilung Allgemeine Technologie
2) SNQ-Projekt, Teilprojekt 3 "Neutronentargetanlage"

Abstract:

As the requirements for the SNQ-target and the target station at all have been well defined, an improved design and essential dimensions and geometries could be fixed recently. Important nuclear data for the uranium and tungsten target have been calculated using the improved technical design of the rotating target. These nuclear data have been taken as a basis for temperature- and stressprofile calculations especially in the hot spot plane of the uranium target pin. Furthermore the feasibility of the target wheel design has been proven in several manufacturing and functional tests.

1. Introduction

The neutron target facility of the SNQ has to meet the following two basic requirements:

1. Generation of neutrons by conversion of protons supplied by the accelerator with as high as possible a yield.

2. Provision of all technical means for optimum utilization of the generated neutron radiation.

The technical realization of the neutron target facility must in addition to these two basic requirements also take into account the following essential conditions:

- safety during normal and abnormal operation situations,
- high availability of the facility (about 6000 hours of operation per year),
- design flexibility of the facility for adaptation to the developing ideas about utilization (probably different operation modes) and for the use of different target materials.

As the basic requirements and the conditions for realization can by no means be met independently of each other, the present overall conceptual design of the neutron target facility is to be regarded as an "optimum technical compromise".

2. General outline of the target facility

The main data of the proton beam determining the design of the target are shown in Tab. 1

final energy	1100 MeV
dc beam current during pulse	200 mA
average time current	5 mA
repetition frequency	100 Hz
beam pulse duration	0,25 ms.

Tab. 1: Main data of the proton beam

The essential part of the facility is the heavy metal target, to be built as a rotating wheel. The target wheel has a diameter of about 2.5 m and is to be rotated at a frequency of 0.5 s^{-1}.

The heavy metal material (depleted uranium; tungsten during start-up phase) is arranged in an annular space of 40 cm width at the periphery of the wheel. Size and rotation frequency of the target wheel prevent the same target material from being hit by two successive proton pulses thus significantly reducing the thermomechanical and irradiation induced stresses of target and structural material (especially of the rotating window) compared with a static arrangement (factor of 200). The part of the target hit by a proton pulse can be cooled down to a fairly low temperature level by relatively simple water cooling within the following 2 seconds until the next impact.

Fig 1 and 2 give an overview of the neutron target facility. Protons from the linear accelerator are guided through a special beam tunnel to the neutron target. The rotating target is imbedded in a shielding block immediately adjacent to the end part of the proton beam tunnel. The target block ensures safe shielding of the radiation emitted from the target, and also contains the main installations for the experimental use of the facility, for instance moderation and extraction of the neutrons generated in the target. The target wheel, positioned in the centre of the target block in a cavern combined with its

drive unit (KLA), which also serves to cool and support the target wheel, is mounted as a substructure on a movable shielding plug. It slides on a track inclined at an angle of 45° in a forward direction relative to the proton beam from the cavern (operation position) to the target cell (handling position). In the target cell all necessary handling of the target disc and all the other components mounted on the plug can be carried out by remote control safely and without delay.
Below the target wheel a lead reflector and an H_2O-moderator are installed. Eight to ten multiple beam tubes with at least two beam switches lead to the H_2O-moderator, two more to a cold source located in the centre of a large reflector above the target. In addition two bundles of six neutron guides lead from the cold source into the neutron guide hall adjacent to the target hall.

Furthermore the neutron target facility comprises ancillary systems, mainly cooling loops with purification and degassing installations, as well as vacuum systems and control equipment (internal control installations) providing for safe operation, as well as for high operational availability. The components of these installations are mainly housed in the basement of the target hall.

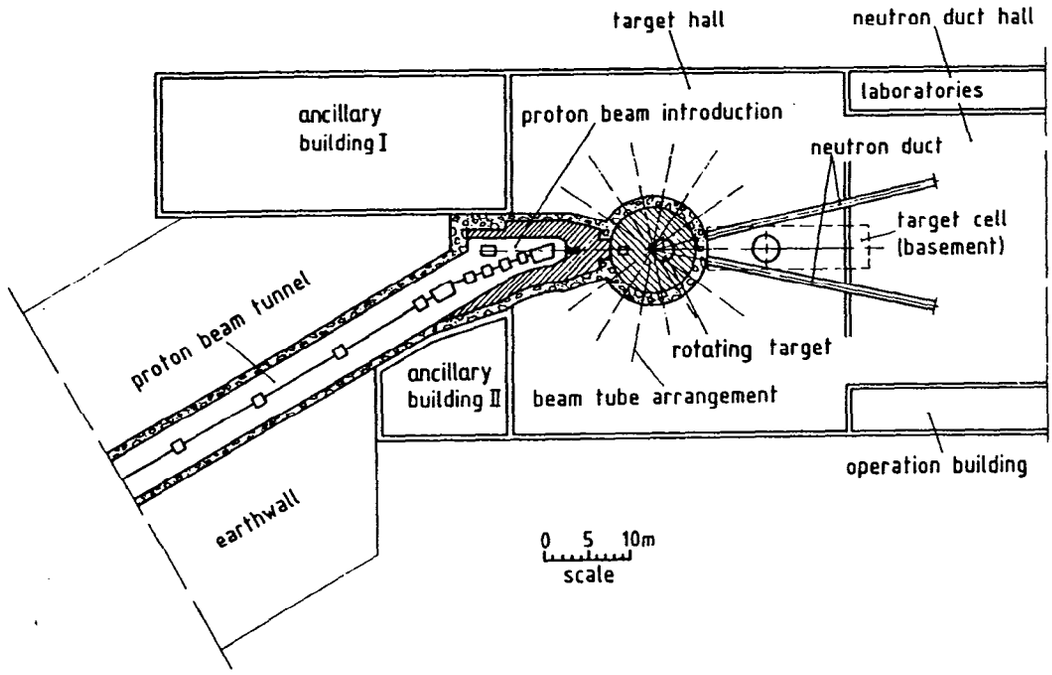

Fig 1: SNQ-neutron target facility (schematic)

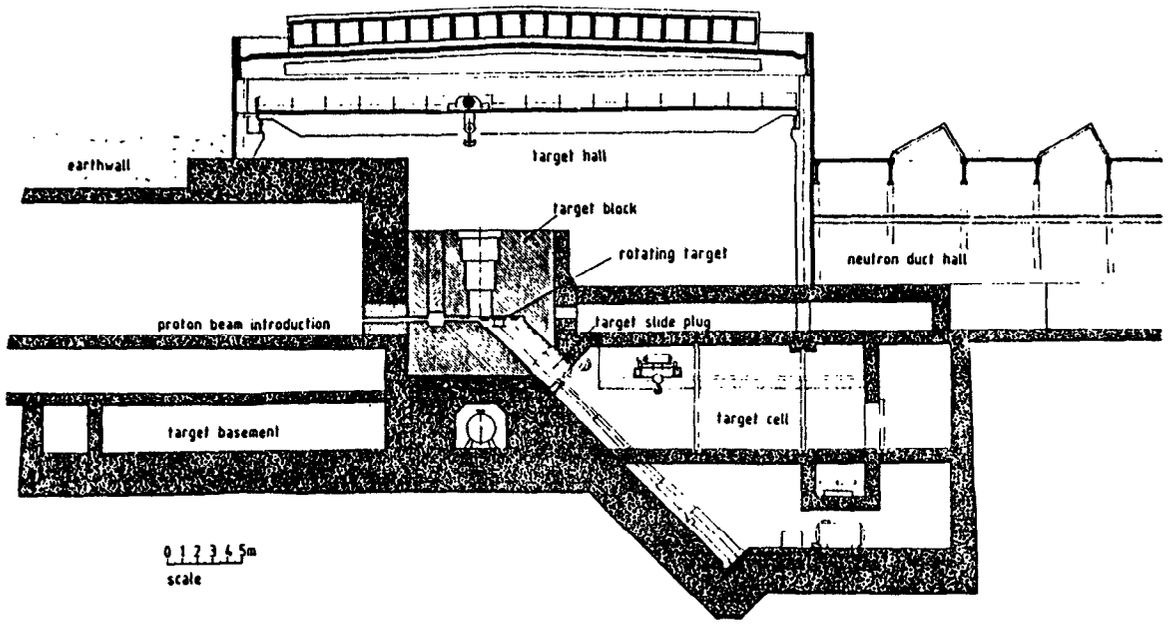

Fig. 2: Neutron target facility (longitudinal section)

3. The rotating target

The rotating target, depicted in Fig. 3, is a combination of the target wheel and the KLA assembly (KLA = german abbreviation of cooling water supply, support bearing, drive).

- The target wheel contains at its periphery the target material from which the heat, generated by the spallation process, is removed within one turn of the wheel by the cooling water.

- The KLA supports the target wheel, rotates it around its axis and connects the cooling water in- and outlet of the target wheel with the stationary substructure.

- The target wheel and KLA are bolted together and the joint is sealed watertight by metallic seals. This joint can be handled remotely.

The rotating target unit is mounted onto the sliding plug as a substructure.

Target wheel

The target wheel unit consists of two subunits

- wheel structure
- target structure.

The structural design of the target wheel is radially symmetric. The evaluation of the various geometric arrangements of the target material inside the target wheel with respect to the influence of temperature, stresses, target material packing density, penetration depth of the proton beam, pressure losses of the flowing cooling water and special manufacturing techniques lead to the so-called "pin target", having the following advantages:

- low thermal stresses in the pins due to the possibility of free expansion in radial and axial direction;

- quasi homogeneous arrrangement of the target material relative to the proton beam axis;

- good cooling water guidance within the target pin arrangement.

Target wheel structure

The design minimizes the number of welding joints by forming the target wheel from three forged parts. Those three forged parts are: the bottom support disc, the lid disc and the rotating window (Fig. 4).

The technical data of the target wheel are presented in Tab. 2.

The cooling water enters the target wheel from the KLA at its centre and flows evenly distributed in a radial direction through the target pin arrangement from the centre to the periphery. At the periphery of the target structure the outgoing cooling water is diverted by the rotating window and returns through channels inside the lid and bottom support disc.

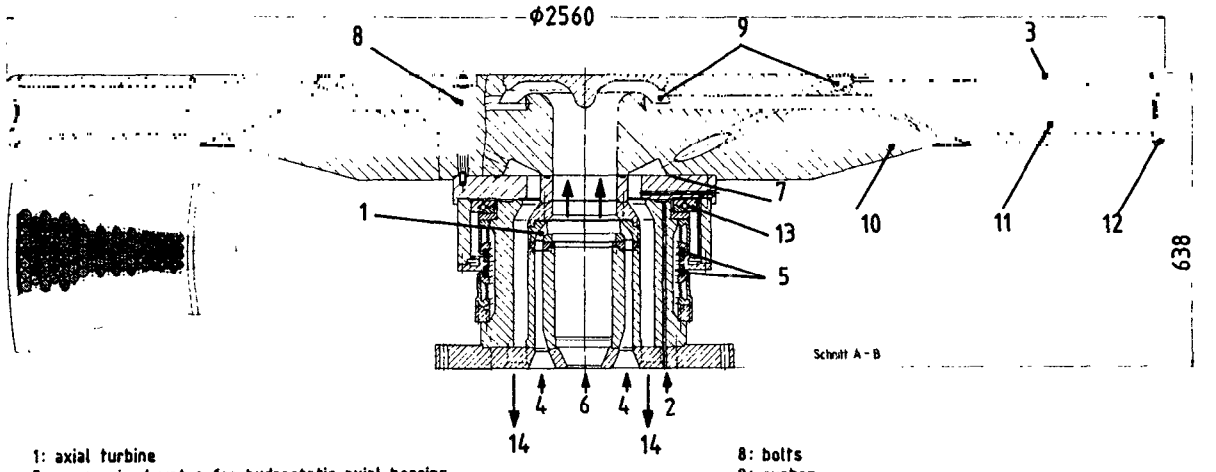

1: axial turbine
2: pressurised water for hydrostatic axial bearing
3: lid disc
4: pressurised water for axial bearing
5: slide ring
6: cooling water
7: metal seal
8: bolts
9: syphon
10: support disc
11: target pin
12: rotating window
13: roller bearing
14: return cooling water

Fig. 3: Target wheel for tungsten or uranium target for 1100 MeV mounted on KLA type II

The channels bored in the lid and bottom support disc are connected by annular channels and the cooling water is guided from the bottom annular channnel in vertical bores into the annular channel of the lid. From the annular channel in the lid the cooling water flows through bores towards the centre of the target wheel, where itreturns through an annular gap arranged concentrically around the water inlet bore. Water in- and outlets of the target wheel are in the form of syphons, so that in the case of pipe rupture in the cooling water system the target pins remain under water.

The design of the target wheel structure facilitates the disassembling after termination of its operation.

The structure of the target wheel carries the weight of the target material and provides for guidance of the cooling water as described above. It easily withstand the tangential acceleration forces caused by the target wheel rotation. The average centrifugal acceleration is less than 10 $m \cdot s^{-2}$ due to the low rotation frequency of 0.5 s^{-1}. The weight load of the target material of about 35 KN is also of minor importance for the stresses of the target wheel structure.

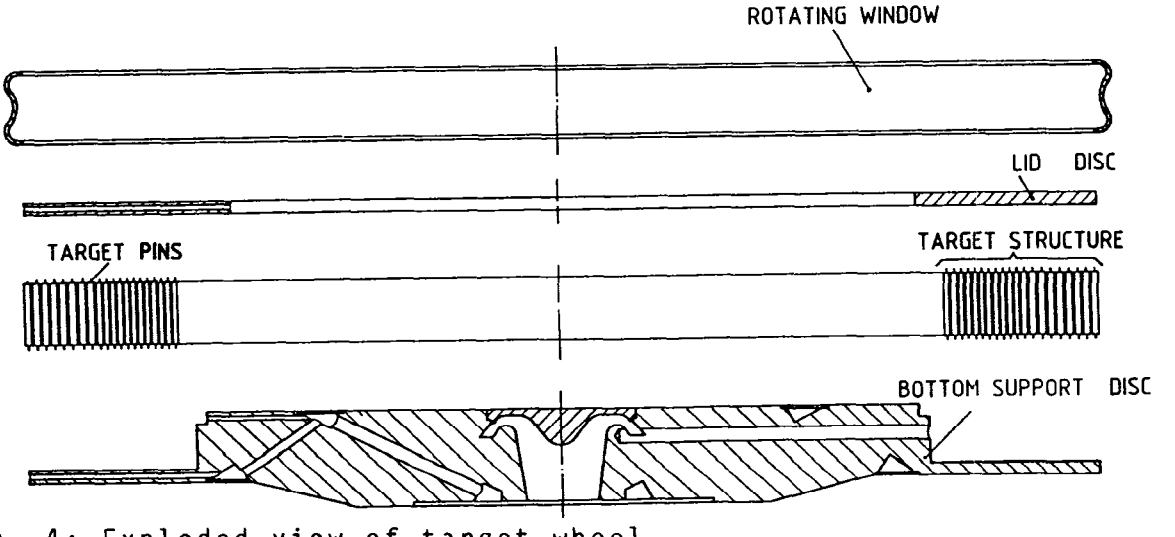

Fig. 4: Exploded view of target wheel

The dominating factor for the dimensioning of the target wheel structure is the static water pressure of 2.5 to 3.5 bars in the target structure. Detailed stress calculations have been carried out.

In order to verify the pressure loss calculations for this complex cooling water channel system in the target wheel, measurements on a 1:1 model are being carried out. In addition welding tests with electron beam and argon arcwelding of target wheel structures on a 1:6 and 1:4 scale are being performed.

revolution frequency	0,5 Hz	
outer dimensions		
diameter	2565 mm	
height	166 mm	
inner structure of target	cylindrical target pins in staggered rows	
technical target depth	362 mm	
number of target pins	8464 mm	
number of staggered rows	23 mm	
outer diameter of target rods	20,2 - 14,3 mm	
clad of target pin		
material	circaloy/AlMgSi1	
clad thickness	0,5 mm	
structural material of target wheel	AlMgSi1	
target material	uranium (UMo 10)	(tungsten)
target cooling		
cooling water flow rate	500 m³/h	(250 m³/h)
temperature increase	21,5 K	(10,3 K)
pressure loss over target depth	1,0 bar	(0,4 bar)
total pressure loss over target wheel	1,5 bar	(0,6 bar)
weight target wheel		
total	4672 kg	(4864 kg)
target material	2957 kg	(3149 kg)
structural material	1715 kg	(1715 kg)

Tab. 2: Target wheel (technical data)

Thermal/nuclear data

Table 3 shows essential thermonuclear data for the uranium and tungsten target which have recently been calculated by Filges et at /1/ using an improved technical design of the rotating target.

	uranium	tungsten
range of protons (cm)	48.3	44.4
target depth for 95% of neutron production (cm)	36.0	36.0
target depth for max. neutron discharge (cm)	8.0	7.5
max. energy deposition (J/cm^3)		
-per pulse	149	99
-during rotation through the proton beam	238	127
temperature increase during rotation through the proton beam in hot spot (K)	107	57
average capacity in target (MW)	12.5	3.0

Tab. 3: Thermal and nuclear data of target

Target structure

Cylindrical target pins in symmetrical geometric arrangement in the interior of the target wheel form the target structure. Each pin consists of an inner target material core covered by a wall (cladding). This clad ends in an upper and a lower cylinder, which fix the target pin in the corresponding positioning bores of the bottom support and the lid disc (see Fig. 5).

The arrangement of the target pins in the target wheel is given for the uranium target for an energy of the proton beam of 1100 MeV (Fig. 3. The target wheel with tungsten target pins is identical in its arrangement).

Target wheels of this arrangement for both heavy metals can most likely also be used for significantly lower proton beam energies (from 600 MeV up). In this target there are 8464 single target pins arranged on 23 concentric circles. 368 target pins are positioned on each of these concentric circles. The angular separation of the pins is the same on each of the circles thus necessitating different diameters of the target pins for each of the circles. Between neighbouring pins there are 1 mm gaps for the cooling water flow. The target pins are cladded (0.5 mm wall thickness) in order to prevent the direct release of spallation products from the pin surfaces of the target material into the cooling water and in addition to avoid the contact of uranium with water. In order to keep the release of spallation products from the surfaces of the cladding material into the cooling water as small as possible, a cladding material with a low atomic weight and a low density will be given preference.

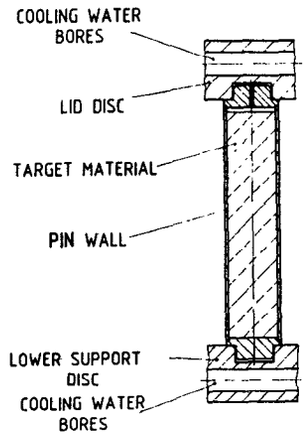

Fig. 5: Target pin

Thermal and stress analysis

The heat energy impact to a target pin is limited to a certain time interval by the rotation of the target wheel. The temperature rise takes place instantaniously within 250 µs because the rotation speed of the wheel is adapted so that each pin is exposed to one full proton pulse only. After this heat-up event the target pin is cooled down by the cooling water flow outside of the proton beam for the time of the wheel revolution of 2 seconds. So the time dependent temperature trend of one pin is also pulsed having of course a significantly smaller repetition frequency (0,5 s^{-1}) compared with that of the proton beam (100 s^{-1}).

The temperature rise for the target pin (hot spot in the pin centre, including proton beam rim effects) is 107 K for the uranium; 57 K for the tungsten material (see Fig. 6).

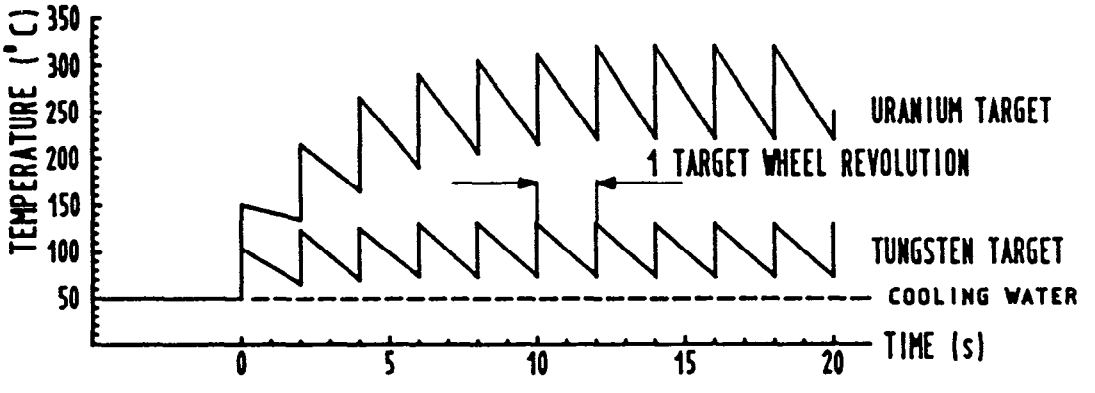

Fig. 6: Time dependent temperature trend for the target pin hot spot (start up behaviour for 1100 MeV, 5 mA, uranium, tungsten).

Due to the different energy impacts and heat conductivities of uranium and tungsten (UMo 10 = 0,16 W/cm K; W: 0,90 W/cm K) the temperature levels in the pin centre at equilibrium are

also different. After start up of the proton beam the temperature equilibrium is achieved for the tungsten target after 4 cycles (8 s) and for the uranium target after 7 cycles (14 s).

To keep the temperature level in the target material as low as possible the cladding tube is solid bonded to the pin to achieve a good heat transfer between the target material and the cladding. The temperature gradient over the pin cross section generates linked mechanical stresses, which are increasing with growing radius. The actual stresses, however, are well below the yield strenght of the target and cladding material (see Fig. 7).

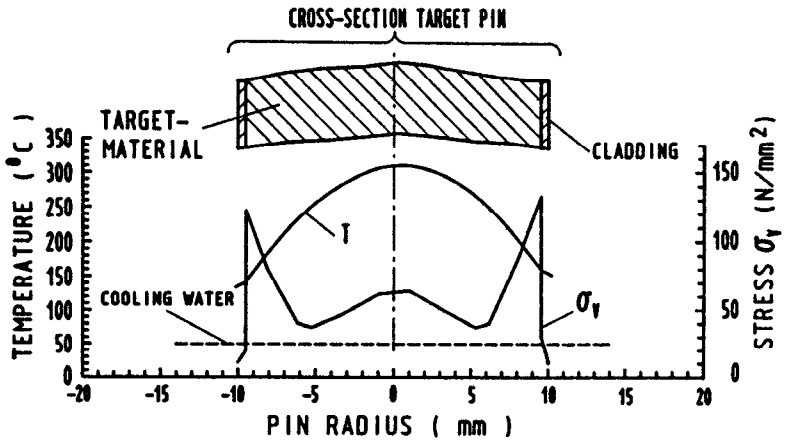

Fig. 7: Temperature and stress profile in the hot spot plan of the uranium target.

KLA-unit

The KLA-unit has to serve the following functions:

- function 1: Providing cooling water flow to and from the target wheel rotating in a vacuum atmosphere where only slight water losses are permitted.

- function 2: Taking up all generated forces, i.e. the weight of the target wheel as an axial force and the effects of imbalance and gyroscopic moment.

- function 3: Effecting the rotation of the target wheel at 30 rpm.

To fulfil function 1 all KLA-versions tested so far need a sliding ring seal. Sliding ring seals are proven standard components. However, in this special case they have to function in a vacuum environment and in a field of high level radiation. Therefore corresponding tests are being carried out at present.

Different approaches are examined to fulfil function 2. In a first tested version the axial and radial forces are taken up by hydrostatic pressurized water bearings.

The experience gained so far and the results of the tests of the KLA type I led to the design of a second version (KLA type II, see Fig. 8). KLA type II also has the proven hydrostatic axial water bearing of type I but has only one radial bearing. This radial bearing is a ball bearing of 430 mm diameter running without additional lubrication in the cooling water. This kind of application is not state of the art, so that corresponding development work and tests on an original-sized ball bearing have been started. Furthermore the KLA type II is equipped with an axial water turbine instead of a radial turbine as used in type I. By this method outside ducts for the cooling water as in type I are avoided, so that all water connections between the support and the KLA are only inside the bottom flange. By this means remote handling is facilitated.

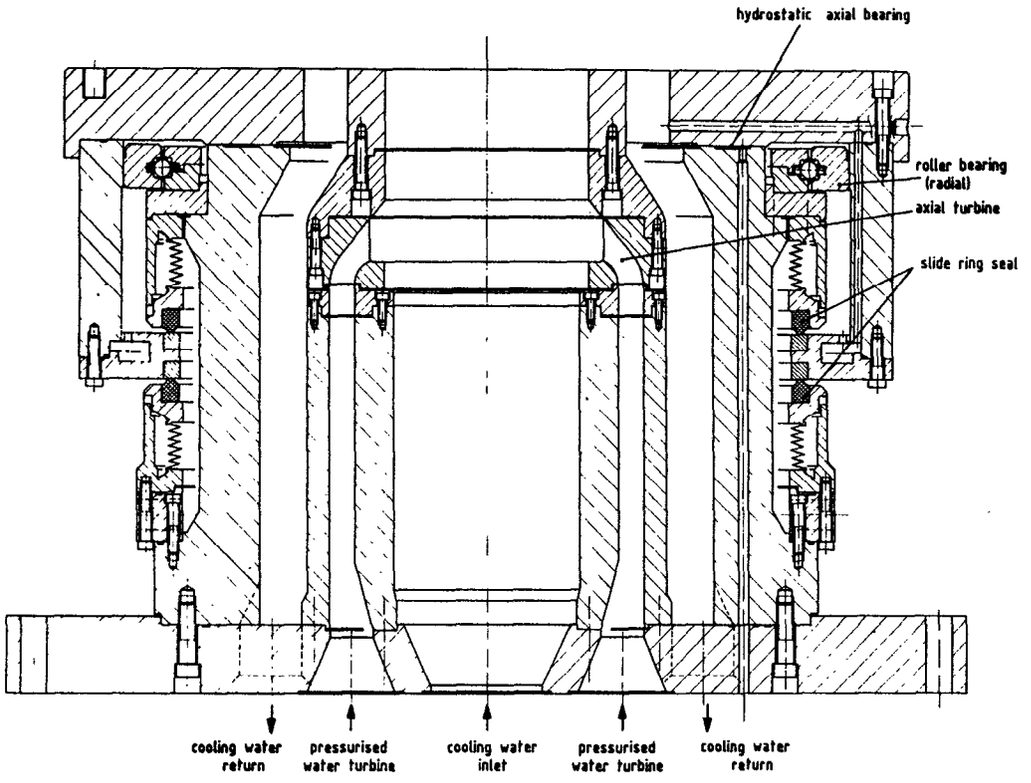

Fig. 8: KLA type II for cooling water supply, support bearing and drive of target wheel (hydrostatic axial bearing, radial roller bearing and axial turbine as drive)

Another difference of the KLA type II to type I is a second sliding ring seal instead of a labyrinth seal. Both form an annular vacuum chamber, that surrounds the first slide ring seal. Thus the monitoring of the leak rate of the first slide ring seal becomes possible. Tests of a corresponding dry running slide ring seal on a 1:1 scale have been started.

The material for the slide ring seals is under development. Since the combination of tungsten carbide against carbon is well established functional and radiation tests for these materials are under way. Furthermore the combination of silicon carbide and carbon is under investigation (reaction bonded SiC, SiC/graphite compound materials, carbon/graphite mate-

rials), because less friction and less radiation damage could be expected for these materials.

The long time tests of a slide ring seal on a 1 : 1 scale with non radiated tungsten carbide under original temperature and pressure conditions show good results with a total water leakrate of about 1 $cm^3 \cdot h^{-1}$ into the surrounding vacuum atmosphere.

References

/1/ D. Filges et al., "Nuclear Aspects in the SNQ Target Design", Proc. ICANS-VIII, Rutherford Appleton Laboratory, 1985 July 8 - 12, this volume

Proceedings of the Eighth Meeting of the International Collaboration on Advanced Neutron Sources (ICANS-VIII)
8-12 July 1985, Rutherford Appleton Laboratory Report RAL-85-110

Thermal Cycling Growth of Uranium Alloys and Fabrication of SNQ Target Pins

P. Krautwasser*, H. Hoven*, H. Kirchhöfer**
*Kernforschungsanlage Jülich GmbH, Institut für Reaktorwerkstoffe
D-5170 Jülich, FRG
** Firma NUKEM GmbH, D-6450 Hauau, FRG

Summary

Targets of neutron spallation sources are exposed to cyclic thermomechanical load induced by the pulsed proton beam. For the development of high power target elements, the cycling growth rates of α -uranium and α-uranium alloys were studied up to 550,000 cycles as a function of the lower cycling temperature T_o and the cycling amplitude ΔT. The growth rates obtained for α -uranium were not constant for given T_o, ΔT and material composition. Depending on the number of thermal cycles accumulated, the growth rate G can be classified in four categories: At cycle numbers $n < 50{,}000$, the G values are high and strongly dependent on T_o and ΔT. In the cycle number intervals 50,000 to 100,000 and about 450,000 to 550,000 most samples tend to shrink, which leads to negative growth rates. At cycle numbers $100{,}000 < n < 450{,}000$ the growth rate is hardly dependent on ΔT and smaller than the initial growth rate. For UMo10 alloys with the bcc γ -phase, no significant dimensional changes during thermal cycling were observed.

For the production of cladded uranium target elements, several fabrication techniques were tested to ensure high thermal conductivity at the uranium/cladding interface during target operation. Based on the material properties of the as-produced target elements, hot isostatic pressing of UMo10 spallation material and Zry-2 cladding gave the best result of all target element variations investigated.

Introduction

The UMo10 alloy is expected to have the best performance of the uranium based spallation materials under thermomechanical cyclic load for the following reasons: a) lack of thermal cycling growth of the bcc γ-phase in contrast to the orthombic α-phase and b) lower corrosion rates in water by a factor of 100 to 2000 compared to uranium.

As the γ-phase is metastable at temperatures below 774 °C, a phase transformation may occur during target operation at temperatures up to 320 °C. Therefore the γ-phase stability under thermal cycling as well as the effect of lower cycling temperature T_0 and cycling amplitude ΔT (Table 1) on the thermal cycling growth of α-uranium and α-uranium alloys were investigated.

Lower Cycling Temperature T_0 (°C)	Cycling Temperature Amplitude ΔT (K)
55	+ 10, + 35, + 65, + 100, + 170, + 205
125	+ 35, + 65, + 100
160	+ 35, + 65, + 100

Table 1: Lower cycling temperature T_0 and temperature amplitude ΔT of the α-uranium cycling program.

Experimental

To study the effect of thermal cycling upon uranium alloys, two methods were used:

a) Sets of up to 12 samples for each Δ T were mechanically transfered between thermostates with silicon oil at different temperatures. The holding time (immersion time) at the lower and uper temperatures was 15 s each, the transfer time of the samples 2 x 2 s. Up to 6 thermostates were placed in a glove box, flushed with nitrogen.

b) A single sample was periodically heated in a 4 kHz medium frequency induction furnace and cooled by a silicon oil containing cooling circuit.

The samples cycled were cylinders, 9 mm in diameter and 50 mm in length for dimensional measurements as well as sets of discs (9 x 2 mm) for metallographic investigations. The materials investigated were uranium, UMo5, UZr3.7, UTi0.7 and "adjusted uranium" with 470 ppm C, 250 ppm Fe and 250 ppm Si (all as α -phase) and UMo10 (as γ -phase).

Evaluation: After given cycle intervals, length and weight of the samples were measured. The changes in length were corrected for sample corrosion, assuming that the weight loss of the samples after cycling is due to an uniform corrosion at the sample surface.

The thermal cycling growth rate (per cycle) was determined in three different ways:

a) by calculating the "integral growthrate" $G_I = \varepsilon / n$ from the total relative change in samples length $\varepsilon = (l_n - l_o) l_o$ at a given cycle number n. (l_o: initial sample length).

b) by calculating the mean of the growth rates for given cycle number intervals and

c) by calculating the growth rate from the slope of the fitted ε -curve.

For optimization of integral target elements, different cladding procedures were applied: hot isostatic pressing (HIP), extrusion, shrink fitting and soldering. UMo10 was used as spallation material with and without a nickel bonding. The Ni coating was deposited either by electrolytic coating or PVD. As cladding material Zry-2, AlMg3 or AlMgSi0,5 was chosen.

The quality of the uranium/(bonding)/cladding interface, which is important for high thermal conductivity, was investigated by optical inspection of metallographic sections and electron microprobe analysis (MPMA) as well as measurements of shearing and tensile strength.

Results

a) Thermal cycling

Uranium and uranium alloys with α-phase: Depending on the number of cycles accumulated, different swelling mechanism occur during thermal cycling at given T_o, ΔT and material composition, leading to variing growth rates. In the cycle number intervall investigated (0 to 550,000 cycles), four categories of growth rates can be distinguished:

- G_o ($n < 50{,}000$) is very sensitive to cycling parameters and increases with increasing ΔT (Fig. 1) and T_o (Figs. 1 and 3), which is in agreement with literature data
- G_1 ($50{,}000 < n < 100{,}000$) is mostly negative
- G_2 ($100{,}000 < n < 400{,}000$) is smaller than G_o and hardly dependent on ΔT, as can be concluded from the similarity of the slopes of the fitted ε -curves in Fig. 2 and the same values for the growth rates G_I in Fig. 3.
- G_3 ($400{,}000 < n < 550{,}000$) is negative for most samples as indicated by the negative slope of the ε -curve above 400,000 cycles in Fig. 4.

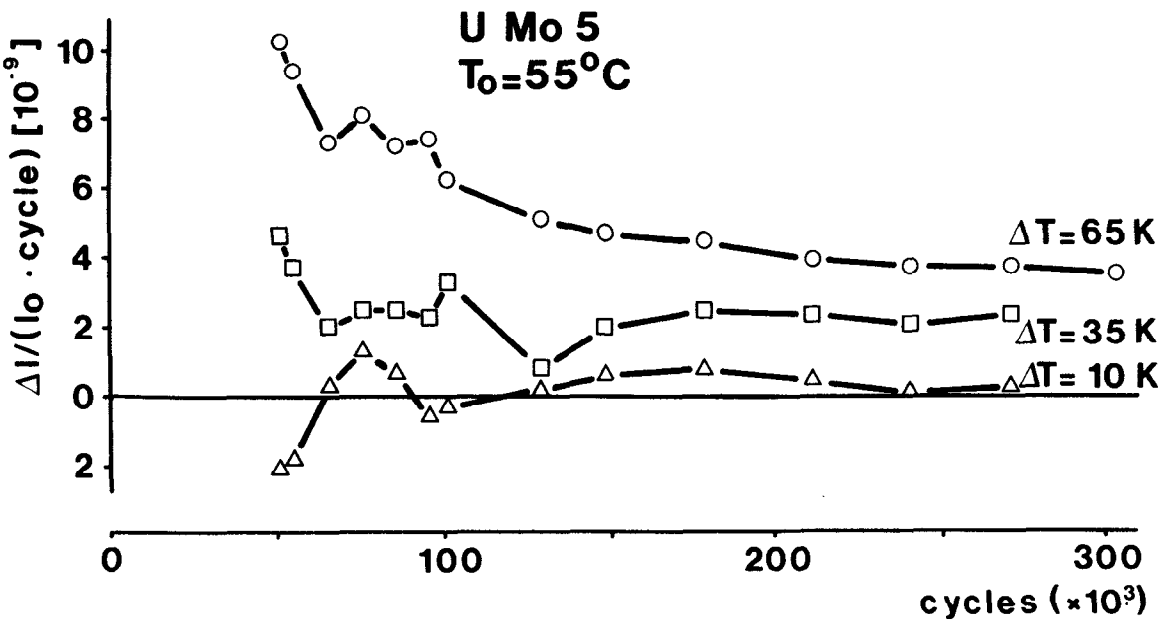

Fig. 1: Cumulative thermal cycling growth rate (per cycle) vs. cycle number of UMo5 at a lower temperature T_0 of 55 °C and ΔT = 10,35 and 65 K

In general α-uranium shows a higher growth rate than the α-uranium alloys investigated. From these, "adjusted uranium" yields the lowest G-values at low T_0 and small ΔT, but the highest growth rates at high T_0 and ΔT.

For the application of α-uranium alloys as target material it is important, that although G_0 is high and proportional to T_0 and ΔT, the thermal cycling growth rate at high cycle numbers is much smaller or even negative and nearly independent of ΔT. The total dimensional changes of the samples measured at a cycle number of 550,000 was, except for uranium, at least a factor of 10 to 30 smaller than these calculated from the G_0 values, assuming a constant initial growth rate up to the above mentioned cycle number.

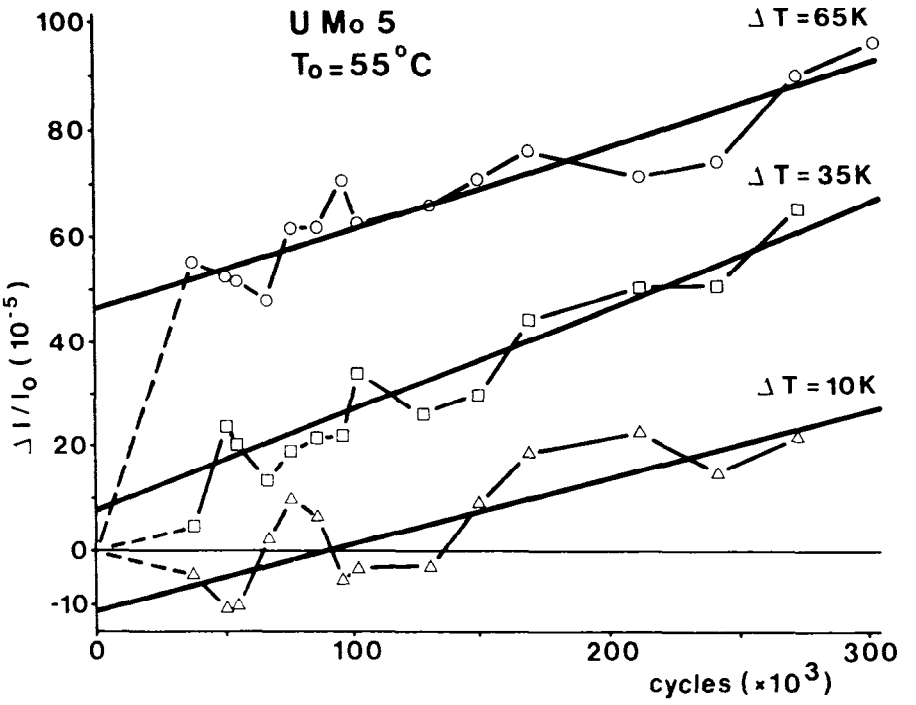

Fig. 2: Relative dimensional changes $\varepsilon = \Delta l/l_0$ vs. cycle number of UMo5 at T_0 = 550 °C and Δ T = 10,35 and 65 K

The UMo10-samples with the metastable bcc γ-phase did not show any significant dimensional change even at the highest T_0 of 160 °C (Δ T = 100 K) or the largest Δ T of 205 K (T_0 = 55 °C)

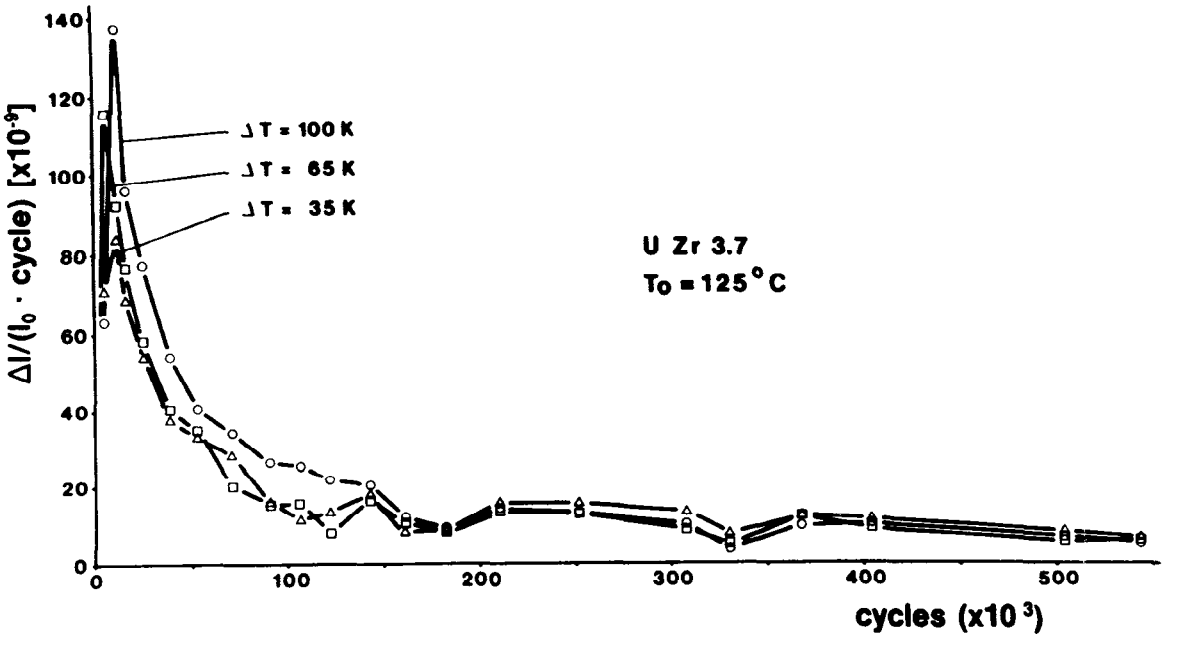

Fig. 3: Cumulative thermal cycling growth rate vs. cycle number of UZr3.7 at T_0 = 125 °C and Δ T = 35,65 and 100 K

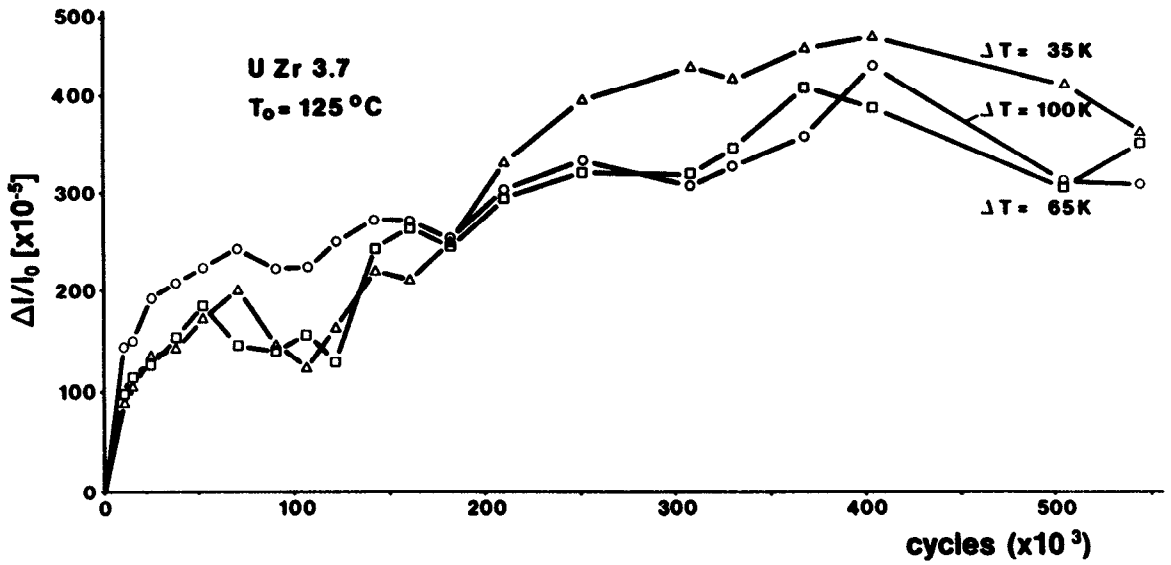

Fig. 4: Relative dimensional changes $\varepsilon = \Delta l/l_0$ vs. cycle number of UZr3.7 at T_0 = 125 °C and ΔT=35,65 and 100 K

With a time at temperature of 15 s per cycle each at the upper and lower temperature, the equivalent temperature treatment during thermal cycling was for example for the samples at T_0 = 160 °C and ΔT = 100 K about 2,500 h (100 d) at 160 °C and at 260 °C respectively.

Samples annealed at 550 °C for 1 to 330 h prior to thermal cycling exhibit an increase in thermal cycling growth with initial annealing time, in qualitative agreement with the degree of γ to $\alpha + \delta$ phase transition as seen in the corresponding metallographic sections after isothermal annealing.

b) Target element fabrication

For the optimization of the UMo10/cladding interface, the thickness of the nickel bonding (0 to 40 um) and the cladding material (Zry-2, AlMg3, AlMgSi0.5) as well as the technique for the bonding deposition and the cladding procedure was varied. Hot isostatic pressing (HIP) showed the best results in encapsulating the UMo10 spallation material, independent whether a Ni-bonding was used or not. In contrast to the other variants

(UMo10/Ni/Zry-2, UMo10/AlMg3, UMo10/AlMgSi0.5, UMo10/Ni/AlMg3, UMo10/Ni/AlMgSi0.5), hot isostatic pressing of UMo10/Zry-2 (without a Ni-bonding) did not lead to numerous intermetallic phases at the UMo10/cladding interface as in the case of the other variants.

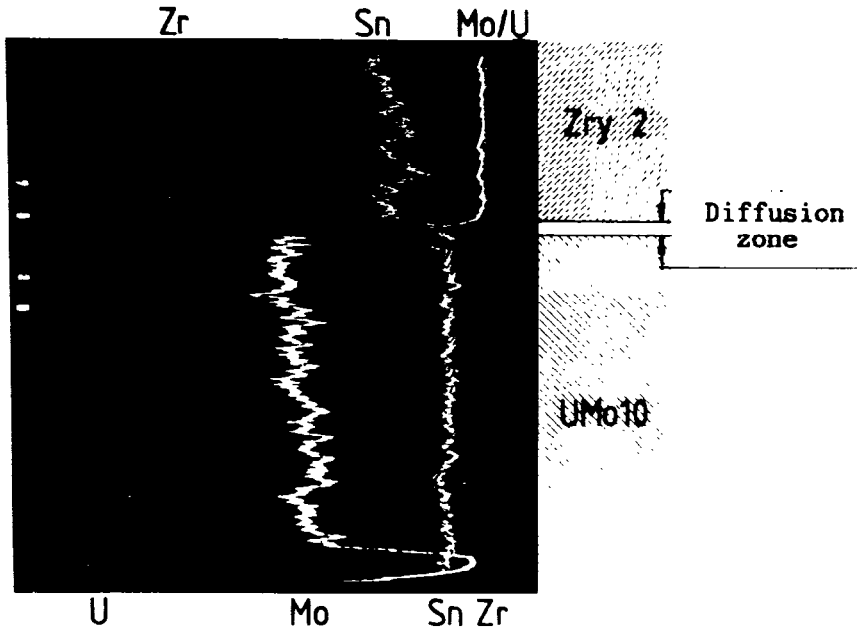

Fig. 5: MPMA linescans of the HIP-interface UMo10/Zry-2. HIP temperature: 800 °C (6 h) (900x).

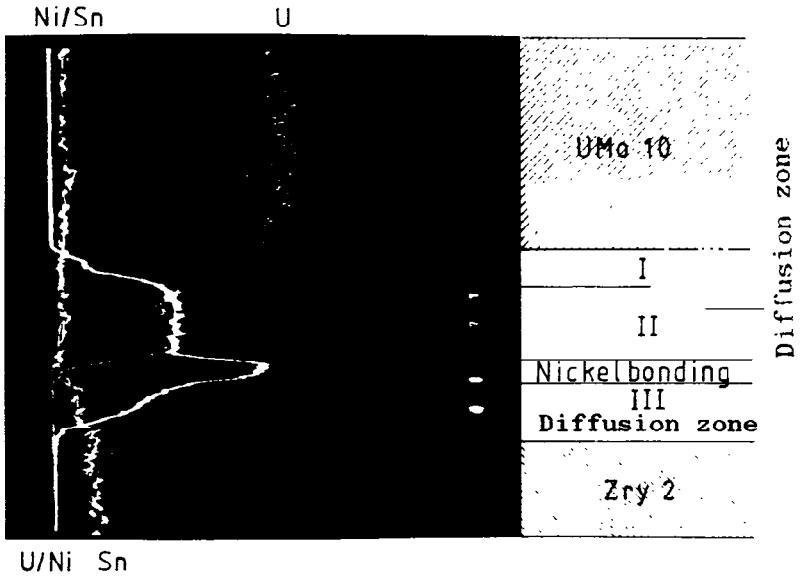

Fig. 6: MPMA linescans of the HIP-interface UMo10/Ni/Zry-2. HIP temperature: 700 °C (6 h). Deposition of Ni-bonding by electrolytic coating; initial layer thickness: 20 µm (900x)

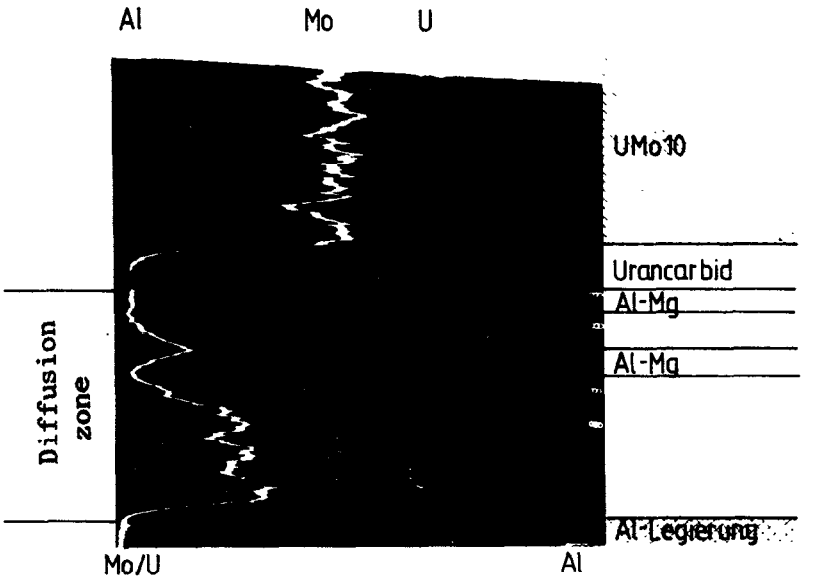

Fig. 7: MPMA linescans of the HIP-interface UMo10/AlMg3. HIP temperature: 550 °C (2 h) (900x).

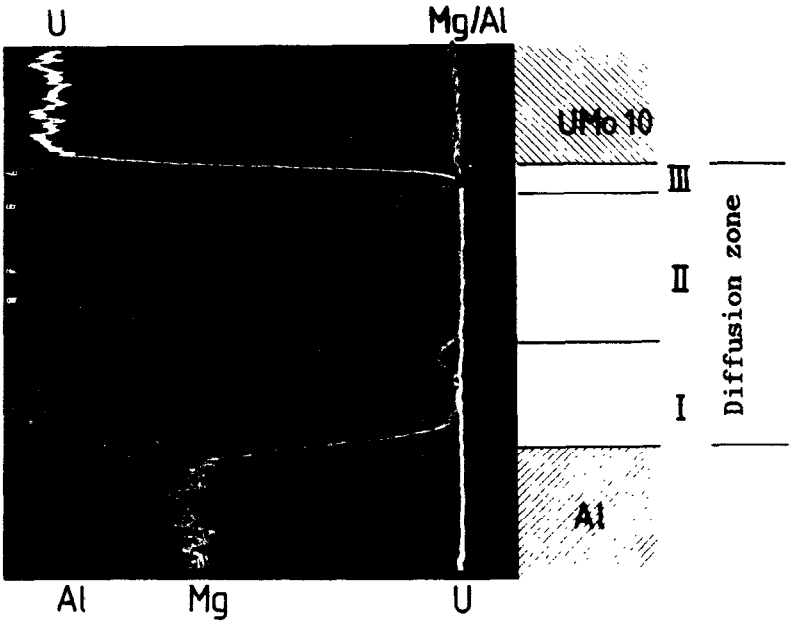

Fig. 8: MPMA linescans of the HIP interface UMo10/Ni/AlMg3. HIP temperature: 550 °C (2 h). Initial Ni layer thickness: 30 µm (900x)

As some of the intermetallic phases are expected to be brittle, cracks may develope during target operation, reducing the thermal conductivity at the interface and the mechanical stability of the cladding. Thus, target elements produced by hot isostatic pressing of UMo10 and Zry-2 without Ni-bonding are expected to perform best.

This assumption is backed by tensile and shearing strength measurements of the UMo10/cladding interfaces. An example is given in Fig. 9, showing the highest shearing strength for the UMo10/Zry-2 interface and a HIP temperature of 800 - 900 °C. In agreement with tensile test data, the shearing strength is lower for the UMo10/Ni/Zry-2 version and the target elements with aluminium-based claddings independent of the presence of a Ni-bonding. The increase in strength with HIP temperture holding time of the UMo10/Ni/Zry-2 interface is due to the reduction of the Ni-bonding layer thickness during hot isostatic pressing.

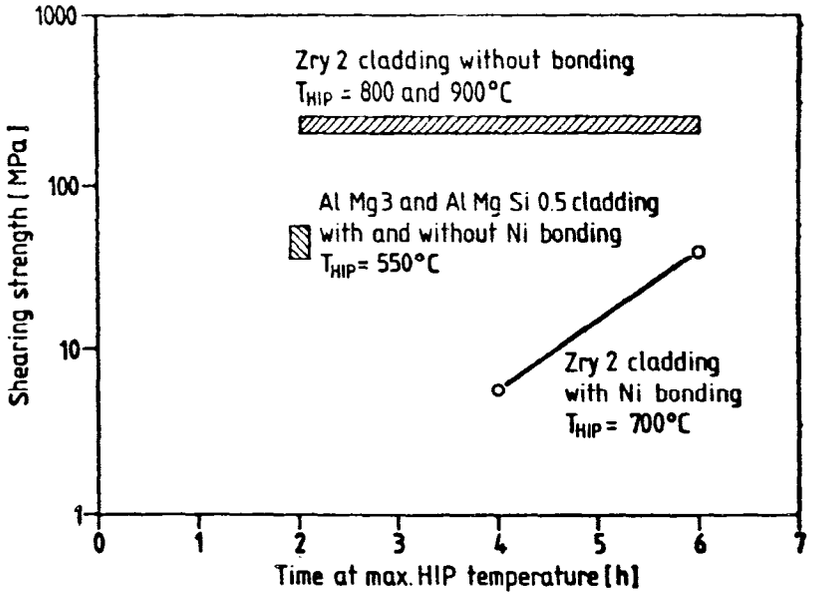

Fig. 9: Shearing strength of different UMo10/(bonding)/cladding interfaces as a function of HIP temperature holding time

Proceedings of the Eighth Meeting of the International Collaboration on Advanced Neutron Sources (ICANS-VIII)
8-12 July 1985, Rutherford Appleton Laboratory Report RAL-85-110

DESIGN FOR REMOTE HANDLING IN THE SNQ TARGET STATION

H. Stechemesser 1), G. Thamm 2),

1) Zentralabteilung Allgemeine Technologie
2) SNQ-Projekt, Teilprojekt 3 "Neutronentargetanlage"

Abstract:

Due to the high radiation exposure the majority of components operated in the SNQ neutron target facility requires remote techniques when being handled for inspection and maintenance and also for replacement. Therefore the technical design of these components has to consider the suitability for remote handling and adequate handling procedures must be planned very carefully. Since the target (uranium) is the most radioactive component which also experiences the highes stresses during beam operation the planned design permits to directly move it mounted on a movable plug into a hot cell which is arranged immediately adjacent to the target block. A short description of the shielding plug and the target cell arrangement and equipment is given.

Furthermore some informations on facilities and procedures necessary for the safe handling of the essential target block components are reported.

1. Introduction

For all components of the SNQ plant which are exposed to high radiation or to thermo-mechanical stresses during operation, inspection and maintenance work at scheduled intervals and also repair or complete replacement of defective components must be planned very carefully in detail. In the neutron target facility effective and above all safe handling procedures are essential, primarily for the target.

The initial (/1/, /2/) design already envisaged that the target should be moved directly into a hot cell in order to be able to use proven standard hot cell equipment for handling. Optimization studies led to the arrangement of the target cell immediately adjacent to the target block below the experiment floor (-8 m) in a forward direction relative to the proton beam and to the design of a movable shielding plug on which the rotating target and other components (KLA-unit, H_2O-moderator) are mounted. This shielding plug slides on a track inclined at an angle of 45° between two positions: operating position (in the centre of the target block) and handling position (in the target cell).

Compared with previous designs (horizontally /1/,/2/ or inclined /3/ - also at 45°, but in a backward direction - connected to the target block) the arrangement now under investigation has the following 4 advantages:

- The proton beam area close to the target block can be designed much narrower giving more usable space for the experiments in the target hall and in addition enabling the installation of two more horizontal beam tubes (10 instead of 8 beam tubes for the H_2O-moderator).

- The end plate of the target shielding plug with its sealing and locking devices and the connection elements as well as the surrounding area will not be activated by neutron radiation, thus allowing the access of personnel to the end plate in case of failure of the remotely operated elements.

- A complete separation of handling of the target and the other components on the shielding plug from handling of the installations in the proton beam area (bending magnets, focussing elements).

- Special supply installations for the proton beam can be located underneath the proton beam tunnel (admittance) in the last 10 to 15 m in front of the target block.

Safe handling must also be provided for several components of the target block of the neutron target facility since stress during operation will probably limit their life. These components (see Fig. 1) are basically the reflector of the cold source, the cold source itself, shutters of beam tubes and neutron guides, choppers, special irradiation devices in the reflector of the cold source and the focussing magnets in the target block. The design for the handling of these components employs a separate handling system comprising a shielded container equipped with a hoist or manipulator and a movable shielding gate.

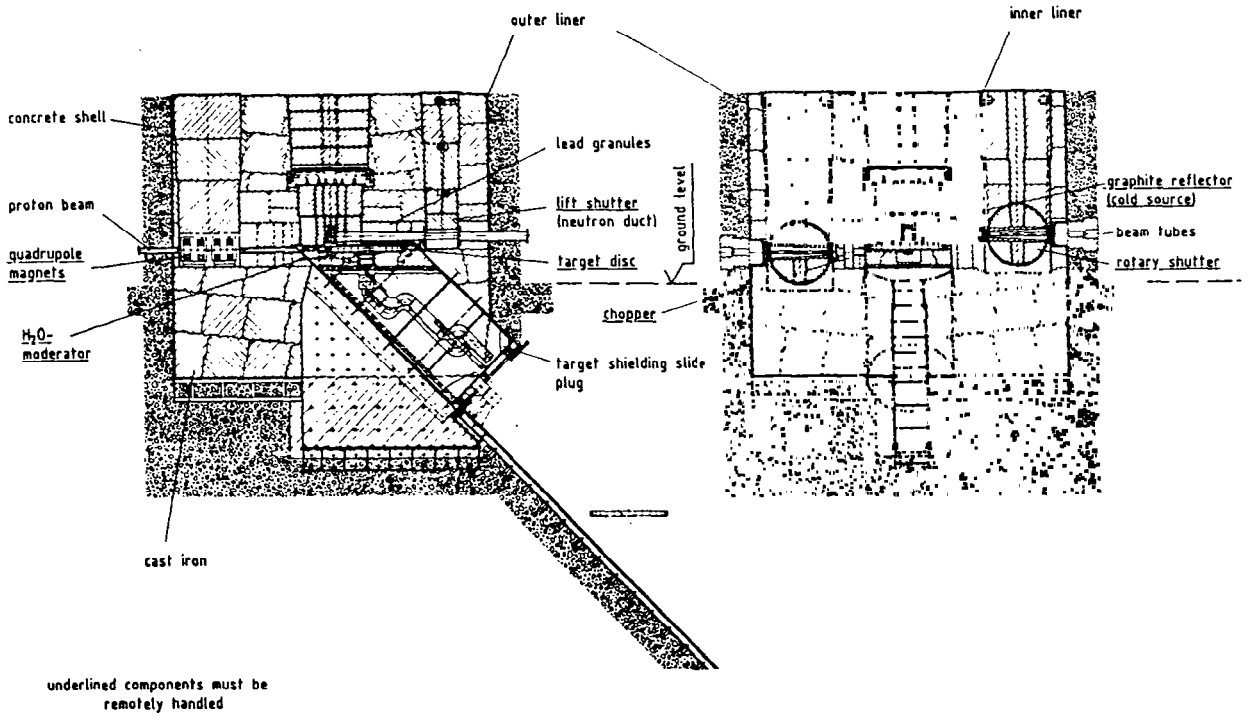

Fig. 1: Target block (vertical view)

2. Target shielding slide plug

The design currently under consideration features a special movable shielding plug with the target disc and KLA-unit fixed on it which can be moved by a hydraulic drive along a slide track inside the cavern which is inclined at an angle of 45° (see Fig. 2). This plug is a steel frame construction of oval or octoangular cross-section in which supply and cooling pipes are imbedded in lead granules for shielding reasons. The plug also carries, the H_2O-fast moderator and its reflector mounted underneath the target disc. The end-plate at the lower side of the plug seals the target cavern (part of the outer liner system). The seal flange of this end-plate is hydraulically placed into the sealing position. All penetrations of pipes and electric cables necessary for supply and measuring are designed vaccum tight. All connections in the design probably will be combined to one coupling device which can be remotely operated.

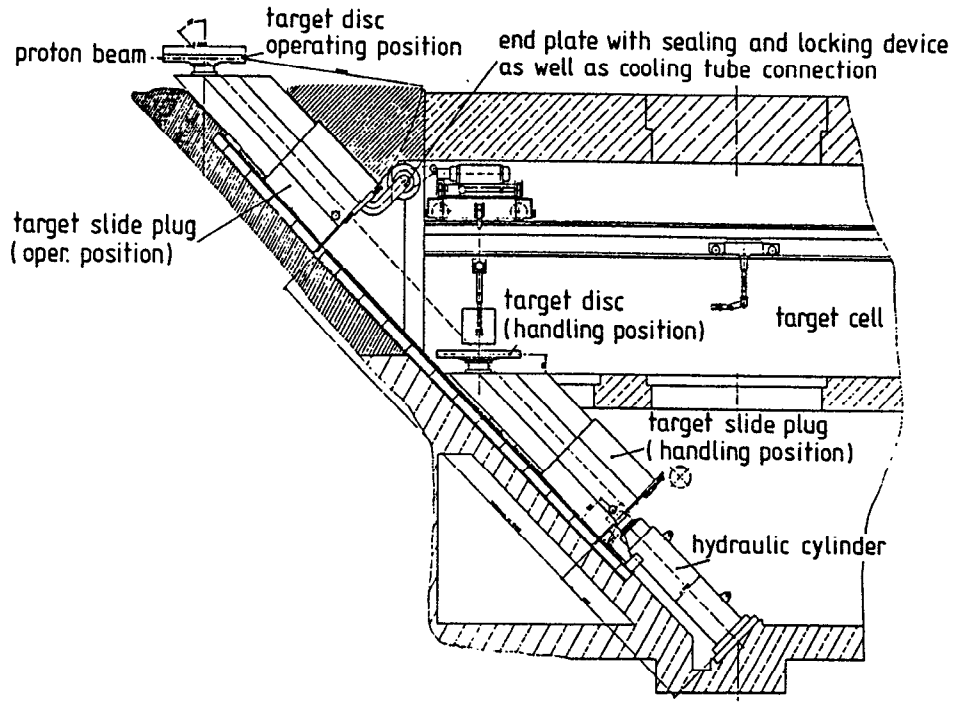

Fig. 2. Target shielding slide plug

In this device the main cooling pipes are arranged concentrically (pressure increasing from inner to outer tube). Alternative designs are being studied at present.

By means of the afore mentioned hydraulic drive (capacity 200 t) the target shielding plug is lowered into the inspection position after disconnecting the connections and locking device. In this position the target disc is in a well shielded cell (target cell) beneath the experiment floor of the target hall. In this target cell all inspection, maintenance and probable repair work as well as replacement or exchange of the target disc and all other components mounted on the plug can be performed by means of the standard equipment of a hot cell.

The feasibility of the tilted arrangement of the target cavern including moving, locking and sealing of the shielding slide plug was demonstrated in a feasibility study carried out by an experienced industrial company.

More information and data of the target shielding slide plug is given in table 1.

– 45° arrangement in a forward direction relative to proton beam, motion on slide track between 2 positions (operation and handling) with special locking (bolts) in upper operation position	
– total weight of slide plug	about 220 t
– dimensions of plug	about 2.5 m octagonal or oval, 6.5 m long
– welded structure	material: mild steel (stainless)
– shielding material	lead granules
– movement by hydraulic drive	
– cylinder force	200 t
– cylinder stroke	12,400 mm
– hoisting and lowering velocity	0.5 m/min
– positioning accuracy of target disc	≤ 5.0 mm

Tab. 1: Target shielding slide plug (essential items and technical data)

3. Target cell

The arrangement, design and geometry of the target cell is presented in Fig. 3. It is subdivided into three areas which are:

- assembly cell,
- workshop cell and
- airlock cell.

The target cell is equipped with a total of 8 pairs of mechanical manipulators. Two pairs each are on opposite sides of the assembly and airlock cell. The other four pairs are mounted in the workshop cell. Each pair of manipulators is mounted above

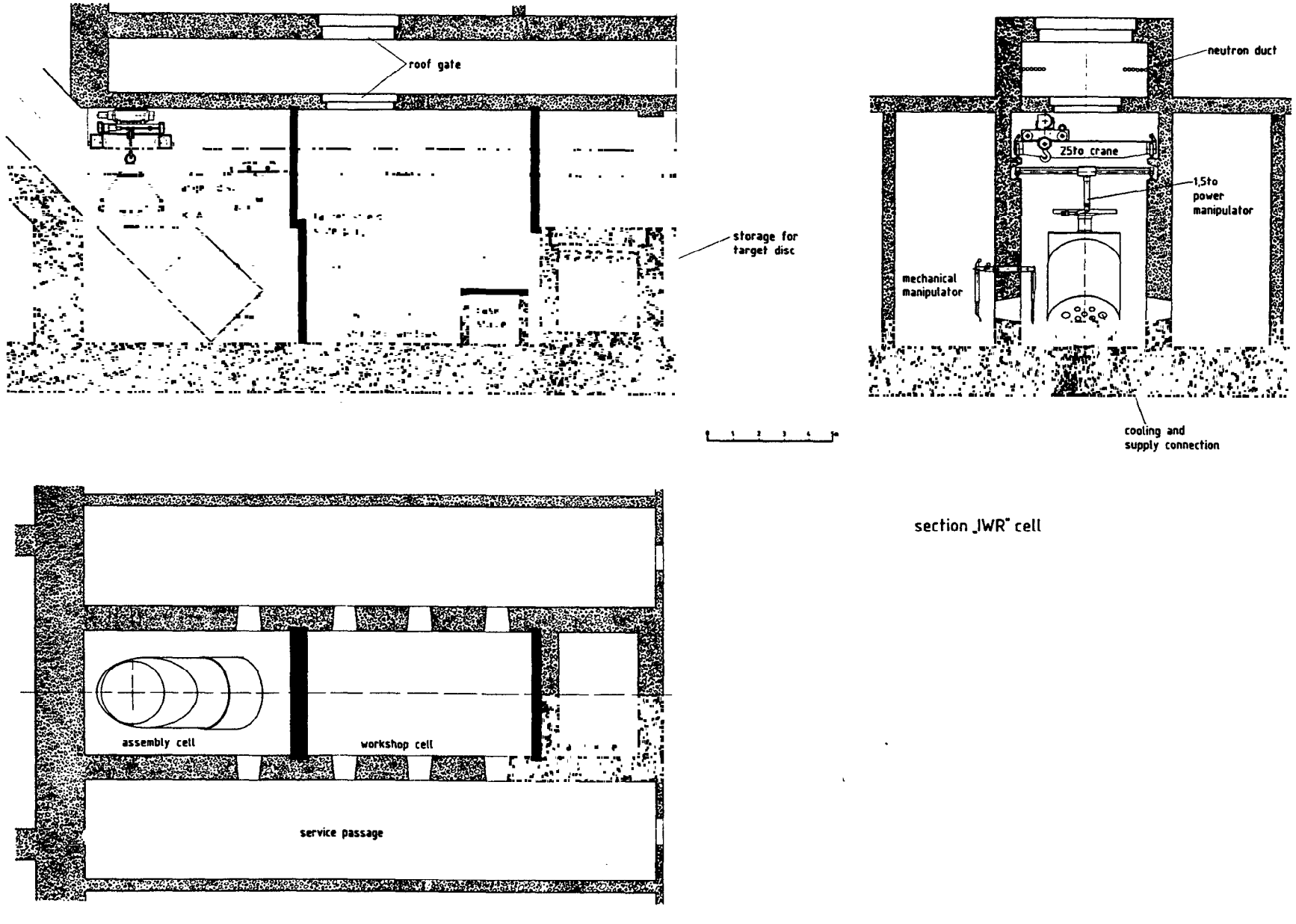

Fig. 3: Target cell

shielding windows in the 1 m thick concrete shielding wall of the cell. In addition there are one retractable viewing plug and wall penetrations in the window frames for supply and control connections into the cell. An overhead crane of 250 KN capacity moves over the total length of the cell.

The basic equipment of the cell also includes a power manipulator with a capacity of 15 KN at the hook of its telescope. The equipment is well proven and available on the market.

Apart from the basic apparatus, auxiliary equipment is needed. These are various tools for maintenance and repair, and also for disassembly especially of the target disc. The type and number of these tools (for instance drilling machines, impact wrenches, cutting machines and so on) will be determined in a test programme which is in progress.

The target cell has several transfer systems, a Padirac system and a one-way system in the workshop cell.

The Padirac-system is already in use in the KFA decontamination department and in the three hot cell facilities thus providing for easy transport to either of the facilities. These will bei used depending on the sort of work to be carried out, for instance waste removal to department of decontamination or post irradiation examination of target rods to the hot cells.

The one-way system only serves to introduce small tools or other items into the cell. Larger components (up to 2.5 m diameter) can be introduced from the target hall into the workshop cell via the cell roof gate.

4. Handling of the target

The uranium target is the most important component as far as the level of radioactivity and afterheat is concerned. Therefore it determines the design of the target cell and special handling procedures. Table 2 presents activity inventory and afterheat data of the uranium target (/4/,/5/), for different times after shut-down of target operation (12000 h, assumed).

Time after shut-down (d)	0	1	5	10	100
Activity inventory (MCi)	45.1	12.6	5.1	3.6	0.8
Afterheat (kW)	415	50	29	20	5

Tab. 2: Activity inventory and afterheat of the uranium target for different times after shut-down (12000 h target operation)

The uranium target will be handled not earlier than 5 days after shut-down of the SNQ target station. At this time the decay heat is about 30 KW, the activity about 5 M curies. Since the corresponding values of the tungsten are significantly lower (about 1/10) the waiting time will be less than 2 days till the target can be moved into the target cell.

The normal H_2O cooling of the target is interrupted during lowering of the target shielding plug into the inspection position and handling of the target in the target cell. Thus the temperature of the target would be increased by about 30 - 40 K per hour under the pessimistic assumption that heat removal (e.g. by conduction, convection or radiation) from the target is not taken into account.

Therefore, after disconnection of the normal cooling pipes (see 2.) the target shielding plug will be connected to a small flexible cooling device that will keep the target at moderate temperatures ($<$100° C) during lowering of the plug and afterwards in the inspection position. If later the small cooling device must be disconnected according to the handling requirements a significant portion of the airflow provided by the ventilation system of the target cell can be directed onto the target disc by means of a movable fan in time intervals to cool the target.

It should be pointed out that the afore described cooling is not needed for safety reasons (release of fission and spallation products according to cladding failure of the target rods) because the temperature of the target will not exceed 300° C due to the heat removal by natural convection and to a smaller extent by radiation of heat when the shielding plug is moved in the cavern or the target is handled in the cell. /3/

5. Handling system for the target block

Fig. 4 shows the concept of this system which is necessary for dismantling, remounting and transportation of the components in the wells of the target block. Its main component, a shielded container, has an inner diameter of about 2.5 metres and a

height of about 2.6 metres. The second component is a movable shielding gate that is to be placed over the top of the well in which the component in question is located. The shielded container can be equipped with either a hoist and a grip or with a manipulator on a telescope for remotely loosening or fastening the connections of the component and lifting or lowering of the component.

At present a design stud y of the system is being carried out in cooperation with an industrial company.

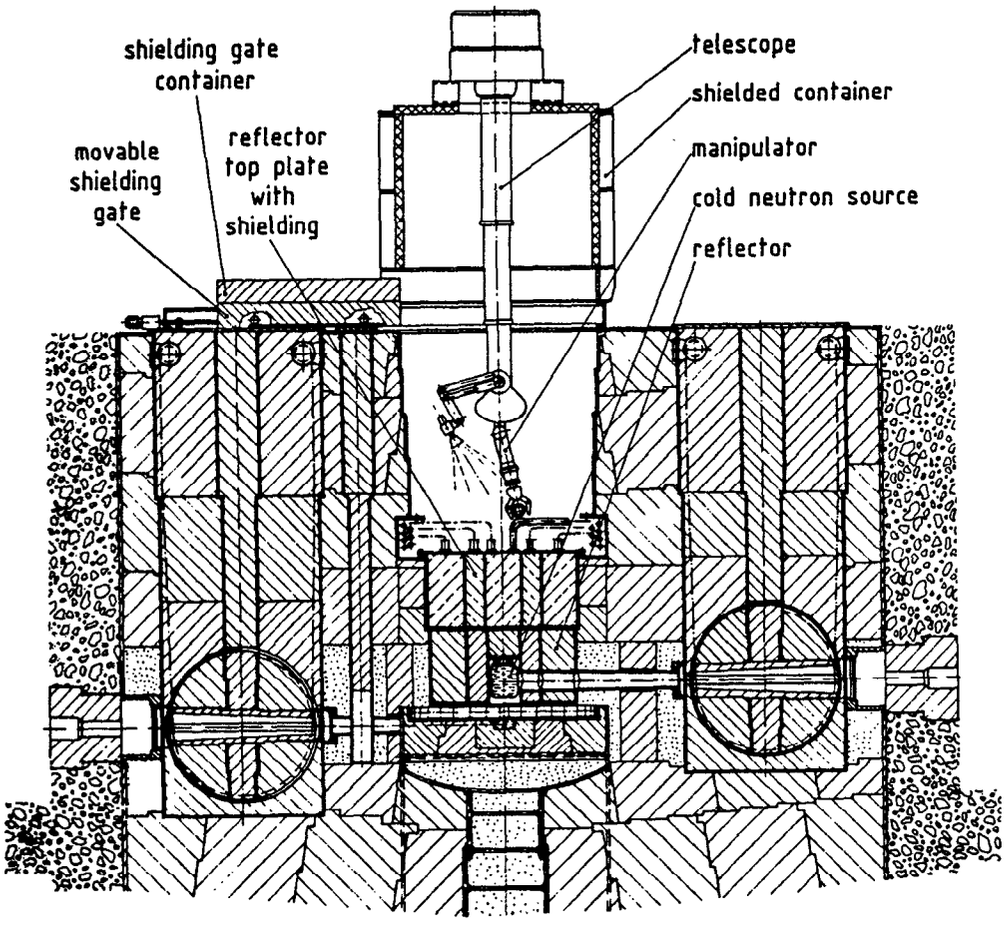

Fig. 4: Handling system for the target block

6. Advanced handling equipment

For the target block handling system, and also for a handling system for accelerator components and of components in the connecting tunnel and close to the target block the design concepts call for advanced handling equipment like robots and/or telemanipulators (electric master-slave manipulators). In a handling test programme both types of equipment have been tested for their suitability. As the main result it can be stated, that for all routine handling operations (for instance preparation for removal of a component) especially adapted robots with the use of programmed control are far more suitable than telemanipulators mainly with respect to speed. Nevertheless it must also be emphasized that in odd cases (deviations from handling routines) a telemanipulator is very useful. An extensive market analysis indicated that out of the large number of types of robots available only a relatively small number of robots combined with appropriate additional equipment seem to be applicable to the requirements for handling in the SNQ. Development of telemanipulators is being carried out in Germany and especially in France. In both cases cooperation with third parties has been initiated. For the SNQ handling test programme in progress a robot has been purchased.

References:

/1/ Jül-Spez-113, KfK 3/75, "Realisierungsstudie zur Spallations-Neutronenquelle, Juni 1981

/2/ H. Buttgereit et al. Proc. ICANS-VII, Chalk River Nuclear Laboratories, 1983 Sept. 13-16

/3/ SNQ 0 /BC 170384, "SNQ-Projektbericht zum Abschluß von Phase B, Februar 1984

/4/ H. Schaal, G. Sterzenbach, "Estimation of Uranium Target Wheel Activation and Afterheat for SNQ Target of 1100 MeV Proton Beam Energy
SNQ 3 I / BH 271184, Nov. 1984

/5/ D. Filges et al, "Nuclear Aspects in the SNQ Target Design", Proc. ICANS-VIII, Rutherford Appleton Laboratory, 1985 July 8-12, this volume

Proceedings of the Eighth Meeting of the International Collaboration on Advanced Neutron Sources (ICANS-VIII)
8-12 July 1985, Rutherford Appleton Laboratory Report RAL-85-110

The development work at the liquid lead-bismuth target for SINQ

Y.Takeda & C.Gerber

Schweizerisches Institut fur Nuklearforschung

CH-5234 Villigen, Switzerland

1 Introduction

The design concept for the SINQ target is to use Lead Bismuth Eutectic (LBE) in the liquid phase in a vertical cylindrical container, with the proton beam entering from the bottom. Natural convection of LBE is to be utilized to tansport the deposited energy to a heat exchanger at the top.
The thermofluid dynamics of this liquid target is one of the important study subjects for a practical design. Numerical calculations were performed to survey effects related to several design parameters <1>. Flow visualization experiments were also made for studying the total flow behaviour in a small scale water model. Results have been reported in an earlier ICANS proceeding <2>.

2 NACOSPANS - Water experiments

A large scale test rig for a water experiment was fabricated. A glass cylinder of 20 cm diameter and 250 cm height is set in a square aquarium of 45 cm side and 300 cm height. A 40 cm long heating rod is inserted from the bottom which has a heat generation decreasing exponentially with a relaxation length of 30 cm. This gives a first approximation to the expected beam heating. A 15 cm diameter glass tube was prepared to be set in a cylinder as a guide tube to stabilize the flow. Approximately 80 thermocouples in total are set in the apparatus to obtain the temperature distribution of water. Experiments were performed with the aim to obtain temperature distributions, to validate the computer program and finally to deduce the flow behaviour from the temperature distribution through computation.

A) Temperature distributions
Temperature distributions were obtained for various heater powers and water heights.

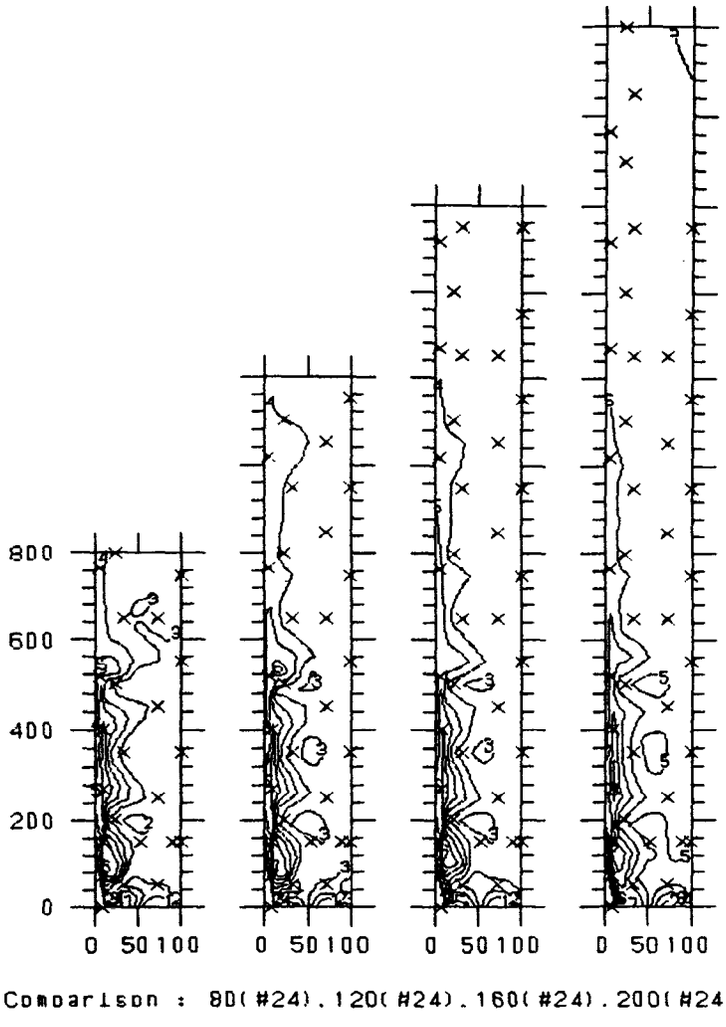

Fig.1 Measured temperature distributions for heights of 80, 120, 160 and 200 cm. Input power is 20 W. Only the half planes are shown (left coordinate coressponds to the center line). Contour lines are for arbitrary unit.

Fig.1 shows examples of distributions for heights of 80,120, 160 and 200 cm. (Heater power, 20 W) For every height, the higher tempearture rising column could be seen in the distribution, however, in the region below the top of the heater the distribution is complicated, showing the stable island of lower temperature. This effect is due to the high aspect ratio of the system and to the existence of the solid surface of the heating rod. This complicated distribution is stronger for higher heater power. From these temperature distributions with temperature islands, we conclude that the flow itself is very complicated, suggesting the existence of bifurcations and some roll structures. Similar patterns of distributions could be seen even in a lower aspect ratio system with lower power.

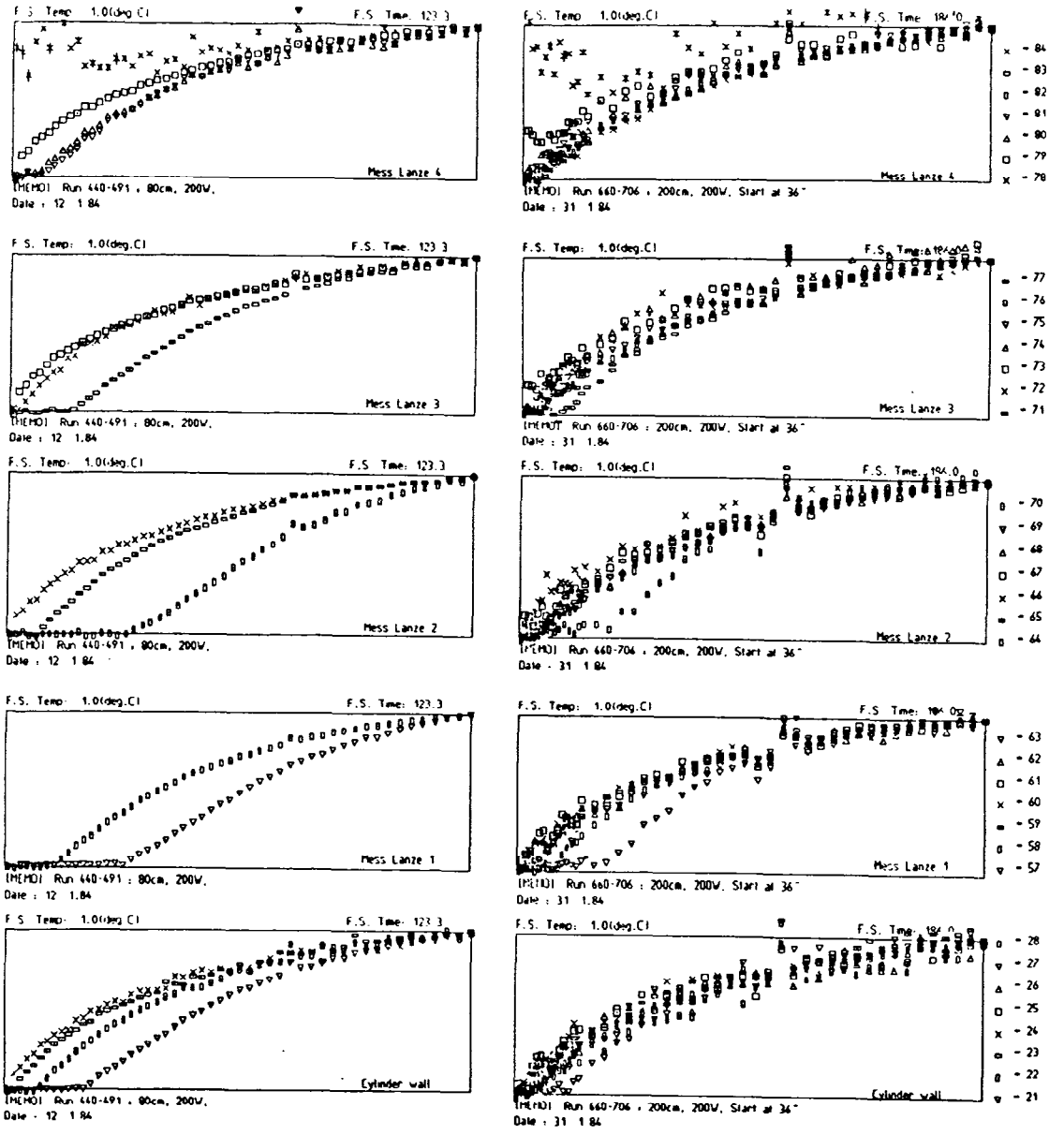

Fig.2 Time variation of the temperature at various positions. Water heights : a-80 cm, b-200 cm, heater power 20 W. Positions of mess lanze in radial direction : 1-72, 2-32, 3-22, 4-5 mm. In the vertiacal direction, the distance between measuring points is 20 cm.

Fig.2 shows the temperature variation at various measuring positions for the systems of heights of 80 and 200 cm. They show splitting lines for the 80 cm system whereas in the 200 cm system lines are almost coalesced. The former shows a rather smooth propagation of temperature increase indicating a smooth circulation but the latter shows the almost simultaneous temperature increases presumably being caused by the roll structure or the chaotic motion of fluids.

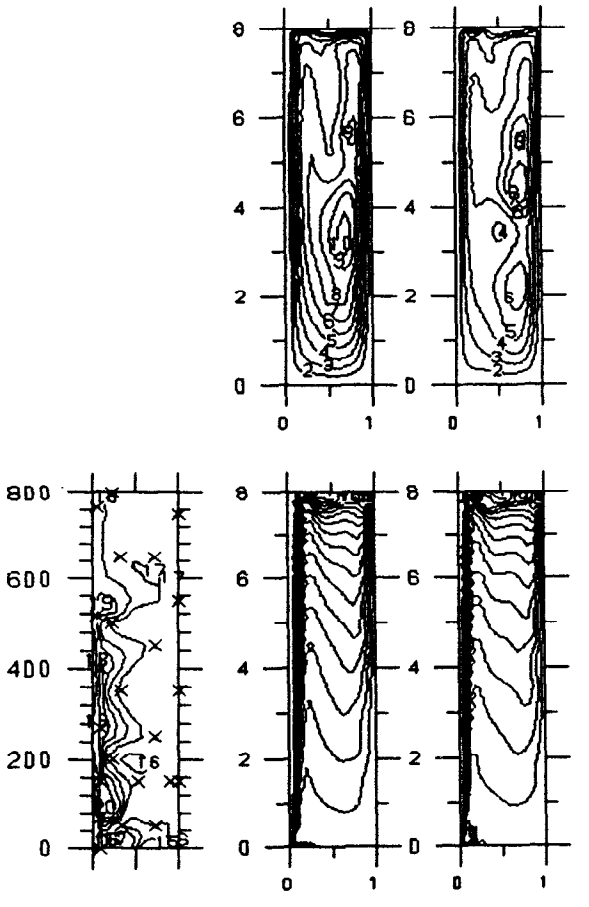

Fig.3 Comparison of (a) measured and (b,c) calculated temperature distributions. Gr : b-1x10^5, c-2x10^5. Upper maps are calculated contour lines of the stream function.

Fig.3 is a comparison of calculated and experimental temperature distributions and streamline contour maps for the corresponding calculations. It was only possible to make calculations with Gr number up to 2x10^5 whereas the experimental Gr value is about 5x10^6. In both cases some bifurcation could be seen at the same position in the system, however, temperature distributions appear to be quite different. We conclude that it is virtually impossible to deduce the flow behaviour from temperature measurements through calculations.

B) Effect of guide tube

Temperature distributions were also measured with a 200 cm guide tube in a system.

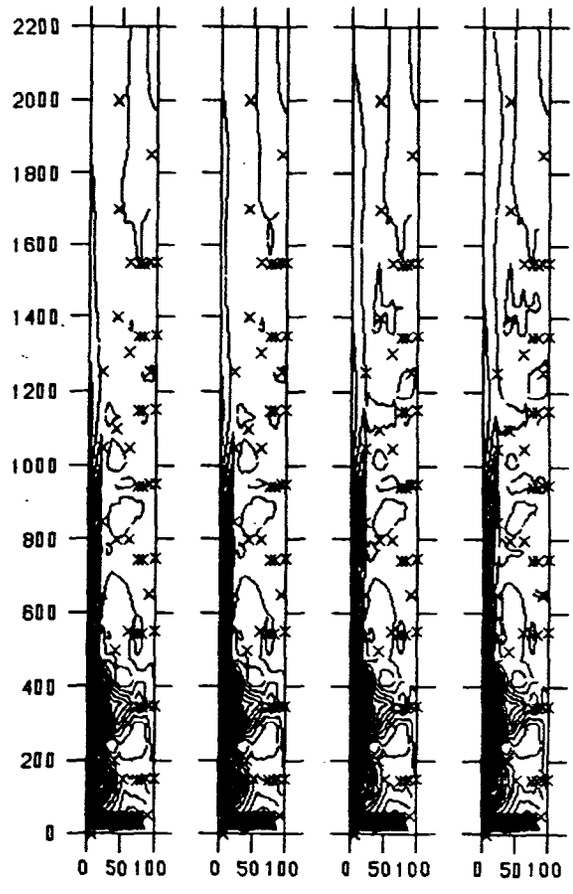

Fig.4 Time variation of temperature distributions. Water height is 220.5 cm, heater power 20 W. Results are from 20 to 30 minutes after the start. Contour lines are for every 1/4 deg. C.

Fig.4 shows part of the time change of these temperature distributions. Although they show complicated distributions with many islands at the lower part of the system, it is clearly seen that a rising column of high temperature is generated, which rises to total height with time. Obviously this result would be caused by the existence of the guide tube which may increase the rising velocity of the fluid and stabilizes the total circulation.

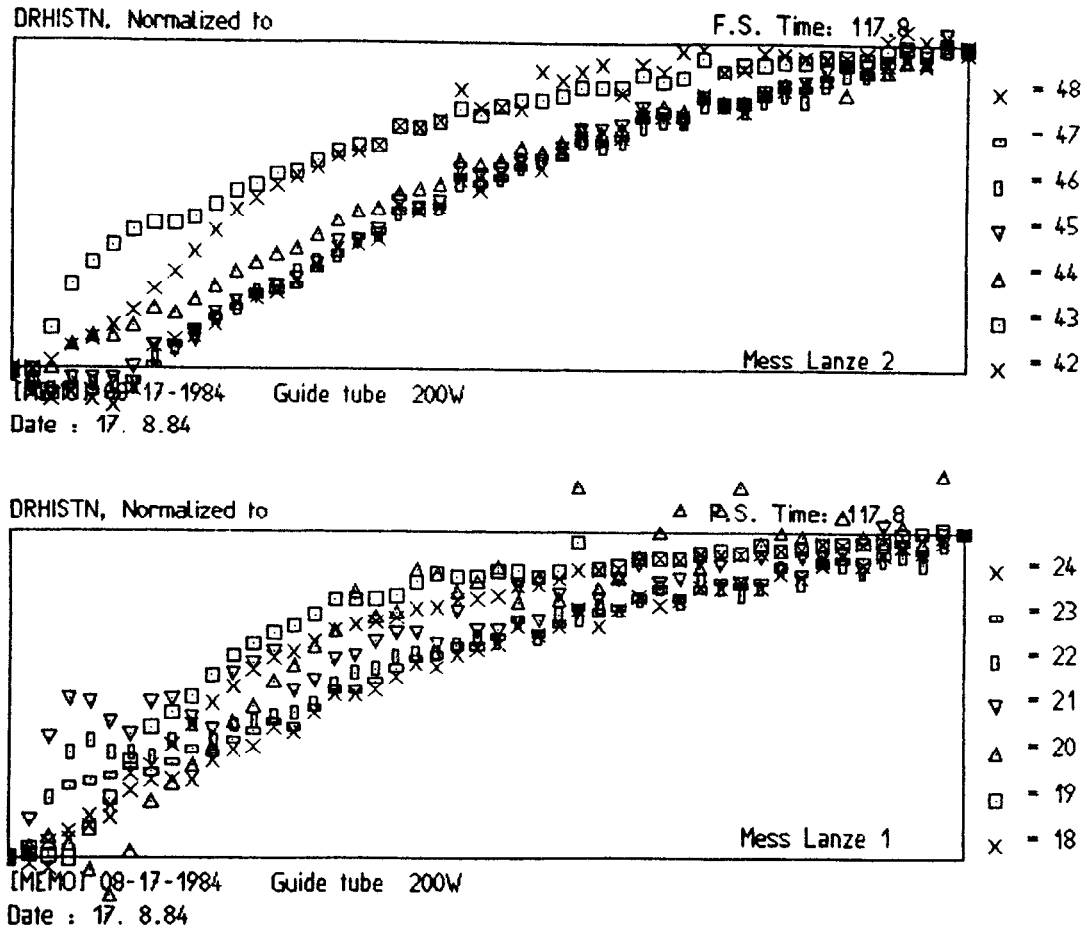

Fig.5 Time variation of the temperature. Mess lanze 1 : inside the guide tube (r=32mm), 2 : outside (91mm).

Fig.5 shows time behaviour of the temperatures inside and outside of the guide tube. At inside, it shows a typical transient behaviour with a small hump immediately after the startup of heating, afterwards the temperature increases monotonically. However, on the outside the temperature changes quite smoothly without any transient characteristics. This also indicates that the guide tube works effectively to stabilize the total circulation of the fluid in the system.

Furthermore, two additional effects were observed; one is a so-called Syphon effect at the top, which is a flow bifurcation. Part of the down-flowing fluid bifurcates, entering back into the guide tube. Another effect is a local circulation which appears in a top plenum. Both effects are strongly related to the position of the guide tube. This should be carefully investigated by a flow visualization experiment which is now prepared.

3 Flow monitoring

From the water experiments described above, we concluded that it is necessary to monitor the flow distribution directly by some other method. Although liquid metal is now extensively used in industry, measurement of flow profiles are not yet properly estabilished. Recently an ultrasound Doppler shift method has been developed for measuring blood flow in human blood vessels. <3> This is a remote measuring technique which has no senser inside the fluid, and could be very suitable also for our target monitoring system. Investigation was made in order to verify its feasibility for general fluid flow and liquid metal flow.

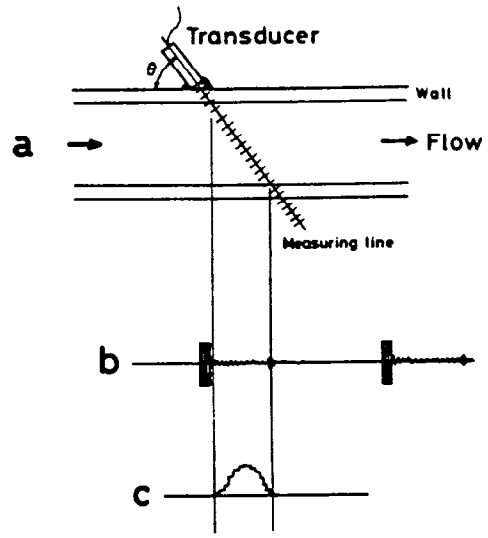

Fig.6 Illustration of the principle of velocity profile measurement by ultrasound Doppler shift method. a : configuration for measurement, b : echo signal c : velocity profile obtained.

Fig.6 shows an illustration of its working principle. Pulsed ultrasound echography is used. The basic frequency of the ultrasound is 4.2 MHz, pulse width ca.5 usec and repetition period 122 usec. The received echo is analyzed to derive its Doppler shift frequency as a function of time after the pulse. This method makes it possible to measure the velocity profile along the measuring line as a function of time. One profile can be measured in ca 16 msec and position resolution is ca 0.7 mm. Investigation was made to apply this method to the Poisoulle flow of water in a pipe and Taylor vortex flow in a rotating double cylinder. Details of the experiment and results are described elsewhere <4>.

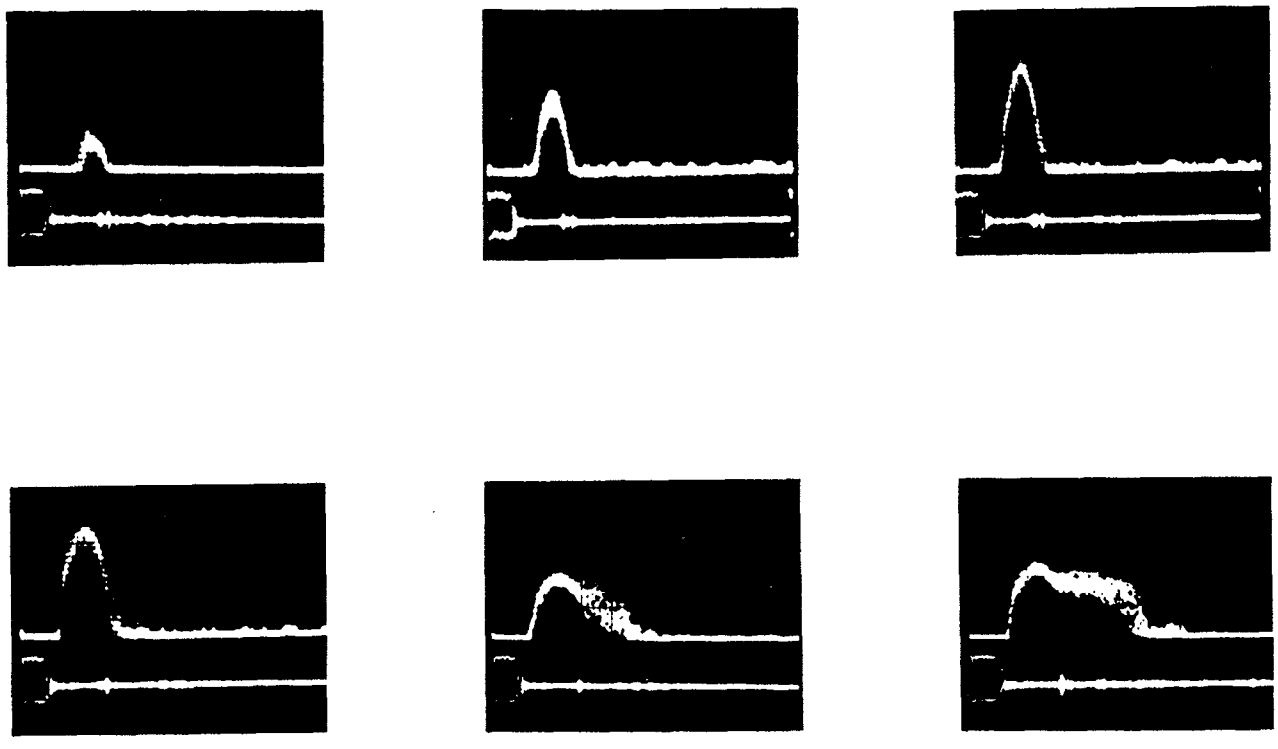

Fig.7 Measured velocity profiles of pipe flow for various Re numbers.

Fig.7 shows examples of change of velocity distributions in a pipe with various Re number.

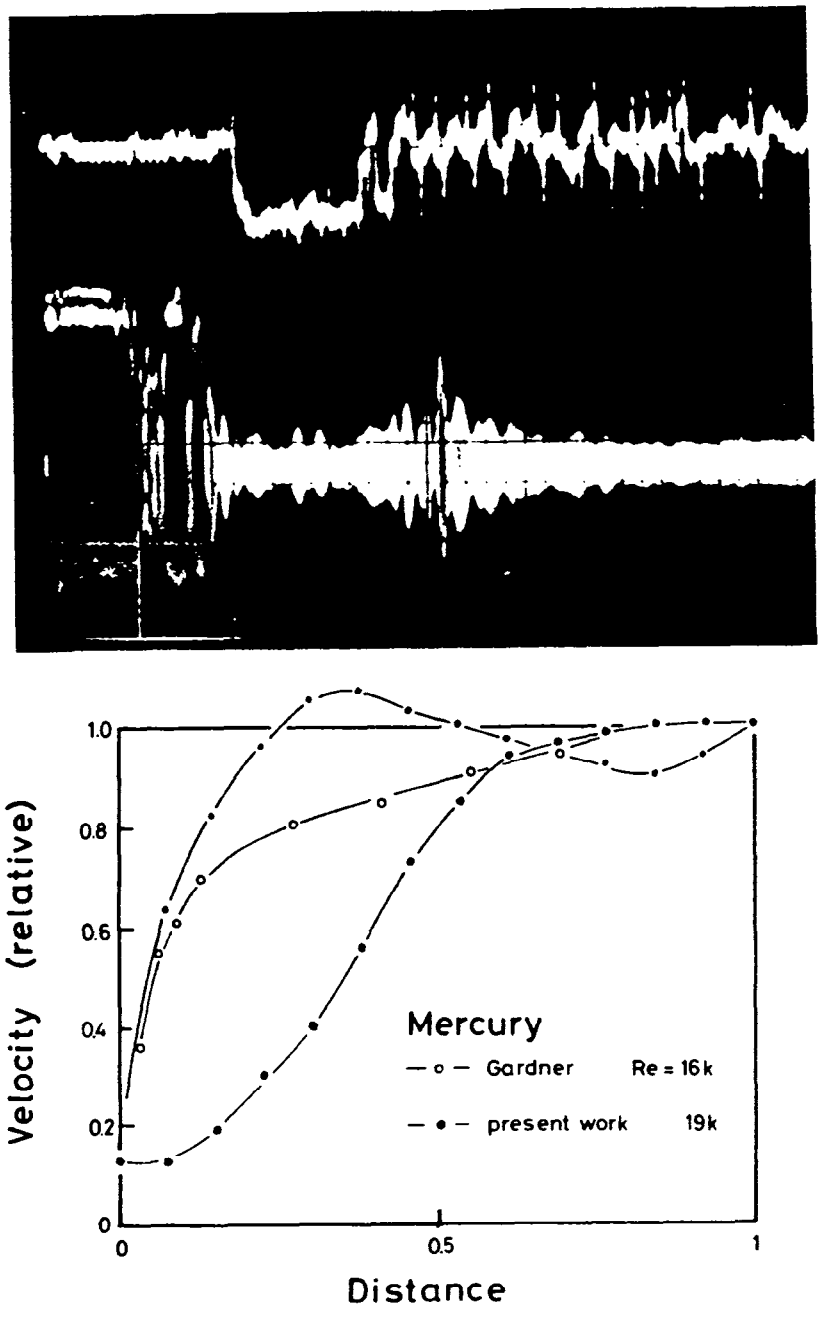

Fig.8 Measured profile of the pipe flow of Mercury.

Fig.8 shows a measured profile of the pipe flow of Mercury and its comparison with the earlier measurement of Gardner & Lukodis by Pitot tube <5>. There is still some disagreement in the profile and some more technical improvement may have to be made for our purpose. However, it was proven that this principle works quite successfully and further development work has been already started in order to use the machine as a target monitoring system.

4 Material study

As a procedure of selecting the target structures materials several tests are planned.

a. Container : Zircalloy 2 & 4 and two kinds of reactor grade Ni free steel were selected as candidate materials for the container and they are to be tested on corrosion properties in high temperature liquid LBE.
b. Window : The window is most heavily loaded by high temperature and proton beam irradiation under contact with LBE. Irradiation tests are under progress at Los Alamos. Results will be reported soon.
c. Heat exchanger : Corrosion and surface contamination by impurity and spallation products may have a significant effects on the heat exchanging properties. Investigations of these effects are planned.

5 Conceptual design

Designing the concept of the target system has been started. The target consists of a double wall containment. The lower part of the target has 190 mm outer diameter and the length is about 1400 mm. The upper part, where the shell and tube type heat exchanger is located, has a diameter of ca. 400 mm and a length of ca. 1600 mm. A guide tube is inserted into the center of the target extending from bottom to top, expecting to stabilize the rising flow of LBE inside this tube. Through the gap of the double wall of the container He gas is circulated for cooling the window and the target itself and for melting LBE before operation is started. At the same time, a part of this He gas is lead to the gas monitoring system in order to monitor leakage of the target container. The empty space above the LBE at the top of the target is to be evacuated in order to extract volatile spallation products generated during the operation.

References

1) Y.Takeda, to appear in the Nuc.Instr.Methods Vol.237 No.3 (1985)

2) Y.Takeda, ICANS-VII Proceedings, 1983, AECL-8488, 1984 Chalk River

3) J.J.Meister, Mesure par echographie Doppler et modelisation therique de l'effet de troubles cardiaques sur la pression et la debit arteriels. These No.504 (1983) Ecole Polytechnique Federale de Lausanne

4) Y.Takeda, submitted to the "International Journal of Heat and Mass Transfer"

5) R.A.Gardner & P.S.Lykoudis, J.Fluid Mech., 47 (1971) 737

Proceedings of the Eighth Meeting of the International Collaboration on Advanced Neutron Sources (ICANS-VIII)
8-12 July 1985, Rutherford Appleton Laboratory Report RAL-85-110

IPNS Enriched Uranium Booster Target*

A. W. Schulke, Jr.
For the IPNS Enriched Uranium Booster Target Design Team
Argonne National Laboratory
Argonne, Illinois 60439 U.S.A.

Introduction

Since startup in 1981, IPNS at Argonne National Laboratory has operated on a fully depleted ^{238}U target. With the booster as in the present system, high energy protons to 450 MeV accelerated by the Rapid Cycling Synchrotron are directed at the target and by mechanisms of spallation and fission of the uranium, produce fast neutrons. The neutrons from the target pass into adjacent moderator where they slow down to energies useful for spectroscopy. The target cooling systems and monitoring systems have operated very reliably and safely during this period. To provide higher neutron intensity, we have developed plans for an enriched uranium (booster) target. The design effort has been underway for the past year and a preliminary design is now in hand. HETC-VIM calculations indicate that the target will produce ~ 90 kw of heat, with a nominal x5 gain (k_{eff} = 0.80). The neutron beam intensity gain will be a factor of ~ 3.

Thermal-hydraulic and heat transport calculations indicate that ~1/2" thick ^{235}U discs are subject to about the same tempeatures as the present ^{238}U 1" thick discs. The coolant will be light demineralized water (H_2O). The coolant flow rate must be doubled to provide adequate cooling and therefore we have designed modifications to the present cooling system. The broadening of the fast neutron pulse width should not seriously affect the neutron scattering experiments. Delayed neutrons will appear at a level about 3% of the total (currently ~ 0.5%). This may affect backgrounds in some experiments, so that we are assessing measures to control and correct for this (e.g., beam tube choppers). Safety analyses and neutronic calculations are nearing completion. Construction of the ^{235}U discs at the ORNL Y-12 facility is scheduled to begin late 1985. The completion of the booster target and operation are scheduled for late 1986. No enriched uranium target assembly operating at the projected power level now exists in the world. This effort thus represents an important technological experiment as well as being a "flux enhancer".

*Work supported by the U.S. Department of Energy

Design and Operating Parameters of the Present and Booster Targets

Target	Depleted U Design Values	Present Operations	Enriched U Design Values
Incident beam	450-600 MeV protons	450 MeV protons	500 MeV protons
Repetition rate	30 Hz	30 Hz	30 Hz
Time-average proton current	22.0 μA	12-14 μA	20 μA
Target power	22.4 kW	8 kW	~ 92 kW
Total number of target discs	8	8	11
Target clad	Zircaloy-2	Zircaloy-2	Zircaloy-2
Target housing vessel	304 SS	304 SS	304 SS
Decoupler material	None	None	^{10}B - Copper
Coolant	Demin. H_2O	Demin. H_2O	Demin. H_2O
Coolant flow	45 gpm	45 gpm	90 gpm
Coolant inlet temp.	122°F	92°F	122°F
Coolant Δ temperature	3.4°F	1.2°F	~ 7.0°F
Max. temp. for 4 cm beam diameter			
at midplane of disc	598°F	94°F	539°F*
surface of disc	225°F	32°F	230°F*

*3 cm beam

Target Assembly Design Requirements and Description

The IPNS-Booster target assembly consists of an alloyed steel cylindrical housing containing zircaloy clad, uranium discs; mechanical devices to restrain the discs; coolant passages for cooling of the discs; instrumentation to monitor the condition of the target; and Boron-copper composite inserts for neutron purposes of decoupling the target from surrounding reflectors and moderators.

Radioactive products from spallation and fission are produced within the target discs. Cladding of the uranium provides for primary containment of these products. Cladding integrity will be determined by monitoring for fission product activity in the cooling system. The existing operating procedures will be used to define operating limits of radioactive contamination of the cooling system.

The target will be subject to the following proton beam conditions during normal operation:

A. The maximum power of the proton current will be a beam of 500 MeV energy and 20 μA current.

B. The proton beam will have a gaussian distribution with a minimum full width diameter at half of peak intensity of 3.0 cm.

C. The beam will be converging at the target face.

The nominal design conditions for operation at maximum proton beam power (described above) are as follows:

A. Maximum center line temperature in the uranium discs is 316°C, 600°F with the maximum differential between cooling water inlet temperature and center line temperature of the discs shall be 248°C, 478°F. The maximum surface temperature of the discs is 126.6°C, 260°F.

B. The coolant temperature differential across the target assembly is 7.0°F. The coolant inlet temperature is 50°C, 122°F.

C. The coolant flow through the target assembly is 5.67 l/S, 90 gpm.

D. The hydraulic pressure differential across the target assembly is 1.0 bar, 15 psi.

F. The maximum hydraulic design pressue of the target housing is 100 psig (corresponds to saturated steam at temperature of 170°C, 338°F).

The uranium targets have been designed to maintain cladding integrity upon loss of coolant and consequent shutdown of the proton beam. The target housing is designed to the requirements of the latest edition of "Section VIII, Div. 1" of the ASME Pressure Vessel Code. The design criteria are for the worst expected conditions. The target coolant could be light and/or heavy water. The target assembly materials will be compatible with coolant chemistry and cooling system components. Maximum surface temperature of the uranium discs will be lower than the saturation temperature of the coolant at the corresponding operating pressure.

Thermocouples inserted into six of the uranium discs sense the centerline temperature of the uranium. The thermocouple leads run through the outlet plenum and into the outlet pipe connection. The leads exit the outlet line at the top of the target extraction tunnel. The uranium discs thermocouples are 0.158 cm (0.062") O.D., 304 SS sheath, MgO insulation, type K calibration (chomel P-Alumel), ungrounded junction, and meet RDT C7-GT Standards. The target discs are secured in the containment housing with provisions for expansion based on expected expansion from all sources.

The booster target discs are made of enriched uranium metal. The total mass in all the discs is still to be determined. Stability of the uranium under proton beam irradiation is provided by additions of elemental C: +100/-200, Fe: 250 +100/-150, Si: 350 +200/-50 in weight percent. The uranium disc faces are clad in nominally 0.020 in. and on the circumference 0.030 in., welded zircaloy-2 jackets, which provide protection from corrosion. Cladding on the faces is minimized in order to consolidate the uranium. A hot isostatic pressing (HIP) operation provides metallurgical bonding between the uranium core and zircaloy-2 clad to provide adequate heat transfer. The bonding parameters should limit the grain size in the uranium to a diameter 0.02 > 0.01 cm. HIP bonding in an enert atmosphere will be controlled to prevent oxidation of the cladding. The discs are expected to remain intact under accident conditions at temperatures up to 1600°F. Decay heat analysis shows the maximum disc temperature to be ~ 1525°F under conditions of complete loss of coolant.

The discs are 4" diameter circular cylinders of two thicknesses. Edges are rounded to a 3/16" radius. Six of the targets contain 1/16" diameter clad thermo wells extending to the centerline from the edge. This provides access for thermocouples which are used for disc temperature monitoring during IPNS operation.

Each disc is supported within a 304 stainless steel container cap, which in turn is stacked within the target housing. The container caps are restained by radial arc cuts in the housing wall. Rotation of the caps is prevented by means of tabs mounted on the container caps. Axial restraint of the disc stack is provided by a spring loaded stainless steel spring assembly located at the back of the housing. Spring material is Inconel 600.

Coolant is supplied and returned through pipe connections located at the back of the target. Channeling in the back of the target housing directs flow to and from the inlet and outlet plenums. The inlet and outlet plenums are formed between the housing walls and the container caps. The container caps' ends are slotted and form parallel flow ducts which connect inlet and outlet plenums when discs and caps are assembled and stacked in the housing. Cooling of the discs' faces is by forced convection in these ducts. An accurate small clearance fit between the container caps and radial arcs machined in the housing walls prevents short circuiting of the coolant around the caps.

The container caps provide support for the source discs and form ducts for coolant flow at the disc face. Each of the source discs is installed in a container cap. The caps are similar except for length and flow area of the ducts. A slot is provided for installation of thermocouples in some of the discs.

Radial support of the source discs is effected by containment within the cylindrical portion of the caps. A radial clearance of 0.007 in. between disc and cap is provided to allow for disc expansion. This design clearance is based on an expected total lifetime expansion of 1.5% of the radius. Axial restraint of the discs is provided by the flat spacers at the end of the caps. A spring loaded assembly at the end of the disc stack causes contact pressure between spacers and disc face.

Rectangular flow ducts are formed between the disc spacers and disc faces. The duct depth (dimension in the axial direction) is determined by the spacer thickness and is equal to 0.063 in. This dimension has been minimized in order to consolidate the uranium. Duct width (dimension in the radial direction perpendicular to the flow) varies with the duct length and is determined by thermal and hydraulic considerations and varies from disc to disc according to the heat flux at the cooled surfaces.

The spring support housing subassembly provides an axial restraint force on the disc stack, and coolant flow separation between inlet and outlet pleniums in the target housing. A boron-copper composite disc is installed toward the front of the spring housing for neutron decoupling purposes.

Axial restraint on the disc stack is provided by a spring loaded backup disc located at the back of the housing. Two concectric Inconel 600 coil springs, each of which is capable, by itself, of providing sufficient axial compression (100 pounds) to restrain the disc stack, are installed behind the back-up disc and cause a separation force between the back-up disc and the front end of the flow distribution chamber. The spring force applied to the front end of the flow distribution chamber pushes this chamber against the back of the target housing while the opposing spring force on the back-up disc is applied to the disc stack. The disc retaining caps are free to move axially along the slides mounted in the target housing, allowing the spring force to be transmitted to each disc face. Since the length of the retaining caps is slightly less than the source disc length, contact between the spacers and the disc faces is assured. The spring force of either spring provides sufficient restraint of the discs to prevent movement during target handling and from hydraulic forces during operation of the target cooling system, but the total spring force does not cause excessive stress concentrations on the disc faces or inhibit final closure of the target housing. Maximum spring deflection and the associated clearances provide for a total lifetime expansion of 2.6% of the total uranium length. the target housing is of welded construction, fabricated entirely of 304 stainless steel.

The target housing provides the containment for the coolant in the target assembly, support for the container caps and spring support subassembly. Also, a layer of Boron-copper composite material is installed in the housing shell for neutron decoupling purposes.

Support of the caps and spring support housing is provided by direct contact with the housing wall. Radial arcs machined in the housing wall at these contact points provide an accurate fit between retaining caps, spring support housing and

the housing wall. Axial restraint of the disc stack is effected by direct contact with the front and back walls of the housing. Final closure of the target housing (weldment of the back wall) deflects the compression spring, thereby spring loading the disc stack.

Target Cooling System Modifications

Fission and spallation of the enriched uranium produce a substantial amount of heat requiring temperature sensing and forced convection cooling to assure satisfactory operation of the target

The increased operating thermal power of the booster target will add ~ 68 kilowatts over the original IPNS-I target design. This increase in thermal power will require twice the primary coolant flow (45 gpm to 90 gpm). To accomplish this, modifications to the two independent cooling systems (Neutron Scattering Target and Radiation Effects Target) will be made for parallel operation. Design considerations will also be given to keep intact the radiation effects cooling system, so that it can be operated if the need arises.

Each cooling system supplies 2.8 l/s (45 GPM) for total flow of coolant of 90 GPM to the target assembly. Total pressure drop across the target assembly at design flow is 1.0 Bars, (15 psi) with a minimum static pressure in the target assembly of 2.4 Bars, (35 psia). Coolant is demineralized light or heavy water with a target inlet temperature of 50 C, (122°F). All wetted parts in the cooling systems are chemically compatible with zircaloy-2 and 304 stainless steel. In order to prevent blockage of flow ducts from solids in the coolant a 3 micrometer* sintered stainless steel in line after filter and a 0.45 micrometer* prefilter are installed in each cooling system. (The minimum width of the flow ducts is 0.16 cm), (1/16"). (* - rated absolute removal in liquids.) Certain sections of the piping will be increased in diameter and the flex-hose will be increased from 1 1/4" to 2" diameter. A pressure relief valve for the target housing will be provided to protect the housing in case of a loss of coolant incident. Due to the increased diameter of the hose a new target linkage and hose connection assembly was is needed. Due to the corrosion problems with the present linkage assembly, the material for the new linkage will be a material (probably stainless steel) to minimize the formation of rust. This should reduce loose contamination problems during maintenance periods.

Tests performed on the present heat exchangers indicate they are adequate for the increased heat load.

The increased decay heat requires maintaining a low coolant flow after operation. Two new smaller pumps will be installed for this purpose. These pumps will be powered by a uninterruptable power supply.

The instrumentation, controls and alarm/shutdown modifications are minimal. Two additional thermocouples and associated instrumentation will be added to the present system. One total primary target flow meter and two decay heat flow meters will be installed. Certain controls and safety interlocks will also be revised.

Reflector Assembly

The target assembly is installed in a graphite reflector assembly cavity. The cavity has the same cross sectional configuration as the target housings with allowance for 0.159 cm, (1/16"), clearance all around. The maximum travel of the target into the cavity is 55.25 cm, (21.75"), from front face of housing to entrance of cavity. The cavity bore tube also contains a Boron-copper composite for neutron decoupling purposes.

Coolant and Reflectors

Cost considerations led us to choose a graphite reflector and light water (H_2O) coolant. The table shows the pulse width from the target with heavy water (D_2O) and beryllium alternatives.

For k_{eff} = 0.80 and nominal gain G=5, and with 1.2 x 10^{22} $^{10}B/cm^2$ decoupling around the target and lining the proton tunnel. We compute the booster pulse width as the product of the gain times the prompt neutron generation time, τ = Gl.

	H_2O	D_2O
Graphite reflector	5 x 68 = 340 nanosec	5 x 51 = 255 nanosec
Beryllium reflector	5 x 62 = 310 nanosec	5 x 43 = 215 nanosec

The results show that the beryllium/D_2O combination is the optimum. Our design goal was a pulse width of less than 500 nanoseconds.

Replacing the light water (H_2O) with heavy water (D_2O) will generally reduce k_{eff} by 0.010 or 0.015 (e.g., from 0.80 to 0.79 or 0.785).

Replacing a graphite reflector with a beryllium reflector will generally increase k_{eff} by 0.020 or 0.025 (e.g., from 0.80 to 0.82 or 0.825).

Analysis Summary

The thermal-hydraulic, thermal-stress and off normal conditions analyses should be completed in the near future.

Mechanical design analysis consist of the following:

Thermal/Hydraulic Analysis

Cooling System Hydraulics

Model existing system	(hydraulic code)
Field tests	
Compare & adj. model	
Model revised system	(hydraulic code)
Run cases	
(a) 2-pumps running	(normal)
(b) 1-pump running	(off normal)
(c) Broken spring case	(off normal)
(d) Blocked channel cases	(off normal)
(e) Parametric study-variable resistances & pump curve	(normal)

Disc Thermal Analysis

Model 1" disc	(ANSYS Code)
Model 1/2" disc	(ANSYS Code)
Cases	
(a) Find worst case disc for given Q & H	(normal)
(b) Broken springs case	(off normal)

(c) Blocked channel cases (off normal)

(d) Insulating effect of space (normal)

(e) Parametric study-variable
Q & H (normal)

Q = Energy Deposition Rate
H = Convective Film Coefficient

Determine transient response of disc

Margin to Channel Boiling Analysis

Decay Heat Analysis (all off normal)

Stoppage of primary coolant flow

Stoppage of secondary coolant flow

Loss of coolant in target (THTB Code)

Target Handling System

The target handling system provides the mechanism for installation of the target assembly into the reflector cavity. The handling system consists of a linkage train and a curved passage way (extraction tunnel) through the shielding.

The maximum target assembly length from the front face of the housing to the first linkage pivot is 32.86 cm, (12.94"). The ovrall cross sectional dimensions of the target assemblies are 13.65 cm, (5.375") by 11.11 cm, (4.375"). This geometry allows for adequate clearance between target assemblies and the curved extraction tunnels.

The transition link is connected to the target assembly by mounting lugs machined in the housing back plate. The transition link is designed for a pull force of 3000 lbs. at the target assembly. The target housing is designed to withstand an external loading equal to or greater than the 3000 lb. pull force. However, the design internal pressure loading of 100 psig and the pull force loading cannot be applied simultaneously.

IPNS Facility Shielding Changes

A review of the IPNS monolith shielding was conducted and the changes required are minor. Recommendations were adding shielding to cover the neutron beam gate drive housings and additional shielding in some areas by the target coolant housings.

There is no increase in groundwater activation to be expected from the operation of the booster target. This is because there is no increase in the intensity of the incident 500 MeV proton beam, which produces the high energy spallation neutrons which are the only ones that can reach the soil.

The booster target has only the effect of producing additional fission neutrons having energies not higher than a few MeV. These neutrons are slowed down by the 5 feet thick steel shield under the target to about 20 KeV (iron window neutron energy). Below the steel shield is a 3 feet thick concrete slab which is sufficient to absorb the iron window neutrons.

Acknowledgements

This work also reports the contributions of people from the IPNS Enriched Uranium Booster Target Design Team. J. L. Bailey, B. S. Brown, J. M. Carpenter, A. G. Hins, R. N. Blomquist, R. J. Armani and A. E. Knox, B. A. Loomis, D. R. Henley.

Proceedings of the Eighth Meeting of the International Collaboration on Advanced Neutron Sources (ICANS-VIII)
8-12 July 1985, Rutherford Appleton Laboratory Report RAL-85-110

Scoping Calculations for a Booster on the RAL SNS

D.J. Picton and T.D. Beynon

A series of preliminary scoping calculations has been performed for two alternative strategies for an upgrade to the SNS at the Rutherford Appleton Laboratory. The first strategy would involve the replacement of the present depleted uranium target with an enriched target of similar dimensions. The second strategy involves the design of a separate booster target which would run in parallel with the present target.

The results give information on the following issues: the relative merits of uranium and plutonium systems, the relationship between enrichment and k_{eff}, and the optimization of decouplers and reflectors.

1. INTRODUCTION

The present SNS target has a design power of 230 kW, corresponding to a neutron production rate of 2.3×10^{16} n/s from a proton beam intensity of 8.7×10^{14} p/s. Undoubtedly it is already one of the most powerful neutron sources available to experimentalists, and the concept of a booster system, to provide substantially higher neutron intensities, requires careful justification.

The main priority in upgrading the SNS in future years will probably involve improvements at energies at which its performance is poor compared with reactor sources. Undoubtedly the main area for improvement is in the cold neutron range below 25 meV, particularly the sub 4 meV range. There are two reasons why the SNS fails to match the performance of reactor sources in this area. Pulsed sources are inherently weak at thermal energies, although their epithermal fluxes are relatively large. The second deficiency is due to the fact that the cold source moderator is "downstream" in its position relative to the SNS target, with a subsequent reduction of the neutron flux incident on the cold moderator due to the attenuation of the proton beam.

The booster project falls into two main areas of study. The first, described in this paper, involves the design of improved targets. The second area will involve the optimization of the moderator.

2. ENRICHED TARGET CALCULATIONS

2.1 General discussion

Two possible strategies for the improvement of the SNS target are described in this paper. This section concentrates on a relatively

unambitious but cheap option, namely the use of a enriched uranium target in place of the present depleted uranium target.

Fig. 1 shows the design of the target station. The target consists of a series of zircalloy-clad uranium plates of varying thickness, cooled by D_2O. Note how the plate thickness increases in inverse proportion to power density.

Fig. 2 shows the arrangement of the moderator chambers on the SNS target. As previously mentioned, the downstream moderators are cold moderators (liquid H_2 and methane.) The most effective design for an enriched target for the improvement of the cold moderators would involve a varying enrichment, increasing in the downstream direction. A uniform power loading throughout the target would be an ideal to aim for.

At this stage, however, we have concentrated on a series of simple scoping calculations to evaluate the overall performance of a uniformly enriched target.

2.2 Calculational Details

The geometry and material used in our calculations is based on a benchmark calculation whose original purpose was code comparison. It has a number of unrealistic features; the uranium density in the target is too high, the geometry is over-simplified, and the target is too well-reflected. Nevertheless, the calculations presented here provide a reasonable semi-quantative estimate of target performance as a function of enrichment.

Fig. 3 shows the enriched target geometry, and Table 1 summarizes the atom number densities used. The system consists of a cylindrical target void in line with a cylindrical target, both of diameter 4.5 cm. Both these regions are decoupled with a 1 cm layer of ^{10}B to prevent the degradation of the fast pulse time distribution via the multiplication of thermal neutrons.

The target and void regions are in turn surrounded by a reflector in the form of a 70 cm cube, containing a mixture of Be and D_2O. The target is D_2O cooled uranium, and the decoupler is ^{10}B.

Two sets of results are presented. The first relates to target performance as a function of enrichment. The second set of calculations involves the optimization of the decoupler density. The calculations presented in this section were performed by the Monte Carlo code Morse-H (1) using the coupled neutron-gamma library DLC37F (2). The fixed source used in these calculations was the result of modelling using the HETC code (3) for spallation neutron production in the SNS target.

2.3 Results

Table 2 presents the results for target performance as a function of ^{235}U enrichment. The quantities calculated in the table are as follows. The multiplication factor M is the ratio of total to primary neutron production. The outgoing current represents the total leakage (over all energy groups) in the outgoing direction and the net current is defined as the (outgoing-incoming) leakage. Rough estimates of target power are also given.

For a 65% enriched system, the enrichment gain (i.e. the ratio of enriched to depleted uranium target performance) has a value of 4.6 for the net leakage at the decoupler-reflector interface. It should be noted that the numerical value of the enrichment gain is not very sensitive to the exact performance indicator used; for example the enrichment gain for outgoing leakage is 4.3 in the above case. This estimate certainly exaggerates the performance of a real target, for the reasons given earlier, ie. the density of fissile material would be lower than used here (and would in fact have to decrease with increasing reactivity to permit effective cooling.) A real system will also be less well reflected in the sense that the reflector will contain voids and will not be in intimate contact with the target.

Table 3 presents the results for the decoupler optimization calculations for the 65% enriched system. Here the ^{10}B density in the decoupler was progressively reduced without changing any other parameter. The main indicator of interest here was the ratio of inward leakage in the thermal group to primary neutron production. At a decoupler density of 0.00125 atoms/($10^{-24}cm^3$) this ratio was about 3%. This unwanted leakage of thermal neutrons into the target would be multiplied and would clearly have an adverse effect on the time distribution of the fast neutron pulse. A firm decision on the decoupler charateristics must await a time-dependent calculation, which has not yet been performed.

3. SIMPLE SCOPING CALCULATIONS FOR A BOOSTER SYSTEM.

3.1 General discussion

A second set of scoping calculations was oriented towards a more elaborate option than that described in the previous section. This alternative strategy would involve a second more specialized booster target which would run in parallel with the existing SNS target.

The optimum performance charcterisitics of a pulsed booster differ considerably from a fast reactor in a number of ways. The neutron leakage at the surface of the booster, and its time distribution, are more relevant performance indicators than total power production. The total neutron multiplication M, defined as in the previous section, is not given by

$$M_o = \frac{1}{1-k_{eff}}$$

In most cases M is larger than M_o because the first few neutron generations are concentrated towards the centre of the booster, and are therefore relatively unaffected by leakage.

Three basic types of booster system were investigated. A simple but rather unpromising option involves a depleted uranium target surrounded by enriched fuel. A second option involves uniformly enriched fuel. The third arises from the observation above concerning $M > \frac{1}{1-k_{eff}}$. In general a system in which enrichment is concentrated in a central region will certainly produce a greater power production, for a given value of k_{eff}, than a uniformly enriched system. This provides a relatively safe means of increasing power production without a potentially risky increase in k_{eff} although, of course, surface leakage rather than power production is the main performance indicator for a booster.

3.2 Computational Details

All the calculations described in this section were performed using the one dimensional neutron transport code ANISN. In all cases, spherical geometry was employed.

Table 4 summarizes the characteristics of the four models described in this section. All the systems under consideration were based on the concept of a ^{235}U or ^{239}Pu-enriched core, surrounded by a 12 cm-thick Ni reflector. No decoupler was specified because nickel does not produce significant thermalization. The net leakage at the core/reflector boundary was used as the main performance indictor for the system. Both integrated intensity and intensity per unit area ("brightness") were evaluated. In all cases the coolant used was sodium uniformly distributed in the core and occupying a volume fraction of 20%.

Model 1 is based on the concept of a highly enriched fissile blanket around a depleted uranium spallation target of similar size to the current SNS target. Model 2 represents the simple case of a uniformly enriched target, and Model 3 represents an attempt to improve performance without increasing k_{eff}, by enhancing the multiplication of the first few neutron generations. An inner area of radius 5 cm was given a higher enrichment.

Models 1-3 are based on current oxide fuel technology (UO_2 or mixed PuO_2/UO_2). However, the use of a uranium alloy (e.g. uranium molybdenum) would in fact be more appropriate for a spallation target. There are two reasons for this; uranium or plutonium oxides contain about half the concentration of metal atoms compared with the parent metal, and the

presence of a large concentration of oxygen in a spallation target would considerably reduce the neutron yield. Model 4 is similar to Model 2 but based on the more realistic concept of uranium or uranium/plutonium metal alloys. In view of the poor characteristics displayed by models 1 and 3, calculations in these geometrics were not repeated using uranium/plutonium metal fuels.

Two basic types of calculation were performed for each case. In the concentration search calculations, the enrichment required to produce a specified value of k_{eff} was determined. In the fixed source calculations, a uniformly distributed fixed source was specified in a central region of radius 5 cm. A ^{235}U fission source was used for the energy distribution.

3.3 Results

Fig. 4 shows the results of the concentration search calculation for Models 1-3. In the case of Model 2, there are two sets of curves for both plutonium-enriched and uranium-enriched systems (ie. ^{238}U enriched with ^{239}Pu or ^{235}U). For models 1 and 3, the results are all for plutonium-enriched systems.

The immediate conclusion which can be drawn in comparing configurations 1 and 2 is that a uniformly enriched system can be considerably more compact than a system containing a depleted uranium core. The difference between the plutonium and uranium systems is as expected from the large difference in critical mass between ^{235}U and ^{239}Pu. At a given enrichment, a uranium system needs about 1.5 times the radius of a plutonium-enriched system to produce the same value of k_{eff}.

Figs 5 to 7 display the results of the fixed source calculations for Models 1-3. Three quantities are presented - integrated net leakage at the core-reflector boundary, net leakage per unit surface area ("brightness") and multiplication factor M (total neutron production per primary source neutron).

One important factor is evident when the curve for integrated leakage is examined. The leakage is a strong function of k_{eff}, but almost independent of radius when k_{eff} is kept constant. It is clear that the inhomogeneous enrichment of Model 3 does not produce a substantial improvement in surface leakage. This is in contrast to the results for neutron multiplication, which demonstrate considerably enhanced power production for Model 3.

For most purposes the "brightness" of the source is more important than integrated leakage. The most important factor in determining brightness is the $\frac{1}{r^2}$-geometric attenuation term. From this point of view it is clear that a system must be reasonably compact in order to provide a bright source for a moderator; Model 1 can be eliminated for this reason.

Fig. 8 to 10 present results for Model 4. Two sets of curves are presented, for $^{235}U + ^{238}U$ fuel and $^{239}Pu + ^{238}U$ fuel.

It is clear from these results that uranium/plutonium metal systems are greatly superior to oxide systems, from a neutronic point of view in addition to the consideration of spallation yield described earlier. Both the uranium and plutonium enriched systems can be substantially more compact than the corresponding UO_2 and mixed $PuO_2 - UO_2$ systems in Model

2. From this point of view, the use of plutonium (with its environmental disadvantages) can be avoided if necessary. This can be seen by comparing figs 4 and 8 for the oxide and all-metal system, respectively. At k_{eff} = 0.9, the minimum radius for the uranium oxide system (fig 4, configuration 2) is approximately 9.5 cm compared with a value of about 6 cm for the uranium metal system (fig. 8). The PuO_2 system (fig 4) would achieve the value k_{eff} = 0.9 at a minimum radius of about 6 cm, and would therefore offer no significant advantages over the uranium metal system. Plutonium metal systems cannot be considered as technologically feasible.

4. FURTHER CALCULATIONS FOR ENRICHED TARGET SYSTEMS.

4.1 General discussion

The calculations presented in the previous two sections were mainly concerned with a few fundamental aspects of booster or enriched target design, i.e. the relationships between size, enrichment and overall neutronic performance. The calculations in this section, however, are concerned with more detailed questions about the choice of materials for the target coolant and reflectors.

In the case of coolant material, the effect of substituting sodium for D_2O was investigated. In addition, the effect of substituting nickel for beryllium as the reflector material was calculated. A somewhat unrealistic nickel reflector, i.e. without coolant or decoupler, was specified in order to evaluate the maximum possible gain in comparison with a more realistic D_2O cooled Be reflector.

A second question which has been addressed concerned the effect of a reflector whose surface is further from the target. A calculation was performed for a system containing a 1 cm void between the target decoupler

and reflector.

4.2 Calculational Details

The geometry used here was based on the modified benchmark geometry in Fig. 3. However, a more realistic composition was assumed for the target, i.e. a homogeneous mixture of uranium (80% volume fraction) and coolant (20% volume fraction).

The two alternative coolant materials used here were sodium and D_2O. For the reflector material, the alternatives were: D_2O cooled beryllium (composition as in section 2, Table 1) or nickel. As in section 2, the beryllium reflected targets were surrounded by a 1 cm thick ^{10}B decoupler (density 10^{22} atoms cm^{-3}). In addition, a case without a decoupler was run for comparison purposes. In the Ni reflected systems, the decoupler material was omitted; a void region was specified in place of the ^{10}B.

In section 2, it was found that the multiplication factor M for systems in the enriched target geometry is always close to

$$\frac{1}{1-k_{eff}}$$

This is not unexpected in view of the small size of the target cylinder in two out of three dimensions. For this reason, a decision was made to maximise computational efficiency by running only k_{eff} calculations for all cases. In general, the cost of fixed source calculation is proportional to M (and becomes infinite at $k_{eff} > 1$). In contrast, the cost of k_{eff} calculations is almost independent of reactivity.

4.3 Results and Discussion

In table 5, the results of the calculation performed for this section are summarized. In addition, selected results are plotted in Fig. 11.

In the case of the heavy water cooled systems plotted in Fig. 11, the substitution of Ni for Be as the reflector material had a significant positive effect on reactivity. However, the difference seen here represents an upper limit. In practice, the Ni reflector would need to be cooled, probably by D_2O. The effect of this would be to soften the reflected spectrum, making it more similar to that of the D_2O cooled Be reflector. In addition, the ^{10}B decoupler density used for the Be reflected systems was probably unnecessarily high. The results presented in Table 3 suggest that the use of an optimized decoupler with a lower density may increase k_{eff} by up to 5%, i.e. enough to match the performance of the Ni reflector.

In the case of the sodium cooled systems, the nickel reflector shows a smaller advantage over Be of the order of 1%. The differences between the sodium and heavy water cooled system are probably attributable to the detailed effects of D_2O moderation on the energy spectrum in the target. The presence of (n,2n) multiplication reactions in beryllium must be taken into account when comparing it with other reflector materials.

5. GENERAL CONCLUSIONS

The calculations presented in this paper provide a considerable amount of information on design concepts for an enriched target or booster for a spallation source.

The results in Sections 1 and 3 provide useful estimates of the necessary degree of enrichment required for an enriched target system of similar dimensions to the existing SNS target. In addition, these results provide useful information on reflectors and decouplers. The ^{10}B decoupler used in most of these calculations appears to have a considerably higher decoupling energy than necessary, although a firm choice of decoupler must await time-dependent calculations. The use of a nickel reflector in place of beryllium appears to present only a marginal advantage. In the case of the coolant material, the use of sodium rather than heavy water carries only a small penalty in reactivity. However, care must be taken in interpreting these results, in the sense that moderators have not been included in the calculations. Any hardening of the spectrum will degrade moderator performance.

In section 2, more basic questions concerning the size, enrichment and choice of fuel for a booster system were answered. A comparison was made between oxide and metal fuels, and between ^{235}U and ^{239}Pu enriched systems. The main conclusion to be drawn is that a uranium metal fuel enriched in ^{235}U is comparable in neutronic performance to a $^{239}PuO_2$ enriched $^{238}UO_2$ system, and would show a large advantage in spallation efficiency. In the absence of a Pu metal fuel technology, the uranium metal system is clearly the only practical option.

References

1. W.W. Engle Jr. Oak Ridge National Laboratory Report No. K1693 (1967).
2. Emmet M.B. The MORSE Monte-Carlo Radiation Transport Code System. Oak Ridge National Laboratory Report ORNL-4972 (1975).
3. T.A. Broome, Rutherford Appleton Laboratory. Private Communication.
4. A.D. Taylor, "Neutron Transport from Targets to Moderators". Meeting on Targets for Neutron Beam Spallation Sources, Jülich, 11-12 June 1979. See also Rutherford Appleton Laboratory Report RL 81 057.

TABLE 1

Particle Number Densities (Atoms/Barn CM)

ZONE	DENSITY	
TARGET		
U-238	0.0166)	
	)	65% enriched case
U-235	0.0308)	
D	0.0093	
O	0.0047	
DECOUPLER		
B-10	0.01	
REFLECTOR		
BE	0.0989	
D	0.0134	
O	0.00669	

TABLE 2

Summary of results for the modified benchmark target (Results are normalized to 1.0 primary source neutron).

Enrichment	0	20	40	65
k eff	0.147	0.455	0.662	0.856
Fission source	0.30	0.98	2.15	6.39
Total source	1.30	1.98	3.15	7.39
Outgoing Current:				
Targ. -Dec.	1.48	2.05	2.97	6.44
Dec. -ref.	1.53	2.12	3.09	6.71
Net leakage:				
Targ. -Dec.	0.910	1.25	1.81	3.89
Dec. -ref.	0.532	0.748	1.11	2.43
Power (MeV)	74	132	228	580
Power / net leakage (Dec. -ref.)	139	176	204	238

TABLE 3

Decoupler optmization for the 65% enriched modified benchmark

B atom density (per 10^{-24} cm^2)	0.01	0.005	0.0025	0.00125
Total source	7.39	8.19	9.50	11.36
Ourgoing current:				
Targ. - Dec.	6.438	7.22	8.44	10.17
Dec. - Refl.	6.708	7.67	9.04	10.98
Net leakage:				
Targ.-Dec.	3.892	4.212	4.756	5.551
Dec.-Refl.	2.437	2.779	3.276	3.964
Ingoing current (thermal group only):				
Dec.-Targ.	0.0	4.0E-5	1.0E-3	3.1E-2

TABLE 4

Booster Model Characteristics.

Model	Zone 1	Zone 2	Zone 3
1	Radius 7.81 cm	Variable thickness	Thickness 12 cm
	80% ^{235}U 20% Na	80% fuel 20% Na Fuel: $^{239}PuO_2$ + $^{238}UO_2$	Ni
2	Variable radius	Thickness 12 cm	-
	80% fuel 20% Na Fuel: $^{239}PuO_2$ + $^{238}UO_2$ or $^{235}UO_2$ + $^{238}UO_2$	Ni	
3	Radius 5 cm	Variable thickness	Thickness 12 cm
	80% fuel 20% Na Fuel: $^{239}PuO_2$ + $^{238}UO_2$	80% fuel 20% Na Fuel: $^{239}PuO_2$ + $^{238}UO_2$ (different enrichment)	Ni
4	Variable radius 80% fuel 20% Na Fuel: ^{239}Pu + ^{238}U or ^{235}U + ^{238}U	Thickness 12 cm Ni	-

TABLE 5

Further results for the enriched target configurations.

Enrichment	Coolant	Decoupler	Reflector	k_{eff}
0	D_2O	^{10}B	Be	0.126±.001
20				0.384±.002
40				0.570±.002
65				0.739±.003
0	D_2O	void	Be	0.128±.003
10				0.610±.006
20				0.718±.006
40				0.889±.007
65				1.045±.007
0	D_2O	void	Ni	0.124±.002
20				0.409±.004
40				0.611±.005
65				0.786±.005
0	Na	^{10}B	Be	0.723±.005
65				0.130±.002
0	Na	void	Ni	0.1360±.0015
65				0.734±.006
0	D_2O	void	void	0.123±.002
65				0.511±.004
0	D_2O	^{10}B*	Be	0.1263±.0015
65				0.721±.004

* surrounded by an additional void region, thickness 1 cm.

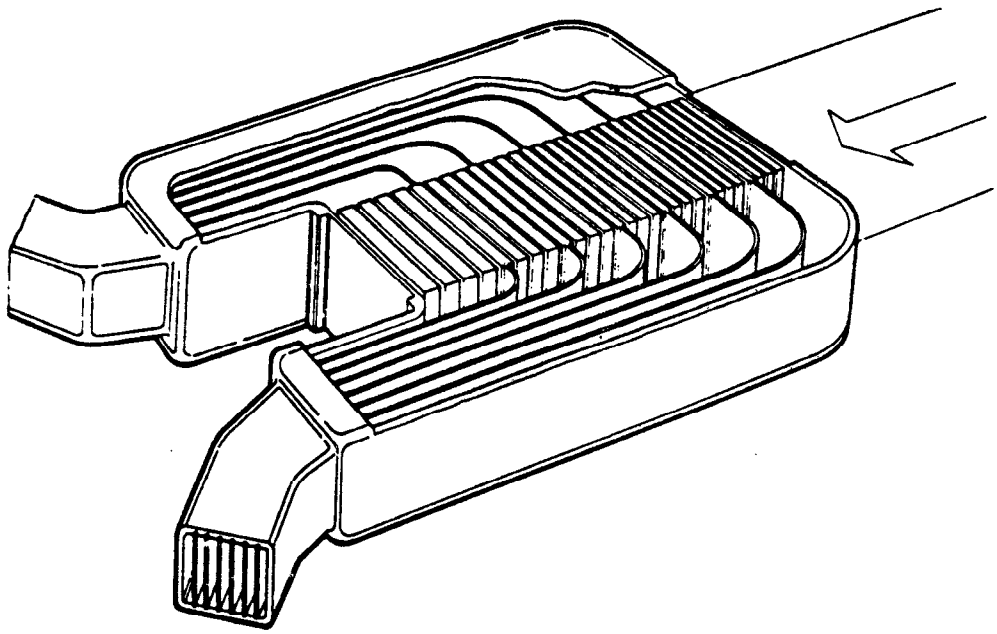

Fig. 1

The high power (200 μA) target for SNS at the Rutherford Laboratory[4]

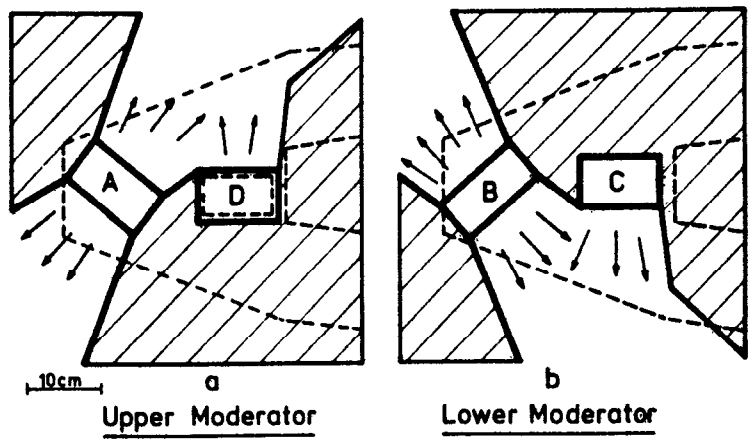

Fig. 2

Schematic representation of the arrangement of the SNS moderators[4] relative to the target.

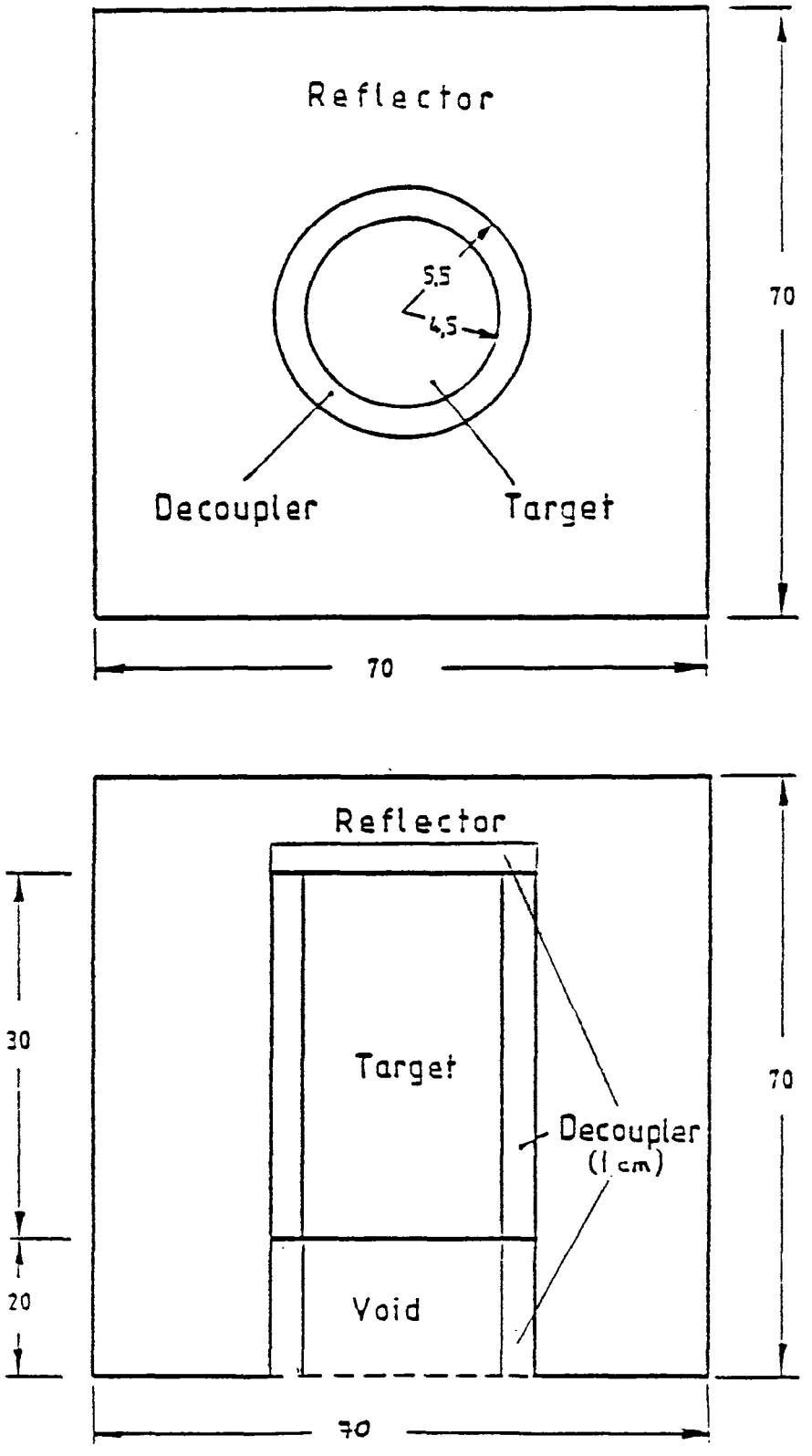

Fig. 3

Model for Transport Calculations (modified)
(Dimensions in cm)

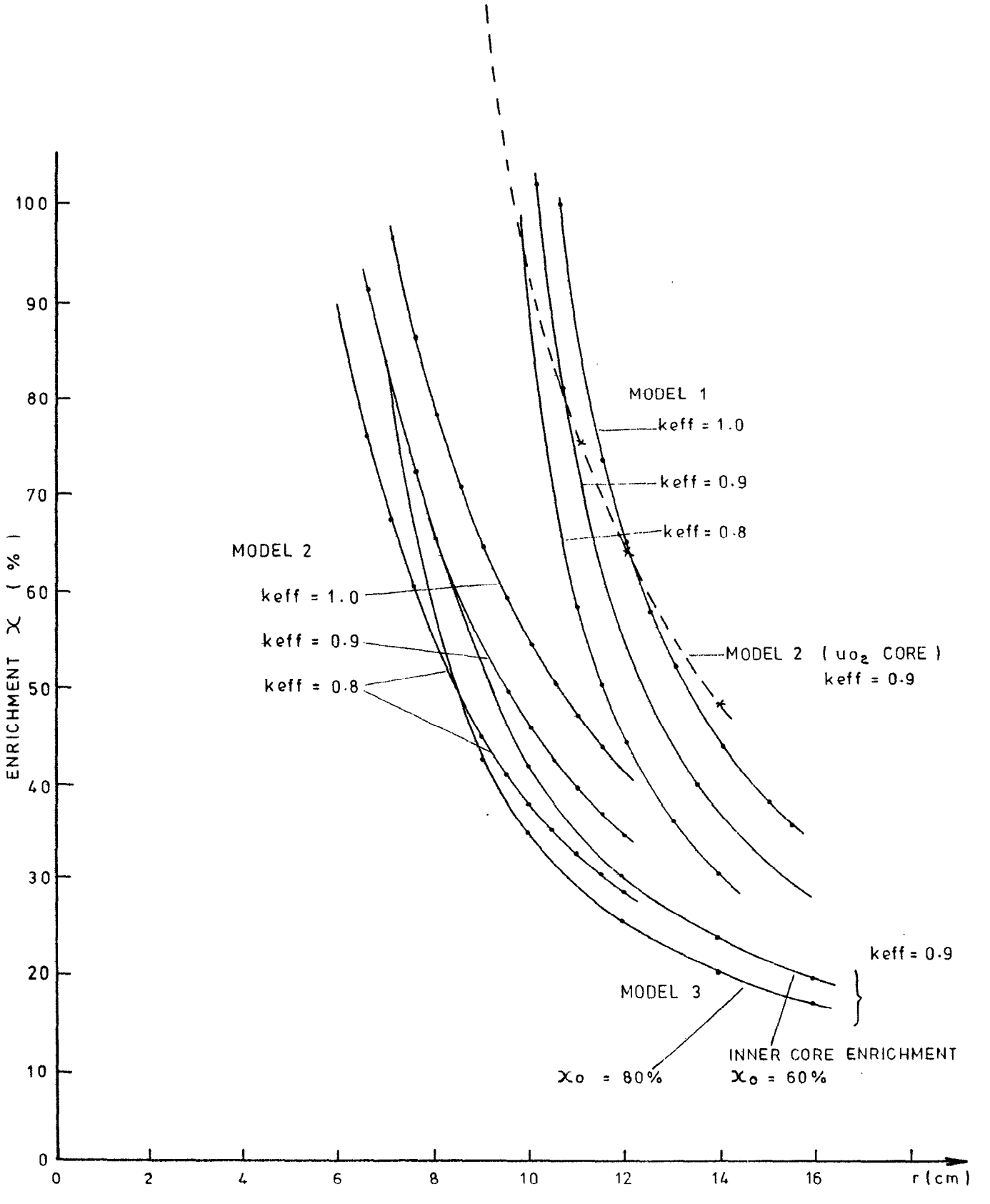

Fig. 4

Enrichment vs core radius for Models 1-3.

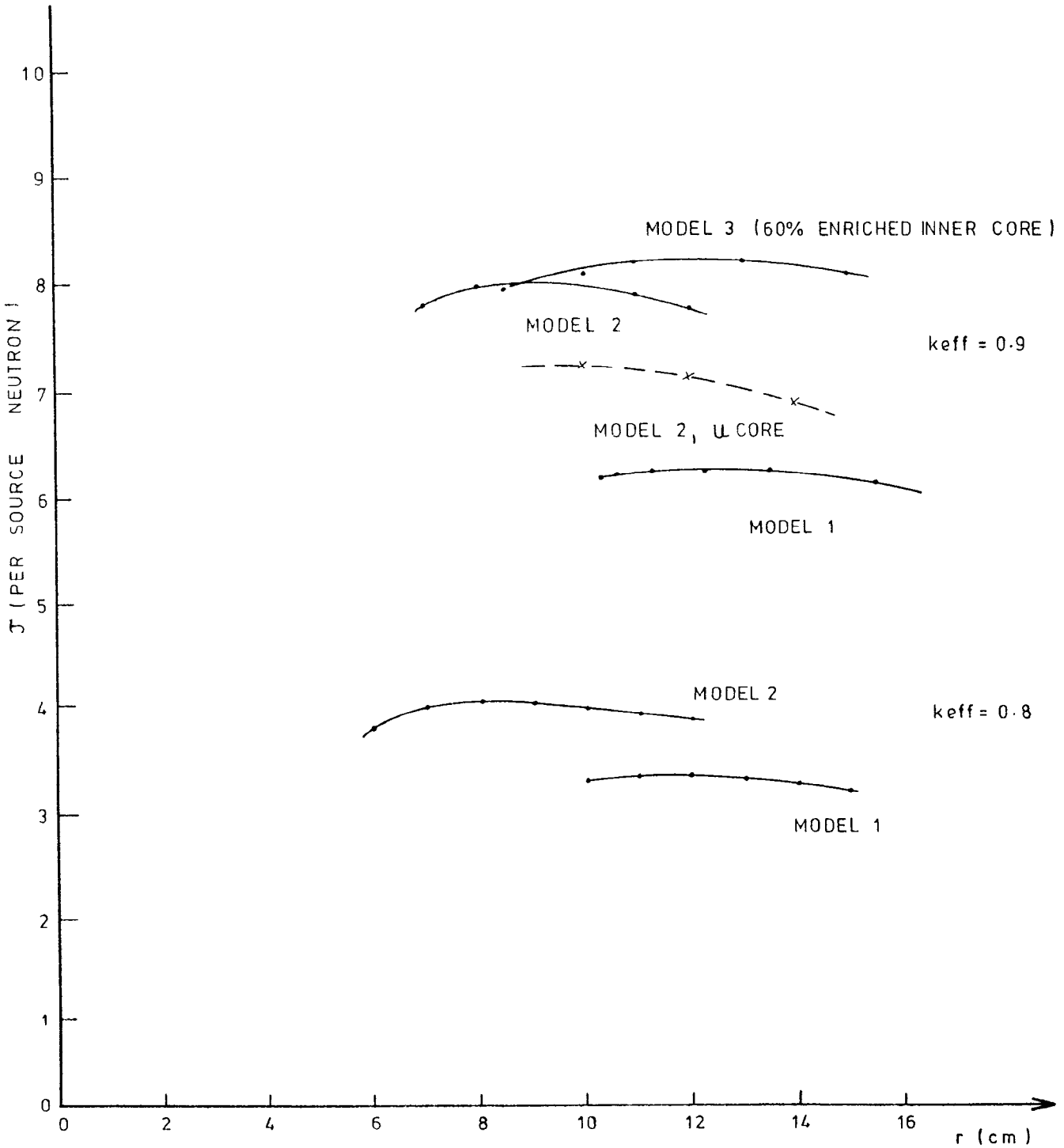

Fig. 5

Integrated net leakage J is core radius r.

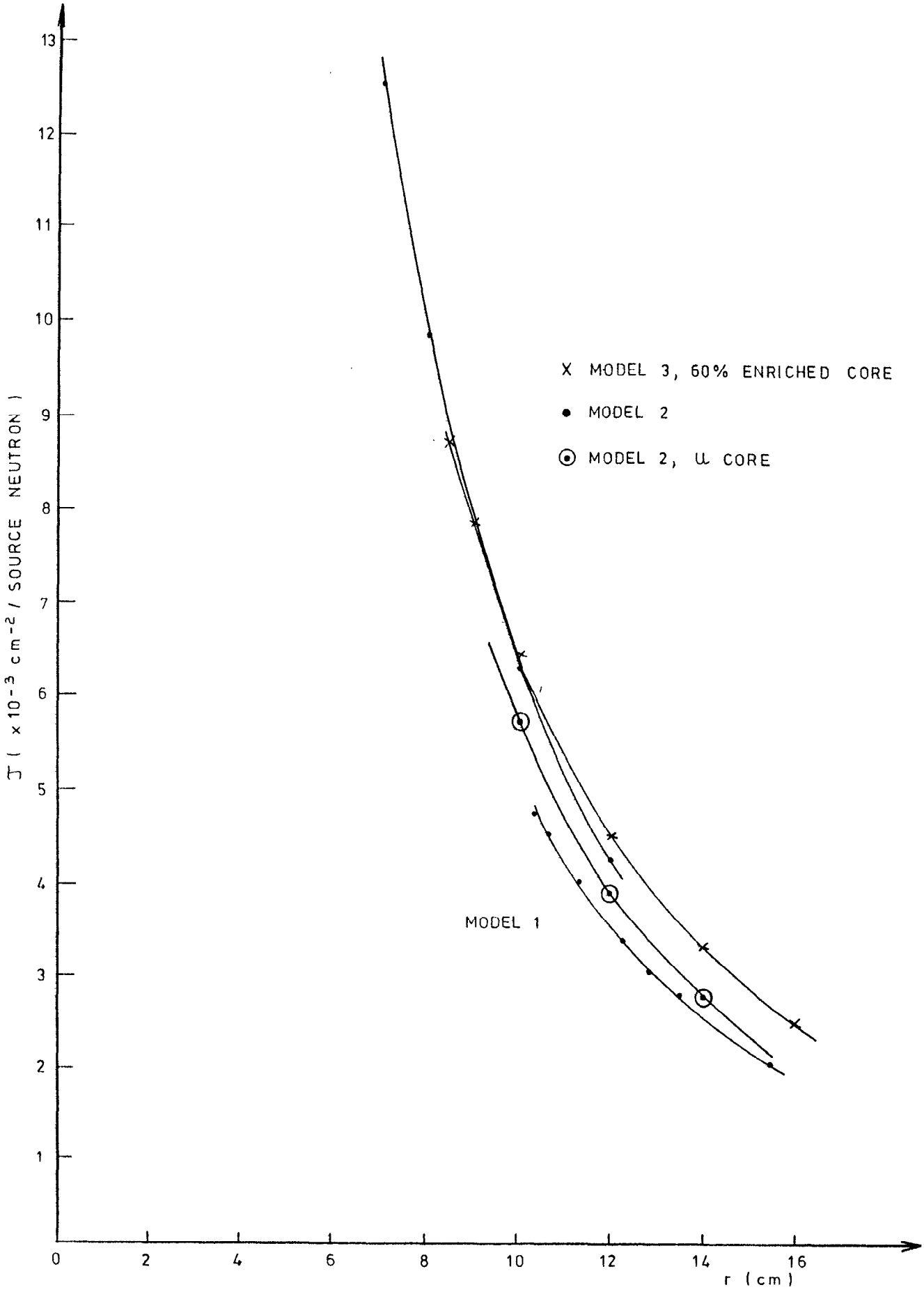

Fig. 6

Leakage per unit area for Models 1-3 (k_{eff} = 0.9)

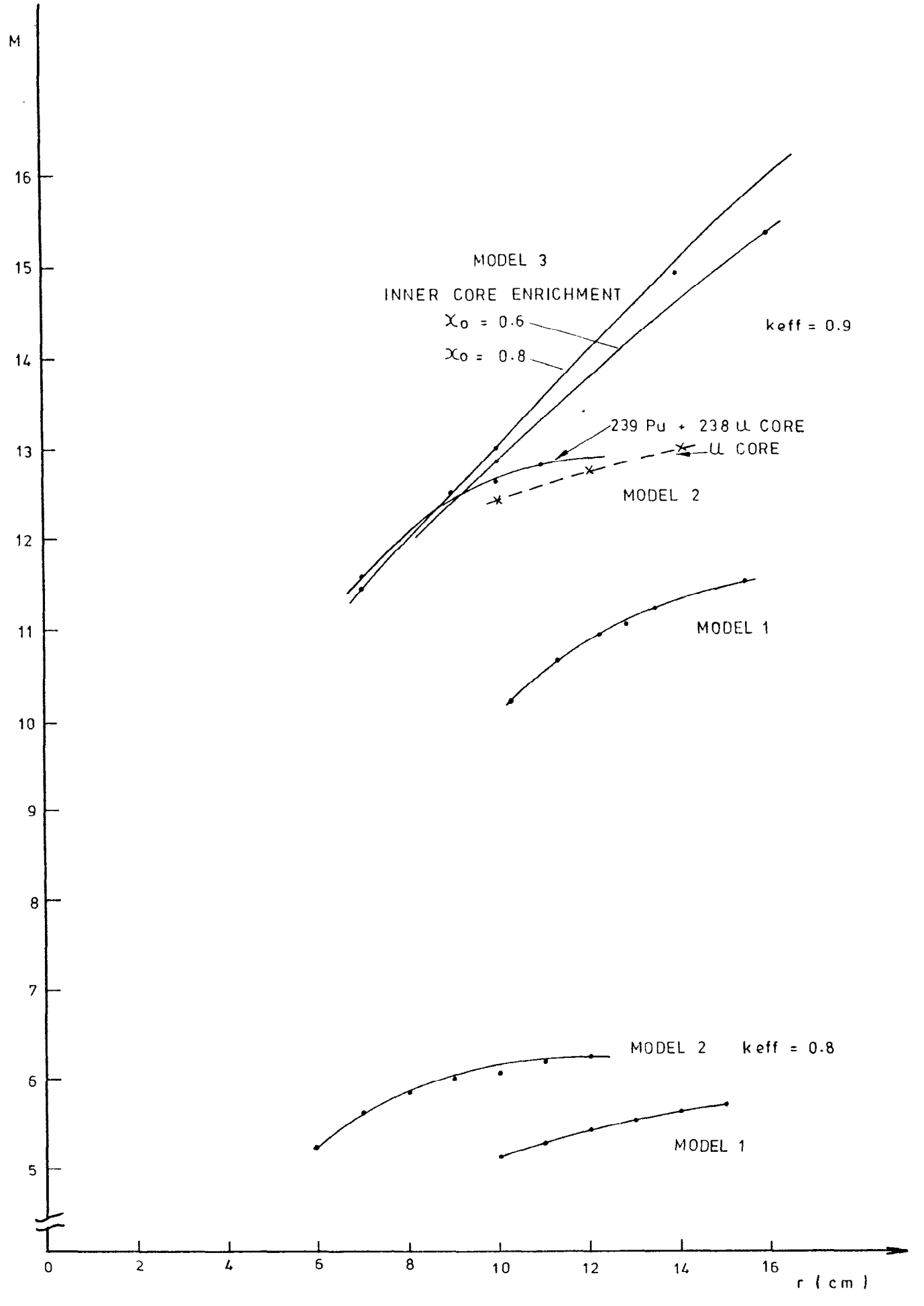

Fig 7

Total Multiplication factor M is core radius for Models 1-3.

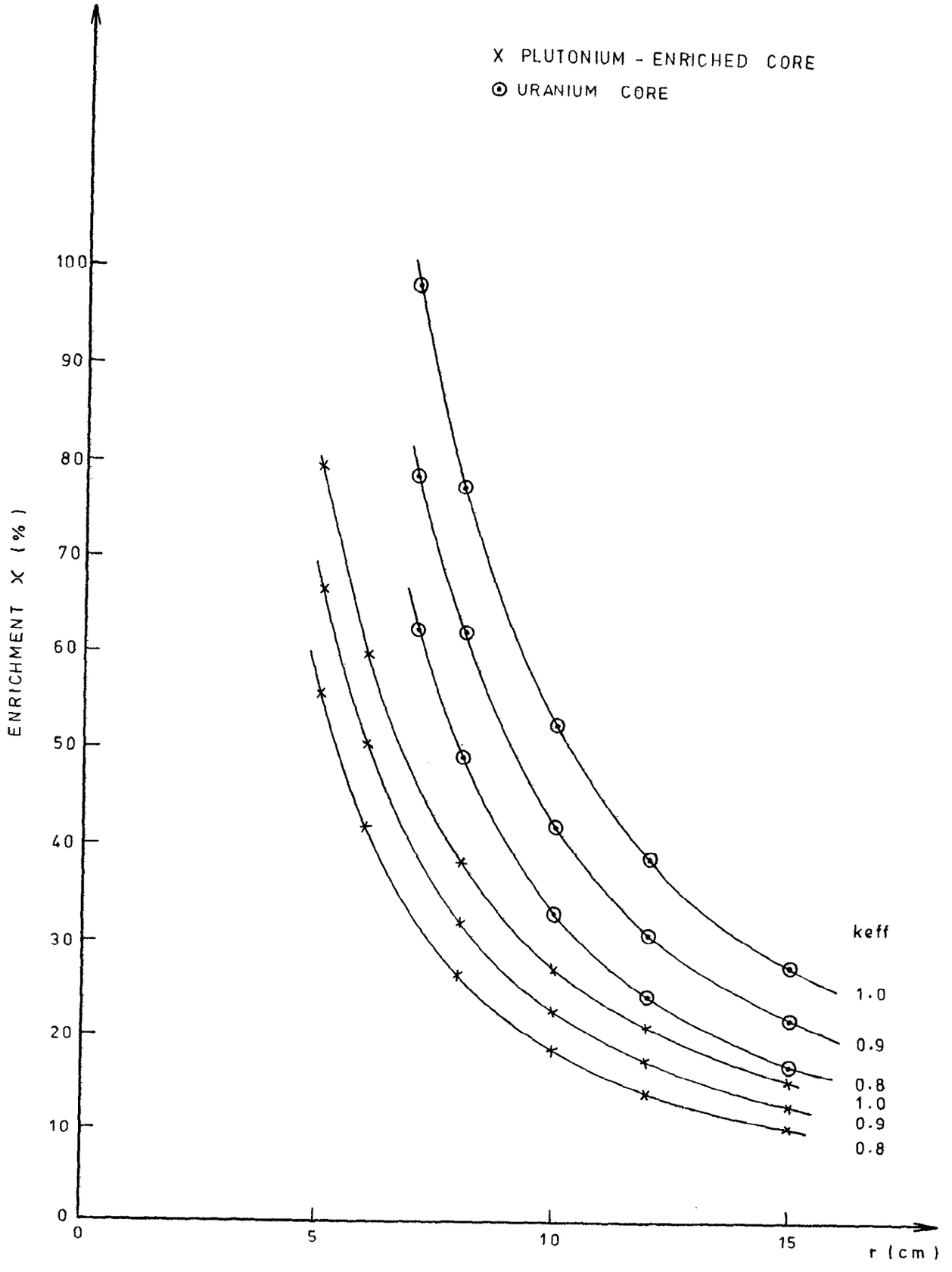

Fig. 8

Model 4: Enrichment vs radius

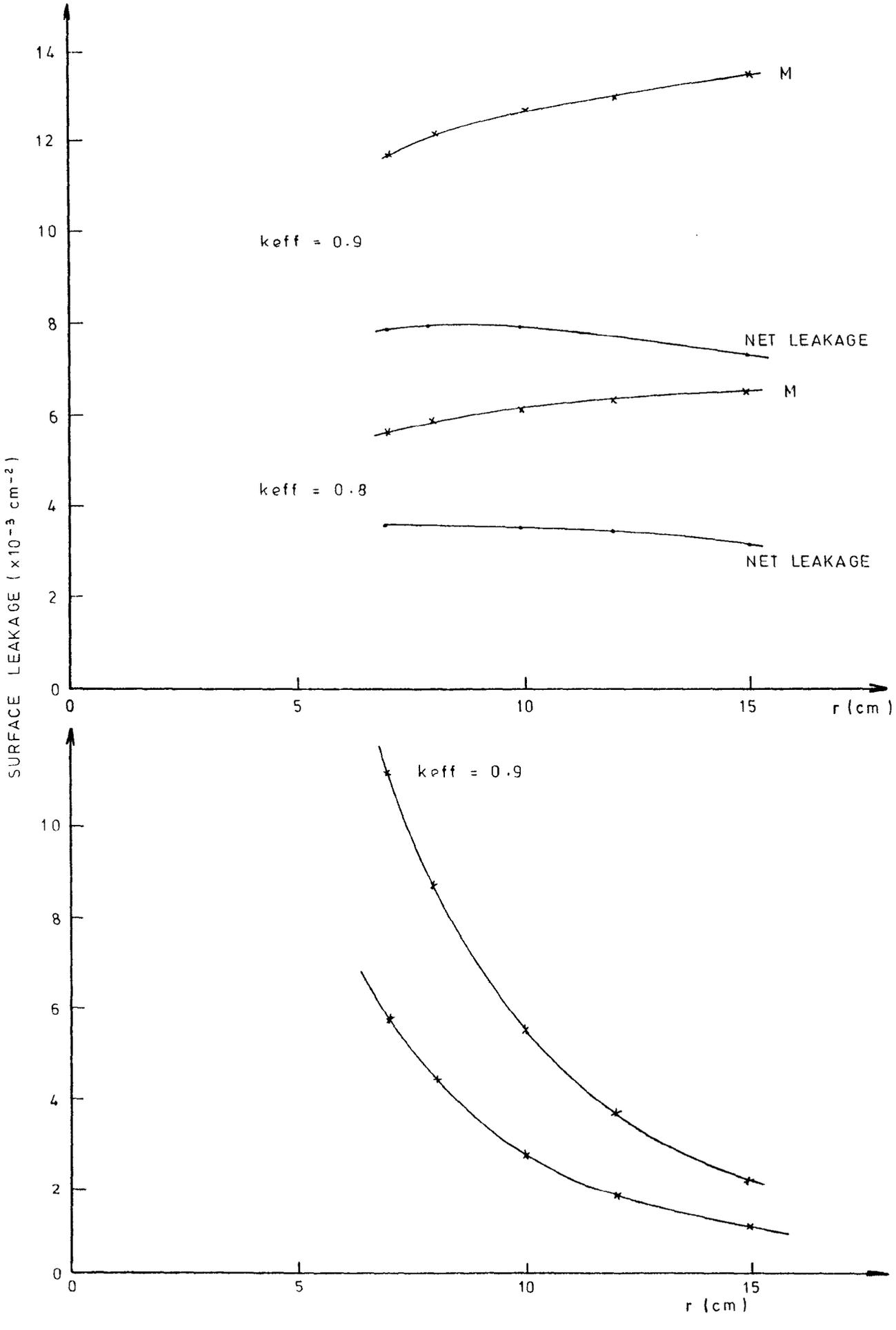

Fig. 9

Fixed source calculation: results for Model 4 (uranium system).

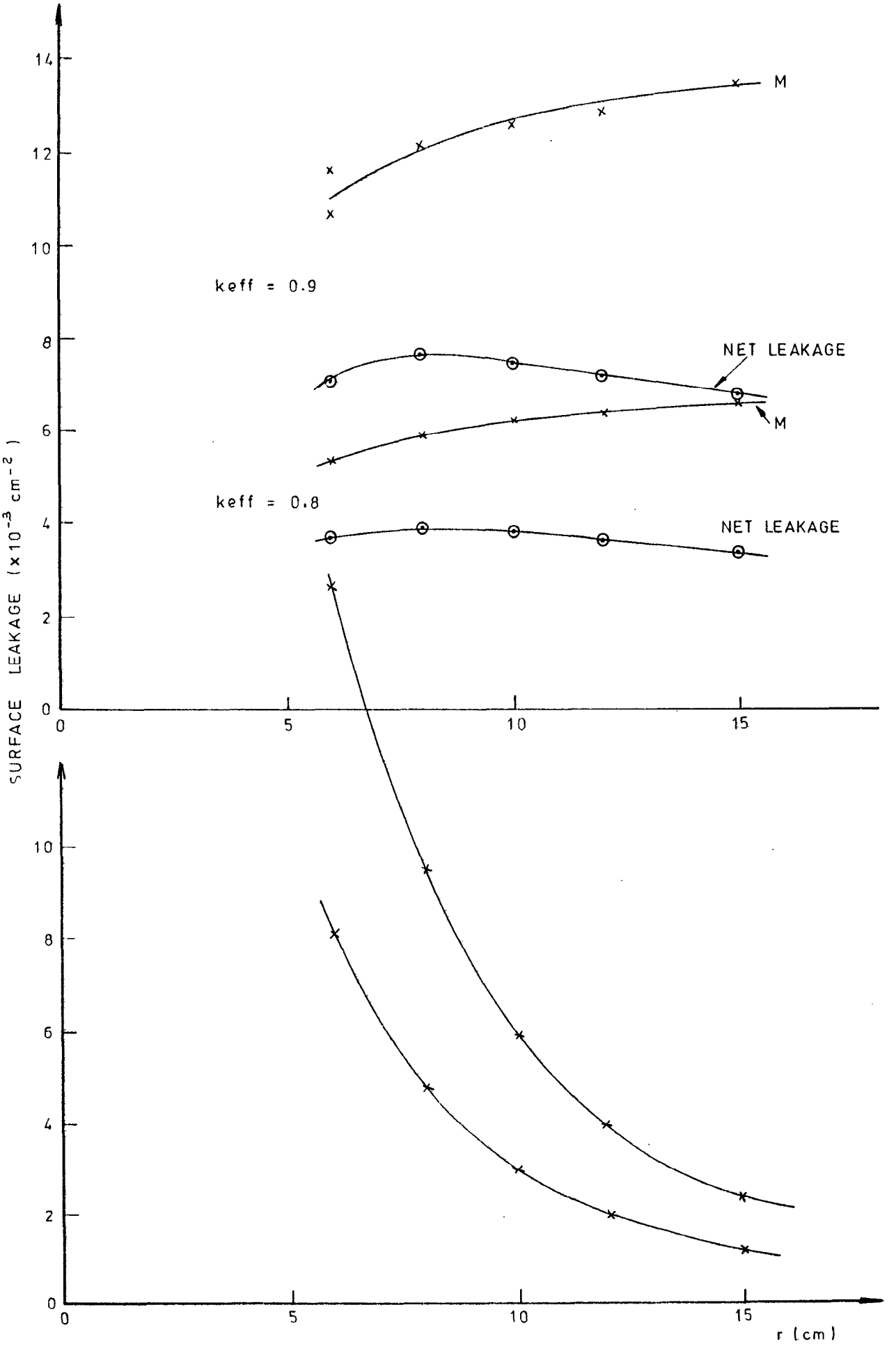

Fig. 10

Fixed source calculations: results for Model 4 (^{239}Pu + ^{238}U system).

Proceedings of the Eighth Meeting of the International Collaboration on Advanced Neutron Sources (ICANS-VIII)
8-12 July 1985, Rutherford Appleton Laboratory Report RAL-85-110

OVERVIEW OF SNS TARGET STATION AMBIENT SERVICES MONITORS AND CONTROLS

D J CLARKE, G H EATON

COMPUTER SYSTEMS

The SNS Target Station has a cooling plant comprising around nine separate water circuits, on which there are more than 200 remotely operated valves and almost as many sensor points. We do not attempt to provide organised hardwired display of this data but feed it into the computer system, and use programmes to show the status of the plant, both past and present, on TV monitors driven from graphics modules.

The main computer is a GEC 4070 minicomputer running GRACES. This is similar to those used on the rest of the SNS (but entirely dissimilar from the VAX computers used for data collection on the experiments). We also use an Intel single-board microcomputer of a certain age to scan around critical parameters and deliver them 'in bulk' to the GEC 4070 minicomputer. This relieves the minicomputer of a tiresome duty, leaving it able to do more interesting things like drawing pictures for the operators to look at it.

The system is now running well. It does sieze up occasionally but its behaviour is otherwise predictable and consistent. We use the programmes to monitor the state of the water circuits to check for shifts in performance, but, as yet, it is too early to see any interesting changes. The minicomputer is networked to the SNS machine control computers so that it is possible to monitor the target station plant from the SNS Main Control Room. However, we still man the Target Station Control Room as certain other systems are not automatic (Shutters, ventilation).

DISPLAY AND CONTROL SYSTEMS

The Target Station plant is controlled from a 'control desk' in the Target Station Control Room. The intention is that the Target Station should run unattended, but a desk is needed for startup and shutdown of the plant, as well as for the setting-up and shakedown going on at present.

The desk hardware used is similar to that elsewhere on the SNS, but we have not indulged in the luxury of touch-screen or colour graphics. Basic equipment is as follows.

VDU 1 - Connected to IGRC*
VDU 2 - Connected to AGRC*
TV 1 - Connected to GREEN
TV 2 - Connected to RED
TV 3 - Connected to BLUE
} Separate outputs from CAMAC Video generators USED AS 3 MONOCHROME SCREENS
TV 4 - Connected to display beam diagnostics

TRACKBALL - Drives cursor on 'GREEN' screen
TWIN 'KNOBS' - For adjusting parameters
TELEPHONE - Used for commissioning all equipment.

* GRACES allows for several concurrent tasks. IGRC and AGRC are both driven from a VDU with keyboard (AGRC, IGRC are but two of six or more current tasks running on the GEC Minicomputer).

DATA ACQUISITION HARDWARE

Because of the fairly respectable radiation dose from activation in the cooling plant, all the sensors and actuators are free of electronic components. This means that all the amplifiers and so on are in the Control Room, (and not distributed about the plant).

Because the computer system is a little prone to crashing, we provide local displays and controls for nearly all the parameters, but there is no attempt to organise them beyond labelling the interface/display with the identifier of the device to which it is connected. This is because we use the computer to organise and display the data for us. (see below).

In order to provide hardwired trips for use on the interlock systems, many of the measured parameters have individual panel meter/trip displays. These are standard commercial hardware. For some tasks e.g. flowmeter readout, proportional valve control and on/off valve control, we have designed and built our own interface hardware.

All communication between the computer systems and the hardware is via MPX hardware, which is an SNS-standard CAMAC-like system. This is fully operational and works well.

SOFTWARE FOR CONTROL AND MONITORING

The complex system of ambient temperature cooling circuits of the SNS Target Station is monitored and controlled by an equally complex suite of computer programs running on the GEC 4070 target station computer. For operator convenience, the large number of programs are menu-driven from the TV monitors according to the desired function i.e.

Start-up/Shutdown and Optimisation of Plant.
Routine monitoring and Optimisation of Plant.
Plotting and Averaging Routines for Plant Parameters.

These menus are used during operation of the ambient systems and have been commissioned successfully during the June-July 1985 period. Reliable and stable operation of both the ambient circuits and the control system has been amply demonstrated. In addition to these menu-driven operational programs, a separate menu-driven suite of programs has been written for filling and draining of the ambient circuits, prior to and after operation. These have also been successfully debugged and commissioned and greatly facilitate these tasks as well as minimising the occurence of operator error.

These programs are all run from the Target Station Control Room. Full descriptions of the Computer Control system is given in RAL-84-103.

Routine monitoring of the ambient circuits and of the two cryogenic moderators, will be handled soon from the SNS Main Control Room (MCR), using two programs specially developed for this task.

The first program displays in the MCR all the critical ambient circuit parameters monitored by the microprocessor computer system.

Should any parameter approach a fault level, this is indicated in the MCR and the operator is able to reoptimize the appropriate circuit in the Target Station Control Room using the full suite of optimisation programs.

A similar program displays the important parameters for the (cryogenic) methane and hydrogen moderators.

INTERLOCKS

The interfaces which deliver digitised parameters to the computer are also, in many cases, fitted with trip outputs in the form of relay closures. These are used to provide hardwired protection against certain calamities. Here is an outline of the interlock system into which these trips are fed.

Target Beam Trip System (TBT).

For those flows and pressures that we consider to be the most sensitive indicators of healthy cooling of the target, and also for the target plate thermocouples, we connect trip contacts in series, in a set of modules known as the Target Beam Trip (TBT) Systems. These are very simple but provide a means of formalising the connections so that faults are easily found and rectified. It is also hard to put an invisible 'frig' onto the system.

The two TBT Systems are now operational and providing a beam-permit signal to the SNS accelerator.

Coolant Control Logic (CCL)

The second type of interlock system on the Target Station is the Coolant Control Logic (CCL).

This will, when completed, provide safety actions by means of three (triple-redundant) Programmable Logic Controllers (PLCs). At present, the wiring of these is about half-complete, but the actuators on the plant are operational, allowing us full control of the plant during startup and shutdown.

The aim of the CCL is to prevent certain actions, by disabling parts of the plant (eg. drain valves) when their operation is not required. This is done at present using 'manual' operation of the CCL actuators by means of simulator boxes plugged in place of the PLCs.

The key to the design of the CCL is that voting (to determine the final outcome of the logic) is done on the plant in a way which is direct. This minimises the effect of single failures, wherever they may occur. The flow of information is therefore as follows:

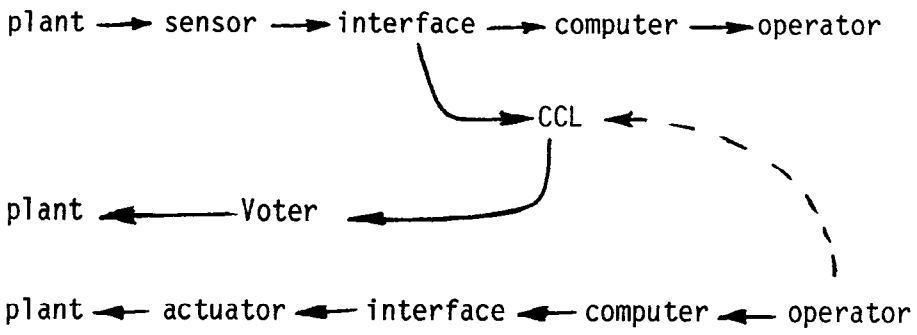

BIBLIOGRAPHY

1. =SNS TARGET STATION SAFETY ASSESSMENT
   =
   =ED A CARNE
   =SNS/PC/P6/82
   = 1982

2. =PROPOSAL FOR AN ON-LINE CLAD FAILURE DETECTION SYSTEM FOR THE
   =SNS TARGET STATION USING HIGH RESOLUTION GAMMA RAY SPECTROSCOPY
   =G H EATON
   =SNS/TS/N10/82
   = 1982

3. =FOR THE PROVISION OF A DEPENDABLE ELECTRICITY SUPPLY
   =FOR THE SNS TARGET STATION
   =D J CLARKE
   =SNS/TS/N4/82
   =APRIL 1982

4. =NODDY'S GUIDE TO MPX MODULES ON THE SNS CONTROL SYSTEM
   =
   =R P MANNIX
   =PRIVATE COMMUNICATION (AVAIL. AUTHOR)
   =APRIL 1984

5. =SNS TARGET STATION CONTROLS BEAM TRIP
   =MECHANISMS - REVISION 2
   =D J CLARKE
   =SNS/TS/N20/83
   =DEC 1983

6. =PRESSURE DROP OF THE TARGET SUBJECT TO FLOW AND
   =GAP BETWEEN PLATES
   =J BLOMBACH
   =SNS/TS/N21/83
   =DEC 1983

7. =SNS TARGET STATION SOFTWARE OPERATORS MANUAL
   =
   =ED M R GEARY
   =RAL-84-103
   =DEC 1984

8. =DISPLAY PROGRAMME FOR THE CONTROL OF THE SNS TARGET STATION
   =
   =G H EATON
   =SNS/TS/N1/82
   =FEB 1982

9. =SOME FEATURES OF THE COMPUTER CONTROL SYSTEM FOR THE
   =SPALLATION NEUTRON SOURCE (SNS)OF THE R A L
   =T R M EDWARDS
   =SNS/CON/N1/84
   =JAN 1984

10. =ON THE QUESTION OF HUMAN INTERVENTION IN THE
    =(SNS) TARGET STATION CONTROLS
    =J BLOMBACH D J CLARKE G H EATON K H ROBERTS
    =SNS/TS/N1/84

11. =SNS TARGET STATION CONTROLS SAFETY SURVEY
    =
    =D J CLARKE
    =SNS/TS/N3/81
    =JULY 1981
    =LOOKS AT THE IDEAS BEHIND MAKING A SYSTEM SAFE

12. =GRACES MANUAL
    =P HASKELL
    =RL-84-043
    =JULY 1984
    =SOFTWARE MANUAL FOR USERS OF THE GRACES LANGUAGE

13. =GRACES HANDBOOK
    =
    =P HASKELL
    =--
    =JULY 1984
    =PROVIDES HELP WITH HOW TO USE GRACES

14. =OUTLINE OF OPERATION OF VALVE CONTROL INTERLOCKS
    =ON SNS TARGET COOLING PLANT
    =D J CLARKE
    =SNS/TS/N9/85
    =JULY 1985

15. =CONCERNING THE INTEGRITY-BY-DESIGN OF THE SNS
    =TARGET STATION CONTROLS
    =D J CLARKE   A J H GODDARD
    =SNS/TS/N6/83
    =JUNE 1983

16. =THE SELECTION OF RADIATION-HARD SENSORS FOR THE
    =MONITORING OF THE SNS TARGET SERVICES PLANT
    =D J CLARKE
    =SNS/TS/N7/82
    =MAY 1982

17. =STRUCTURE OF THE SNS TARGET STATION CONTROLS
    =
    =D J CLARKE
    =SNS/TS/N7/81
    =NOV 1981

18. =CONCERNING COMPUTER CONTROL OF THE SNS EXTRACTED PROTON
    =BEAM AND TARGET STATION
    =D J CLARKE   G H EATON
    =SNS/TS/N6/81
    =SEPT 1981

19. =TARGET TEMPERATURE MONITORING
    =
    =D J CLARKE
    =SNS/TS/N5/81
    =SEPT 1981

20. =FAIL-SAFE FEATURES OF THE TARGET STATION MONITORING
    =CONTROL AND INTERLOCK SYSTEMS
    =D J CLARKE G H EATON
    =SNS/TS/N17/83
    =SEPT 1983
    =

21. =SNS TARGET STATION HAZARD SURVEY
    =
    =SNS TARGET STATION STAFF
    =SNS/ENV/N1/ REV1
    =SEPT 1983

Proceedings of the Eighth Meeting of the International Collaboration on Advanced Neutron Sources (ICANS-VIII)
8-12 July 1985, Rutherford Appleton Laboratory Report RAL-85-110

LANSCE HIGH POWER (200 μA) TARGET-MODERATOR-REFLECTOR-SHIELD

G. J. Russell, C. D. Bowman, E. R. Whitaker, H. Robinson and M. M. Meier

Los Alamos National Laboratory
P.O. Box 1663
Los Alamos, New Mexico 87545, U.S.A.

We are in the process of upgrading the high-current target area at the Los Alamos Neutron Scattering Center (LANSCE, alias WNR)[1] to accept 200 μA of 800-MeV protons from our Proton Storage Ring.[2] In addition to higher-power operation, we had to consider changes in the LANSCE Target-Moderator-Reflector (TMR) system to accomodate an expanded user program.[3] Our recently retired 'T'-shape TMR (see Fig. 1) was a proven, efficient neutron production system;[4,5] other spallation neutron source target systems are hard-pressed to match its neutron production efficiency. The 'T'-shape TMR utilized wing-geometry, and had the ability to simultaneously service nine of the twelve LANSCE target area flight paths (see Fig. 2). Note in Fig. 2 the layout of the twelve LANSCE flight paths; there are four flight path clusters (three flight paths per cluster) at 90° to each other. This flight path arrangement presents an interesting challenge for moderator layouts with acceptable neutronic performance. A requisite requirement for the upgraded LANSCE target system was that all twelve flight paths be serviced simultaneously by moderators with specific neutronic characteristics.

As described in Reference 6, we have powerful calculational and experimental capabilities at Los Alamos to study spallation neutron source problems. We have done numerous computations (using the Los Alamos HETC/MCNP/HTAPE Monte Carlo code package)[7] for the new upgraded, high-performance LANSCE TMR system. We also made benchmark calculations of the 'T'-shape geometry (see Fig. 1) to compare with the enhanced LANSCE TMR design. We performed a benchmark experimental measurement of the LANSCE TMR geometry to verify computational predictions.

The new LANSCE target system design has four unique features:

- There is no crypt per se (a void region) surrounding the TMR.
- The target is not one piece, but split into two unequal segments separated by a void.

- Moderators are not located adjacent to the target as in conventional wing-geometry design. In the LANSCE target system, the moderators are located where there is no target material (that is, next to a void region).

- A conventional all beryllium reflector is not used; the LANSCE TMR employs a composite reflector/shield arrangement.

Results of our LANSCE target system studies can be summarized as follows:

- Compared to the customary all beryllium reflector used in pulsed spallation neutron sources, thermal neutron performance can be enhanced by 10-20% if a composite reflector-shield (inner beryllium region and outer nickel region) is used (see Fig. 3). The outer nickel region also acts as a neutron shield; hence, we can talk about a Target-Moderator-Reflector-Shield (TMRS). There may also be a cost benefit for the composite arrangement. The new LANSCE target system utilizes the TMRS concept.[8] Since the outer nickel region is cooled, the effect is the same as cooling the inner portion of a bulk shield. We are pursuing a split-target design. By splitting the target into upper and lower sections, we can position moderators between the targets in a 'flux-trap' geometry. These flux-trap moderators are viewed by the twelve existing LANSCE flight paths. Our split-target TMRS concept is illustrated in Fig. 4.

- We are continually trying to better understand and optimize the split-target, TMRS design. We recently performed a measurement of thermal neutron yields and pulse widths in 'standard' reflected wing-geometry for both solid and split targets. A cursory look at our experimental results show: a) the difference in thermal neutron yields between solid and split targets was as predicted, and b) for a cylindrical void space between targets of 5 cm diam x 10 cm long, there was no discernable difference in the thermal neutron pulse widths. It is also possible to 'significantly' enhance the moderator neutron yield from a flux-trap moderator by increasing the field-of-view (FOV) above the canonical 100 cm^2. For example, compared to a 10 x 10 cm FOV, a 12 x 12 cm FOV increases the moderator thermal neutron yield by a factor of 1.34 with a decrease in the average source brightness of ~10%; these effects are illustrated in Figs. 5 and 6. One significant advantage of our flux-trap geometry is that all flux-trap moderators are high intensity. Our calculations show that for realistic moderator locations (moderators starting 8 cm from proton beam center), there is no difference in moderator thermal neutron yield between wing geometry with a beryllium reflector and flux-trap geometry with a composite beryllium/nickel reflector.

- As seen in Fig. 4, there are four flux-trap moderators in the initial (startup) LANSCE TMRS. Three of the moderators are ambient temperature water. Two of the water moderators are heterogeneously poisoned at 2.5 cm with gadolinium and have cadmium decoupler/liners. These two moderators are referred to as 'high-intensity' moderators. The third water moderator is heterogeneously poisoned with gadolinium at 1.5 cm and has a boron decoupler/liner (1/e transmission at ~3 eV). This moderator is called the 'high-resolution' moderator. The poison neutronically defines the thickness of a moderator viewed by an experiment. The decoupler surrounds the moderator per se to neutronically isolate the moderator from the reflector. The liner is a material which 'lines' the void region through the reflector-shield where neutrons are extracted for experiments; the liner neutronically isolates the moderator 'viewed surface' from the reflector-shield. We recognize the need and importance of cold moderators, and the fourth flux-trap moderator is liquid para-hydrogen at 20-25 K.[9] Our liquid hydrogen moderator has a gadolinuim decoupler and a cadmium liner. Neutron yields, mean-emission-times, pulse widths, and pulse shapes for the high-intensity and high-resolution water moderators and the liquid hydrogen moderator are shown in Figs. 7-13. For a (decoupled) depleted uranium target with Rutherford Appleton Laboratory Spallation Neutron Source (RAL SNS) target design parameters,[10] the calculated average energy deposition (at the flux-trap moderator location) is ~2.7 $mW/cm^3-\mu A$, ~0.89 $mW/cm^3-\mu A$, and ~1.5 $mW/cm^3-\mu A$ for water, liquid hydrogen, and aluminium, respectively.

- As described in Reference 2, there will be a need for the LANSCE TMRS to service more flight paths (in addition to the twelve shown in Fig. 2) to support an expanded user program. As seen in Fig. 4, these 'future' moderators are depicted as wing-moderators adjacent to the upper target. In reality these moderators would be adjacent to the void region upstream of the target (the moderators could also overlap part of the upper target as well). The feasibility of this approach is demonstrated in Fig. 14, where the location of a wing-moderator relative to the target is indicated. As can be seen in Fig. 14, the penalties in neutron intensity (relative to the optimum moderator location) are roughly the same whether the moderator is located fore or aft of the optimum position. The feasibility of drilling additional flight paths through the LANSCE bulk shield has been successfully demonstrated.

- Our initial LANSCE target is solid tungsten. The upper target size is 10-cm diameter by 7-cm long; the lower target size is 10-cm diameter by 27-cm long. The void region between the targets is 10-cm diameter by 14-cm long. After accounting for the effects of proton beam windows, the upper target length was set at the optimum value for thermal neutron yield (see Fig. 15). The calculated power in both tungsten targets is ~49 kW for 100 μA of 800-MeV protons.

- We intend to design and implement a depleted uranium (0.20 a% ^{235}U) target capable of handling 200 μA of 800-MeV protons. In our depleted uranium target studies, we found that neutrons resulting from low-energy (E < 20 MeV) neutron induced fissions in ^{235}U cause the following problems: a) artificial enhancement of the thermal neutron intensity, b) broadening of the thermal neutron pulses, and c) additional (unwanted) power generation in the target. For 200 μA of 800-MeV protons and a light water cooled depleted uranium target neutronically coupled to the LANSCE TMRS, we found:

  - About 7% of the thermal neutron intensity at the surface of a moderator originate with low-energy neutron induced fissions in 235-U. In general, these neutrons do not contribute to the useful neutron beam current, and may require decoupling a depleted uranium target.

  - The calculated standard deviation of the thermal neutron pulse at the moderator surface was ~78 μs (compared to ~23 μs for a decoupled target).

  - About 25 kW (out of ~215 kW total) of target power is attributable to low-energy neutron induced fissions in 235-U.

- The calculated neutronic gain for a decoupled depleted uranium target is compared to a tungsten target in Fig. 16; the gain in thermal neutron intensity for depleted uranium relative to tungsten is 1.42 ± 0.04. For this comparison we used decoupled RAL SNS target design parameters;[10] the tungsten target was solid. This comparison should be valid for proton currents where a tungsten target can be solid (up to ~100 μA of 800-MeV protons) and a depleted uranium target needs to be segmented for adequate cooling. For a coupled depleted uranium target, the calculated thermal neutron intensity gain (relative to tungsten) is 1.52 ± 0.06.

- For spallation neutron source applications, depleted uranium is a booster-target (albeit a relatively inefficent one - 2.8 fissions/proton giving 3.5×10^{15} fissions/sec for 200 μA of 800-MeV protons). We will be studying more efficient booster-targets with a useful thermal neutron gain (the gain in neutron beam current to an experiment) of three over that attainable from a depleted uranium booster-target. Other possible booster-target

materials are ^{233}U, ^{235}U, ^{237}Np, and ^{239}Pu. A scoping calculation of a ^{237}Np booster-target, yielded a power of ~2 MW (k_{eff} 0.80-0.84) for 200 μA of 800-MeV protons.[11] This preliminary calculation did not account for any engineering realities necessary in an actual high power booster-target design. High power booster-targets will present significant technological design problems (particularly in the areas of heat removal and materials). The advantages and disadvantages of booster-targets with respect to cost, complexity, gain in useful neutron beam current, beam current quality (signal-to-noise ratio, gamma-ray contamination, etc.) need further study.

Acknowledgements

We appreciate the continuing support of Dick Woods for this work and on going useful discussions with Dick Prael. We acknowledge the help of K. J. Hughes, A. Bridge, R. A. Spencer, G. L. Legate, J. R. Baldonado, and R. E. Meyer in the crucial task of designing, assembling and installing the LANSCE TMRS.

One of the authors (G. J. Russell), would like to acknowledge the opportunity he had to work with Rex Fluharty; interacting with Rex was both a challenge and an inspiration - I will miss him.

This work was performed under the auspices of the U.S. Department of Energy.

References

1. G. J. Russell, P. W. Lisowski, S. D. Howe, N. S. P. King, and M. M. Meier, "Characteristics of the WNR - A Pulsed Spallation Neutron Source," Nuclear Data for Science and Technology, K. H. Bockhoff, ed., pp. 831-835, 1983.

2. F. A. Morse, "Project Status Report LANSCE the Los Alamos Neutron Scattering Center," Eighth Meeting of the International Collaboration on Advanced Neutron Sources (ICANS-VIII), Oxford, England, July 8-12, 1985.

3. C. D. Bowman, "Status Report on the WNR/PSR Pulsed Spallation Neutron Source at the Los Alamos National Laboratory," Seventh Meeting of the International Collaboration on Advanced Neutron Sources (ICANS-VII), Chalk River Nuclear Laboratories, September 12-16, 1983.

4. G. J. Russell, M. M. Meier, J. S. Gilmore, R. E. Prael, H. Robinson, and A. D. Taylor, "Measurements of Spallation Target-Moderator-Reflector Neutronics at the Weapons Neutron Research Facility, "Proc. of Fourth Meeting of the International Collaboration on Advanced Neutron Sources (ICANS-IV), KEK, Tsukuba, Japan, October 20-24, 1980, KENS Report II, pp. 210-241 (March 1981).

5. G. J. Russell, M. M. Meier, H. Robinson, and A. D. Taylor, "Preliminary Neutronics of a 'T'-Shape Premoderator/Moderator for the Weapons Neutron Research Facility," Proc. of Fifth Meeting of the International Collaboration on Advanced Neutron Sources (ICANS-V), Juelich, West

Germany, June 22-26, 1981, Juelich-Conf-45, ISSN-0344-5789, pp. 389-416 (October 1981).

6. G. J. Russell, "Applied Spallation Physics Research at Los Alamos", Los Alamos National Laboratory report, LA-UR-84-778 (1983).

7. R. E. Prael, "User Guide to the HETC Code System," Los Alamos National Laboratory internal report (April 1985).

8. G. J. Russell, "WNR High Power (200 μA) Target-Moderator-Reflector-Shield," Los Alamos National Laboratory internal report, TN-GJR/P9-006 (October 1983).

9. H. Robinson, G. J. Russell, E. D. Tucker, E. R. Whitaker, K. D. Williamson, and F. Edeskuty, "Liquid Hydrogen Moderator System Hardware, Characteristics, and Operation," Eighth Meeting of the International Collboration on Advanced Neutron Sources (ICANS-VIII), Oxford, England, July 8-12, 1985.

10. B. Boardman, "Spallation Neutron Source: Description of Accelerator and Target," Rutherford Appleton Laboratory report RL-82-006 (March 1982).

11. G. J. Russell, "Some Preliminary Thoughts on WNR Booster-Target Characteristics," Los Alamos National Laboratory internal report, TN-GJR/P-9-001 (February 1984).

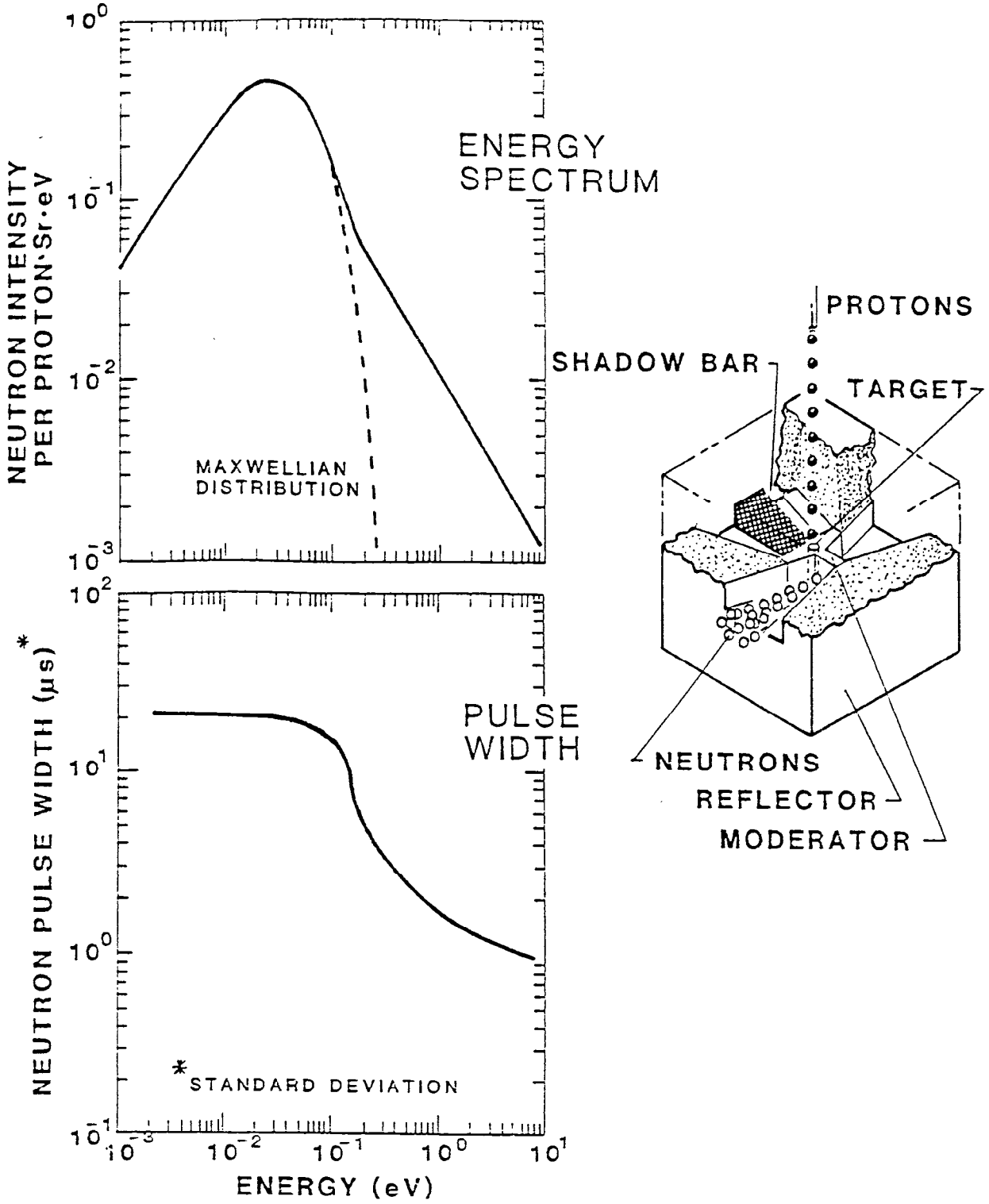

Fig. 1. Neutron surface-current and pulse width characteristics for the reflected T-shape (H_2O) moderator with a 10 by 10 cm field-of-view. The moderator is heterogeneously poisoned by Gd at a depth of 2.3 cm, and decoupled from the Be reflector by Cd.

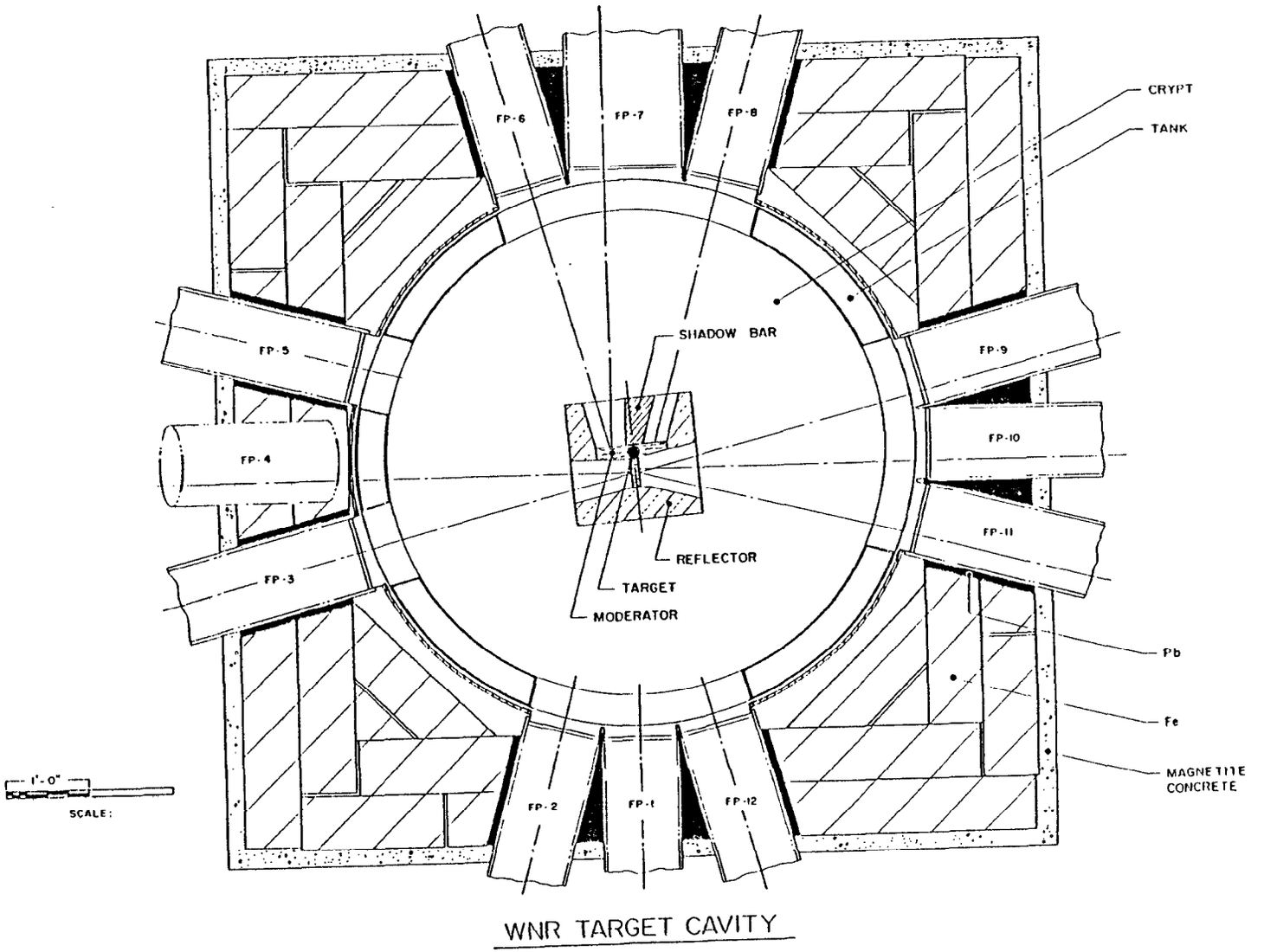

Fig. 2. Section thru the original WNR target cavity showing the orientation of the TMR (with the 'T'-shaped moderator) and the flight path configuration.

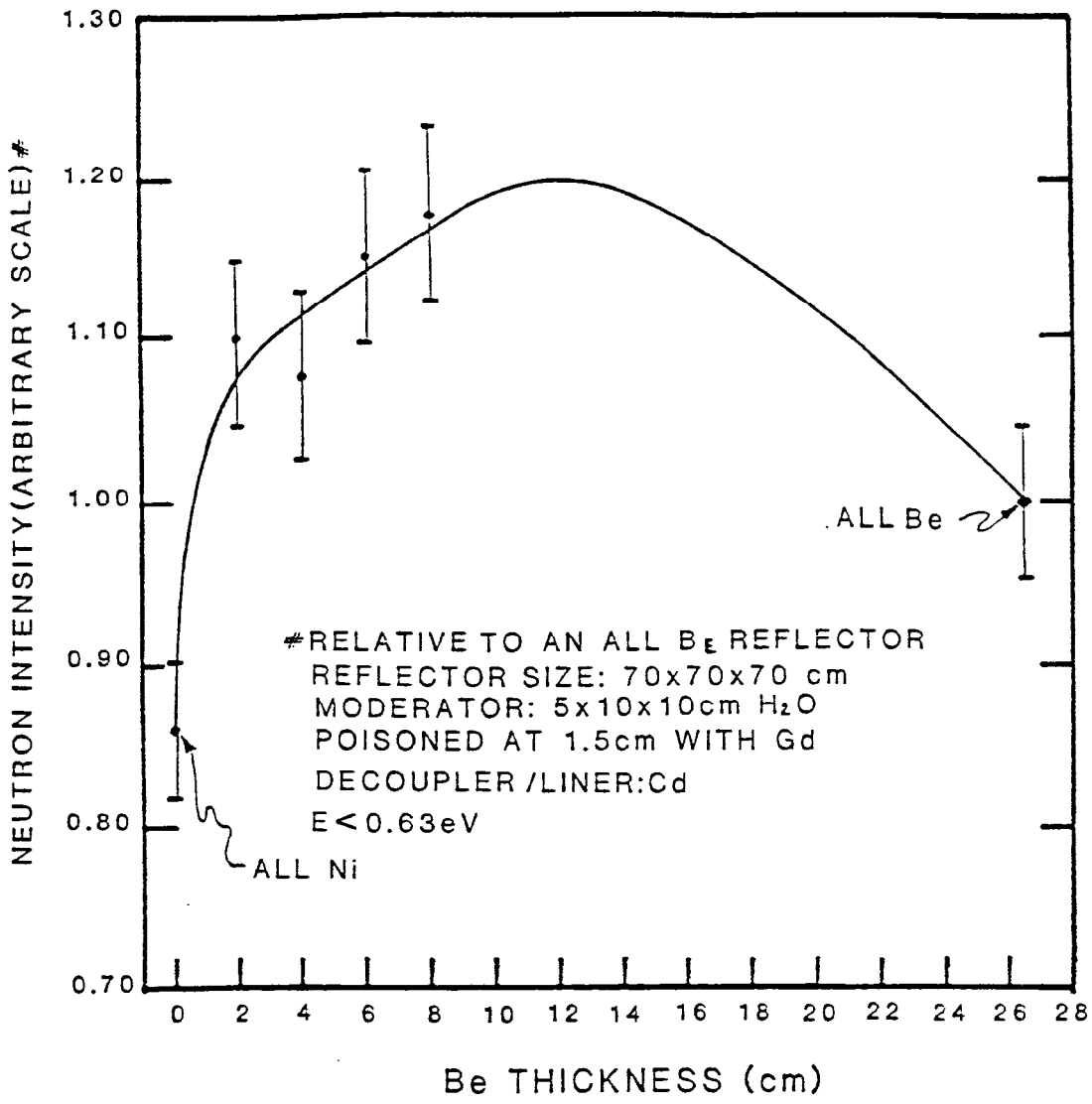

Fig. 3. Neutron surface-current for a composite beryllium/nickel reflector-shield. The computations were done for a moderator in wing-geometry. More definitive computations are underway.

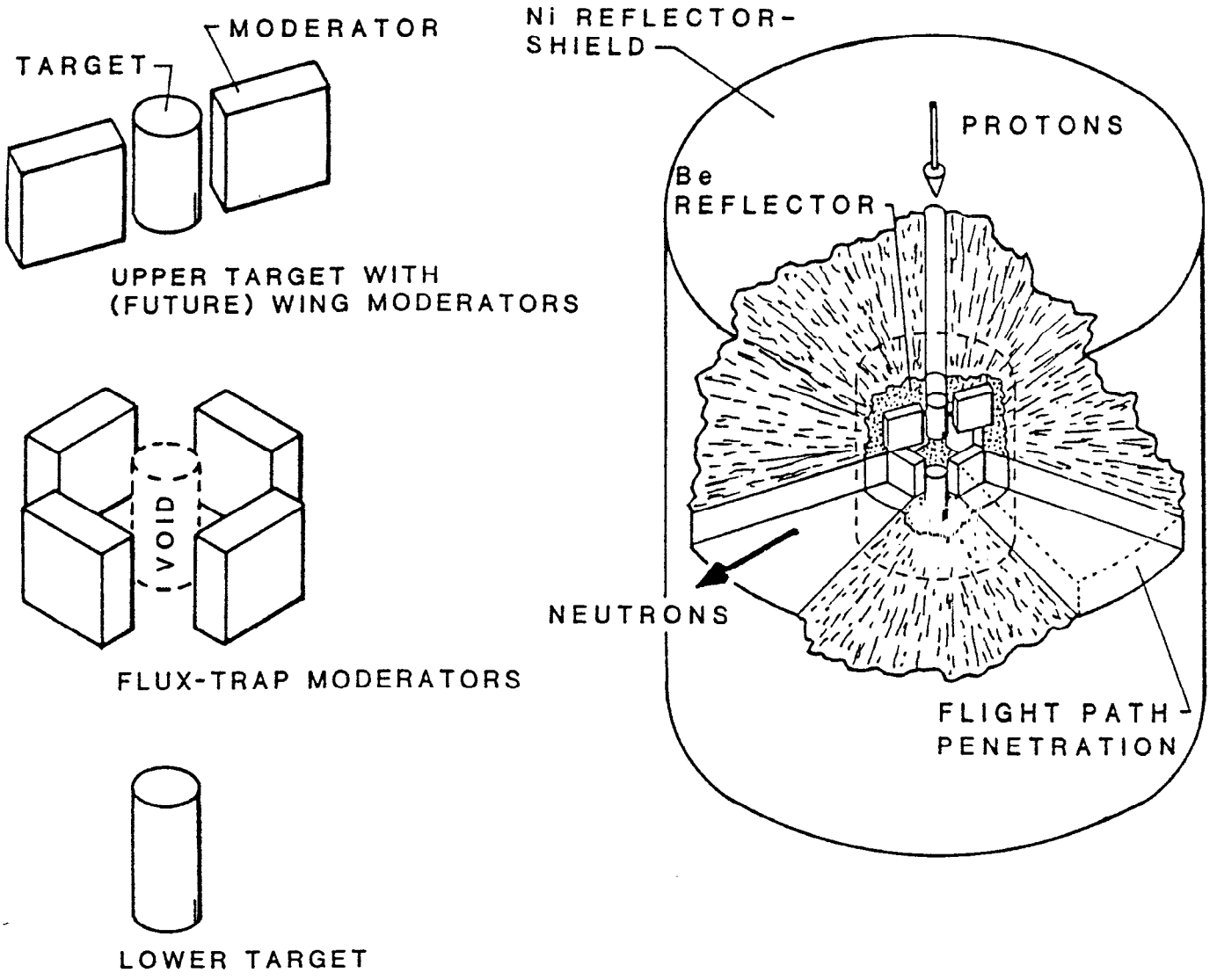

Fig. 4. Illustration of the upgraded/enhanced TMRS configuration for the LANSCE high-current target area. The 1-m-high assembly consists of a split-target, an inner Be reflector region, and an outer Ni reflector/shield. The twelve existing flight paths view the flux-trap moderators; new flight paths would look at wing-moderators in the upper target position.

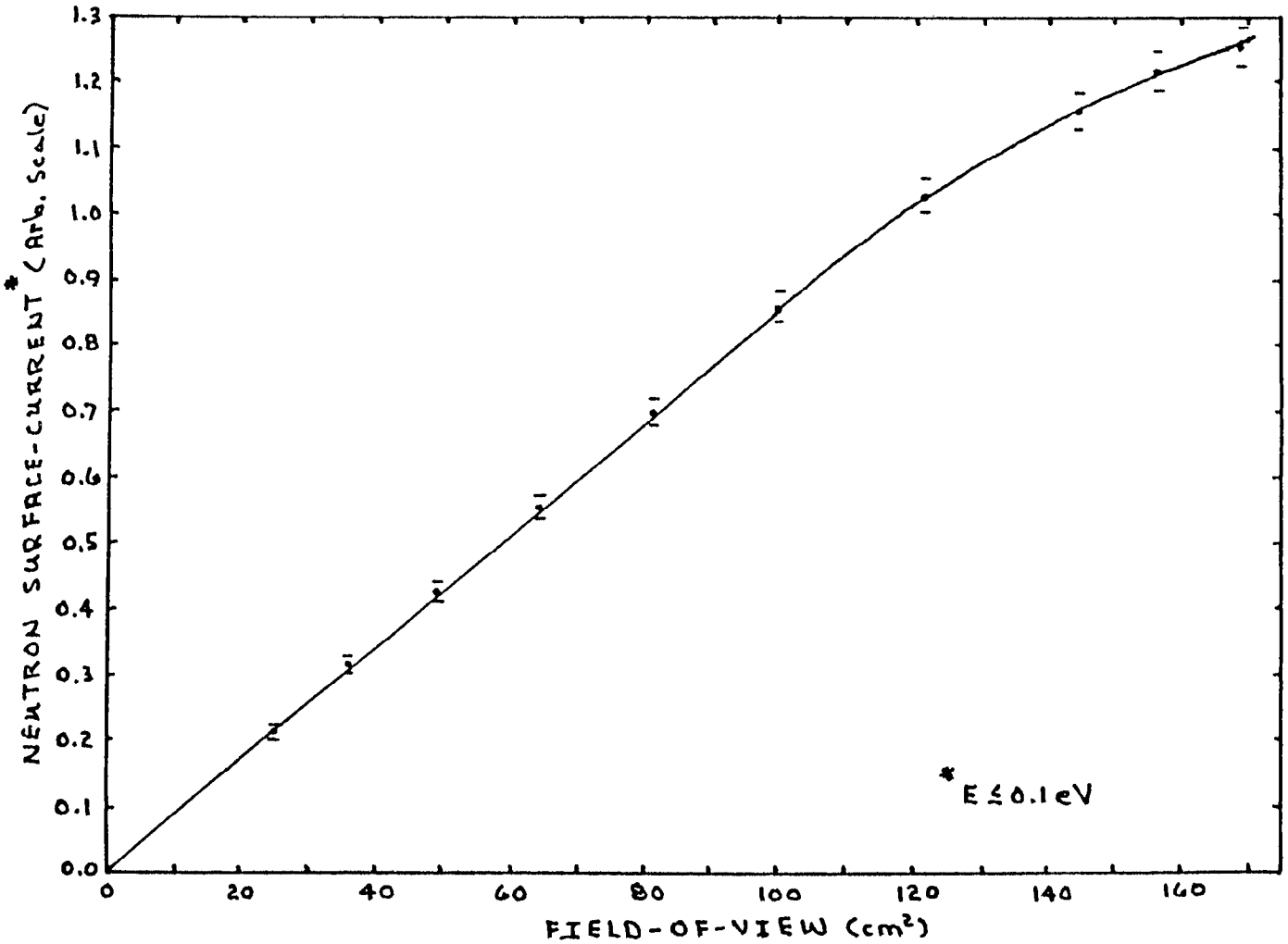

Fig. 5. Neutron surface-current from a high-intensity flux-trap H_2O moderator versus moderator field-of-view.

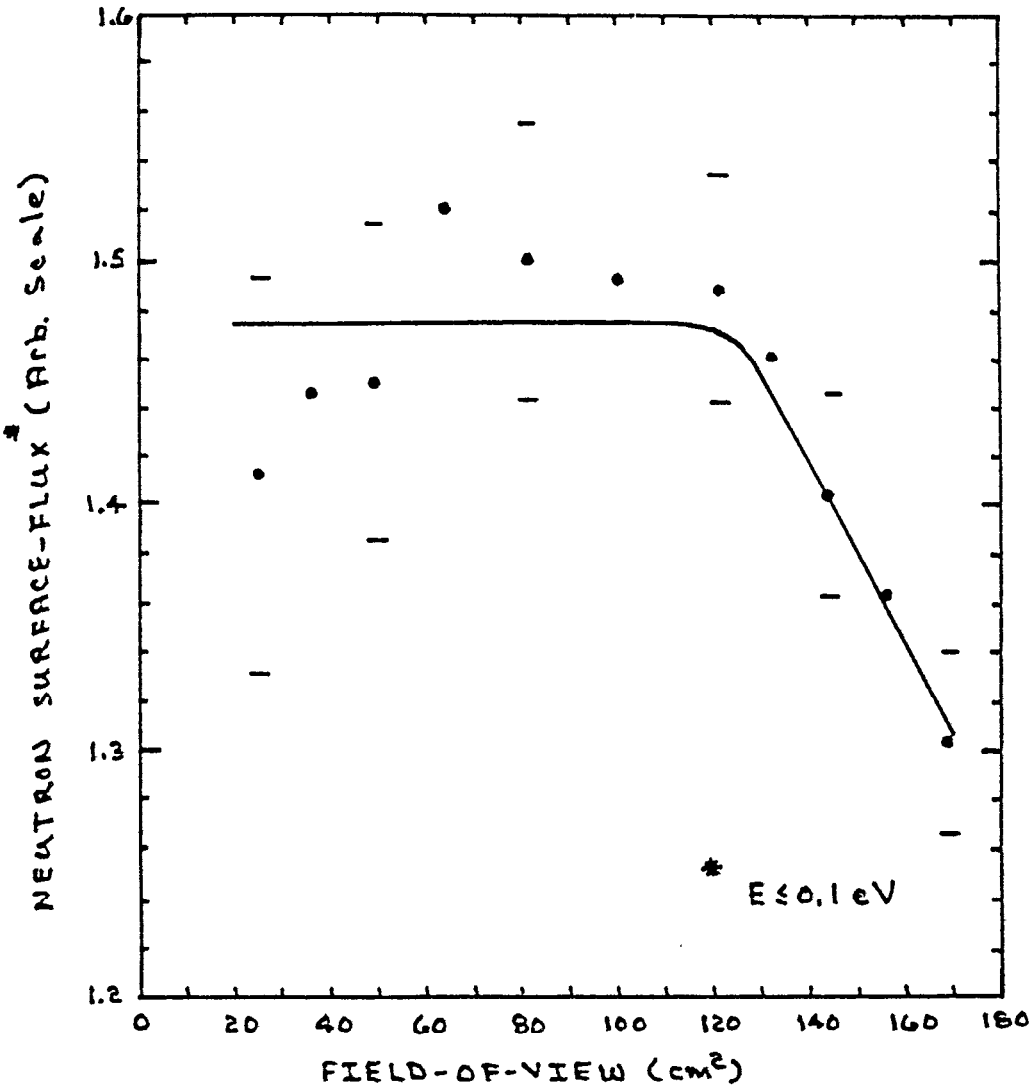

Fig. 6. Neutron surface-flux from a high-intensity flux-trap H_2O moderator versus moderator field-of-view. Neutron surface-flux is indicative of moderator brightness. The relative error in the calculation is approximately ±5%.

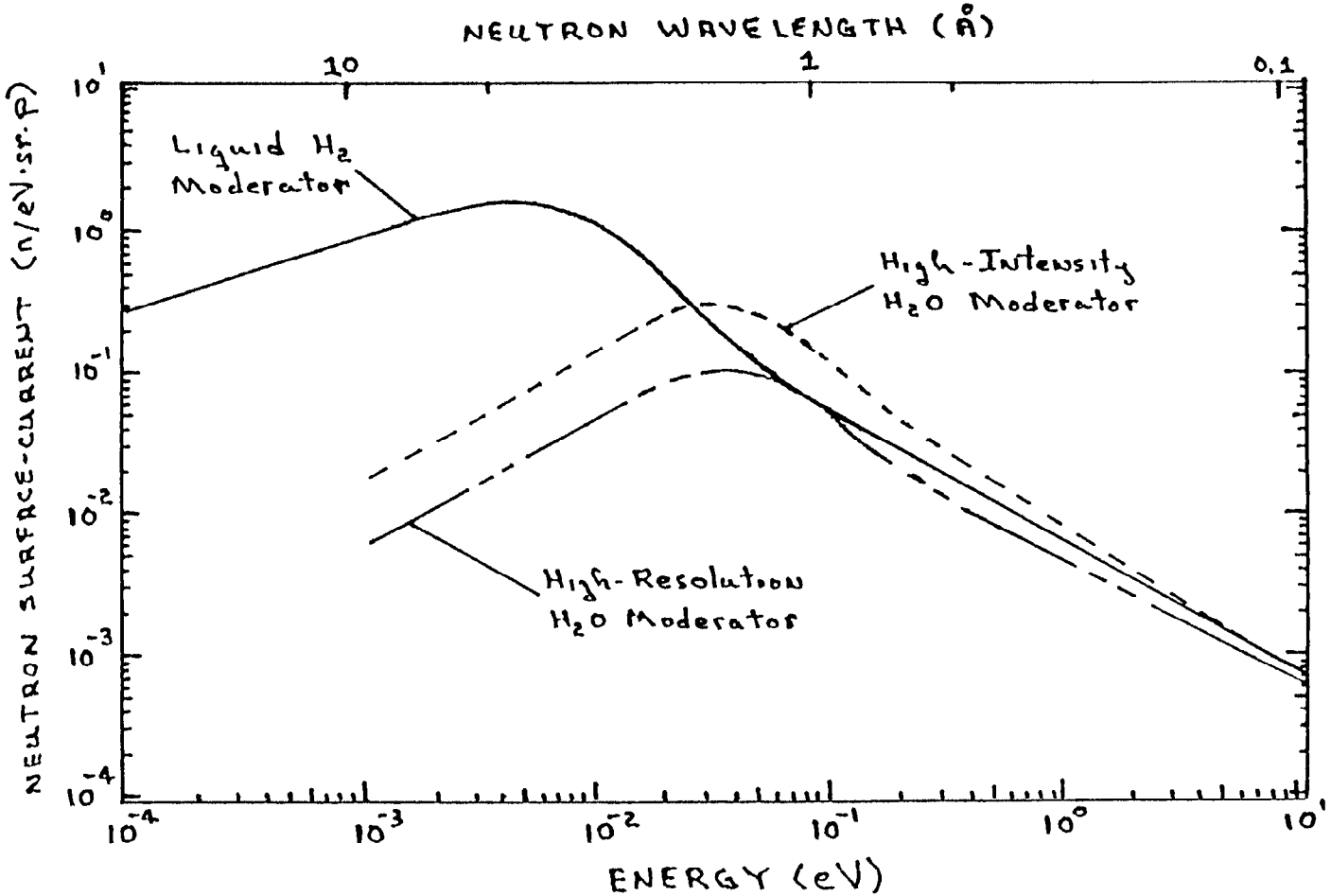

Fig. 7. Calculated neutron surface-current for various flux-trap moderators with a 10-cm-diam tungsten split-target. The moderator field-of-view was 100 cm^2.

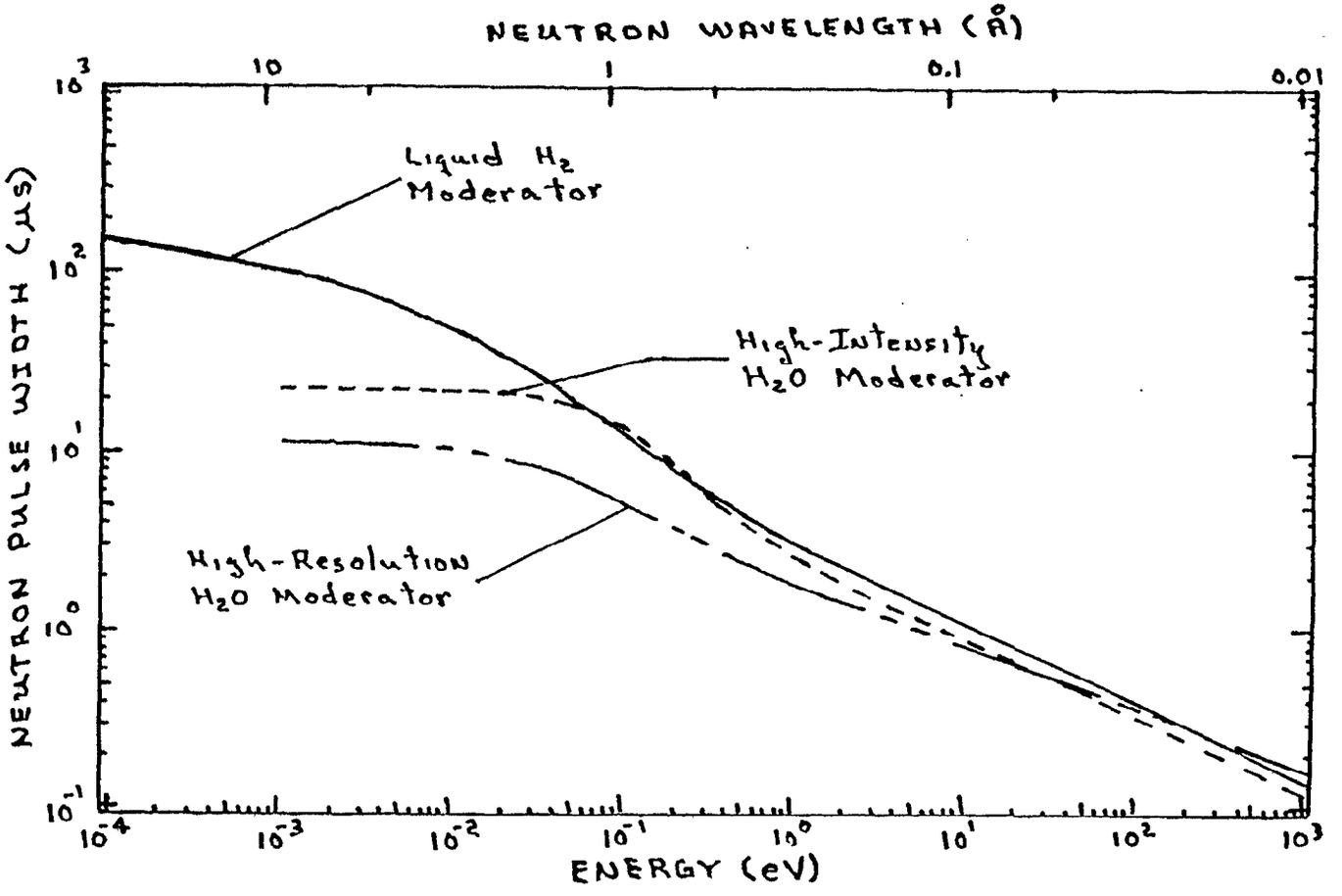

Fig. 8. Calculated standard deviation of neutron pulse for various flux-trap moderators with a 10-cm-diam tungsten target. The moderator field-of-view was 100 cm^2.

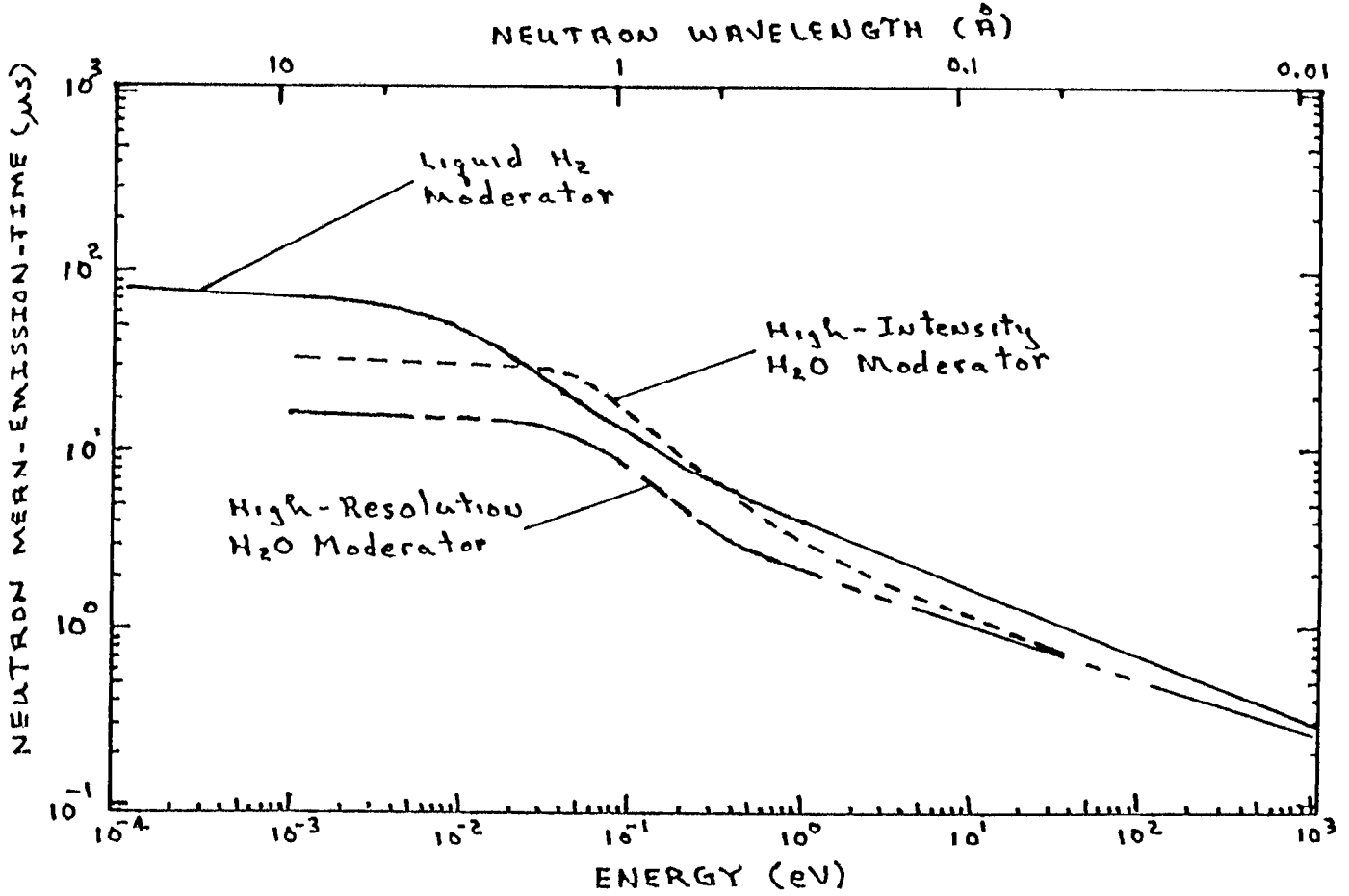

Fig. 9. Calculated neutron mean-emission-time for various flux-trap moderators with a 10-cm-diam tungsten split-target. The moderator field-of-view was 100 cm^2.

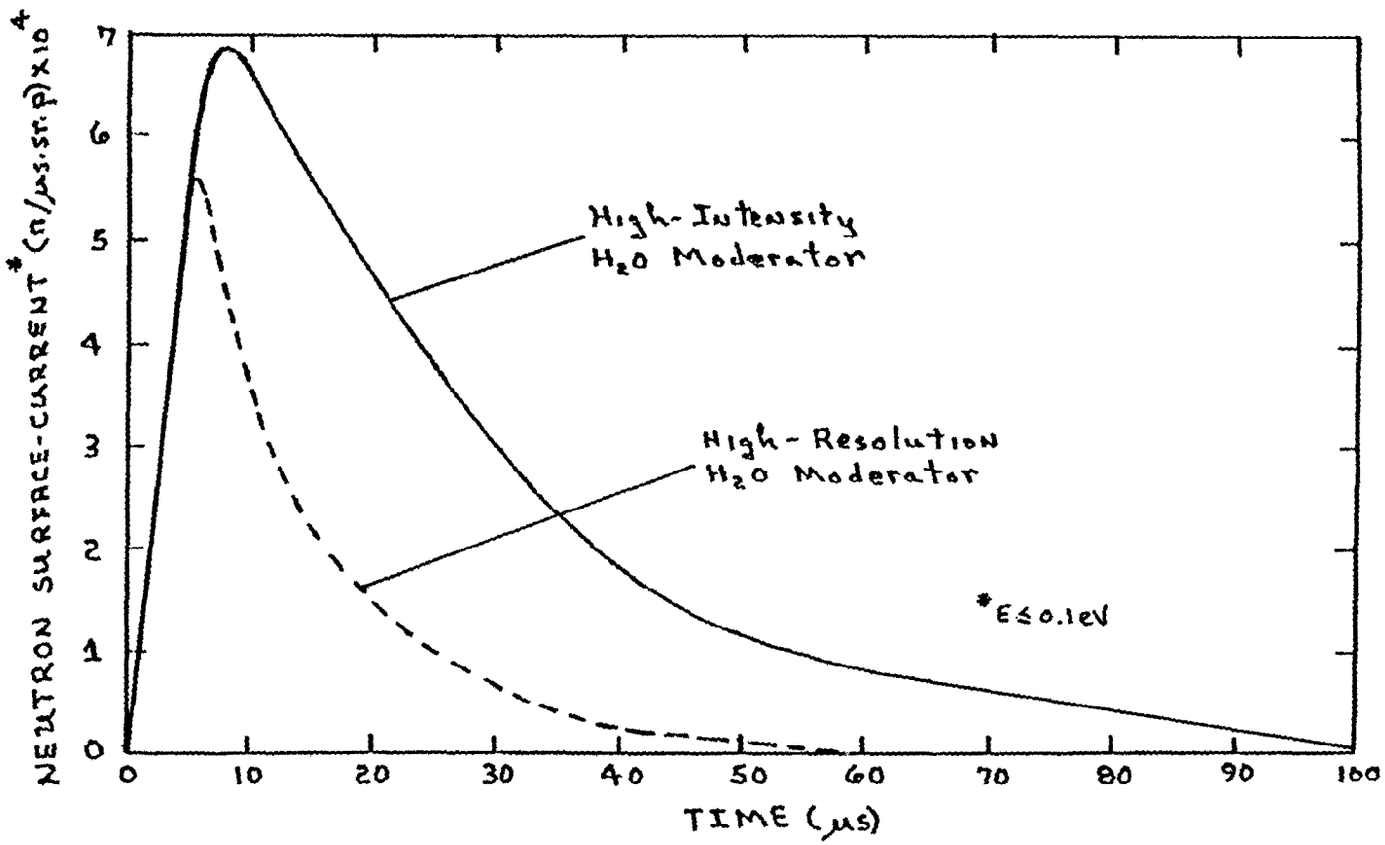

Fig. 10. Calculated neutron time distribution for high-intensity and high-resolution water flux-trap moderators with a 10-cm-diam tungsten target. The moderator field-of-view was 100 cm^2.

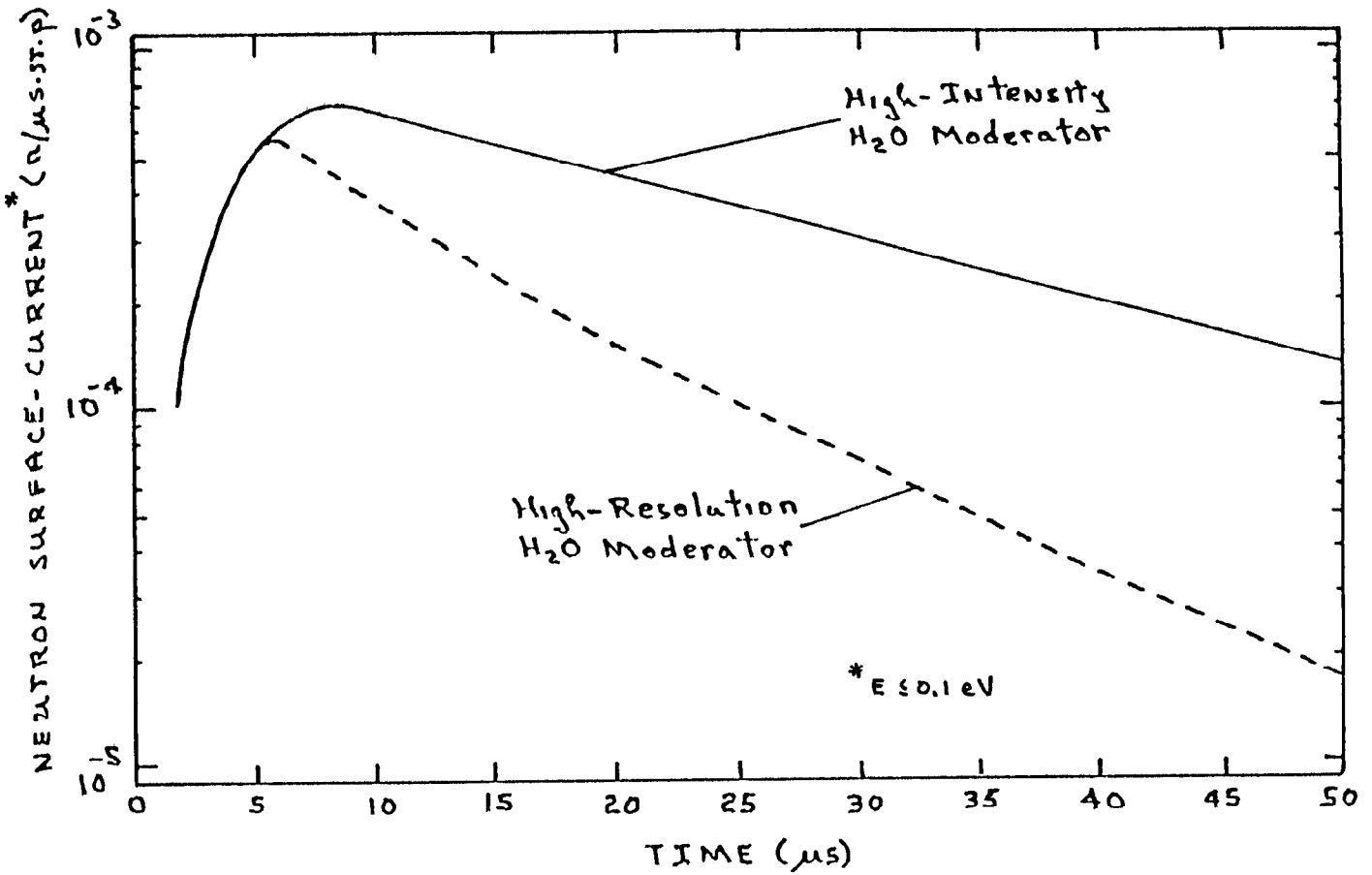

Fig. 11. Calculated neutron time distribution for high-intensity and high-resolution water flux-trap moderators with a 10-cm-diam tungsten target. The moderator field-of-view was 100 cm^2.

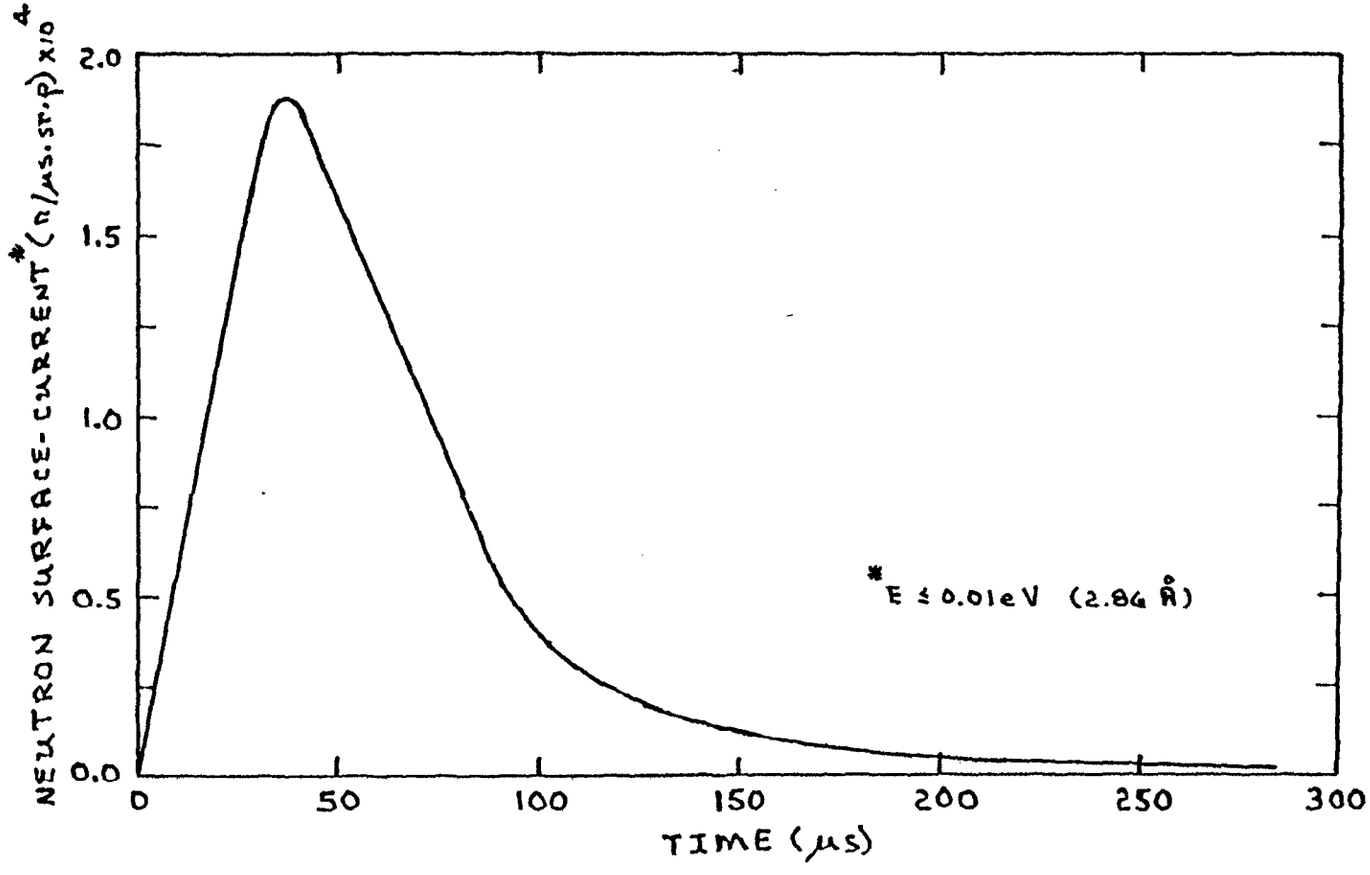

Fig. 12. Calculated neutron time distribution from the liquid hydrogen moderator with a 10-cm-diam tungsten target. The moderator field-of-view was 100 cm^2.

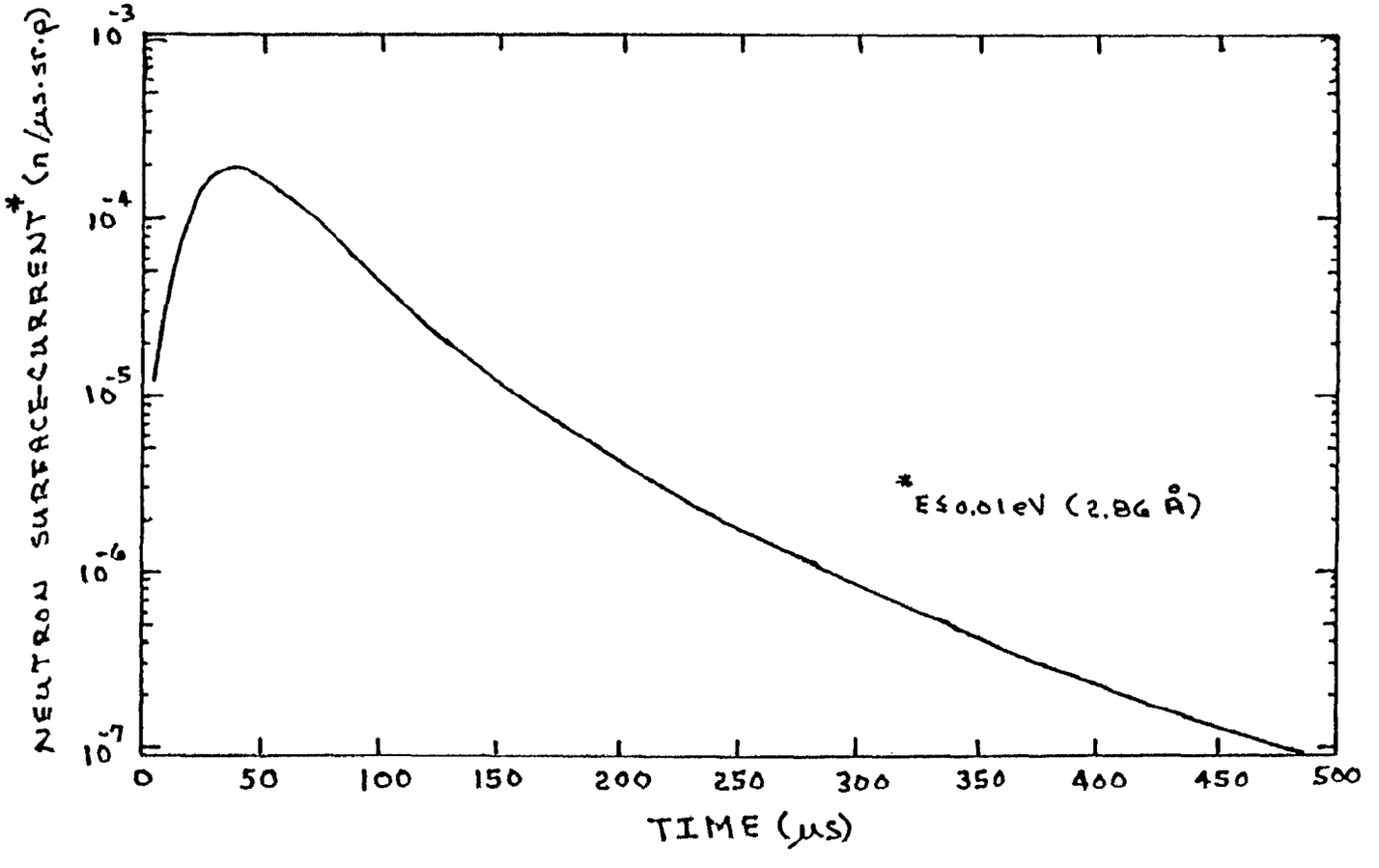

Fig. 13. Calculated neutron time distribution from the liquid hydrogen moderator with a 10-cm-diam tungsten target. The moderator field-of-view was 100 cm^2.

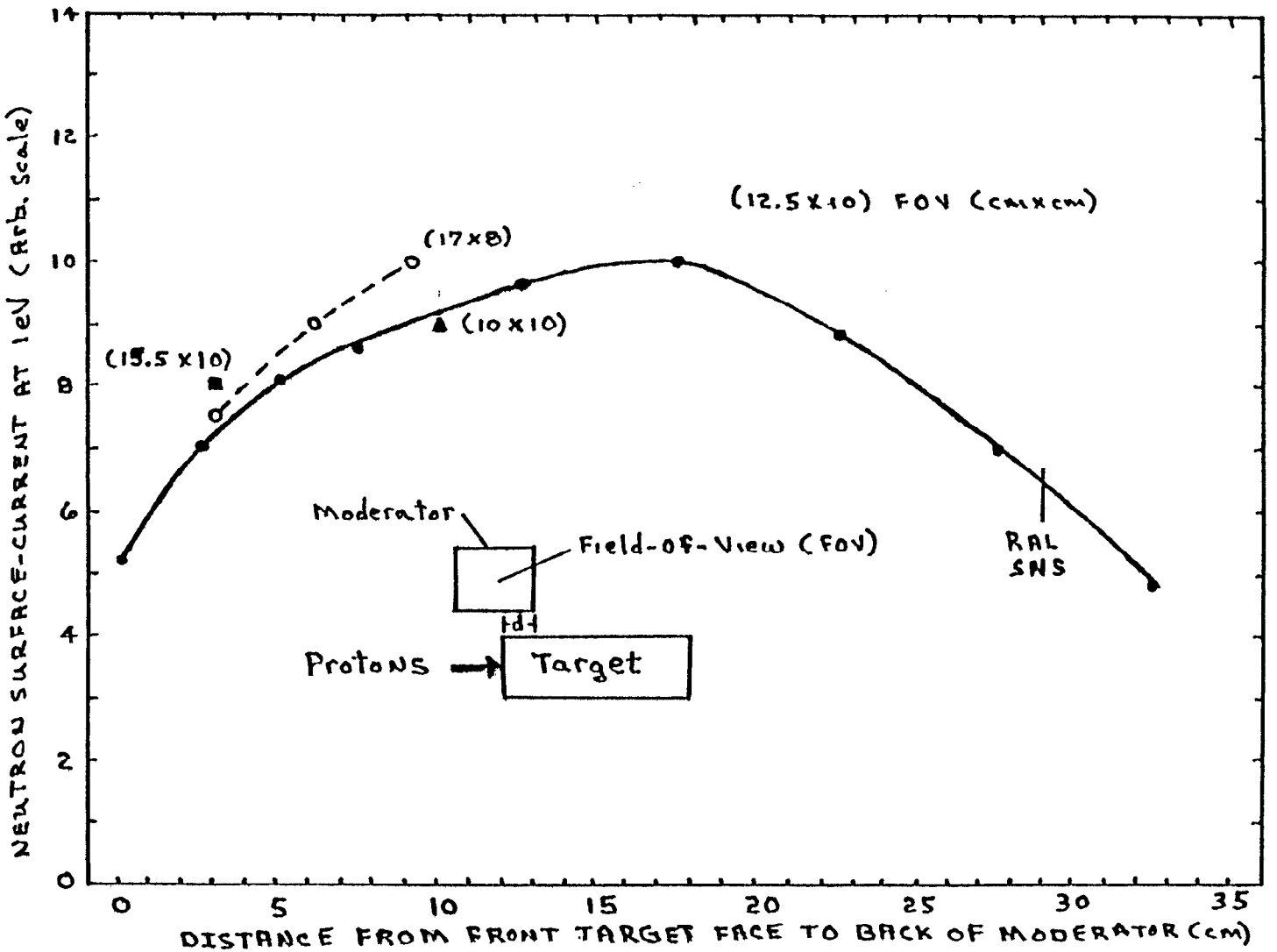

Fig. 14. Neutron surface-current versus location of moderator relative to target in reflected single-wing geometry.

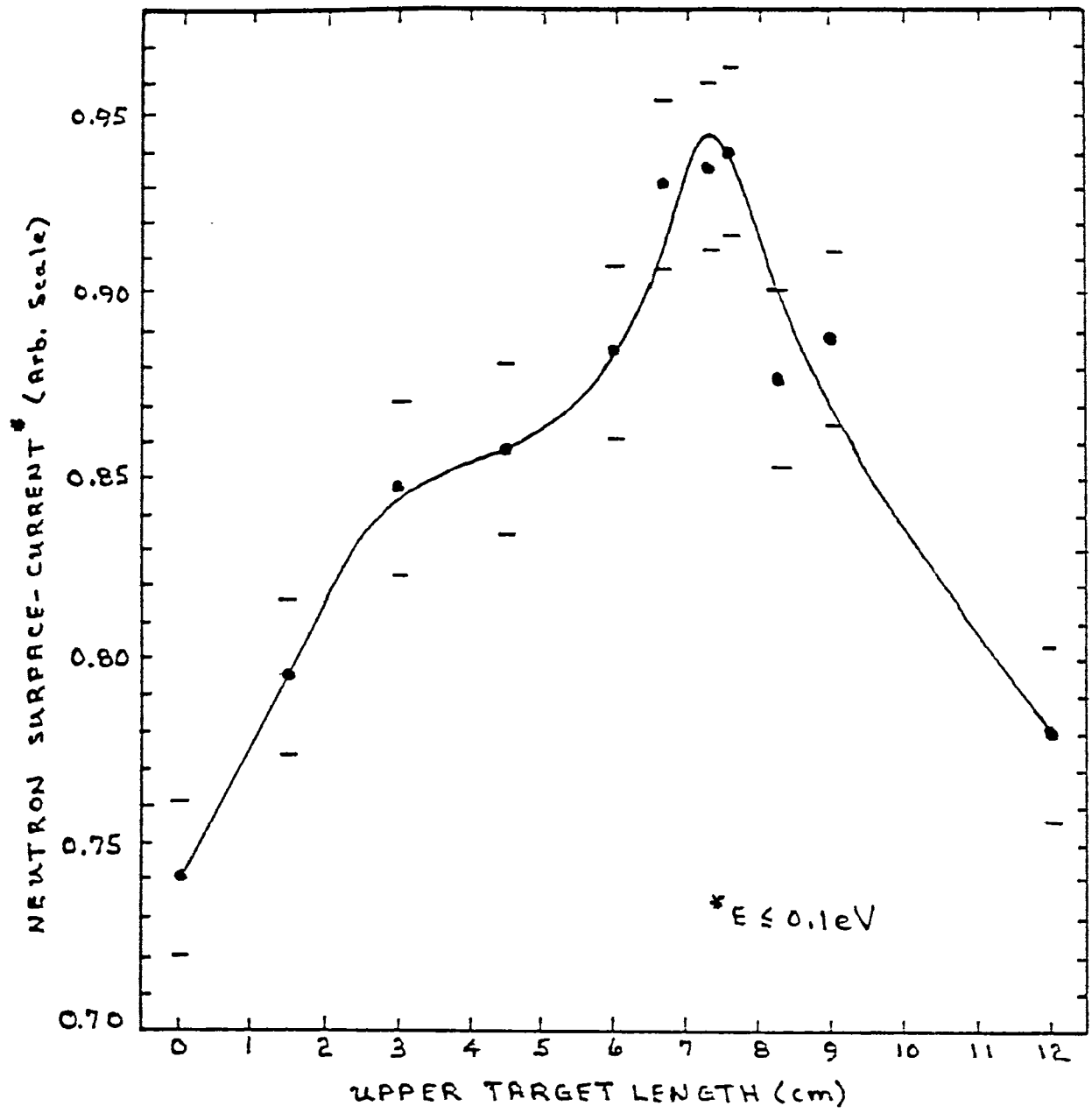

Fig. 15. Neutron surface-current from a high-intensity water moderator as a function of the length of the upper tungsten (10-cm-diam) target. The moderator field-of-view was 11.5-cm from proton beam center.

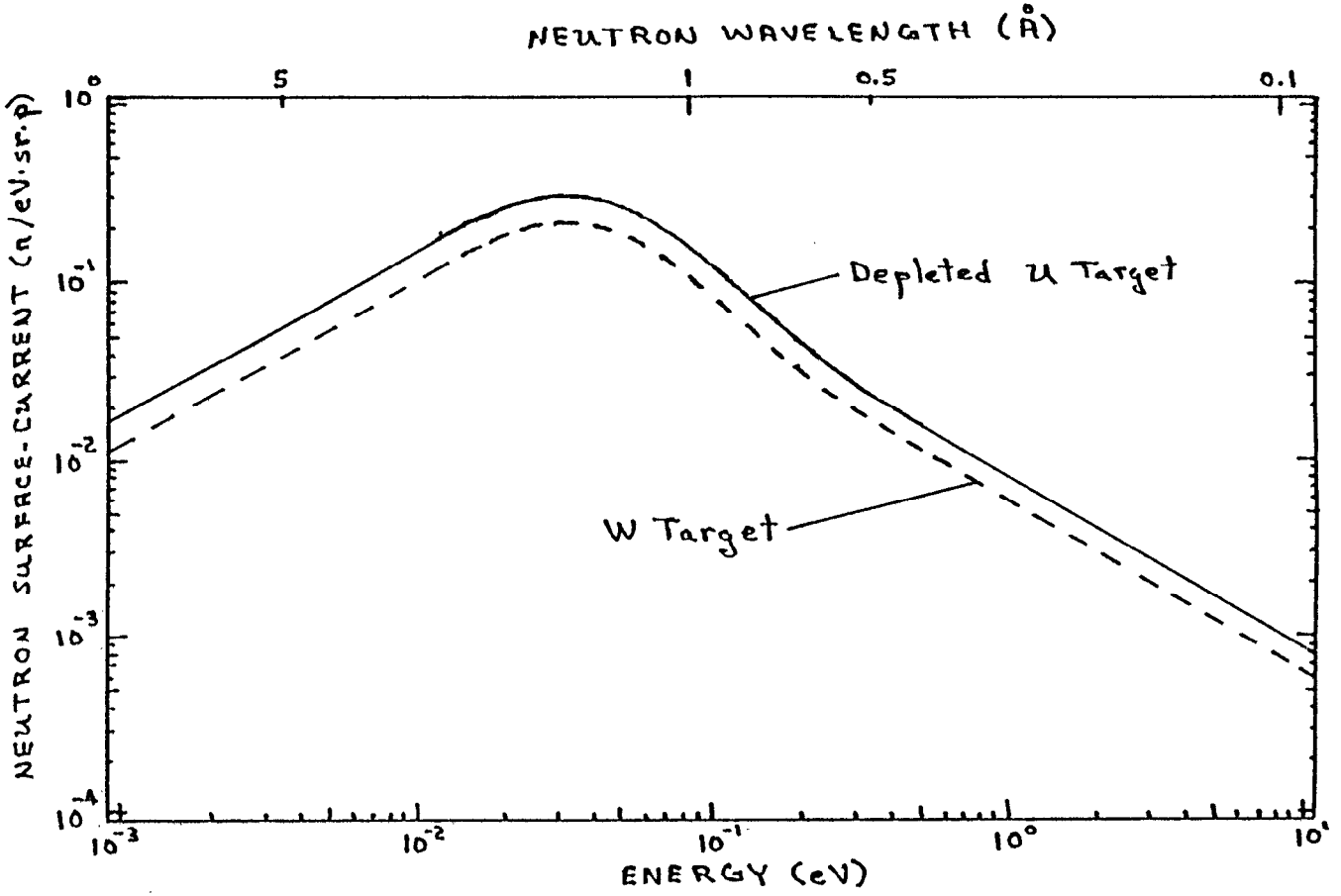

Fig. 16. Neutron surface-current from a high-intensity water moderator for split-targets. The 100 cm^2 moderator field-of-view was 11-cm from proton beam center.

Proceedings of the Eighth Meeting of the International Collaboration on Advanced Neutron Sources (ICANS-VIII)
8-12 July 1985, Rutherford Appleton Laboratory Report RAL-85-110

LANSCE LIQUID HYDROGEN MODERATOR SYSTEM HARDWARE-CHARACTERISTICS-OPERATION

H. Robinson, G. J. Russell, E. D. Tucker,
E. R. Whitaker, K. D. Williamson, Jr. And F. J. Edeskuty

Los Alamos National Laboratory
P.O. Box 1663
Los Alamos, NM 87545
USA

Introduction

In this paper, we report the current status of the hardware development and testing program for a liquid hydrogen moderator system currently being fabricated for installation into the Los Alamos Neutron Scattering Center (LANSCE) upgraded target system.[1][6]

Facility Upgrade

The PSR has been commissioned with first beam[2] and the WNR/LANSCE proton transport system was upgraded to transport the higher current beam required for the PSR era[3][4](Figure 1). The upgrade work for the target crypt and the TMRS assembly is progressing. All new target crypt shielding and a new water-cooled beam stop have been installed. The new 500 KW target/shield cooling system has been fabricated. The ambient temperature moderator cooling package is to be delivered this month. Our objective for completing all remaining tasks is August 1985.

Hardware and Design Considerations

1. Refrigerator

   We were very fortunate to locate a Koch 1400 He Liquifier/Refrigerator unit as surplus equipment at our laboratory. The unit was equipped with the three compressor option. Although it was a 1975 model, it had relatively few operating hours on it, 2500 total. After talking to the manufacturer of the unit about our intended application, it was suggested that we return it to the factory for modifications to give a cooling capacity of 450-500 watts. Upon the return of this unit to Los Alamos, it was put through a heat-load test(Figure 2). Preliminary studies indicated a desirability

to have 300 Watts of cooling capacity inside the upgraded TMRS. The total capacity of the refrigerator (450-500 watts) gives us a margin for line losses and heat leaks in our cryogenic exchange unit.

2. He/H_2 Heat Exchanger Assembly

Having watched the hydrogen moderator design progress our colleagues at the SNS Project[5] were making, we decided to pursue a similar approach by using a circulating pump for the liquid hydrogen. Lacking any cryogenic expertise within our group at Los Alamos, we sought help from another division for developing the fabrication specification for such an assembly (Table I). The design and fabrication package for the heat exchanger and transfer line components was awarded to a vendor with a history of cryogenic dewar fabrication. A simplified heat exchanger schematic is shown (Figure 3). The process of fabrication and testing proved to be a learning experience for both the vendor and ourselves.

3. Thermodynamic Operation

We initially favored a low-pressure, subcritical operating region for the hydrogen with the intent that this would permit us to design a thinner moderator canister. Actual testing demonstrated that our pump would not efficiently circulate the hydrogen gas during cooldown. Thus the liquid that condensed in the heat exchanger was pumped through warm transfer lines resulting in surges that equalled the supercritical range. Our earlier decision to design all components for 17 ATM of operation permitted us to cooldown and charge at the supercritical level of 15 ATM. This mode of operation eliminated the pressure surge problem.

4. Ortho-Para

In order to attain a known ortho-para concentration, we have designed a hydrogen catalyst chamber to be installed into the loop at a later date. Because of the added pressure drop across such a unit, we will initially use the long cooldown approach to attain an equilibrium mixture with an ortho-para ratio of 99.8% para-hydrogen at liquid temperatures.

5. Moderator Canister

Since our test program had forced us into the 15 ATM operating region, we looked into the flat verses curved shaped approaches for

the canister walls. After discovering the cost and time delay to investigate the complex curved shapes by finite element analysis, we have elected to start with a flat head approach(Figure 4). This design can be improved at the same time we upgrade the target material to uranium. We selected to go with 6061 aluminum because of its mechanical properties and history of use for cryogenic applications. The canister dimensions are 13cm H x 13cm W x 5cm D with viewing side thickness of 6.4 mm.

6. System Location

The moderator is located in the TMRS assembly adjacent to the target flux-trap[1](Figure 5). This TMRS assembly is in the center of the target crypt and is viewed by 12 flight paths that pass through the biological shield and into the experimental hall. The hydrogen moderator will be viewed by three of these flight paths. The area above this crypt, the target cell, houses the proton beam transport components responsible for bending the beam from its horizontal transport plane into a vertical plane for transport into the target crypt(Figure 6). Remote handling equipment for servicing the TMRS assembly is also in this room. Maintenance to equipment within the target cell is a "hands on" operation with the beam off. The He/H_2 heat exchanger is located above and to the side of the target crypt with the hydrogen transfer lines passing up through the shielding connecting the moderator to the heat exchanger. This gives a very close couple for the hydrogen system. The He transfer lines route up from the heat exchanger and out into the service area where the refrigerator is located. The compressor trailer is positioned outside of the building. Since the heat exchanger has no organic dynamic seal applications, the moderate radiation levels in this vacinity during beam-on conditions should not effect its operation at this location.

7. Safety

Our approach in designing for safety was to keep the hydrogen volume as small as possible and dump the hydrogen into the vent stack upon any system malfunction. The hydrogen system volume has been minimized by the close mounting of the components. Total system volume is ~ 6 liters, which is the liquid equivalent of one size H hydrogen cylinder. The hydrogen components are located in three places - the target crypt, the target cell, and the service area(Figure 7). If a size H cylinder of gas was completely dis-

charged into either the target cell or the service area, any dispersion would result in the hydrogen air ratio being well below the flammability level. However, two hydrogen monitor heads have been located in critical positions. The target crypt is always under a vacuum of at least 100 microns when we are operating. Any rise in vacuum pressure brought about as a result of a hydrogen leak will shut the system down venting the remaining hydrogen up the vent stack. This target crypt vacuum provides the triple containment for the moderator. The transfer lines and the heat exchanger enclosure have a double containment and are also monitored for a rise in vacuum pressure. Control of these safety features is by relay logic. All vacuum pump exhausts are vented into the hydrogen vent stack.

System Testing

The He/H_2 heat exchanger assembly and transfer lines arrived at the Laboratory as an untested unit. The transfer lines had been fabricated to reach the required positions for the operating mode. This resulted in locating the test set-up in a somewhat awkward manner, adjacent to the target cell(Figures 8 & 9). A test moderator canister was simulated by joining the transfer lines with an enlarged tube section. The support systems for the test ie. instrumentation and controls, and vacuum and vent piping were fabricated by our group. As I indicated earlier, our tests were not at all boring. Our initial attempts to cooldown at the lower pressure settings created temperature and pressure surges that resembled bolt threads when data plots were made. Our vendor was not without fault himself. For example, pump housing seals failed; heaters burned up, melting diodes; rupture diaphrams blew out; noncalibrated diodes were installed; and electrical feedthroughs were overtightened, shearing wires.

After these minor setbacks were corrected, we increased our charging pressure to 15 ATM giving the results as shown(Figure 10). Cooldown at the supercritical region went quickly and very smoothly. The heat load was applied on the hydrogen piping inside the heat exchanger enclosure. While the pump flow appears less than we had specified, we believe we can maintain the required temperature at 300 watts of load. Additional testing is planned when we finish the production moderator prior to inserting it into the crypt.

Cost

A cost summary is listed in Table II.

Acknowledgements

The authors gratefully acknowledge the assistance of the following people who have contributed to this program: R. Candler, S. Ortiz, R. Reed, and D. Vigil for the assembly assistance, and G. Gallegos for the graphics work. This work was performed under the auspices of the U.S. Department of Energy.

References

1. G. J. Russell, C. D. Bowman, E. R. Whitaker, H. Robinson, and M. Meier, (1985) LANSE High Power (200μA) Target-Moderator-Reflector-Shield, ICANS VIII
2. F. Morse, (1985) Status Report On the Los Alamos WNR/PSR Facility, ICANS VIII
3. G. P. Lawrence, (1984) Los Alamos Proton Storage Ring, ICANS VII
4. C. D. Bowman, (1984) Status Report on the WNR/PSR, ICANS VII
5. B. R. Diplock, (1983) Cryogenic Moderator Design, ICANS VI
6. G. J. Russell, (1983) "WNR High-Power (200μA) Target-Moderator-Reflector-Shield," Los Alamos National Laboratory Internal Report, TN-GJR/P-9-006

TABLE I

SYSTEM SPECIFICATIONS

He GAS REFRIGERATOR

KOCH PROCESS SYSTEM, INC.

MODEL 1400 3 COMPRESSORS + LN2

MAXIMUM CAPACITY- 450 WATTS

FLOW RATE : 13.8 G/S

SUPPLY TEMPERATURE: 13 K - 20K

H2 MODERATOR

CANISTER SIZE: 13 Cm H- 13 Cm W- 5 Cm D

CANISTER VOLUME : ≃.86L

CANISTER MATERIAL : ALUMINUM 6061

PIPING SIZE : 19mm

H2 SYSTEM VOLUME : ≃ 8L

H2 CHARGING PRESSURE - 15 ATM (SUPERCRITICAL)

TEMPERATURE . 26K

DESIGN HEAT INPUT : 300 WATTS

DESIGN FLOW RATE : 40 G/S

TRANSFER LINE LENGTH : ≃10m TOTAL

TABLE II

SYSTEM COST

	U.S. DOLLARS
* He REFRIGERATOR REWORK	46K
REFRIGERATOR INSTALLATION	2.5
He / H2 HEAT EXCHANGER	44
INSTALLATION HARDWARE	6
INSTRUMENTATION & CONTROL	12
MODERATOR FABRICATION	3.5
REFRIGERATOR CONSULTANT	1.2
DESIGN CONSULTANT	20
DESIGN & INSTALLATION SUPPORT	40
TOTAL	175.2 K

* REFRIGERATOR ACQUIRED FROM SURPLUS- REPLACEMENT COST $ 260 K

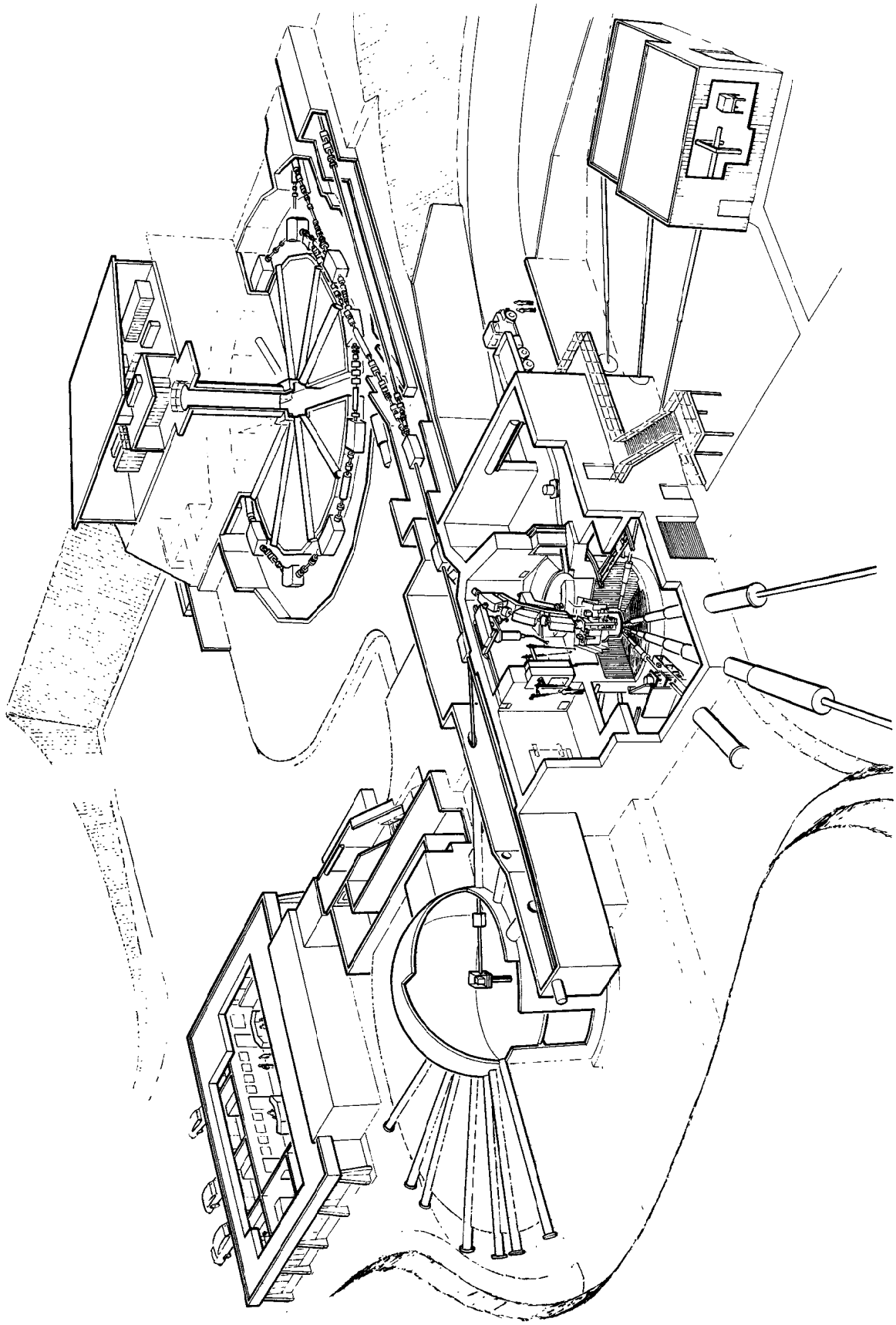

Figure 1. WNR-PSR/LANSCE Facility

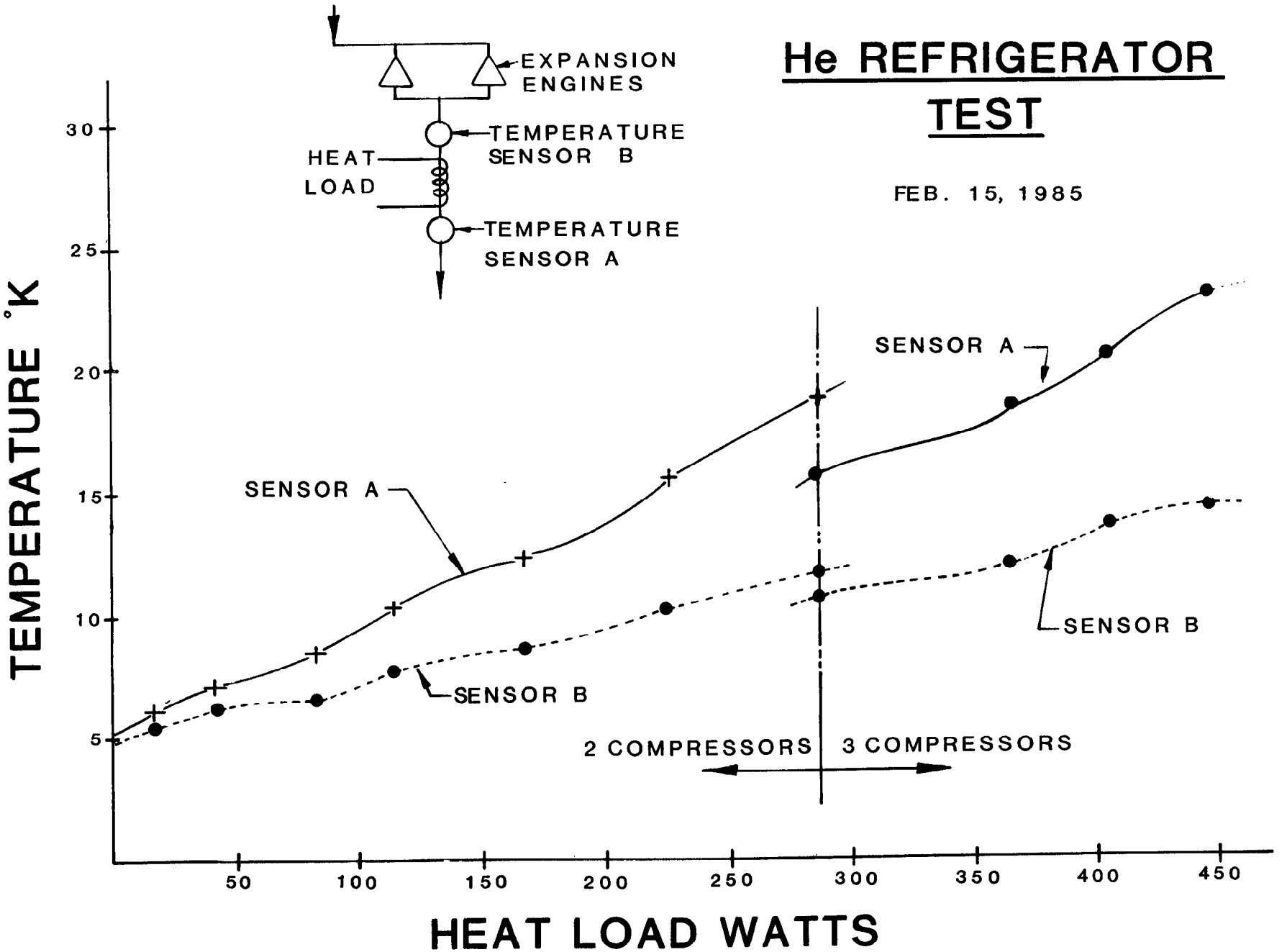

Figure 2. He Refrigerator Test

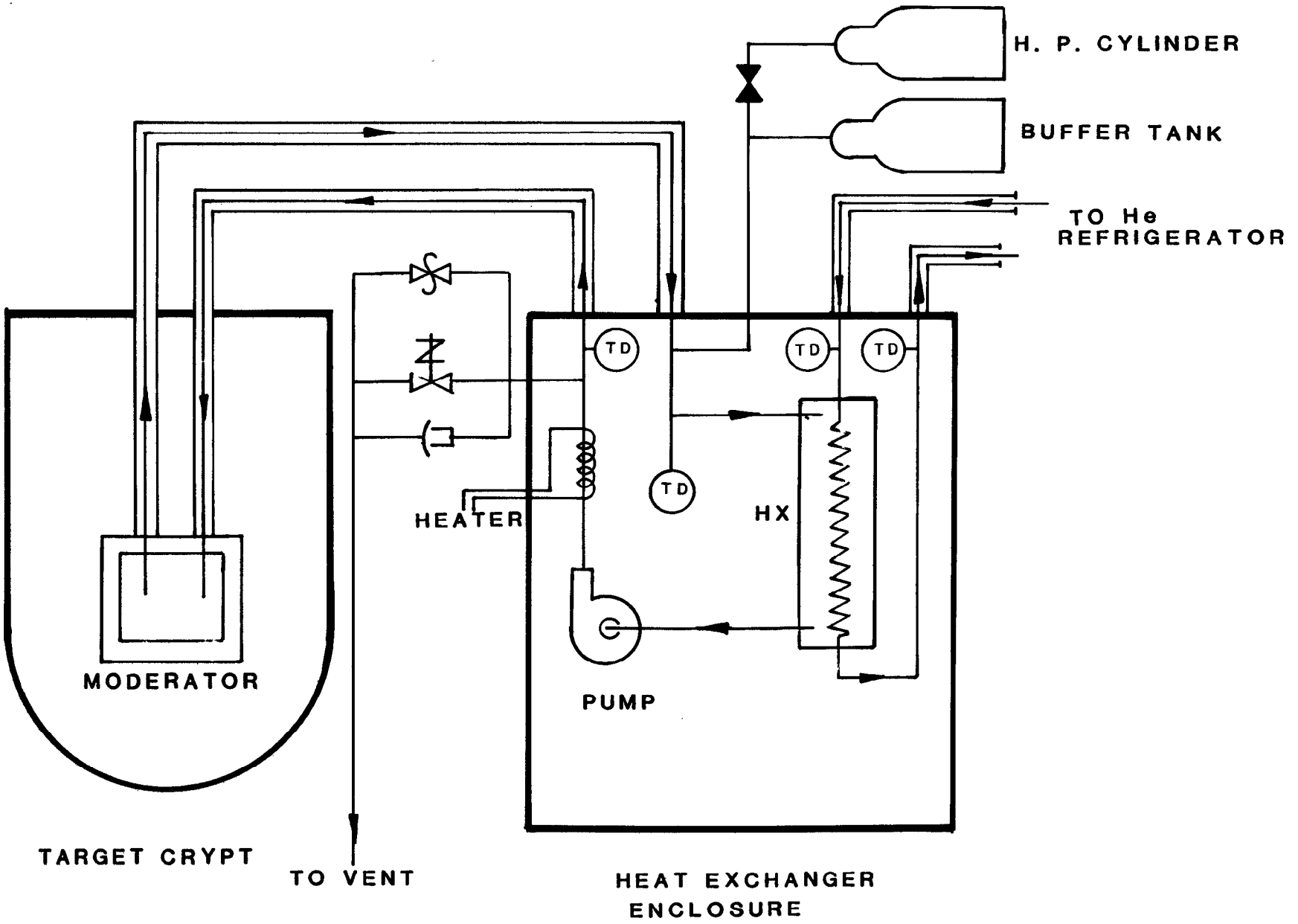

Figure 3. He/H_2 Heat Exchanger Schematic

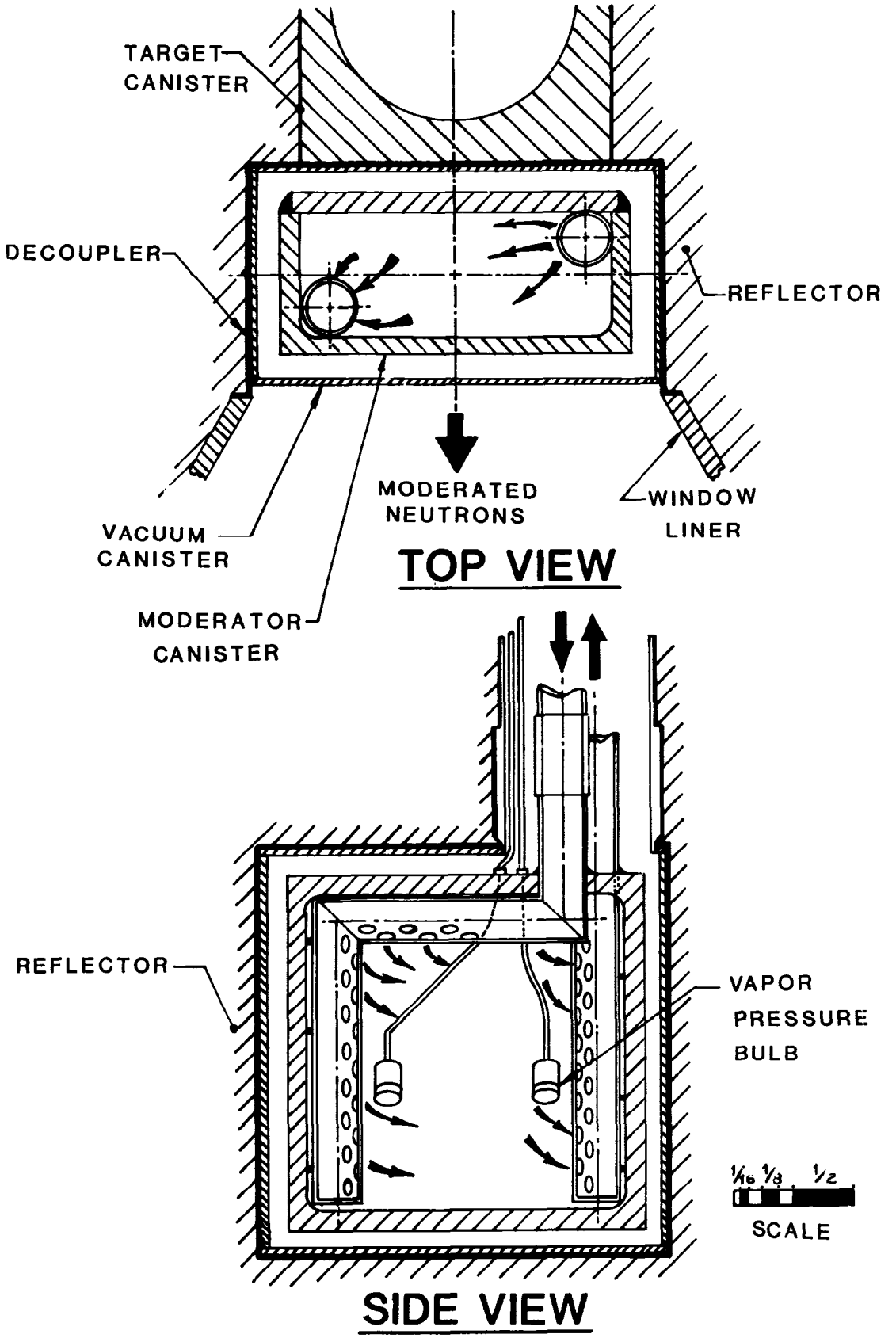

Figure 4. Moderator

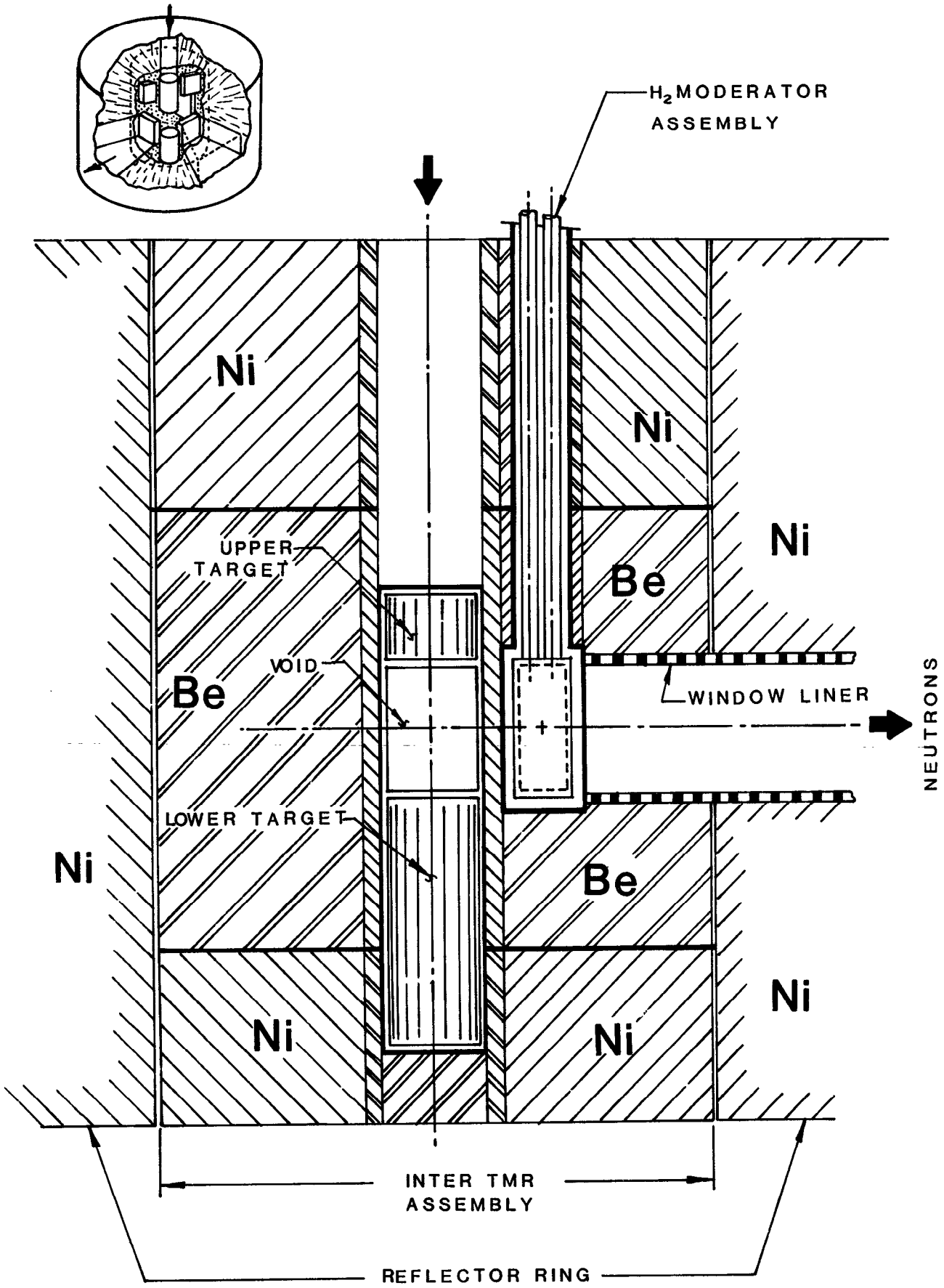

Figure 5. TMRS Assembly

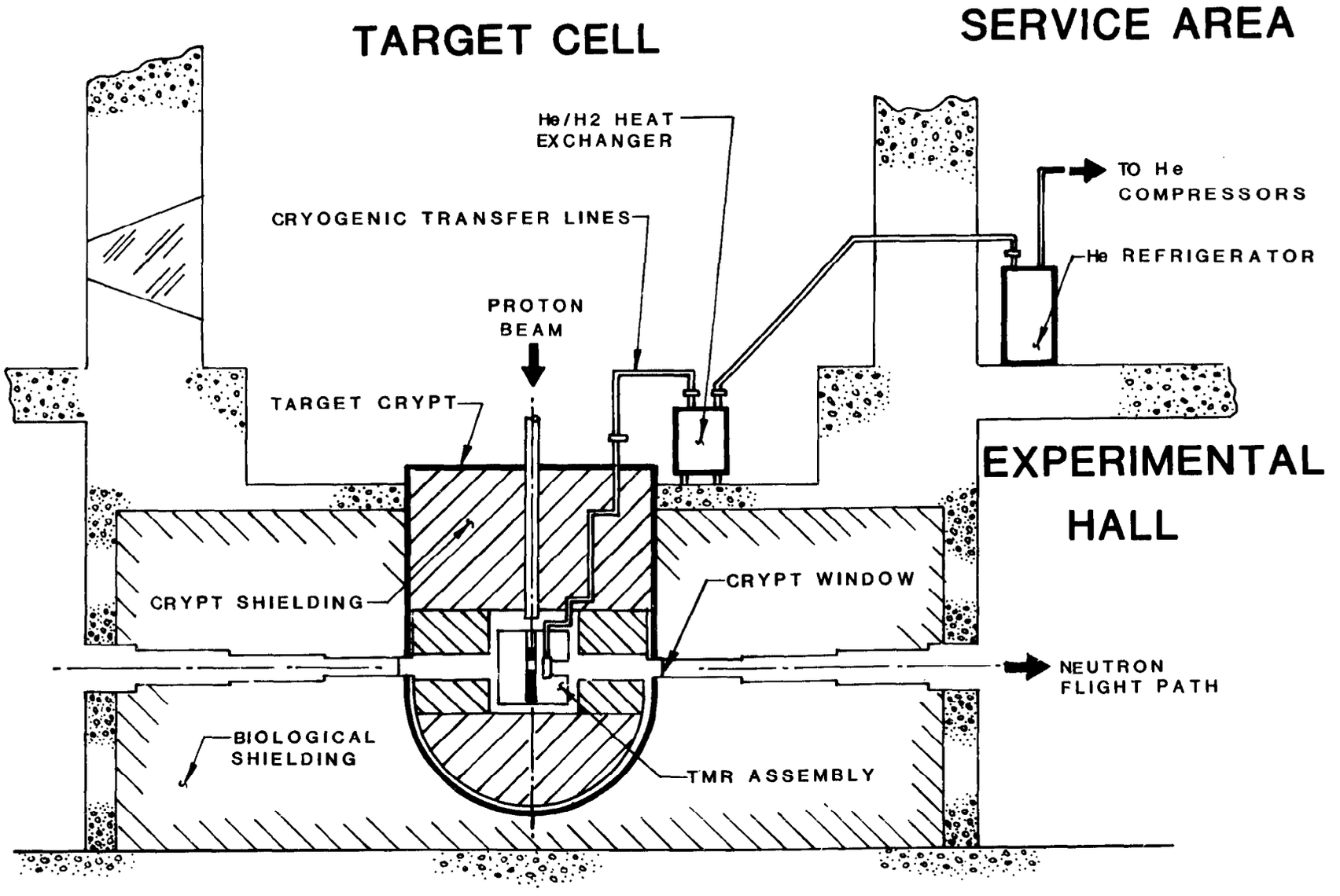

Figure 6. Target Cell Layout

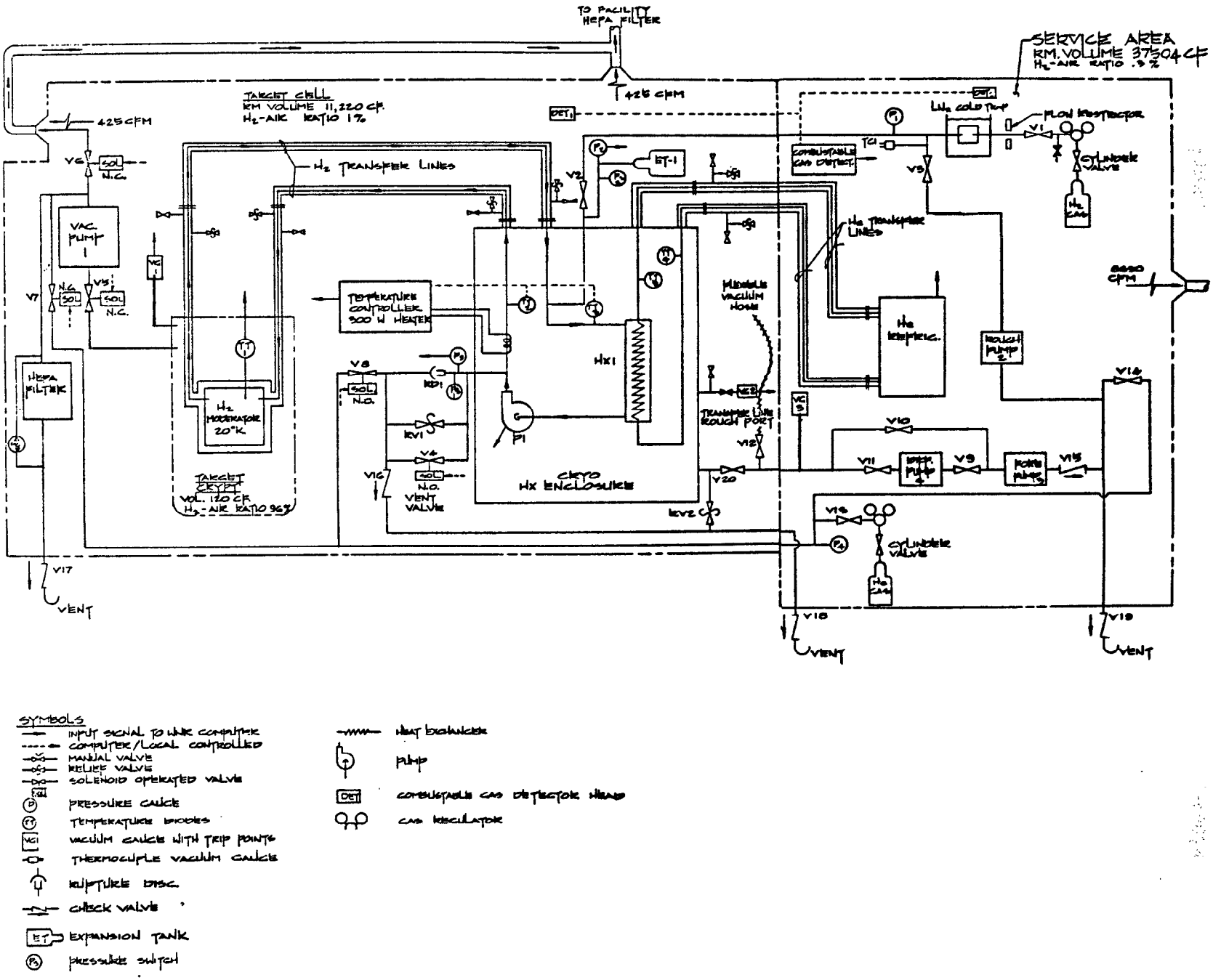

Figure 7. System Schematic

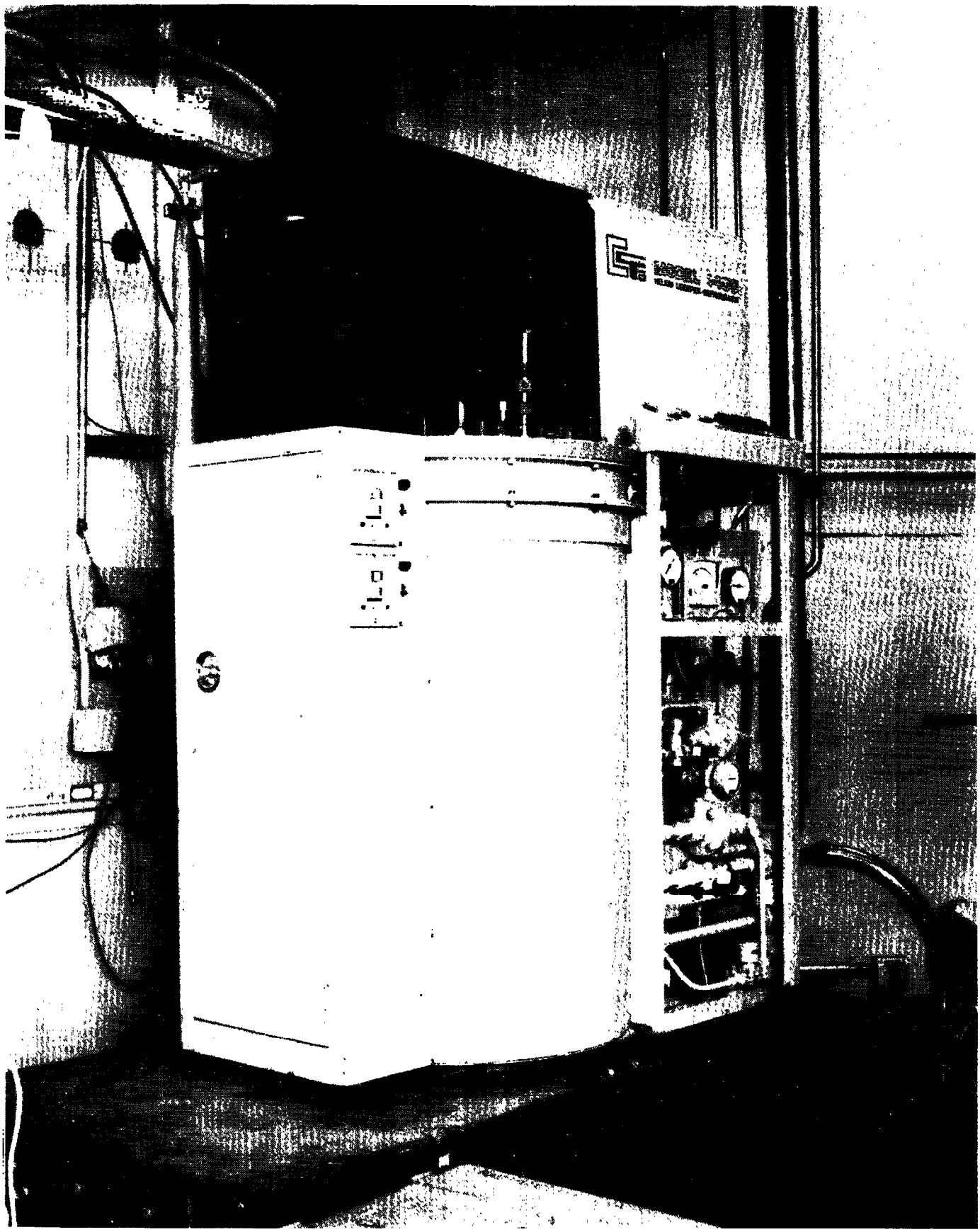

Figure 8. He Refrigerator

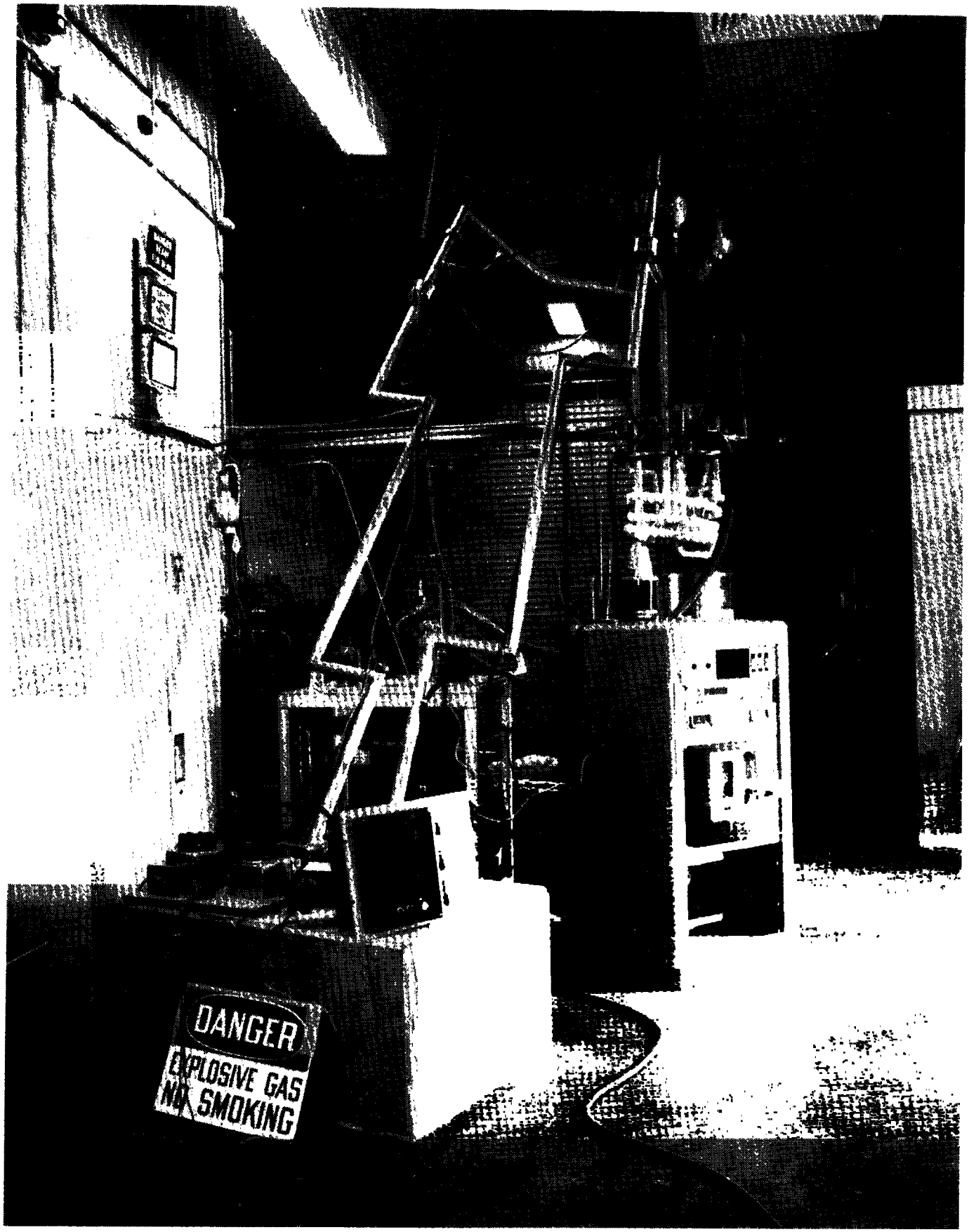

Figure 9. Test Setup

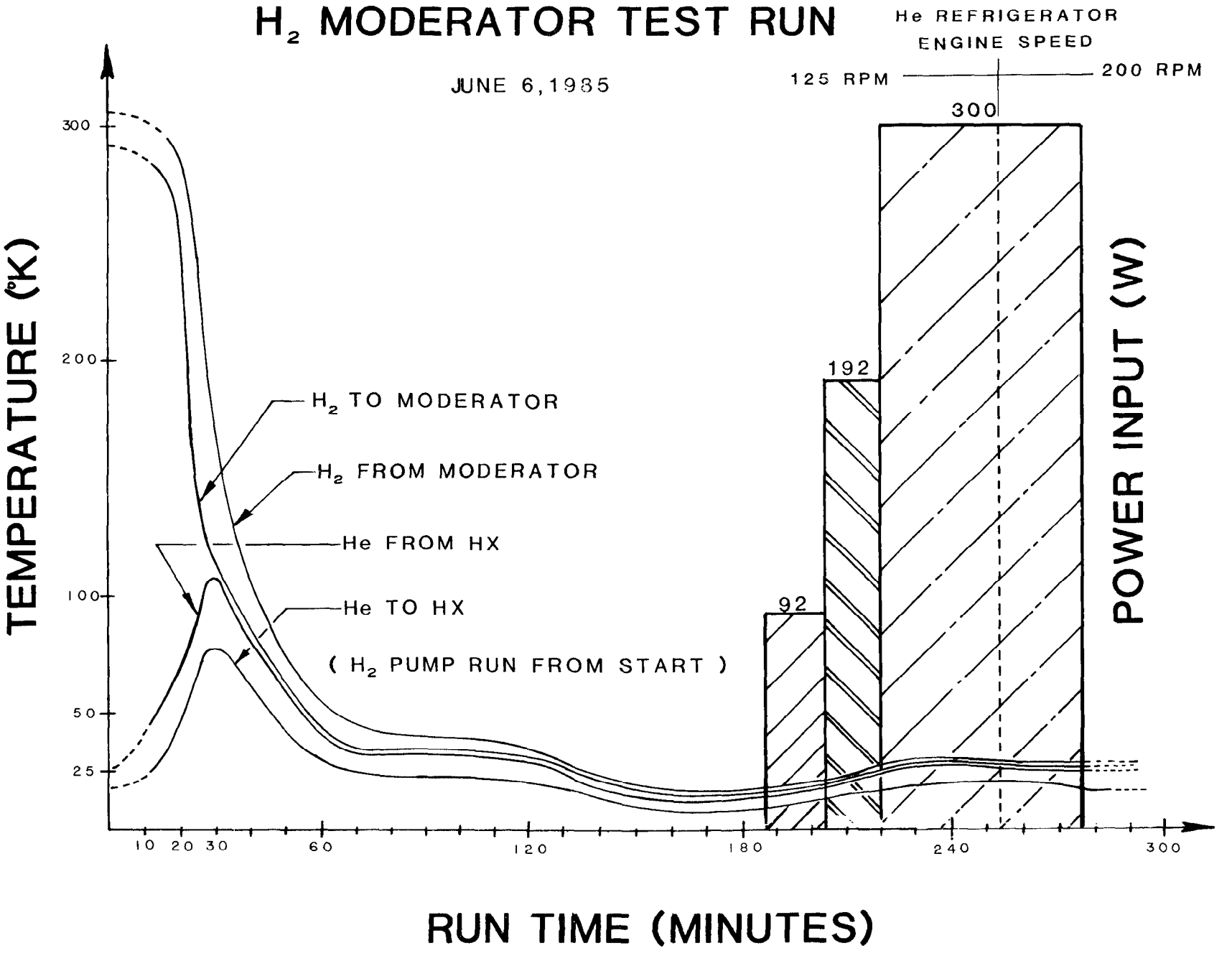

Figure 10. Test Results

Proceedings of the Eighth Meeting of the International Collaboration on Advanced Neutron Sources (ICANS-VIII)
8-12 July 1985, Rutherford Appleton Laboratory Report RAL-85-110

The IPNS Grooved, Solid Methane Moderator*

John M. Carpenter, August W. Schulke,
Terry L. Scott, Denis G. Wozniak
Argonne National Laboratory
Argonne, Illinois 60439 U.S.A.
and
Burton E. Benson and Bryan D. Leyda
Energy Research and Generation, Inc.
Oakland, California U.S.A.

Introduction

There are two motives for using cold moderators in pulsed neutron sources, to provide higher fluxes of long-wavelength neutrons, and to extend the epithermal range with its short pulse structure to lower energies. For both these purposes solid methane, operated at the lowest possible temperatures, is the best material we know of. Two problems accompany the use of solid methane in high power sources, namely heat transport in view of the low thermal conductivity of solid methane, and deterioration due to radiation damage. We have designed a system suitable to operate in IPNS, subject to nuclear heating of about 25 W, which incorporates an aluminum foam matrix to conduct the heat from within the moderator. We report the results of the first few months' operation, and of a few tests that we have performed.

Design of the Grooved Cold Moderator

The goal of the design of the grooved solid methane moderator was to provide as low a spectral temperature as possible, with no constraint on resolution. While the goals need not to have been qualified for the Small Angle Diffractometer, the Polarized Beam experiment which also views this moderator, requires reasonable intensity for 4 Å wavelengths and nearby, and resolution of about 100 μsec. The tests of Inoue, et al.[1] indicate that the spectrum from 10 K methane would not be so cold as to diminish significantly the flux of 4 Å neutrons, and that by a grooved design similar to that now in use at KENS would satisfy the resolution requirement.

However, experience at KENS[2] and our own calculations indicated that with the power densities expected at IPNS, temperature gradients would be too great in pure solid methane. Thus we were led to provide a metal matrix within the solid methane volume to conduct the heat to the cooled walls of the container. Aluminum metal foam seemed to provide the required small subdivision of the methane and the required increase in bulk thermal conductivity, and to be fabricable using well-developed techniques, while the required sacrifice in methane density is small and acceptable. The foam is brazed to the cooled flat surface of the container.

A closed-cycle refrigerator provides approximately 7 K circulating helium gas for cooling. Figures 1 and 2 show the design of the grooved moderator container. A room temperature aluminum can provides the insulating vacuum enclosure. The

*Work supported by the U.S. Department of Energy

thermocouple is a 0.063 inch (1.6 mm) diameter stainless steel sheathed type T junction. In operation, the moderator is decoupled from the surrounding graphite reflector by 0.05 cm cadmium. The normal mode of operation is to fill the system by condensing the methane into the system at the beginning of a run cycle. At the end of each cycle, (typically about 400 hours), after waiting for decay of short-lived isotopes (^{11}C, etc.) we allow the system to warm up and release the gas to the facility exhaust system. Normally we fill the system so that the filling tubing contains an overpressure greater than one atmosphere absolute, with the motive to prevent leakage of air into the system.

Thermal Analysis

Argonne retained the Materials Division of ERG under contract to perform the thermal analysis, design, fabrication, and tests of the Inner Cannister of the Solid Methane Moderator for the IPNS program. ERG was selected because of its unique Duocel Foam Metal which is used extensively in solid thermal mass heat exchangers for various applications such as Infra-red Surveillance Satellites. The material is ideally suited to provide nearly isothermal conditions in the solid methane cryostat.

Doucel foam metal is an open-cell, reticulated, skeletal structure that is manufactured with average cell sizes between 10 and 40 pores per inch (PPI), and density varying from 3% to 12% that of the bulk metal. The pore structure is more or less regular and the ligaments display a purity equal to that of drawn wire or cast aluminum. The conductivity is isotropic because of the uniformity of the matrix.

ERG determined the alloy, density, and pore size to meet the goals of the program. 6101-T6 aluminum foam would provide the best conduction, and would enable brazing to the cooled back plate. The alloy also has superior strength in the heat treated condition. 6101 alloy contains 0.5% Si, 0.5% Mn and other trace constituents, yet retains high thermal conductivity at low temperature. ERG's prior experience with this alloy cycling to low temperature in other applications also indicated its use.

The predominant factor in foam metal heat transfer is the cross sectional area of the ligament. For like densities the coarsest material gives the largest ligament diameter, which means the largest conduction area. For the specified conditions, the mean diameter of the solid methane cells in the 10 PPI material provides for adequate heat transfer from the solid methane to the aluminum ligaments. Thus ERG recommended the 10 PPI foam metal.

The remaining variable in the design is the density of the material required to provide an adequate conductance path for transporting the 25 W of nuclear heating to the back plate. The cross sectional area of the foam ligament varies as the cube root of the density; for example, foam of 3% density has a ligament diameter of 0.012 inches (0.0047 cm), while 6% dense material has a ligament diameter of 0.015 inches (0.0059 cm).

We adopted a worst-case approach to arrive at the required foam density. We found that there is a cross sectional area within the moderator 1.375 in (3.49 cm) high by 1.19 inch (3.02 cm) wide and extending 1.375 inches (3.49 cm) from the cooled back plate, through which all the heat generated within it must be conducted to the back plate. The highest temperature within the moderator would then be expected at this section, 3.49 cm into the foam. Assuming uniform nuclear heating power density we found that this volume would have a total power of 1.067W. With these assumptions we employed a simple one-dimensional finite element analysis to determine the temperature rise.

$$Q = [C_{alum} \times \text{Area} \times (\text{foam density}/2.8) + C_{methane} \times (1. - \text{foam density})] \times \Delta T/\Delta x$$

where

Q = total power in the section,

C = thermal conductivity,

A = area of section,

1./2.8 is the fraction of metal in the direction of the heat flow (only 33% of the ligaments' mass lies in the flow direction). This factor adjusts for the effect of percolation of heat through the random matrix.

ΔT = temperature increment,

Δx = length increment in the finite element analysis.

We used the following thermal conductivities:

$C_{methane}$ between 10 K and 20 K = 0.003 W/cm-K

C_{alum} for 6101-T6 alloy

10 K	= 0.750
11 K	= 0.845
13 K	= 1.035
15 K	= 1.225
17 k	= 1.415
19 K	= 1.605
20 K	= 1.700

For our adopted worst case we found the following temperature increments

Distance	Temperature rise
0.0 - 1.0 cm	5.36 K
1.0 - 2.0 cm	2.48 K
2.0 - 3.0 cm	1.24 K
3.0 - 3.5 cm	0.39 K

which we illustrate below.

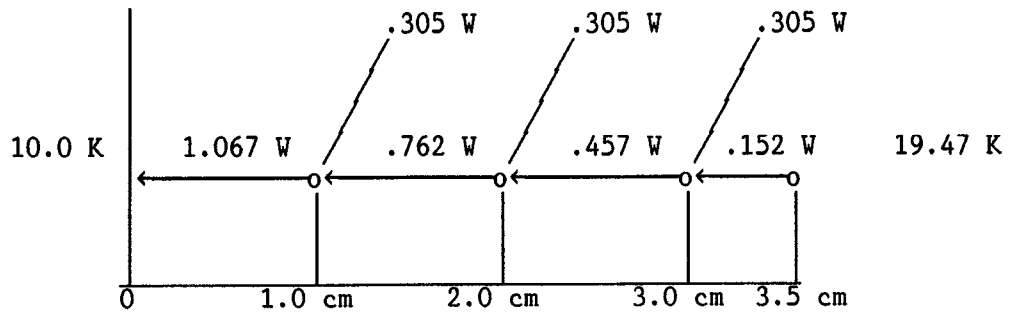

The calculation indicates that with a 6 % density, 10 PPI, 6101-T6 Duocel foam metal a maximum temperature of 19.47 K can be expected at the hottest point in the moderator. The moderator actually operates with the full heat load and with helium gas at 7 K, at a temperature of 12 K at the location of the thermocouple.

The Spectrum

We determined the spectrum of the neutron beam emerging from the new moderator, using the "1/v" monitor detector of the Small Angle Diffractometer, approximately 6.4 m from the moderator. Figure 3 shows the resulting counting rate distribution. With the IPNS delivering about 12 μA of 450 MeV protons to the ^{238}U target, the temperature at the location of the thermocouple was approximately 12 K during the measurement. The three lines indicate the locations of aluminum Bragg edges present in the spectrum due to the structural components and the windows in the beam, and verify the wavelength scale. Analysis of the spectrum indicates a Maxwellian temperature 19.9 K, and a thermal to epithermal flux ratio of 4.4 when referred to the slowing-down spectrum in the range 10 - 20 meV. By throttling the flow of cooling helium gas, we briefly operated the moderator with the internal thermocouple indicating 24. K; then the spectral temperature was 36. K and the thermal-to epithermal flux ratio was 5.6. Detailed analysis of the spectrum indicates that it falls below the Maxwellian function due to absorption and scattering of long wavelength neutrons in the beam path, which have not been corrected for in the data.

Operating Experience

The system has operated quite well since its installation in January, 1985. Approximately the expected volume (375. stp liters) of methane gas condenses without difficulty into the container after opening the cooled system to the filled ballast tank, and empties without problems upon turning off the refrigerant flow. However, periodically (about every 30 hours during operation) the system suffers "indigestion", in which the internal thermpocouple temperature rises abruptly to 50 or 60 K, the temperature of the outer can decreases about 10 or 20 degrees from its normal 50 C, and the pressure in the insulating vacuum space (normally 10^{-5} Torr) rises to about 10^{-3} Torr. Mass spectrometer leak detector measurements made during these episodes indicate that the gas in the insulating space is not helium. The radiation monitor on the facility exhaust gas system shows a transient release of ^{11}C, which returns to normal in about 3 minutes.These events (except one, which occurred within a few minutes after shutdown) have occured only during full power operation. We suspect a leak in the methane system, which opens due to the release of stored radiation damage energy. Normally the system recovers from these episodes within about 5 minutes, so that they have no noticable effects on the measurements. After two months' operation, the system developed a leak which appears when the system is warm, but closes when the system is cold. Since that time there have been several major lapses of performance in which the problems persist for several hours and some methane is lost from the system; except for their duration, these appear like the brief events, and have led us to design a new system which will be installed during the summer, 1985 shutdown.

Transient Tests

To determine the response time and the temperature change due to nuclear heating, we recorded temperatures for a period of steady operation before shutting down the acceleartor, and following shutdown. The resulting transient relaxed in an exponential fashion with a time constant of approximately one minute, while the temperature change was approximately 1.K for prior 12 μA, 450 MeV operation. The measurement cannot be considered definitive, since the temperature recording device had a digitizing error only slightly smaller than the change in thermocouple emf.

Radiation Deterioration

Following one 15-day-long cycle, during which the synchrotron delivered 6.5×10^{19} protons to the ^{238}U target, we collected the volatile products in a previously-evacuated tank, following the warming up of the methane. Table I gives the results.

Table I

Analysis of Volatile Products of Radiolysis of Methane from the IPNS Solid Methane Moderator

Product	Mole fraction* of gas, %
H_2	5.38
CH_4	91.37
H_2O	<0.04
C_2H_4	0.20
C_2H_6	2.30
N_2	not determined-used as mixing gas
O_2	0.17
Ar	0.04
C_3H_8	0.42

* Exclusive of N_2. Average after two periods of mixing, 45 min and 100 min.

The results indicate substantial deterioration of the material, and do not include whatever gases remained in the tubing between the moderator and the collecting tank, nor any non-volatile products. These findings are roughly consistent with those for the KENS solid methane moderator,[2] but our product yields are somewhat smaller, in spite of the fact that the IPNS ^{238}U target produces about twice as many neutrons per proton as the KENS W target. This may have to do with the coupling between the KENS moderator and the KENS target, which is superior to the target-moderator coupling for this moderator in IPNS.

Conclusions

We have developed a successful low temperature solid methane moderator, which operates under conditions of higher power density than can be accomplished in pure solid methane. The measured spectral temperature is the lowest that we know of from all cold neutron sources in existence.

References

[1] K. Inoue, Y. Kiyanagi, H. Iwasa, N. Watanabe, S. Ikeda, J. M. Carpenter and Y. Ishikawa, ICANS VI, p 392, (1983).

[2] Y. Ishikawa, S. Ikeda, N. Watanabe, K. Kondo, K. Inoue, Y. Kiyanagi, H. Iwasa, and K. Tsuchihashi, ICANS VII, p 230, (1984).

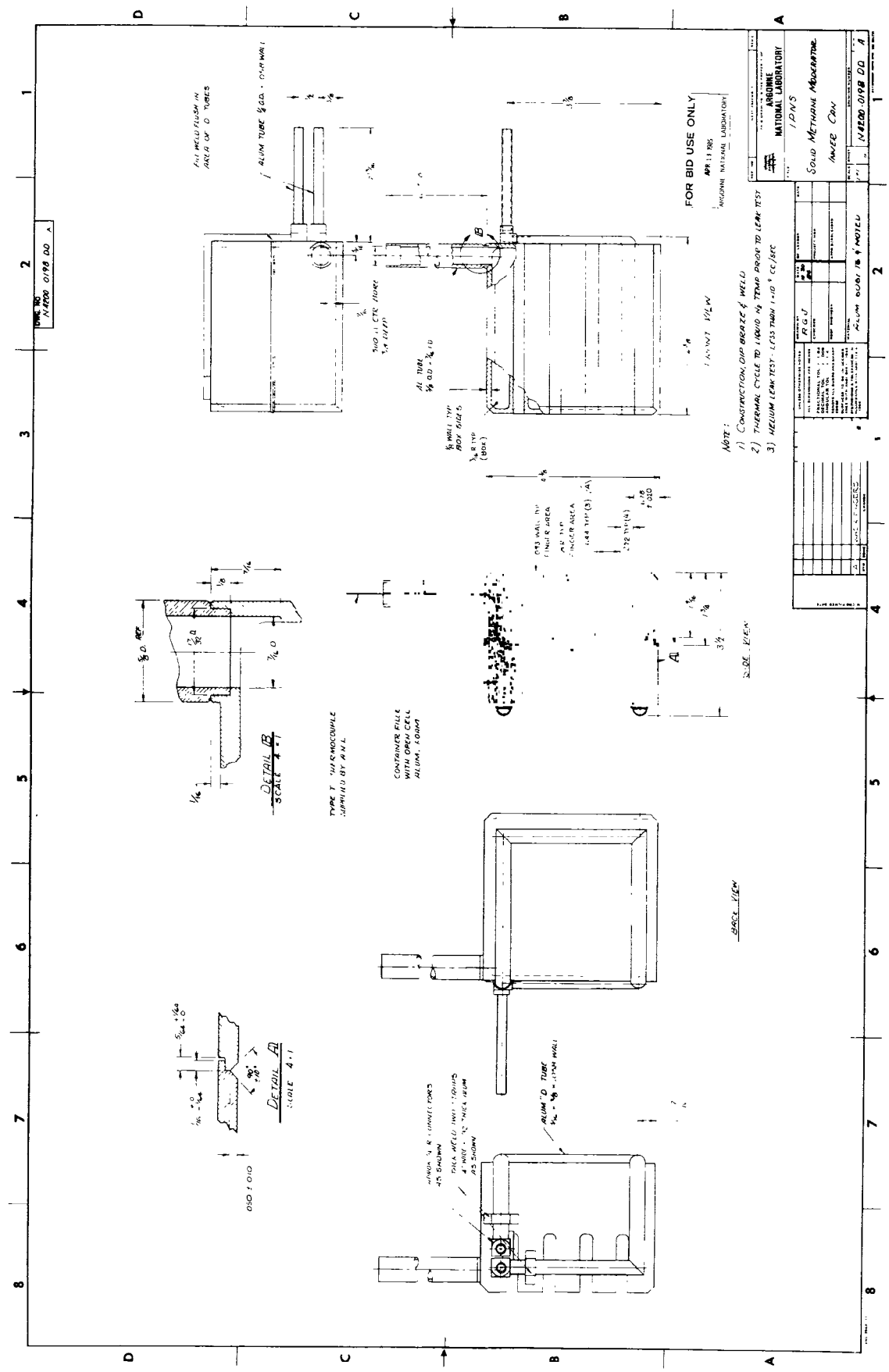

1. Design of the inner cannister of the grooved solid methane moderator.

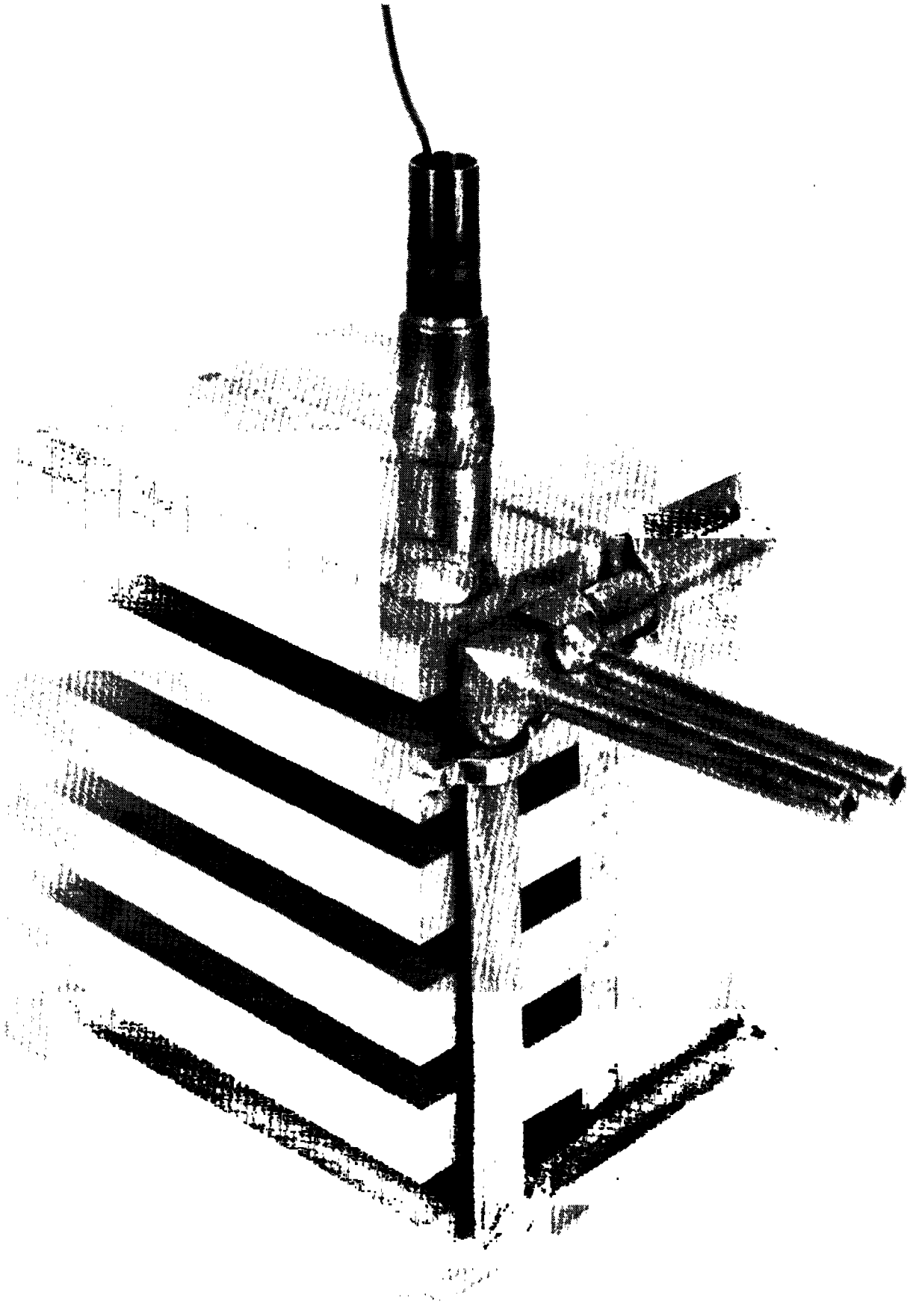

2. Photograph of the inner cannister of the grooved solid methane moderator.

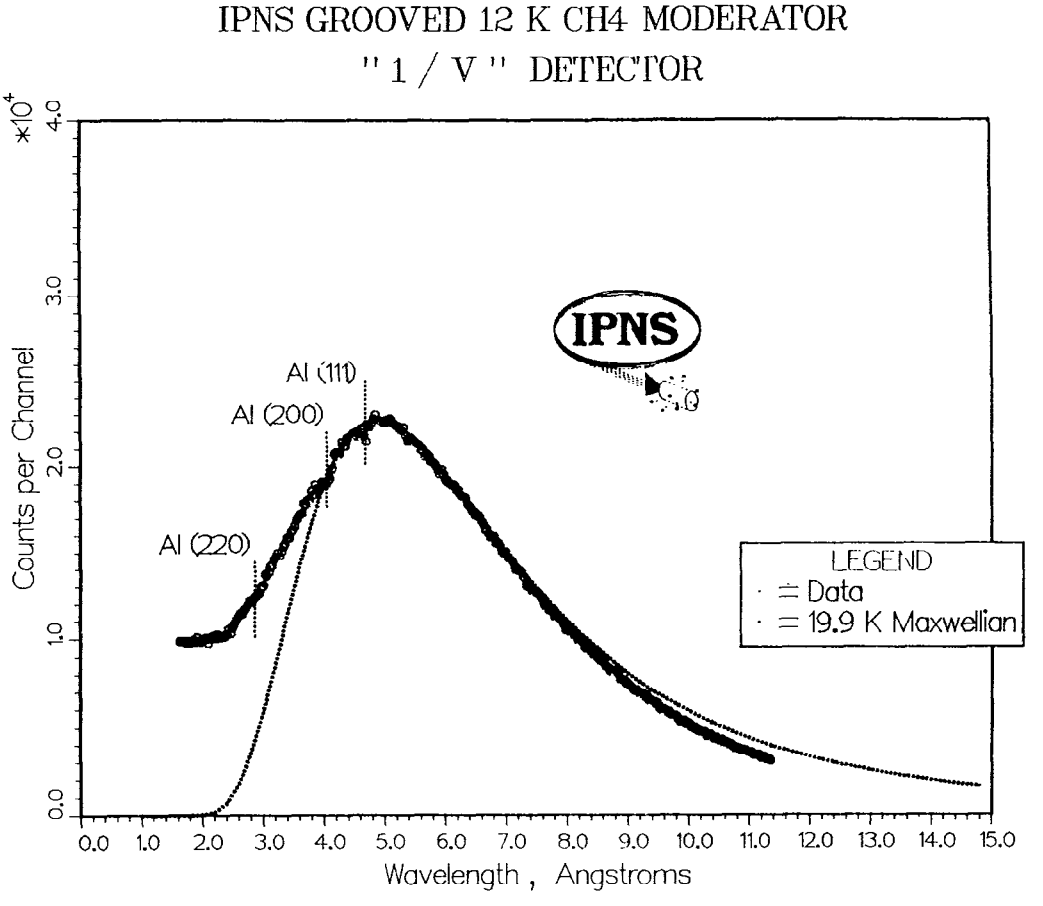

3. The counting rate distribution measured with a "1/v" detector in the beam from the grooved solid methane moderator. The maximum temperature in the moderator at the time of the measurement was 12 K. The dips in the spectrum are aluminum Bragg edges due to structural and window components in the beam.

Proceedings of the Eighth Meeting of the International Collaboration on Advanced Neutron Sources (ICANS-VIII)
8-12 July 1985, Rutherford Appleton Laboratory Report RAL-85-110

SNS MODERATOR PERFORMANCE

A D Taylor
Neutron Division
Rutherford Appleton Laboratory
Chilton, Oxon, OX11 0QX
UK

INTRODUCTION

The SNS moderators are designed to optimise the production of a wide variety of beams with spectral and resolution characteristics which are matched to the envisaged suite of neutron scattering instruments [1]. Four independent moderators are used in reflected wing geometry, two above and two below the target (see Figure 1). The reflector is D_2O cooled beryllium. To facilitate heat removal and to minimise radiation damage, the moderator materials are fluids. The four moderators are a 4.5cm thick liquid methane moderator at 95K poisoned with gadolinium at a depth of 2.25cm; a 4.5cm thick ambient water moderator asymmetrically poisoned with gadolinium to give 1.5cm and 3.0cm effective thicknesses; an 8cm thick supercritical hydrogen moderator at 25K; and a 4.5cm thick ambient water moderator poisoned with gadolinium at a depth of 2.25cm. Important aspects of the physical design of the moderators are summarised in Table I. Further details may be found in references [2,3], and predictions of their neutronic performance in reference [4].

In its initial configuration SNS has

- -seven beams viewing the high intensity, high resolution liquid methane (CH_4) moderator, which is optimised for pulse structure;

- -three beams viewing a very high intensity face (A) and three beams

viewing a high intensity, high resolution face (AP) of an ambient moderator;

-three beams of long wavelength neutrons from the liquid hydrogen (H_2) moderator, which is optimised for intensity;

-and the remaining two beams viewing an intermediate resolution ambient moderator (D).

During the initial commissioning run of SNS in December 1984, six neutron beamlines viewing four different moderator faces were specially instrumented to obtain the maximum amount of information from the limited experimental run. In addition to measuring the performance of the moderators, several other experiments were performed simultaneously on each beamline, and the results from these are described in reference [5].

SPECTRAL PROPERTIES OF THE MODERATORS

The spectral distribution of the SNS moderators was measured using the primary time-of-flight monitors on each beamline. Physical parameters of these monitors are described in reference [5] and details of the analysis given elsewhere [6]. The monitor spectra were corrected for detector efficiency and residual air attenuation and transformed to an energy scale. The spectra were then described [4] as the sum of a Maxwellian term

$$\phi_{max}(E) = J \frac{E}{T^2} \exp\{-E/T\} \qquad (1)$$

where J is the Maxwellian integral, E the energy in eV and T the Maxwellian temperature in eV, and a slowing down term

$$\phi_{epi}(E) = \frac{1}{E^A} \qquad (2)$$

where A is a leakage parameter. These parts are combined using a switch function $\Delta(E)$, and multiplied by a constant ϕ_o, the differential neutron current at 1 eV, to give the absolute value (discussed below)

$$\phi(E) = \phi_o\{\phi_{max}(E) + \Delta(E)\ \phi_{epi}(E)\}$$
$$= \phi_o \cdot \phi_{tot}(E) \qquad (3)$$

Typical fits for each of the three types of moderator are shown in Figure 2. Data rate problems on the SXD beamline viewing the ambient water moderator (A) prevented a quantitative analysis being performed on data from this moderator.

These parameters are given in Table II and compared with the design values taken from Table II of reference [4]. The agreement is excellent for the major parameters such as J, T and A and in good accord for the somewhat empirical switch function.

ABSOLUTE NEUTRONIC PERFORMANCE OF SNS

The absolute neutronic performance of SNS was determined by white beam activation of thick gold foils on each beamline. These data were then analysed using the appropriate spectral distribution measured by the time-of-flight monitor and corrected for multiple interactions by a numerical technique [6]. The absolute performance of the moderators, taken from reference [6] and corrected for viewing angle, is compared in Table III with the predicted performance [4], appropriate to 550 MeV. An independent measure of ϕ_o for each beamline may also be obtained from the time-of-flight monitors by assuming their calibrated efficiencies. These parameters again corrected for viewing angle are also presented.

The overall agreement is excellent for all three moderators. The error is almost entirely due to proton normalisation and is not present in relative measurements, such as a comparison of two beamlines viewing the same moderator, where only random errors of a few percent are important. The discrepancy between the TFXA and HET measurement of the ambient poisoned moderator referred to in [6] resulted from an error in the location of the gold foil (11.5m rather than 10m). The discrepancy between the LAD and HRPD measurements of the liquid methane moderator, seen by both the gold foil and time-of-flight technique, may still be significant. Possible explanations are a misalignment of the shutter-collimator system or an angular flux distribution from the moderator face which is more strongly peaked than the anticipated cosine-like distribution.

TIME STRUCTURE OF THE NEUTRON PULSE

Detector saturation problems on TFXA and IRIS prevented a full pulse shape analysis from the ambient water and liquid hydrogen moderator and the purposely large beam on HRPD led to sample geometry contributions to the methane data. However, long time decay constants were obtained from all three moderators (see Table II) which were in excellent agreement with the predictions from reference [4]. Additional confirmation of the quality of the pulse shape came from the low data rate (but correspondingly poor statistics) run on TFXA and the fact that HRPD achieved its design resolution of $\Delta d/d = 0.0004$ (see reference [5]). An additional long time decay constant ($\sim 35\lambda$ Å-μs) was observed in the pulse from the non-decoupled liquid hydrogen moderator and this led to the decision to decouple the hydrogen moderator with cadmium for subsequent operation.

CONCLUSION

The neutron intensity and spectral properties of the SNS moderators have been measured and were found to be in excellent agreement with the design values.

REFERENCES

[1] A J Leadbetter, 'Instrumentation for Pulsed Sources'. Proc IAEA Conference 'Neutron Scattering in the 90s', Julich, 219 (IAEA, Vienna, 1985).

[2] A Carne, 'Review of the SNS Target Station', in Proceedings of ICANS-IV (1980), p136, KENS Report-II (1981).

[3] B R Diplock, 'Cryogenic Moderator Design', in Proceedings of ICANS-VI (1982), p327, Argonne Report ANL-82-80.

[4] A D Taylor, 'SNS Moderator Performance Predictions' Rutherford Appleton Laboratory Report RAL-84-120 (1984).

[5] A J Leadbetter et al 'First Neutron Results from SNS', Rutherford Appleton Laboratory Report RAL-85-030 (1985).

[6] T G Perring, A D Taylor and D R Perry, 'Absolute Neutronic Performance of SNS from Gold Foil Activation', Rutherford Appleton Laboratory Report RAL-85-029 (1985).

TABLE I

MODERATOR	Front Ambient		Liquid Methane		Liquid Hydrogen	Rear Ambient
Mnemonic	AP	A	CH_4		H_2	D
Material	H_2O		CH_4 (4 atm)		p-H_2 (15 atm)	H_2O
Temperature (K)	316		95		25	316
Position	Top Front		Bottom Front		Bottom Rear	Top Rear
Height (cm)	12		11.5*		12*	12
Width (cm)	12		12*		11*	12
Thickness (cm)	4.5		4.5*		8*	4.5
Poison	0.05 mm Gd		0.05 mm Gd		--	0.05 mm Gd
Poison Depth (cm)	1.5	3.0	2.25	2.25	--	2.25
Beam Lines (Angle to Moderator Normal)	N7(0) N8(14) N9(27)	S1(14) S2(1) S3(12)	N1(14) N2(1) N3(12)	S6(13) S7(0) S8(14)+ S8(14)+ S9(27)	N4(13) N5(0) N6(13)	S4(13) S5(0)
Decoupler	Boron^x		Boron^x		None	Boron^x
Void Liner	Boron^x	Boron^x	Boron^x	Boron^x	Boron^x/Cd	Boron^x

Notes: * Maximum dimension. Moderator containment is a pressure vessel whose faces have radii of 25 cm.

\+ S8 beam line is multiplexed with two guides.

x 1/e transmission of boron layer at 3.6 eV.

TABLE II

MEASURED SPECTRAL DISTRIBUTION PARAMETERS FOR THE SNS MODERATORS
(DESIGN VALUES IN PARENTHESES)

Moderator:	AP	A	CH_4	H_2
Maxwellian parameters				
J	2.3 (2.4)	--	2.1 (1.8)	2.4 (2.6)
T (meV)	32 (33.9)	--	11 (11)	2.1 (2.8)
Epithermal parameters				
A	0.95 (0.9)	--	0.92 (0.9)	0.95 (0.9)
Joining function parameters				
W1	120 (90)	--	55 (54)	15.5
W2	10 (8.9)	--	7 (6.7)	3.1
W3	--	--	--	11
W4	--	--	--	0.254
W5	--	--	--	0.0275
Time structure parameter: μs	22 ± 5 (20)		31 ± 2 (32)	23λ ± 2λ (25λ)

TABLE III

COMPARISON OF DESIGN VALUES OF ϕ_o WITH GOLD FOIL AND MONITOR MEASUREMENTS.
Units: 10^{10}n/eV.sr.100cm^2.μA.s

		Gold Foil	Design	Monitor
Ambient Poisoned Moderator	TFXA(13°)	2.8 ± 0.5	2.3	2.9
	HET(27°)	2.7 ± 0.4		2.4
Liquid Hydrogen Moderator	IRIS(13°)	1.9 ± 0.4	2.1	2.0
Liquid Methane Moderator	LAD(0°)	2.6 ± 0.4	1.9	2.3
	HRPD(14°)	1.1 ± 0.3		1.1

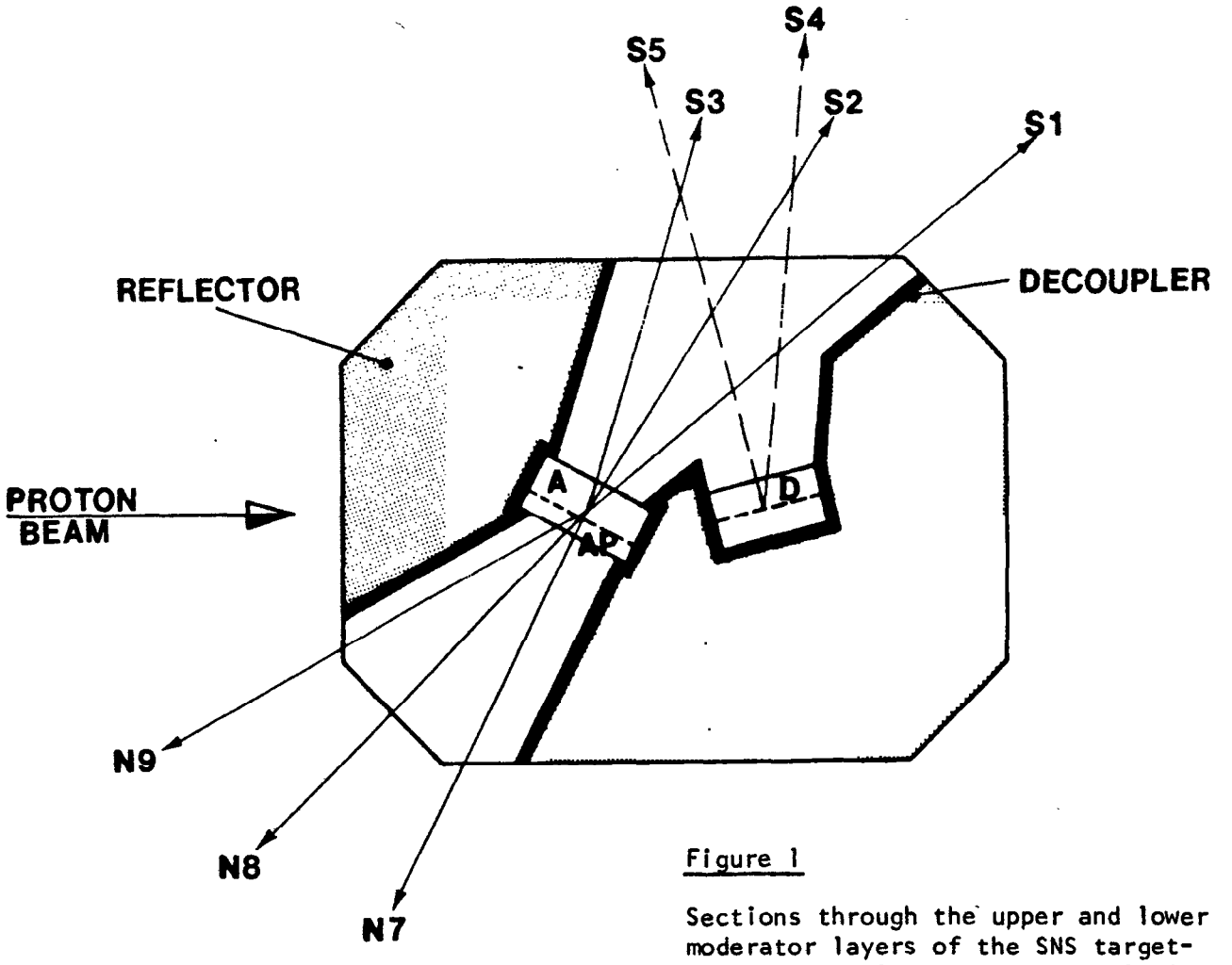

Figure 1

Sections through the upper and lower moderator layers of the SNS target-moderator-reflector system. N1-N9 are the beam directions on the North side of the experimental hall and S1-S9 are the beam directions on the South side of the hall

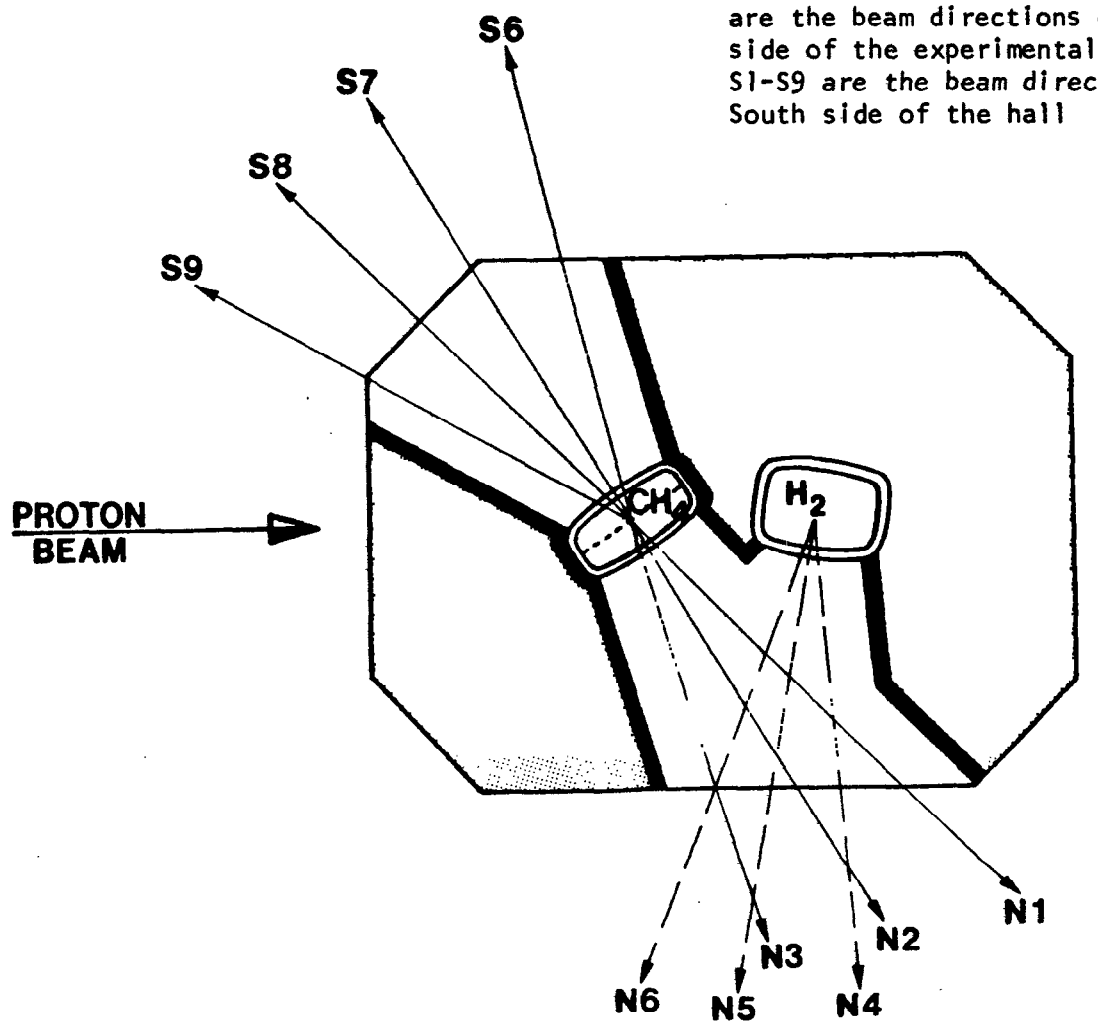

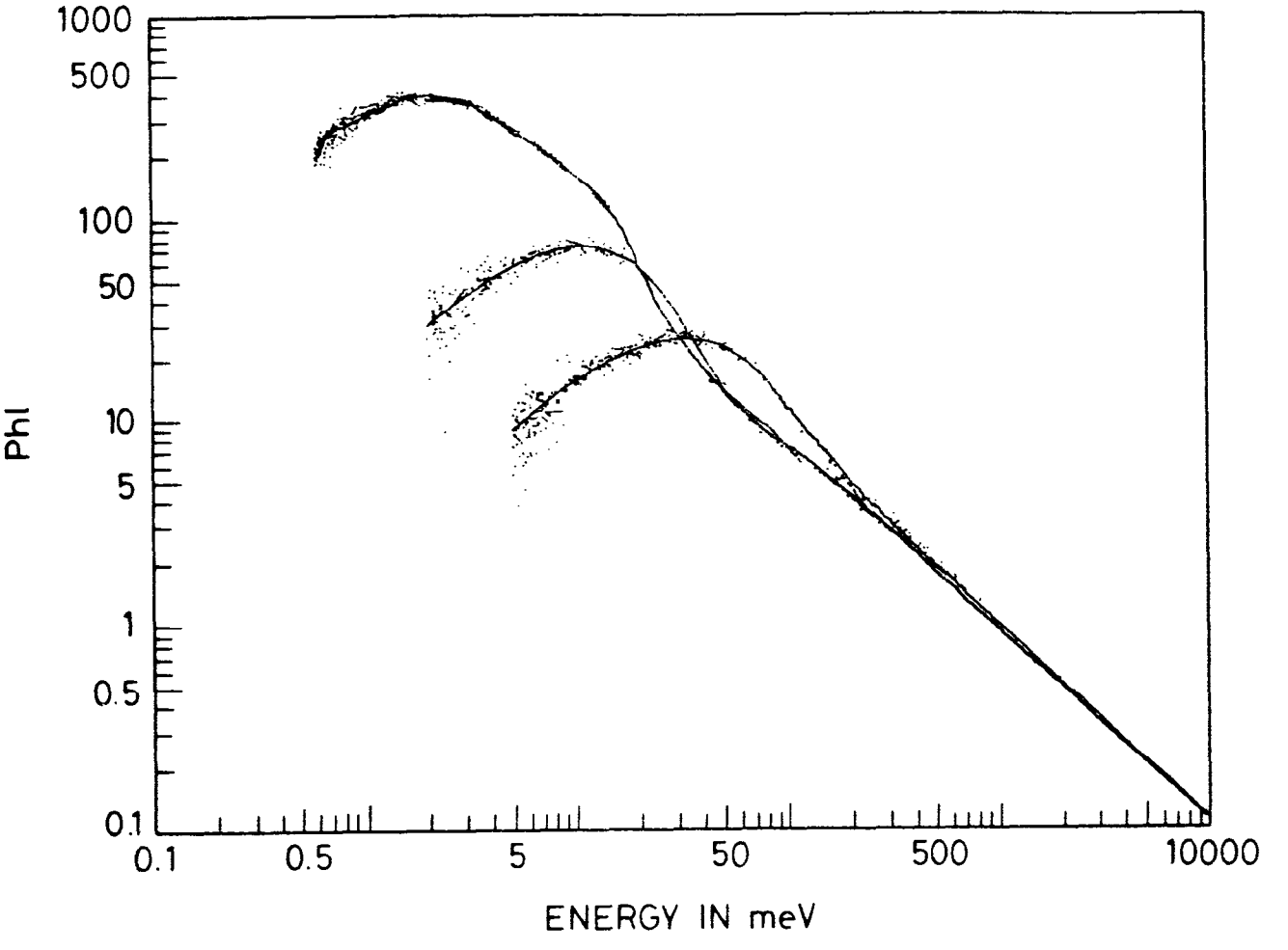

Figure 2 The observed (points) and fitted spectral distribution from (a) the ambient poisoned moderator (TFXA); (b) the 100K liquid methane moderator (LAD); and (c) the 25K liquid hydrogen moderator. The solid line is equation (3) and the fitted parameters are summarised in Table II.

Proceedings of the Eighth Meeting of the International Collaboration on Advanced Neutron Sources (ICANS-VIII)
8-12 July 1985, Rutherford Appleton Laboratory Report RAL-85-110

Mock-Up Experiments for KENS-I' Cold Moderator

Y. Ishikawa, M. Furusaka and S. Itoh
Physics Department, Tohoku University, Sendai
and
S. Ikeda and N. Watanabe
National Laboratory for High Energy Physics, Tsukuba
and
K. Inoue and H. Iwasa
Department of Nuclear Engineering, Hokkaido University, Sapporo

Abstract

A mock-up experiment has been performed for the KENS-I' solid methane cold moderator in order to establish the method for removing the neutron heating of order of 20 W deposited inside solid methane. It has been suggested that the insertion of 0.5 mm Aℓ plates with a distance of 10 mm can keep the moderator temperature below 20 K by employing the present refrigerator (PGH, 105)

1. Introduction

The cold neutron moderator and the experiments employing cold neutrons are one of the most important success of the KENS, because it gave a promissing aspect of the spallation neutrons even for the cold neutron scattering[1]. Therefore the installation of the cold neutron moderator is also indispensable for the KENS-I' where the neutron intensities are expected to be increased by a factor 8. Since the heat deposit in the KENS-I' becomes quite substantial, we carried out a mock-up experiment of the cold moderator to find the best method for removing the heat deposit.

We have reported in a paper[2] presented in the previous ICANS meeting at Chalk River the result of successful operation of the grooved cold moderator as well as the heat deposit we estimated for two different types of cold moderators used in KENS-I. The estimation was made from the temperature rise of hydrogen thermometer by neutron heating and the results are reproduced in Table 1 with a slight modification. We should remark here that the heat deposit was order of 1.5 W in a flat moderator, but it increased to 5 W in a grooved one. The increase is partly due to the increase of volume, but mainly because of the decrease of the effective thermal conductance of solid methane. In the course of present mock-up experiment, we also found that our previous estimation of head deposit of 1.2 W was underestimated as will be described later. The revised value of heat deposit was somewhat 16 W $\sim$ 20 W for the flat moderator and it would go up to 50 W $\sim$ 60 W for the grooved moderator. Therefore we need to establish the method for removing the heat deposit corresponding to 20 $\sim$ 60 W in the KENS-I' cold moderator.

2. Mock-up experiments

Mock-up experiments have been performed by employing the KENS-I flat cold moderator, the layout of which is shown in Fig. 1. The solid methane was cooled by a heat exchanger placed at the top of the moderator case and methane was cooled by thermal contact with the moderator case wall made by pure Aℓ. The neutron heating was simulated by electric heater plates embedded inside the solid methane.

The heaters' positions were determined so that the temperature gradient attained by them became identical to that we can expect for neutron heating. The heat deposit Q(x,y,z) will obey an exponential function,

$$Q(x,y,z) = Ae^{-\Sigma z} , \tag{1}$$

with A given by

$$A = \frac{q\Sigma}{1-e^{-\Sigma \ell_z}} , \tag{2}$$

where q (w) is heat power, $\Sigma = 0.31\ cm^{-1}$, macroscopic cross section of neutrons and $\ell_z = 15$ cm is a total length of the moderator. Fig. 2 displays the temperature distribution observed for a given heat power. It was found from the figure that, with a heating power of 15 W, the maximum temperature at a central position almost attained to 60 K, but the temperature rise was rather small near the moderator case wall where the hydrogen thermometer was located.

In order to improve the situation, we inserted in solid methane an Aℓ wire lattice of 10 x 10 mm^2 with 1 mmϕ Aℓ, the top of the wires being screwed to the top of the moderator case. The results are shown in the lower part of Fig. 3, indicating that the temperature increase is substantially reduced, but still not enough for the KENS-I' cold moderator.

In Fig. 4 we plotted the temporal evolution of the temperatures at various different positions, when a heat deposit was supplied to solid methane with Aℓ lattices. The results are quite instructive; the temperature increase was relatively small at the position of heat exchanger ②, the coolant temperature was still less than 20 K even if the heat power went up to 20 W. However the temperature of moderator case wall, ③ or ⑧ rose to 30 K, suggesting the existence of a large resistance between the heat exchanger and moderator case. The increase of the temperature inside solid methane was of course quite of significance.

3. Simulation calculation

In order to find a better solution, we have made a three

dimensional calculation based on the differential equation of heat transport given by

$$\frac{\partial T}{\partial t} = \frac{K}{C\rho}\left(\frac{\partial^2 T}{\partial x^2} + \frac{\partial^2 T}{\partial y^2} + \frac{\partial^2 T}{\partial z^2}\right) + \frac{Q(x,y,z)}{C\rho} \quad , \tag{3}$$

where Q (x,y,z) is given by eq (1), K,C. and ρ being thermal conductivity, specific heat and density respectively.
In case of solid methane with Aℓ wires, K and Cρ are replaced by averaged values $\bar{K}$ and $\overline{C\rho}$ defined by

$$\begin{aligned} \bar{K} &= S_{A\ell}K_{A\ell} + S_{me}K_{me} \qquad (S_{A\ell} + S_{me} = 1), \\ \overline{C\rho} &= S_{A\ell}C_{A\ell}\rho_{A\ell} + S_{me}C_{me}\rho_{me} \quad , \end{aligned} \tag{4}$$

where $S_{A\ell}$ and S_{me} are the relative cross sections of Aℓ and methane in a unit area perpendicular to the direction of heat flow. Therefore the temperature T(x,y,z) obtained by this calculation gives an average temperature of a given small area (1 x 1 cm^2). For K, C and ρ of Aℓ and solid methane, we used the reported values at each temperature.

The results of temperature distribution calculated by this equation for 1.2 W heat deposit are compared with observation in Fig. 5, where "1. neutron simulation" corresponds to the case where eq (1) was used for Q (z), while "2. heater simulation" represents the case of actual heater's heating. The agreement between the calculation and observation is quite satisfactory in three directions, assuring the computer simulation calculation we made. In Fig. 6 (a) we plot the temporal evolution of the temperature at a middle part of solid methane obtained by simulation calculation, which is quite similar to what was observed by the mock-up experiment, giving also a good support to our simulation calculation. Note that the simulation calculation does not agree with the temperature increase of the hydrogen thermometer as shown in Fig. 5(b). The final temperature rise is only 0.7 K for 1.2 W heat deposit, while the simulation calculation expects the rise of 1 K for this heat deposit. The discrepancy may be due to the thermometer tube made by copper which decreases the temperature of the thermometer by heat flow through it. The results suggest that the heat deposit corresponding to the temperature increase of 1.0 K of the hydrogen thermometer should be modified from 1.2 W to 1.8 W which is listed as "corrected values" in

Table 1.

The comparison of the calculation and observation was also done for higher heat deposit of 10 W in Fig. 7. The agreement between the calculation and observation is again reasonably good in both cases of without and with Aℓ wires, suggesting the correctness of the values of parameters we adopted in the calculation. Note, however, that the calculation of the case with Aℓ wires does not agree with the observation, if we assume that the wires contact perfectly with the moderator case wall which we assumed to be 16.5 K. The thermal contact of the wire to the case wall would not be good in our experiment. Therefore we assumed that there is a thermal resistance between the wire and case, the value of which was determined so as to explain the experimental data for a given heat deposit. The result with this calculation (NC) explains well the observed temperature distribution as well as the dependence of the maximum temperature on supplied heat power as shown in Figs. 7 and 8 respectively.

The results of calculation in different cases are summarized in Fig. 8, where we shows the results of two cases of inserting 1 mmϕ Aℓ wires and 0.5 mm Aℓ plates. We found that either Aℓ wires with a lattice of 5 x 5 mm^2 or 0.1 mm Aℓ plates placed in a distance of 10 mm satisfies the requirement that the temperature of solid methane should be less than 20 K for the heat deposit of 20 W. The latter case is recommanded because it has a better packing factor than the former case and is easy to fabricate.

4. Conclusion

We have found that the insertion of 0.5 mm Aℓ plates with a distance of 10 mm can keep the solid methane temperature below 20 K for the heat deposit of 20 W, if we can keep the temperature of moderator case wall at 18.5 K and makes the plates good thermal contact with the wall. In order to realize this situation, the moderator case should be cooled more directly and the present refrigerator (PHG 105) has an enough cooling power for it. We need, however, to give up the grooved moderator, because the insertion of Aℓ plates is not simple for this moderator. Furthermore our refrigerator power would not be enough to keep solid methane in the grooved moderator below 20 K. In addition to it, the grooved moderator was

found not suitable for the high resolution powder spectroscopy which uses the cold moderator. The decrease of the intensity by adopting the flat moderator can be partly remedied by improving the reflector system.

We should note finally that the insertion of Aℓ sponge (Duocel Foam Metal) is one of the most convenient method to increase the effective thermal conductivity of solid methane as successfully adopted for the IPNS solid methane cold moderator[3] We have, however, decided not to adopt this method because we doubt if a curious phenomenon of "burps", phenomenon of a sudden increase of local temperature and pressure which occurs once a day in the IPNS cold moderator[3], would be related with the use of this Aℓ sponge. It is almost sure that the "burps" is related with the hydrogen gas created by radiation decomposition which may be accelerated by the presence of Aℓ sponge. Further studies will be required to examine this possibility.

References

1) Y. Ishikawa, Y. Endoh and K. Inoue, Proc. Conf. Neutron Scattering in the nineties IAEA (Vienna) (1985) 285.

2) Y. Ishikawa, S. Ikeda, N. Watanabe, K. Kondo, K. Inoue, Y. Kiyanagi, H. Iwasa and K. Tsuchihashi, Proc. ICANS-VII (Chalk River) (1983).

3) J. Carpenter private communication.

Table 1

Heat Deposit in Cold Moderators in KENS-I by Nuclear Radiation[2)]

	Flat Moderator (Jul. 1980)	Flat Moderator (Feb. 1983)	Grooved Moderator (Jul. 1983)
Proton Intensity (current I, μA)	7.3×10^{12} protons/sec (1.2)	8.0×10^{12} protons/sec (1.3)	6.5×10^{12} protons/sec (1.0)
Volume V (cm^3)	900	900	1,544
Bottom Area S (cm^2)	60	60	131
Temperature Rise (K)	1.0	1.4	2.0
Thermal Conductance K(J/K·sec)	1.08	1.09	2.46
Total Heat Deposit q (W)	1.2	1.7	4.9
Normarized Heat Deposit (= $q/N\eta I$) ($mW/cm^3 \cdot \mu A$)	1.11	1.44	2.75
Corrected Heat Deposit* q (W)	1.8	2.4	6.9 W

* corrected based on the present mock-up experiment

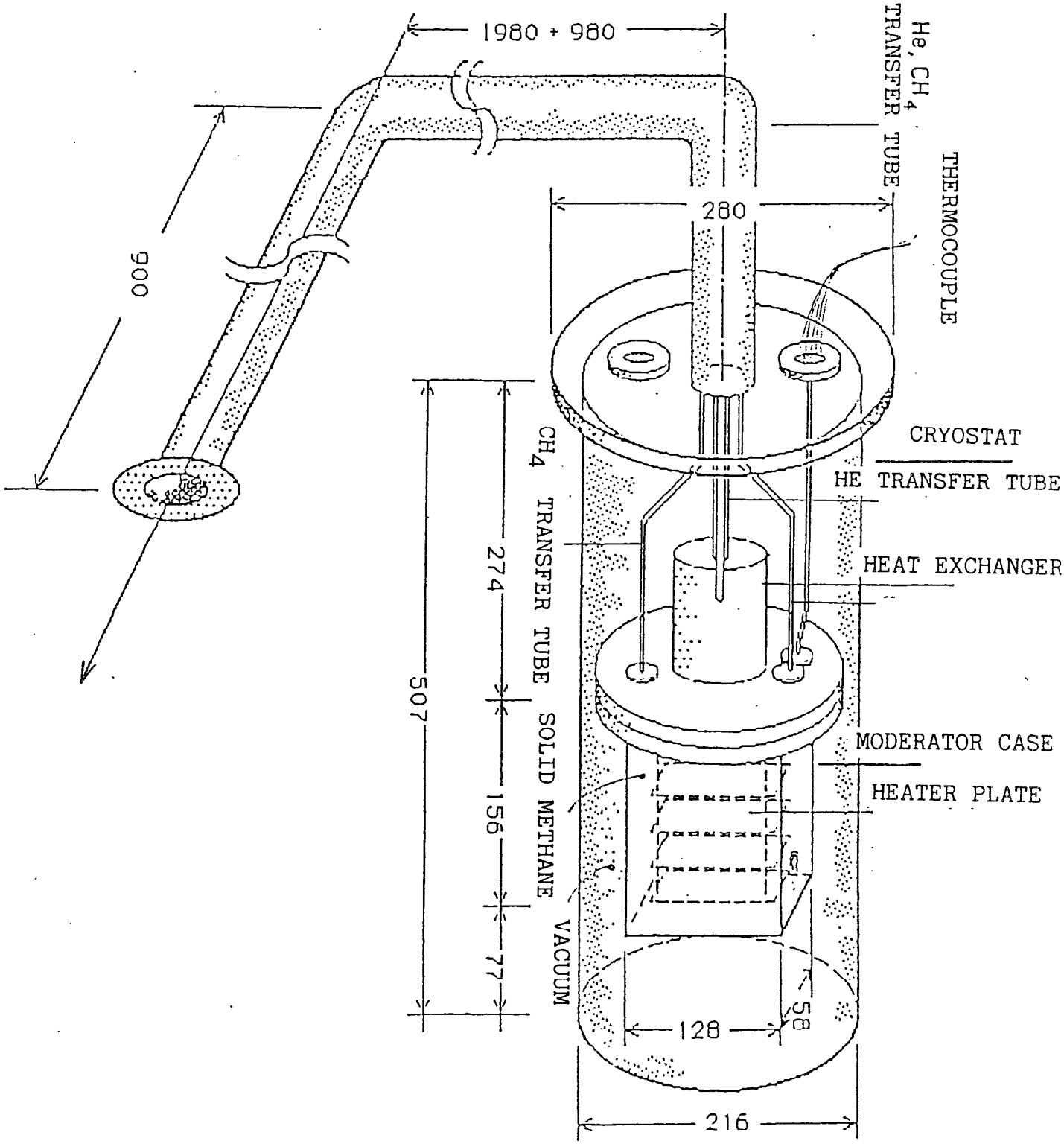

Fig. 1 Layout of mock-up experiment

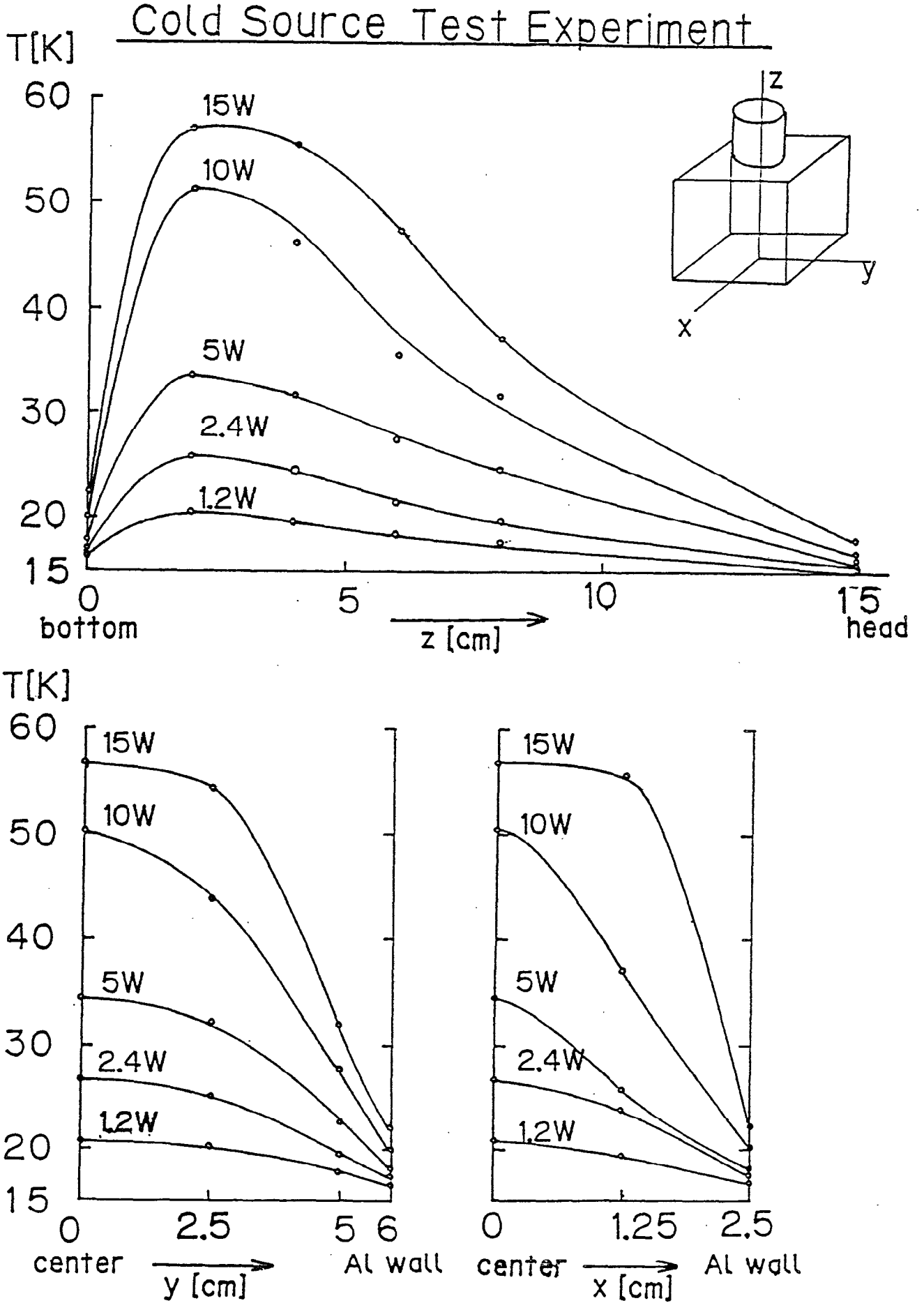

Fig. 2 Temperature distribution inside solid methane when a heat deposit is given by electric heaters

Mock Up Experiments for KENS Cold Moderator

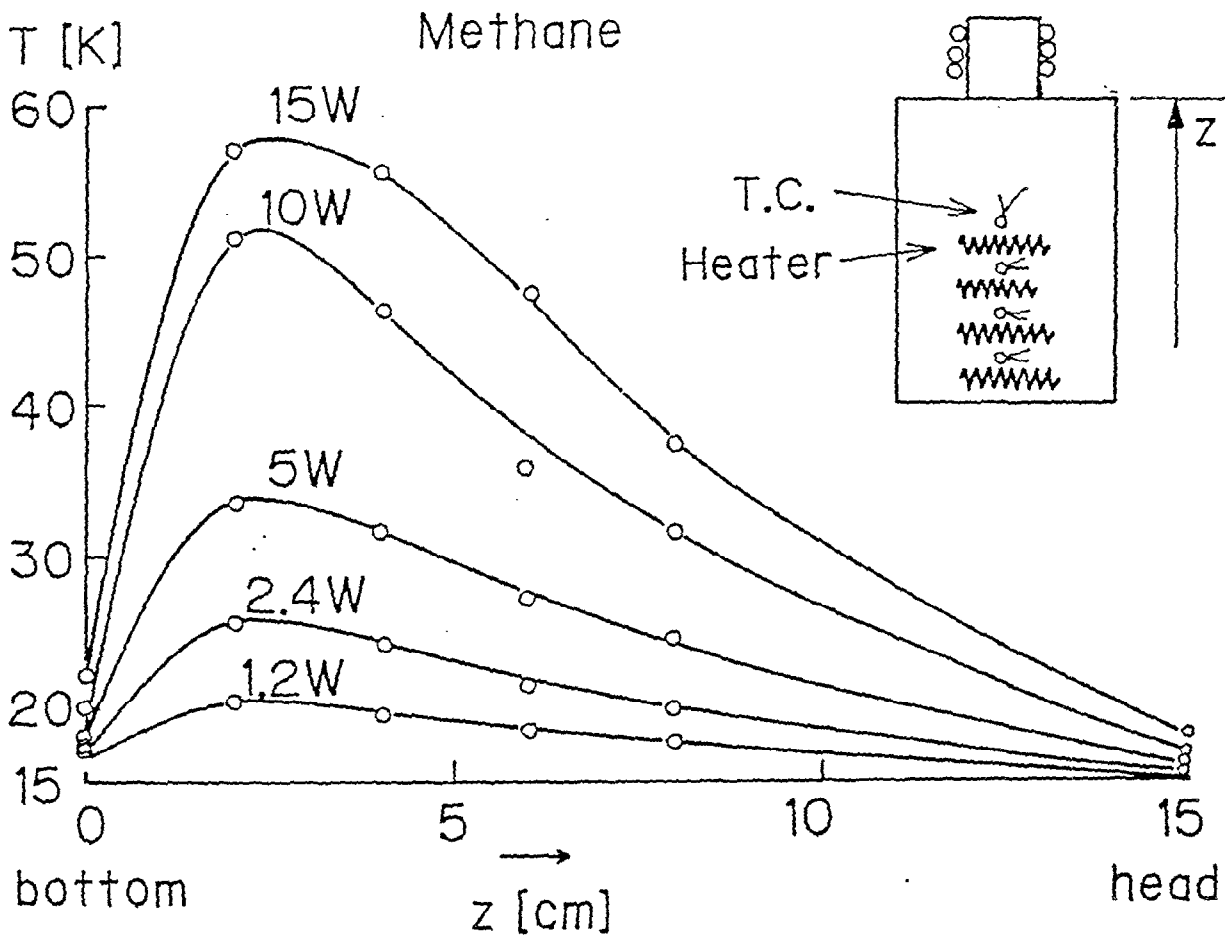

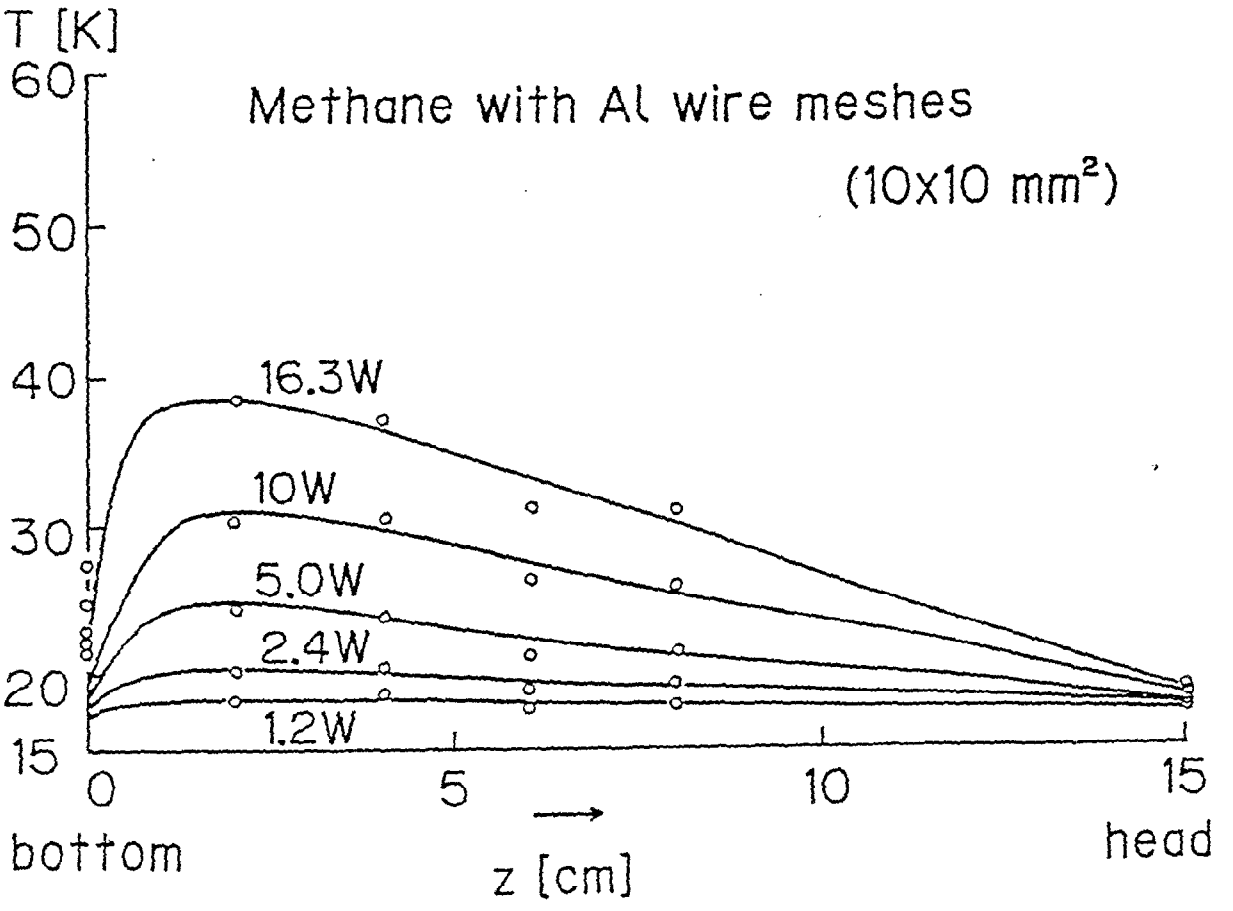

Fig. 3 Temperature distribution of solid methane with 1 mmϕ Aℓ wire lattice when a heat deposit is supplied by electric heater. (lower figure)

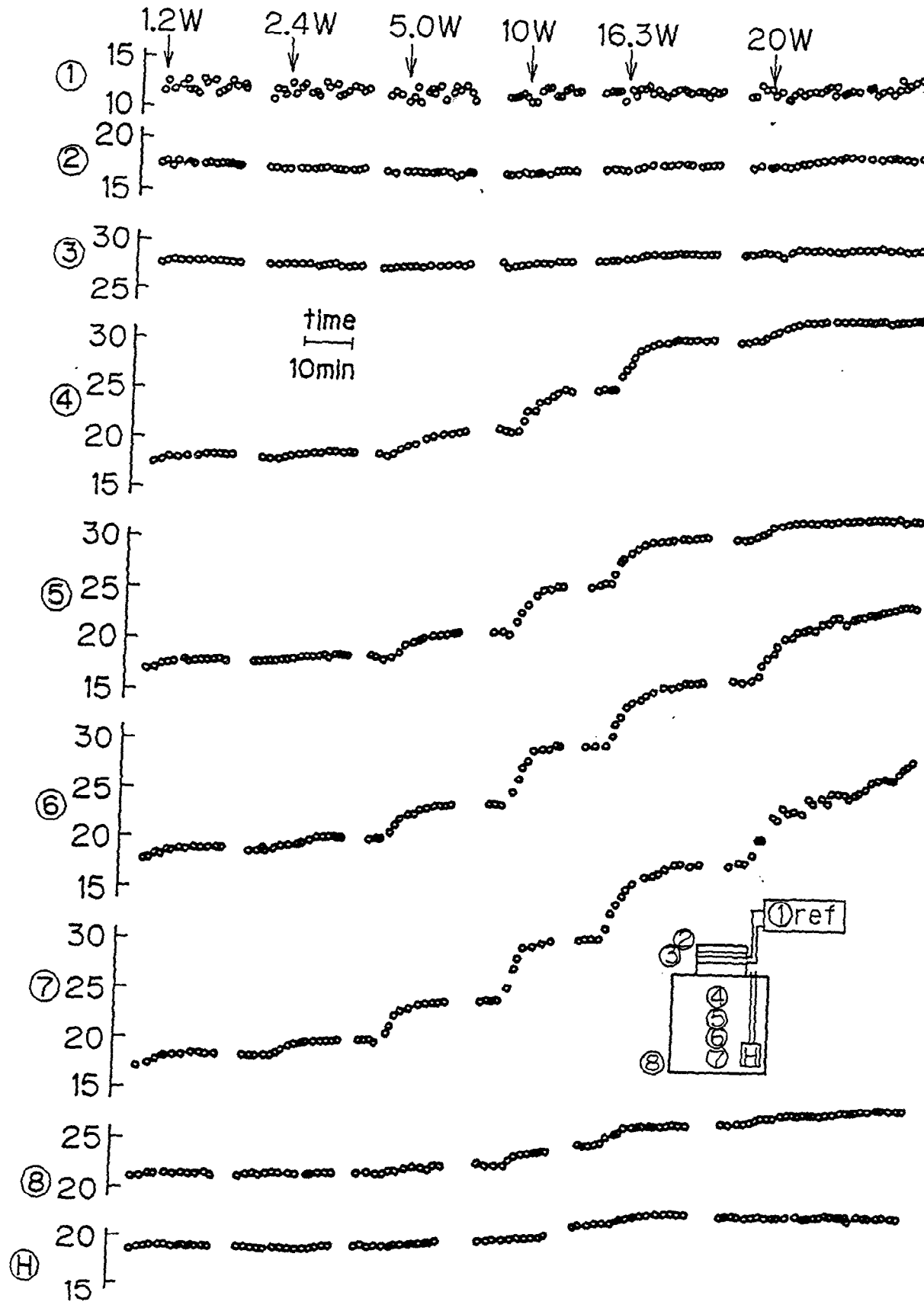

Fig. 4 Temporal evolution of temperatures at several positions inside solid methane marked by numbers in the figure when a heat deposit is given by electric heaters.

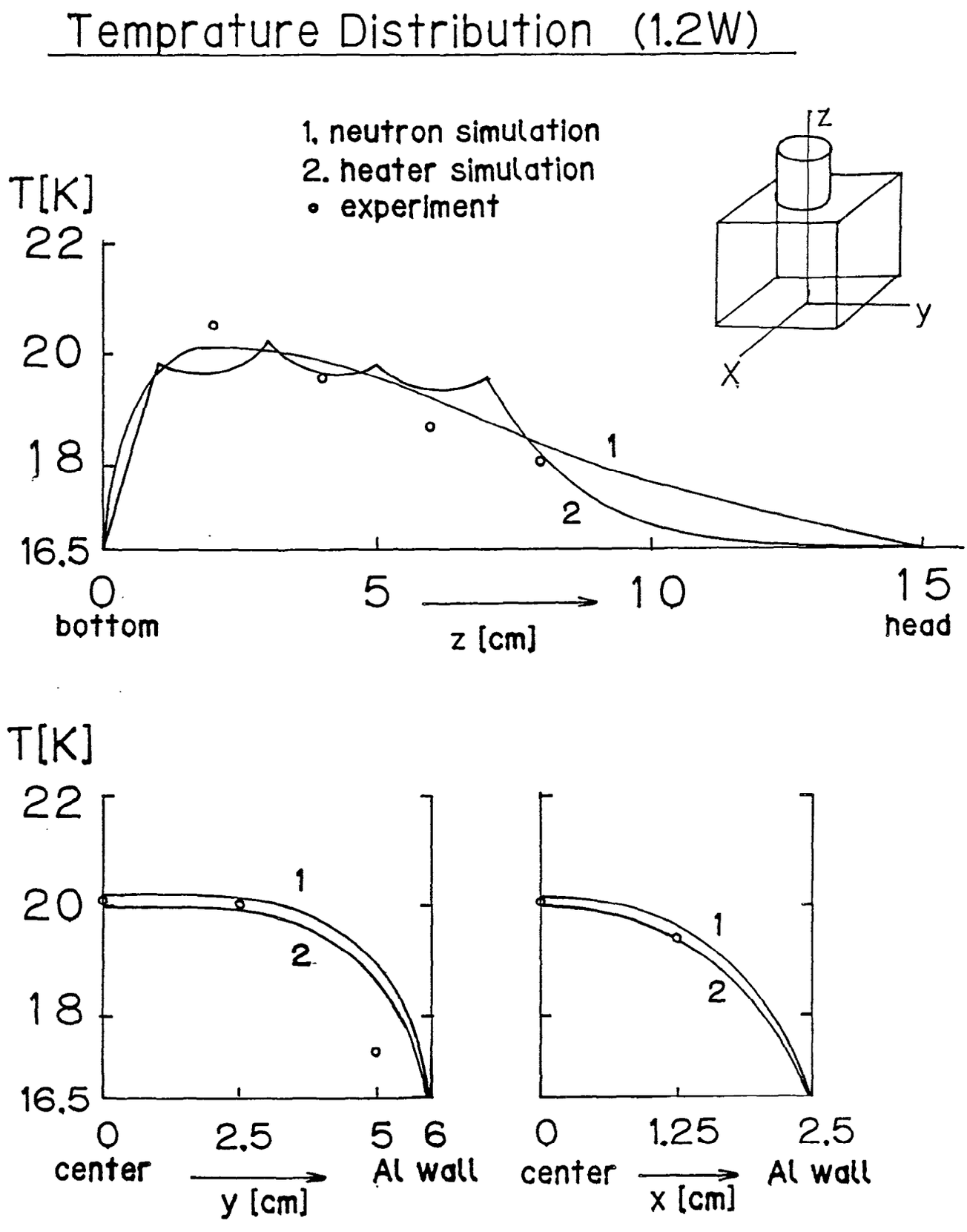

Fig. 5 Temperature distribution of solid methane estimated by three dimensional calculation of heat transport equation (eq(3)) and comparison with observation (o) for Q = 1.2 W.

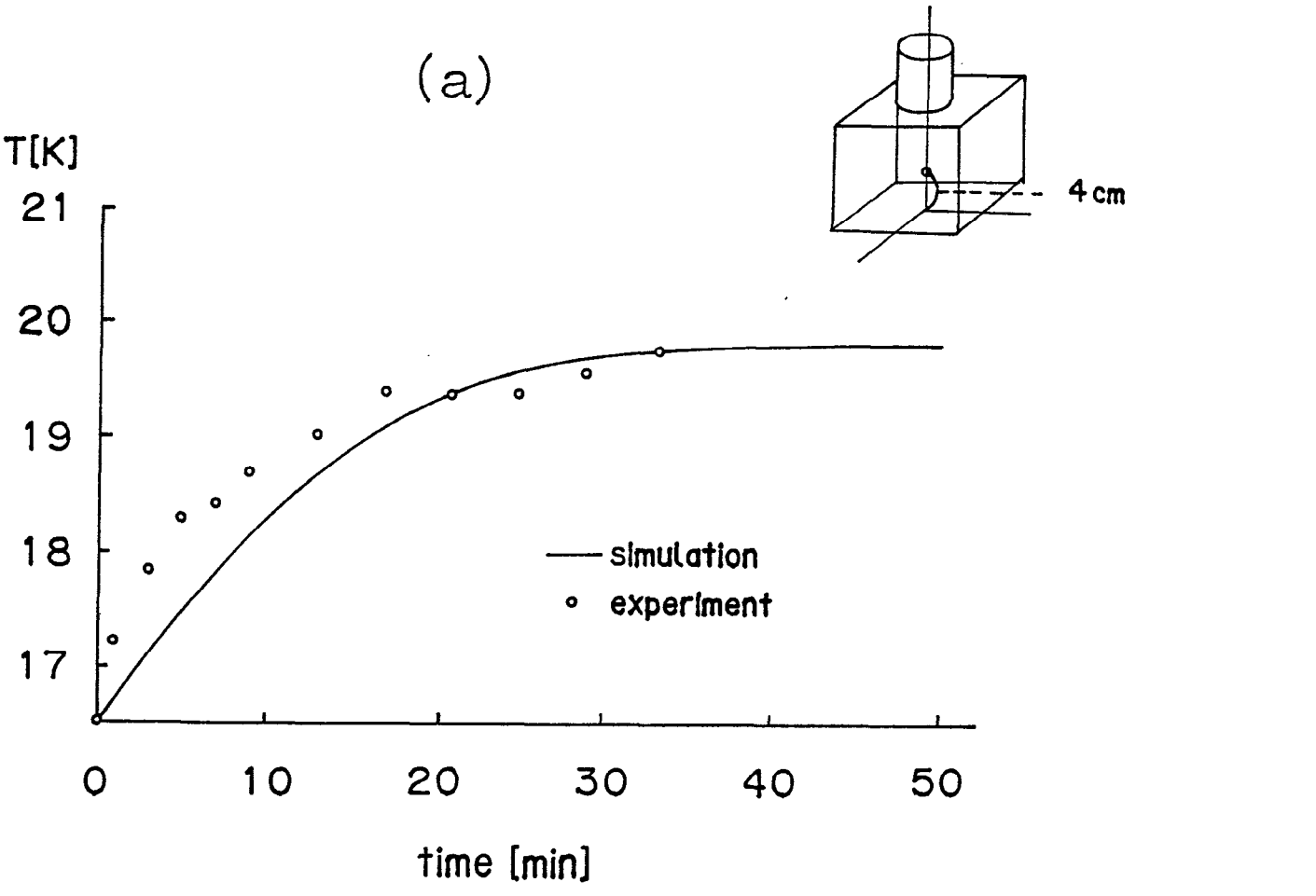

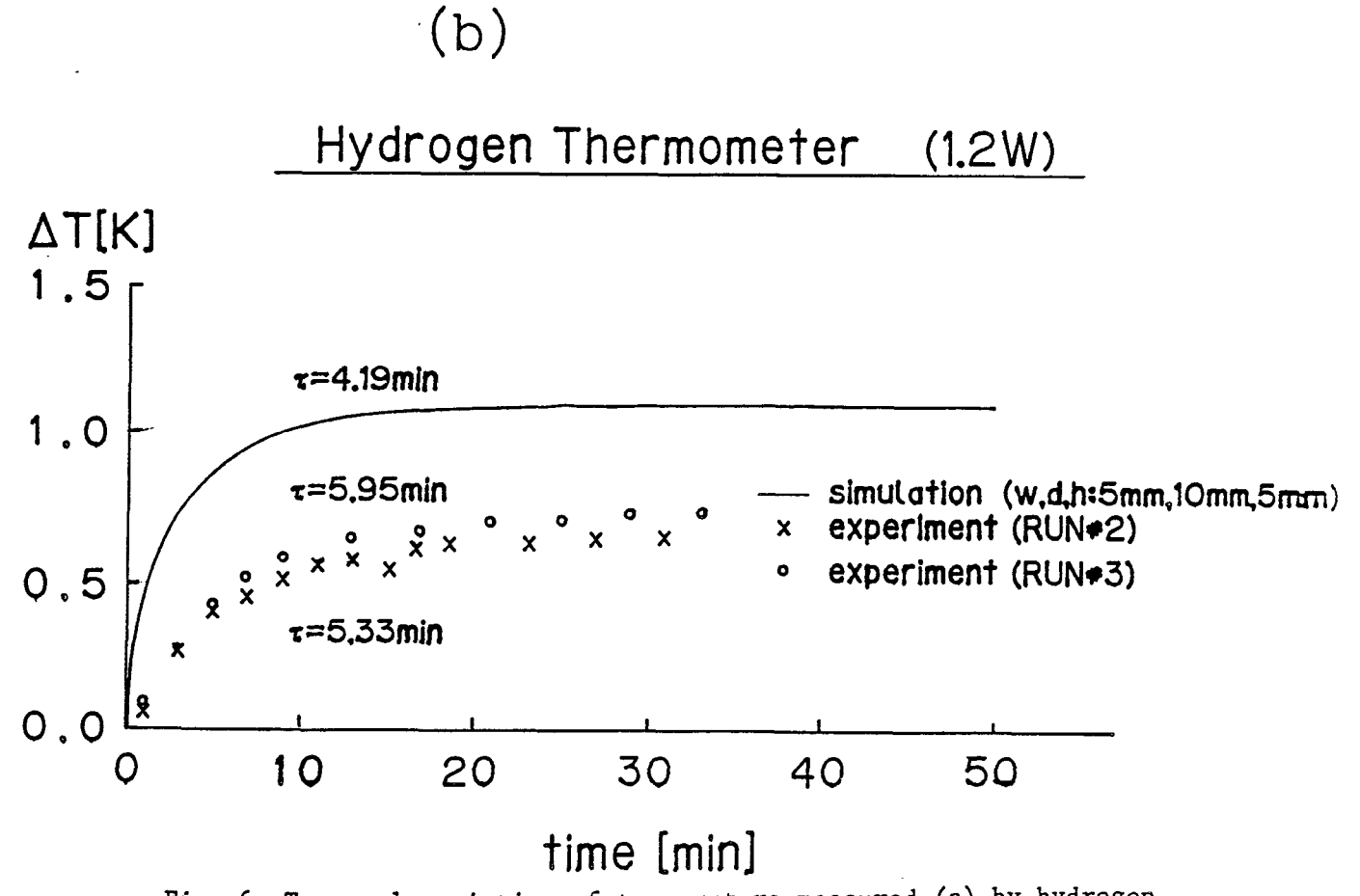

Fig. 6 Temporal variation of temperature measured (a) by hydrogen thermometer and (b) by a thermo-junction at the center and comparison with three dimensional simulation calculation based on eq (3) (solid lines).

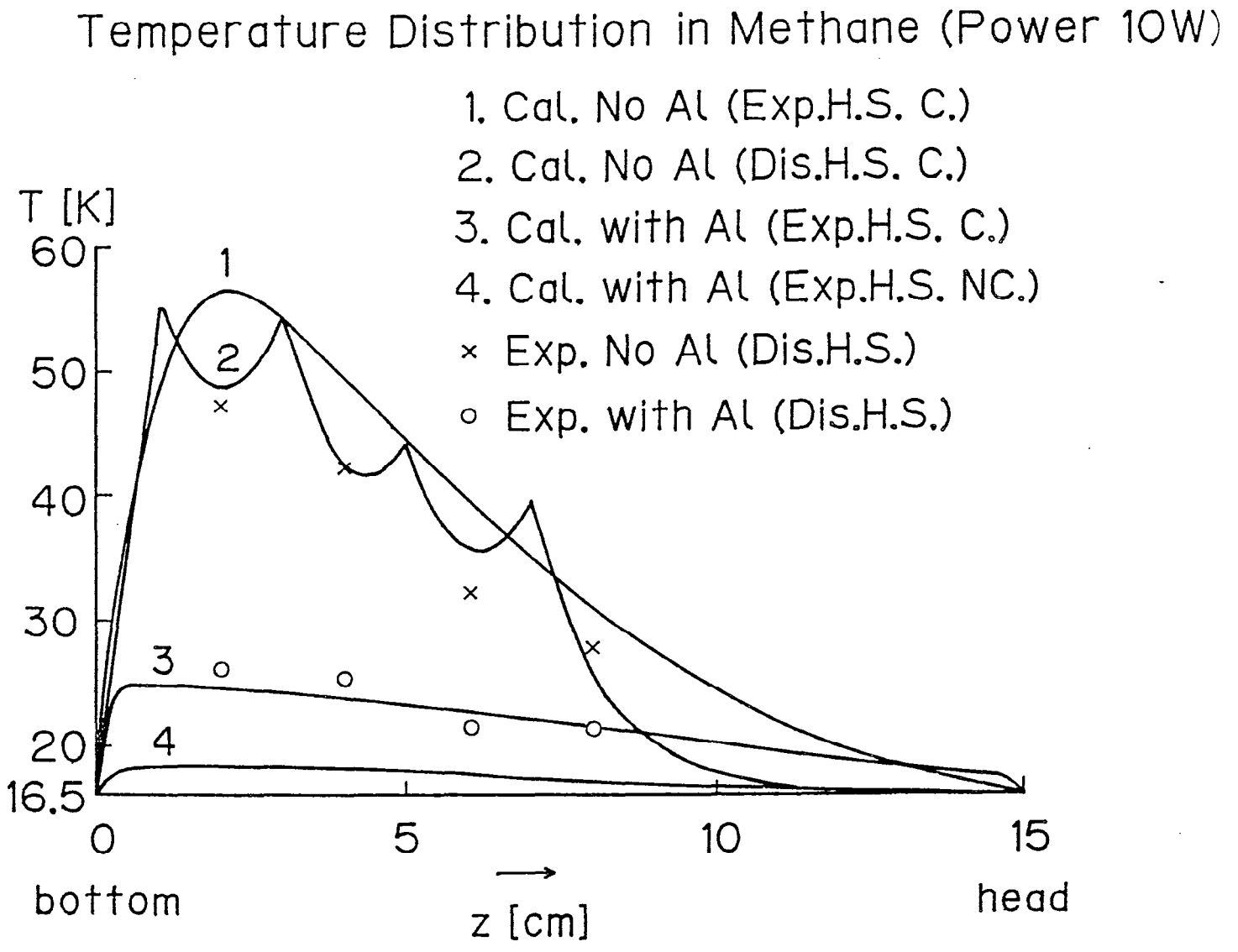

Fig. 7 Temperature distribution of solid methane estimated by three dimensional simulation calculation based on eq (3) for Q = 10W and comparison with observation.

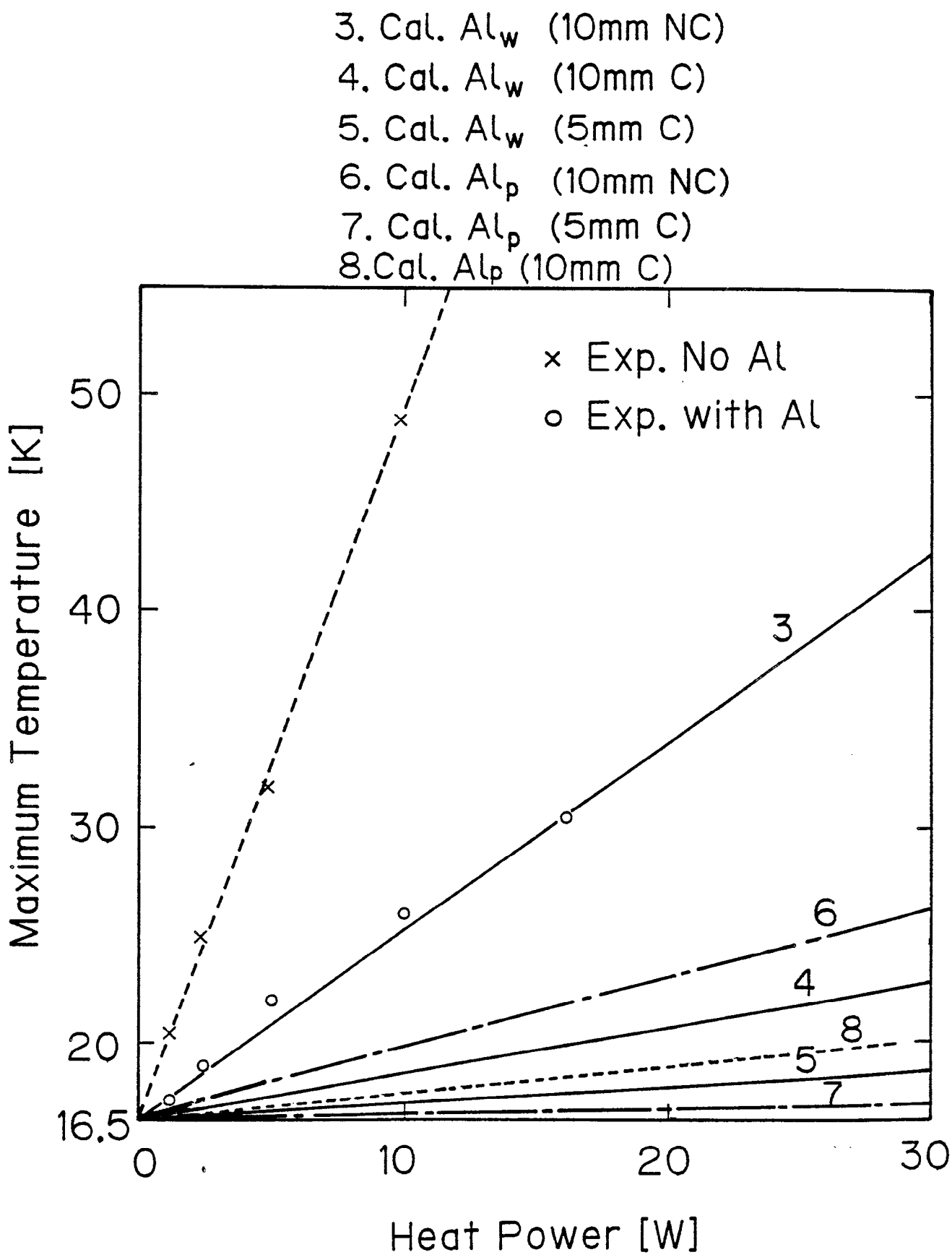

Fig. 8 Calculated maximum temperature of solid methane with various cooling devices plotted against heat deposit.

Proceedings of the Eighth Meeting of the International Collaboration on Advanced Neutron Sources (ICANS-VIII)
8-12 July 1985, Rutherford Appleton Laboratory Report RAL-85-110

LEAKAGE FLUX, LIFE-TIME AND SPECTRA OF COLD NEUTRONS FROM H_2-MODERATORS WITH VARIOUS REFLECTORS

G. Bauer[1], H. Conrad[2], W. Fischer[3], K. Grünhagen[1] and H. Spitzer[2]

1) Projekt Spallationsneutronenquelle, KFA Jülich GmbH, D-5170 Jülich, FRG
2) Institut für Festkörperforschung, KFA Jülich GmbH, D-5170 Jülich, FRG
3) Schweizerisches Institut für Nuklearforschung, Villigen, Switzerland

Abstract

Results are presented of leakage flux, neutron life-time and spectra measurements of nine different cold hydrogen moderators (grooved and flat vessels of varying size) embedded in heavy water, graphite and lead reflectors respectively. Nearly no shape and size dependence of the leakage fluxes from the different vessels in a D_2O reflector was observed. Both graphite and lead reflectors yielded lower average fluxes than heavy water, but lead gave the highest peak flux value due to the shortest neutron life-time of that moderator-reflector combination. The neutron temperature was found to be about 80 K in almost all cases, therefore being much higher than the thermodynamic value. Correspondingly, lower gain factors than for deuterium cold sources will be expected.

1. Introduction

The measurements and results presented here are part of an experimental programme for optimizing the cold moderator of the German spallation source SNQ. Although according to the feasibility study (Bauer, 1981) and the project proposal (SNQ project staff, 1985) a liquid deuterium source is the design choice for one of the two moderators placed on both sides of the target wheel, we started our experiments with a comprehensive study of light hydrogen sources. Admittedly, on the one hand, hydrogen is known to give lower gain factors than deuterium sources. This is because of the higher neutron temperatures only obtainable due to strong cold neutron absorption. On the other hand, however, hydrogen sources are much smaller than deuterium sources. Therefore, higher peak flux values are expected as compared to large deuterium sources. This is due to the shorter neutron life-time in a

small volume of high slowing-down density medium like liquid hydrogen. Furthermore, the technical problems (related to the large nuclear heat deposition in a 30ℓ deuterium containing vessel) are much less severe with a 0.5-ℓ-vessel for hydrogen.

As besides a high peak flux value the SNQ concept also requires the biggest possible time average flux, a high performance reflector tightly coupled to the cold moderator is inevitably necessary. Both large average flux and large peak flux may be contradictory demands, the reconciliation of which may finally be a matter of compromise. With respect to this problem we investigated three different reflector materials: D_2O, graphite and lead. The two moderating reflectors are expected to contribute essentially to the effective neutron life-time, consequently resulting in low peak flux values. Accordingly, the non-moderating lead reflector should yield a higher peak flux and presumably a lower time average flux.

The ultimate goal of this study, the first part of which is presented here, is the optimization of the cold source with respect to at least three parameters: gain factors for cold neutrons, time average flux and peak flux. Therefore the conclusions drawn in this paper from the hydrogen data may have to be revised on the basis of the results from the forthcoming deuterium experiments.

2. Experimental

The measurements have been performed with the 600 MeV protons at SIN (Swiss Institute for Nuclear Research), where since a couple of years an SNQ target-moderator-reflector mock-up has been utilized for basic neutronics experiments. The arrangement is depicted in Fig. 1. It mainly consists of a large rectangular tank (1.7 x 1.7 x 2.5 m^3) into which targets, moderators and reflectors are installed. The targets (Pb or ^{238}U) are placed on a table, which also serves as a support for the solid reflectors piled around the cold moderator chamber above the target. In the case of a D_2O-reflector the whole tank is flooded up to a level of 85 cm above the target midplane. For technical reasons the space below the target could not, according to the SNQ design, filled with lead and iron, representing the reflector of the ambient temperature moderator and part of the shielding. The neutron reflecting action of both these non-moderating materials was simulated in the present experiments by filling the tank with D_2O up to the lower target surface and decoupling the D_2O by a 0.1 cm Cd layer just below the target.

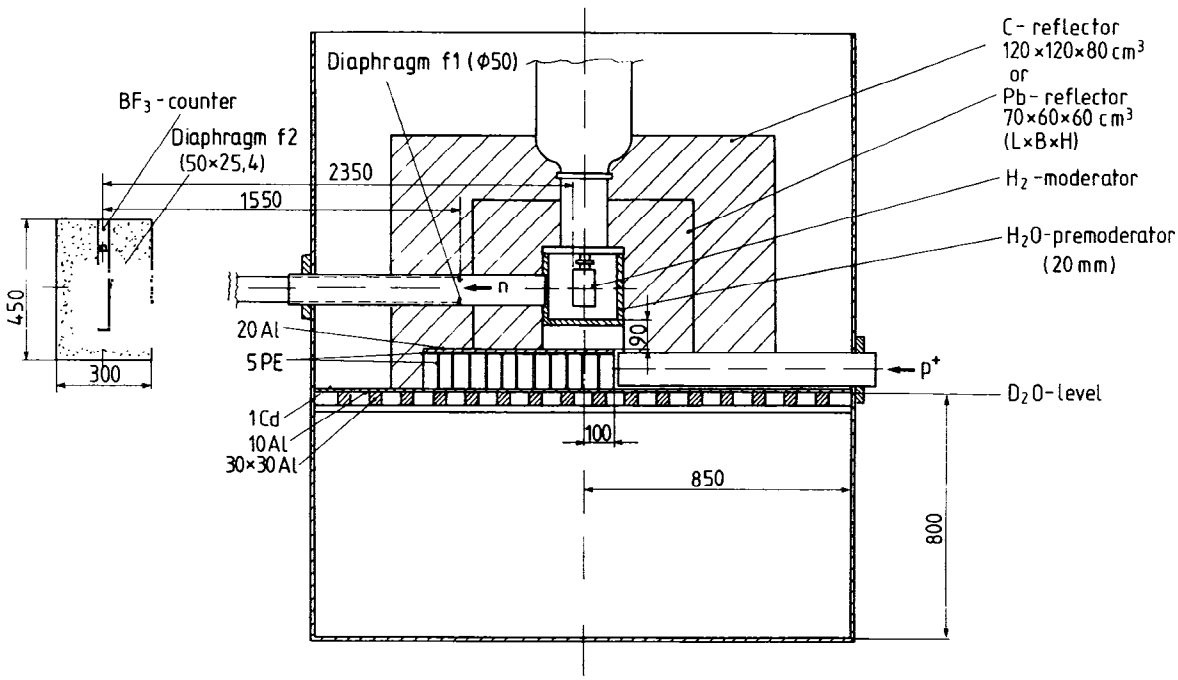

Fig. 1 Schematic representation of the experimental set-up
(For the sake of simplicity both carbon and lead reflectors are shown together. They were not used together in one measurement.)

The hydrogen has been liquified in situ employing the evaporation of liquid helium within a heat exchanger plate, which served as the common support onto which the different moderator chambers have been tightly attached. Each vessel was permanently connected to a surge tank ($V \approx 1\ m^3$) filled with gaseous hydrogen up to 2 bars. The pressure decrease during condensation has been used as a measure of the filling level of the cold chambers. Altogether four pairs of moderator vessels have been investigated. Each pair consisted of a flat and grooved vessel, both having the same volume and the same dimensions perpendicular to the neutron beam hole. Thus, the four pairs differed only in the "effective" thickness along the neutron beam direction, being equal to 2.5, 3.6, 5.6 and 7.8 cm respectively. In all but one case both the normal and the para-modification have been measured. The para-modification has been generated by submerging a Fe_2O_3 catalyst into the liquid hydrogen. The completed conversion has been determined by the vapour pressure increase in the isochorous system.

The neutron life-time in the cold moderators has been measured with a small

boron-10-depleted BF_3 counter mounted on the vacuum container wall. This counter has been shielded against thermal neutrons from the reflector by a cadmium cover. The neutron counts have been stored time-dependently, the time-zero signal being generated by a pick-up unit on the proton chopper. The proton pulses had nearly triangular shape of about 250 µs FWHM. The cold neutron spectra have been recorded simultaneously with the life-time data, the latter being the "resolution" function for the former ones. The flight path used was the 235 cm long beam channel shown in Fig. 1. The leakage fluxes have been measured in the same configuration but with a continuous proton beam on target.

3. Data Evaluation and Results

3.1 Leakage Fluxes

The absolute values of the time average cold neutron fluxes have been deduced from measurements of the neutron current at the end of a beam hole of

Target	Moderator thickness [mm] f = flat g = grooved		time average cold neutron fluxes $\overline{\phi}_{sth}$ [10^{14} cm^{-2}s^{-1}]				
			Reflector D_2O hydrogen modification		C + premoderator		Pb + premod.
			n	p	n	p	n
Pb	25	f	3.2 ± 0.2	3.3	-	-	-
		g	3.3	-	-	-	-
Pb	36	f	3.1	3.0 ± 0.2	2.9 1.9(no premod.)	2.8	2.3
		g	3.4	3.4	3.0 2.8(refl.cooled)	-	2.2
Pb	56	f	2.9	3.0	-	-	-
		g	3.1	2.9	-	-	-
Pb	78	f	2.7	2.8	-	-	-
		g	3.1	2.9	-	-	-
Pb	96	f	3.0	-	2.5	2.5	2.2
^{238}U	36	f	-	5.8 ± 0.4	-	-	-

Table 1 Time average fluxes for various cold H_2-moderators in different reflector environments

known geometry. The neutron counting rates have been corrected for epithermal background (cadmium difference data), energy dependent detector efficiency and geometrical factors. By simultaneously counting the protons via a scintillator telescope viewing a scatterer in the proton beam, the absolute fluxes given in the Tab. 1 have been obtained by scaling the proton current to 10 mA. This corresponds to the SNQ design values of 5 mA at 1100 MeV.

The results from Table 1 obtained with the complete set of moderator vessels, filled with both normal and para hydrogen, and measured with the D_2O reflector are shown in Figure 2.

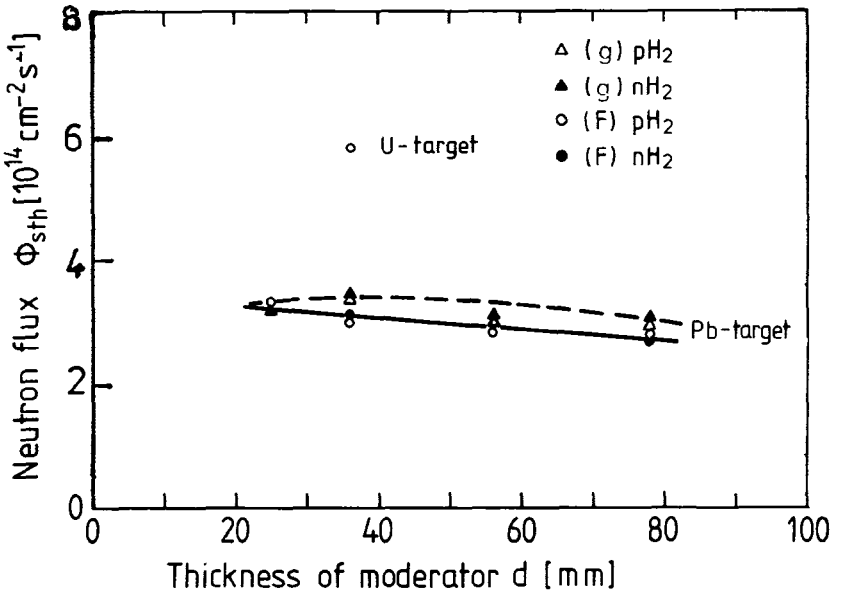

Fig. 2 Time average cold neutron fluxes (D_2O reflector) as a function of moderator thickness d. Full symbols denote normal hydrogen, open symbols the para modification. Circles stand for flat vessels, triangles for grooved ones. Data connected by guide lines for the eye have been obtained with a Pb target, the single data on top is for a ^{238}U target.

3.2 Life-times of cold neutrons in H_2 moderators in different reflector environments

The build-up and decay of the neutron field in the moderator has been measured with a small counter attached to the vacuum container as mentioned

above. Although the time dependence of the overall neutron signal is determined both by the proton pulse shape and the decay constants of the moderator, the latter ones solely describe the signal shape for times greater than the proton pulse duration. From a semilogarithmic plot of the time signal the decay constants can be obtained without any deconvolution of the data. Figure 3 shows such plots for the "optimum" moderator in D_2O, graphite and lead reflectors respectively.

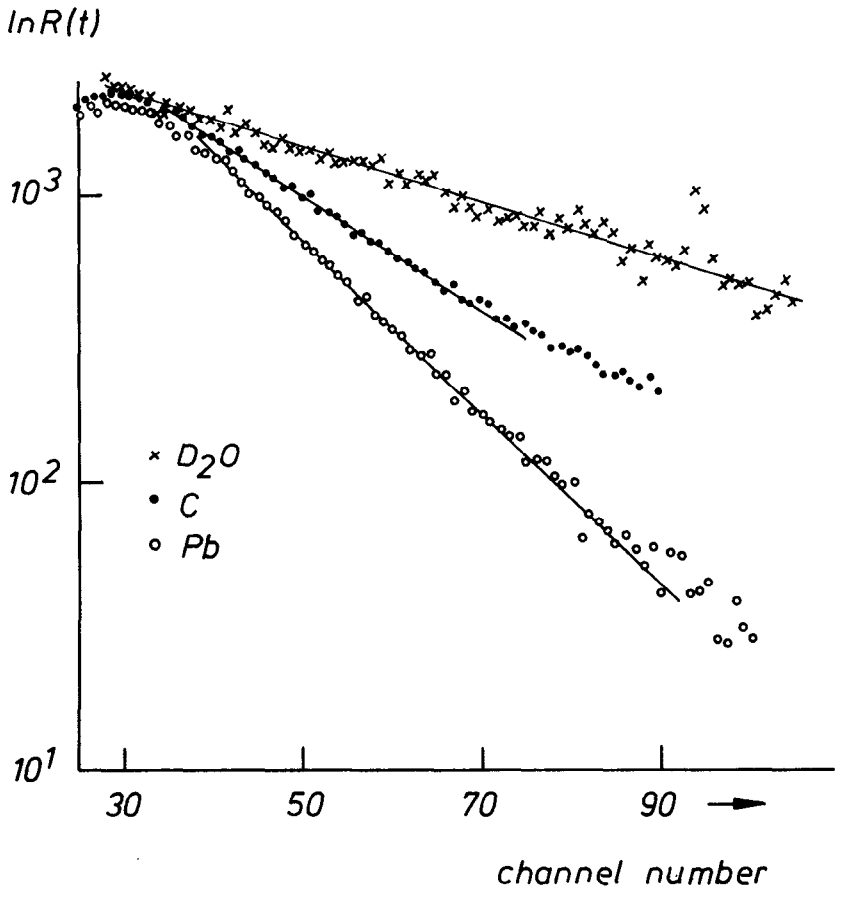

Fig. 3 Semilogarithmic plots of the time signal obtained for the optimum moderator in various reflector environments. (The channel width is 16 μs.)

The decay constants determined from the slopes of the semilogarithmic plots are (in units of microseconds):

710	for	D_2O
350	for	graphite
230	for	lead.

The consequences of these figures will be discussed in section 4.

3.3 Spectra and Neutron Temperatures

In order to deduce the neutron temperature from our measured time-of-flight spectra we proceeded in the following way. Firstly, we assumed that a Maxwellian velocity distribution is the proper description of the equilibrium part of the spectra and that the slowing-down process may be described by a simple $1/E^{1-\alpha}$ law. Secondly, we had to compute convolution-like integrals containing both the above expressions and the time signal from section 3.2 as the resolution finction for the Maxwellian as well as the proton pulse shape as the generating function of the slowing-down peak. In this step we also took into account both the unavoidable overlap contribution of the low velocity tail of the Maxwellian and a correction for detector efficiency. Thirdly, we fitted by a numerical procedure the resulting expression (eq. 1) to the experimental data.

$$I(t) = \int_{t_o}^{t} P(t')E(t-t')\varepsilon(t-t')dt' + \int_{o}^{t} R(t')M(t-t')\varepsilon(t-t')dt' + \int_{o}^{t_c} R(t')M(t + t_c - t')\varepsilon(t + t_c - t')dt' + B \qquad (1)$$

The notations are: proton signal P(t) with t_o as its starting time, the slowing-down spectrum E(t)

$$E(t)dt = E_o \cdot t^{-(1+2\alpha)}\, dt/(1 + 5^7(t/t_T)^{14})$$

where the denominator acts as a joining function to the Maxwellian. R(t) is the experimental resolution function for the Maxwellian, i.e. the time behaviour of the moderator neutron field measured during one chopper period t_c. The energy-dependent detector efficiency is denoted by $\varepsilon(t)$, a time-independent background by B. The third term of equation (1) describes the frame overlap from one previous chopper cycle. The Maxwellian assumes the form

$$M(t)dt = M_o \cdot t^{-5} \cdot \exp(-t_T^2/t^2) \cdot dt.$$

The fit parameters have been E_o, α, M_o, t_T and B. The neutron temperature T is given by the expression

$$T = 3.35 \cdot 10^{-4}(Ks^2) \cdot t_T^{-2}$$

In Table 2 is presented a compilation of selected neutron temperature data from various cold moderators in different reflecting environments.

Target	Moderator thickness [mm] and shape F = flat G = grooved		Effective neutron temperature T_N[K]							
			Reflector							
			D_2O				C + premoder.		Pb + premoder.	
			normal-H_2	para-H_2	moderator decoupled n-H_2	moderator decoupled p-H_2	n-H_2	p-H_2	n-H_2	p-H_2
Pb	25	F	94 ± 7	82 ± 5	-	-	-	-	67±18	68±24
		G	88 ± 6	-	-	-	-	-	-	-
Pb	36	F	82 ± 5	78 ± 5	-	-	76±5	-	72±7	-
		G	84 ± 6	-	54±9	53±11	81±6	-	81±8	-
Pb	56	F	76 ± 5	82 ± 4	58±7	-	-	-	-	-
		G	83 ± 6	87 ± 6	-	-	-	-	-	-
Pb	78	F	83 ± 5	81 ± 4	-	-	-	-	-	-
		G	79 ± 5	78 ± 5	57±7	53±7	-	-	-	-
Pb	96	F	-	-	-	-	73±4	72±4	-	-
^{238}U	36	F	-	-	-	-	-	-	-	79±5

Table 2 Selected results from the numerical determination of the neutron temperature

A typical set of experimental data, i.e. the proton signal, the time behaviour of the neutron field and a time-of-flight spectrum, the latter together with the fitted curve, is shown in Figure 4.

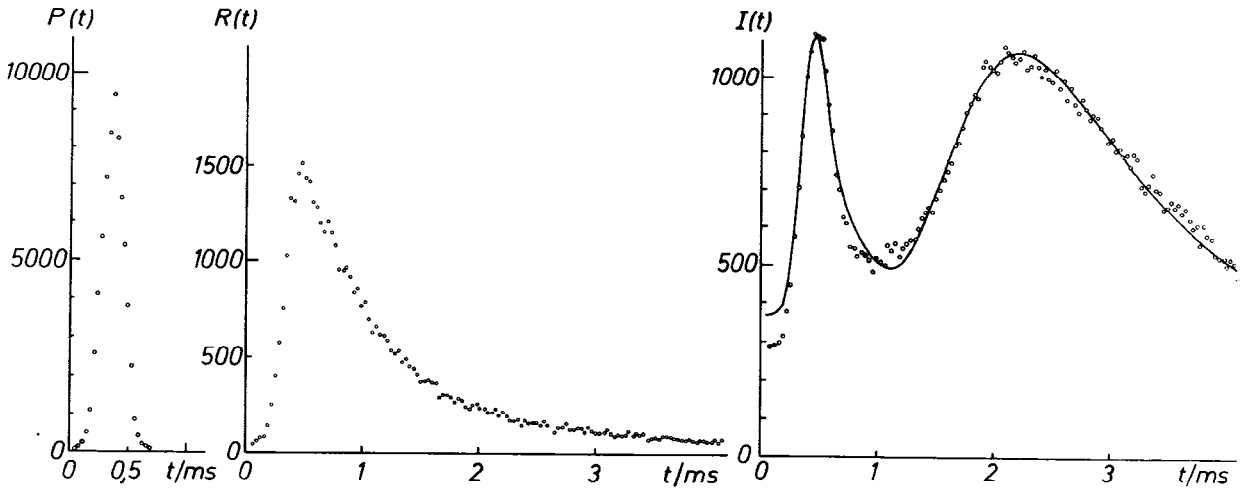

Fig. 4 Example of experimental proton signal, neutron time signal and time-of-flight spectrum with fitted theoretical curve. The corresponding neutron temperature is T = 78 ± 5 K.
(para-H_2, vessel F36, D_2O reflector)

4. Discussion and conclusions

Surprisingly, the leakage flux values do neither depend significantly on hydrogen modification nor on moderator "thickness" (i.e. vessel dimension perpendicular to neutron beam) and shape. Apparently, gain factors of 2, as obtained with ambient temperature moderators with grooved survaces (Bauer et al. 1981) are missing with cryogenic moderators. A possible explanation might be the fin width of 1.3 cm, which was the same for all vessels and adapted to the about 60% longer scattering mean free path of slow neutrons in liquid hydrogen as compared to H_2O, but which nevertheless might be too large because of stronger absorption of cold neutrons. Absorption may also be the reason for the missing flux dependence upon vessel thickness. Obviously, the "radiating" depth of the H_2 moderator is only about 2.5 cm, the thickness of our smallest vessel, therefore the trivial vanishing of the flux with vanishing moderator volume could not be observed. With increasing

vessel thickness no decrease is observed as the increased number of primary fast neutrons from the target intercepted by the moderator may be just cancelled by absorption of the slow neutrons. Only a weak, if any dependence at all on moderator thickness is expected for the para modification as observed. In this case absorption plays only a minor role as the "escape path" is much shorter due to the large scattering mean free path of about 8 cm.

An essential feature in optimizing both time average flux and peak flux is the action of a premoderator between cold moderator and reflector. For solid state reflectors, which potentially yield higher peak fluxes than D_2O, only the use of a premoderator (in our case a 2 cm layer of H_2O all around the cold vessel) gave comparable time average fluxes like D_2O. With graphite, for example, the gain in time average flux using a premoderator amounted to more than 50% (compare Table 1). Including the unavoidable losses due to the reflector coolant, the time average flux with graphite reflector plus premoderator is more than 80% of the D_2O value (compare Table 3 below). The highest peak flux has been obtained with the lead reflector, the time average flux in this case being about 65% of the D_2O-value. The summary Table 3 gives a concise compilation of the most essential results of the fluxes and neutron life-times and the deduced neutron pulse widths.

reflector material, dimensions [cm³]	average cold flux $\overline{\phi}_{sth}$ [10^{14} cm^{-2}s^{-1}]	neutron life-time [10^{-6}s]	$\frac{\hat{\phi}}{\overline{\phi}}$	neutron pulse width [10^{-6}s] (for proton pulse duration of 250 µs)	peak flux $\hat{\phi}$ [10^{14}cm^{-2}s^{-1}]
D_2O 170x170x85	6.6 ± 0.4	710	12	620	79.
C (cooled) 120x120x80	5.4 ± 0.4	350	20	390	108.
Pb 60x60x60	4.3 ± 0.3	230	27	320	116.

Table 3 Results for a liquid H_2-source (11x11x3.5 cm³) grooved, ^{238}U-target

Inspection of Table 3 shows that a gain in peak flux is paid for by a loss in time average flux and vice versa. It seems that the graphite reflector is a good compromise.

Let us finally discuss the results of the spectra measurements. The high

neutron temperatures deduced from the time-of-flight data are at least qualitatively consistent with experimental results of wavelength-dependent gain factors of hydrogen sources (P. Ageron et al. 1969). A quantitative agreement can hardly be expected because the experiments are never performed in the sense of the definition of the gain factors, i.e. replacement of the cold moderator by an ambient temperature one. In an experiment the gain factors are determined by comparing the intensities of the filled, cold vessel with those of the empty one. Nevertheless, assuming a neutron temperature of 70 K (compare our results!) the experimental gain factors for a hydrogen source can be verified.

Whether this surprisingly high temperature is due to a spectral hardening because of absorption, or due to insufficient moderation or a combination of both, can only be clarified in a high resolution time-of-flight experiment. In such an experiment possible deviations from the Maxwellian could be observed. In the experiments planned for the study of deuterium sources, such high resolution measurements will be performed by chopping the neutron beam adequately. (In the present experiment we chopped the proton beam.) A very interesting phenomenon was observed by completely decoupling the cold moderator from the D_2O reflector: the neutron temperatures fell significantly below the values obtained in the undecoupled cases (compare Table 2). As the fluxes also decreased drastically (about an order of magnitude), thereby impressively demonstrating the importance of the reflector, this decoupling makes no sense as a means in lowering the effective neutron temperature.

References

P. Ageron, Ph. De Beaucourt, H.D. Harig, A. Lacaze and M. Livolant (1969), Cryogenics, Feb. 1969, 42-50.

G. Bauer, H. Sebening, J. Vetter, H. Willax (eds.) (1981), Jül-Spez-113, Teil I

Proceedings of the Eighth Meeting of the International Collaboration on Advanced Neutron Sources (ICANS-VIII)
8-12 July 1985, Rutherford Appleton Laboratory Report RAL-85-110

SNQ-MODERATOR OPTIMIZATION

V. Drüke, P. Cloth, D. Filges, R.D. Neef
Institut für Reaktorentwicklung, Kernforschungsanlage Jülich

SNQ-Moderator Optimization

Fast moderators have to be optimized in their geometrical dimensions as well as in their structural material components. Experiments /1/ show in special cases that "grooved" moderators give higher responses for thermal neutrons than solid moderators.

In the design calculations for the SNQ-target-moderator-reflector system details like the surface structure of the fast moderator originally were not considered. Therefore, a study to optimize the moderator structure (size, surface, and material) was initiated.

A special fast running 3-D geometry model for HETC/MORSE Monte Carlo calculations was developed. The advantage of this geometry model is easy parameter variation for overall size of the moderator and description of grooves and fins including structural and moderator material. Point detector estimation of escaping neutron fluxes in energy, time and space with importance sampling is used.

Figure 1 represents the geometrical model for moderator optimization calculations which have been performed for an uranium target with 1100 MeV incident proton beam.

Figure 2 shows that variation of the H_2O-moderator width from 7 to 21 cm in the direction of the beam tubes (curve A) has no influence on the detector response at 6 m distance from moderator at the end of the beam tubes. A detector response curve for grooved moderators with 12 grooves (depths 1/3 of geometrical width) is plotted in the same figure as curve B. All curves represent theoretical values because in these calculations the grooves are without structural material. The maximum flux at detector positions is 5.7×10^{-7} n/cm^2 per proton compared to 2.90×10^{-7} n/cm^2 per proton in case of an ungrooved moderator shows a possible gain factor of nearly 2 for a grooved moderator. The optimum grooved moderator has an effective width of about 16 cm, i.e. geometrical width of 24 cm and groove depth of 8 cm. All other dimensions are not yet optimized. Variation of the groove depth at constant geometrical width of 18 cm (curve C) shows that the optimum response is obtained with 7 cm groove depth (11 cm effective moderator thickness). In the above calculations the distance between target material and moderator was taken as 5 cm. In case of 2.5 cm distance the gain factor is 1.25. Further calculations show that a 1 mm thick aluminium structure of the grooves reduces the detector response by 30 %. Therefore, the final detector response will be comparable to the case without grooves and without beam tubes.

The results of the calculations are summarized in Table I. The calculation for a moderator optimized in beam tube direction give a flux value of 4×10^{-7} n/cm^2 per incident proton at detector position B (see Figure 1) taking into account all losses in structural materials.

Also given in Table I are values for the "equivalent isotropic flux", denoted as "EIF". This is a commonly used basis for comparison in relating the neutrons measured at the end of a beam tube to the magnitude of the thermal neutron source.

Table I: Thermal neutron fluxes from fast moderator (uranium target, 1100 MeV proton beam energy)

Position	Thermal Neutron Fluxes		
	Φ_{th} (a) (n/cm^2 per proton)	Φ_{th} (b) (n/cm^2 s)	Φ_{th} (c) (n/cm^2 s)
A	2.80×10^{-2}	8.3×10^{14}	3.3×10^{16}
B (ungrooved)	2.75×10^{-7}	8.6×10^{9}	3.4×10^{11}
B (grooved)	4.0×10^{-7}	1.25×10^{10}	5.0×10^{11}
"EIF" (d)	4.6×10^{-2}	1.4×10^{15}	5.6×10^{16}

(a) Neutron fluence per beam proton
(b) Average neutron flux for $\bar{I} = 5$ milliamperes
(c) Peak neutron flux for $\hat{I} = 200$ milliamperes
(d) "EIF" = "Equivalent Isotropic Flux"

To make sure that the Monte Carlo models used are adequate for this problem a series of benchmark experiments was started. These experiments do not aim directly on the optimization of the SNQ fast moderator, but on validation of computational methods. These benchmark experiments were performed with 14 MeV neutrons.

Figure 3 shows a comparison of calculated neutron escape spectra from the fast moderator. Case a) represents the results of a calculation using the 1100 MeV proton beam induced neutron spectrum and source distribution of the SNQ design calculations. The moderated neutrons are transported to the end of flight path. This calculated neutron spectrum is compared with a spectrum originating from a 14 MeV point source (case b) in the same target-moderator-geometry.

No significant differences between the two cases can be recognized. Therefore, benchmark experiments investigating the neutronic behaviour of fast moderators of spallation sources can be performed using D-T-neutron generators.

The experimental arrangement of the experiments is shown in Figure 4. Ungrooved or grooved polyethylene moderators of various thickness are surrounded by lead reflectors of 20 cm x 60 cm x 60 cm dimension. The escape spectra of different fast moderators are measured at the end of the 5.4 m long flight path. Fixing the outer dimensions of the moderator the groove depth and the number of grooves and fins were varied. In Table II several results of the first experimental runs and the corresponding calculations are summarized. Figures 5 to 11 show the normalized measured and calculated neutron spectra of the different moderators. The calculations fit the experiments quite well. In the energy range below 0.02 eV a number of groups should be added to the used 53 group library. The integrated normalized fluxes show the same tendency in experiments and calculations, but in absolute numbers some minor differencies remain.

Table II: Benchmark Experiments and their Flux Yields

Groove Depth in cm	Number of Grooves	Thickness in mm	Normalized integrated flux 0.457E-2 – 1.0 eV	
			Experiment	Calculation
Reference	–	–	1.0	1.0
5	6	10	1.72	1.40
5	12	5	1.86	1.59
5	30	2	1.83	1.63
6	6	10	1.56	1.39
6	12	5	1.75	1.50
6	30	2	1.72	1.71
3	6	10	1.44	1.32
3	12	5	1.57	1.38
3	30	2	1.68	1.56

References

/1/ G. Bauer et al.
Realisierungsstudie zur Spallationsneutronenquelle, Teil B
Jül-Spez-113, June 1981

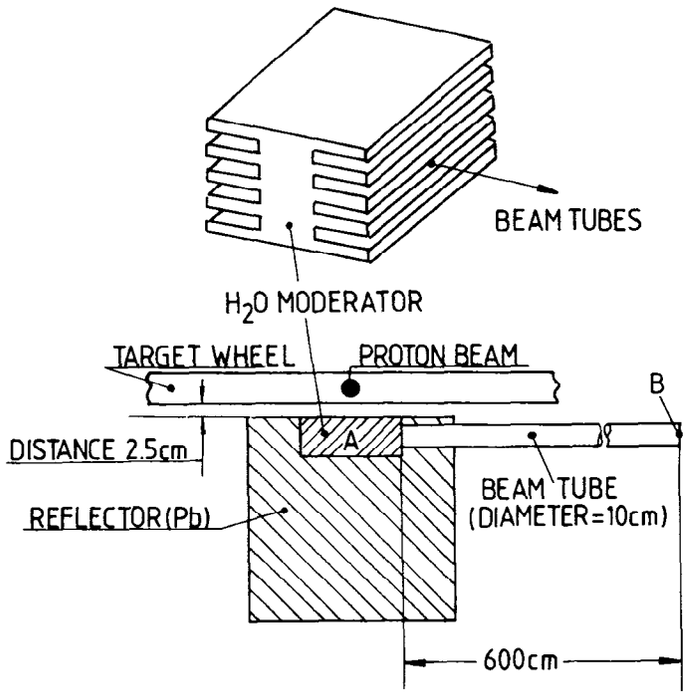

Fig. 1: Model for fast moderator design

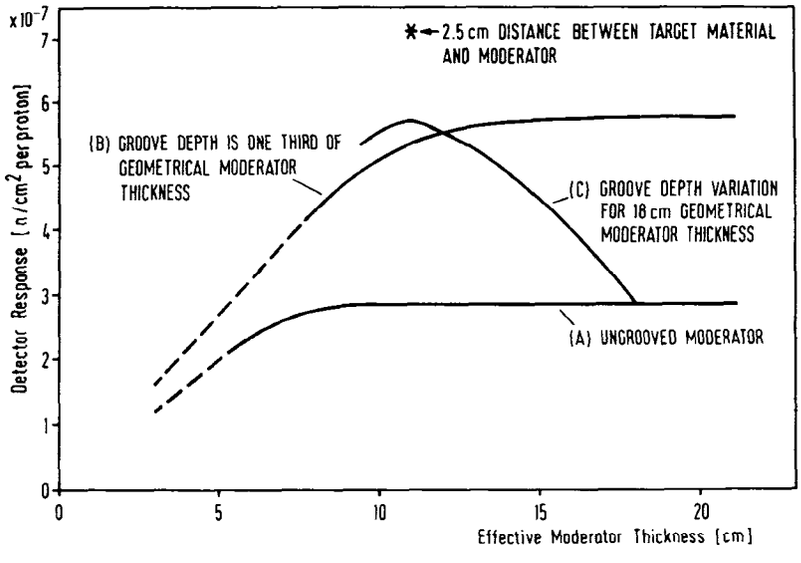

Fig. 2: Moderator optimization by Monte Carlo Calculation: Comparison of detector responses (thermal energy 10^{-5} - 0.4 eV) for solid and grooved moderators

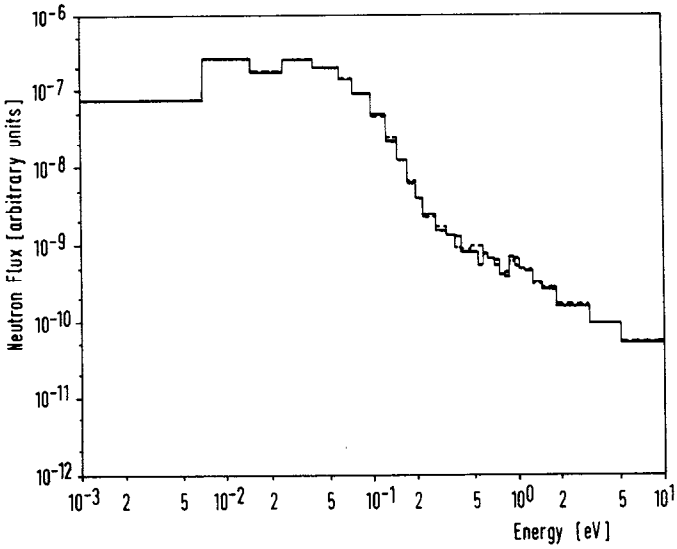

Fig. 3: Comparison of neutron flux spectra from fast moderator at the end of flight path (_____) 14 MeV Neutron Source (-----) Spallation Source

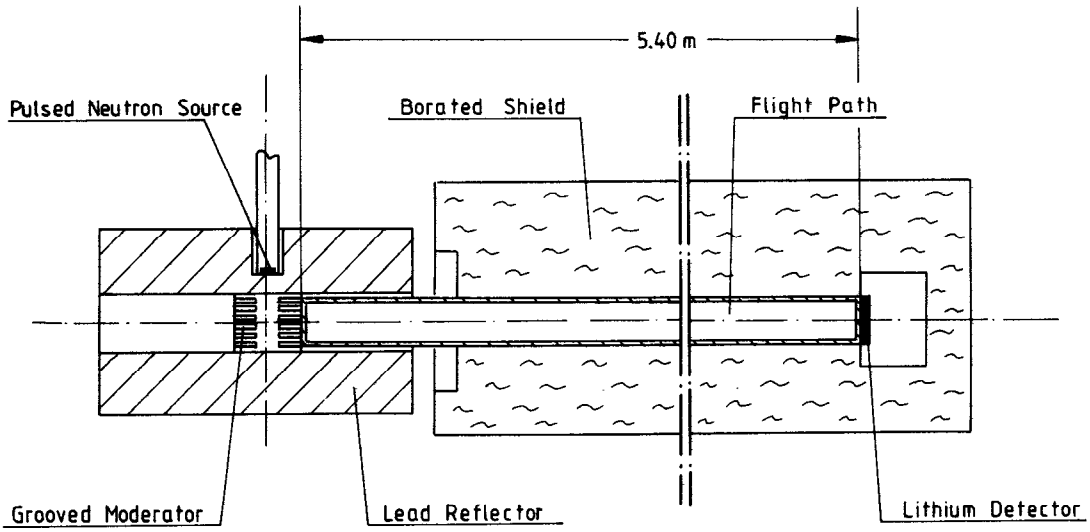

Fig. 4: Horizontal view of measurement assembly

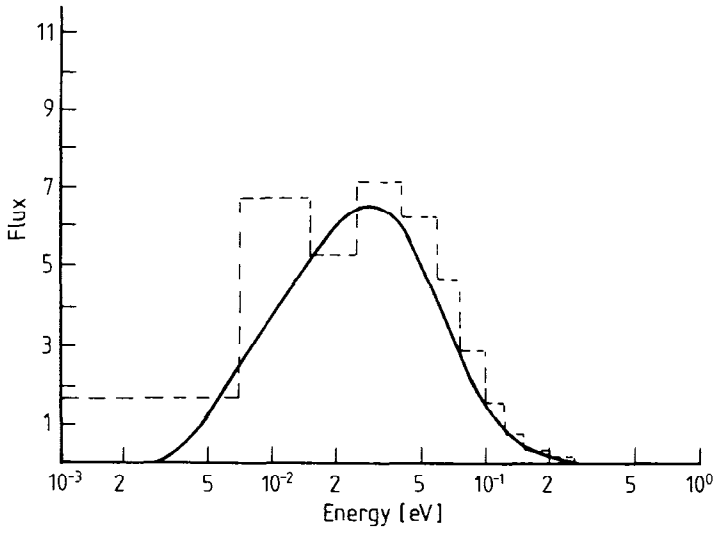

Fig. 5: Reference Moderator without Grooves

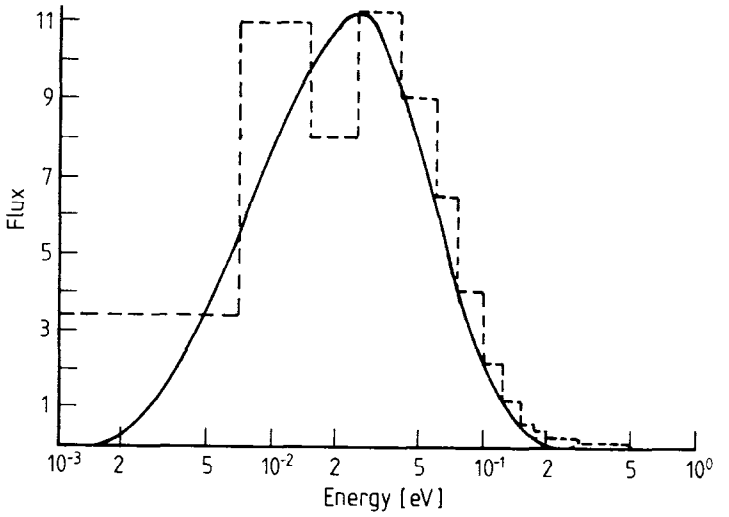

Fig. 6: 6 Grooves of 5 cm Depth

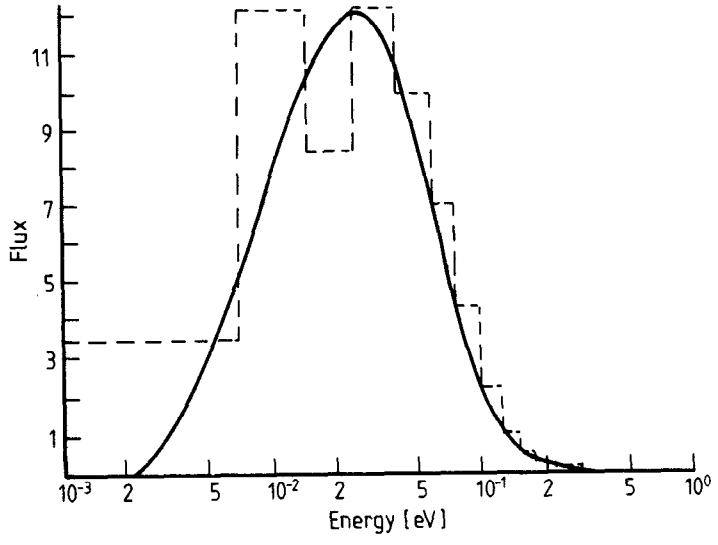

Fig. 7: 12 Grooves of 5 cm Depth

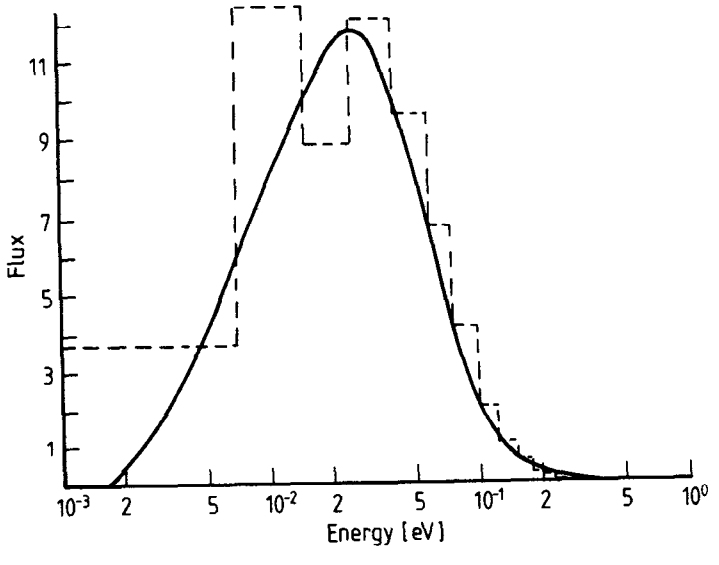

Fig. 8: 30 Grooves of 5 cm Depth

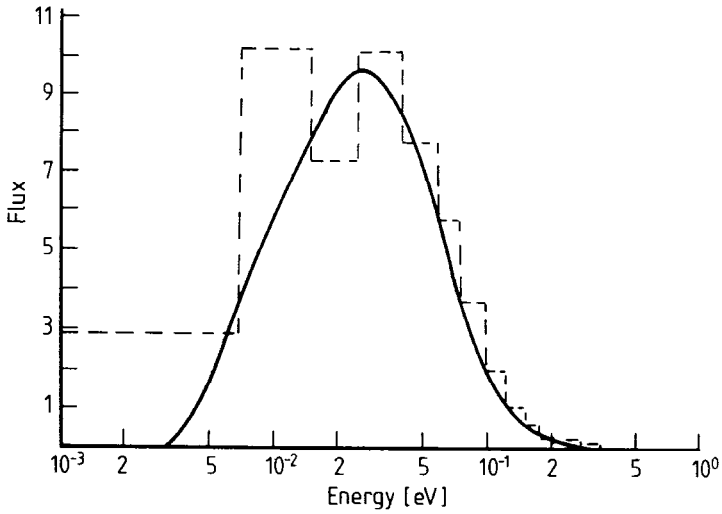

Fig. 9:
6 Grooves of 3 cm Depth

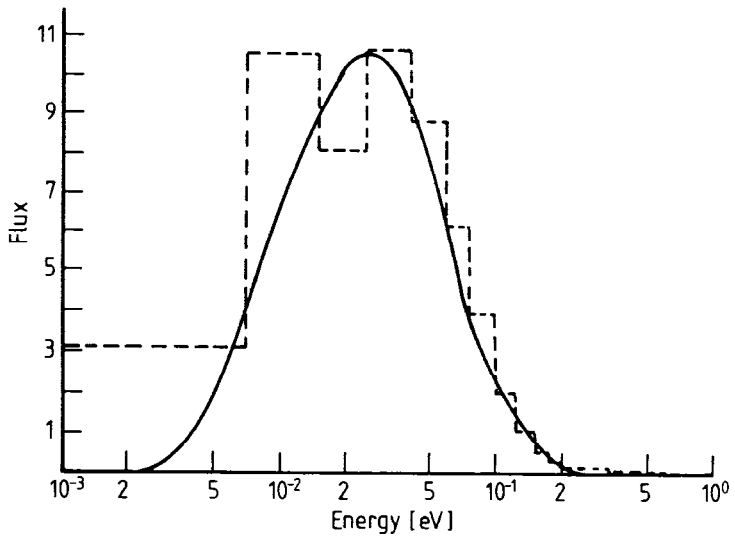

Fig. 10:
12 Grooves of 3 cm Depth

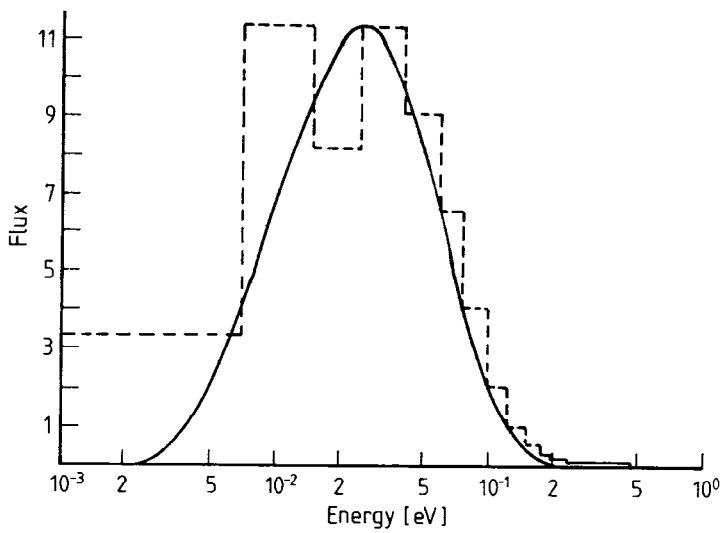

Fig. 11:
30 Grooves of 3 cm Depth

INDEX OF AUTHORS